PACIFIC EARTHQUAKE ENGINEERING RESEARCH CENTER

Proceedings of the

First NEES/E-Defense Workshop on Collapse Simulation of Reinforced Concrete Building Structures

6–8 July 2005
Berkeley, California

Sponsors:

National Research Institute for Earth Science and Disaster Prevention
Pacific Earthquake Engineering Research Center
Japan Ministry of Education, Culture, Sports, Science and Technology
U.S. National Science Foundation

PEER 2005/10
SEPT. 2005

Proceedings of The First NEES/E-Defense Workshop on Collapse Simulation of Reinforced Concrete Building Structures

6–8 July, 2005
Berkeley, California

Organizers:

Jack P. Moehle
Pacific Earthquake Engineering Research Center
University of California, Berkeley

Toshimi Kabeyasawa
Earthquake Research Institute
University of Tokyo

Research Report

Sponsors:

National Research Institute for Earth Science and Disaster Prevention
Pacific Earthquake Engineering Research Center
Japan Ministry of Education, Culture, Sports, Science and Technology
U.S. National Science Foundation

PEER Report 2005/10
Pacific Earthquake Engineering Research Center
College of Engineering
University of California, Berkeley

September 2005

Published September 2005

PREFACE

BACKGROUND

Research collaboration agreements for earthquake disaster prevention are in progress between U.S. and Japanese organizations: the George E. Brown, Jr. Network for Earthquake Engineering Simulation (NEES) and the National Science Foundation (NSF) on the U.S. side, and the National Research Institute for Earth Science and Disaster Prevention of Japan (NIED) and the Ministry of Education, Culture, Sports, Science and Technology of Japan (MEXT). Collectively these organizations are known as the “NEES/E-Defense Earthquake Engineering Research Collaboration.” The purpose of the joint research is to improve scientific knowledge and engineering practice in earthquake-resistant design and retrofit of built infrastructure by conducting experimental research in earthquake engineering using NEES facilities in the U.S. and E-Defense, the world's largest shake table, located in Miki City outside Kobe, Japan. The agreements will enable earthquake engineering researchers to participate in joint research initiatives and to have mutual access to the testing facilities in both countries. The Joint Technical Coordinating Committee (JTCC) is coordinating the implementation of this agreement and the joint research program.

On the U.S. side, NEES is funding research proposals under this joint research framework. On the Japan side, three research themes, (1) steel building structures, (2) bridge structures, and (3) information technology, have been selected and funded as the joint research project for five years beginning in 2005, including the test plans at E-Defense from 2007. Matching funds from both countries are to be coordinated mainly for the three research topics.

Another five-year national project of Japan, “Special Project for Earthquake Disaster Mitigation in Urban Areas,” or the “DaiDaiToku” project in Japanese, begun in 2002, covers (1) wooden structures, (2) reinforced concrete building structures, and (3) soil and foundation. The full-scale or large-scale tests at E-Defense have been planned and conducted for the second phase of this project, from 2005 to 2006. U.S.-Japan research collaboration would be possible in these areas as well under the DaiDaiToku project or under post-DaiDaiToku projects if the common research themes could be coordinated with U.S. researchers funded by NEES for the joint research program.

In the area of reinforced concrete building structures, past collaboration was successful under the "U.S.-Japan Cooperative Research in Urban Earthquake Disaster Mitigation" project sponsored by MEXT and NSF. Activities were coordinated by the Pacific Earthquake Engineering Research Center (PEER), University of California, Berkeley, in the U.S., and by the Earthquake Research Institute, University of Tokyo, in Japan. The proceedings of the first through fifth workshops on Performance-Based Earthquake Engineering Methodology for Reinforced Concrete Building Structures, from 1999 to 2003, have been referred to worldwide with related reports, papers, and guidelines. Evaluation methods for performance criteria, especially on reparability, have been developed by the joint research, while experimental and analytical simulation of seismic collapse, and economical retrofit technologies are still under way in both the U.S. and Japan. Economical retrofit technologies are also the main objectives of the DaiDaiToku project.

The First NEES/E-Defense Workshop on Collapse Simulation of Reinforced Concrete Building Structures was organized as a kickoff or preliminary meeting towards possible collaboration in the field. The objectives of the workshop were:

(1) to identify past experimental and analytical research and the present state of knowledge and practice of collapse simulation;

(2) to exchange information on ongoing research and future plans in related NEES and E-Defense projects;

(3) to apply traditional and new analytical methodologies to the preliminary simulation of the full-scale test plan at E-Defense; and

(4) to discuss future research needs and possible collaborations focused on collapse simulation.

The first workshop was held 6 to 8, July 2005, in the Hotel Durant at Berkeley, California. It was attended by 15 participants from Japan, 11 from the U.S., 2 from Taiwan, and one from Canada, as well as several observers. The participants are identified in the following table.

U.S. SIDE	JAPAN SIDE
Vitelmo Bertero, UC Berkeley Craig Comartin, CD Comartin, Oakland Greg Deierlein, Stanford U. Jack Moehle, UC Berkeley Jose Pincheira, U. Wisconsin Adolfo Matamoros, U. Kansas John Wallace, UCLA James Jirsa, U. Texas at Austin Julio Ramirez, Purdue U. Mark Moore, Rutherford & Chekene, Oakland Kent Yu, Degenkolb, Portland	Toshimi Kabeyasawa, U. Tokyo Taizo Matsumori, NIED Shaohua Chen, NIED Toshikazu Kabeyasawa, U. Tokyo Tomoya Matsui, Toyohashi UT Yousok Kim, U. Tokyo Yasushi Sanada, U. Tokyo Hiroshi Kuramoto, Toyohashi UT Susumu Kono, U. Kyoto Jun Tagami, Kajima Kazutaka Shirai, Ohbayashi Hideo Katsumata, Ohbayashi Taiki Saito, BRI Koichi Kusunoki, BRI Takuya Nagae, U. Kyoto

OTHER COUNTRIES
Chiun-lin Wu, NCREE, Taipei Ken Elwood, U. British Columbia Shyh-Jiann Hwang, NCREE, Taipei

HOST ORGANIZATIONS AND SPONSORS

The workshop was organized as a preliminary meeting under the auspices of the NEES/E-Defense Earthquake Engineering Research Collaboration with funding by the George E. Brown, Jr. Network for Earthquake Engineering Simulation (NEES) and the National Science Foundation (NSF) on the U.S. side, and the National Research Institute for Earth Science and Disaster Prevention (NIED) and the Ministry of Education, Culture, Sports, Science and Technology (MEXT) of Japan.

On the U.S. side, this workshop was supported in part by the Pacific Earthquake Engineering Research Center through the Earthquake Engineering Research Centers Program of the National Science Foundation under Award number EEC-9701568. Any opinions, findings, and conclusions or recommendations expressed in this material are those of the author(s) and do not necessarily reflect those of the National Science Foundation.

On the Japan side, the workshop was supported as part of the (2) Reinforced Concrete Building Structures, Theme II Significant Improvement of Seismic Performance of Structures, "Special Project for Earthquake Disaster Mitigation in Urban Areas (DaiDaiToku Project)," a grant to the National Research Institute for Earth Science and Disaster Prevention (NIED) by the Ministry of Education, Culture, Sports, Science and Technology (MEXT) of Japan.

The technical program was developed by Professor Toshimi Kabeyasawa, Professor, Division of Disaster Mitigation Science, Earthquake Research Institute, the University of Tokyo, and by Professor Jack P. Moehle, Professor and Director, Pacific Earthquake Engineering Research Center, University of California, Berkeley.

The efforts of Yolanda West of the Pacific Earthquake Engineering Research Center to make local arrangements and finalize the program administrative details are especially appreciated. Janine Hannel and YouSok Kim organized the submission of manuscripts and finalized the publication of the workshop proceedings.

The workshop proceedings in the same edition are to be published both from PEER on the U.S. side and from NIED on the Japan side.

CONTENTS

SESSION 5: SEISMIC BEHAVIOR OF SHEAR WALLS
Chaired by Shyh-Jiann Hwang and Kazutaka Shirai

SESSION 6: AXIAL FAILURE OF STRUCTURAL MEMBERS
Chaired by Chiun-lin Wu and Susumu Kono

SESSION 7: DYNAMIC LOADING TESTS
Chaired by Julio Ramirez and Takuya Nagae

LIST OF ORAL PRESENTATIONS

SESSION 1: WELCOME, INTRODUCTION, AND KEYNOTE REPORTS

Chaired by

♦ Jack Moehle and Toshimi Kabeyasawa ♦

DEVELOPING CONSENSUS ON PROVISIONS TO EVALUATE COLLAPSE OF REINFORCED CONCRETE BUILDINGS

Gregory G. DEIERLEIN[1] and Curt B. HASELTON[2]

ABSTRACT

Research and development of methods and tools to assess building collapse are advancing to the stage to warrant concerted efforts to formalize these techniques into consensus guidelines. Extending concepts proposed in FEMA 273/356, ATC 40, and the SAC Guidelines for Steel Buildings, this paper outlines a methodology for collapse assessment under development by the Pacific Earthquake Engineering Research (PEER) Center. The methodology is based on the use of nonlinear analysis to either simulate building sideway collapse response directly or to provide input to component damage (fragility) models to assess loss in vertical load carrying capacity. Validated nonlinear component simulation and fragility models, which are expressed in a statistically robust format, are a key ingredient of the assessment procedures.

1. INTRODUCTION

The primary goal of the seismic design requirements of building codes is to protect life safety of building inhabitants during extreme earthquakes. First and foremost, this requires controlling the likelihood of structural collapse to an acceptably low level. While experience with modern code-conforming buildings has generally been good, the empirical nature of current codes and standards do not provide the means to assess the risk of collapse.

Emerging performance-based design approaches seek to enable more accurate and transparent assessment of both life-safety risks and damage control through the use of advanced analysis models and design criteria. A critical element toward achieving this vision is an accepted framework to integrate the supporting research and development. The first generation of performance-based assessment provisions, such as FEMA 273 and 356 (ASCE 1997; ASCE 2000b) and ATC 40 (ATC 1996), provided an excellent first step towards codifying approaches that embrace nonlinear analysis to simulate system performance and articulate performance metrics for the onset of damage up to structural collapse. As such, these documents marked the

[1] *Professor, Director of Blume Earthquake Engrg. Research Center, Dept. of Civil and Envir. Engrg., Stanford University, Stanford, CA, USA*
[2] *Ph.D. Candidate, Dept. of Civil and Envir. Engrg., Stanford University, Stanford, CA*

first major effort to develop consensus-based provisions that went beyond the traditional emphasis on linear analysis and specification of component strengths, which have long been the mainstay of engineering practice and building code provisions.

In this paper, we examine ways to extend the concepts of the first generation of performance-based provisions to more realistically simulate structural performance, with particular emphasis on models and criteria for predicting structural collapse. By advancing some key concepts to a comprehensive performance assessment framework, the ultimate goal is to promote, through professional consensus, the formalization of procedures, models, and criteria for assessing structural collapse risk.

1.1 Overview of Previous Developments

Over the past fifteen years, there have been a number of important developments that helped provide the framework for current initiatives to develop accurate methods to assess building performance. Two that relate most directly to research of the Pacific Earthquake Engineering Research (PEER) Center are the SAC Joint Venture Steel Project (ASCE 2000a) and the development of the FEMA 273/356 provisions (ASCE 1997; ASCE 2000b).

The SAC Joint Venture Project (ASCE 2000a), which was undertaken to address unexpected fractures to steel frames that occurred in the 1994 Northridge earthquake, led to two important advancements in methods to assess building safety. One is the formalization of a probabilistic methodology to determine the collapse safety of a structure based taking into account uncertainties in ground motions and the nonlinear structural response analysis. The SAC approach describes collapse safety in terms of a mean annual frequency of collapse with a specified prediction confidence level; the process is described in FEMA 350 (ASCE 2000a) with supporting background reported by Jalayer et al. (2003), Foutch et al. (2004), and others. A related aspect of the SAC study is development of nonlinear component models for simulation of collapse behavior of steel-framed buildings, taking into account strength and stiffness degradation due to yielding, local buckling, and connection fracture (Lee 2000).

The FEMA 273/356 project (FEMA, 1997; ASCE, 2000) was an important milestone in codifying degrading nonlinear models and procedures to explicitly evaluate structural collapse. A key component of these procedures is the specification of nonlinear structural component models in the form of monotonic backbone curves that define characteristic force-deformation behavior of the components as a function of seismic detailing parameters. For example, FEMA 356 specifies backbone curve parameters that define the nonlinear moment-rotation response of reinforced concrete beam-columns as a function of longitudinal and horizontal reinforcement and axial and shear demands. While these models have some limitations (e.g., being highly idealized and generally conservative in deterministic representation of response), they are noteworthy in terms of their breadth (modeling the full range of behavior for a wide variety of structural components for all major forms of building construction). Equally important is the integration of the element modeling guidelines within formal nonlinear assessment methods. This was a major advancement over traditional design specifications which have primarily focused on strength design, where deformation response and capacity is considered implicitly through empirical detailing requirements.

1.2 Extension of Collapse Simulation Procedures and Models

The Pacific Earthquake Engineering Research (PEER) Center has extended these previous developments toward a comprehensive probabilistic framework to evaluate building collapse caused by earthquakes. The PEER methodology provides a general probabilistic framework (Krawinkler and Miranda 2004; Deierlein 2004) that is used in conjunction with the collapse simulation to complete the overall collapse risk assessment. PEER has also developed the OpenSees computer platform (OpenSees 2005) for implementing the detailed structural component models to simulate nonlinear degradation and collapse. Model development pertinent to our particular study includes concentrated hinge models by Ibarra and Krawinkler (Ibarra 2003) for global sidesway collapse; Haselton, Taylor Lange, Liel, and Deierlein (Haselton et al. 2006) for RC beam-column calibrations; Elwood and Moehle (Elwood and Mohle 2005; Elwood 2002) for shear failure and loss of axial capacity in RC beam-columns; and Aslani and Miranda (Aslani and Miranda 2005; Aslani 2002) for fragility-type models to detect loss of vertical load capacity of shear critical columns and slab-column connections.

The authors and others are working to extend and standardize these developments. Specific efforts described in this paper are to: (a) review key aspects of the assessment methodology and modeling needs specifically related to collapse assessment, (b) extend the element backbone models for reinforced-concrete beams to include cyclic deterioration and "post-failure" negative stiffness, so collapse can be directly simulated, and (c) extend the concept of backbone response models to explicitly incorporate modeling uncertainties. The concepts are then applied to evaluate the collapse performance of a modern (code-complying) reinforced concrete special moment frame building.

2. GLOBAL METHODOLOGY AND PROBABILISTIC FRAMEWORK

Figure 1 outlines the global performance assessment framework under development by PEER, which divides the process into the four stages of hazard, structural, damage and loss analysis. Data between each stage is distilled into the four variables: ground motion Intensity Measure (IM), Engineering Demand Parameter (EDP), Damage Measure (DM), and one or more Decision Variables (DV). In concept, each stage of the analysis account for uncertainties in the process and the resulting decision/performance variables are described probabilistically. While the procedures are general and account for the full range of performance, this paper deals only with collapse assessment. As Figure 1 shows, collapse assessment circumvents the loss analysis and relies on data from the structural and damage analysis to evaluate collapse. As the emphasis in this paper is on the structural response aspects, the reader is referred to other references for issues associated with the selection and scaling of ground motion records for input to the nonlinear response analyses (see Baker, 2005; Haselton and Goulet et al. 2005; and Kramer, 1996).

To the extent possible, it is desirable to evaluate the collapse risk directly through simulation by modeling the deterioration modes and dynamic behavior that leads to structural instability. However, explicitly modeling structural collapse is a difficult problem. While researchers have long tried to explicitly model the nonlinearity and dynamic instability that cause collapse, only in recent years has research progressed close to this goal (Ibarra 2003; Ibarra and Krawinkler 2004; Elwood 2002; Lee and Foutch 2000). Still, for many collapse failure modes, such as loss of axial capacity in columns, accurate simulation models are not yet available. As indicated by the flowchart of Figure 1, the collapse assessment assumes that the element models for frames and other important aspects of the simulation, such as large displacement geometric effects, are sufficiently well developed to directly simulate sidesway collapse (SC). On the other hand, localized loss of vertical carrying capacity (LVCC), such as loss of axial load capacity in a shear

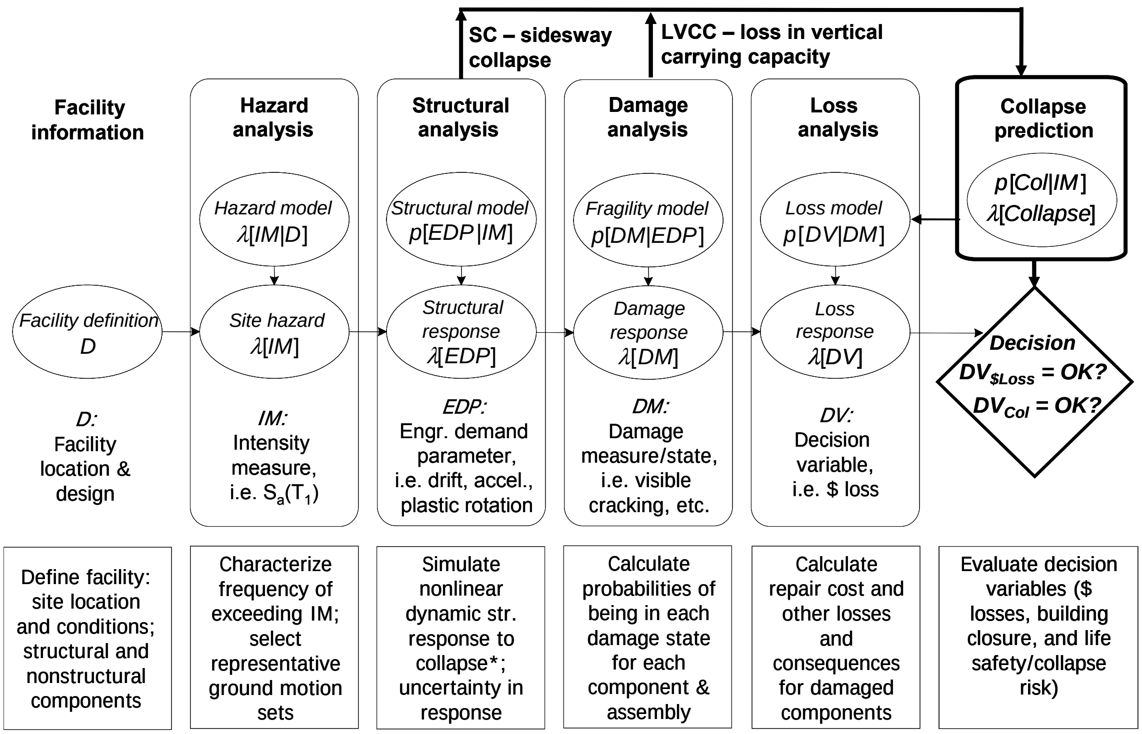

Fig. 1: PEER methodology framework to probabilistically quantify collapse and other performance measures (after Porter 2003)

critical RC column or punching failure of slab-column connections, is evaluated using a damage (fragility) function. Damage functions describe the probability of observing a particular local collapse mode as a function of the simulation data (e.g. probability of vertical collapse of slab given story drift ratio, see Aslani 2005).

The probability of collapse is calculated using the total probability theorem to combine the probabilities of SC and LVCC as follows (Aslani 2005):

$$P[C \mid IM = im] = P[C_{SIM} \mid IM = im] + P[C_{DM} \mid NC_{SIM}, IM = im] \cdot P[NC_{SIM} \mid IM = im] \tag{1}$$

where C is collapse (from either type of collapse mode), NC is non-collapse, C_{SIM} is a collapse captured directly in the simulation, C_{DM} is a collapse captured by a damage model, IM is the ground motion intensity level (i.e., spectral acceleration at first mode period).

3. DETERIORATION AND COLLAPSE MODES

The identification of all deterioration modes that could lead to local or global collapse of the structural system is an obvious, but critical, portion of the collapse evaluation. To illustrate this step, consider the reinforced concrete building system shown in Figure 2. The building consists of a reinforced concrete (RC) perimeter moment resisting frame with a flat-plate gravity system. The markers (A to F) in Figure 2 refer to locations of possible deterioration, which are related to specific structural component deterioration modes in Table 1. Table 1 also summarizes the current availability and maturity of models to simulate and/or assess the various deterioration modes. Next, Table 2 summarizes potential collapse scenarios for sidesway and vertical collapse, each of which are described in terms of the various deterioration modes in Table 1. Finally, the likelihood of the various collapse scenarios is identified in Table 3 for three categories of seismic moment frame systems (ordinary, intermediate, or special), as specified in U.S. building codes. As Table 3 indicates, the more stringent detailing and design provisions for intermediate and special frames tend to reduce the number of expected collapse scenarios.

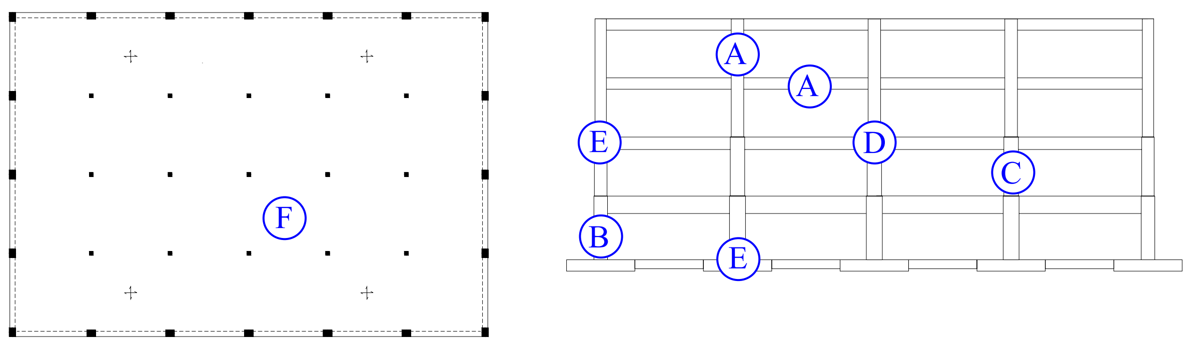

Fig. 2: Reinforced concrete frame building plan and elevation views, to show deterioration and collapse modes

4. SIMULATION AND DAMAGE MODELS

Ideally, we would like to explicitly model all deterioration and collapse modes, so the simulation will directly predict collapse. This is an ideal, but still far from being realized — particularly for building systems, such as ordinary moment frames (OMF) that are less ductile and are vulnerable to many failure modes. The collapse modes that cannot be directly predicted in the simulation must be dealt with by using damage (fragility) functions that relate key building response parameters (e.g. story drift ratio) to the onset of a collapse mode (e.g., vertical collapse of a column after shear failure). A codified model to predict structural collapse should incorporate both modeling guidelines to predict the collapse modes that can be directly simulated and damage functions to capture the collapse modes that cannot be directly simulated.

Table 1: Deterioration modes of RC frame elements

Deterioration Mode	Element	Behavior	Simulation Model Availability	Fragility Model Availability	Description
A	Beam-column	Flexural	4	NR	Concrete cracking Concrete spalling Reinforcing bar yielding Concrete core crushing Reinforcing bar buckling (incl. stirrup fracture) Reinforcing bar fracture
B	Beam-column	Axial compression	2	4	Concrete crushing, longitudinal bar yielding Stirrup rupture, longitudinal bar buckling
C	Beam-column	Shear Shear + Axial	1	4	Concrete shear cracking Transverse tie pull-out Possible loss of axial load carrying capacity
D	Joint	Shear	3	2	Panel shear failure
E	Reinforcing bar connection	Pull-out or Bond-slip	2	2	Reinforcing bar bond-slip or anchorage failure at joint Reinforcing bar lap-splice failure Reinforcing bar pull-out (especially at footings)
F	Gravity frame slab-column connection	Punching shear	2	3	Punching shear at slab-column connection Possible vertical collapse of slab

(*1) Model Maturity (0: Non existent, 1-5: 1 - low confidence to 5 - high confidence; NR - Not required; behavior can be simulated)

Table 2: Collapse scenarios of RC frame systems

Sidesway Collapse Scenarios

	Element Deterioration Mode						
Scenario	**A**	**B**	**C**	**D**	**E**	**F**	**Description**
FS1	■						Beam and column flexural hinging, forming sidesway mechanism
FS2	■						Column hinging, forming soft-story mechanism
FS3	■		■				Beam or column flexural-shear failure, forming sidesway mechanism
FS4	■			■			Joint-shear failure, likely with beam and/or column hinging
FS5	■				■		Reinforcing bar pull-out or splice failure, leading to sidesway mechanism

Vertical Collapse Scenarios

	Element Deterioration Mode						
Scenario	**A**	**B**	**C**	**D**	**E**	**F**	**Description**
FV1			■				Column shear failure, leading to column axial collapse
FV2	■		■				Column flexure-shear failure, leading to column axial collapse
FV3						■	Punching shear failure, leading to slab collapse
FV4						■	Failure of floor diaphragm, leading to column instability
FV5		■					Crushing of column, leading to column axial collapse; possibly from overturning effects

Table 3: Likelihood of scenario for RC frames

Systems	Sidesway Collapse					Vertical Collapse				
	FS1	FS2	FS3	FS4	FS5	FV1	FV2	FV3	FV4	FV5
SMF	H	L-M	L	L	L-M	L	L	L	L	L-M
IMF	H	M	L	L-M	M	L	L	M	M	L-M
OMF	H	H	H	M	H	M	H	M	M	M-H

SMF: Special reinforced concrete moment frame
IMF: Intermediate reinforced concrete moment frame
OMF: Ordinary reinforced concrete moment frame
H: High
M: Medium
L: Low

The following discussion focuses on the evaluation of a special reinforced concrete moment frame (RC-SMF), where the governing collapse mode is assumed to be sidesway collapse that can be simulated directly (collapse scenario FS1 in Table 2). We are using a beam-column element model that was developed by Krawinkler and Ibarra (Ibarra 2003) and is available in OpenSees (OpenSees 2005). This model is based on a concentrated plastic hinge model, which incorporates the nonlinear properties described below.

Figure 3 shows the monotonic trilinear backbone of the element model, which is described by five parameters (M_y, θ_y, K_s, θ_{cap}, and K_c); and Figure 4 shows the cyclic behavior. The model captures four modes of cyclic deterioration (Ibarra 2003): basic strength deterioration, post-cap strength deterioration, unloading stiffness deterioration, and accelerated reloading stiffness deterioration (not used for RC elements; Haselton et al. 2006). Each mode of cyclic deterioration is based on an energy index that has two parameters: normalized energy dissipation capacity and an exponent term to describe how the rate of cyclic deterioration changes with accumulation of damage. Each of the cyclic deterioration modes can be calibrated independently, for a total of eight cyclic deterioration parameters. To reduce complexity and make the calibration tractable, simplifying assumptions are applied to consolidate the cyclic deterioration parameters from eight to two.

In summary, the element model for use in collapse simulation requires the specification of seven parameters must to control both the monotonic and cyclic behavior of the model: M_y, θ_y, K_s, θ_{cap}, K_c, λ, and c; where each is defined in terms of the physical properties of the beam-column.

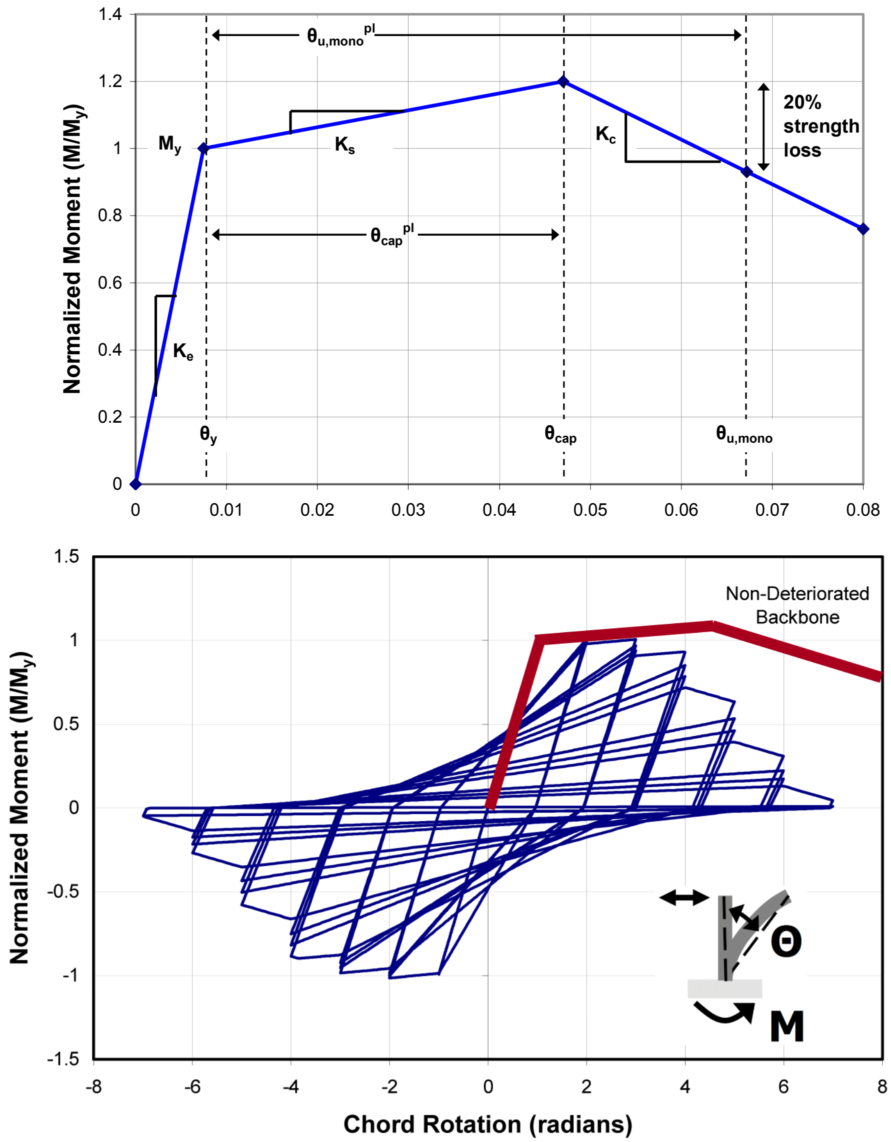

Fig. 4: Illustration of element model cyclic deterioration (Ibarra 2003)

Creating empirical functions for these seven model parameters is the topic of our ongoing research. Parameter definitions should be described in terms of mean (characteristic) values along with appropriate statistical measures of the uncertainty in the predicted response. This is in contrast to traditional philosophy of defining nominal or "lower bound" values equations that define component response. For example, building code design provisions for new buildings are usually based on conservative models of component strengths. Similarly, the backbone curves of FEMA 273/356 are based on conservative estimates of component response, which indirectly account for cyclic deterioration.

4.1 Relating Physical Properties to Model Parameters: Past Research for θ_y and θ_{cap}

Berry and Eberhard (Eberhard 2005; PEER 2005; Berry and Eberhard 2003) assembled a web-accessible available database of cyclic test results of rectangular and circular RC columns. Of 301 rectangular columns, the experimental reports classified 226 as having a flexural failure mode. From these data, Berry and Eberhard created empirical equations that can be used to predict the plastic rotations at the onset of spalling and rebar buckling.

Fardis et al. (Fardis et al. 2003; Panagiotakos et al. 2001) assembled a comprehensive database of experimental results of RC element tests. The database includes a total of 1802 tests, 727 of which are cyclic tests of rectangular columns having conforming detailing and failing in a flexural mode. From these data Fardis and Panagiotakos created empirical equations to predict the chord rotation of RC elements at yield and "ultimate," where "ultimate" is defined as a reduction in load resistance by at least 20% under either monotonic or cyclic loading (equations are provided for each). Berry's predictions for rebar buckling lie between θ_{cap} and $\theta_{u,mono}$, which confirms consistency between the two. The equations proposed by Fardis for θ_y and $\theta_{u,mono}{}^{pl}$ (Fig. 3) are given below:

$$\theta_y = \phi_y \frac{L_s}{3} + 0.00275 + a_{sl} \frac{\varepsilon_y}{(d-d')} \frac{0.2 d_b f_y}{\sqrt{f'_c}} \tag{2}$$

$$\theta_{u,mono}{}^{pl} = \alpha_{st}{}^{pl}(1+0.55a_{sl})(1-0.4a_{wall})(0.2)^{v}\left(\frac{\max(0.01,\omega')}{\max(0.01,\omega)} f'_c\right)^{0.225}\left(\frac{L_s}{h}\right)^{0.375} 25^{\left(\alpha\rho_s \frac{f_{yw}}{f'_c}\right)} 1.3^{100\rho_d} \tag{3}$$

where θ_y is the chord rotation at yield, ϕ_y is yield curvature, L_s is distance from point of maximum to point of zero moment, a_{sl} is a bond-slip indicator (1 if boundary conditions allow bond-slip past point of maximum moment), ε_y is longitudinal steel yield strain, (d-d') is distance from top to bottom longitudinal steel, f_y is longitudinal steel yield strength ($f_{y,w}$ is for stirrups), f'_c is concrete strength, $\theta_{u,mono}{}^{pl}$ is monotonic plastic rotation from yield to point of 20% strength loss, α_{st} is a coefficient for type of steel, a_{wall} is a coefficient to indicate if the member is a wall, v is the axial load ratio ($P/A_g f'_c$), ω and ω' are reinforcement ratios, h is the height of the section, α is a confinement effectiveness factor, ρ_s is the area ratio of transverse steel parallel to direction of loading, and ρ_d is ratio of diagonal reinforcement.

Berry et al. and Fardis et al. both made valuable contributions to the field and their work has been a useful basis for this current work. Even so, their predictions are not directly applicable and/or have some limitations that need to be overcome before this beam-column model and empirical predictive equations can be codified. In particular, while Berry et al. quantify the onset of the rebar buckling, their model does not provide a quantitative link to the associated degradation parameters (θ_{cap} and K_c). On the other hand, whereas the model by Fardis et al. does provide explicit equations of the degraded plastic rotations (e.g., $\theta_{u,mono}^{pl}$), they do not provide an equation for θ_{cap}. Thus, one must resort to inferring θ_{cap} based on $\theta_{u,mono}^{pl}$ and the negative cap stiffness, K_c, which has a high degree of uncertainty. Fardis' empirical equations for $\theta_{u,mono}^{pl}$ are also unconservatively biased for "non-conforming" columns (Fardis 2003, pg. 526). The next section describes how we are improving the beam-column model calibration based on a combination of past research and new experimental data.

4.2 Relating Physical Properties to Model Parameters: Current/Future Research

The goal our research is create empirical functions to relate all seven model parameters to the physical properties of the column, including quantifying uncertainty in each prediction and the correlations between the model parameters (correlations are necessary for system reliability studies). Table 4 outlines the relationships between the seven model parameters, physical behavior, and the physical properties of the beam-column. To create the link between model parameters and the beam-column physical properties, we have calibrated the element model (previously shown in Figure 4) to the 226 flexurally dominated cyclic tests of RC columns in Eberhard's database (Eberhard 2005; PEER 2005). Figure 5 shows an example of such calibration. Based on the 226 calibrations, we are in the process of developing empirical functions to predict model parameters using the physical properties of the beam-column. During this process, we will use the past research (Berry et al. 2003; Fardis et al. 2003) for comparison and to determine appropriate predictors and functional form for each empirical function (Haselton et al. 2006).

Accurate quantification of the model uncertainty is an important aspect of the models — providing data to determine the resistance factors for use in a codified model and for quantifying uncertainties in system reliability analyses. Table 5 lists the estimated uncertainties in the prediction of each model parameter, based on past research. Our ongoing calibration studies will help refine these using the beam-column database.

Table 4: Description of model parameters and associated physical behaviors/properties

Model Parameter	Description	Physical Behavior Contributing to Parameter	Physical Properties / Possible Predictors	Reference(s)
M_y	"Yield" moment	Longitudinal rebar yielding, concrete cracking (flexure and shear), concrete crushing (for over-reinforced)	Whitney stress block approach or fiber analysis (section geometry, axial load (ratio), material strengths and stiffnesses)	Basic beam theory; Fiber moment-curvature; Fardis, 2003; Panagiotakos, 2001
θ_y	Chord rotation at "yield"	(same as above)	Section geometry (d-d', rebar diameter), level of shear cracking (shear span, shear demand/capacity), axial load (ratio), material stiffnesses/strengths	Fardis, 2003; Panagiotakos, 2001; Fiber moment-curvature;
θ_{cap}	Chord rotation (mono.) at onset of strength loss (capping)	Longitudinal rebar buckling/fracture, concrete core failure for high axial loads and/or minimal lateral confinement (stirrup fracture)	Confinement (amount, spacing, type and layout, effectiveness index), axial load (ratio), end conditions (possibility of bond-slip), geometry (shear span, etc.), reinforcement ratio	Fardis, 2003; Panagiotakos, 2001; Berry 2003; Haselton, 2006
K_s	Hardening stiffness	Steel strain hardening, nonlinearity of concrete, bond-slip flexibility	Steel hardening modulus, section/element geometry, presence of intermediate longitudinal steel layers	Fiber moment-curvature and plastic hinge length approach; Haselton, 2006
K_c	Post-capping stiffness	Research still needed - Post- rebar buckling behavior, behavior after loss of core concrete confinement	To be determined - Rebar slenderness between stirrups (large stirrup spacing), and over several stirrups (small stirrup spacing)	Haselton, 2006; PEER, 2005
λ	Normalized hysteretic energy dissipation capacity (cyclic)	Research still needed - Progression over cycles of concrete crushing, stirrup fracture, rebar buckling, longitudinal steel fracture	To be determined - Confinement (amount, spacing, effectiveness index), stirrup spacing, axial load (ratio)	Haselton, 2006; PEER, 2005
c	Exponent term to model rate of deterioration (cyclic)	(same as above)	(same as above)	Ibarra, 2003; Haselton, 2006; PEER, 2005

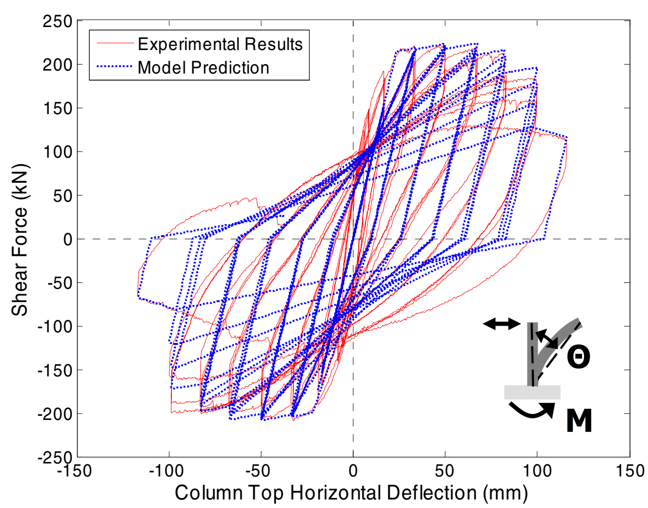

Fig. 5: Calibration of RC beam-column model to experimental test by Saatcioglu and Grira, specimen BG-6 (Saatcioglu 1999; Haselton 2006; PEER 2005)

Table 5: Predictions of mean and uncertainty of model parameters

Model Parameter	Mean Estimate	Coefficient of Variation	Reference(s)	Notes
M_y	1.00**	0.12	Ellingwood, 1980; Fardis, 2003; Panagiotakos, 2001;	
θ_y	1.00*	0.36	Fardis, 2003; Panagiotakos, 2001;	
θ_{cap}	1.00*	0.60	Fardis, 2003; Panagiotakos, 2001; Berry, 2003	
K_s	0.50**	0.50	Fardis, 2003; Wang, 1978; Paulay, 1992	1/2 factor to account for bond-slip and shear deformations at ultimate
K_c	$-0.075K_e$	0.60	Haselton, 2005; Eberhard, 2005	
λ	120	0.50	Haselton, 2005; Eberhard, 2005	
c	1.2	n/a	Haselton, 2005; Eberhard, 2005	Held constant during calibration, so all cyclic deterioration variability in λ

* value is a fraction of the predicted value (from references)
** value is a fraction of prediction using fiber analysis with expected material parameters and axial load, with plastic hinge length from Paulay

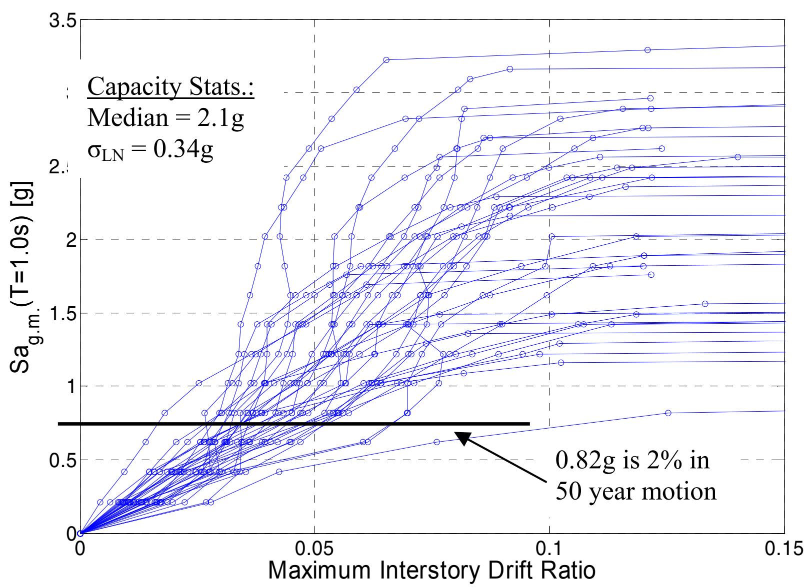

Fig. 6: Incremental dynamic analysis of four-story RC SMRF (Haselton et al. 2005)

4.3 Use of Element Model to Directly Simulate Sidesway Collapse

To directly simulate global sidesway collapse caused by dynamic instability in one or more stories, we use the Incremental Dynamic Analysis (IDA) technique (Vamvatsikos 2002). This technique is composed of repetitively scaling-up the ground motion intensity level, Sa(T_1), and running a nonlinear dynamic analysis until a further increase in ground motion intensity causes large drifts of one or more stories of the structure (dynamic instability). Figure 6 shows an IDA diagram using 36 ground motions for the new code-conforming RC SMF building shown in Figure 2 (Haselton et al. 2005).

Figure 7a shows the probabilistic collapse capacities predicted in Figure 6 (at each point of dynamic instability, when the IDA becomes a flat line), assuming a lognormal fit. In addition, Figure 7a shows how the modeling uncertainty impacts the collapse capacity prediction (Haselton et al. 2005; Haselton et al. 2006). Figure 7b shows the hazard curve for a site in Los Angeles, California to illustrate how the collapse CDF and the hazard curve can be integrated together to obtain the collapse risk (mean annual frequency of collapse). In this example, the integration of the collapse capacity CDF with the hazard curve leads to a mean annual frequency of collapse estimate of 1.8×10^{-5} using only record-to-record variability and 1.7×10^{-4} with both record-to-record and modeling variability included.

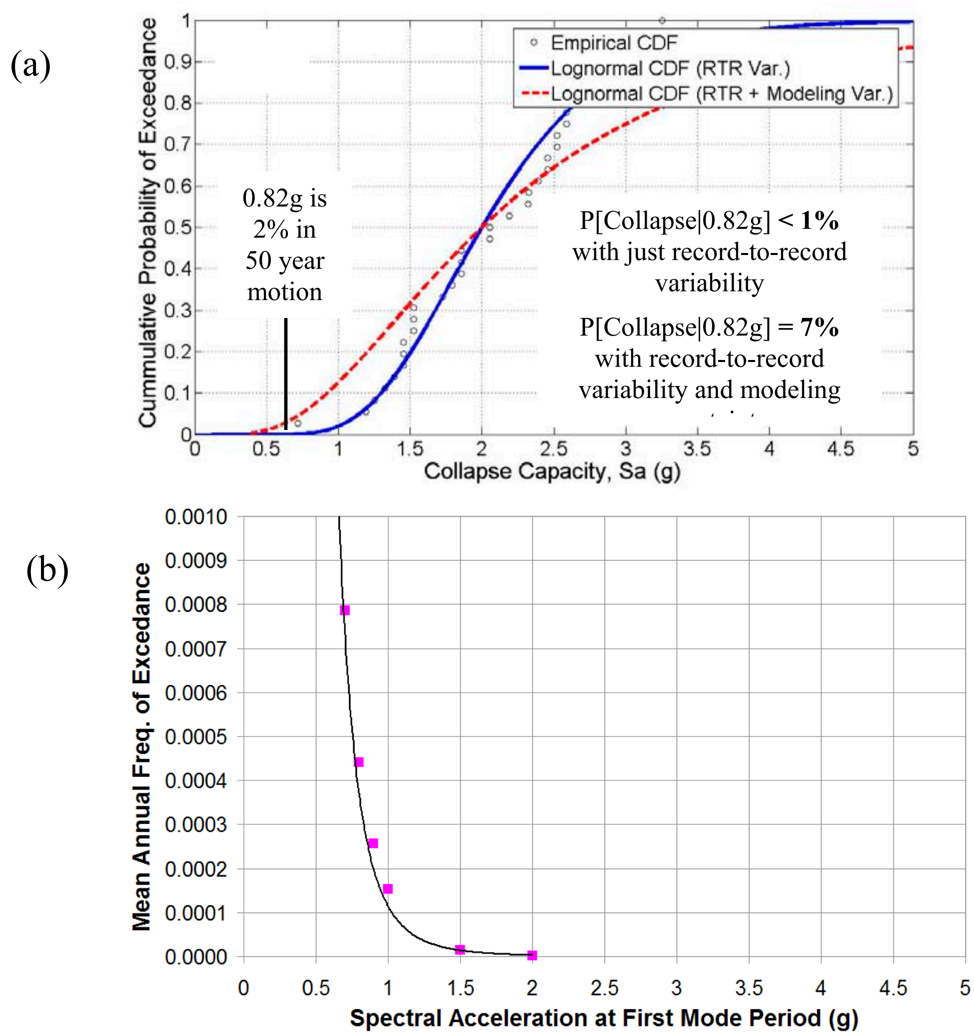

Fig. 7: (a) Collapse capacity CDFs (b) hazard curve (Haselton et al. 2005)

4.4 Damage Models to Capture Non-Simulated Collapse Modes

The collapse modes that are not captured directly by the structural simulation should be accounted for in a post-processing mode by using damage models to relate some aspect of the structural response (e.g., story drift, etc.) to the onset of the collapse mode of interest (e.g. axial collapse of a column after shear failure). Based on detailing and capacity design requirements for new RC special moment frame buildings (ACI 2005), we have ruled out many of these premature failure modes for the sample building presented in this paper; so this paper does not illustrate this step of the collapse assessment. More detailed consideration of local collapse modes can be found in work by Aslani and Miranda (Aslani 2005).

5. CONCLUDING REMARKS

Modeling and assessment of structural collapse has long been a goal in earthquake engineering, and modern scientific developments in performance-based earthquake engineering are helping to realize this vision. The approach summarized herein combines emerging concepts in probabilistic seismic hazard and risk analysis together with nonlinear structural behavior and simulation. While the intent is for the methods and tools to be based on scientific models and principles, the full implementation requires considerable interpretation and engineering judgment. Therefore, widespread acceptance of these methods and models in practice will require a concerted effort to develop guidelines and criteria that reflect the judgment and consensus of the earthquake engineering community. It is hoped that the research described in this paper will contribute to such a consensus process and result in codified guidelines for assessing structural collapse risk.

6. ACKNOWLEDGMENTS

This research was funded by the Pacific Earthquake Engineering Research Center through the Earthquake Engineering Research Centers Program of the National Science Foundation under award number EEC-9701568 this support is much appreciated. The authors would also acknowledge the valuable input and assistance with the element calibration from Professors Helmut Krawinkler and Eduardo Miranda and undergraduate researcher Sarah Taylor Lange. In addition, the authors appreciate the contributions of Jiro Takagi and Abbie Liel.

REFERENCES

Altoontash, A. (2004). *Simulation and Damage Models for Performance Assessment of Reinforced Concrete Beam-Column Joints*, Dissertation, CEE Dept., Stanford University.

American Concrete Institute. (2002). *Building Code Requirements for Structural Concrete (ACI 318-02) and Commentary (ACI 318R-02)*, Farmington Hills, MI.

American Society of Civil Engineers. (2000b). "FEMA 356: Prestandard and Commentary for the Seismic Rehabilitation of Buildings", Report No. FEMA 356, ASCE/FEMA Agency.

American Society of Civil Engineers. (2000a). "FEMA 350: Recommended Seismic Design Criteria for New Steel Moment-Frame Buildings", Report No. FEMA 350, ASCE/FEMA Agency.

American Society of Civil Engineers. (1997). "FEMA 273: "NEHRP Commentary on the Guidelines for the Seismic Rehabilitation of Buildings", Report No. FEMA 273, ASCE/FEMA.

American Society of Civil Engineers. (2002). *Minimum Design Loads for Buildings and Other Structures*, Reston, VA.

Applied Technology Council (ATC) (1996). *Seismic Evaluation and Retrofit of Concrete Buildings (ATC40),* Applied Technology Council, Redwood City, CA.

Aslani, H., and E. Miranda. (2005). *Fragility assessment of slab-column connections in existing non-ductile reinforced concrete buildings*. Journal of Earthquake Engineering, 9(4), pp. 1-28.

Aslani, H. (2005). *Probabilistic Earthquake Loss Estimation and Loss Disaggregation in Buildings*, Ph.D. Dissertation, Dept. of Civil and Environ. Engr., Stanford University.

Baker, J. (2005). *Vector-Valued Ground Motion Intensity Measures for Probabilistic Seismic Demand Analysis*, Ph.D. Dissertation, Dept. of Civil and Environ. Engr., Stanford University.

Berry, M., and M. Eberhard. (2003). *Performance Models for Flexural Damage in Reinforced Concrete Columns*, Report 2003/18, PEER Center, University of California, Berkeley.

Cornell, C. A., F. Jalayer, R. O. Hamburger, and D. A. Foutch. (2002). "Probabilistic Basis for 2000 SAC Federal Emergency Management Agency Steel Moment Frame Guidelines," *Journal of Structural Engineering*, Vol. 128, No. 4, April 2002, pp. 526-533.

Deierlein, G. G. (2004). "Overview of a Comprehensive Framework for Earthquake Performance Assessment," *Performance-Based Seismic Design Concepts and Implementation, Proceedings of an International Workshop*, PEER Report 2004/05, UC Berkeley, p. 15-26.

Eberhard, M. (2005). *Structural Performance Database*, Department of Civil and Env. Engineering, Univ. of Washington, http://maximus.ce.washington.edu/~peera1/ (March 10, 2005).

Ellingwood, B., T.V. Galambos, J.G. MacGregor, and C.A. Cornell. (1980). *Development of a Probability-Based Load Criterion for American National Standard A58*, National Bureau of Standards, Washington, DC, 222 pp.

Elwood, K.J. (2002). *Shake Table Tests and Analytical Studies on the Gravity Load Collapse of Reinforced Concrete Frames*, Ph.D Dissertation, CEE Dept., UC Berkeley.

Elwood, K. J., and J. P. Moehle. (2005). "Axial Capacity Model for Shear-Damaged Columns," *ACI Structural Journal*, July-August 2005, No. 4, pp. 578-587.

Fardis, M. N., and D. E. Biskinis. (2003). "Deformation Capacity of RC Members, as Controlled by Flexure or Shear," *Otani Symposium*, 2003, pp. 511-530.

Haselton, C. B., J. Mitrani-Reiser, C. Goulet, G. G. Deierlein, J. Beck, K. A. Porter, J. Stewart, and E. Taciroglu (2005). *An Assessment to Benchmark the Seismic Performance of a Code-Conforming Reinforced-Concrete Moment-Frame Building*, Report 2005/##, Pacific Engineering Research Center, University of California, Berkeley, California, (in preparation).

Haselton, C. B., S. Taylor Lange, A. B. Liel, and G. G. Deierlein (2006). *Beam-Column Element Model Calibrated for Predicting Flexural Response Leading to Global Collapse of RC Frame Buildings*, Report 2006/##, Pacific Engineering Research Center, University of California, Berkeley, California, (in preparation).

Ibarra, L. (2003). *Global Collapse of Frame Structures Under Seismic Excitations*, Ph.D. Dissertation, Dept. of Civil and Environ. Engr., Stanford University.

Ibarra, L., and H. Krawinkler. (2004). *Global Collapse of Deteriorating MDOF Systems*, 13th World Conf. on Earthquake Engrg., Vancouver, B.C., Canada, August 1-6, 2004, Paper No. 116.

International Code Council. (2003). *2003 International Building Code,* Falls Church, VA.

Jalayer F., 2003. *Direct probabilistic seismic analysis: Implementing non-linear dynamic assessments*, Ph.D. Dissertation, Dept. of Civil and Environ. Engr., Stanford University.

Kramer, S.L. (1996). *Geotechnical Earthquake Engineering*, Prentice Hall, New Jersey, ISBN: 0-13-374943-6.

Krawinkler, H., E. Miranda, Y. Bozorgnia, and V. V. Bertero. (2004). "Chapter 9: Performance Based Earthquake Engineering,", *Earthquake Engineering: From Engineering Seismology to Performance-Based Engineering*, CRC Press, Florida.

Lee, K., and D.A. Foutch. (2000). "Performance prediction and evaluation of steel special moment frames for seismic loads." *SAC Background Document SAC/BD-00/25*, SAC Joint Venture, Richmond, Ca.

Open System for Earthquake Engineering Simulation (OpenSees). (2005). PEER Center, University of California, Berkeley, http://OpenSees.berkeley.edu/.

Panagiotakos, T. B. and Fardis, M. N. (2001). "Deformations of Reinforced Concrete at Yielding and Ultimate," *ACI Structural Journal*, Vol. 98, No. 2, March-April 2001, pp. 135-147.

Paulay, T., and M. J. N. Priestley.(1992). *Seismic Deign of Reinforced Concrete and Masonry Buildings*, John Wiley and Sons Inc., New York.

Porter, K. A. (2003). "An Overview of PEER's Performance-Based Earthquake Engineering Methodology," *Conference on Applications of Statistics and Probability in Civil Engineering (ICASP9)*, Civil Engrg. Risk and Reliability Assoc. (CERRA), San Francisco, CA, July 2003.

PEER (2005). *Pacific Earthquake Engineering Research Center: Structural Performance Database*, University of California, Berkeley, http://nisee.berkeley.edu/spd/ (March 10, 2005).

Saatcioglu, M., and M. Grira. (1999). "Confinement of Reinforced Concrete Columns with Welded Reinforcement Grids," ACI Structural Journal, Vol. 96, No. 1, Jan.-Feb. 1999, pp. 29-39.

Seung-Yul, Y., R. O. Hamburger, C. A. Cornell, D. A. Foutch. (2002). "Seismic Performance Evaluation of Steel Moment Frames," *JSCE*, ASCE, 128(4), April 2002, pp. 534-545.

Vamvatsikos, D. (2002). *Seismic Performance, Capacity and Reliability of Structures as Seem Through Incremental Dynamic Analysis*, Ph.D. Diss., CEE Dept., Stanford University.

Wang, P., Shah, P. Surendra, A. E. Naaman. (1978). "High-Strength Concrete in Ultimate Strength Design," *Journal of the Structural Division*, ST11, November 1978, pp. 1761-1773.

KEYWORDS: collapse, sideways collapse, local collapse, consensus, codification, failure modes, cyclic deterioration, flexural failure, deformation capacity, beam-column model

SESSION 2: OUTLINE OF THE FULL-SCALE TEST AT E-DEFENSE

Chaired by

♦ Greg Deierlein and Hiroshi Kuramoto ♦

DESIGN OF THE FULL-SCALE SIX-STORY REINFORCED CONCRETE WALL-FRAME BUILDING FOR TESTING AT E-DEFENSE

Toshimi KABEYASAWA[1],

Taizo MATSUMORI[2], Hideo KATSUMATA[3], Kazutaka SHIRAI[4]

ABSTRACT

A full-scale three-dimensional earthquake simulation test on reinforced concrete building structure has been planned using the shaking table at E-Defense. The test is to be conducted as a part of the second phase of a five-year national research project, called DaiDaiToku project. In the first phase of the project, preliminary experimental and analytical researches have been performed, including the trial design and analysis of the specimen, towards the full-scale testing at E-Defense. With the results of these preliminary design analyses, RC committee on the DaiDaiToku project discussed on possible research themes and objectives, and selected a six-story wall-frame building as the first test structure. The structure was designed based on the past Japanese code of design and practice in 1970s. This paper reports on the allowable stress design procedure, the sectional design details as a result and pushover analyses of the test structure as well as the main research objectives of the test plan. The construction of the test specimen started outside from July 2005 towards the test on the table in January 2006. Detailed preliminary static and dynamic analyses of the test specimen are to be reported independently in several other papers for the presentation at this workshop. These analytical simulations, as blind simulations before the test, may be verified after the test with the observed behavior.

1. INTRODUCTION

The Opening Ceremony and Inauguration International Symposium were held at E-Defense on January 15 and 16, 2005. E-Defense has the world largest three-dimensional earthquake simulator, which is a shaking table of 20mx15m size carrying a specimen up to 20m height and 1200ton weight. The design speculations of the table motion in the horizontal direction in terms of the maximum horizontal acceleration, velocity and displacement are 0.9G, 200cm/s. and 100cm, respectively, and those in the vertical direction are 1.5G, 70cm/s. and 50cm, respectively. Therefore, a medium-rise full-scale reinforced concrete building could be tested under a severe earthquake motion to collapse. E-Defense has been under trial condition towards the first phase main tests starting from October 2005. The first phase main test series in 2005 and 2006 are to be

[1] *Earthquake Research Institute, The University of Tokyo*
Email: kabe@eri.u-tokyo.ac.jp
[2] *Hyogo Earthquake Research Center, National research Institute for Earth science and Disaster prevention*
Email: taizo@eri.u-tokyo.ac.jp
[3] *Technical research Institute, Obayashi Corporation*
Email: katsumata.hideo@obayashi.co.jp
[4] *Hyogo Earthquake Research Center, National Research Institute for Earth Science and Disaster Prevention*
(formerly, Technical Research Institute, Obayashi Corporation)
Email: shirai@bosai.go.jp

conducted on timber structures, reinforced concrete structures, and soil and foundation structures as part of the second phase of the Dai-Dai-Toku project.

A full-scale test has been planned for a reinforced concrete building structure, which is to be conducted in the winter of 2005, and probably another one or possibly two specimens in the winter of 2006 as well. In the first phase of the Dai-Dai-Toku project, from 2002 to 2004, preliminary analytical and experimental researches were conducted for the full-scale testing at E-Defense, which includes shaking table tests with scaled specimens, component tests under static and dynamic loading, and development of analytical models, especially for the simulation of collapse behavior, as well as plan and design of the full-scale test specimen. Considering the results of the preliminary design analyses, the DaiDaiToku committee on RC project (Chair: Kabeyasawa) has discussed on the possible research themes and objectives, and has selected a six-story wall-frame building as the first reinforced concrete test structure of the project at E-Defense.

Procedure and the selected design of the test specimen are outlined in this paper with the objectives of the test plans. Detailed preliminary static and dynamic analyses of the test specimen are reported in several other papers, which are still under progress in detail towards the dynamic test in January 2006.

2. PLANNING OF THE FULL-SCALE TEST

2.1 Objectives of the Test

Possible research objectives of the full-scale testing of reinforced concrete buildings have been discussed in the RC committee as well as at US-Japan (NEES-E-defense) meeting in April 2004. They are analyzed and classified as follows here:

(1) ***Objective types of structures:*** (S1) Existing structures before/after strengthened, (S2) Non-ductile/ductile structures, (S3) Irregular/regular structures, (S4) Innovative structural systems with isolation and/or dampers, (S5) Non-engineered structures such as infilled RC, reinforced/bare masonry, adobe, (S6) Structures with fixed/flexible/inelastic foundation, (S7) Structures with non-structural components/installation/furniture;

(2) ***Objective types of performances:*** (B1) Overall/story/progressive collapse mechanism, (B2) Ductile/limited ductile/brittle failure mode, (B3) Earthquake/gravity load carrying capacity, (B4) Higher mode/3-D/torsional response, (B5) Damping or energy dissipation capacity, (B6) Structural integrity/stability, (B7) Post-earthquake residual capacity, (B8) Fail-safe capacity;

(3) ***Objective demand characteristics:*** (D1) earthquake intensity: moderate/strong/extreme, (D2) Characteristics of earthquake motions: far field/near field motion, (D3) 1D/2D/3D earthquake motion;

(4) ***Objective limit states:*** (L1) Serviceability/reparable damage limit, (L2) Safety/ultimate limit, (L3) Overall structural collapse or overturning;

(5) ***Objective tools:*** commonly experimental verification for (T1) Seismic performance of structures, (T2) Evaluation methods for design, (T3) Analytical models, (T4) Sensing technologies, (T5) Post-earthquake assessment methods.

2.2 Selected Research Items

2.2.1 Prerequisites in the Plan

As the first test at E-Defense, there are several prerequisites in the viewpoints of not only research oriented but also demonstration to public, such as:

(1) The specimen shall be "**full-scale,**" in "**3-Dimentional**," behavior up to 800 tons, 15mx20m area and 20m height. A lot of possible plans were drawn and a 6-story and 2x3 bay frame was selected.

(2) The specimen shall be tested under the capacity of the table "**to collapse**." Therefore the ultimate base shear coefficient at the formation of mechanism would preferably be less than 0.5, for which one wall is good enough to attain the capacity.

(3) The specimen shall be planned as "**a part of long term plan**," although only one specimen is available in 2005 and probably another in 2006. Therefore, several research objectives shall be included considering possible other serial projects in the future.

(4) "**Standard experimental technique**" for full-scale testing on reinforced concrete structures shall be established, such as instruments for measurement, backup for safety, and setup and remove. A new method of testing shall also be tried.

(5) The test results shall be the "**benchmarks"** for conventional and future analytical tools, which would be verified as generally as possible. Therefore, the structure shall not be too simple but not too complicated, and shall represent practically designed structures in general.

(6) The available term for E-Defense table is fixed as "**two months"** from 1 December 2005 to 31 January 2006.

(7) The budget was fixed in January 2005, which would be available for "**one full-scale specimen**," for the fiscal year 2005.

2.2.2 Selection of the Structural Plan

We could select either from the following alternatives, and we have selected basically the first one for the structural plan in the first test:

(1) **<u>Regular</u> vs. Irregular**: Regular type would be necessary even if irregular type is adopted

(2) **<u>Wall-frame</u> vs. Open frame**: Open-frame would be too simple as benchmark for analytical modeling

(3) **<u>Existing</u> vs. New construction**: Research themes on existing structures are more general than new development, such as non-ductile collapse mechanism of structure, which should be investigated further in detail, while ductile and stable behavior would be too simple.

As a result, the structural plan and elevation shown in Figure 1 and Figure 2 are selected for the test specimen.

2.2.3 Research Themes for the Full-Scale Testing

Main research items have been discussed by the committee, which could generally be assigned to past, current and future projects as follows, although some of them were duplicated among several projects.

(1) Past project on pilot is (1999-2003): Soft first story

(2) Preliminary tests 2002-2004: Eccentricity, Dynamic effect, Flexible/fixed foundation, Multi-directional input

(3) Full-scale test 2005: **Collapse behavior, Wall-frame interaction, Damage evaluation, Scale effect, Non-structural component**

(4) Full-scale test 2006: **Design code or detail, Strengthening, Repair, Flexible foundation**

(5) Future full-scale projects: Damper, Sensor, Monitor, IT, Base-isolation, Vertical motion, Slab integrity, Beam-column joint, etc.

3. DESIGN PROCEDURE

3.1 Design Method

The task group members of the RC committee (Kabeyasawa, Matsumori, Katsumata, Shirai) conducted the trial design and analysis of the full-scale test structure, which was then discussed and approved by all the committee members. The design and calculation were made with the following policy.

(1) The building is planned and designed as a specimen for the full-scale earthquake simulation test at E-Defense.

(2) The selected scale is almost full but strictly about 0.8 times of Japanese buildings in practice, considering the capacity of the table, such as payload and practical height limitation.

(3) The maximum acceleration of the table is 900cm/sec^2 with the full payload of 1200ton so that the lateral load carrying capacity should not be too high, preferably should not be greater than 400tonf in terms of base shear.

(4) Considering the method of construction outside and setting up on the table, the total weight of the specimen shall be less than 800ton, which is the limitation of the crane. The volume of the specimen had been kept less than the above value at the planning of the specimen until the limitation would not be critical when the budget was fixed January 2005 and a new method of moving the specimen to the table would be available.

(5) In order to observe various damages of members and to obtain various findings as possible from one specimen, the structure is planned as the combination of frames or components with different characteristics. The spandrel non-structural walls are added to the beams in one of the two open-frames, so that the inner heights of the columns become short, or relatively non-ductile.

(6) Although the dynamic test is subjected to three-dimensional earthquake motions, the principal direction of the motions is planned so that the maximum response and the failure mechanism would be formed in the longitudinal direction (Y-direction in the figure).

(7) In the span direction (X-direction), sidewalls are added to the center columns of the outer frames, so that enough resistance is given to control response of the direction within certain level and less than that of the longitudinal direction.

3.2 The Specimen

(1) The structure is a six-story building, which has three spans in the longitudinal (Y) direction, two spans in the orthogonal or span (X) direction. The center bay of the central frame in the longitudinal direction has a continuous wall with boundary walls from the first story to the top. In the orthogonal direction, the central columns of the outer frames have continuous sidewalls from the first story to the top with small-size boundary columns or confined region.

(2) The additional mass was considered in the first stage with the slab thickness of 12cm due to total weight limitation, although the slab thickness was increased to 15cm in the medium floor and 19cm in the roof floor after the new set up method on the shake table was adopted.

3.3 Structural Calculation

(1) The test structure is to represent a reinforced concrete building designed following the Japanese code of design and practice for buildings in 1970s. Therefore, the structural calculation was conducted in accordance with the AIJ standard of 1975 edition and Building Standard Law and the Corresponding Enforcement Order in 1970s, although a current computer program was used for structural calculation.

(2) The dead load G and live load P specified in the BSL is considered. Calculation for earthquake load K is shown. The earthquake load then was specified as the lateral seismic coefficient of 0.2, which means that the building weights concentrated at each floor are multiplied by 0.2 and applied in the lateral direction.

(3) The allowable stresses of material were used in design.

(4) The building was analyzed as frame structure with shear wall.

(5) The increase of the stiffness and the strengths by the spandrel walls to the beams in the frame C were neglected in accordance with the common practice in the structural calculation in 1970s. The assumption was approved and considered to be safe side then because these effects give additional strength to the structure.

(6) The sidewalls in the frames 1 and 4 in the orthogonal direction are considered in the calculation. The sections of the sidewalls were changed from the original plan.

(7) The wall base and column base is assumed as fixed.

(8) A three-dimensional matrix method, which was not yet popular in 1970s, was used for frame analysis to calculate actions in members due to gravity loads and earthquake loads.

(9) Although the calculation for seismic action is based on elastic stiffness of members, stiffness degradation is considered in the member as shown in Table 2, considering the cracking of concrete where the larger stress is expected.

(10) Effective width of slab for T-beam and stiffness of beam-column joints are determined in accordance with the AIJ standard.

(11) Longitudinal reinforcement in the column and the beam sections are calculated based on flexural theory and allowable stress. Maximum of reinforcement ratios (1) required for gravity load actions, (2) required for gravity plus earthquake load actions, and (3) minimum requirement are taken as the design required amount.

(12) Foundation and foundation beams are designed independently, which gives enough strength and stiffness for the specimen partially supported by the load cells on the shaking table.

(13) Design for shear is based on AIJ standard. Although the equation is in a form of allowable stress method, the equation is approximation of ultimate strength and still being used in the current practice. Minimum requirements are also the same as the current code: the shear reinforcement ratio of 0.002 for column and beam, and the maximum spacing is 100mm for column and 1/2 of beam depth nor 250mm for beam. The design seismic forces for shear are amplified by 1.5 times from analytical actions under earthquake loading or calculated from ultimate flexural moments at both ends. Therefore, flexural yielding prior to shear failure is assured basically for all the beams and columns.

4. SECTION DETAILS

4.1 Material Properties

4.1.1 Concrete

Normal concrete with standard strength of F_c = 180 kgf/cm^2 is assumed to be used. In design calculation, allowable strengths were determined for the standard strength. In the non-linear analysis and dynamic analysis shown in other papers, σ_B = 240 kgf/cm^2 is used as probable strength in the test specimen.

4.1.2 Steel

Deformed bars with nominal diameter of D19 (bar sectional area: 2.865cm^2), D16 or D22 and nominal strength of SD345 are used for column and beam main bars, while bars of D10 (0.713cm^2) or D13 (1.267cm^2) and SD295 are used for column hoops, beam stirrups, wall shear reinforcement, and slab bars. yield strengths of σ_y = 3500 kgf/cm^2 and σ_y = 3000 kgf/cm^2 are used as the nominal strengths for SD345 and SD295, respectively, in the past engineering system units. Allowable stresses of concrete and steel are given in Table 1. Note that in the preliminary pushover and dynamic analysis shown in other papers, 365 Mpa for SD295 and 380 Mpa for SD345 are assumed commonly as probable average strengths of the bars, which will be used in construction of the specimen.

4.2 Weight of the Structure

In the original design, the weight of the structure was calculated in detail. Several changes were made for plan, assumed section sizes such as slab thickness, balcony slab, wing walls in the orthogonal direction, steel stairs and so on. Finally, the constant averaged mass of 125 ton (1225kN) for each floor from the second to the roof was assumed commonly in the preliminary pushover and dynamic analyses.

4.3 Designed Reinforcement Details

The sectional and reinforcement details of all members of the full-scale test structure are listed in Table 3, for (a) columns, (b) beams, (c) walls, (d) wing walls, (e) slabs and (f) floor beams, as designed. The main reinforcing bars of beams shown in the table are those of the latest version, which have been coordinated from the original design for the construction of the specimen. Because these have been several changes in design and the final design analysis was conducted to fix the design for construction in July 2005, an old version of the design has been assumed in the preliminary response and pushover analyses. The old version was shown in the footnote of the table. The analyses shall be conducted rigorously assuming the latest version and actual material strength, although the results would not be different much due to these changes.

4.4 Non-Structural Components

Some of the floors of the specimen are to be completed with finishing to observe damages to non-structural components, such as spandrel walls, partitions, windows, glasses, sealing, and furniture. The details are being planned and designed.

5. ULTIMATE CAPACITY

5.1 Pushover Analysis

Although the design is completed as above in accordance with the code of practice in 1970s, the ultimate lateral carrying capacity is calculated by pushover analysis as is required in the second phase design of the Japanese current practice. Two types of lateral load distribution were assumed: (a) Rectangular and (b) Inverted triangular. The earthquake force distribution in the past code was similar to the former (a) and the current code to the latter (b). Under the inverted triangular distribution, the calculated ultimate shear strength of the wall, which is also shown in the figure, is larger than by 1.3 times than the ultimate shear force at the deformation angle of 1/100. Therefore, the wall may be defined as flexural type based on the current code calculation.

5.2 Nonlinear Time-History Dynamic Analysis

In addition to the linear analysis and pushover analysis for the design of the specimen shown as above, the task group members for preliminary analysis (Kabeyasawa, Matsumori, Chen, Sanada, Shirai, Kim, Kabeyasawa) have been doing pushover analyses and nonlinear time-history analyses using their own modeling independently. The results are to be reported and discussed in each paper, with special emphasis on each specific response behavior, such as strength decay of the wall or the short columns, shear distribution into the wall and the columns, side-story failure in the first or the second, and the torsional responses.

6. INSTRUMENTS FOR MEASUREMENT AND SAFETY

6.1 Instrumentation for Measurement

A total of 960 channels are available for measurement at E-Defense with the sampling intervals of 2000Hz (32ch with 1000000Hz).

6.1.1 Measurement of Floor Acceleration and Displacement

In the current plan of measurement, 150 channels are allocated for floor accelerations and 100 channels for relative inter-story displacements. Floor displacements relative to the base (the table) are not to be measured directly except for the second floor in the test because the rigid gauge flame is not available on the table.

6.1.2 Measurement of Strain and Local Deformations

120 channels are allocated for measuring local member deformations, such as column and beam hinge rotations, elongation of wall boundary columns, and wall panel and beam elongations. 300 channels are allocated for measuring strains in reinforcement such as main bars of columns, beams, and walls, hoops of columns, wall shear reinforcement and slab reinforcement.

6.1.3 Measurement of Reaction Forces at the Base

One of the main objectives of the test is to measure the dynamic reactions, shear and axial forces, at the base independently for a wall and columns with sidewalls. A total of 24 three-dimensional load cells are placed under the foundations in X2-frame of the specimen as shown in Figure 2(b). The foundations of X1- and X3-frames are fixed to the table directly, the shear carried by which will be calculated as the residual.

6.1.4 Damage Observation

The balcony slabs with hangover length of 1.0m are placed around the main frames at each floor level. Efficient direct observation of residual cracks after each run will be available on the exterior surface of the building. A lot of records by video cameras are also planned during the shake table tests.

6.2 Other Techniques for Testing

In addition to measurement techniques, there are several other important techniques for full-scale shaking table test. Some of them have been developed and tried in the preliminary tests, but the followings will be new trial in the full-scale testing.

6.2.1 Method of Setup

The specimen is to be constructed outside of the testing facility and then moved inside after the construction and set up on the table. A special technique with temporary steel slide rails is to be used for transfer and set up of the specimen on the table.

6.2.2 Safety Protection against Pancake Collapse

Steel box frames are placed on the table and on each floor from the 1st to the 6th, which are used for the measurement of relative inter-story displacements. The frames are also designed to carry the weight of the building above, if the vertical elements could not sustain its gravity load due to a brittle failure or collapse. Steel wires are also placed to protect overturning.

7. CONCLUSION

The full-scale three-dimensional earthquake simulation test on reinforced concrete building structure, being planned for testing at E-Defense as the second phase of DaiDaiToku Project from 2005 to 2006, are outlined. Considering the results of the preliminary design analyses, DaiDaiToku committee on RC project has selected a six-story wall-frame building as the first RC test structure at E-Defense, for which the design is based on the past Japanese code of design and practice in 1970s. The allowable stress design procedure and additional pushover analysis for the selected design of the test specimen are outlined in this paper with the research objectives and the test plans.

ACKNOWLEDGEMENT

The study was carried out as a part of “National research project on mitigation of major disaster in major city/ Theme II Improvement of seismic performance of structures using E-defense/ Reinforced concrete structures (DaiDaiToku/RC project)” of MEXT. The full-scale test will be carried out in January 2006 at E-Defense, NIED in Miki. The variable discussions and joint efforts on the test planning by the members of the DaiDaiToku RC research committee on RC structures are gratefully acknowledged.

REFERENCES

[2] AIJ, "AIJ Standard for Structural Calculation on Reinforced Concrete Structures (1975 and Japanese version)," AIJ, 1975.

Keywords: Reinforced concrete building, Shear wall, Shaking table test, Full-scale test, Collapse

Table 1: Allowable stresses of concrete and steel

	Long term					Short term				
	Comp	Ten	Shear	Bond		Comp	Ten	Shear	Bond	
				Beam Upper	Others				Beam Upper	Others
SD345	2200	2200	2000	12	18	3500	3500	3000	18	27
SD295	2000	2000	2000	12	18	3000	3000	3000	18	27
Concrete	60	—	6	—	—	120	—	9	—	—

(Unit: kgf/cm^2)

Table 2: Member stiffness degradation ratios in linear analysis

Story	Column	Beam (general)	Boundary Beam	Wall (flexure)	Wall (shear)
R	—	1.0	0.5	—	—
6	1.0	1.0	0.5	0.5	0.5
5	1.0	1.0	0.5	0.5	0.5
4	1.0	1.0	0.5	0.3	0.3
3	1.0	1.0	0.5	0.3	0.3
2	1.0	1.0	0.5	0.2	0.2
1	1.0	1.0	1.0	0.2	0.2

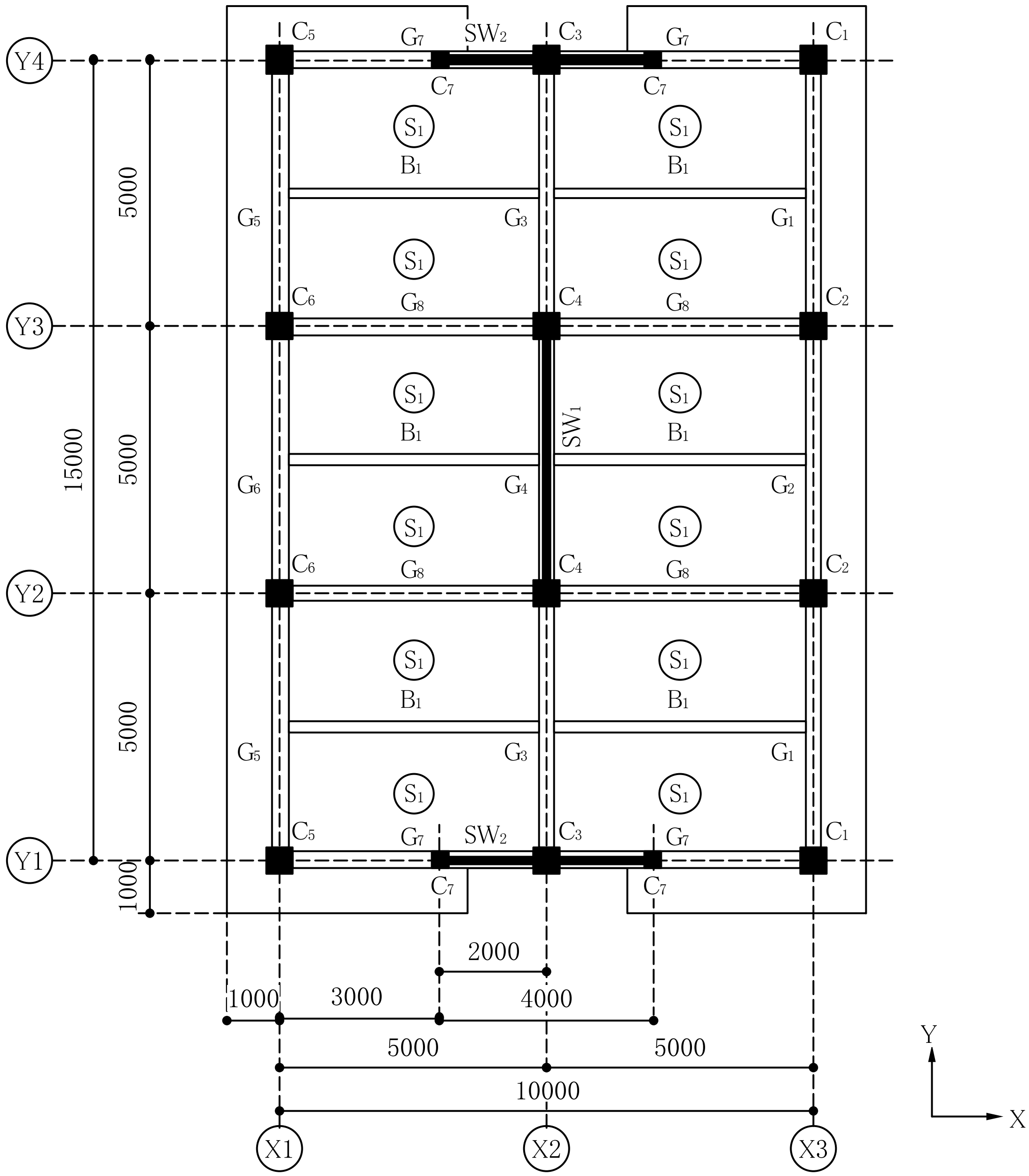

(a) second to fifth floor

Fig. 1: Plan of the full-scale test

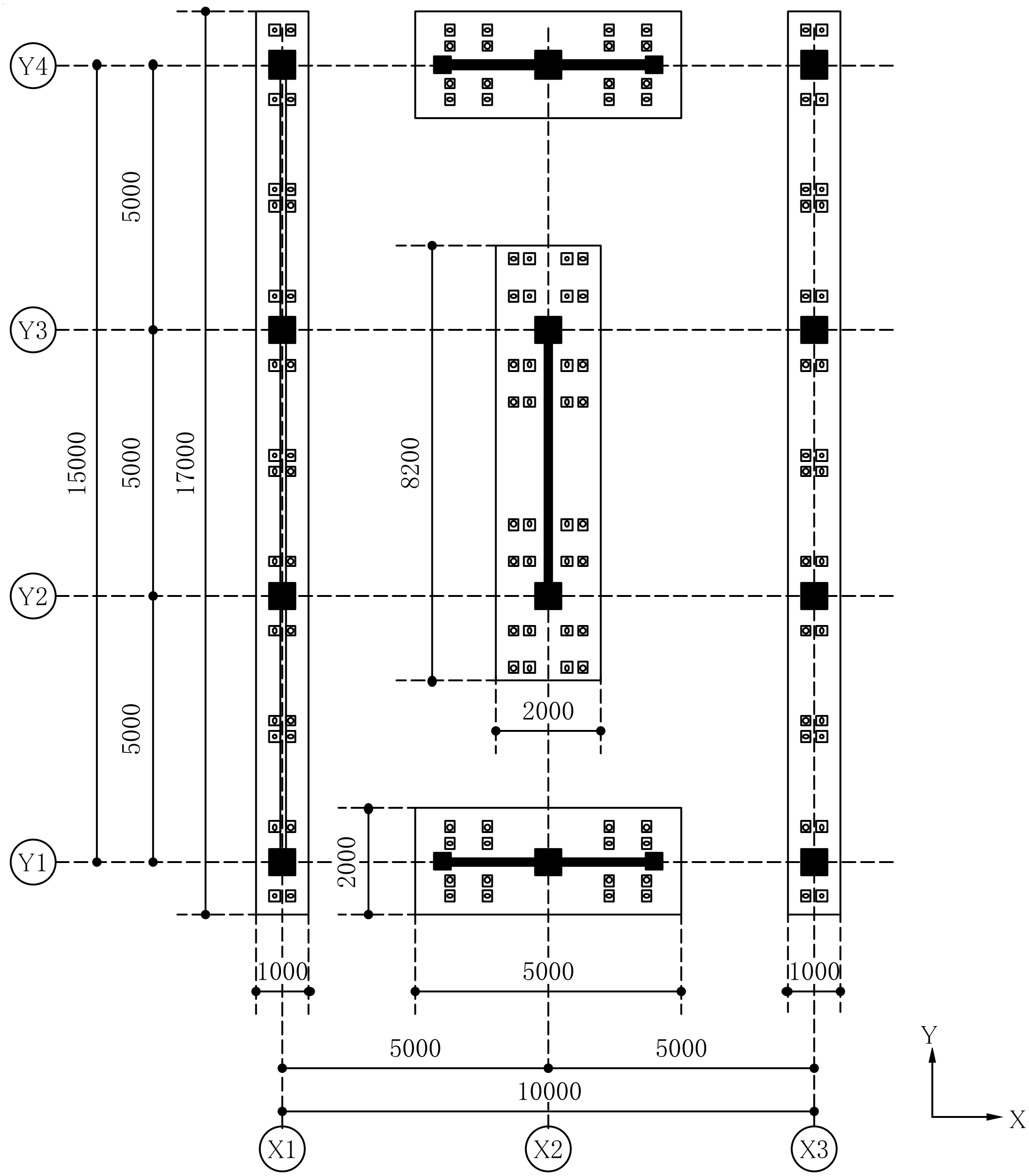

(b) base floor

Fig. 1: ***continued***

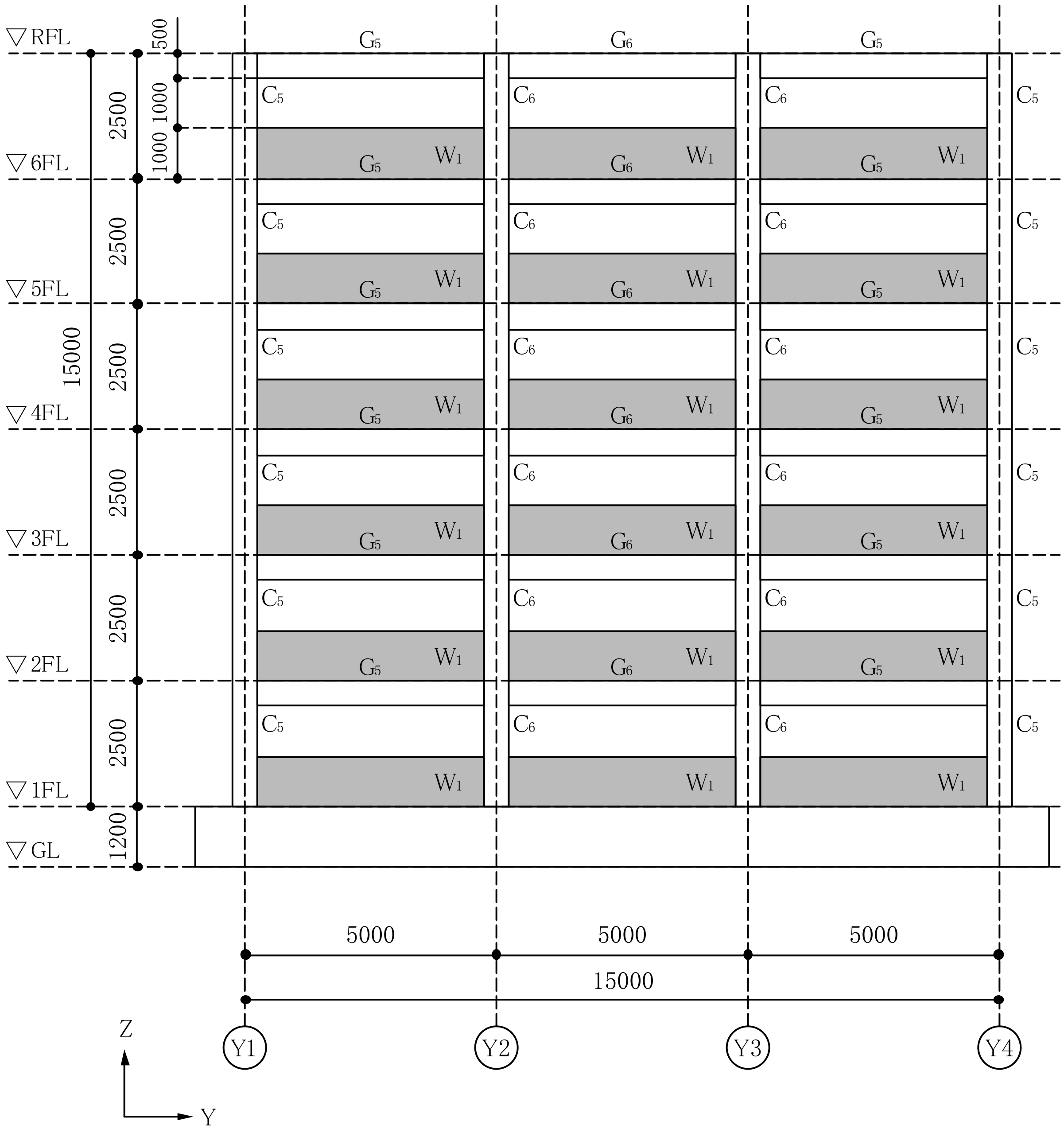

(a) X1-frame

Fig. 2: Elevation of the full-scale test structure

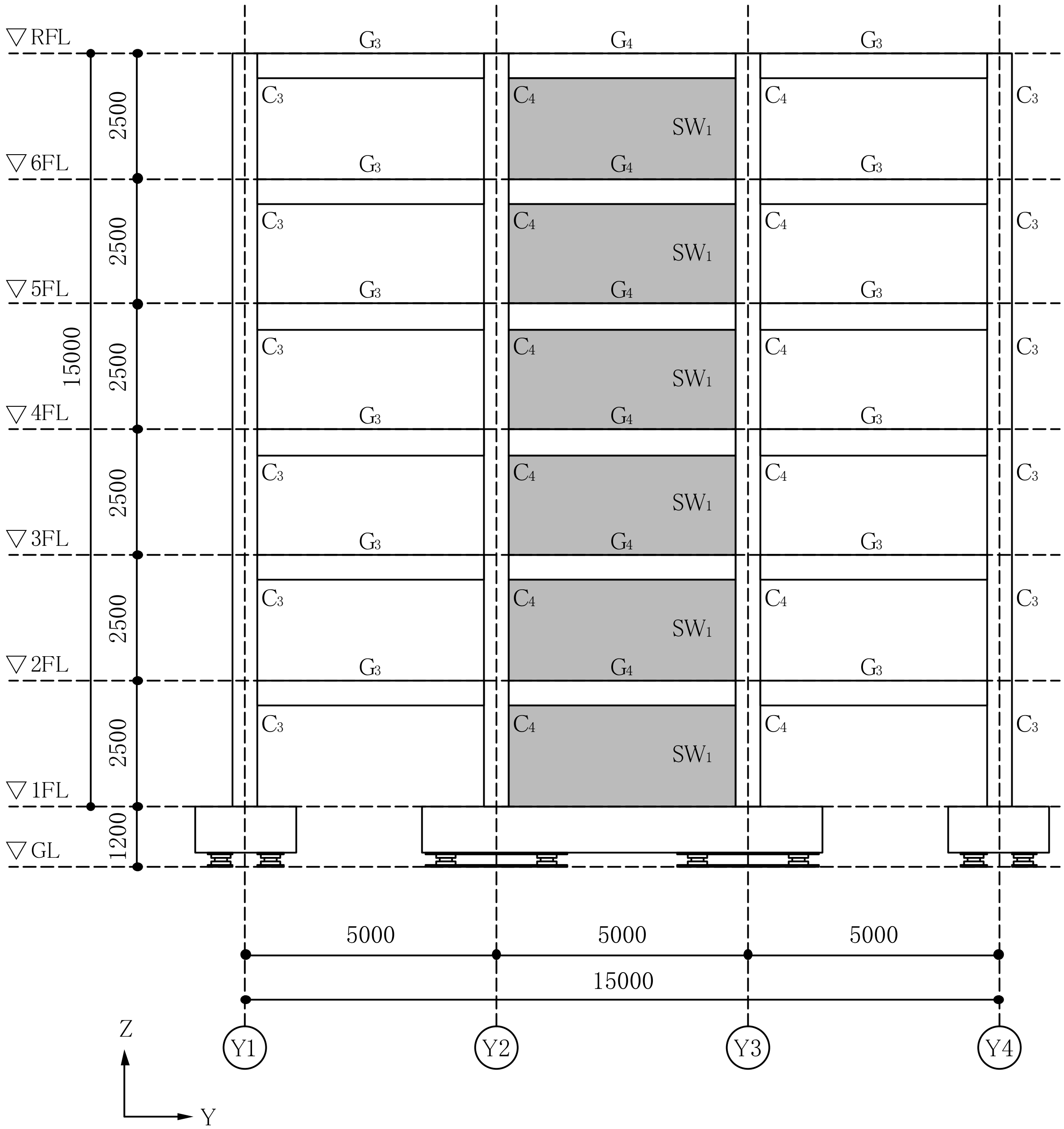

(b) X2-frame

Fig. 2: ***continued***

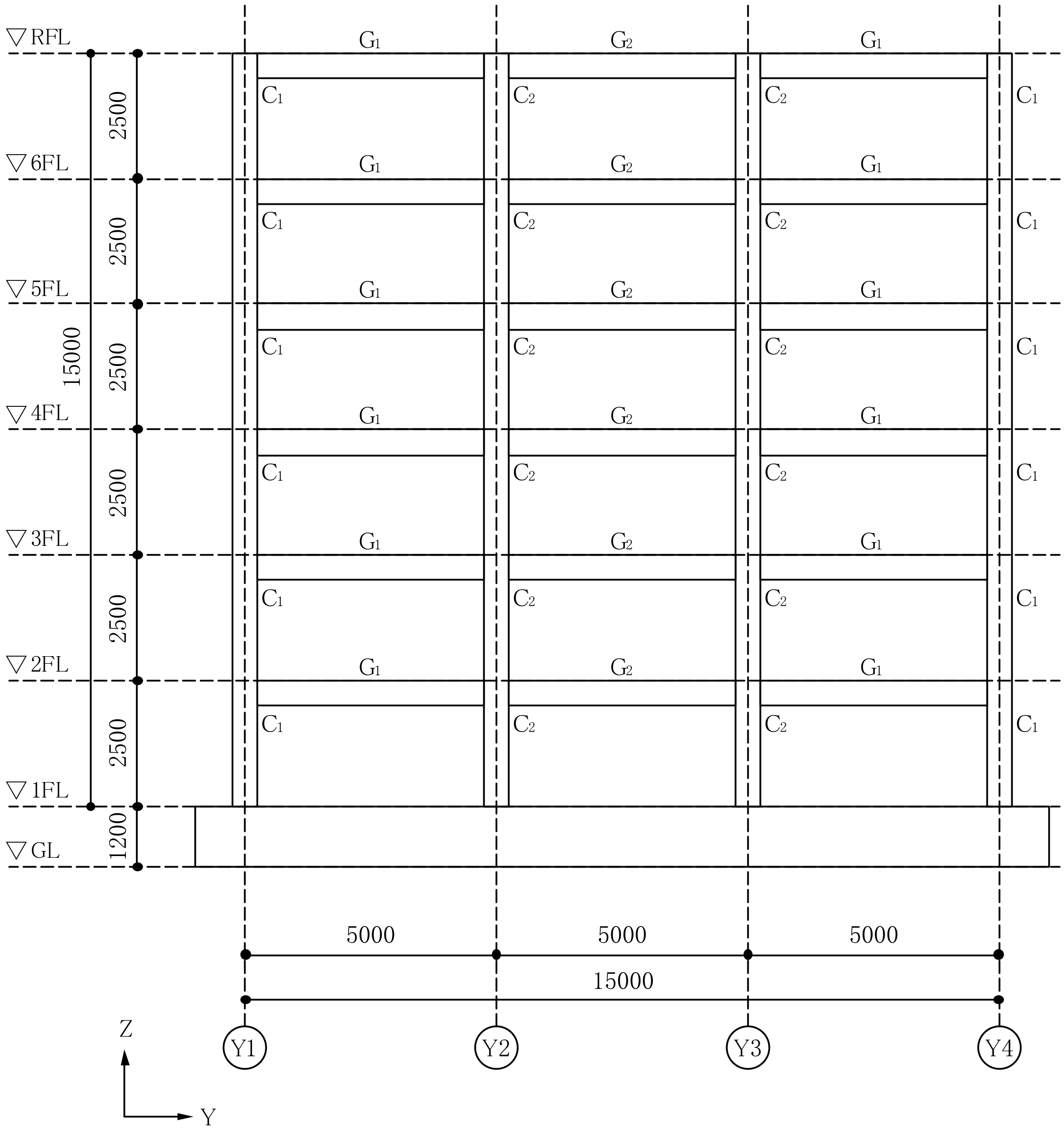

(c) X3-frame

Fig. 2: ***continued***

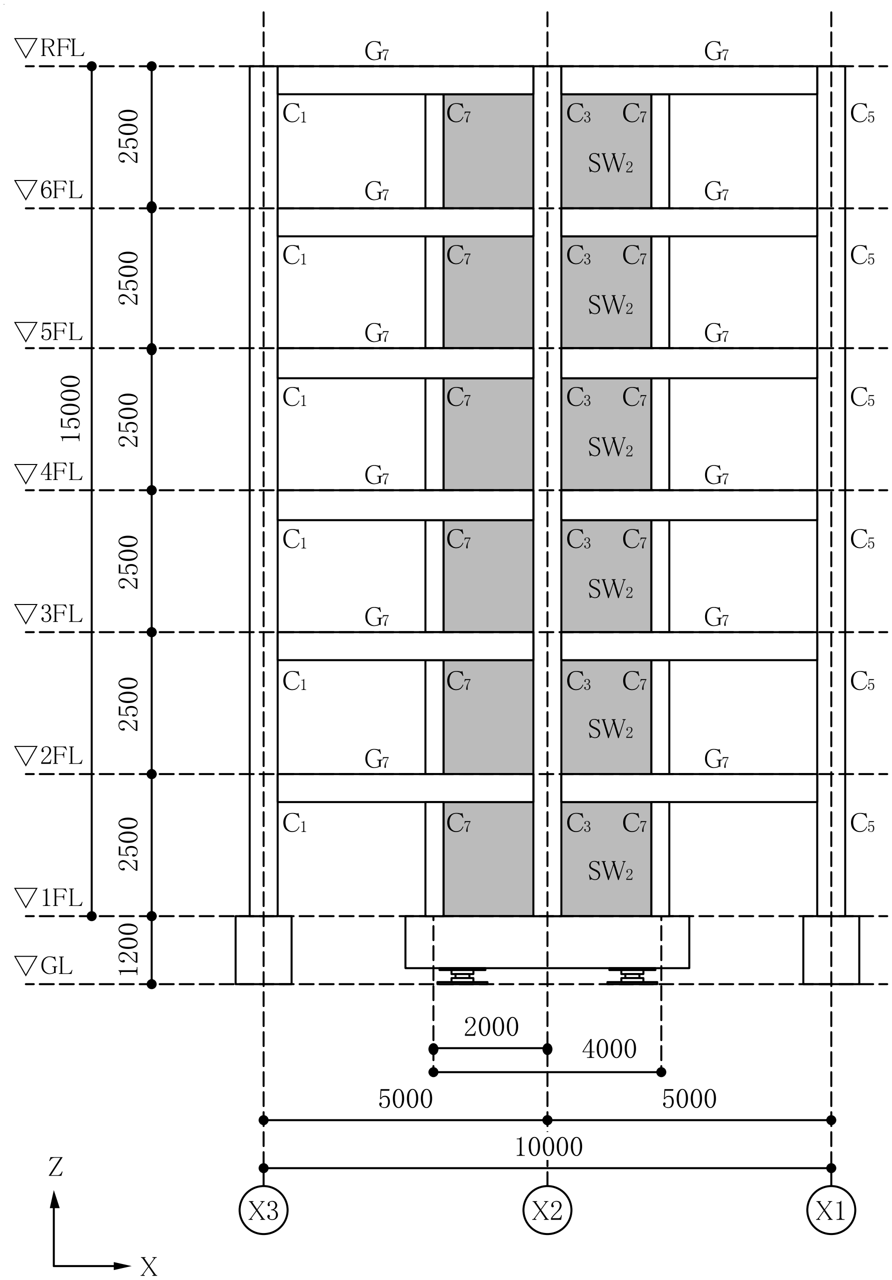

(d) Y1-frame and Y4-frame

Fig. 2: ***continued***

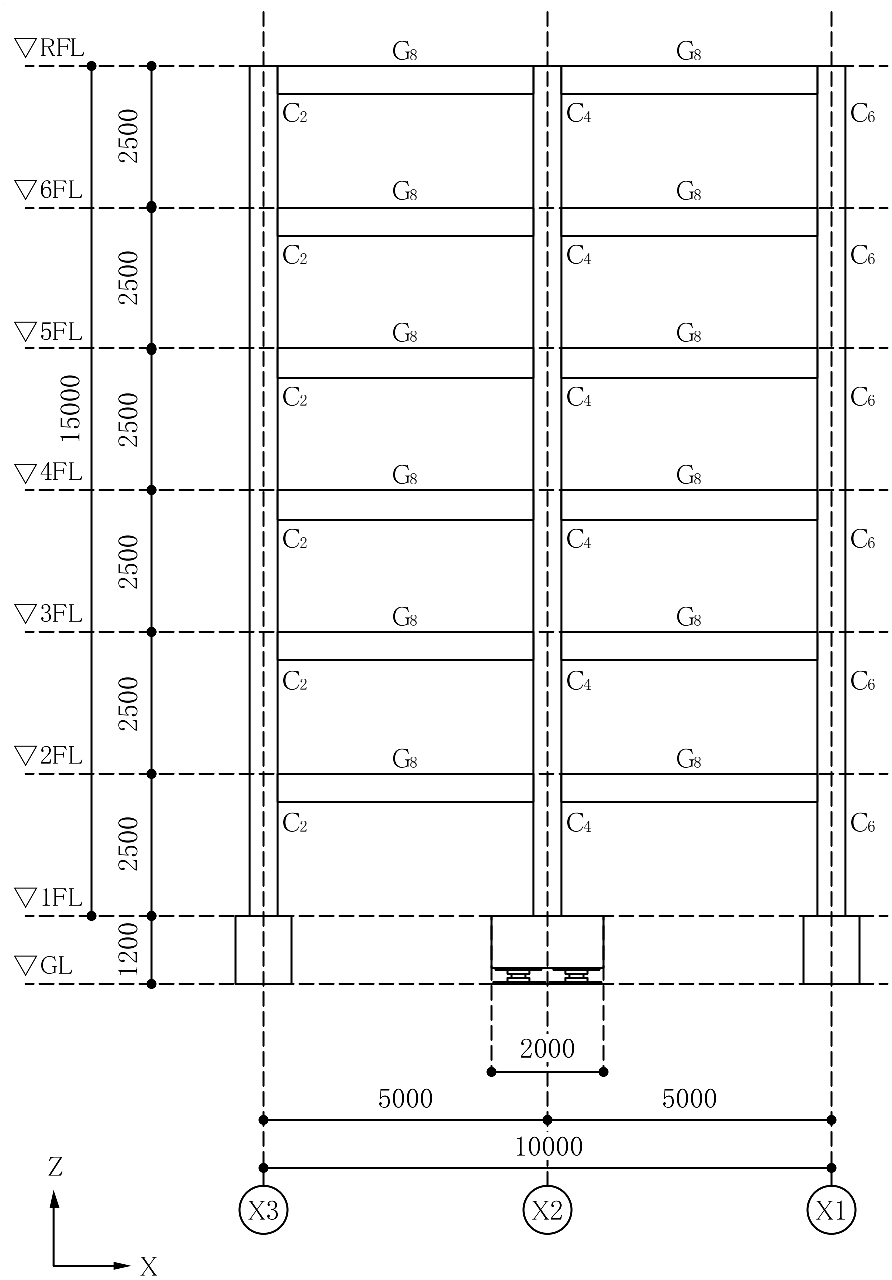

(e) Y2-frame and Y3-frame

Fig. 2: ***continued***

Table 3: Sectional details of the full-scale test structure

(a) Column sections

Story	C_1～C_6	C_7、C_8
1–6	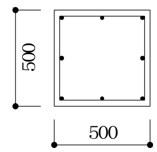	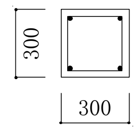
Main bars	8-D19	4-D19
HOOP	□-D10@100	□-D10@100

(c) Wall sections

Story	SW_1		SW_2	
	Thickness(mm)	Re-bars	Thickness(mm)	Re-bars
1-6	150	2-D10@300	150	2-D10@300

(d) Wing wall sections

Story	W_1	
	Thickness(mm)	Re-bars
1-6	120	1-D10@200

(e) Slab

Floor	S_1	
	Thickness(mm)	Re-bars
2-5	150	2-D10@200
R	190	2-D10@200

(f) Floor beams

Story	B_7			
	Width (mm)	Depth (mm)	Reinforcement	Stirrup
2-R	200	400	Top2-D19 Bottom2-D19	□-D10@200

Table 3: *continued*

(b) Beam sections (final design)

Floor	G_1	G_2	G_3
R~5	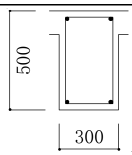	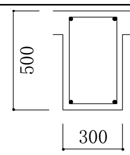	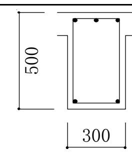
Top	2-D19	2-D19	3-D19
Bottom	2-D19	2-D19	2-D19
Stirrup	□-D10@200	□-D10@200	□-D10@200
4~2	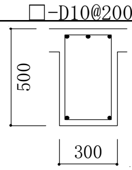	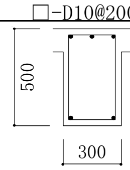	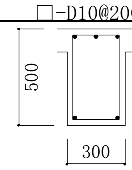
Top	3-D19	3-D19	3-D19
Bottom	2-D19	2-D19	2-D19
Stirrup	□-D10@200	□-D10@200	□-D10@200
Base	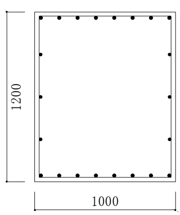	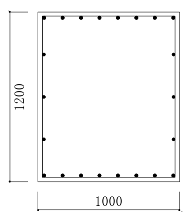	None
Top	8-D25	8-D25	
Bottom	8-D25	8-D25	
Mid	3x2-D22	3x2-D22	
Stirrup	□-D16@100	□-D16@100	

Floor	G_4	G_5	G_6
R~5	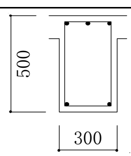	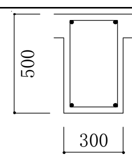	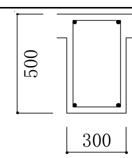
Top	3-D19	2-D19	2-D19
Bottom	2-D19	2-D19	2-D19
Stirrup	□-D10@200	□-D10@200	□-D10@200
4~2	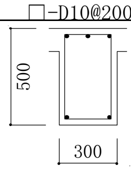	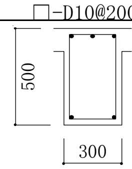	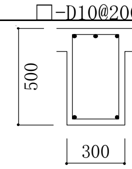
Top	3-D19	3-D19	3-D19
Bottom	2-D19	2-D19	2-D19
Stirrup	□-D10@200	□-D10@200	□-D10@200
Base	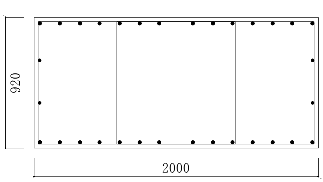	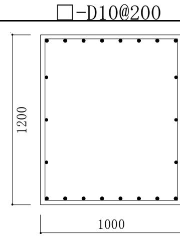	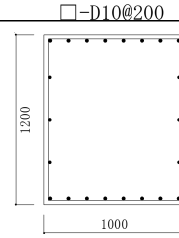
Top	14-D25	8-D25	8-D25
Bottom	14-D25	8-D25	8-D25
Mid	2x2-D22	3x2-D22	3x2-D22
Stirrup	□□□-D16@100	□-D16@100	□-D16@100

Table 3 *continued*

Floor	G_7	G_8
R~5	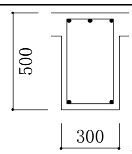	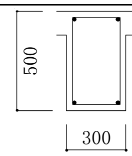
Top	3-D19	2-D19
Bottom	2-D19	2-D19
Stirrup	□-D10@200	□-D10@200
4~2	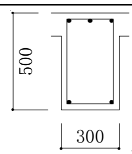	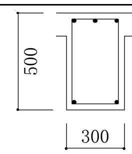
Top	3-D19	3-D19
Bottom	2-D19	2-D19
Stirrup	□-D10@200	□-D10@200
Base	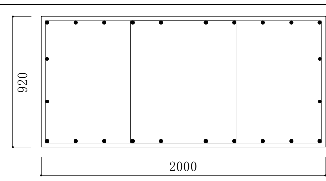	None
Top	10-D25	
Bottom	10-D25	
Mid	2x2-D22	
Stirrup	□□-D16@100	

At the previous design stage and for analysis in this and other papers, the following sections are changed as:
G4 →Top 4D19 /Bottom 2D19 /Stirrup -D10@200 (RF)
Top 3D19 /Bottom 2D19 /Stirrup -D10@200 (6F~2F)
G8 →Top 3D19 /Bottom 2D19 /Stirrup -D10@200 (RF~5F)
G9 →Top 2D19 /Bottom 2D19 /Stirrup -D10@200 (RF~5F) (deleted)
G9 →Top 3D19 /Bottom 2D19 /Stirrup -D10@200 (2F) (deleted)
and the middle of beam sections was different from the end as:
G1,2,3,5→middle：Top 2D19 /Bottom 2D19 /Stirrup -D10@200
G4,7,8 →middle：Top 2D19 /Bottom 3D19 /Stirrup -D10@200
G6 →middle：Top 2D19 /Bottom 2D19 /Stirrup -D10@200 (RF~5F)
middle：Top 2D19 /Bottom 3D19 /Stirrup -D10@200 (4F~2F)
G9 →middle：Top 2D19 /Bottom 2D19 /Stirrup -D10@200 (deleted)
and tow ends are different as:
G3 →Top 3D19 /Bottom 2D19 /Stirrup -D10@200 (5,6F outer end)
Top 2D19 /Bottom 2D19 /Stirrup -D10@200 (5,6F inner end)
G5,9 →Top 3D19 /Bottom 2D19 /Stirrup -D10@200 (4F outer end)
Top 2D19 /Bottom 2D19 /Stirrup -D10@200 (4F inner end)
Base G8 →same as Base G7

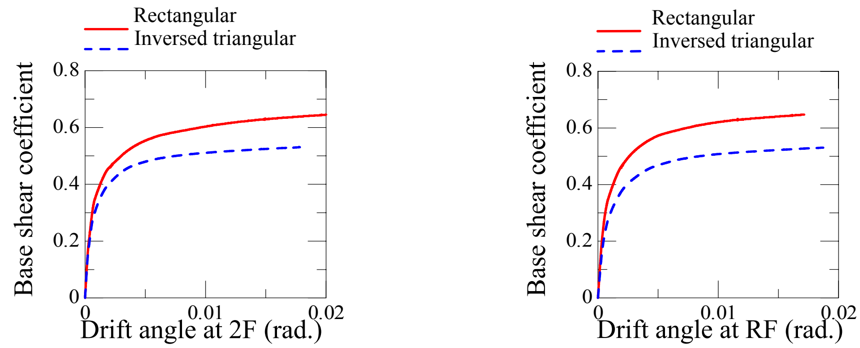

(a) base shear coefficient vs. drift angle (Y-direction)

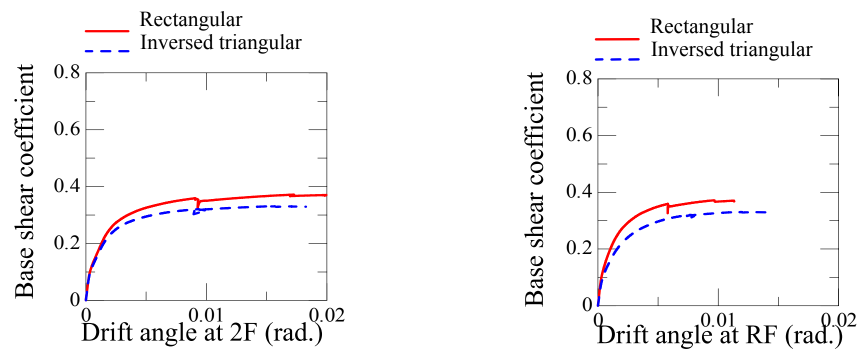

(b) base shear coefficient vs. drift angle (X-direction)

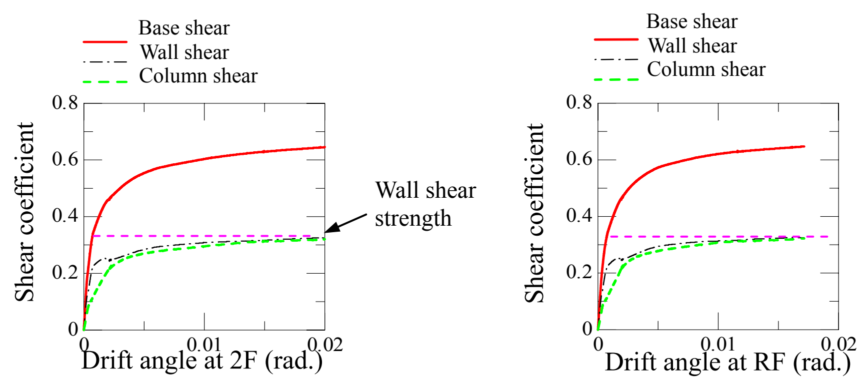

(c) shear coefficient of 1st story vs. drift angle (Y-direction, rectangular)

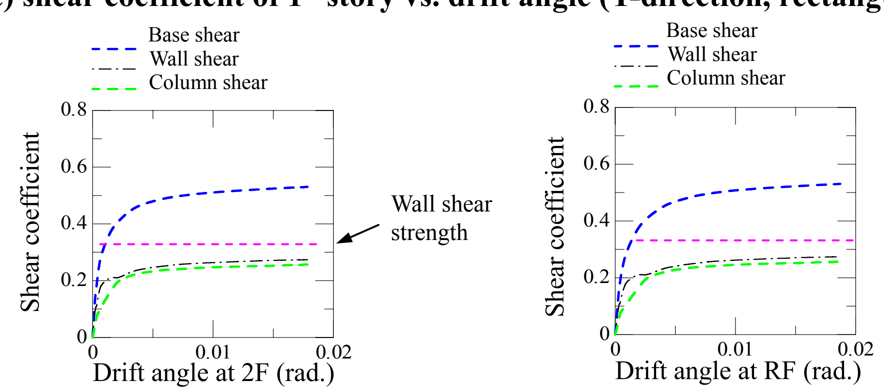

(d) shear coefficient of 1st story vs. drift angle (Y-direction, inversed triangular)

Fig. 3: Shear coefficient of 1st story vs. drift angle (Y-direction, inversed triangular)

A SIMPLE APPROACH FOR DISPLACEMENT-BASED ASSESSMENT OF REINFORCED CONCRETE COLUMNS

Hossein MOSTAFAEI[1], Toshimi KABEYASAWA[2]

ABSTRACT

A simple method is presented for displacement-based evaluation of reinforced concrete columns. The main concern in the approach is consideration of axial-shear-flexural interaction in the analytical process. Flexural mechanism is modeled based on conventional methods such as section analysis or fiber model in one-dimensional stress field. An integration point, representing the average strain-stress relationship of the element, simulates the shear behavior of the reinforced concrete columns. The strain-stress relationship for the integration point is developed on the basis of the smeared reinforcement and smeared rotating crack concept. Shear-flexural-axial interaction is considered by equilibrium satisfaction and realizing the compatibility in the averaged deformations. Axial strain of the model is obtained from the summation of axial strains caused by flexural, axial and shear mechanisms. Pushover analyses were carried out to evaluate the performance of shear, shear-flexural, and flexural dominated reinforced concrete column specimens applying the proposed method. The analytical results such as ultimate lateral forces and ultimate lateral drift ratios show reasonable agreement with that of the test results. Consistent correlations were also obtained for post-peak responses between analytical and experimental outcomes.

1. INTRODUCTION

Behavior of reinforced concrete columns in shear and flexure has been studied for decades. In case of flexural behavior, traditional section analysis or, more precise method, fiber model in one-dimensional stress field, gives acceptable prediction in terms of ultimate strength and yielding-deformation. In shear, there were several studies that the results leaded to various approaches mainly truss and arch mechanisms in addition to the empirical models. However shear strengths estimated by these methods are varying in a wide range and none of them can be applied in order to attain an acceptable deformation at the ultimate strength. Later Modified Compression Field Theory, (MCFT) (Vecchio et al, 1986) was developed in order to solve this analytical lack and to estimate shear behavior of an in-plane reinforced concrete element subjected to shear and axial stresses. The theory was verified by applying on a large number of reinforced concrete elements loaded in shear or shear with axial stresses. However, in order to

[1] *Earthquake Research Institute, The University of Tokyo*
Email: mhossein@eri.u-tokyo.ac.jp
[2] *Earthquake Research Institute, The University of Tokyo*
Email: kabe@eri.u-tokyo.ac.jp

predict flexural-shear behavior of a reinforced concrete element such as a column by MCFT, the structure should be discretized into a large number of biaxial elements and conducting a non-linear finite element analysis, which results in a fastidious computation. Later, the concept of MCFT was extended to the sectional analysis approach (Vecchi et al., 1988) in order to assess the response of reinforced concrete beams loaded in combined shear, moment, and axial forces. In this approach, biaxial elements are applied as concrete fibers, instead of uniaxial elements used in the conventional section analysis. In another word, a reinforced concrete beam is composed of a series of concrete biaxial elements and longitudinal steel elements. Then considering the compatibility and equilibrium conditions, each of the concrete elements is analyzed individually in in-plane stress field based on MCFT. The results obtained from this method were also verified by experimental data. The latest implementation of such a method is applied in a program called Response-2000 (Bentz, 2000).

In this study, considering the simplicity of the section analysis in uniaxial stress filed, the main objective is to modify the conventional section analysis approach for shear behavior to be applicable for displacement-base evaluation of reinforced concrete columns and beams subjected to shear, flexural and axial loads. In the approach traditional section analysis or fiber model in one-dimension stress field is applied to assess axial-flexural behavior and one integration point in in-plane stress conditions, applying MCFT, is considered to determine axial-shear behavior. Axial deformation is the main interaction consideration in the proposed method as well as equilibrium and compatibility satisfaction. It is approved by experimental results that load-deformation of a single reinforced concrete column, considering the symmetric condition, can be accurately predicted by applying only one section analysis at the end section and one in-plane stress integration point representing the behavior of the length of the column from the end to the inflection point. The pullout effect due to joint bond-slip is also modeled and considered in the analytical process. It is likely that the approach can be extended to three-dimensional analysis by applying fiber model, simulating the flexure and in-plane shear model subjected to the resultant shear stress caused by biaxial flexural mechanism. By applying the new model, three reinforced concrete columns specimens in three failure modes; shear, shear-flexural, and flexural were tested and analyzed. The results were verified with the experimental data for the ultimate strengths and deformations as well as post-pick response including axial failure accuracy.

2. ANALYTICAL MODEL

Traditional section analysis is a very handy and convenient approach to predict flexural performance of a reinforced concrete column or a beam. In order to contribute shear behavior in section analysis, a new analytical process is presented considering axial, shear and flexural interaction. The method consists of three mechanisms of axial, shear and flexure, in which axial-flexural mechanism is modeled by traditional uniaxial section analysis and axial-shear mechanism is modeled by only one biaxial shear element. The three mechanisms are connected as series springs and interrelated in stress-strain field, considering equilibrium and compatibility. Total lateral drift of the column, γ between two sections, is considered equal to the summation of shear strain γ_s and flexural drift ratio γ_f between the two sections. Furthermore, total axial strain of the column ε_x between the two sections, is obtained by summation of axial strains due to axial ε_{xa}, shear ε_{xs} and flexural ε_{xf} mechanisms.

$$\gamma = \gamma_s + \gamma_f \qquad\qquad \varepsilon_x = \varepsilon_{xs} + \varepsilon_{xf} + \varepsilon_{xa} \tag{1}$$

Section analysis gives axial strain caused by axial and flexural mechanisms, $\varepsilon_{xa}+\varepsilon_{xf}$ which is the centroidal strain. On the other hand in-plane shear model gives axial strain due to axial and shear mechanisms, $\varepsilon_{xa}+\varepsilon_{xs}$.

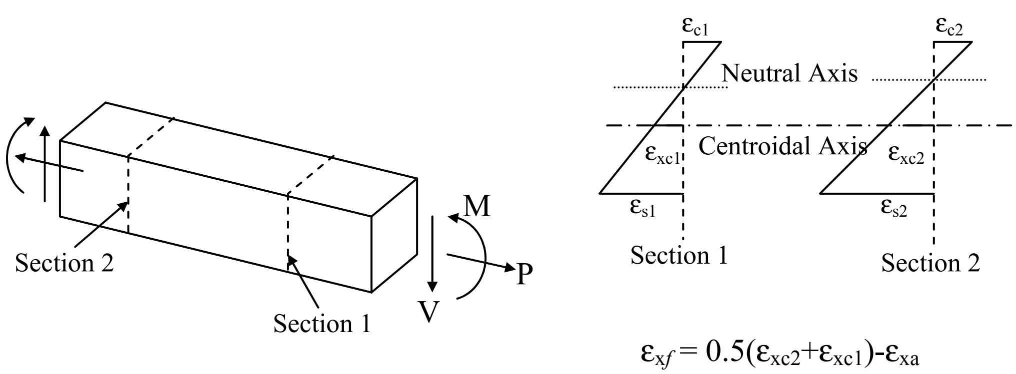

ε_{xf} :Axial strain due to flexure

ε_{xa}: Average axial strain due to the applied axial

Fig. 1: Average centroidal strain due to flexure to be contributed in the in-plane shear element

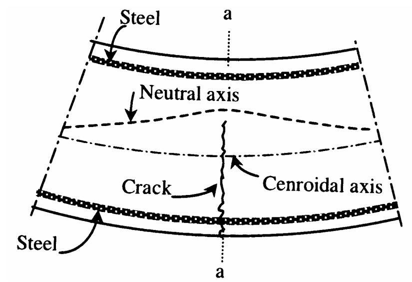

Fig. 2: Centroidal and neutral axes in a cracked section

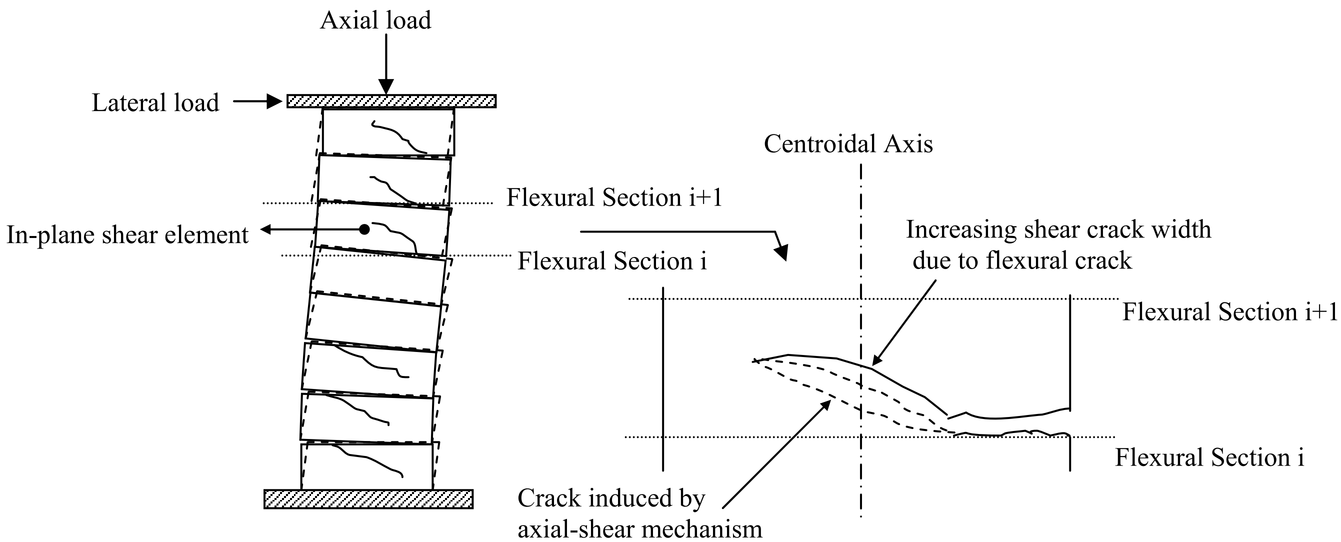

Fig. 3: Conceptual illustration for effect of flexural deformation and crack at centroidal axis on shear crack widening in a reinforced concrete column

Therefore, to obtain ε_x in equation (1), it is necessary to extract ε_{xf} from section analysis, and to determine ε_{xs} from in-plane shear model considering axial strain due to axial mechanism ε_{xa}. In this study, the main role of in-plane shear integration point is to model shear behavior of an element between two flexural sections. Therefore, only shear deformation is determined by the in-plane shear model and axial mechanism is modeled by fiber model.

Figure 1 shows strain distributions in two sections of a reinforced concrete column. Axial strain caused by flexural mechanism between two sections, ε_{xf} is computed by deducting the average axial strain due to axial mechanism, ε_{xa} from the average centroidal strains, assuming a linear strain relationship between the two sections. By the same concept, axial strain due to shear mechanism ε_{xs} is determined by subtracting the average axial strain due to axial mechanism, ε_{xa} from total axial strain of the in-plane shear element.

Considering linear strain relationship between two flexural sections of a column, average axial strain component, due to axial mechanism, of the element between two sections, ε_{xa} might be defined as Eq. (2).

$$\varepsilon_{xa}=0.5(\varepsilon_{xa1}+\varepsilon_{xa2}) \tag{2}$$

Where, ε_{xa1} and ε_{xa2} are axial strains of the two consecutive flexural sections due to axial mechanism.

$$\varepsilon_{xa1}=\frac{\sigma_o}{k_{xa1}},\qquad k_{xa1}=\frac{\sum E_{1i}A_{1i}}{A_{1i}},\qquad \varepsilon_{xa2}=\frac{\sigma_o}{k_{xa2}},\qquad k_{xa2}=\frac{\sum E_{2i}A_{2i}}{A_{2i}} \tag{3}$$

where, K_{xa1}, and K_{xa2}= axial stiffness, E_{1i}, E_{2i}= elasticity modulus of fiber i and A_{1i}, A_{2i}= fiber i section area for two consecutive flexural sections at the corresponding loading step. In another words, ε_{xa}, at any loading step, is the axial strain of an element when lateral loads at the corresponding loading step are omitted and the element is subjected only to the axial load.

Concept of axial strain due to flexural mechanism, ε_{xf} can be explained by means of cracked and non-cracked reinforced concrete sections. In a non-cracked reinforced concrete section the centroid and neutral axes are identical and the centroidal strain due to flexure is zero. However, for a cracked section the two axes are not in the same position, which is the cause of centroidal strain or axial strain due to flexural mechanism, ε_{xf} as shown in Figure 2. Given the flexural sections and in plane shear elements, illustrated in Figure 3, the width of the shear crack is increased due to the crack caused by flexure mechanism.

Equilibrium of shear and axial stresses obtained from section analysis τ_f, σ_{xf} and in-plane shear model τ_s, σ_{xs} , respectively, are satisfied simultaneously through the analysis.

$$\sigma_{xf}=\sigma_{xs}=\sigma_o \qquad \tau_f=\tau_s=\tau \tag{4}$$

Where σ_{xf}: Axial stress in axial-flexure mechanism, σ_{xs}: Axial stress in axial-shear mechanism, σ_o: Applied axial stress, τ_f: Shear stress in axial-flexure mechanism, τ_s: Shear stress in axial-shear mechanism, and τ: Applied shear stress.

Stresses in axes perpendicular to the axial axis of the column, or clamping stresses σ_y, and σ_z are neglected due to equilibrium between confinement pressure and hoops stresses. This is a basic assumption also in (AASHTO, 2000) code provisions, for estimation of shear strength of reinforced concrete beams.

$$\sigma_y=\sigma_z=0 \tag{5}$$

Axial strain due to flexure, ε_{xf} can be added to the axial strain of in-plane shear model by adding the flexibility stiffness for the flexural-axial component to the corresponding flexibility stiffness element of the in-plane shear element. Flexibility stiffness for the flexural-axial component, f_{xf}, can be obtained by Eq. (6).

$$f_{xf}\sigma_o = \varepsilon_{xf} \tag{6}$$

where, σ_o= applied axial stress of column. In case of beams that axial load might be zero, in order to avoid producing an indefinite value in the process of analysis, a small enough value should be considered as σ_o, however the value should not be changed in the process of computation. Considering the in-plane stress field, a strain-stress relationship in terms of flexibility matrix may define as:

$$\begin{bmatrix} f_{11} & f_{12} & f_{13} \\ f_{21} & f_{22} & f_{23} \\ f_{31} & f_{32} & f_{33} \end{bmatrix} \begin{Bmatrix} \sigma_x \\ \sigma_y \\ \tau \end{Bmatrix} = \begin{Bmatrix} \varepsilon_x \\ \varepsilon_y \\ \gamma \end{Bmatrix} \tag{7}$$

where, f_{ij}(i,j=1,2,3)= flexibility components of the in-plane shear model, ε_y= strain of hoops or lateral reinforcement. Axial strain due to flexure, ε_{xf} can be simply contributed into the in-plane stress field, as Eq. (8), by adding corresponding flexibility value, obtained from Eq. (6), into Eq. (7). Considering x-axis as the main axis of the column, stress in x direction is assumed equal to the applied axial stress $\sigma_x = \sigma_o$. Stress in y direction is considered zero, σ_y=0, satisfying the equilibrium between confinement pressure and hoops stresses.

$$\begin{bmatrix} f_{11}+f_{xf} & f_{12} & f_{13} \\ f_{21} & f_{22} & f_{23} \\ f_{31} & f_{32} & f_{33} \end{bmatrix} \begin{Bmatrix} \sigma_o \\ 0 \\ \tau_s \end{Bmatrix} = \begin{Bmatrix} \varepsilon_x = (\varepsilon_{xs}+\varepsilon_{xa})+\varepsilon_{xf} \\ \varepsilon_y \\ \gamma_s \end{Bmatrix} \tag{8}$$

Where, $(\varepsilon_{xs}+\varepsilon_{xa})$= axial strain due to shear and axial mechanisms determined from the in-plane shear model.

The same approach can be applied for fiber model to add axial strain due to shear, ε_{xs} to the total axial strain. Therefore, considering the two sections in Figure 1, total axial strain for the two sections, $\varepsilon^*_{xc2}, \varepsilon^*_{xc1}$, are modified as:

$$\varepsilon^*_{xc1}=\varepsilon_{xc1}+\varepsilon_{xs} \quad \text{and} \quad \varepsilon^*_{xc2}=\varepsilon_{xc2}+\varepsilon_{xs} \tag{9}$$

Thus, for computing axial strain due to flexural mechanism in Figure 1, ε_{xs} should be deducted from the obtained total axial strain as:

$$\varepsilon_{xf}= 0.5(\varepsilon^*_{xc2}+\varepsilon^*_{xc1})-\varepsilon_{xa}-\varepsilon_{xs} \tag{10}$$

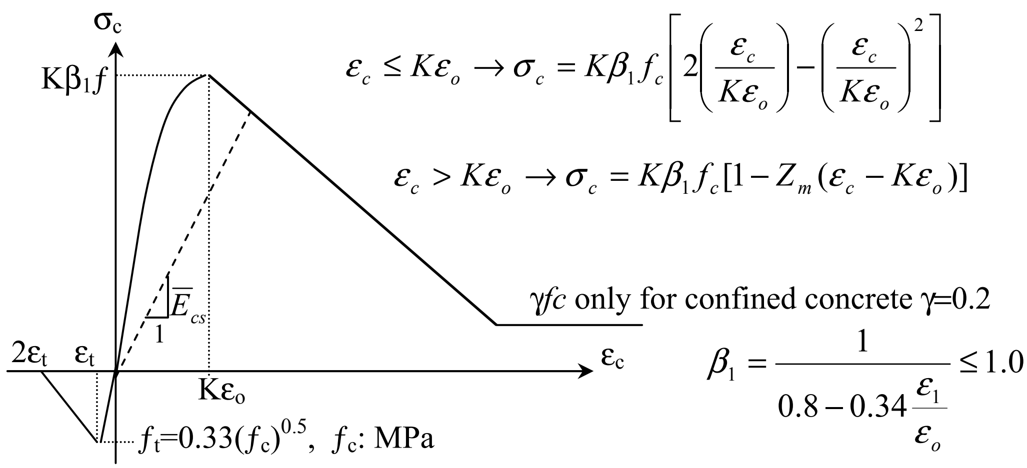

(a) Concrete constitutive law for uniaxial fiber model in section analysis

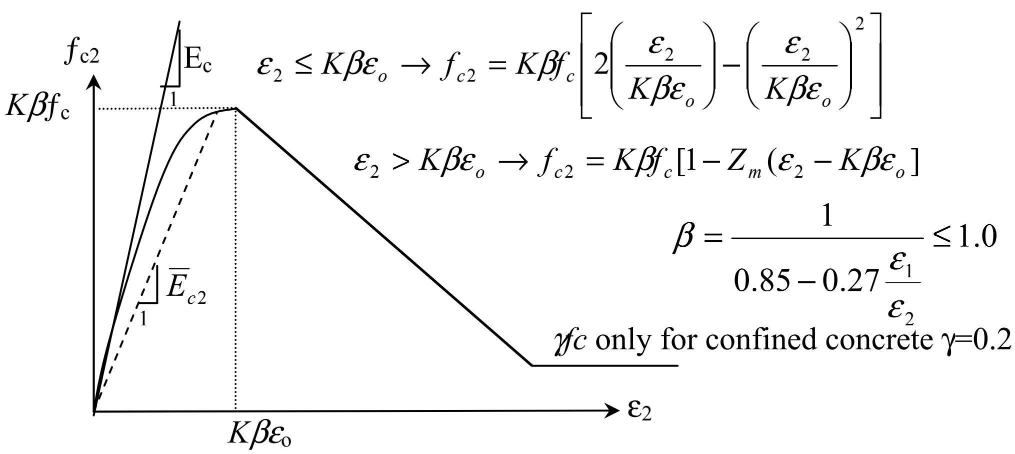

(b) Concrete in principle compression direction for in-plane stress field

Fig. 4: Constitutive laws and secant moduli used in the analytical process for concrete and reinforcement

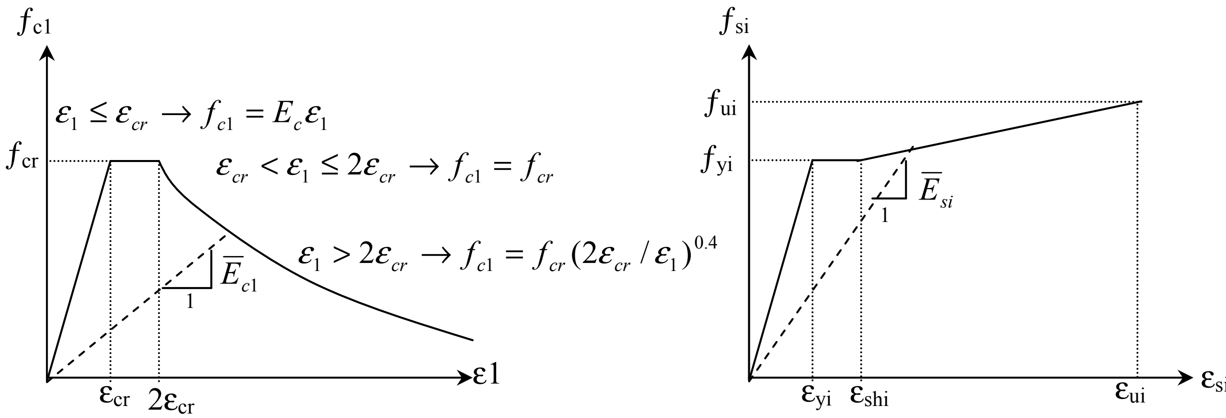

(c) Concrete in principle tensile direction **(d) Reinforcing bars**

Fig. 4: *continued*

Contribution of shear-axial strain, ε_{xs} into flexure mechanism, may give a lower estimated or a conservative strength for an element when concrete compression failure is the dominant failure mode of the element. This is due to decreasing compression strain by adding tensile shear-axial strain, ε_{xs} to the total compression strain. Therefore, for design purpose, it might be acceptable to neglect contribution of shear-axial strain, ε_{xs} into the section analysis.

Given the compatible stress-strain fields, secant moduli might be applied for the concrete and reinforcement. Constitutive laws and secant moduli used in the analytical process for one-dimensional section analysis and the in-plane shear integration point are shown in Figure 4. In Figure 4-a, parameter K and Z_m is computed based on modified Kent and Park model for stress-strain relation of concrete confined by rectangular steel hoops (Park, et al., 1982).

$$K = 1 + \frac{\rho_s f_{yh}}{f_c'}, \quad Z_m = \frac{0.5}{\dfrac{3 + 0.29 f_c'}{145 f_c' - 1000} + \dfrac{3}{4}\rho_s \sqrt{\dfrac{h''}{s_h}} - K\varepsilon_o} \tag{11}$$

Where, ρ_s=ratio of volume of rectangular steel hoops to volume of concrete core measured to outside of the peripheral hoop, f_{yh}= yield strength of steel hoop (MPa), f_c= concrete compression cylinder strength (MPa), h'' = width of concrete core measured to outside of the peripheral hoop, and S_h= center-to-center spacing of hoop sets.

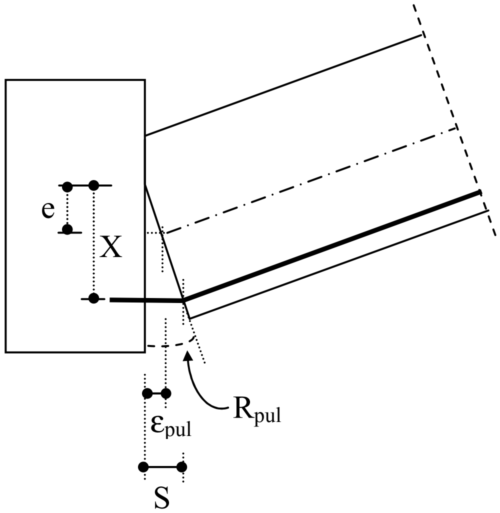

$\gamma_{pul}=R_{pul}=S/X$
$\varepsilon_{pul}=(e.R_{pul})/(Lin)\geq 0.0$
Lin: Distance between the end joint and inflection point

Fig. 5: Deformations due to pull-out of steel bars at the joint section

In addition to shear and flexural deformations, slip of steel bars under tension stress at the section adjacent to section with larger thickness should be consider in the total deformation of the reinforced concrete element. As shown in Figure 5, there are two components of deformation, rotation and axial deformation that contributed in the total performance of the column. The pull out element is considered series with springs of flexural and shear mechanisms. Pullout model and strain-slip relation of steel bars subjected to tensile stress applied in the analytical process are presented in Figure 6 (Okamura and Maekawa, 1991).

In order to contribute the effect of pull out, centroidal strain due to pullout, ε_{pul}, should be added to the total axial deformation of the column. The total lateral drift of the element is computed as summation of total shear and flexural lateral drift and pullout rotation, $R_{pul.}$

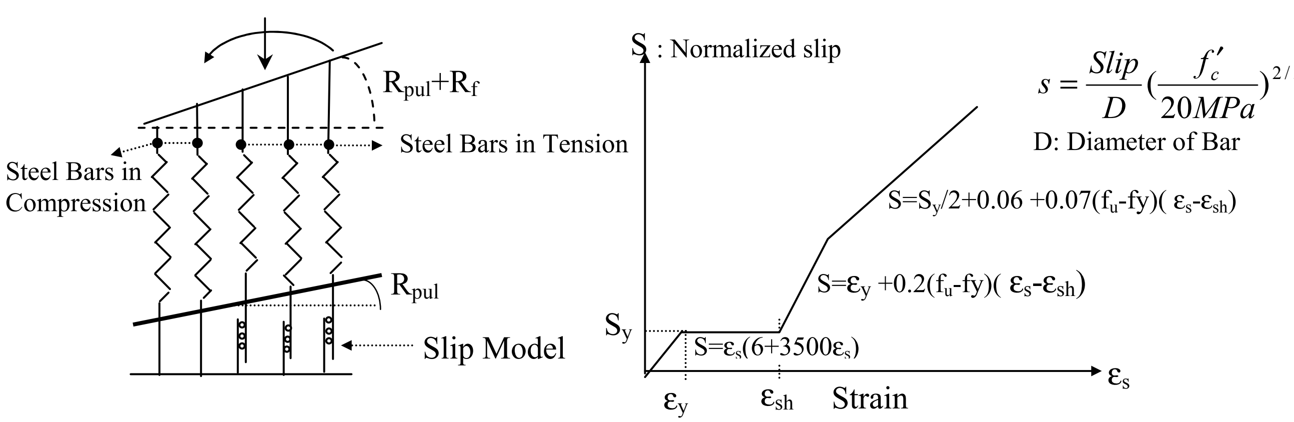

Fig. 6: Pull-out and slip models for steel bars at the joint section

As mentioned before, section analysis can be implemented by applying fiber model in one-dimensional stress field. In case of a reinforced concrete column section, fiber model can be introduced with two variables of curvature ϕ and axial strain ε_o. The idealization of fiber model, strain and force relationships are presented in Fig7.

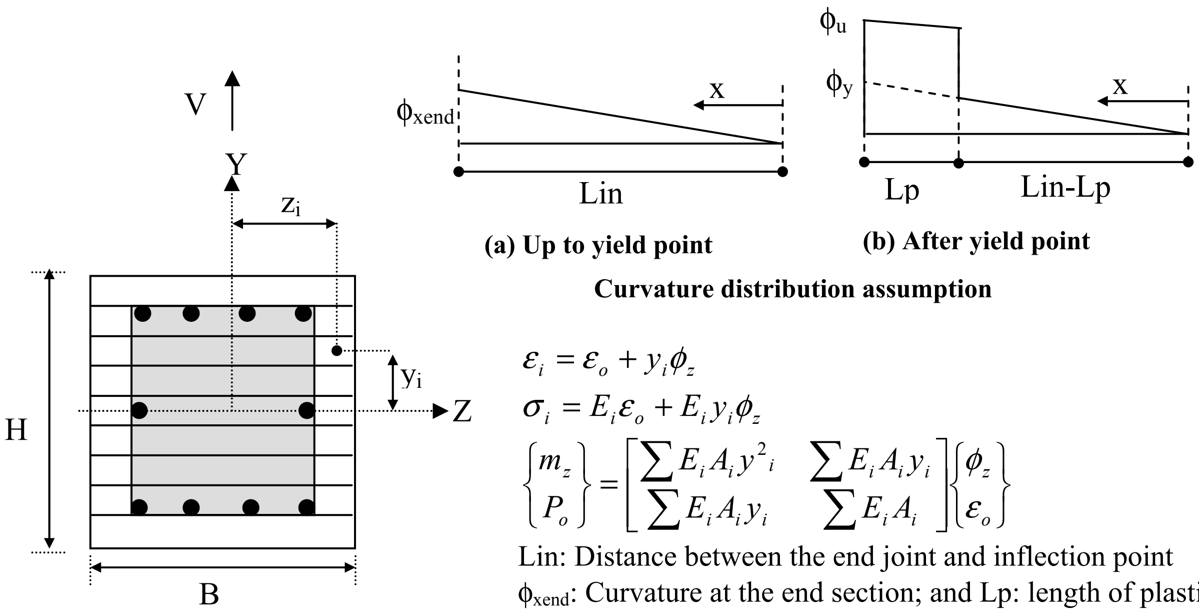

$$\varepsilon_i = \varepsilon_o + y_i \phi_z$$

$$\sigma_i = E_i \varepsilon_o + E_i y_i \phi_z$$

$$\begin{Bmatrix} m_z \\ P_o \end{Bmatrix} = \begin{bmatrix} \sum E_i A_i y^2{}_i & \sum E_i A_i y_i \\ \sum E_i A_i y_i & \sum E_i A_i \end{bmatrix} \begin{Bmatrix} \phi_z \\ \varepsilon_o \end{Bmatrix}$$

Lin: Distance between the end joint and inflection point

ϕ_{xend}: Curvature at the end section; and Lp: length of plastic zone

Fig. 7: Fiber model for a section under axial load and lateral load in y direction

Since the analytical process is implemented in strain-stress field therefore results of moment, axial load and curvature should be converted into shear stress, axial stress and lateral drift (rotation) respectively.

Considering x as the axis of the column or normal axis of the flexural sections, average shear stress and axial stress can be computed from equilibrium as:

$$\sigma_x = \frac{P_o}{BH}, \quad \tau_{xy} = \frac{V}{BH}, \quad \tau_{yx} = \frac{(m_x / d)}{BLin} \quad \tau = \tau_{xy} = \tau_{yx} \Rightarrow V = \frac{Hm_x}{dLin} \qquad (12)$$

Where, V: Lateral Load, P_o: applied axial load, m_z: moment at the section and d: distance from the extreme tension bar and extreme compression fiber of the concrete, Lin: distance from an end to the inflection point of the column, B: width of the section, and H: height of the section.

Lateral drift of a column, γ_f, when one section is considered for the analysis at the end, can be determined based on the curvature distribution in Figure 7 between the end and the inflection point.

Therefore, flexural deformation γ_f corresponding to the shear stress τ can be related by a stiffness of K_f.

$$K_f = \frac{\tau}{\gamma_f} \quad \text{where, } \gamma_f = \frac{\delta}{Lin} = \frac{1}{Lin}\int_0^{Lin} x\phi dx \tag{13}$$

Where, δ: lateral drift, x: distance variable from inflection point, ϕ: curvature, function of x, and Lin: distance from an end to the inflection point of the column.

Then a spring with stiffness of K_f is contributed in series with the shear spring with stiffness of K_s as well as pullout spring with stiffness of K_{pul}. Therefore, the total stiffness K_γ corresponding to shear strain, γ_s, flexural drift ratio γ_f, and pullout rotation, γ_{pul}, is determined as:

$$\frac{1}{K_\gamma} = \frac{1}{K_f} + \frac{1}{K_s} + \frac{1}{K_{pul}} \qquad K_\gamma(\gamma_s + \gamma_f + \gamma_{pul}) = \tau \tag{14}$$

where, shear spring stiffness, K_s, and pullout spring stiffness, K_{pul}, are computed as:

$$K_s = \frac{\tau}{\gamma_s}, \quad K_{pul} = \frac{\tau}{\gamma_{pul}} \tag{15}$$

Where, γ_{pul} can be determined based on equation provided in Figure 5. For axial springs, since the contribution of flexural-axial strain is considered in equation (8), therefore total axial stiffness $K_{\varepsilon x}$ is determined by considering the axial stiffness $K_{s\varepsilon x}$, obtained from the in-plane stress field model, and axial strain stiffness $K_{pul\varepsilon x}$ obtained from pullout axial strain ε_{pul}.

$$K_{s\varepsilon x} = \frac{\sigma_x}{\varepsilon_x}, \quad K_{pul\varepsilon x} = \frac{\sigma_x}{\varepsilon_{pul}}, \quad \frac{1}{K_{\varepsilon x}} = \frac{1}{K_{s\varepsilon x}} + \frac{1}{K_{pul\varepsilon x}}, \text{ therefore: } K_{\varepsilon x}\varepsilon_{x-total} = \sigma_x \tag{16}$$

where, $\varepsilon_{x\text{-total}}$ = total axial deformation

$$\varepsilon_{x\text{-total}} = \varepsilon_{xa} + \varepsilon_{xf} + \varepsilon_{xs} + \varepsilon_{pul} \tag{17}$$

3. PROCESS OF ANALYSIS

The new analytical approach described here is mainly based on contribution of three mechanisms of shear, flexure and axial and their interaction as well as pullout of the tensile steel bars at joint section. In order to provide a simple explanation of the approach, process of the computation is described for a reinforced concrete column considering one section at the end of the column and one integration point representing the shear behavior of the column from the section to the inflection point, as shown in Figure 8.

In addition to the deformation illustrated in Figure 8, axial strain and lateral drift due to pullout of tensile steel bars in the flexural section are computed and contributed in the total deformations of the column based on equation provided in Figures 5 and 6. Flowchart of the analytical process is illustrated in Figure 9.

Since the shear integration point is an in-plane stress field without contribution of geometrical parameters, the approach can be simply modified for three-dimensional analysis. In order to do so, fiber model in three dimensions is applied and in-plane stress field will be developed for the resultant of the shear stresses in the two directions of the column.

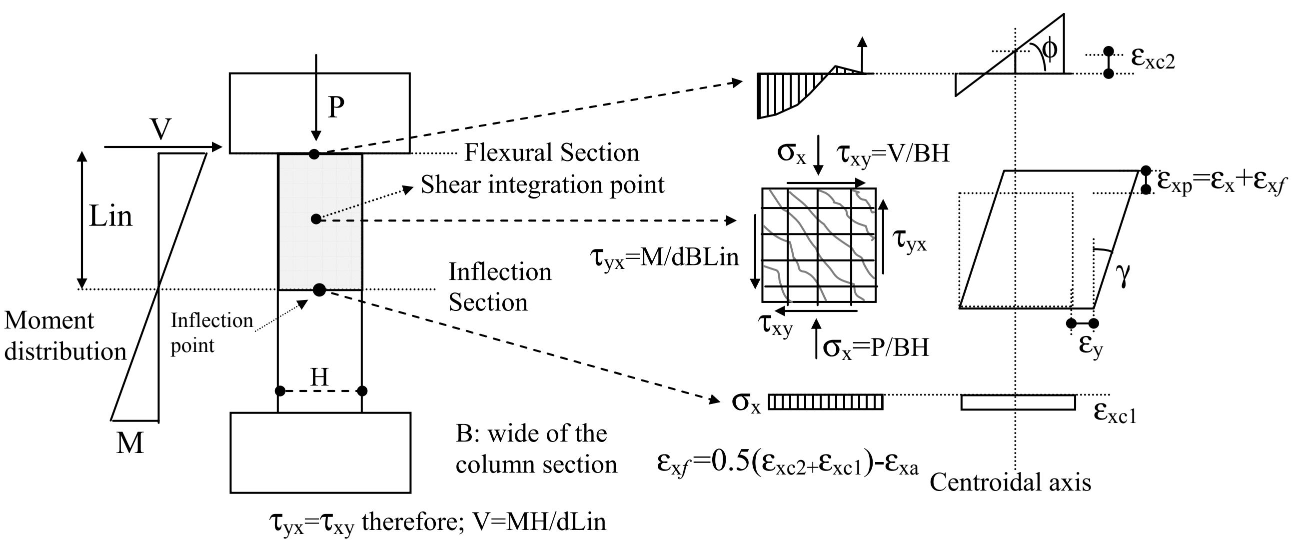

Signs; compression negative and tension positive

Fig. 8: Illustration of the new analytical model, stress and strain distributions

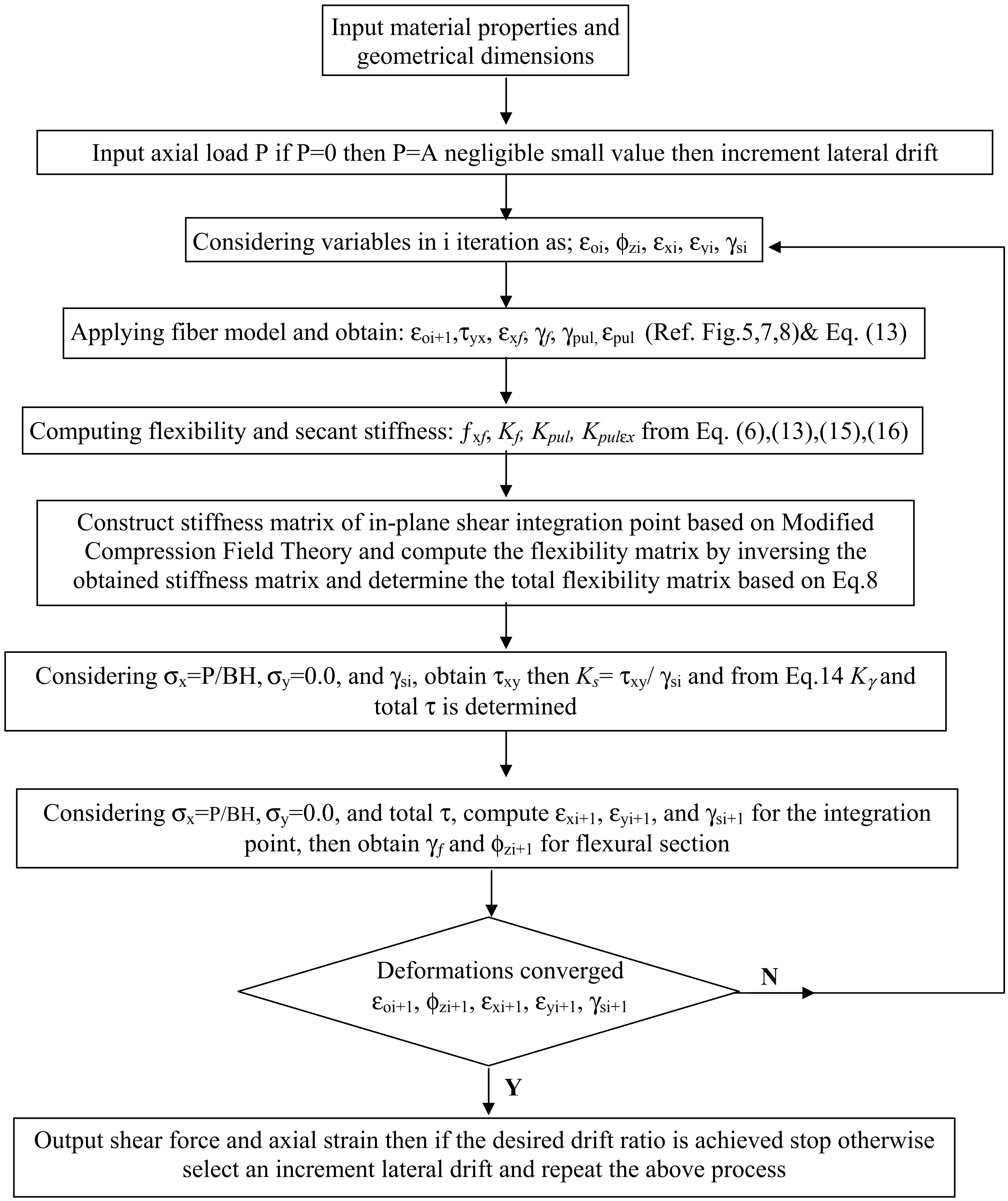

Fig. 9: Flowchart for the new analytical approach in displacement based

4. VERIFICATION OF ANALYTICAL APPROACH

Three reinforced concrete columns were loaded under constant axial load and static cyclic unidirectional reverse lateral (Ousalem et al., 2003). The tested specimens are scaled to 1/3 of actual columns, representing of a column located in the first floor of a building with moderate high. Cross section of all columns is 300×300mm^2. Geometrical detail and material properties are depicted in Figure 10 and Table 1.

The three columns have almost the same characteristics except for lateral reinforcement ratios. Column No. 12 has the lowest lateral steel ratio and expected to fail in shear. Specimen No.15 is design to have flexural response with high hoop ratio. Finally the behavior of column No.14 is expected to be between that of the two previous columns as flexural-shear failure. Both ends of the columns were considered as moment resistant connections with rotation of zero.

Table 1: Material properties of the specimens

<table>
<tr><th>Specimen</th><th>Height (mm)</th><th>Shear span ratio</th><th>Concrete strength σ_B (MPa)</th><th>Axial load ratio η</th><th>Longitudinal reinforcement (MPa)</th><th>Transverse reinforcement (MPa)</th></tr>
<tr><td>No.12</td><td rowspan="3">900</td><td rowspan="3">1.5</td><td>28.15</td><td>0.21</td><td rowspan="3">16-D13
ρ_g=2.258%
σ_y=399</td><td>2-D6@150
ρ_w=0.14%</td></tr>
<tr><td>No.14</td><td rowspan="2">26.1</td><td rowspan="2">0.23</td><td>2-D6@50
ρ_w=0.43%
σ_{wy}=398</td></tr>
<tr><td>No.15</td><td>4-D6@50
ρ_w=0.85%</td></tr>
</table>

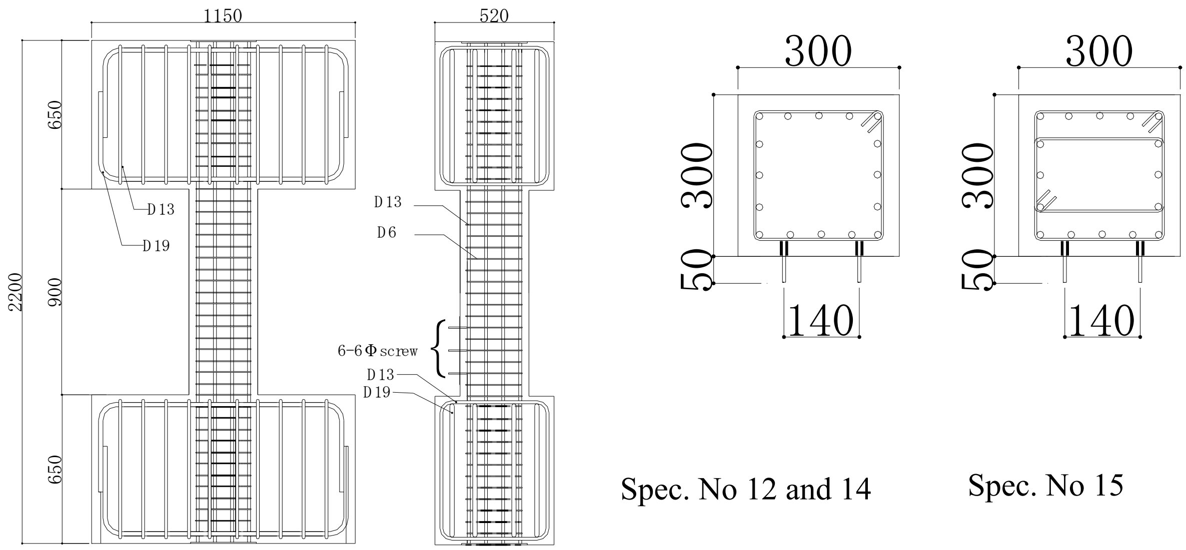

Fig. 10: Detail of reinforcement for three tested reinforced concrete columns

Symmetric conditions are considered and half of the columns' height, from inflection point to one end, is modeled in the analysis. Fiber model discretization is applied for the end section analysis. One integration point is representing the in-plane shear model from inflection point to the end's section. Since moment at inflection point is zero, stress-strain relationship is simply computed based only on axial mechanism. Pushover analysis was implemented according to the new analytical approach presented in Figure 9 and lateral load-drift ratio responses for three columns were estimated. In addition results of the relationships between lateral drift-axial deformations are obtained for the specimens. The analytical results as well as experimental outcomes are presented and compared in Figures 11, 12, and 13. The comparisons between the results show consent agreement for the three tested reinforced concrete columns. In the process of the computation, axial failure or gravity collapse is defined as the stage that equilibrium in vertical direction in section analysis cannot be satisfied any more. Based on this definition, axial collapse points are obtained and depicted in the performance responses of the three columns as shown in the figures.

(a) Specimen after failure and loading system

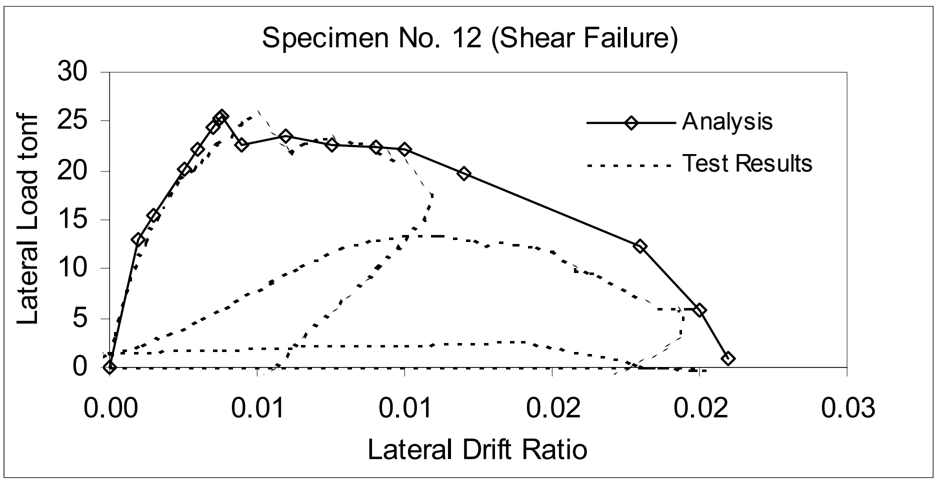

(b) Lateral drift-force relationship

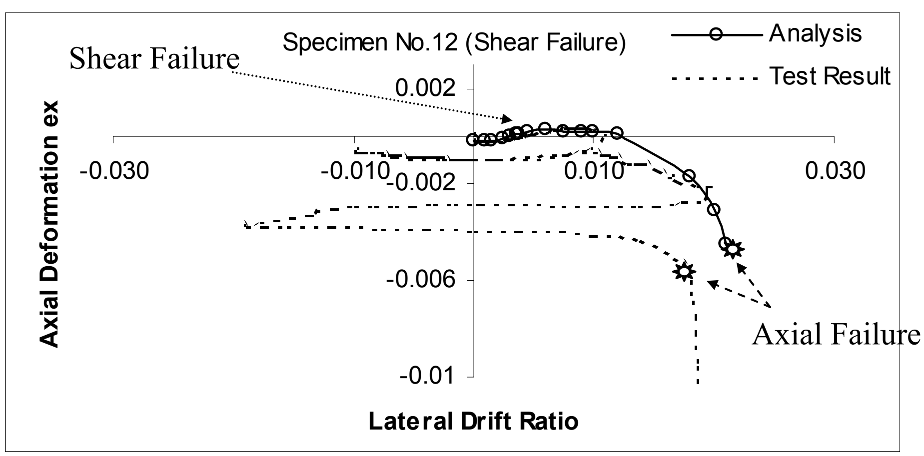

(c) Lateral drift-axial deformation relationship

Fig. 11: Experimental and analytical results for specimen No. 12 with shear failure response

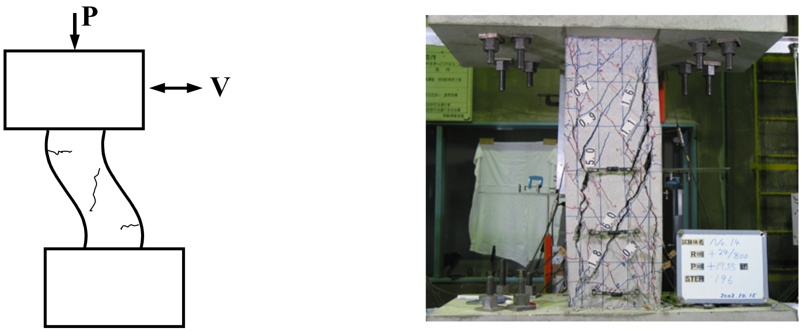

(a) Specimen after failure and loading system

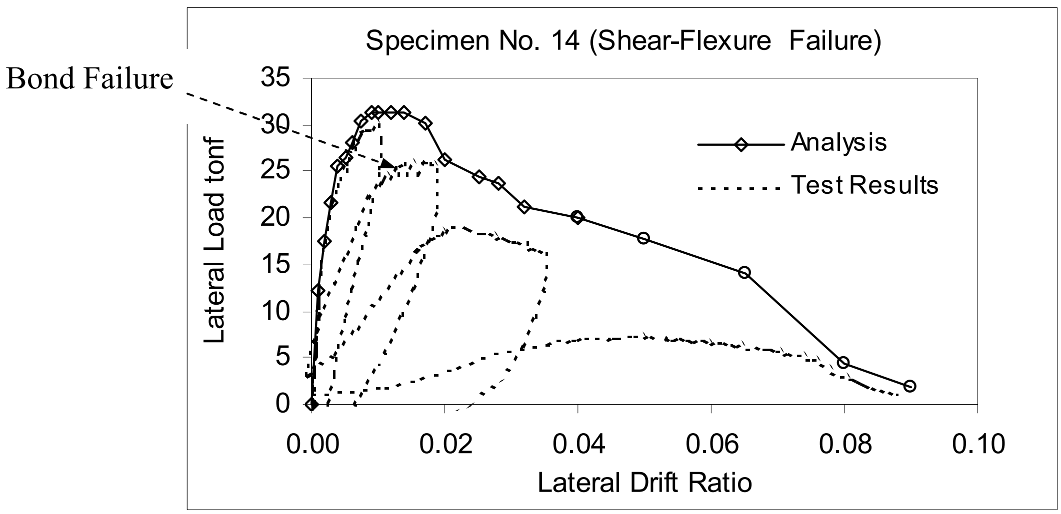

(b) Lateral drift-force relationship

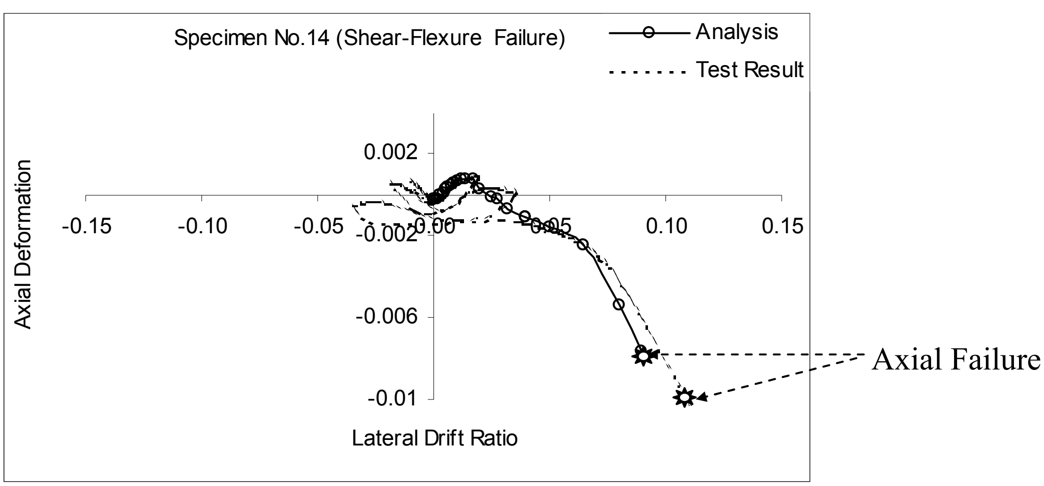

(c) Lateral drift-axial deformation relationship

Fig. 12: Experimental and analytical results for specimen No. 14 with shear-flexure failure response

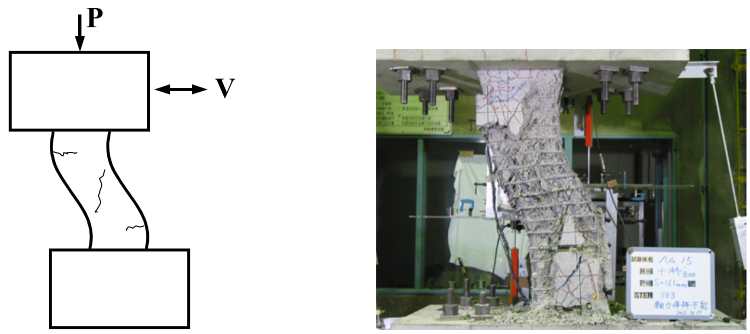

(a) Specimen after failure and loading system

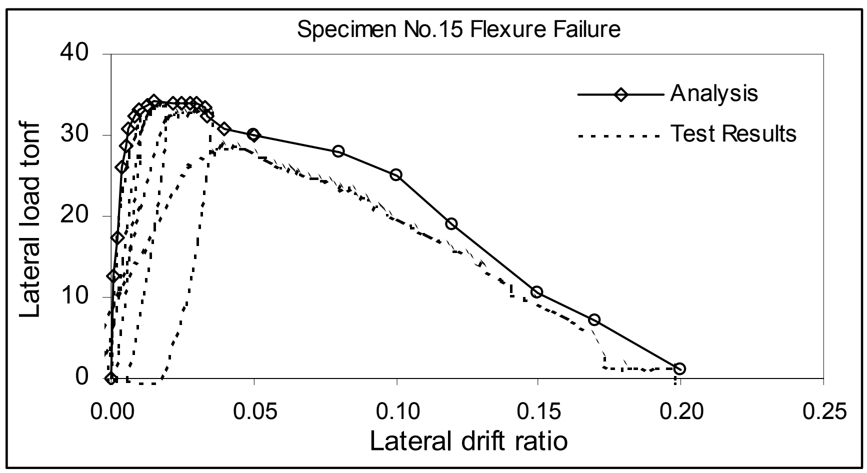

(b) Lateral drift-force relationship

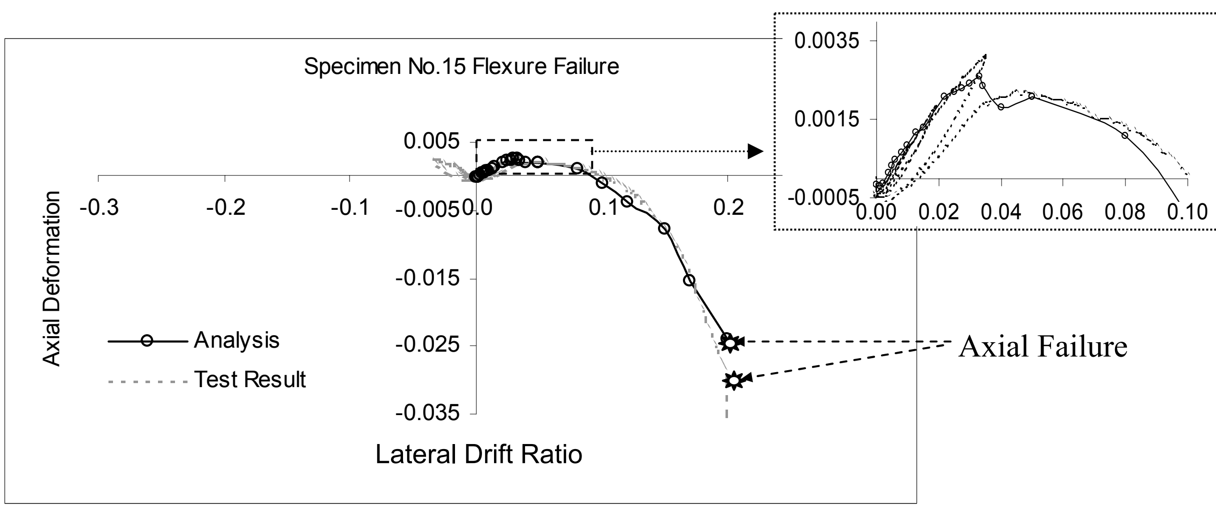

(c) Lateral drift-axial deformation relationship

Fig. 13: Experimental and analytical results for specimen No. 15 with flexure failure response

Experimental result for specimen No. 14 with shear-flexure failure shows lower lateral strength from 0.012 to 0.018 lateral drift ratios, as shown in Figure 12-b. This could be due to bond failure of longitudinal steel bars, observed in the test operation. Therefore the analytical approach should be improved for consideration of bond failure mechanism.

It is important to mention that by decreasing the compression strength of concrete in the compression fiber, bond stress in compression reinforcement is reduced. Therefore compression stresses in compression steel bars are gradually decrease corresponding to the bond stress reduction and buckling of the steel bars. Thus, compression steel bars cannot carry its stress capacity and slip occurs along the bars. This phenomenon should be considered in the post-pick response of compression fibers. All three specimens, presented in this paper, were modeled for the section analyses by applying fiber model, considering the confined concrete for core concrete and unconfined concrete for cover concrete. Stresses in compression steel bars are reduced as the concrete compression strength degrades. However total strain in compression fiber is considered as the summation of normalized slip and strain of steel bars. In each flexural section, linear strain distribution is assumed throughout the linear and nonlinear stages of the analysis.

5. CONCLUSION

A new displacement based evaluation approach for reinforced concrete columns is presented based on modification of fiber model considering the two mechanisms of shear and flexure. Flexure mechanism can be modeled based on conventional section or fiber model analysis. Shear behavior is expressed based on in-plane stress filed considering the smeared reinforcement and rotating crack, applying modified compression field theory, MCFT. Shear-flexural-axial interaction is developed assuming three components of axial deformations as axial strain due to axial load, axial strain caused by in-plane shear stress field and average axial strain induced by flexural mechanism. Concrete compression strength degradation is considered for section fibers simultaneously equal to compression softening reduction factor obtained from in-plane stress field. The new displacement based evaluation approach was verified by comparing the analytical results with experimental outcomes in terms of ultimate strengths, ultimate deformations, and post pick responses. The method can be referred also as modified fiber model in shear.

REFERENCES

AASHTO (2000) “AASHTO LRFD Bridge Design Specifications and Commentary,” 2nd Ed. (1998) and 2000 update, American Association of State Highway Transportation Officials, Washington D.C. 1998.

Bentz, E. C.(2000), *Sectional Analysis of Reinforced Concrete Members*, Ph.D. Thesis, University of Toronto, 198pp.

Okamura H., Maekawa, K.(1991), *Nonlinear Analysis and Constitutive Models of Reinforced Concrete,* Gihodo Shuppan Co., Ltd.

Ousalem H., Kabeyasawa T., Tasai A., Iwamoto J.(2003), Effect of Hysteretic Reversals on Lateral and Axial Capacities of Reinforced Concrete Columns, *Proceedings of the Japan Concrete Institute*, Vol.25, No.2, 2003, pp.367-372

Park R, Priestley MJN, Gill WD (1982), Ductility of square confined concrete columns, *Journal of Structural Division ASCE*, 108(4): 929–950.

Vecchio, F. J., Collins, M.P.(1986), The Modified Compression Field Theory for Reinforced Concrete Elements Subjected to Shear, *ACI Journal*, Vol. 83, No. 2, pp. 219-231.

Vecchio, F. J., Collins, M.P.(1988), Predicting the Response of Reinforced Concrete Beams Subjected to Shear Using Modified Compression Field Theory, *ACI Journal*, Vol. 85, No. 3, pp. 258-268

Vecchio, F. J. (1989), Nonlinear Finite Element Analysis of Reinforced Concrete Membranes, *ACI Journal*, Vol. 86, No. 1, pp. 26-35.

SHAKING TABLE TEST OF A ONE-THIRD-SCALE MODEL OF A SIX-STORY WALL-FRAME R/C STRUCTURE

T. MATSUMORI [1]

J. KIM, and T. KABEYASAWA [2]

ABSTRACT

A one-dimensional shaking table test was carried out to study structural performance of a one-third-scale model of a 6-story wall-frame R/C structure. The test specimen was subjected to a series of earthquake motions in increasing intensity. Although the test specimen was designed to develop large flexural ductility, the 1st-story structural wall failed in shear at relatively early stage. Maximum shear force carried by the 1st-story wall was larger than predicted by pushover analysis. Dynamic distribution of lateral forces was much different from the constant distribution assumed in the push-over analysis.

1. INTRODUCTION

Quite a number of existing reinforced concrete buildings in Japan are wall-frame structures, which are constituent of structural walls coupled with a set of beam-column frames. As a part of DaiDaiToku Project, response of a 6-story wall-frame structure to earthquake motions was investigated by testing a one-third-scale model specimen on the one-dimensional shaking table. This paper describes the outlines of the test method used and the test results.

2. TEST DESCRIPTION

The shaking table test was conducted using NIED's one-dimensional shaking table. The test specimen was a one-third-scale model of a 6-story wall-frame structure.

2.1 Test Specimen

2.1.1 Geometry of Specimen

The structure consisted of three three-bay frames (Y_1, Y_2, and Y_3) parallel to the longitudinal direction, and four two-bay frames (X_1, X_2, X_3, and X_4) in the transverse direction. The span widths were 2.0m each in the longitudinal and transverse direction. Shaking was applied in the

[1] *National Research Institute for Earth Science and Disaster Prevention, Japan*
E-mail: taizo@bosai.go.jp
[2] *Earthquake Research Institute, The University of Tokyo, Japan*
E-mail: kabe@eri.u-tokyo.ac.jp

longitudinal direction. The inter-story height was 1.0m each from the 1st to the 6th story, and overall height was 6.69m. Figure 1 shows an outline of the test specimen; Figure 2 shows the typical floor plan; and Figure 3 shows the structural elevation above the 1st-story columns.

Of the three frames in the longitudinal direction in which the shaking was applied, frame Y_2 had a structural wall (60 mm in thickness) in the central bay continuous from the 1st to the 6th story. Frames Y_1 and Y_3 were three-span open frames. All frames in the transverse direction were open frames. Wing walls (60mm in thickness; 300 mm in width) were installed to X_1Y_2- and X_4Y_2-columns so as to reduce the torsional and transverse displacement of the test specimen.

The dimensions of a column section were 200x200 mm throughout the test specimen. X_2Y_2- and X_3Y_2-columns, which were the boundary columns for the structural wall, were reinforced with 4-D10 bars and 4-D6 bars (D10 bars were placed in the corner). Gross total longitudinal reinforcement ratio p_g was 1.03%. Perimeter hoops of D4 deformed bars were spaced at 40mm over the total height of the columns. Shear reinforcement ratio p_w was 0.31%. Only for the 1st-story boundary columns, supplemental tie of 1-D4 bar was provided at an 80mm spacing (p_w= 0.39% in total) to improve the flexural deformation performance. Independent columns other than the boundary columns of the structural wall were reinforced with 8-D10 bars (p_g=1.43%). Perimeter hoops of D4 deformed bars were spaced at 40mm.

The size of girders parallel to the shaking direction was 140x200mm. The girders were reinforced with 2-D10 at both top and bottom. Tensile reinforcement ratio p_t was 0.51%. Hoops of D4 bars were spaced at 80mm. Shear reinforcement ratio p_w was 0.22%. The dimensions of a transverse beam were 140x200mm in frames X_2 and X_3, and 150x250mm for the beams in frames X_1 and X_4.

The multi-story continuous structural wall had a thickness of 60 mm, and was reinforced with 1-D4 bar at a spacing of 60mm in the vertical and horizontal directions. Shear reinforcement ratio p_s was 0.35%.

The floor slabs were 100mm thick throughout the specimen, and was reinforced with D4@100 mm at the top, and D6@100 mm at the bottom. The thickness of the floor slabs was not scaled down to one third.

Due to the time limit on the availability of the shaking table and the load capacity (300 kN) of the overhead travelling crane, the test specimen was manufactured in the open air, split into three, transported, and reassembled on the shaking table.

The test specimen was split at the 3rd and 5th story; independent columns and columns with wing walls were split at the mid-height, and the structural walls were split at the bottom. Each steel plate above and below the splitting plane was welded to the longitudinal reinforcing bars of the columns or walls beforehand, and the splitting or unification of the test specimen was made possible by detaching the two steel plates or bolting them together.

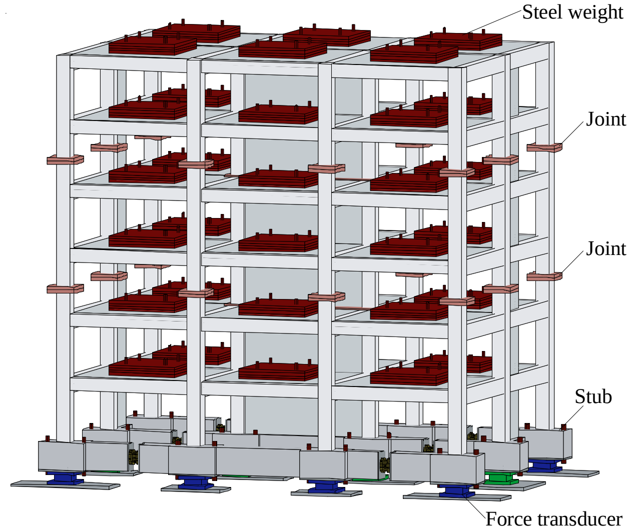

Fig. 1: Schematic drawing of test specimen

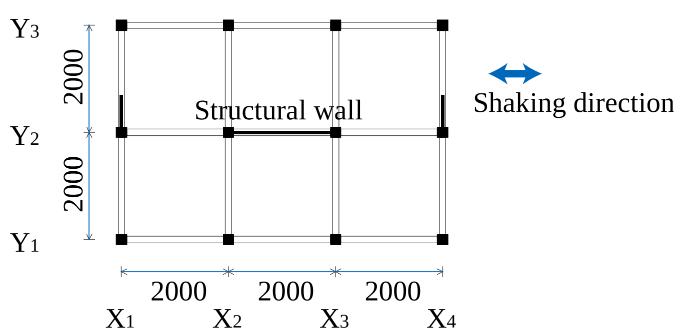

Fig. 2: Typical floor plan

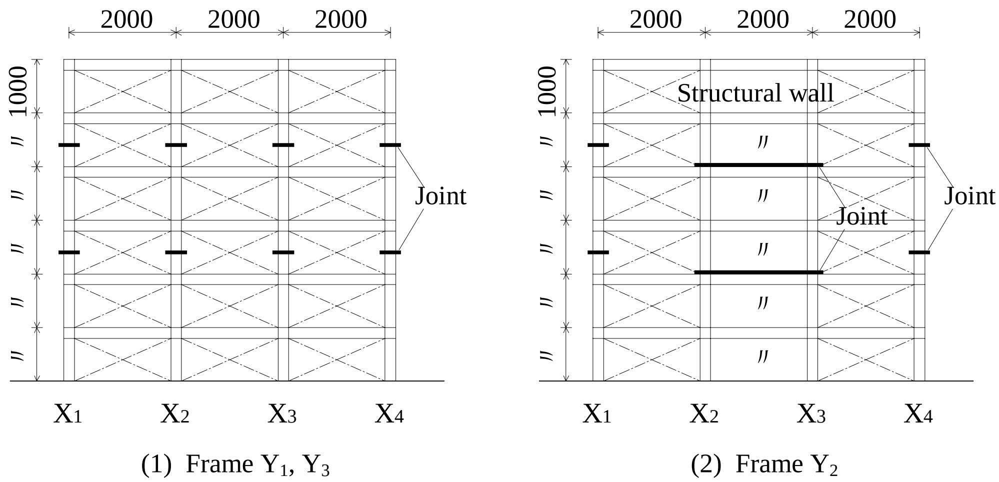

Fig. 3: Structural elevation

2.1.2 Details of Foundation

Figure 4 shows a detailed drawing of the foundation structure. Foundation stub was installed under each column. The size of foundation stubs were all 700 (X) x 410 (Y) x 425 (in height) mm^3. In order to measure the reaction force from the shaking table, 12 load cells (8 three-component-force transducers and 4 two-component-force transducers) were instrumented at the base of every foundation stub.

The four foundation stubs, which stood in a line in the X direction, were connected by footing beams in order to suppress Y-axis rotation. The cross section of the footing beam was 240 x 425 mm. No foundation slabs or footing beams in the Y direction were to be placed so that the forces could not be transferred between Y-frames in the foundation. Two-component-force transducers were also instrumented in the mid-span of the footing beams between X_1 and X_2 and between X_3 and X_4. Shear force carried by the structural wall or columns in the 1st story can be obtained by summing or subtracting axial or shear forces recorded by the load cells instrumented at base of the foundation stubs, or in the footing beams.

2.1.3 Mass of Floor

Additional mass was installed so that axial and shear stresses in the specimen corresponded to those in the prototype structure. Each slab was made thicker (100 mm) than one-third scale, and a steel weight (mainly 1,000x1,000x320 mm) was placed in the center of each span on every floor.

The mass of each floor, calculated as the sum of the products of the bulking values of the reinforced concrete body and the steel weight multiplied by their specific gravity, 2.3 and 7.86, respectively, ranged between 22.8 and 24.3 tons. An upper-floor mass was defined as the mass above the mid-height of columns and walls, while a lower-floor mass was defined as that thereunder. The total mass, including the foundation, amounted to 148.6 tons.

Natural period became $(1/3)^{1/2}$ times for scaling down and additional mass. Time axis was compressed by $3^{1/2}$ to obtain a representative relation between the natural frequency of the structure and the frequency content of the earthquake motion.

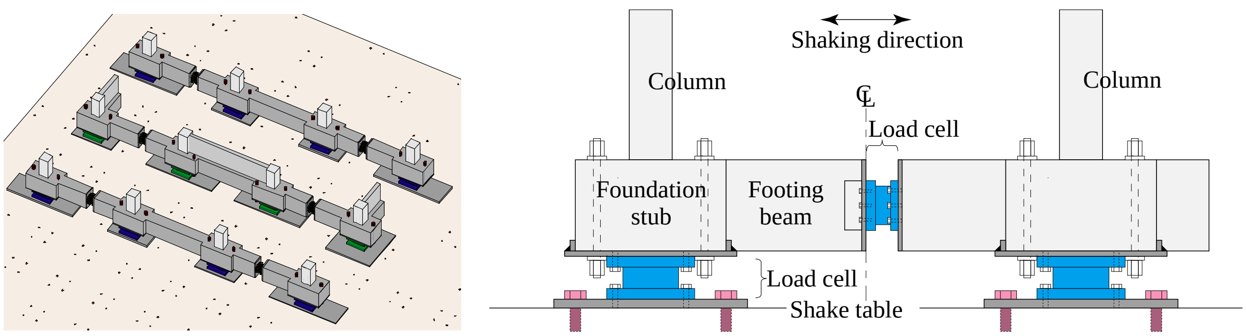

Fig. 4: Detailed drawing of foundation structure

2.2 Design of Test Specimen

The structure was designed to form a total yield mechanism of weak-beam strong-column type; i.e., flexural yield hinges were planned to form at the base of first-story columns and wall and at the ends of all floor girders. The vertical distribution of design story shear was determined in accordance with the Building Standard Law Enforcement Order. As to the longitudinal direction, base shear coefficients were 0.45 and 0.30, for the longitudinal and transverse direction, respectively. The yield moment at the planned yield hinges was determined as the flexural moment calculated by the linear analysis, and the yield moment at locations other than planned yield hinges was assumed to be 1.7 times the elastic moments.

Figure 5 shows story shear vs. story drift relationships obtained by a push-over analysis for the longitudinal direction. The vertical distribution of lateral force was determined in accordance with the Building Standard Law Enforcement Order. For columns and girders, all inelastic rotational deformation was assumed to concentrate at the member ends. Girder-column connections were assumed to be rigid. The moment-rotation relationship of a member was idealized by a tri-linear relation with stiffness changes at flexural cracking and yielding points. The wall was idealized as three vertical line elements with rigid beams at the top and bottom floor. Two outside line element represented the axial stiffness of the boundary columns. The central vertical element was a beam model in which vertical, horizontal and rotational springs were concentrated at the base.

The structure developed flexural yielding at the base of the 1st-story boundary column of the wall at base shear coefficient of about 0.3. Base shear coefficient increased due to the resistance of the compression side boundary columns and moment-resisting frames; the maximum base shear coefficient was about 0.44. The shear force carried by the 1st-story structural wall was 83% of the shear strength calculated by using the following empirical Hirosawa Equation.

$$Q_{su} = \left[\frac{0.0679\, p_t^{0.23} (\sigma_B + 18)}{\sqrt{M / QL + 0.12}} + 0.85 \sqrt{\sigma_{wh}\, p_{wh}} + 0.1 \sigma_0 \right] b_e j \qquad (1)$$

The elastic period was 0.168 sec in the analytical model structure.

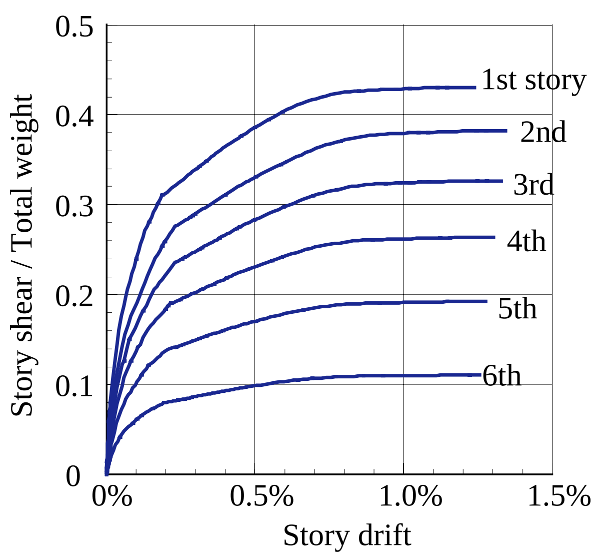

Fig. 5: Story shear vs. story drift relationships

2.3 Material Properties

Specified design strength of concrete was 21 N/mm^2. Concrete was cast in nine portions. The age of concrete ranged from 79 to 138 days at the shaking tests. Compressive strength tests were conducted for three test pieces for each casting before and after the shaking tests. Table 1 shows the mean value for a total of six test pieces. Young's modulus tests and the splitting tensile strength tests were conducted only for the concrete of the 1st-story column, and the results were 26.2 kN/mm^2 and 2.95 N/mm^2, respectively.

Table 2 shows the properties of reinforcement. Only D10 exhibited clear yield plateaus. For D6 and D4, yield strengths were determined at a 0.2% offset.

Table 1: Properties of concrete

Member	Compressive strength	Age at shaking tests
6th-story columns ~ Roof slabs	25.7 N/mm^2	78 days
5th-story columns ~ 6th-floor slabs	33.7 N/mm^2	89 days
5th-story columns (lower part)	24.7 N/mm^2	96 days
4th-story columns ~ 5th-floor slabs	30.2 N/mm^2	99 days
3rd-story columns ~ 4th-floor slabs	29.8 N/mm^2	106 days
3rd-story columns (lower part)	21.3 N/mm^2	113 days
2nd-story columns~ 3rd-floor slabs	26.3 N/mm^2	117 days
1st-story columns~ 2nd-floor slabs	33.0 N/mm^2	126 days
Foundation	33.1 N/mm^2	138 days

Table 2: Properties of steel

Size	Grade	Nominal area	Yield stress	Young's modulus
D10	SD295A	71.3 mm^2	350 N/mm^2	179 kN/mm^2
D6	SD295A	31.7 mm^2	348 N/mm^2	178 kN/mm^2
D4	SD295A	13.2 mm^2	408 N/mm^2	200 kN/mm^2

2.4 Measurement Plan

Approximately 250 responses of the specimen to the base motions, such as absolute acceleration, horizontal displacement, strains in reinforcing bars in hinge zones, and axial and shear forces in the load cells instrumented at the foundation, were recorded in sampling rate of 1000 Hz.

Horizontal displacement was measured by differential transducers at each floor level relative to the reference steel frame which was installed side by side with the test specimen on the shaking table.

3. TEST RESULTS

3.1 Input Shake Table Motions

The test specimen was subjected to a series of test runs in increasing intensity. Two earthquake ground motion records were used in the test runs, i.e., NS component of the 1940 El Centro record, and NS component of the 1995 Kobe Marine Observatory record of Japan Meteorological Agency. The amplitude of each earthquake motion in prototype structure was scaled to the maximum ground velocity of 0.25, 0.50 or 0.85 m/sec as shown in Table 3. For time axis was compressed by $3^{1/2}$ as mentioned above, velocity of the table motion to the test specimen was $1/(3)^{1/2}$ time the velocity in prototype.

Table 3: Properties of input of earthquake motions

RUN	Earthquake data	$V_{t\ max\ proto}$	$A_{t\ max}$	$A_{r\ max}$	$V_{r\ max}$	$V_{r\ max\ proto}$
1	1940 El Centro NS	0.25 m/s	2.40 m/s^2	2.39 m/s^2	0.153 m/s	0.265 m/s
2	1940 El Centro NS	0.25 m/s	2.40 m/s^2	2.54 m/s^2	0.157 m/s	0.272 m/s
3	1940 El Centro NS	0.50 m/s	4.80 m/s^2	4.39 m/s^2	0.275 m/s	0.477 m/s
4	1940 El Centro NS	0.50 m/s	4.80 m/s^2	3.91 m/s^2	0.261 m/s	0.452 m/s
5	1995 JMA Kobe NS	0.85 m/s	8.10 m/s^2	9.91 m/s^2	0.517 m/s	0.896 m/s
6	1995 JMA Kobe NS	0.67 m/s	6.40 m/s^2	5.63 m/s^2	0.358 m/s	0.620 m/s
7	Simulated earthquake	1.40 m/s	8.10 m/s^2	8.95 m/s^2	0.814 m/s	1.401 m/s

$V_{t\ max\ proto}$: Maximum target velocity in prototype structure
$A_{t\ max}$: Maximum target acceleration in test specimen
$A_{r\ max}$: Measured maximum acceleration in test specimen
$V_{r\ max}$: Measured maximum velocity in test specimen
$V_{r\ max\ proto}$: Calculated maximum velocity in prototype structure

Before and after the input of each test run, a random wave (frequency range of 0.1 to 40 Hz; maximum acceleration of approximately 0.15 m/s^2) was input to observe the change of the natural frequency of the damaged specimen.

3.2 Initial Frequency Response

The initial response transfer function and frequency response were obtained by the input of a random wave before the input of the earthquake motions. The measured initial natural period was 0.199 sec, which was longer than the calculated value. It may have been affected by damage when the test specimen was hoisted onto the shaking table or by shrinkage due to dryness.

3.3 Damage Process

Table 4 shows the maximum roof-level response acceleration and displacement at each test run, and the measured natural period before each test run. Figure 6 shows the damage observed in Frame Y_2 at the 1st and 2nd stories after RUN-5.

Table 4: Maximum response

RUN	Earthquake motion	T_1	$A_{roof\ max}$	$D_{roof\ max}$
1	1940 El Centro NS (0.25 m/s)	0.199 sec	5.30 m/s^2	8.52 mm
2	1940 El Centro NS (0.25 m/s)	0.212 sec	6.31 m/s^2	11.71 mm
3	1940 El Centro NS (0.50 m/s)	0.218 sec	10.35 m/s^2	30.47 mm
4	1940 El Centro NS (0.50 m/s)	0.266 sec	12.20 m/s^2	50.06 mm
5	1995 JMA Kobe NS (0.85 m/s)	0.291 sec	14.06 m/s^2	155.27 mm
6	1995 JMA Kobe NS (0.67 m/s)	0.538 sec	10.55 m/s^2	125.04 mm
7	Simulated earthquake (1.40 m/s)	N/A	10.11 m/s^2	> 300 mm

T_1 : Natural period before test run
$A_{roof\ max}$: Maximum roof-level acceleration
$D_{roof\ max}$: Maximum roof-level displacement

The damage process during test run is as shown below:

3.3.1 Before Tests

In Tsukuba area, an earthquake with a Japanese seismic intensity of 5- occurred at midnight on the day before the shaking tests. Flexural cracks were developed in some footing beams, at the top of the 6th-story columns, and at the ends of some girders on the 2nd floor. The natural period changed from 0.194 sec to 0.199 sec.

3.3.2 RUN-1

Flexural cracks were observed on the top of the slabs at the ends of the girders on every floor. The cracks were remarkable at the 5th and 6th floors.

3.3.3 RUN-2

The crack patterns observed after the earthquake motion were similar in appearance to those after RUN-1. The maximum roof drifts (roof-level displacement divided by the overall height) increased to 1/512 at RUN-2 from 1/704 at RUN-1.

3.3.4 RUN-3

Many shear cracks were observed in the structural walls between the 1st and 3rd stories. Flexural cracks were observed at the ends of girders in all locations. According to the displacement transducers for the measurement of the opening at the ends of girders, the width of the cracks reached around 0.5 mm. The longitudinal bars yielded at the girder ends adjacent to the walls on every floor, and at the base of the 1st-story columns. The vertical reinforcing bars in the wall panel also yielded at the base of the 1st story. The maximum roof drifts was 1/197.

3.3.5 RUN-4

Flexural cracks at the ends of girders widened; the maximum crack width increased to 0.7 mm. The residual shear crack width was 0.3 mm in the 1st-story structural walls. The maximum roof drifts increased to 1/120.

3.3.6 RUN-5

Sliding shear failure was observed in the multi-story continuous structural walls at the 1st story; concrete crushed, and the reinforcing bars were partially exposed and buckled. Shear cracks reached to both-side boundary columns, at around the top of X_2Y_2-column and around the base of X_3Y_2-column. In frames Y_1 and Y_3, the longitudinal bars yielded at the ends of the girders from the 2nd to the 6th floor, and at the top of the 6th-story columns. The maximum response displacement at the level of the 2nd floor was 35.5 mm (story drift of 1/28) and the residual displacement was 9.1 mm. The test specimen was able to sustain constant axial load even after the test run.

3.3.7 RUN-6

Crushing of concrete along the sliding shear failure surface in the 1st-story structural wall progressed.

3.3.8 RUN-7

The test specimen collapsed due to the flexural failure of the 1st-story columns, except for the boundary columns of the structural wall.

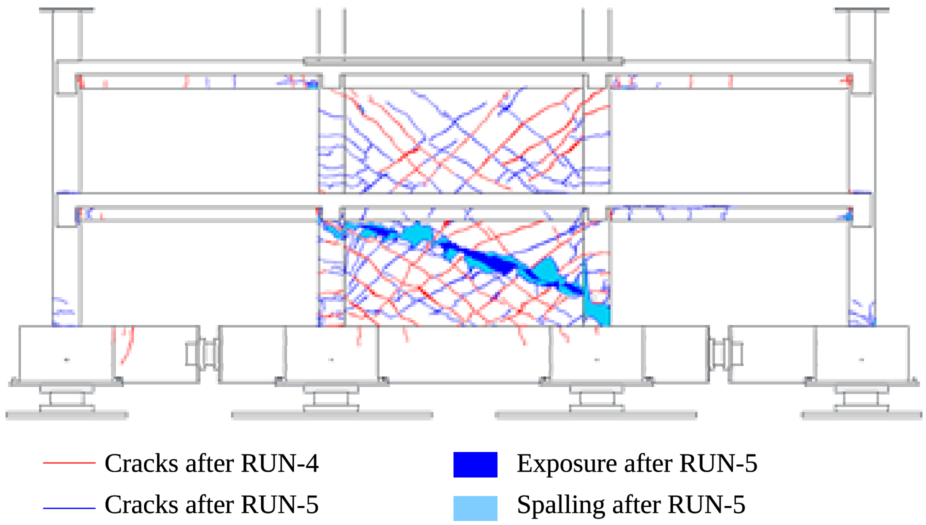

Fig. 6: Crack patterns in structural wall

3.4 Force-Displacement Relationship

The base shear and overturning moment at the base were calculated by using the recorded acceleration and the calculated value of the mass of each floor. The mass of each floor was assumed to be concentrated at the measuring point of acceleration. The base shear was assumed to be the sum of the inertial forces acting on all floors, and overturning moments at the base was calculated as the algebraic sum of the products of the inertial forces and corresponding height of the levels from the base. The damping force was ignored.

Figure 7 shows the relation between overturning moment at the base and roof-level displacement. Deformation abruptly increased during RUN-5. Resistance and stiffness degradation became significant in RUN-6 and 7. The relations show a regular curve pointing to the maximum response point in the past.

Figure 8 shows the relation between the base shear and 2nd-floor-level displacement during RUN-5. Shear force carried by the structural wall was calculated by using recorded forces by the load cells instrumented in the foundation. Shear strength of the structural wall was calculated by using Eq. (1). Maximum total base shear and wall shear force were larger than calculated values by the push-over analysis. Ratio of wall shear force to total base shear was approximately 50% in elastic stage, 42% at the stage when total base shear reached maximum, and 57% at the stage when absolute value of wall shear force reached maximum. Maximum wall shear was comparable with calculated shear strength.

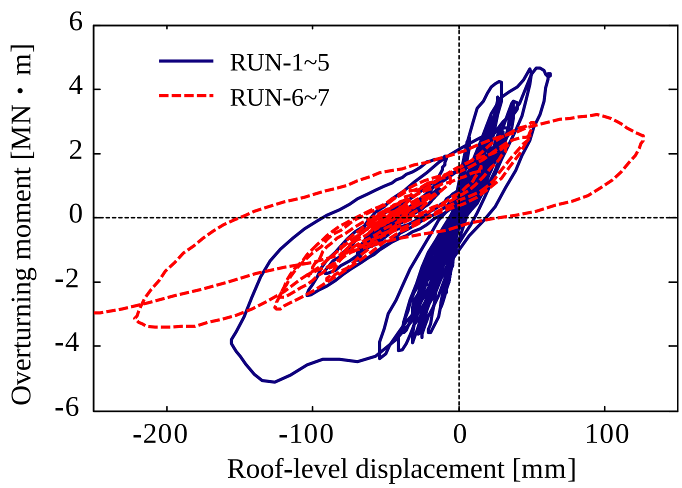

Fig. 7: Overturning moment vs. roof-level displacement relationships

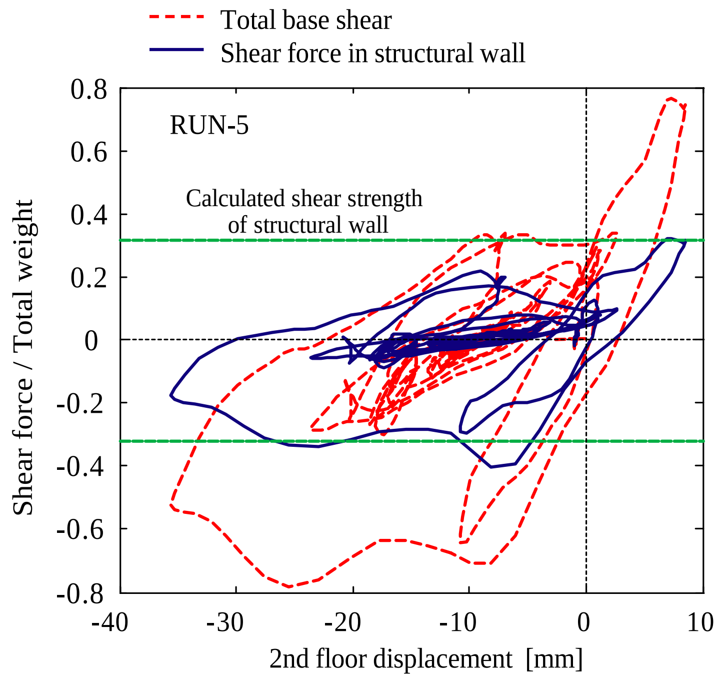

Fig. 8: Base shear vs. 2nd floor displacement relationships

3.5 Vertical Distribution of Inertial Force and Story Shear

Figure 9 shows the vertical distribution of inertial force and story shear at three stages in RUN-5. Inverted triangle type force distribution was observed for inertial force distribution at the stage when total base shear reached maximum. This distribution agreed favourably with the distribution used in the push-over analysis. On the other hand, bottom heavy force distribution was observed at the stage when absolute value of wall shear force reached maximum. At this stage, because inflection point in the structural wall was located nearer to the base, the structural wall was loaded with larger shear force in the 1st story even though bending moment at the base was equivalent.

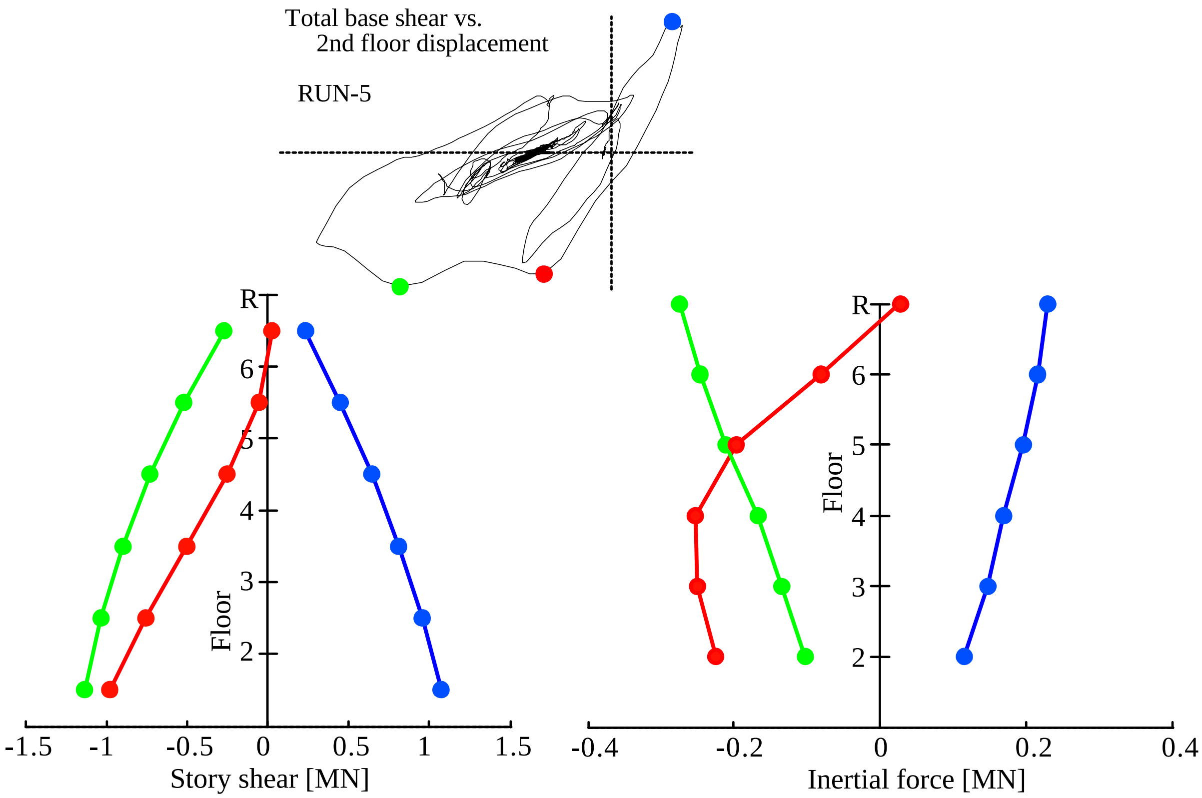

Fig. 9: Vertical distribution of inertial force and story shear

4. CONCLUSION

Test results of a shaking table test on one-third scale R/C 6-story wall-frame structures are summarized as follows:

1. Although flexural yielding was observed at the base of the 1st-story wall prior to shear failure as planned, the 1st-story wall failed in shear without a large flexural ductility.

2. Maximum shear force carried by the 1st-story structural wall was larger than predicted by pushover analysis because large inertial force acted at the lower levels of the test specimen.

3. Maximum wall shear was comparable with shear strength evaluated by the empirical equation.

ACKNOWLEDGMENTS

The writers would like to express acknowledgment to Tokyo Soil, Dr. Hirade, Dr. Kato and Dr. Kusunoki (all three belong to Building Research Institute) for lending us without compensation

some steel weights, dynamic strain amplifiers, displacement transducers and two-component force transducers, respectively.

Photo 1: Overall view before test

Photo 2: Structural wall after RUN-5

Photo 3: Overall view after test

Photo 4: Structural wall after test

COLLAPSE ANALYSIS OF REINFORCED CONCRETE STRUCTURE UNDER EARTHQUAKES

Shaohua CHEN[1], Tomoya Matsui[2], Taizo Matsumori[3], Toshimi KABEYASAWA[4]

ABSTRACT

Because of the improvements of material constitutive and the understanding of material mechanics properties of reinforced concrete, many analytical models for structural elements (such as multi-spring model, fiber model and frame-element model for column and beam, also the panel model for shear wall) were developed based on material mechanics properties, and it becomes possible to do nonlinear earthquake response analyses for reinforced concrete structure until structure collapse with these analytical models.

The purpose of this study is to predict collapse process of full-scale reinforced concrete wall-frame structure that is planed to be tested on E-Defense by DaiDaiToku Research Project. Using frame-element model for columns and beams, and panel model for shear walls, verification analyses of the analytical program are done with 2-story shear wall dynamic test, a good correspondence between analytical and experimental results is obtained. By static and dynamic analysis with the analytical program, response prediction of the full-scale reinforced concrete wall-frame structure is done.

1. ANALYTICAL MODEL

1.1 Panel Model for Shear Wall

Using a 4-node panel under plane stress state to represent the wall effect and axial springs for outside columns, shear wall model is idealized as Figure 1. Interaction of moment, axial force and shear force can be considered in this model; also the influence of varying axial force on the performance of shear wall can be considered automatically using stress-strain relationships. The analytical accuracy of this model is better than uniaxial line models (such as Beam Model, Truss Model, Three Vertical Line Model, Fiber Model, etc.) either in case of flexural yielding or in case of shear failure (Chen, 2000). Setting the nodes on the joints of columns and beams, this model remains the concept of frame structure members, is different from normal FEM model. Based on nonlinear material mechanics properties, collapse analysis is possible for wall-frame structure.

[1] Hyogo Earthquake Research Center, National Research Institute for Earth Science and Disaster Prevention, Miki, Hyogo, Japan
Email: sh_chen@bosai.go.jp
[2] Department of Architecture and Civil Engineering, Toyohashi University of Technology, Toyohashi, Aichi, Japan
Email: matsui@tutrp.tut.ac.jp
[3] Hyogo Earthquake Research Center, National Research Institute for Earth Science and Disaster Prevention, Miki, Hyogo, Japan
Email: taizo@bosai.go.jp
[4] Earthquake Research Institute, The University of Tokyo, Tokyo, Japan
Email: kabe@eri.u-tokyo.ac.jp

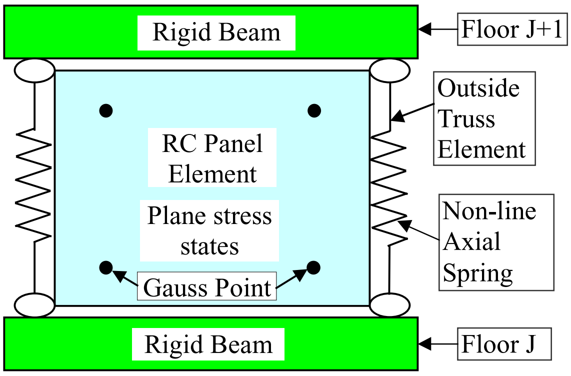

Figure 1: Panel Model for Shear Wall

1.2 Frame-element Model of Columns and Beams

In order to do nonlinear analysis for reinforced concrete structure until collapse, material mechanics properties based model should also be developed for columns and beams. There are three deformation combination types for columns and beams as axial deformation only, axial and one direction flexural deformations, axial and two direction flexural deformations, but shear deformation is not considered by the analytical model in this study. Frame-element model is adopted in this study (Figure 2). Shape functions and displacement functions are shown in equation (1), and deformations of element can be calculated by equation (2) from displacements $\{d\}$ of the two end nodes. Using solution of finite element method (FEM), stiffness of a member between end forces and end displacements can be derived (Chen, 2004).
The section of a reinforced concrete member is divided into core concrete cells, cover concrete cells and steel bars. Core concrete has properties of confined concrete with higher strength even after concrete compressive strength, but tension stiffening effect is weaker. On the contrary, cover concrete looks as reinforced concrete with stronger tension stiffening effect, but the strength will be rapidly reduced after concrete compressive strength.

$$\begin{cases} N_3 = \frac{3}{2l}(1-S^2), \quad N_4 = -\frac{1}{4}(1-S)(1+3S), \quad N_5 = -\frac{1}{4}(1+S)(1-3S) \\ N_6 = \frac{1}{4}(1-S)^2(2+S), \quad N_7 = \frac{1}{4}(1+S)^2(2-S), \\ N_8 = \frac{l}{8}(1-S)^2(1+S), \quad N_9 = -\frac{l}{8}(1-S)(1+S)^2 \end{cases} \tag{1}$$

$$\begin{Bmatrix} w \\ \theta_x \\ \theta_y \end{Bmatrix} = \begin{bmatrix} 0 & 0 & N_1 & 0 & 0 & 0 & 0 & N_2 & 0 & 0 \\ 0 & N_3 & 0 & N_4 & 0 & 0 & -N_3 & 0 & N_5 & 0 \\ -N_3 & 0 & 0 & 0 & N_4 & N_3 & 0 & 0 & 0 & N_5 \end{bmatrix} \{d\} \tag{2}$$

$$\{d\} = \{u_1 \quad v_1 \quad w_1 \quad \theta_{x1} \quad \theta_{y1} \quad u_2 \quad v_2 \quad w_2 \quad \theta_{x2} \quad \theta_{y2}\}^T$$

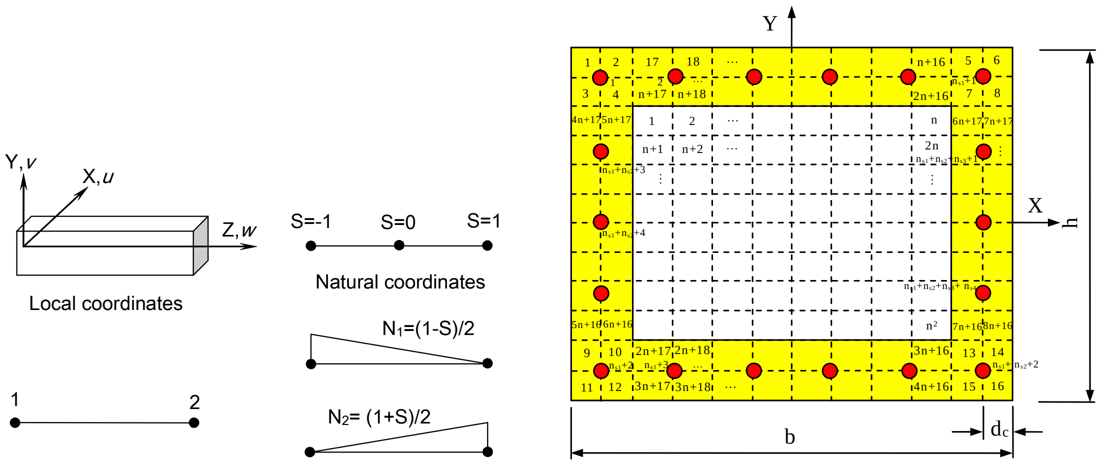

Figure 2: Frame-element Model for Column and Beam

1.3 Average Stress-strain Relation of Concrete

Considering bond effect between steel bar and concrete, tension stiffening concrete model is adopted for tension envelope [Izumo, Shima and Okamura, 1989]. Under plane stress status for panel model of shear wall, Modified Compression Field Theory (MCFT) is adopted for compression envelope [Vecchio and Collins, 1982]. In our study, average stress-strain relation and hysteretic rules of concrete shown as Figure 3 is adopted.

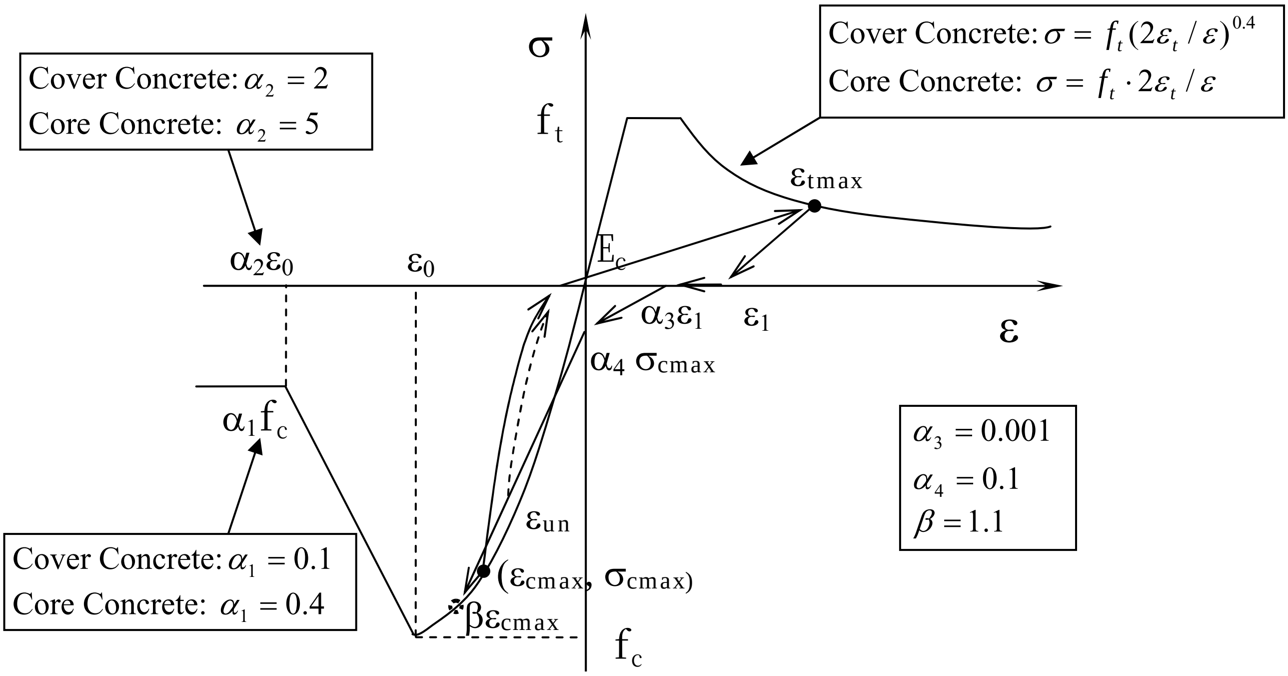

Figure 3: Average Stress-strain Relation of Concrete

1.4 Average stress-strain relation for steel bar

The skeleton curve of bare steel bar is often simplified by O-A-B-C, but the skeleton curve of bar embedded in concrete can be simplified as a bi-linear model like O-A'-C' (Figure 4). Here, ε_h=0.015, E_{sp}=0.025E_s are adopted. The parameters of bilinear model (Chen, 2004) can be decided by equation (3), and hysteretic loops of steel bar are shown as Figure 5.

$$\begin{cases} \dfrac{f_y^*}{f_y} = 1 - 1.5\dfrac{\sqrt{n}}{\rho}\left(\dfrac{f_t}{f_y}\right)^{1.5} \\ \dfrac{f_y^{'}}{f_y} = 0.51 + 0.42\dfrac{f_y^*}{f_y} \\ \dfrac{E_{sp}^{'}}{E_{sp}} = 0.45 + 0.26\dfrac{f_y}{100} + \left(0.23 - 0.25\dfrac{f_y}{100}\right)\cdot\left(\dfrac{f_y^*}{f_y}\right) \end{cases} \tag{3}$$

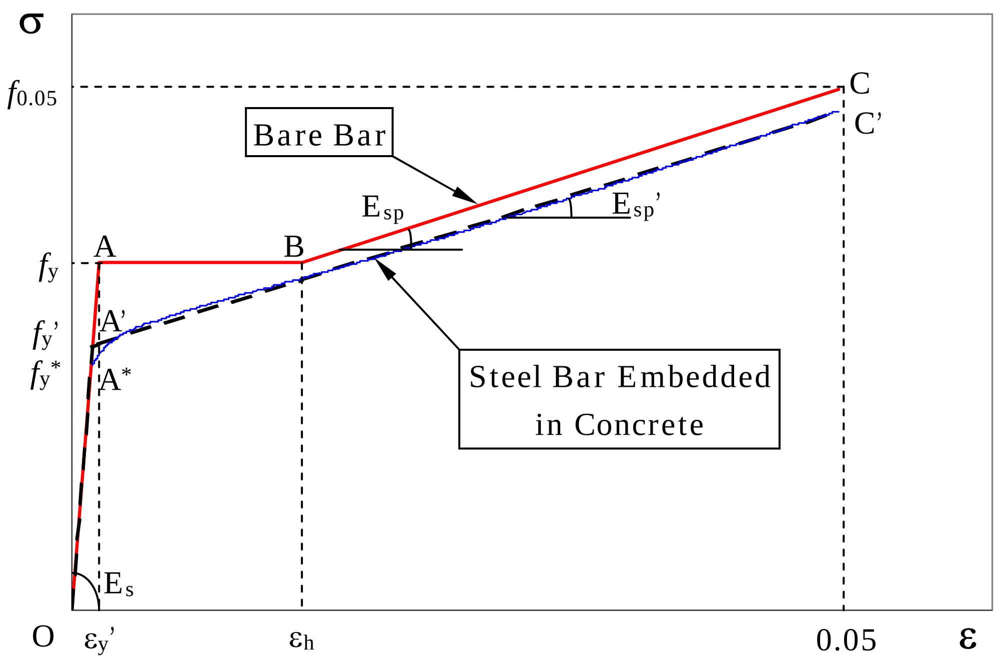

Figure 4: Stress-strain Relationship of Steel Bar

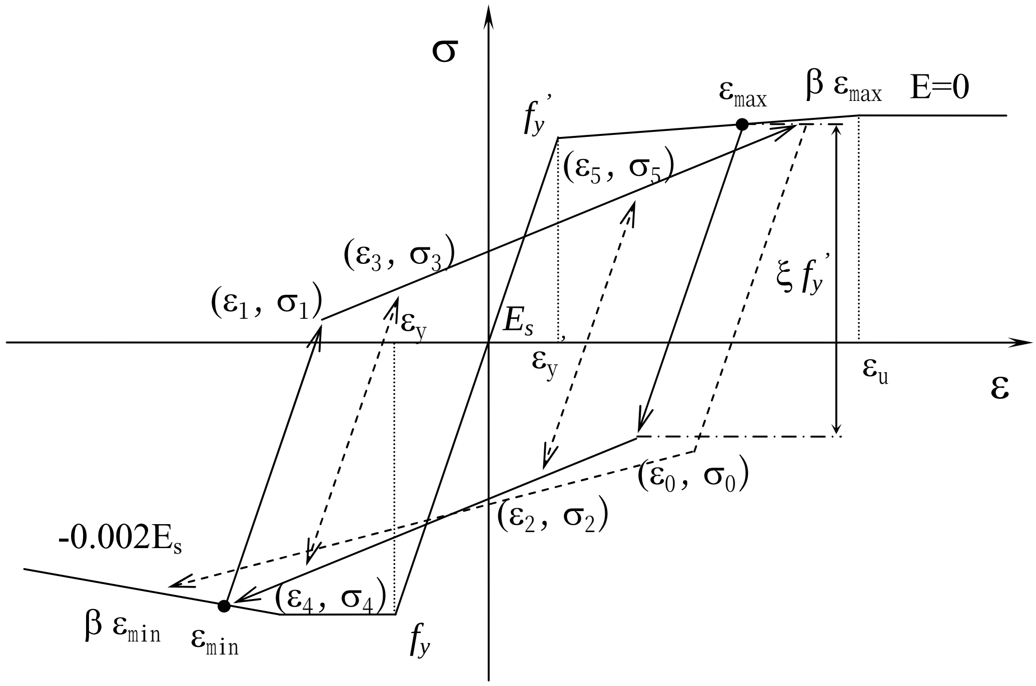

Figure 5: Hysteretic Loops for Steel Bars

2. 2-STORY SHEAR WALL DYNAMIC ANALYSIS

2.1 General Instruction of Analysis

Two specimens with different shear span were tested. The specimen Wall_A has low shear span and the specimen Wall_B has high shear span. Dimensions of the 1/3-scale 2-story shear wall specimens (Matsui, 2004) are shown in Figure 6. The strength of concrete is 25.2-30.0MPa; and the yield strengths of steel bar of D6 (for wall), D10 (for beam) and D13 (column) are 377MPa, 366MPa and 434MPa. The reinforcement of the column (200x200mm) is 12-D13, and the beam (150x200mm) is 4-D10, and the wall is D6@100.

The specimens are modeled as 3-story wall-frame structure shown in Figure 7. The top story represents the weight added to the specimen, and it's seemed as a rigid wall in analysis. The numbers in parentheses is for the specimen (Wall_B). In the analyses, the acceleration data (shown in Table 1) measured for footing stab is used. Rayleigh type damping is adopted, mass proportional damping coefficient is 0.005, and stiffness proportional damping coefficient is 0.002. The same damping is used for the full-scale structure analysis at next chapter. The weight (7.4tonf) of the specimen is concentrated at top stab level, and the additional weight (37.7tonf) is concentrated at virtual top level.

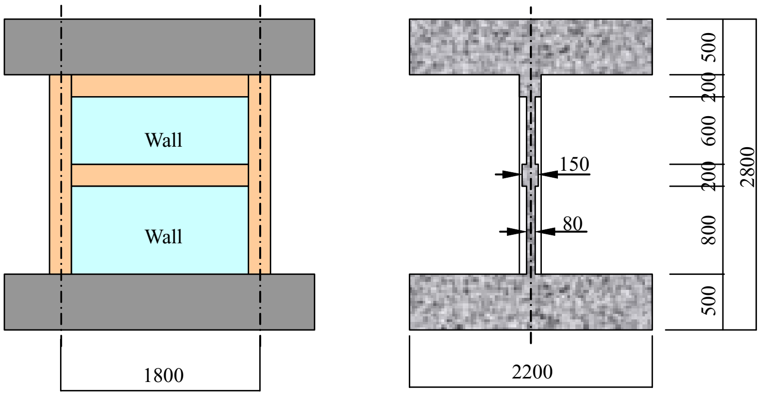

Figure 6: Dimensions of the Specimens

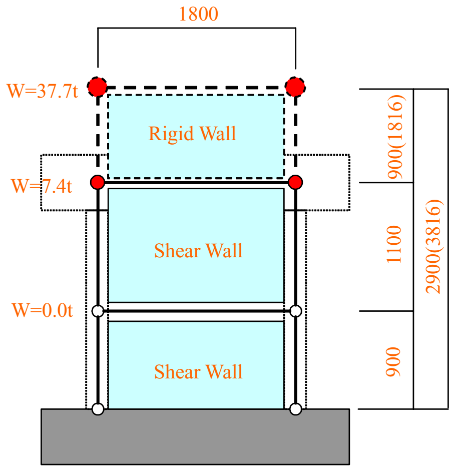

Figure 7: Analytical Model for the Testing Specimens

Table 1: Input Earthquake Waves

Name	Max. Acc.(gal)	Max. Vel.(kine)	Duration(Sec)
TOH25	154.9	14.4	25(26.6)
ELC37	375.9	21.4	25(31.0)
JMA50	492.4	28.9	12.5(34.6)
JMA75	738.5	43.3	12.5(34.6)
CHI60	796.0	34.6	50(57.7)
JMA100	984.7	57.7	12.5(34.6)
CHI50	619.1	28.9	50(57.7)
TAK125	605.5	72.2	15(23.1)
CHI70	884.4	40.4	50(57.7)

*Numbers in () are the durations in experiment.

2.2 Analysis Results

Comparisons between analytical results and experimental results are made. Figure 8, Figure 9 and Figure 10 are for specimen Wall_A, and Figure 11 is for specimen Wall_B by relationship between shear force and displacement. Good accuracy is obtained for each specimen under each input wave by the analyses.

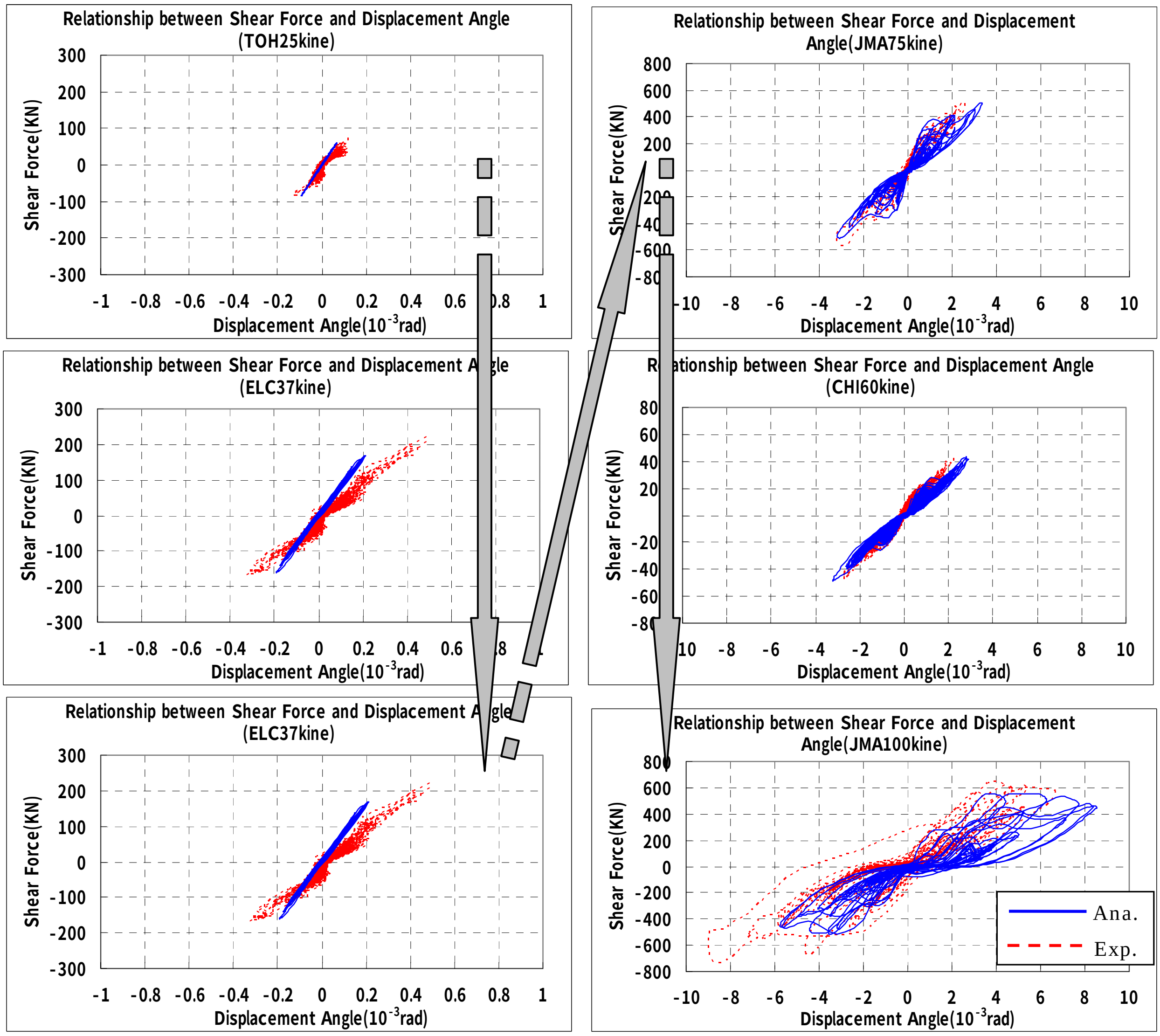

Figure 8: Comparison by the First 6 Waves for Wall_A

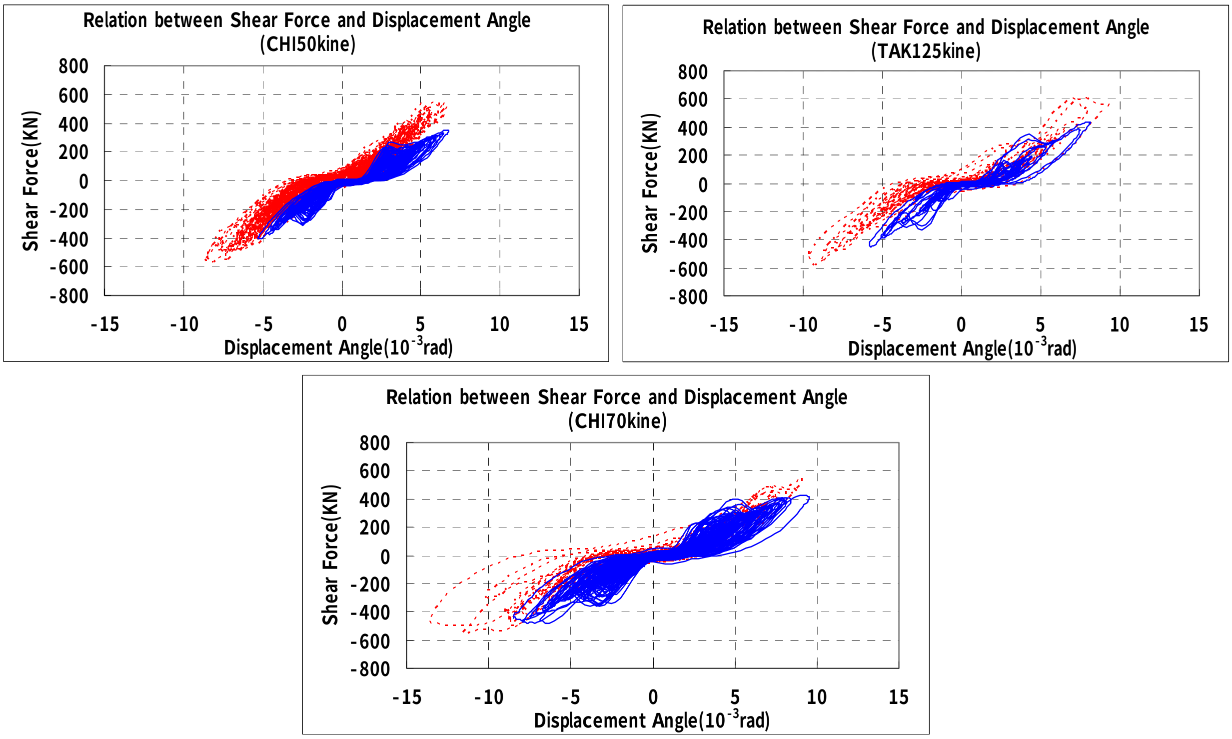

Figure 9: A Comparison by the Last 3 Waves for Wall_A

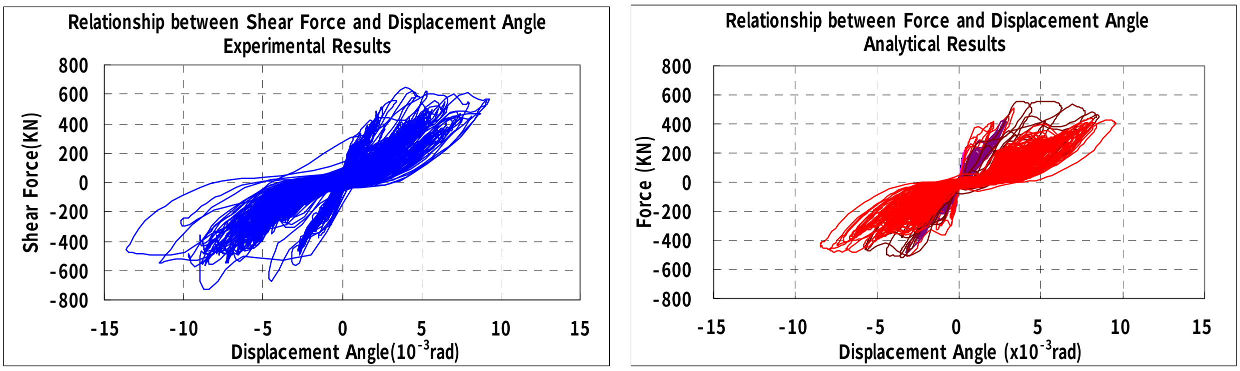

Figure 10: Comparison with All Input Waves for Wall_A

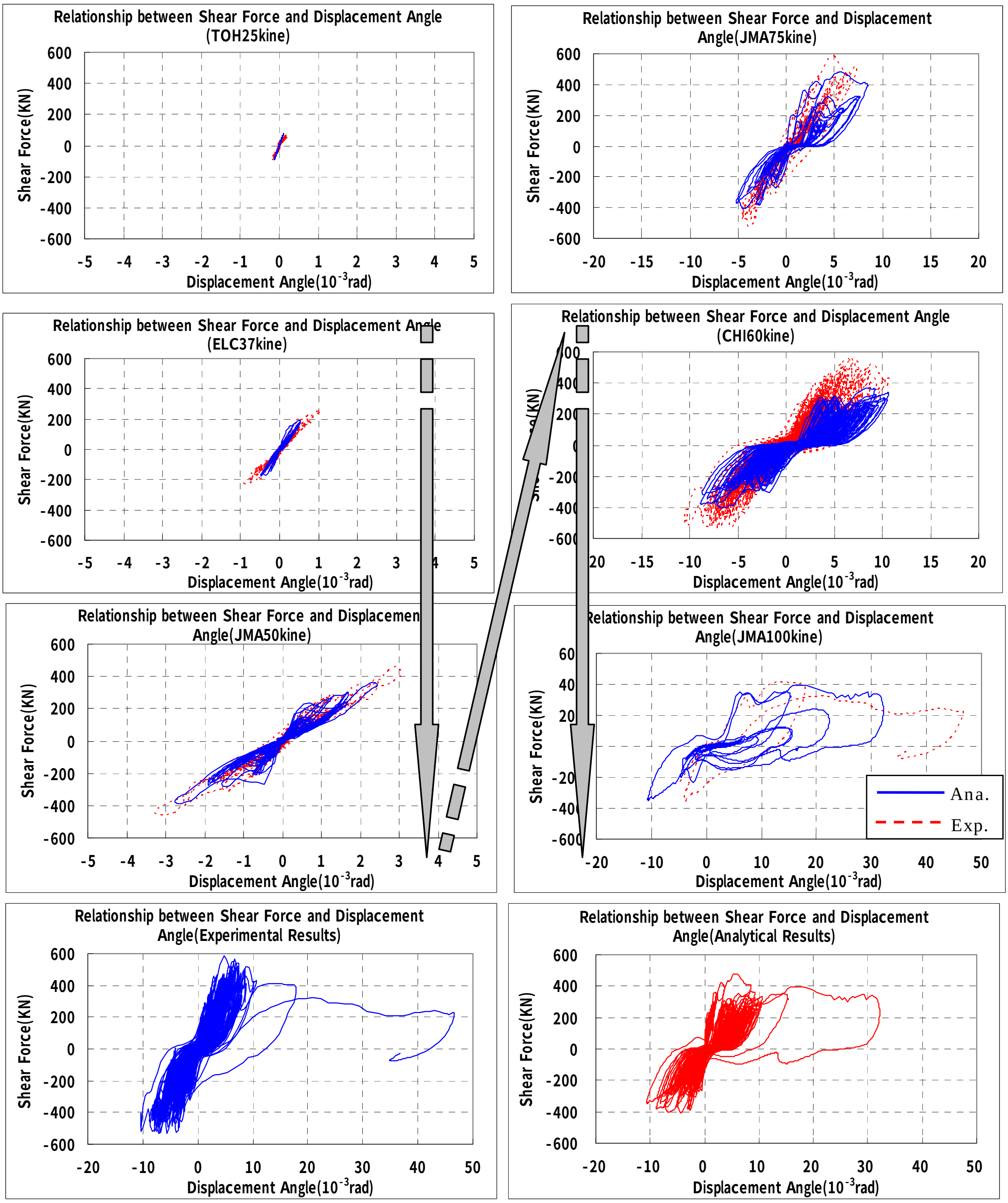

Figure 11: Analytical Results and Experimental Results of Wall_B

3. PREDICTION ANALYSIS OF FULL-SCALE WALL-FRAME STRUCTURE

3.1 General Instruction of Analysis

The dimensions of the specimen are shown in Figure 12-14. The mass of each floor (excluding ground level) is designed 125tonf; total mass of upper structure is 750tonf.
In analytical model, nodes are not only set at joints of column and beam but also in the middle of columns and beams. Wing walls are considered as shear walls and modeled by Panel Model. Standing walls are also considered by reinforced concrete panels. The floors are assumed as rigid in the plane.
Compressive strength of concrete is assumed as 24.0MPa; and yield strength of steel bar above D19 (for beam and column) is assumed as 380MPa, steel bar below D16 (for walls, etc.) is 354MPa. The reinforcement of the columns (500x500mm) is 8-D19, and the beams (300x500mm) are 4-D19 or 5-D19; the shear walls (150mm) and wing walls (150mm) are double D10@300, but standing walls (120mm) are single D10@200.

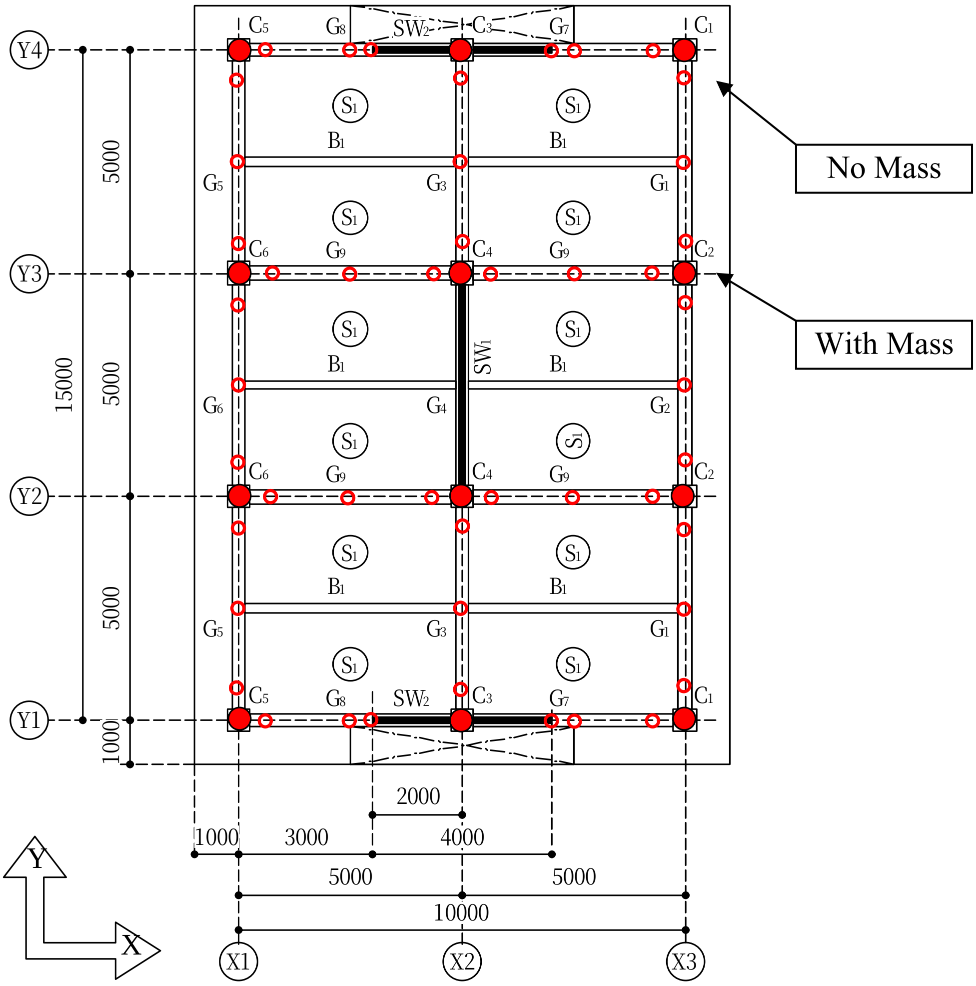

Figure 12: Plan of the Specimen

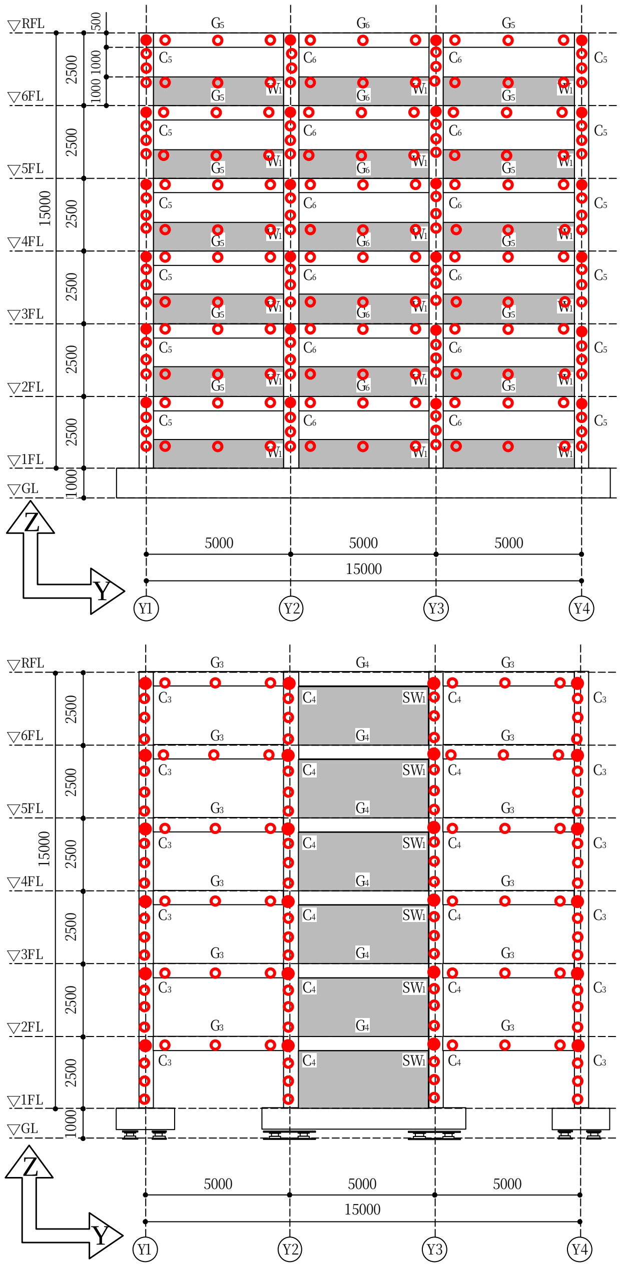

Figure 13: Frame of X1 (the Left), X2 (the Right)

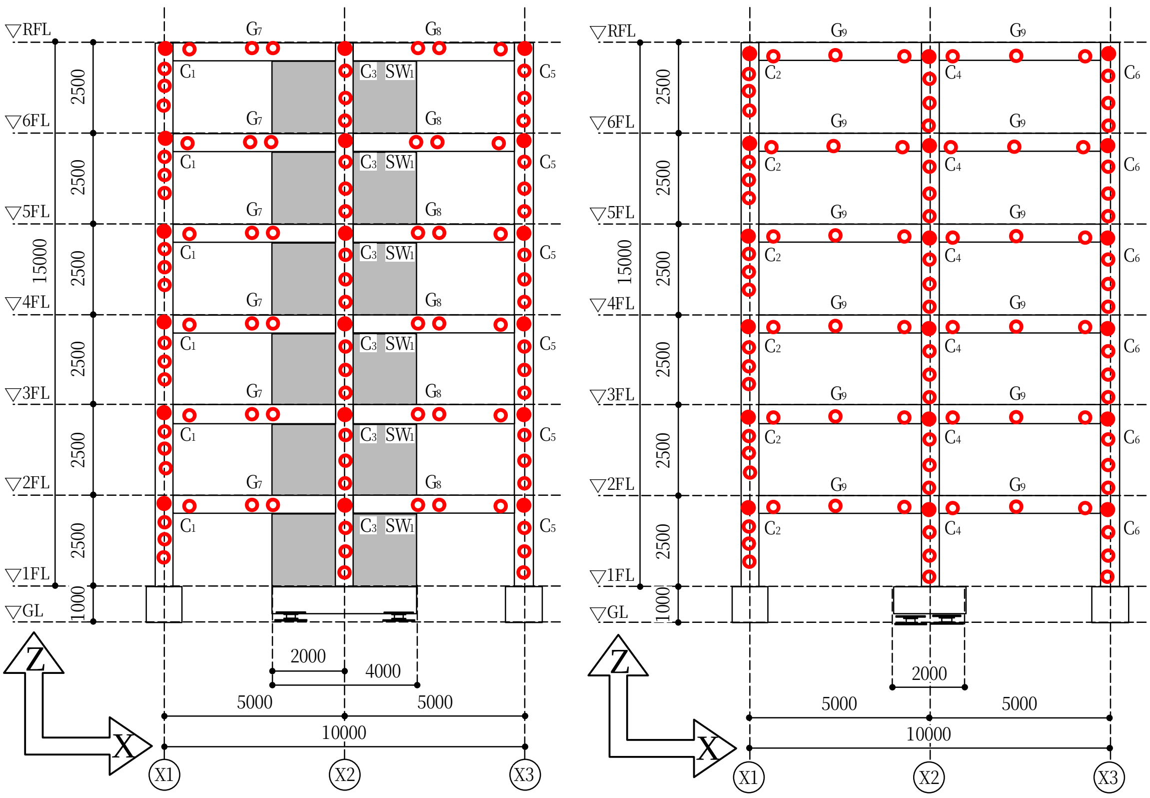

Figure 14: Frame of Y1, Y4 and Y2, Y3

3.2 Input Waves for Analysis

JMA Kobe Waves are selected for the input waves in analysis. Y-direction is assumed as main damage direction, so the JMA Kobe wave is rotated -45 degree (in clockwise). The orbit of input waves in X, Y directions is shown in Figure 15; the broken line is for the original waves and solid line is in -45 degree direction. Histories of input waves in three dimensions are shown in Figure 16.

Analyses are done continuously by 0.8 times and 1.0 time input of JMA Kobe Waves. Pushover analyses are also done by inverted triangle and uniform distributed loads in each horizontal direction and by inverted triangle distributed loads in two direction of X direction and Y direction (loads in X direction is 0.8 times of loads in Y direction).

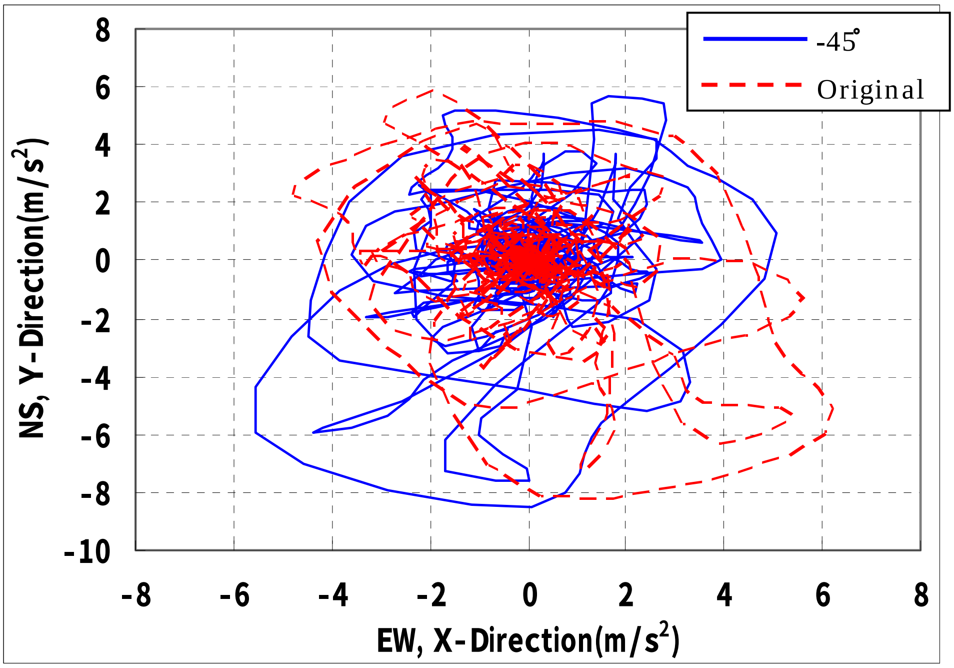

Figure 15: Orbit of Input Waves in Horizontal Directions (JMA Kobe)

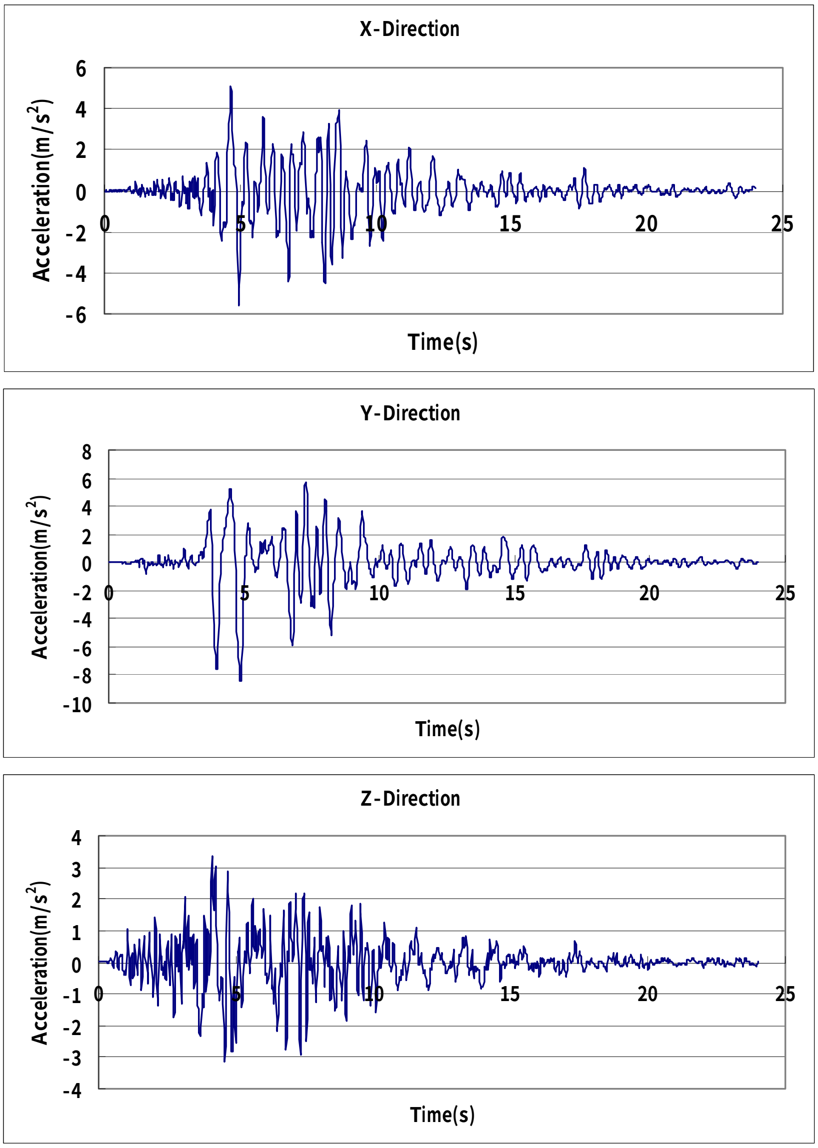

Figure 16: Input Original Waves for Analysis (JMA Kobe)

3.3 Analytical Results

3.3.1 Y-direction Analytical Results

At first, relationships between base shear force coefficient and roof level drift angle in Y-direction are shown in Figure 17. Analytical result of static inverted triangle loading has a better correspondence with dynamic result than static uniform loading. 0.8 times input of JMA Kobe Waves will yield the structure and the drift angle at roof level will be less than 1%. But the structure will be collapsed by 1.0 time input of JMA Kobe Waves and the drift angle at roof level will be more than 2%.

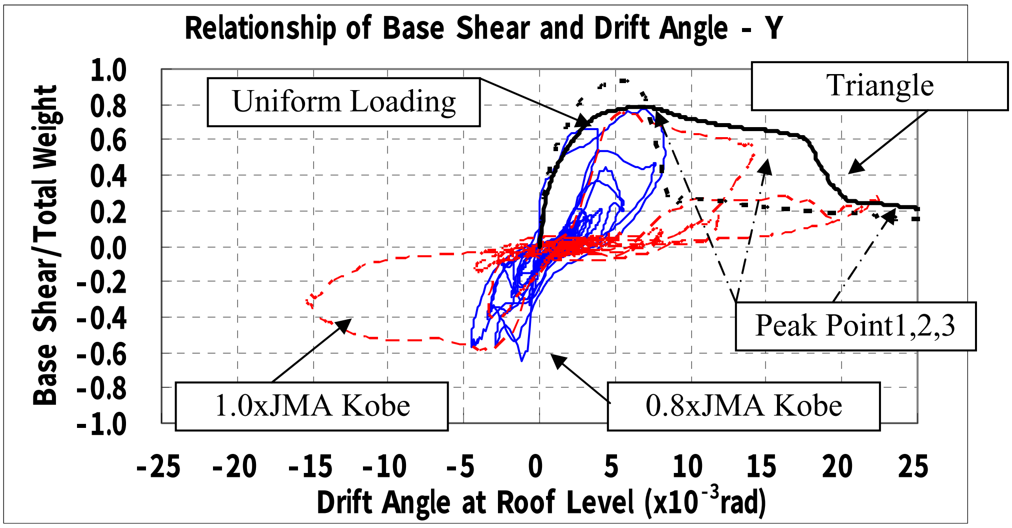

Figure 17: Relationship of Base Shear Force and Roof Level Displacement

A comparison of shear force contribution of shear wall is made between static inverted triangle loading and dynamic loading (Figure 18). The maximum of base shear force coefficient is 0.78, and about 50% of total shear force is contributed by shear wall in case of dynamic loading. In case of static loading, the maximum of base shear force coefficient is same as dynamic loading, and about 45% of total shear force is contributed by shear wall. Almost same performance can be got either in case of static loading or dynamic loading. The performance of shear wall is shown in Figure 19.

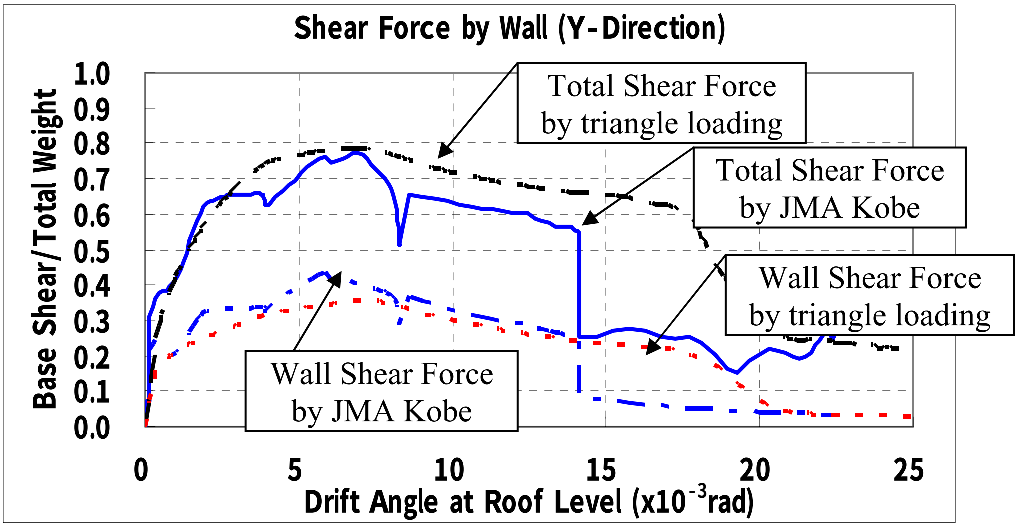

Figure 18: Shear Force Contribution by Shear Wall in Y-direction

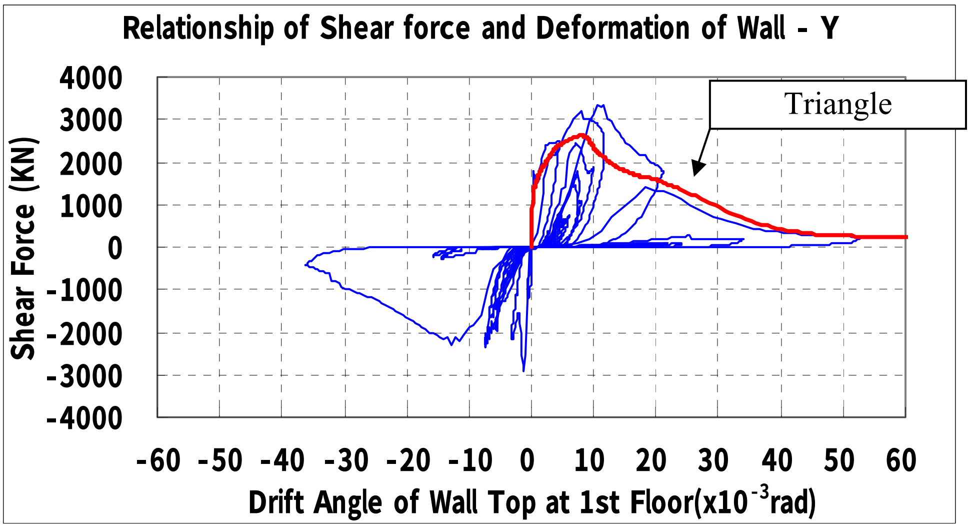

Figure 19: Performance of Shear Wall

Distributions of displacement at vertical direction are shown for peak point 1, 2, 3 in Figure 20. From peak point 1 to point2, 3, it is known that shear deformation is excelled at 1st level. The relationship between base shear force and 1st level drift angle is shown in Figure 21, and the specimen will be collapsed by 1.0 time input of JMA Kobe Waves because of the ground level collapse, the drift angle of 2nd level will be more than 1/20.

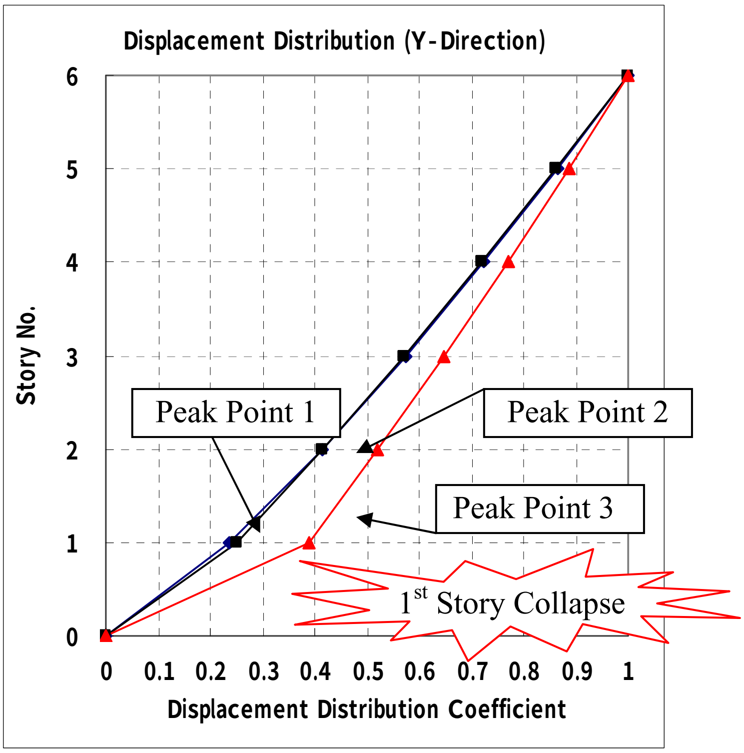

Figure 20: Distribution of Displacement along Vertical Direction in Y-direction

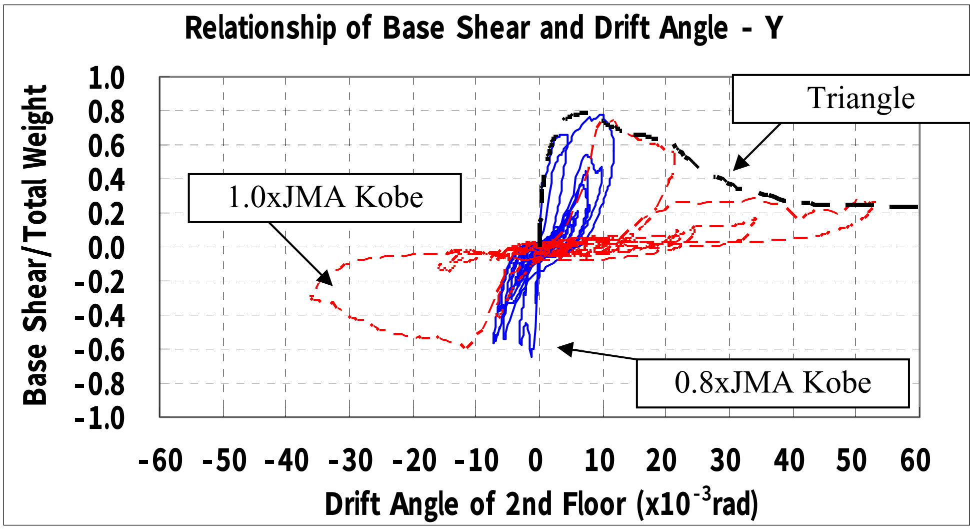

Figure 21: Relationship of Base Shear Force and 1st Level Displacement

3.3.2 X-direction Analytical Results

At first, relationship between base shear force coefficient and roof level drift angle in X-direction is shown in Figure 22. Analytical results of static loading are seriously different from dynamic results. The maximum of base shear force coefficient is 0.66 in case of static inverted triangle loading, but it is 0.58 in case of dynamic loading. 0.8 times input of JMA Kobe Waves will yield the structure and the drift angle at roof level will be less than 1/100. Even by 1.0 time input of JMA Kobe Waves, the drift angle at roof level will be less than 15/1000.

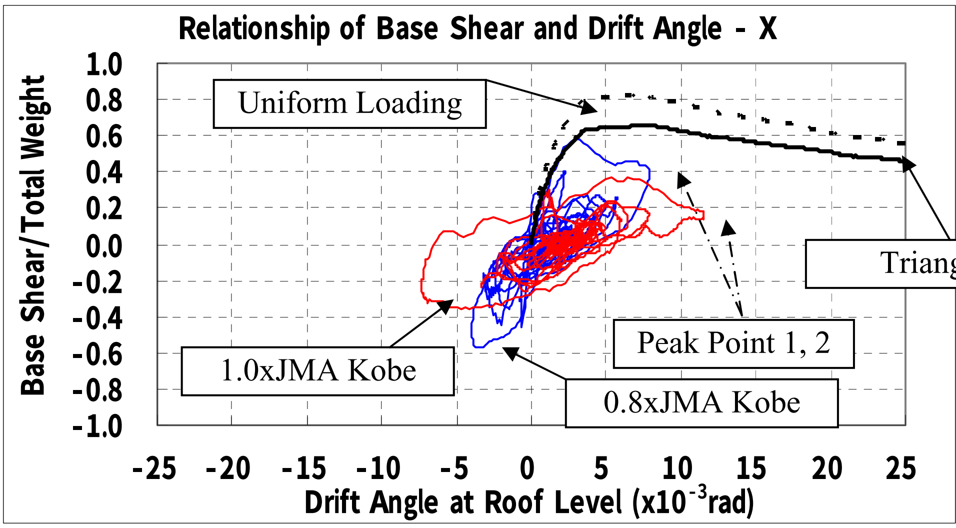

Figure 22: Relationship of Base Shear Force and Roof Level Displacement

To investigate the reason, the performance of wing walls (in frame Y1 and Y4) is shown in Figure 23, and the performance of all columns is shown in Figure 24. It can be known that the wing walls will remain good performance under dynamic loading, but the columns can't give full ability of shear resistance after 1/400 deformation under 3-dimension dynamic loading.

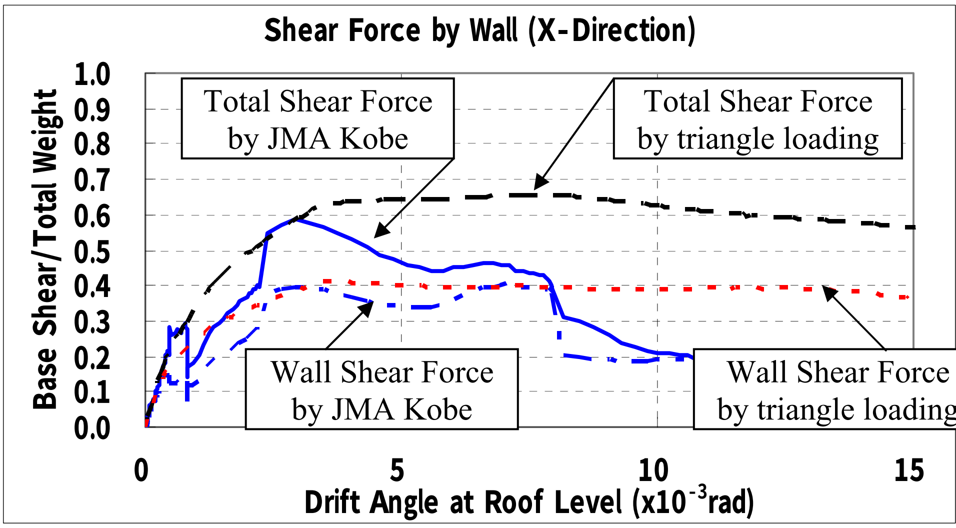

Figure 23: Total Performance of Wing Walls in X Direction

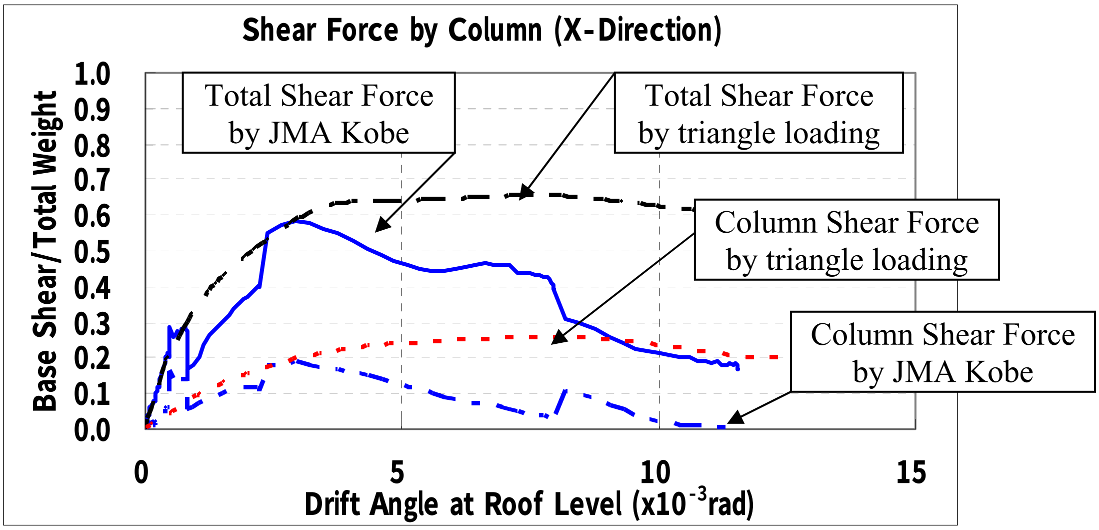

Figure 24: Total Performance of Columns in X Direction

Distributions of displacement along vertical direction are shown for peak point 1, 2 in Figure 25. No story will be collapsed. The relationship between base shear force and 1st level drift angle is shown in Figure 26. The drift angle of 2nd level will be not more than 15/1000 even in case of 1.0 time input of JMA Kobe Waves.

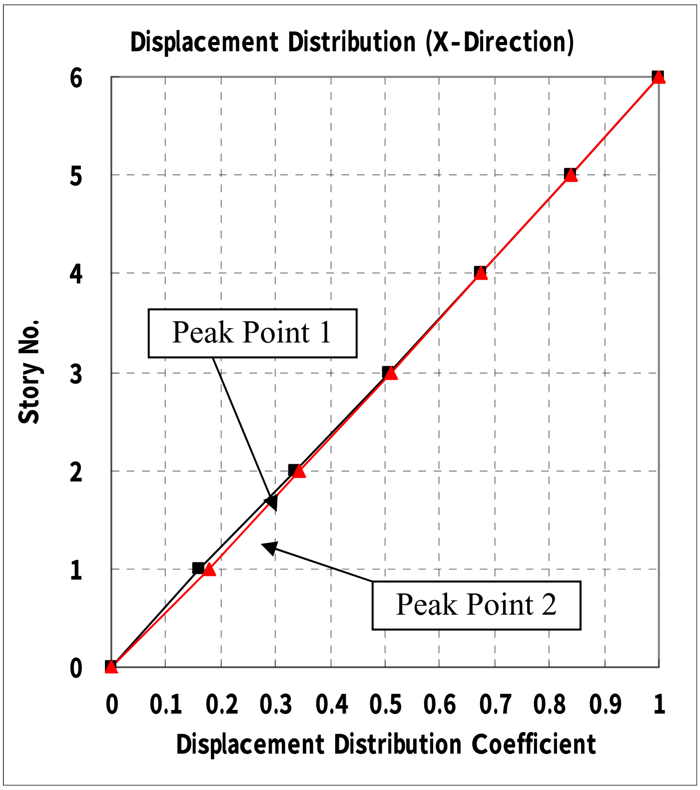

Figure 25: Distribution of Displacement along Vertical Direction

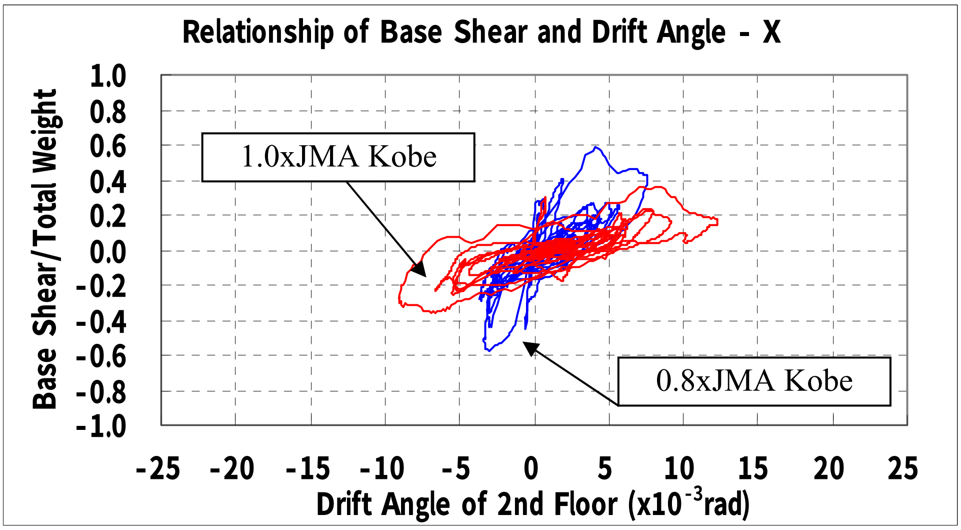

Figure 26: Relationship of Base Shear Force and 1st Level Displacement

3.3.3 Static Loading in Two Directions

The dynamic analysis is done by 3-dimension input of JMA Kobe Waves, but static analyses shown above are done by 1-direction loading only. It seems that analysis of 2-direction static loading will be better for comparison with dynamic analysis. Inverted triangle distribution load is selected to add in Y direction, and 0.8 times of Y direction load is added to X direction at the same time. Comparisons between dynamic and static loading are shown in Figure 27 (Y direction) and Figure 28 (Y direction). It is known that base shear by dynamic loading is higher than by static loading.

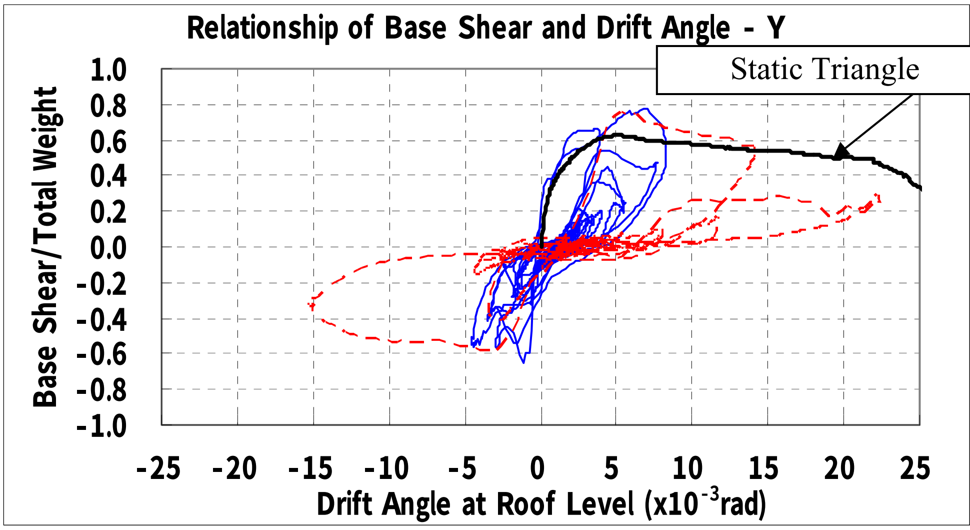

Figure 27: Performance Comparison between Dynamic and Static Loading in Y Direction

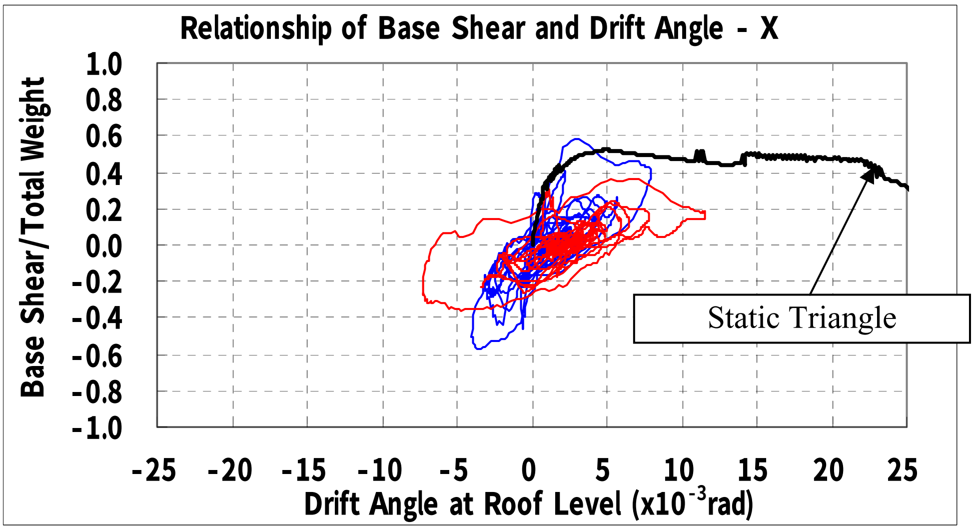

Figure 28: Performance Comparison between Dynamic and Static Loading in X Direction

3.3.4 Torsion Deformation

Torsion deformations of roof are shown in Figure 29 for 0.8 times input of JMA Kobe Waves, and Figure 30 for 1.0 time input. Analytical results of static loading are seriously different from dynamic results. If the columns (especially short columns) are not collapse by shear failure, the maximum torsion angle will reach to about 2.0% in case of 1.0 time input of JMA Kobe Waves.

In other words, difference of x-direction displacements between frame Y1 and Y4 will be to about 30cm.

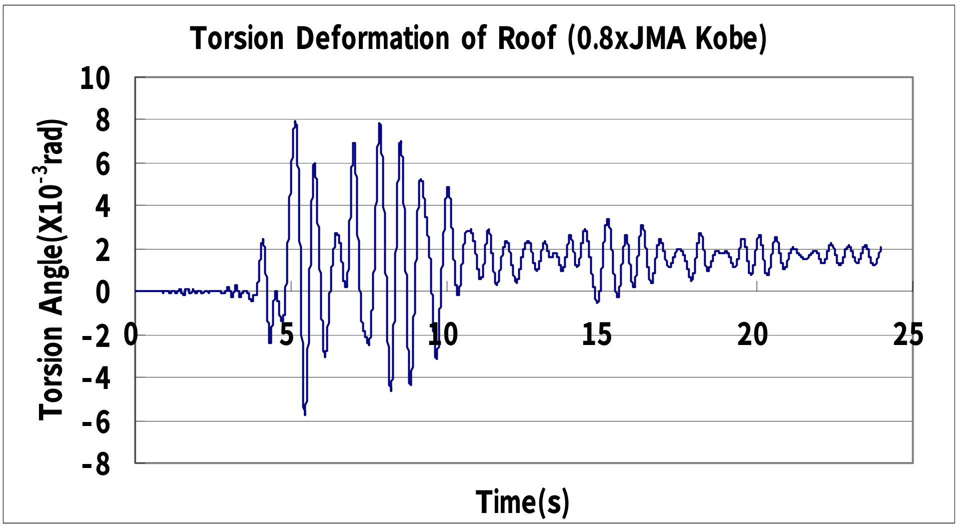

Figure 29: Torsion Deformation of Roof by 0.8xJMA Kobe Waves

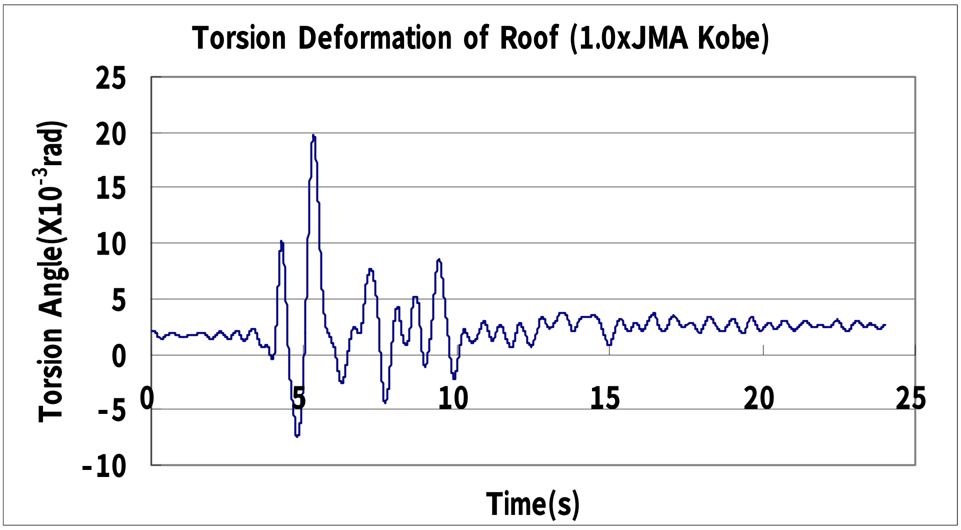

Figure 30: Torsion Deformation of Roof by 1.0xJMA Kobe Waves

4. RESULTS

The results of this paper can be concluded by the following points.

1. Good accuracy was obtained for 1/3-scale 2-story shear wall specimens by the proposed analytical methods.
2. The full-scale specimen will be collapsed at Y-direction because of the ground level collapse by excitation of JMA Kobe Waves in -45 degree direction.

3. The maximum of base shear force coefficient will reach 0.78 in Y-direction under JMA Kobe Waves; the maximum of X-direction is 0.58.
4. The drift angle at roof level will be more than 2% in Y-direction by excitation of JMA Kobe Waves; the drift angle of 2nd level will be over 5%.
5. The drift angles of X-direction at roof level and at 2nd level will be less than 1.5% in by JMA Kobe Waves.
6. Torsion deformation will be occurred, the maximum torsion angle at the roof level will reach to 2.0%.

5. REFERENCES

Chen, S. and Kabeyasawa T. (2000). Modeling of reinforced concrete shear wall for nonlinear analysis. *12th World Conference on Earthquake Engineering, CD-ROM*, Paper No.1596.
Chen, S. and Kabeyasawa T. (2004). Macro-FEM model of reinforced concrete column and beam only considering flexural deformation. *Proceedings of the Japan Concrete Institute*, 26:2:25-30
Chen, S. and Kabeyasawa T. (2005). Average stress-strain relationship of steel bars embedded in concrete. *13th World Conference on Earthquake Engineering, CD-ROM*, Paper No.3290.
Izumo, J., Shima, H. and Okamura, H. (1989). Analytical Model for RC Panel Elements Subjected to In-plane forces. *Concrete Library International, JSCE,* 2:155-181.
Matsui, T., Kabeyasawa T., Kato A., Kuramoto H., and Nagashima I. (2004). Shaking Table Test and Analysis of Reinforced Concrete Walls, *13th World Conference on Earthquake Engineering, CD-ROM,* Paper No.419.
Vecchio, F.J. and Collins, M.P. (1982). Response of Reinforced Concrete to In-Plane Shear and Normal Stress. *Department of Civil Engineering, Publication 82-03, University of Toronto.*

6. KEYWORDS

Panel model, prediction analysis, collapse analysis, full-scale, reinforced concrete, DaiDaiToku, E-Defense

SESSION 3: EVALUATION OF COLLAPSE PROCESS

Chaired by

♦ Craig Comartin and Taizo Matsumori ♦

COLLAPSE TESTS OF LIGHTLY CONFINED REINFORCED CONCRETE COLUMNS AND FRAMES

Wassim M. GHANNOUM[1], Yoon Bong SHIN[1], and Jack P. MOEHLE[2]

ABSTRACT

Collapse of older-type reinforced concrete buildings is investigated in a series of experiments, model developments, and computer simulations. A primary focus of the collapse study is axial-load failure of columns following shear failure. Past and ongoing studies consider individual columns under slowly-varying lateral load tests, shake table studies of single-story structures, and shake-table studies of multi-bay, multi-story structures. Analytical model development includes models for shear strength, deformation at shear failure, and deformation at axial failure. The models are implemented in computer software to simulate earthquake response to collapse.

1. INTRODUCTION

Post earthquake studies show that the primary cause of reinforced concrete building collapse during earthquakes is the loss of vertical-load-carrying capacity in critical building components leading to cascading vertical collapse. In cast-in-place beam-column frames, the most common cause of collapse is failure of columns, beam-column joints, or both. Once axial failure occurs in one or more components, vertical loads arising from both gravity and inertial effects are transferred to adjacent framing components. The ability of the frame to continue to support vertical loads depends on both the capacity of the framing system to transfer these loads to adjacent components and the capacity of the adjacent components to support the additional load. When one of these conditions is deficient, progressive failure of the building can ensue.

Of primary interest in this research effort is the behavior of reinforced concrete columns with relatively light transverse reinforcement and with proportions that enable the column to yield in flexure prior to developing shear or axial failure. Columns with these details and proportions may be able to sustain moderately large lateral deformations prior to failure; a challenge is to estimate the lateral drift at which failure occurs. Past laboratory studies have identified primary variables that contribute to loss of shear as well as axial-load capacity of such columns. These variables have been implemented in the nonlinear dynamic analysis platform OpenSees allowing the simulation of building collapse during earthquake shaking. Current research efforts are looking into the interaction of columns of different ductilities in terms of global structural system

[1] *Graduate Student Researcher, Pacific Earthquake Engineering Research Center, UC Berkeley.*

[2] *Professor and Director, Pacific Earthquake Engineering Research Center, UC Berkeley, Email: moehle@berkeley.edu*

behavior. As well, effort is being put into testing a 3-story, 3-bay reinforced concrete frame that would allow better assessment of the mechanisms involved in reinforced concrete frame system collapse.

2. PREVIOUS WORK

2.1 Shear and Axial Load Failure Tests of Reinforced Concrete Columns

For a column that yields in flexure, the lateral strength is limited to the flexural strength, and therefore can be calculated with relatively high accuracy. The column subsequently may sustain apparent shear failure. Although the details of the mechanism leading to shear failure are not fully understood, it is postulated that crack opening and tensile strains reduce the shear-carrying capacity of the concrete, while spalling and bond distress lead to degradation of the reinforcement contribution. To identify if shear failure is likely, it is necessary to estimate whether the shear strength will degrade to less than the flexure strength.

Sezen and Moehle (2002) conducted full scale tests on columns with light transverse reinforcements and proportions that would induce longitudinal steel yielding prior to column shear failure. Axial loads were varied in the tests with two distinct levels at $0.15A_gf'_c$ and $0.60A_gf'_c$ as well as variable axial load simulating frame action on a column. Lateral loading was either cyclic or monotonic. These tests combined with previous literature data allowed the development of a shear capacity model for such columns which accounts for the ductility demand on shear capacity. The shear strength was defined as:

$$V_n = V_s + V_c = k\frac{A_{st} f_{yt}\, d}{s} + k\left(\frac{0.5\sqrt{f'_c}}{a/d}\sqrt{1+\frac{P}{0.5\sqrt{f'_c}A_g}}\right)0.8A_g \quad \text{(MPa)} \qquad [1]$$

where V_s and V_c are shear contributions assigned to steel and concrete; k is a parameter equal to 1 for $\mu_\delta \le 2$, equal to 0.7 for $\mu_\delta \ge 6$, and varies linearly for intermediate μ_δ values; μ_δ = displacement ductility; A_{st} = area of shear reinforcement parallel horizontal shear force within spacing s; f_{yt} = yield strength of transverse reinforcement; d = effective depth (=0.8h, where h = section depth parallel shear force); P = axial compression force; f'_c = concrete compressive strength (MPa); A_g = gross section area, and a/d = shear span/effective depth (value limited between 2 and 4). Figure 1 compares measured and calculated shear strengths. The mean ratio of measured to calculated strength and its coefficient of variation are 1.05 and 0.15.

These tests provided a good basis for reckoning whether shear failure would follow flexural yielding. However, the horizontal drifts at shear and axial failures especially under dynamic loading, as well as dynamic response for strength-degrading structures, remained unknown. To assess these effects Elwood and Moehle (2004) performed dynamic tests of two single-story frame assemblages with mixed ductile and non-ductile columns. The non-ductile columns had details replicating those of Sezen (2002) with axial loads on non-ductile columns either $0.15A_g f'_c$ or $0.24A_g f'_c$.

Elwood and Moehle (2004) proposed an empirical expression for the drift at shear failure based on statistical analysis of the data shown in Figure 1. Shear failure was defined as the loss of twenty percent of the maximum shear strength. The data show that deformation at shear failure decreases with increasing shear stress, increasing axial stress, and decreasing transverse reinforcement index. According to the model, deformation at shear failure is defined as

$$\delta_s = \frac{3}{100} + 4\rho'' - \frac{1}{40}\frac{v}{\sqrt{f'_c}} - \frac{1}{40}\frac{P}{A_g f'_c} \geq \frac{1}{100} \quad \text{(MPa units)} \qquad [2]$$

where ρ'' = transverse steel ratio and v = nominal shear stress. Figure 2 compares results from tests and from Equation 2. The mean ratio of measured to calculated strength and its coefficient of variation are 0.97 and 0.34.

Axial load failure may coincide with onset of shear failure or may occur at larger drift. Elwood and Moehle (2004) used concepts of shear-friction and experimental data to derive an expression for the drift at axial load failure of columns initially yielding in flexure, then developing shear failure, and finally developing axial failure. The drift at axial failure is estimated as

$$\delta_a = \frac{4}{100}\frac{1+\tan^2\theta}{\tan\theta + P\left(\dfrac{s}{A_{st} f_{yt} d_c \tan\theta}\right)} \qquad [3]$$

in which θ = critical crack angle (assumed = 65 deg) and d_c = depth of the column core measured parallel to the applied shear. Figure 3 compares results of tests and Equation 3.

It is important to note that the models presented were for columns with rectangular cross section, relatively light and widely spaced transverse reinforcement, subjected to unidirectional lateral load. Additional data are needed to validate models for other conditions.

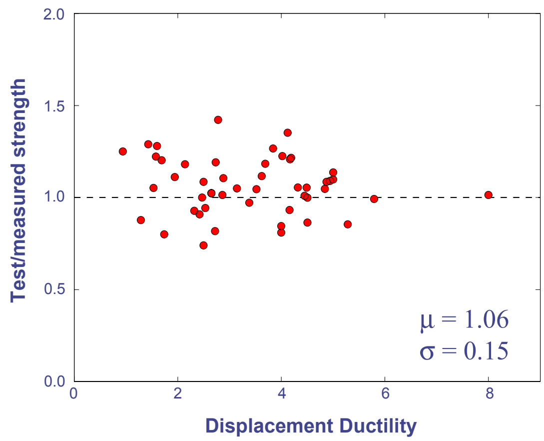

Fig. 1: Ratios of strengths measured during tests to strengths calculated by the strength model

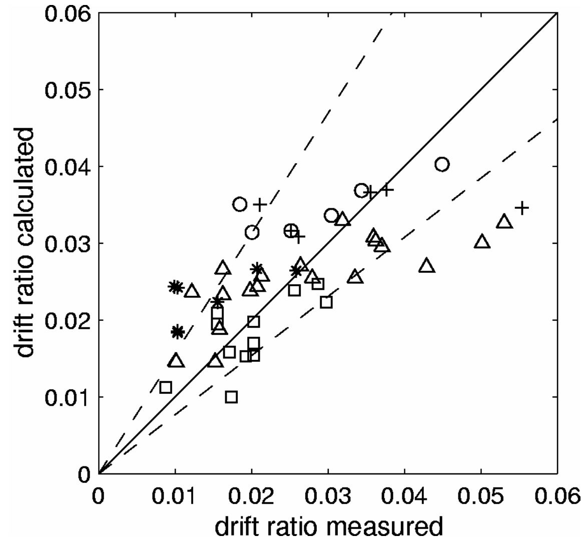

Fig. 2: Displacement capacity measured and calculated by Equation 2

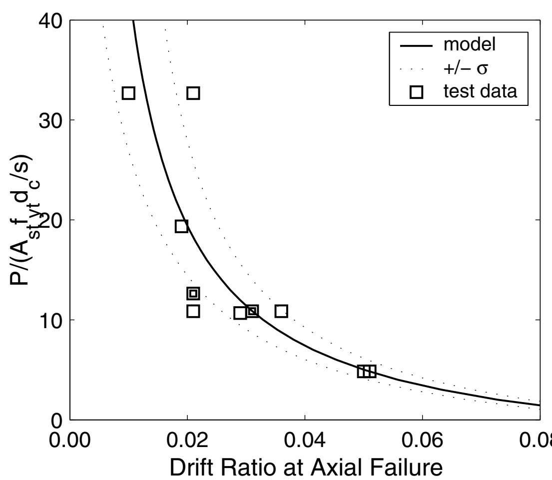

Fig. 3: Drift capacity curve based on shear-friction model

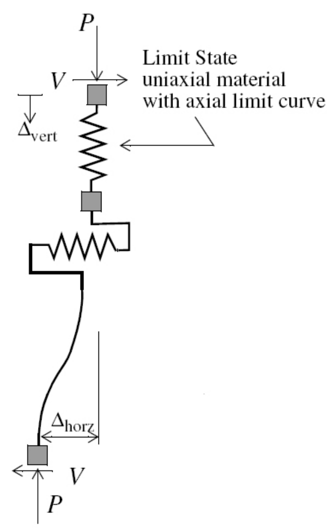

Fig. 4: Zero-length springs (Elwood 2002)

2.2 Implementation of Axial Failure Model in OPENSEES

Shear and axial failures are modeled in OpenSees by adding at the end of the columns zero-length Limit State spring elements developed by Elwood (2002) (Fig. 4). These elements have differing backbone curves before and after failures are detected. Prior to shear failure, the shear springs are elastic with stiffness corresponding to the shear stiffness of the column. Once the element reaches the limit curve defined by an empirical shear-drift relation (Elwood 2002) the shear spring backbone curve is modified to a degrading hysteretic curve (Fig. 5). The shear degrading slope Kdeg is calibrated based on observations from previous tests (Nakamura and

Yoshimura 2002), which have shown that axial failure is initiated when shear strength degrades to about zero.

Similarly, the zero-length axial springs have a "rigid" backbone prior to reaching the axial load-drift limit curve (Elwood 2002) (Fig. 5). This limit curve is defined by the shear-friction model and, hence, assumes that shear failure has already occurred in the element. Once the column element reaches that drift limit curve its axial load-vertical deformation backbone is modified to a degrading hysteretic material model. Because the shear-friction model only describes compression failures, the backbone is only redefined for compressive axial loads. Beyond the initiation of axial failure, a coupling effect exists between the horizontal and vertical deformations where an increase in horizontal drift causes an increase in vertical deformation. This effect is modeled in the vertical spring element with an iterative procedure that keeps the column response on the horizontal drift-axial load curve defined by the shear-friction model. When the earthquake motion reverses direction, the vertical spring backbone is redefined to an elastic response with a reduced elastic stiffness to account for the damage in the column. This modification also halts the axial degradation in the column as it is assumed that the critical shear crack closes which prevents any further sliding along that crack.

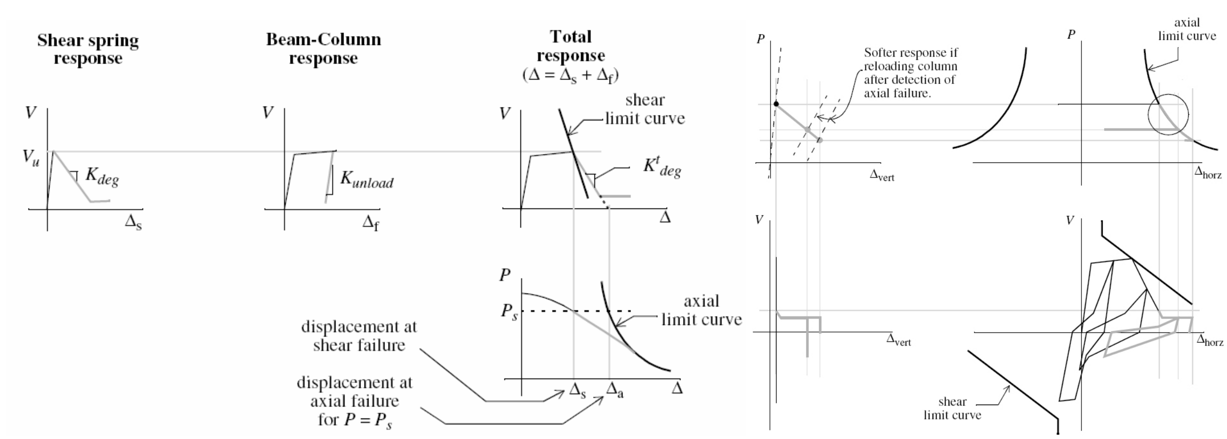

Fig. 5: Shear and axial zero-length element responses and limit curves (Elwood 2002)

3. CURRENT OBJECTIVES AND RESEARCH EFFORTS

Much progress has already been made towards the understanding and predicting the collapse behavior of reinforced concrete columns with light transverse reinforcements and flexure-shear-axial failure sequence. Under this research effort numerical and analytical models have been developed to simulate the behavior of such columns up to complete collapse. However, this behavioral knowledge at the component level is not sufficient to fully predict the global frame system behavior as collapse of one or several columns is initiated. Sezen (2002) demonstrated in his tests the importance of load history on the collapse behavior of such columns. This load history is greatly affected by the framing system in which the columns reside. Load redistribution due to softening of weak columns will generate additional load demand on adjacent beams, beam-column joints and columns which may soften as well due to the additional loads. On a system level, the softening of columns and adjacent elements will produce shifts in the apparent periods of the structure as well as reduction in capacity, which in turn modifies the seismic demand on the structure and feeds back into the component load history.

The next stage of this research program is focusing on frame system behavior. Two experiments are currently under way. In the first project, a series of 12 tandem-column dynamic tests will be performed at the University of California, Berkeley, shake table facility to observe dynamic response of strength-degrading systems. Series variables are axial load, tie spacing and ground motions. The second project will dynamically test a third-scale, 3-bay, 3-story, planar frame structure at the same test facility to observe effects of internal force redistribution associated with collapse. These projects are described in more detail below.

4. CURRENT RESEARCH ON DYNAMIC RESPONSE OF OLDER-TYPE REINFORCED CONCRETE FRAMES

4.1 Single-Story Shake Table Test

These tests involve several planar, two-column, single-story structures having different column behavioral characteristics ranging from ductile to strongly strength-degrading. The objective is to improve understanding of the dynamic response of strength-degrading concrete structures. A specific test structure will have either two ductile columns, a ductile column and shear-critical column, or two shear-critical columns to control the rate and amount of strength degradation. Two ground motions (one relatively shorter duration with strong velocity pulses and one relatively longer duration without strong velocity pulses) will be used (Fig. 6). Each setup will have two axial load cases (0.1 fc’Ag and 0.24 fc’Ag) (Table 1).

Table 1: Test matrix

Setup	Reinforced Concrete Columns	Ground Motion
I	Ductile + Ductile	Chile 1985: Llolleo Station - Component 100 Kobe 1995: JMA Record - North/South
II	Ductile + Shear Critical	Chile 1985: Llolleo Station - Component 100 Kobe 1995: JMA Record - North/South
III	Shear Critical + Shear Critical	Chile 1985: Llolleo Station - Component 100 Kobe 1995: JMA Record - North/South

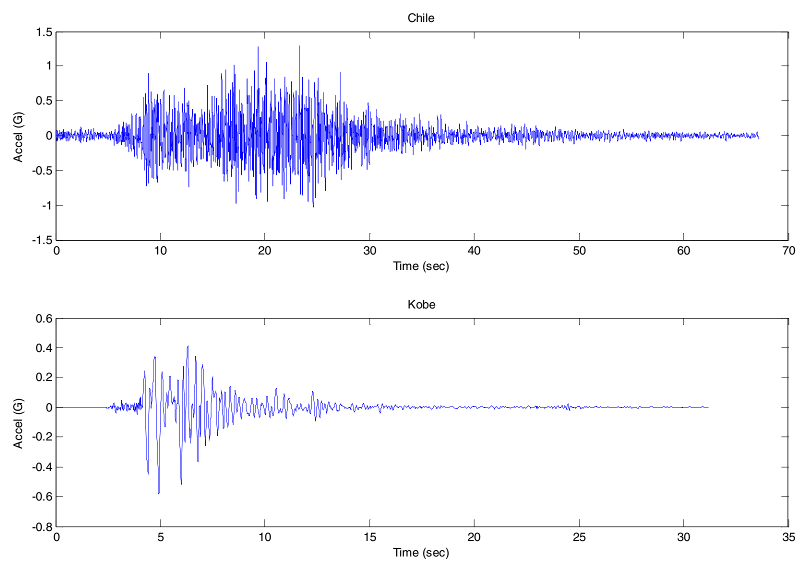

Fig. 6: Ground motions

The non-ductile columns are one-third-scale models of a prototype column tested previously by Sezen (2002). Specimens are designed to have a concrete strength of 21 MPa with 10mm diameter 400 MPa longitudinal reinforcement. Figure 7 shows the details of the specimens.

The basic test setup comprises two reinforced concrete columns fixed at the bottom to the shake table and at the top to a stiff steel beam. Lead weights attached to the steel beam act as gravity loads (0.1 fc'Ag axial load on a single column) and inertial mass. For the 0.24 fc'Ag axial load case, pneumatic jacks reacting between the shake table and steel beam will provide additional axial load. Out of plane bracing reduces movement of the specimen in the out of plane direction. To prevent the specimen from collapsing onto the shaking table, a steel frame (independent from the specimen) is placed beneath the specimen to support after axial failure occurs in the columns (Fig. 8).

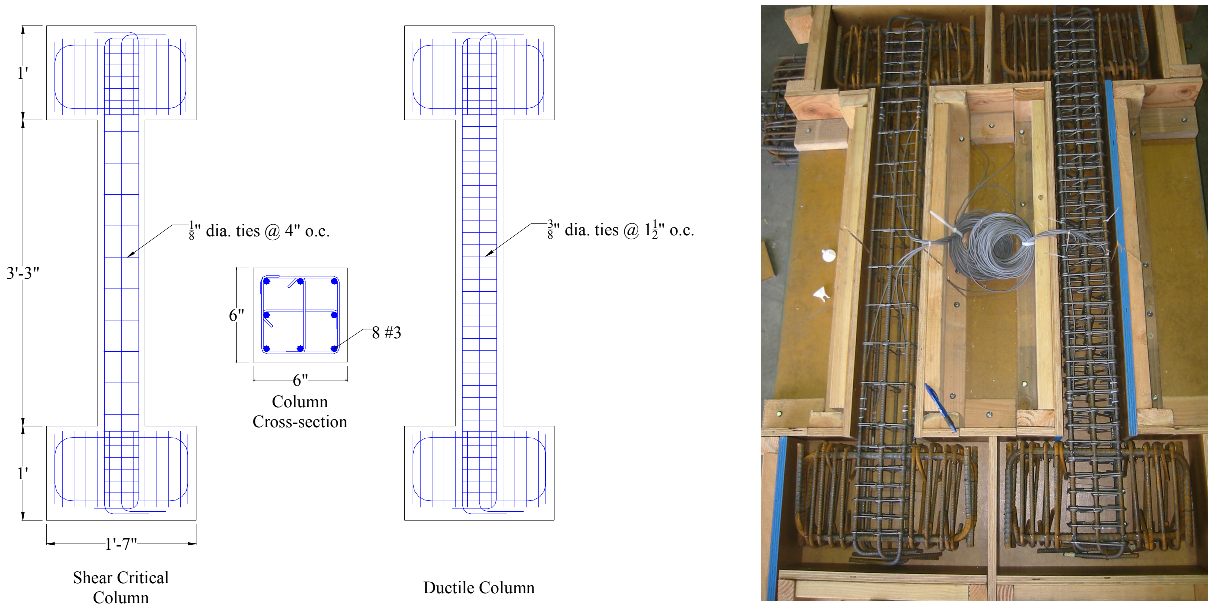

Fig. 7: Reinforced concrete specimens

The ground motions are applied to the concrete specimen in one horizontal direction. There are two types of earthquakes considered (Chile, Kobe). The ground motions are scaled to meet the on-third-scale similitude requirement by multiplying a time factor of √3 to the time domain. The magnitude of the ground motions are scaled to observe shear and axial failure in the columns.

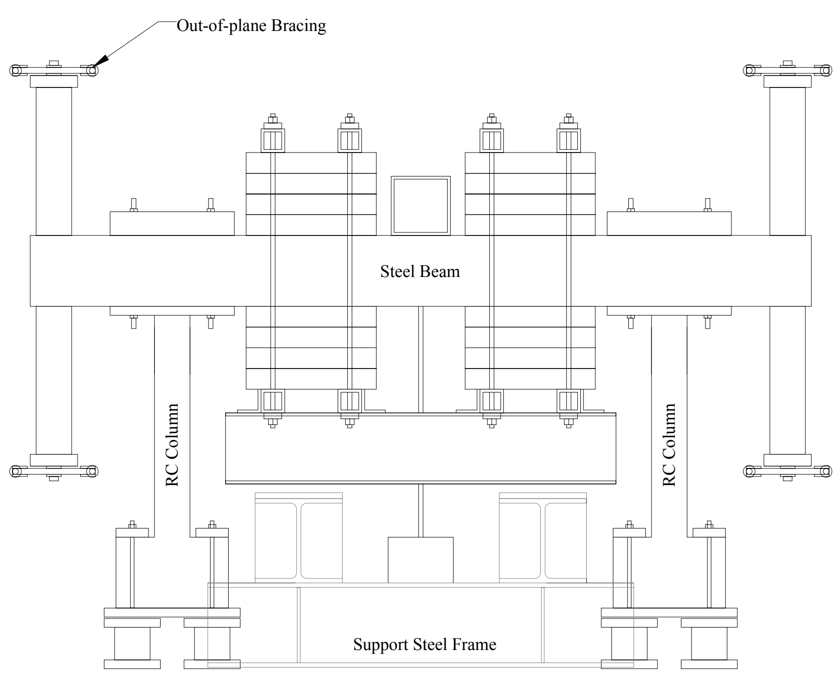

Fig. 8: Test setup

OpenSees has been used to conduct a preliminary analysis of the test setup. The shear critical reinforced concrete column uses the zero-length Limit State spring elements with a nonlinear beam column element (described previously), and the ductile column is modeled with a nonlinear beam-column element. The steel beam is modeled with an elastic beam column element. Figures 9a and 9b show calculated results of setup II and III with two axial load cases with Chile and Kobe ground motions. Of interest is to be able to estimate the maximum displacement response for strength-degrading structures.

<u>Kobe</u>

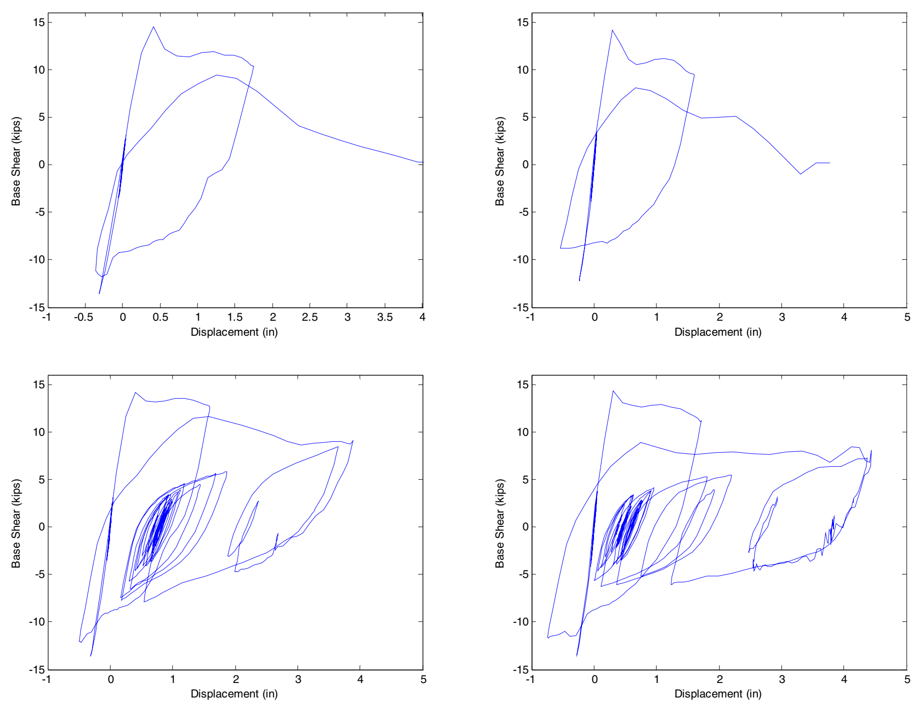

$0.10\, f'_c A_g$ Axial Load $\qquad$ $0.24\, f'_c A_g$ Axial Load

Fig. 9a: Preliminary analysis results

Chile

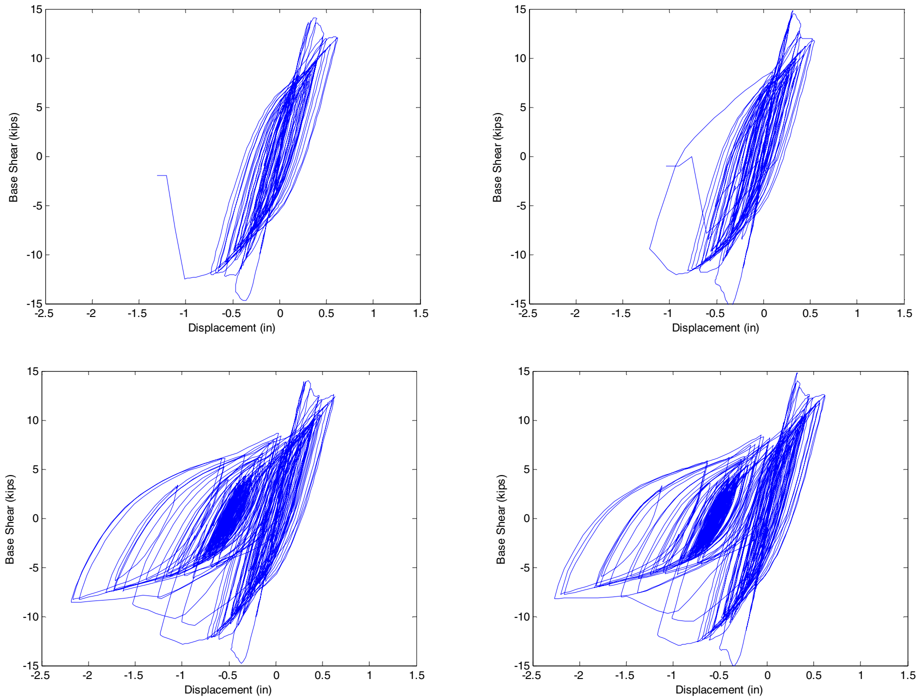

0.10 $f'_c A_g$ Axial Load   0.24 $f'_c A_g$ Axial Load

Fig. 9b: Preliminary analysis results

4.2 Three-Story, Three-Bay Frame Shake Table Test

4.2.1 Specimen Description

A third-scale reinforced concrete frame specimen with three bays and three stories is currently under construction at the University of California, Berkeley (Fig. 10). This frame test is aimed at better understanding and modeling the system collapse behavior of non-ductile reinforced concrete frames. This frame was proportioned to typical 1960s and 1970s office building construction in California with typical span lengths and floor heights.

Fig. 10: Frame construction

Figure 11 shows the frame dimensions and reinforcement details. Two columns in the frame have ductile detailing as per ACI 318-2002 while the other two have the same "non-ductile" reinforcement details as in Sezen (2002) and Elwood (2004). The mixed column-ductility arrangement of this frame was chosen so that the dynamic interaction between columns of different ductilities could be observed. Also, this provides greater resistance to collapse in part of the frame which in turn would force greater load redistribution through the elements. Closely spaced ties were placed in the beam-column joints on the ductile side of the frame as per ACI 352-2002 recommendations, whereas no ties were placed in the joints of the "non-ductile" side. This is intended to provide comparison data for the two types of joint details while keeping the details of both sides of the frame consistent with ductile and non-ductile detailing.

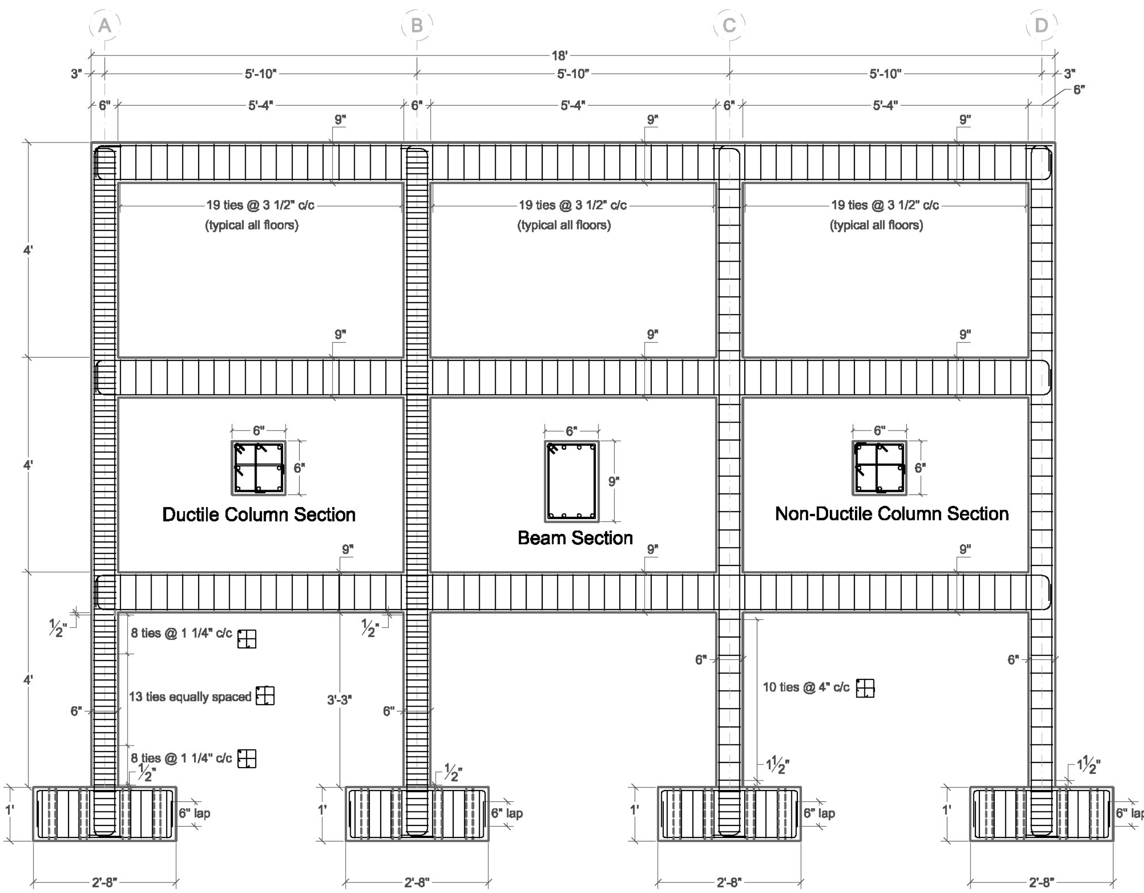

Fig. 11: Frame details

Beam depth and reinforcements were chosen to create a weak-column strong-beam mechanism as well as to reduce joint shear stresses. This should result in the concentration of damage in the non-ductile columns which will force axial collapse in these columns at high drifts. The beam reinforcement details are typical of those in moment-resisting frames built in the 1960s and 1970s in California.

Masses that will be added to the frame were chosen to generate approximately 0.15Agf'c axial load on the first-floor center columns and half that for the end columns. The advantage of this 3-bay frame arrangement is that it will provide columns of similar reinforcement detailing having two axial load levels and differing axial load histories due to the framing action. Finally, target concrete cylinder strength f'c is 3000psi for the specimen while steel yield strength is taken as fy=69 ksi.

4.2.2 OpenSees Modeling

All columns in the model are discretized into 12 displacement-formulation fiber-section elements. Displacement formulation was used for numerical stability purposes and the 12 element discretization produced very close results to the "exact" force-formulation alternative. The use of fiber sections rather than lumped plasticity was to account for the variable axial loads produced in the columns by the framing action. Fiber section concrete material is modeled using the OpenSees concrete01 uniaxial material model (Kent-Scott-Park model with a degraded unloading/ reloading stiffness according to Karsan and Jirsa). Concrete is modeled with no tension strength. Fiber section steel is modeled using the OpenSees steel01 uniaxial material model which has a bilinear response with kinematic hardening.

Beams in the model have the same formulation as columns with the same material model properties while joints and footings were considered to be rigid at this stage. Bar slip in footings and joints was modeled using rotational springs at the ends of columns as well as beams, and calibrated to previous tests results (Elwood 2004). At the ends of the "non-ductile" columns, zero length elements with shear and axial Limit-State materials (Elwood 2004) were introduced to simulate the shear and axial failures.

Splices were not included in the test model and their effects were not modeled. Damping used was mass and stiffness proportional (1st and 3rd mode) with an equivalent damping ratio of 3%. Mass is lumped in the model as it will be in the test setup.

The ground motion chosen for this test is a scaled up record from the 1985 Chile earthquake at Valparaiso. This record is a long duration record which will allow a longer observation period and a more gradual collapse. The resulting modeled structure had an initial elastic first-mode period of 0.34 sec and an effective first-mode period near collapse of about 0.55 sec.

4.2.3 Preliminary Analysis Results and Future Work

Dimensioning and detailing of the frame were chosen to concentrate damage in the non-ductile columns at the first floor level, with little or no damage in the upper floor columns prior to collapse. A non-linear pushover analysis with a first mode loading pattern was performed to identify the critical response and damage stages for the structure (Fig. 12). The calculated response and damage sequence for the frame is as follows:

1. Yielding of all first floor column longitudinal steel occurs at a first floor horizontal drift between approximately 0.7% and 1.0%.
2. At higher drifts, the opening of cracks in the yielded areas initiates shear failure in the non-ductile columns. This occurs at about 2.2% horizontal drift.
3. Between approximately 2.2% and 7% horizontal drift, there is a gradual loss of shear capacity in the non-ductile columns until a residual shear/friction capacity is reached.
4. At that drift level loss of axial load capacity in the non-ductile columns is initiated. It is important to note that these particular drift levels are mainly a function of the axial load on the columns as well as the flexure-then-shear failure sequence in the columns.
5. As the structure is pushed to even higher drifts, it collapses on the non-ductile side of the frame dragging the ductile side with it. A drift of 8% on the first floor was deemed the collapse drift for this frame. This final stage can be altered by choosing "stronger" framing on the ductile side in which case only a partial collapse would have been observed.

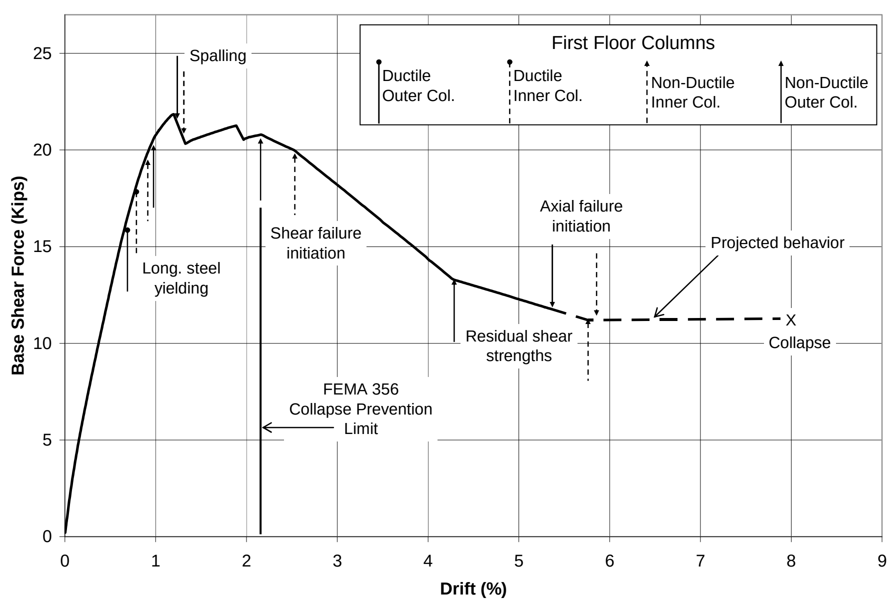

Fig. 12: First floor drift versus base shear response

It should be noted from Figure 12 that the pushover curve terminated at a drift of about 5.5%. This is because numerical instability is encountered when axial load degradation is initiated in a static analysis. This consistently occurs in static analyses using the axial Limit State material where the dynamic equations of equilibrium are lacking.

The collapse limit state for this structure was compared with the FEMA 356 Collapse Prevention Performance Level for a structure with shear critical primary columns. FEMA 356 guidelines define Collapse Prevention in this case as "the deformation at which shear strength is calculated to be reached". This state occurs at a first floor drift of about 2.2% for this frame whereas the model predicts collapse to occur at a much higher drift of 8%. It is clear in this case that the FEMA 356 guidelines can be too conservative for this type of structures, particularly for low axial loads. One can define the Collapse Prevention Performance Level as the stage at which axial load carrying capacity begins to degrade (drift of 5.5%) essentially neglecting the load redistribution capacity of a structure. However, even with this more conservative definition, the FEMA 356 guidelines are still too conservative by comparison.

The same model was subjected to a dynamic analysis simulating the Chile earthquake to which the physical specimen will be subjected to. Figure 13 illustrates the frame displacements at different key stages as obtained form the OpenSees analysis results. This figure demonstrates the capabilities of the current models to simulate the collapse of column elements. Figure 14 plots the column shear force versus floor drifts for all columns, while Figure 15 plots the axial deformations versus horizontal drifts and axial loads versus horizontal drifts for all columns.

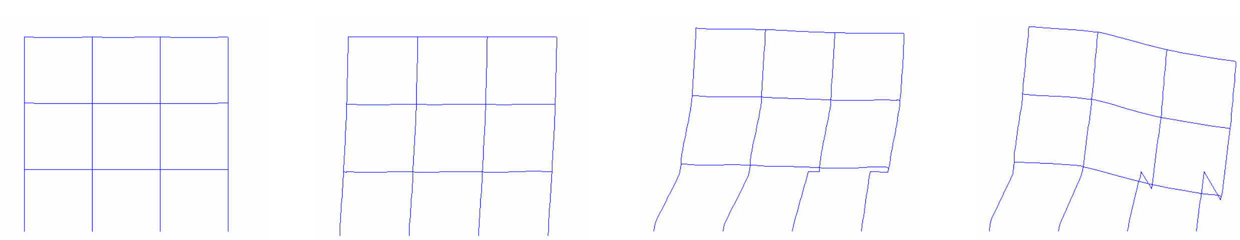

Fig. 13: Frame displaced shapes

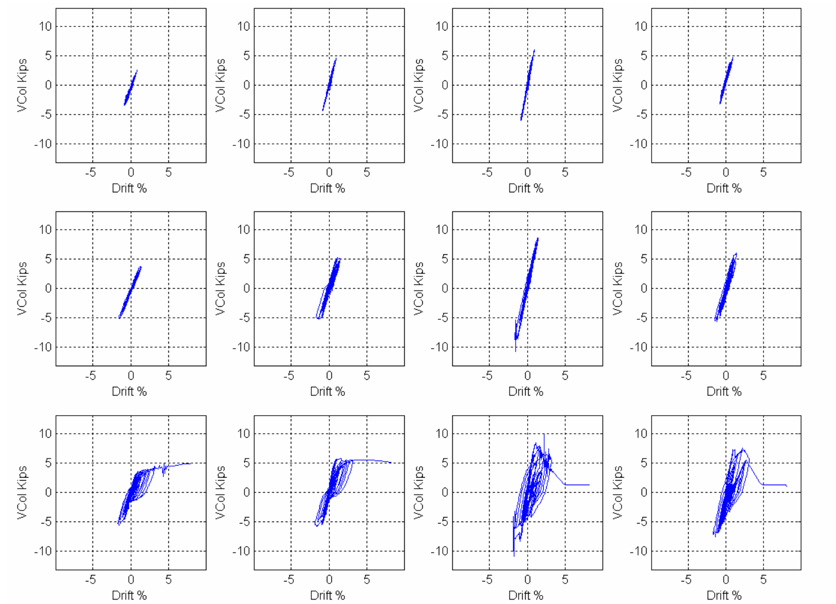

Fig. 14: Column shear forces vs. floor drifts (arranged as per frame geometry)

At this stage, these preliminary analyses are useful to set up the physical test and to target shake-table input motions likely to induce collapse. After the completion of the test, OpenSees joint elements will be input in the model to be tested and the LimitState material models will be refined (especially for column behavior during axial degradation). The ultimate goal of this project is to achieve an analytical model that simulates the physical test with good accuracy.

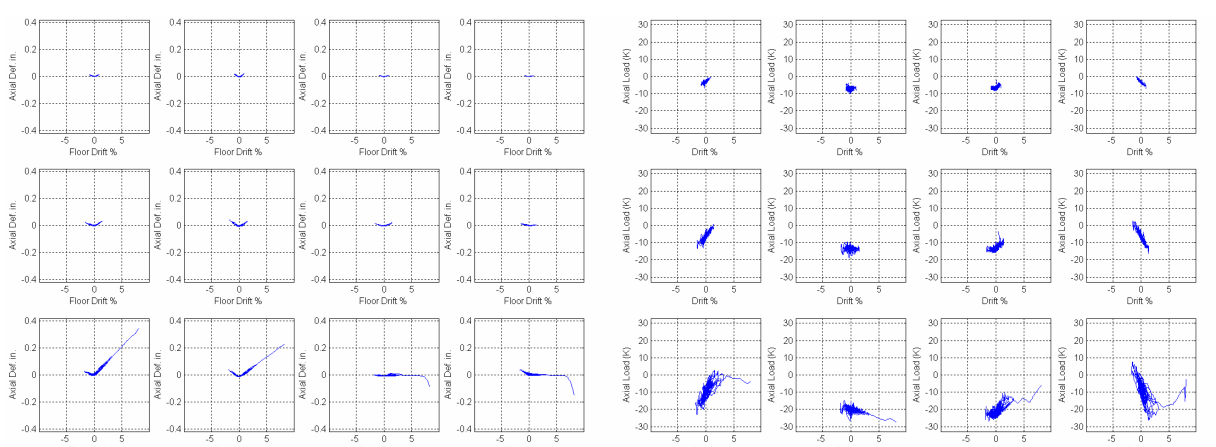

Fig. 15: Column axial loads and deformations vs. floor drifts (arranged as per frame geometry)

5. SUMMARY

A series of tests are planned at the University of California, Berkeley to improve understanding of the dynamic behavior of older-type concrete frames susceptible to collapse. One series of tests will examine dynamic response of single-story models with different degrees and rates of strength degradation subjected to different types of input ground motions. Another test will examine behavior of a three-story, three-bay planar frame shaken to collapse. The ultimate aim of this research is to improve simulation capabilities for non-ductile concrete buildings so that truly dangerous buildings can be identified and mitigation efforts can be directed toward them.

6. REFERENCES

Elwood, K. (2002). Shake Table Tests and Analytical Studies on the Gravity Load Collapse of Reinforced Concrete Frames. *Doctoral Dissertation,* University of California at Berkeley.

Elwood, K. and J. P. Moehle (2004). Evaluation of existing reinforced concrete columns. *Proceedings, 13th World Conference on Earthquake Engineering*, Vancouver.

FEMA 356 (2000). Prestandard and Commentary for the Seismic Rehabilitation of Buildings. *Federal Emergency Management Agency*, Washington, D.C.

Nakamura, T. and M. Yoshimura (2002). Gravity Load Collapse of Reinforced Concrete Columns with Brittle Failure Modes. *Journal of Asian Architecture and Building Engineering*, Vol. 1, No. 1, pp. 21-27.

OpenSees (2004), *Open System for Earthquake Engineering Simulation*, http://opensees.berkeley.edu, Pacific Earthquake Engineering Research Center, University of California, Berkeley.

Otani, S. (1999). RC Building Damage Statistics and SDF Response with Design Seismic Forces. *Earthquake Spectra*, Earthquake Eng. Research Institute, Vol. 15, No. 3, pp. 485 - 501.

Sezen, H. (2002). Seismic Behavior and Modeling of Reinforced Concrete Building Columns. *Doctoral Dissertation*, University of California at Berkeley.

Sezen, H., and J. P. Moehle, (2002). Seismic Behavior of Shear-Critical Reinforced Concrete Building Columns. *7th US National Conference on Earthquake Engineering*, Boston, MA, Earthquake Engineering Research Institute.

GLOBAL DYNAMIC COLLAPSE OF SDOF RC FRAMES UNDER EXTREME EARTHQUAKE LOADING

Chiun-Lin WU,[1] Yuan-Sen YANG,[2] and Chin-Hsiung LOH[3]

ABSTRACT

During the September 21 (local time) 1999 Chi-Chi Taiwan earthquake, a large number of older buildings built before 1982 sustained severe damage, and many others suffered from complete failure. These old buildings, having low ductility RC columns, are known to have poor seismic performance in terms of ductility and energy-dissipation capacity during severe seismic events. Therefore, it is the main concern of structural engineers and to the benefit of building owners to retrofit these old buildings to match stricter requirements of the next generation of building codes to get better odds to survive probable future earthquake events. To reach this goal, dynamic nonlinear behaviors of these low ductility columns must first be thoroughly studied. Shake table tests using near-fault input motions were conducted to yield experimental data on structural post-peak behaviors involved in global collapse mechanism. In addition, preliminary numerical simulation is carried out to present limitations of current OpenSees embedded models.

INTRODUCTION

While considerable advances have been made in the use of analytical and/or numerical methods to evaluate seismic performance of civil structures, recently there is a clear trend that more RC collapse experiments are being conducted or planned worldwide to gain more knowledge on failure mechanism in view that the fundamental characteristics of structural collapse are not easily amenable to an analytical/numerical treatment at the present stage. On the other hand, older buildings built before 1982 in Taiwan are known to demonstrate poor seismic performance in terms of ductility and energy dissipation capacity during severe seismic events. During the September 21 (local time) 1999 Chi-Chi Taiwan earthquake, a large number of older buildings sustained severe damage and many others suffered from complete failure.

Shake table tests, therefore, were conducted in this study to investigate global low-ductility collapse of old RC columns due to poor detailing. In the meantime, shake table test results will be very helpful in validating numerical hysteretic models with consideration of post-peak behaviors, and finding key parameter values of such models. Although not many, a few collapse experiments had been conducted to this date. Among those are gravity load collapse of ½-scale RC frames by Elwood (2002), small-scale steel frame tests by Vian et al. (2003), and a

[1] *National Center for Research on Earthquake Engineering, Taipei 106, Taiwan; email: clwu@ncree.org.tw*
[2] *National Center for Research on Earthquake Engineering, Taipei 106, Taiwan; email: yuansen@ncree.org.tw*
[3] *Department of Civil Engineering, National Taiwan University, Taipei 106, Taiwan; email: lohc@ncree.org.tw*

few others (Kim and Kabeyasawa 2004, etc.) This type of instrumented observations on dynamic collapse help gain further insight into dynamic stability problems. During our tests, digital camcorders were used to record the progress of structural collapse; displacement histories were obtained through both Temposonic LDTs and image processing technique, the latter of which was shown more effective when collapse or large displacement was expected. Different failure patterns were observed in two individual experiments, which implies column design and loading history both play an important role in collapse mechanism. Collapse analysis usually indicates involvement of discontinuum mechanics; however, experimental data show that hysteretic modeling approach could be sufficient in matching the needs of engineering practice in description of nonlinear dynamic response at structural collapse. In this regard, the authors' experience in using OpenSees shows that more efforts still need to be made among engineering community in order to predict structural response with more accuracy, and, as such, experimental data from collapse tests provide a great platform for setting up benchmark problems for verification of new numerical simulation methods. If a higher hazard level at 2% exceedance probability in 50 years and near-fault ground motions are to be considered in performance-based earthquake engineering, global/local collapse consideration needs to be carefully accounted for in structural dynamic analysis.

DESIGN OF SHAKE TABLE TESTS

Specimen Design

The test frame was designed to represent a real 4-story commercial-resident complex, which is quite popular in the central part of Taiwan. The two columns, interconnected by a strong beam, represent those at the soft 1st story (vertical irregularity) of the building, which is also typical in this type of open-front commercial complex. Beams and footings were designed strong enough to ensure plastic behavior occurs only in columns. The column design is aimed to reproduce genuine local engineering practice in Taiwan before 1982, in contrast to the new design code documents introduced after 1997. Its cross section is shown in Figure 1. A 1:2 scale model is selected following the design steps recommended by Tassios (1992) and bearing capacity limitation of NCREE's shake table. Acceleration, stress, and geometry are the three independent scale factors selected for the 1:2 scale experiment. Gravitational acceleration, density, viscous damping ratio, modulus of elasticity, and Poisson's ratio are the 4 physical quantities, scale factors of which remain unchanged. It, however, should be noted that the material related properties may not be the same as the prototype structure because of a more or less inevitable deviation in material properties (e.g., concrete compressive strength) due to the mix design of microconcrete material and production of D4 steel wires that were used for transverse reinforcements. D4 steel wires were made through cold-rolling operation on bars of a slightly larger diameter, with a consequence of an increase in its yield strength and a significant ductility loss because appropriate heat treatment (anealing) was not performed. However, the 90°-hook ties opened up before yielding could occur on these D4 wires. Also, stress and strain rates will be slightly accentuated since a time compression factor of $\sqrt{1/2}$ is used. While it is unlikely to manufacture reinforced concrete scale specimens to be true replica models, additional masses were provided to better reproduce inertia effects, column's stress state, and corresponding natural period of the target 4-story building, considering that in many cases the level of action-effects due to gravity forces (or, axial load) is of paramount importance for the ductility capacity of RC columns. Specific similitude requirements are imposed based on the following understandings:

1. Geometric similitude is considered essential due to constraints of the shake table specifications.
2. The stress-strain curves for model and prototype materials should be as much similar as possible both in compression and tension.
3. Strains in the model and prototype at failure are at a similar level.

In addition to the above-mentioned similitude requirements, it is also hoped that the ratio of vertical load, overturning moment and lateral excitation of the model structure can be kept close, as much as possible, to its prototype counterpart, but in the meantime out-of-plane instability of the test frames is alleviated to a considerably lower level. Based on the above criteria, the time scale of input earthquake motions was scaled down accordingly. A total weight of 21 ton lead ballast ($0.1f_c^{'}A_g$) was added to reproduce axial loads of 1st story columns.

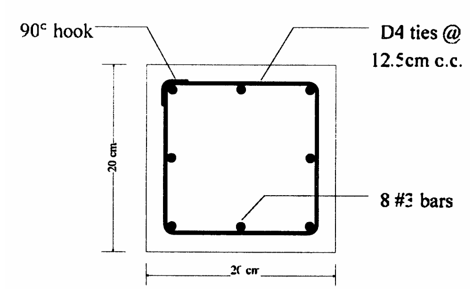

Fig. 1: Cross section and reinforcement details of column

Construction, and Material Strength Tests of Concrete and Steel Rebars

The frame specimens were constructed in an upright position and were moved into NCREE laboratory for storage 5 weeks after construction job was complete. The concrete mix was cast in two lifts, footings, and then columns and beams with a 1-week interval in between. After the construction was complete, wet curing was continued for another 2 weeks. Standard concrete cylinders (15cm diameter by 30cm high) were cast at the days of concrete pour, and then cured at the same condition as frame specimens. Compressive strength tests of concrete cylinders were conducted at the same days of the tests. Their strength at different age after casting is shown in Figure 2, and tensile test result of #3 bars used as the longitudinal reinforcement of columns is also shown.

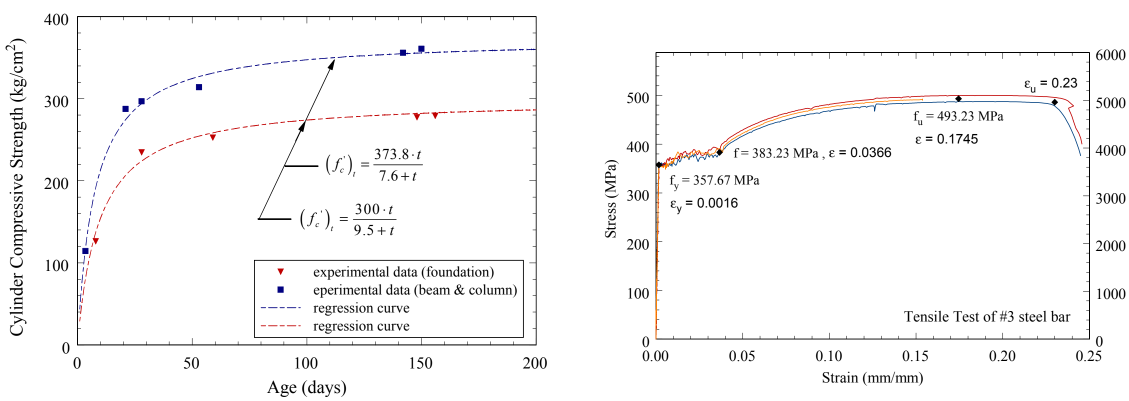

Fig. 2: Concrete cylinder compressive strength (left), and #3 steel bar tensile strength tests (right)

Experimental Setup

A photographic view of the experimental setup is shown in Figure 3. The test frame configuration and reinforcement details can be referred to in Loh et al. (2004). A supporting steel frame system was provided inside the table to prevent out-of-plane movement of the frame specimen. Another protective beam system was installed outside the table to catch the specimen from hitting the shake table when global collapse occurred. The experimental setup aims for instrumented observation of global dynamic collapse of low ductility columns. To do so, load cells, accelerometers, Temposonic linear displacement transducers (LDTs), inclinometers, and strain gages were employed to collect experimental data of engineering interest, which are helpful in finding how a negative slope takes place and how specimen is capable of remaining in position when negative slope does occur. All these observations are very helpful in finding numerical solution methods related to dynamic stability problems to solicit the introduction of performance-based earthquake engineering.

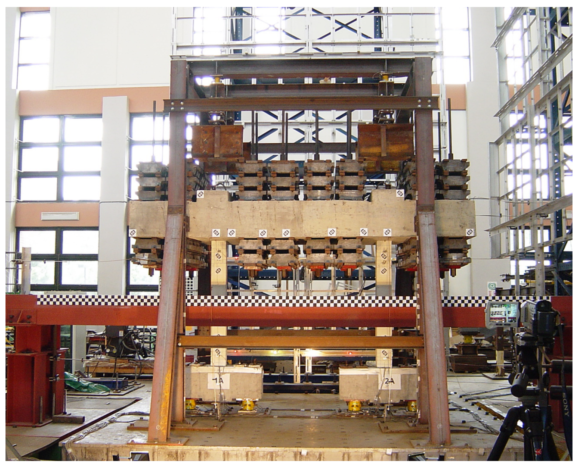

Fig. 3: Photographic view of the experimental setup

Input Ground Motions

Because a 1:2 geometric scale factor was taken for the test specimen, input ground motions should then be adjusted using a time compression factor of $\sqrt{0.5}$ on the basis of keeping unchanged acceleration scale factor (= 1). In the tests, the NS component of TCU076 accelerogram and the EW component of TCU082 accelerogram from the 1999 Chi-Chi Taiwan earthquake were applied to Specimens 2 and 3 as input ground motions, respectively, based on the following considerations:

1. Representative of main characteristics of near-fault earthquake motions in Taiwan. Especially, these 2 stations are located in central Taiwan, and are close to the target building studied. TCU076, stationed at Nantou Elementary School, is less than 250m from the 4-story target building, while TCU082 is some 30km away from the building. Frequency

contents of these two records consist of dynamic velocity pulses, but static fling step pulses, however, are not in the consideration of this study.

2. In addition to long-period velocity pulses, the frequency contents also consist of short to intermediate period motions such that a wide range of frequencies could be covered, and non-stationary evolution of frequency contents as observed in ordinary earthquake motions could be put into consideration. As such, excitation force will be able to remain in the same intensity level even when columns sustain damage and structural period lengthens accordingly.
3. Finally, spectral values of selected ground motions have to meet the capacity limitation of the shake table.

The selected ground motions, after modulated with a trapezoidal frequency domain filter from 0.2Hz to 20Hz, were scaled to the PGA levels at which test specimens will experience global collapse. In Figure 4, shake table capacity is given in the performance spectrum, including maximum displacement, maximum velocity, and maximum acceleration for a given operating frequency either with a bare table or with a payload of test specimen. It is seen that achieved table motion is of a broadband nature, but still contains velocity pulses.

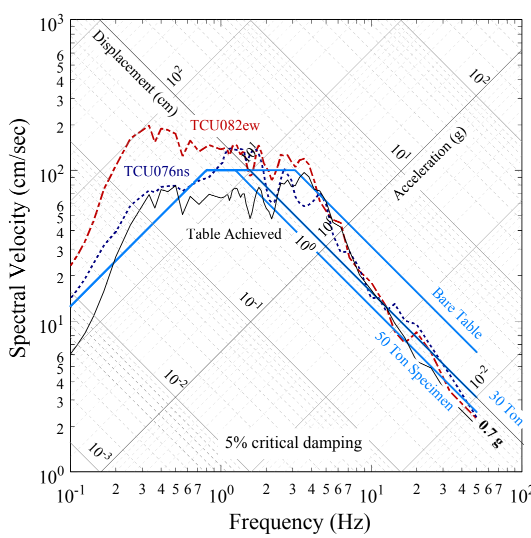

Fig. 4: Tripartite response spectrum of table achieved motion applied to Specimen 3 at 0.63g PGA level. Also shown are table performance curve and tripartite response spectra of TCU076NS and TCU082EW.

TEST PROCEDURES AND RESULTS

A total of 3 portal frames with the same design were built. There was a pre-collapse test of Specimen 1 (Wu et al. 2004) before the actual collapse tests took place. This paper, however, will focus on discussing collapse test results of Specimens 2 and 3. Before full intensity input earthquake motions were applied, low-level 25-gal white noise excitation was first employed to determine structural periods of test frames; results of these are shown in Table 1. Full intensity motions were applied to specimens for observation of the flexural-shear-axial failure sequence. Progressive collapse snapshots are shown in Figs. 5-6. In Specimen 2 more flexural deformation was observed, while in Specimen 3 shear deformation made a major contribution in the column failure. In Specimen 2, flexural hinges were completely formed shortly after shear cracking initiated.

Displacements of test frames were monitored using both Temposonic LDTs and consumer mini DV camcorders, and comparisons are plotted in Figure 7. Displacement histories were obtained from video films through image processing techniques. For this purpose an small in-house computer code ImPro was written, which in general should feature the following components: (1) conversion of pixel into length unit (e.g., mm, in, etc.), (2) automatic tracking of target, (3) calibration of image distortion due to optical lenses, and stereo distortion resulted from geometric relationship between specimen and camcorder, (4) synchronization between video films, (5) synchronization of initial time and sampling rates between video films (1/30s) and shake table data acquisition system (0.005s). Since camcorders were zoomed in to record small local areas of the column hinges and were elevated at appropriate heights as the column hinges to minimize distortions as much as possible to a negligible level, the 3rd component abovementioned thereby was not implemented in ImPro at the current stage. In addition, it is advised that fixed-focus filming is always preferred to minimize computational efforts in calibrating image distortion. For those who have sufficient budget and also need high accuracy, high-speed cameras will be a much better choice because they record non-interlaced images and usually have a high resolution of at least 1000×1000 pixels. In this study, a resolution of 640×480 pixels was obtained in the avi-format files of Matlab regardless of the resolution of camcorders, and finally an accuracy of ±0.42mm ~ ±1.15mm was achieved depending on the area that the camcorder taped. From Figure 7, numerical results from image processing look satisfactory, and observations show that camcorders yield longer displacement histories than Temposonic LDTs since Temposonic sensors reached their stroke limit before tests could be completed. Obtained hysteretic loops are shown in Figure 8. Specimens went through a couple of hysteretic cycles with negative slopes before they actually collapsed.

Although both specimens demonstrated basically a flexural-shear-axial failure pattern, yet there is distinct difference between the two specimens most likely because of the difference in input motions. Axial load, shear force, vertical displacement, and lateral drift are plotted in Figures 9-10. The loss of gravity load carrying capacity of columns is not obvious in Specimen 2, because flexural hinge made a significant contribution to structural collapse. It is mentioned that hysteretic model is not capable of predicting serious fluctuation observed at the final stage of the collapse test, so this collision-induced fluctuation is not plotted in Figures 8–10.

The experimentally obtained hysteretic loops impose important implications on engineering practice; especially the segment with negative slope will help in determining failure point of structural components and system. Figure 10 plots together the backbone curves suggested by Elwood (2002) with our experimental results. Included in the figure are base shear strength converted from nominal moment capacity following ACI procedures and shear strength calculated according to Sezen (2000). The comparison shows that Moehle and his co-workers proposed a conservative backbone curve prediction, which at the current stage is very positive in promoting collapse consideration among engineering community. With more collapse experiments conducted worldwide in the near future, the Moehle empirical formula should be able to evolve into a new form with adequate accuracy. Also plotted in Figure 10 are static pushover results calculated through OpenSees software, in which the numerical model used will be described in the next section.

Table 1: Structural periods obtained from white noise excitation results

Specimen No.	Weight (metric ton)		½-scale T_1 (sec)	½-scale f_1 (Hz)	Prototype 4-story T_1 (sec)	Lead Packets (metric ton)
2	8.72	Beam: 7.373 Columns: 0.347 Foundations: 1	0.366	2.73	0.518	21.35
3	9.42	Beam: 8.073 Columns: 0.347 Foundations: 1	0.427	2.344	0.604	21.35

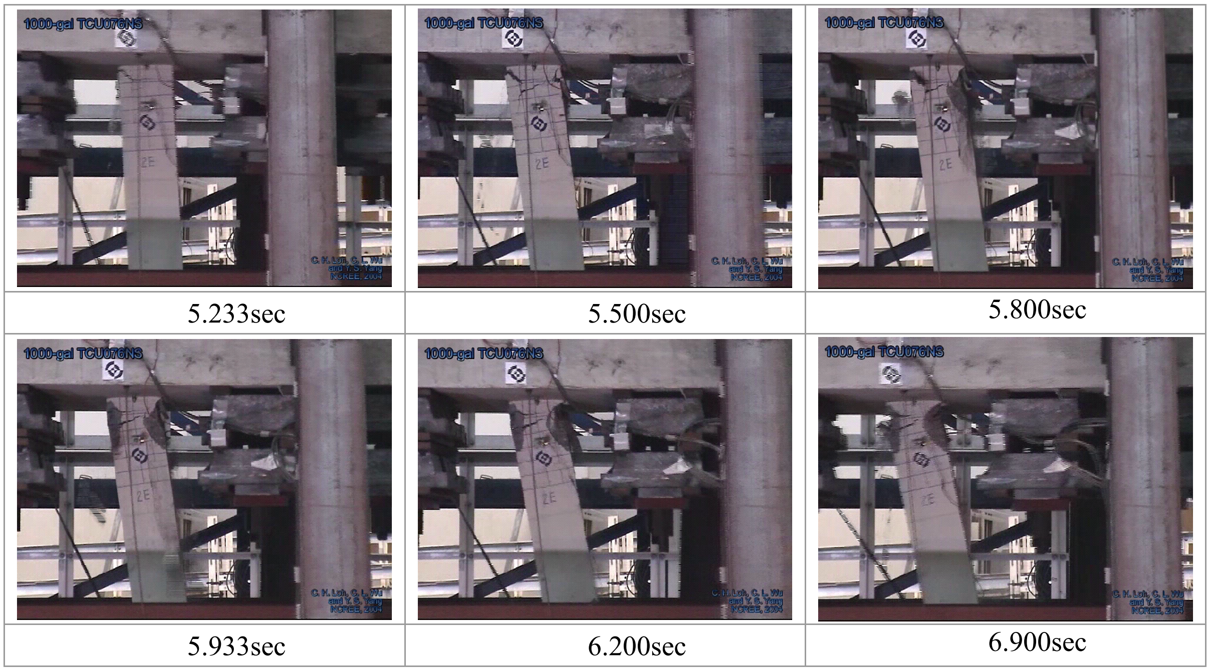

Fig. 5: Close up snapshots of collapse mechanism at the top of Specimen 2 north column

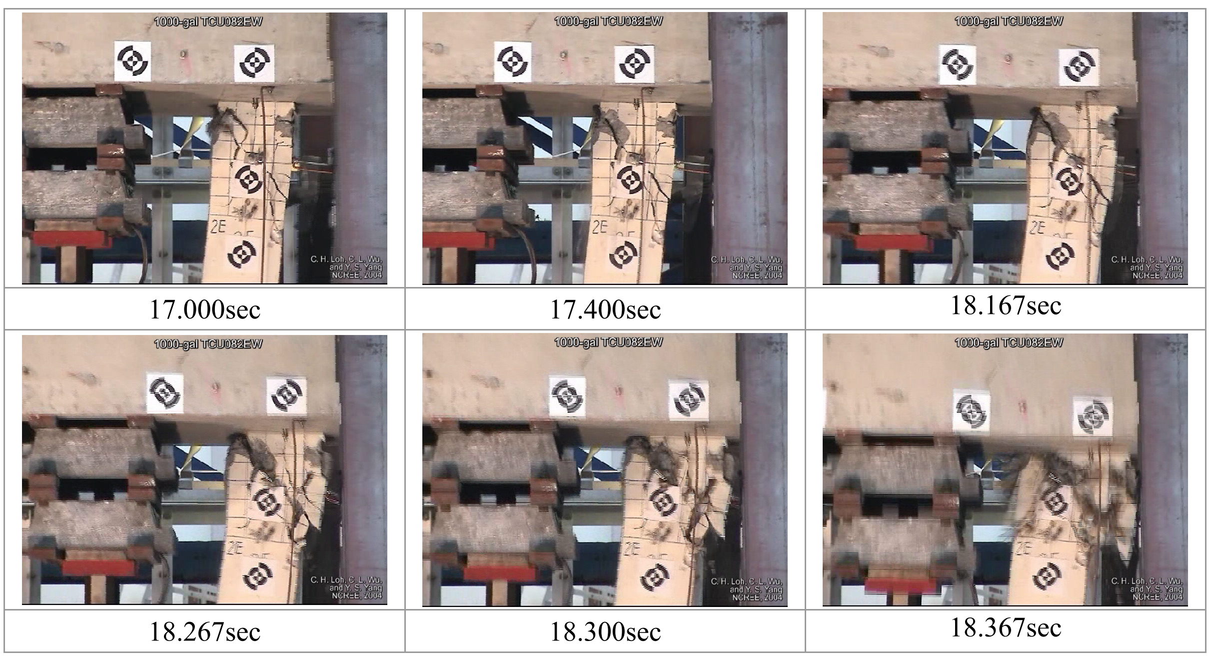

Fig. 6: Close-up snapshots of collapse mechanism at the top of Specimen 3 north column

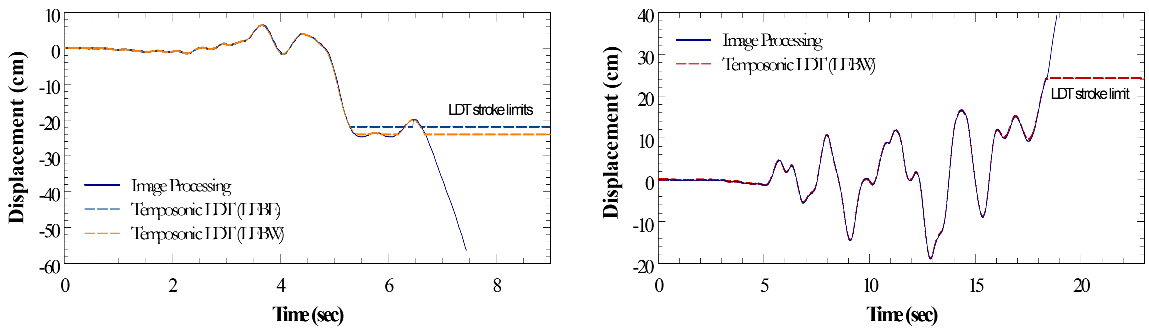

Fig. 7: Comparison of roof drift histories obtained by Temposonic LDTs and image processing technique: Specimen 2 (left) and Specimen 3 (right)

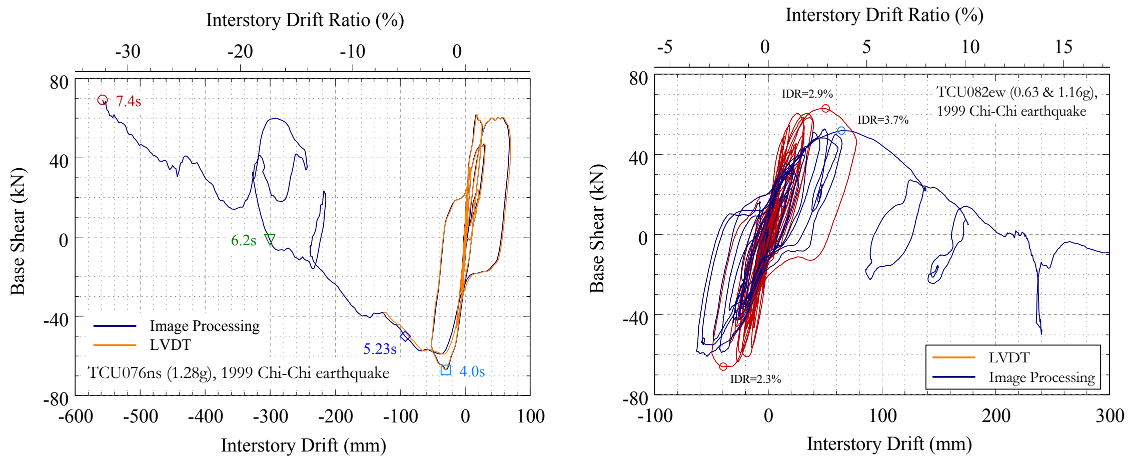

Fig. 8: Base shear vs. interstory drift hysteretic loops: Specimen 2 (left) and Specimen 3 (right, red trace subjected to TCU082ew at 630gal, and blue trace 1.16g PGA)

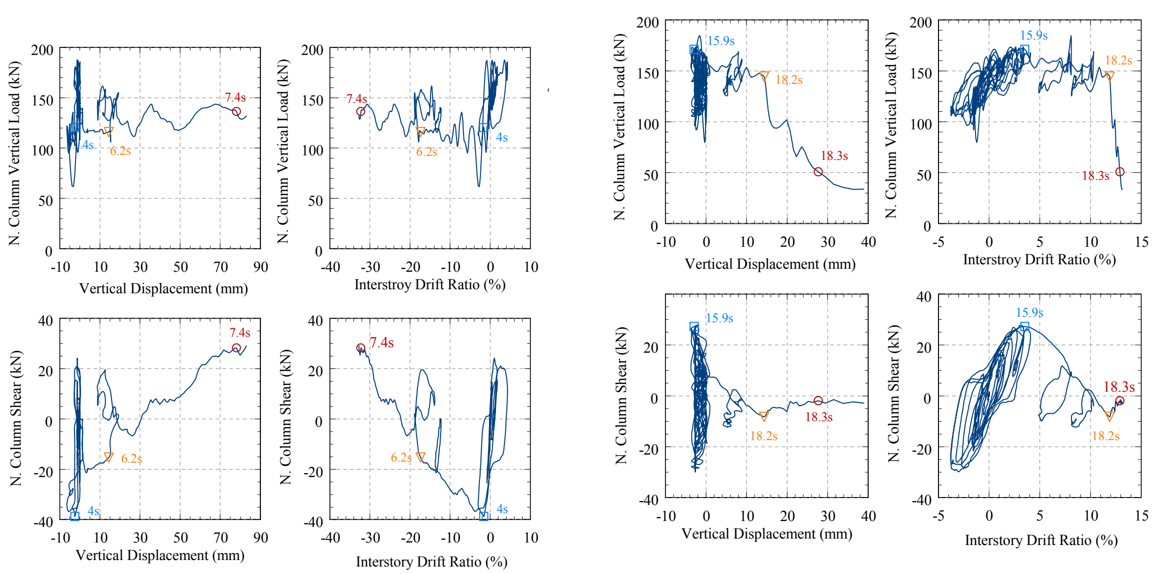

Fig. 9: Relations between north column axial load, vertical displacement, shear force, horizontal displacement of Specimen 2 (left) and Specimen 3 (right)

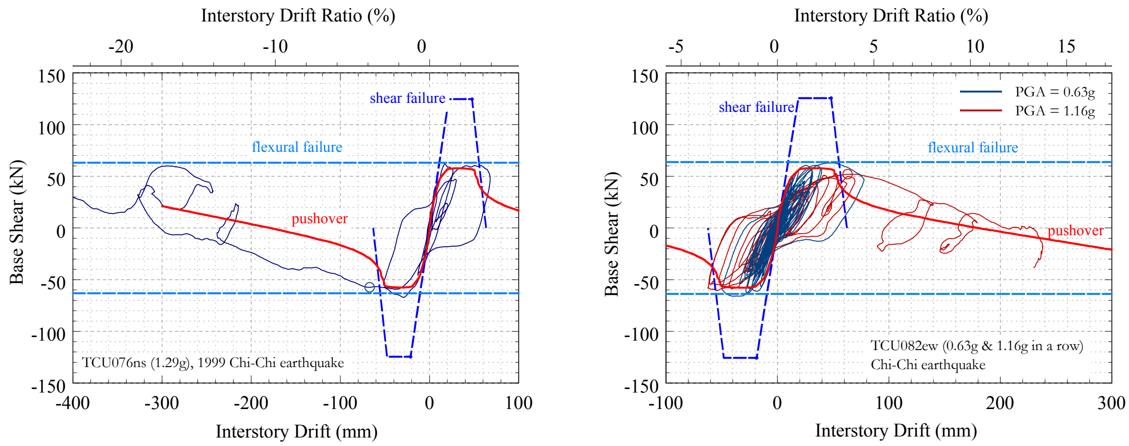

Fig. 10: Experimentally obtained hysteretic loops in comparison with Elwood-Moehle empirical curves: Specimen 2 (left) and Specimen 3 (right); also shown are pushover analysis results (red lines)

PRELIMINARY NUMERICAL SIMULATION

Numerical dynamic simulation was conducted to investigate the capability and limitation to simulate the collapse experiment using beam-column-based finite element analysis technology. Fiber section technique was employed to simulate the complicated nonlinear properties of steel-concrete composite sections. In this work, a well known finite-element based analysis package OpenSees 2004 was used. This section presents the numerical analysis result of both specimens subjected to TCU076ns and TCU082ew near-fault motions, respectively.

Figure 11(a) shows the numerical model of the frame specimen. OpenSees displacement-based nonlinear beam-column elements were used to model the strong beam and two low-ductility columns. Added masses were rigidly fixed onto the beam. The protective beam system (i.e., the giant red steel beam in Fig. 3) was simulated by two vertical beam-column elements at both sides, which used a gap material and would take effect to support the specimen beam whenever the specimen collapsed and its strong beam dropped down by 45 centimeters. The displacement-based element type requires a section model to represent flexural, axial, torsional and shear mechanical properties on the integration points along an element. In this work, the section model for the two columns was aggregated by a fiber section model and a torsional section model. The fiber section model was composed of steel fibers and concrete patches. The torsional section was given a high stiffness because the specimen mainly maintained an in-plane movement during the entire test. Figure 11(b) shows the levels of steel/concrete materials, sections and the beam-column element model. In the fiber section of columns, a confined concrete patch was assumed for the core concrete inside the perimeter hoop, while unconfined concrete patch was assumed for cover concrete outside the hoop. The steel and concrete material behavior was described by OpenSees embedded steel02 and concrete02 models based on material strength test results. The actual table-achieved motions during the experiments were used as the input ground motions in our numerical simulation. More detailed description of the numerical model can be referred to Yang et al. (2005).

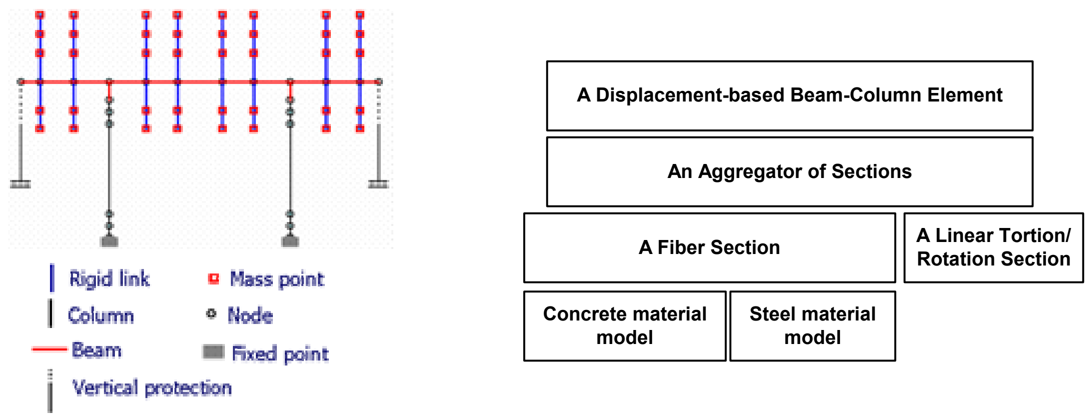

Fig. 11: (a) Schema of the numerical model; (b) levels of steel/concrete materials, sections and the beam-column element model

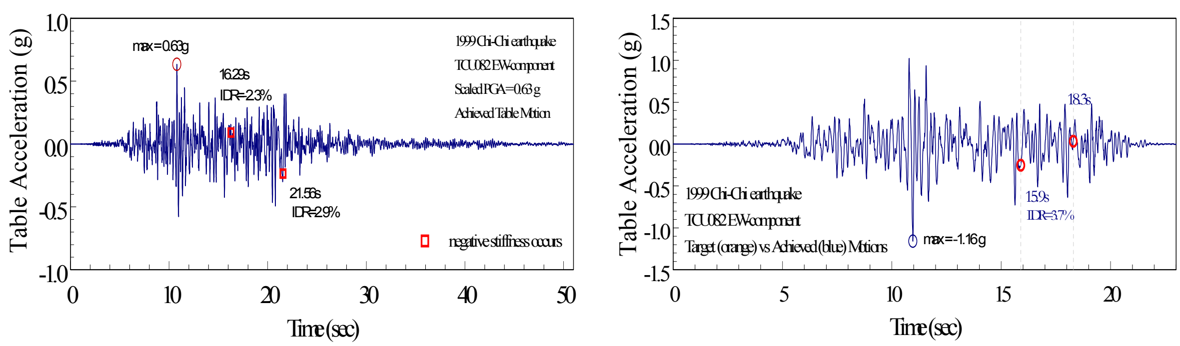

Fig. 12: Specimen 3 subjected to (a) first input motion at 0.63g; (b) second input motion at 1.16g

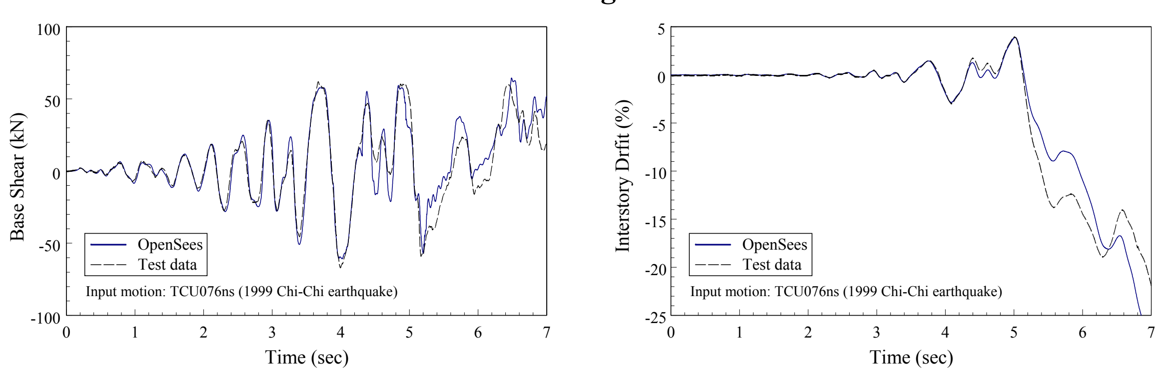

Fig. 13: Comparison of OpenSees simulation and test results of Specimen 2: (a) total base shear time history, (b) roof drift time history

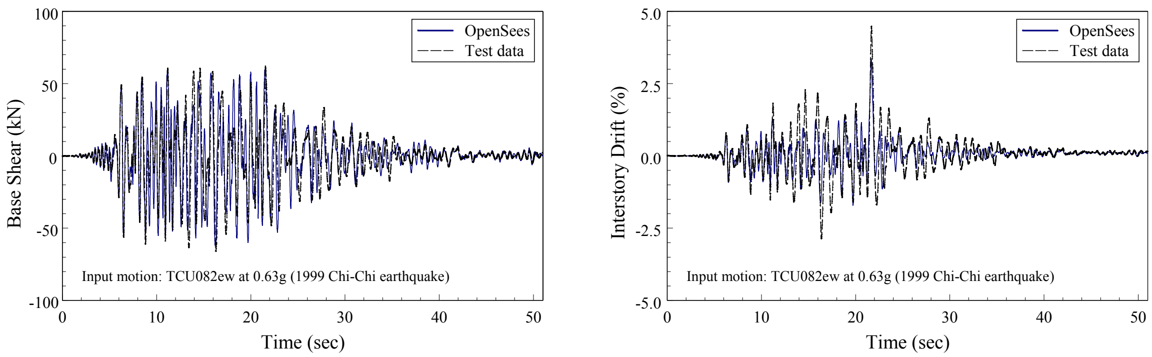

Fig. 14: Comparison of OpenSees simulation and test results of Specimen 3 (loading protocol TCU082ew at 0.63g): (a) total base shear time history, (b) roof drift time history

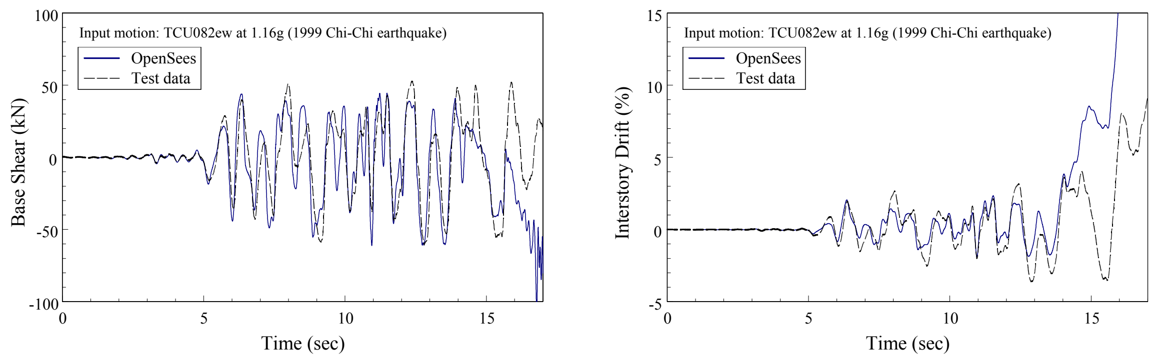

Fig. 15: Comparison of OpenSees simulation and test results of Specimen 3 (loading protocol TCU082ew at 1.16g): (a) total base shear time history, (b) roof drift time history

Two different ground motions, both of near-fault characteristics, were used in this study. Specimen 2 was subjected to TCU076ns at 1.28g PGA level, while Specimen 3 was subjected to TCU082ew at 0.63g and 1.16g intensity levels in a row in order to reach its structural collapse. OpenSees simulation results were presented in Figures 13–16. Because Specimen 2 shows more flexural behavior in its response, numerical analyses using OpenSees embedded element models well predicted base shear and roof drift time history. On the other hand, Specimen 3 demonstrated more shear deformation in its structural failure as seen in Figure 6. Current OpenSees model takes into account only the flexural contribution such that roof drift prediction still needs to be improved. Same could be said to the calculated hysteretic loops (Fig. 16). Generally speaking, the numerical analyses well predicted maximum base shear force. This is because shear force does not vary significantly in the nonlinear plateau. It is mentioned that at the final stage of structural collapse high-frequency fluctuation in the shear force time history will be observed because of the impact force between the test specimen and the (physical/numerical) protective beam.

CONCLUSIONS

Global collapse and dynamic structural post-peak behaviors were presented in this study using low-ductility columns and near-fault ground motions in the 1999 Chi-Chi earthquake. It is observed that failure mechanism varies for frames with the same design detail but subjected to different motion histories. This unique observation needs further investigation before confident conclusions can be drawn. Test results obtained provide a great database for calibrating existing numerical simulation methods to account for post-peak behaviors. This type of shake table tests may be used as benchmark problems for establishment of advanced numerical simulation methods. In addition, image processing technique was introduced to monitor large displacement of the specimen with success.

ACKNOWLEDGEMENTS

This research is funded in part by the National Science Council of Taiwan under grant number NSC92-2811-E-002-023. This financial support is gratefully acknowledged. Experimental facilities and technical support from NCREE are much appreciated. Special thanks are extended to Pei-Yang Lin and Lu-Sheng Lee for their assistance in conducting shake table tests. All opinions expressed in this paper are solely those of the authors, and, therefore, do not necessarily represent the views of the sponsor.

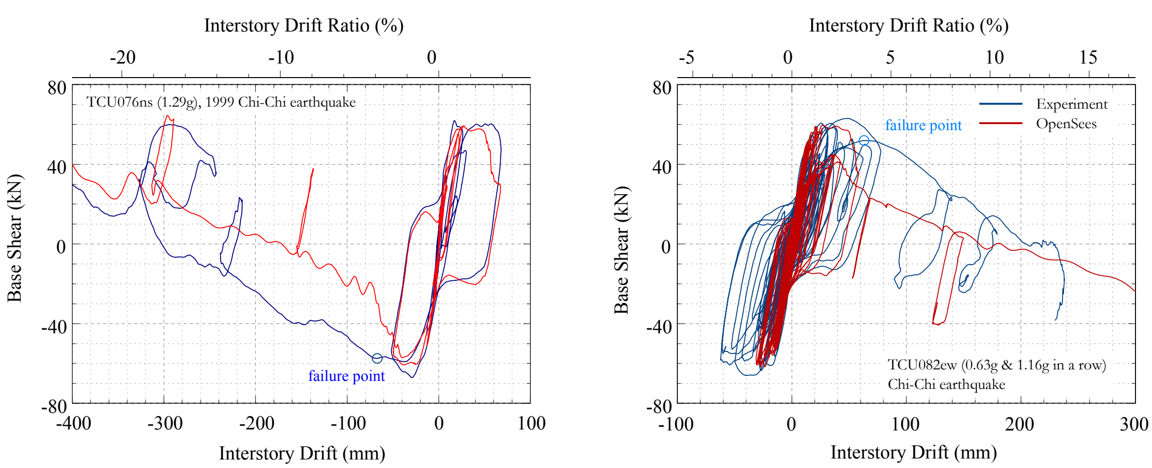

Fig. 16: Calculated base shear vs. roof drift hysteretic loops compared with test results: Specimen 2 (left), and Specimen 3 (right)

REFERENCES

Elwood, K. (2002). *Shake table tests and analytical studies on the gravity load collapse of reinforced concrete frames*, PhD dissertation, Department of Civil and Environmental Engineering, University of California, Berkeley (adviser: J.P. Moehle).

ImPro (2004). Program developers: Y.S. Yang and C.L. Wu, in-house computer code, National Center for Research on Earthquake Engineering, Taiwan.

Kim, Y. and Kabeyasawa, T. (2004). "Dynamic test and analysis of an eccentric reinforced concrete frame to collapse," *Proc. of the 13th World Conference on Earthquake Engineering*, Paper No. 381, Vancouver, B.C., Canada, August 1-6.

Yang, Y. S., Wu, C. L., and Loh, C. H. (2005). *Numerical Simulation of Shake Table Tests on Gravity Load Collapse of Low-Ductility RC Frame*, Technical Report (in preparation), National Center for Research on Earthquake Engineering, Taiwan.

Loh, C. H., Hong, L. P., Wu, C. L., Liao, W. Y., and Yang, Y. S. (2004). "Evaluation of maximum drift demand for seismic performance assessment of RC buildings," *International Conference in Commemoration of 5th Anniversary of the 1999 Chi-Chi Earthquake*, September 8-9, Taipei, Taiwan.

OpenSees (2002). *Open System for Earthquake Engineering Simulation* (opensees.berkeley.edu), Berkeley, Calif.: Pacific Earthquake Engineering Research Center, University of California.

Sezen, H. (2000). *Seismic Behavior and Modeling of Reinforced Concrete Building Columns*, PhD dissertation, Department of Civil and Environmental Engineering, University of California, Berkeley (adviser: J.P. Moehle).

Tassios, T. P. (1992). "Modelling of structures subjected to seismic loading" in Noor, F. A. and Boswell, L.F. (Editors), *Small Scale Modelling of Concrete Structures*, 229-271, Elsevier Science, New York.

Vian, D. and Bruneau, M. (2003). "Tests to structural collapse of single degree of freedom frames subjected to earthquake excitations." *ASCE Journal of Structural Engineering*, 129(12), 1676-1685.

Wu, C. L., Loh, C. H., Yang, Y. S. and Lin, C. H. (2004). "Consideration of collapse and residual deformation in reliability-based performance evaluation of buildings," *Proc. of the 13th World Conference on Earthquake Engineering*, Paper No. 716, Vancouver, B.C., Canada, August 1-6.

A NONLINEAR MODEL FOR THE SEISMIC ASSESSMENT OF RC COLUMNS WITH SHORT LAP SPLICES

José A. PINCHEIRA[1] and Jae-Yeol CHO[2]

ABSTRACT

Short, poorly confined lap splices are a common deficiency in columns of reinforced concrete frames built in the 1970s in the United States. The available experimental evidence shows that such columns may fail prematurely with reduced lateral strength and deformation capacity. In this paper, a modeling and analysis procedure for estimating the response of columns with short lap splices subjected to cyclic load reversals is presented. The model is based on local bond stress-slip relationships and is compared with experimental data on isolated columns from three independent investigations. The results show that the strength of the columns can be predicted very well using local bond-slip models derived from isolated anchored bars. In addition, the lateral load and deformation response as well as the calculated failure mode are found to be in very good agreement with the observed values.

1. INTRODUCTION

Reinforced concrete frames constructed in the early 1970s or before in the United States were generally designed and detailed to resist much lower lateral forces than those required by today's standards. In particular, building columns were often considered as compression members with lap spliced bars designed to transmit only compressive forces. The splice length specified in these columns was often short (20 or 24 longitudinal bar diameters) and poorly confined. The typical construction practice was to locate lap bar splices immediately above the slab in each floor where large moment reversals may be expected to occur during strong ground motion. Because of the limited tensile capacity of the splices, the section at the base of the column is often susceptible to premature lap splice failure before yielding of the longitudinal bars. Even if yielding of the longitudinal reinforcing bar is developed, splice failure can still occur shortly after yielding of the bar.

In this paper, the results of a nonlinear analysis procedure to compute the seismic response of reinforced concrete columns with short lap splices are presented. The reliability and accuracy of the modeling procedure is evaluated by comparing the calculated response with experimental data obtained from three independent research programs.

---

[1] *Associate Professor, Dept. of Civil and Env. Engr., University of Wisconsin - Madison, USA*
[2] *Former Post Doctoral Fellow, Dept. of Civil and Env. Engr., University of Wisconsin - Madison, USA*

2. DESCRIPTION OF THE MODEL

In lap splices, the bars interact with each other in a complex force transfer mechanism. The majority of the experimental work on lap splices has been conducted on beams, and it has focused primarily on splice strength rather than on the local bond transfer and deformation mechanism in the splice region (Darwin and Graham 1993, Plizzari et al. 1996, Azizinamini et al. 1999). More recent studies on columns with short lap splices (Aboutaha et al. 1996, Lynn et al. 1996, Melek and Wallace 2004) have yielded valuable information in terms of the overall response of columns with such details and provided further insight into their deformation capacity. However, specific studies on the local bond–slip behavior of lap splices do not exist. Experimental studies have found, however, that the cracking and splitting behavior of splices is similar to that of anchored bars. For simplicity and in the absence of appropriate relations for lap spliced bars, it is postulated that the local bond stress and slip relations obtained for a single bar embedded in concrete may be used to simulate the behavior mechanism of lap spliced bars. Based on this assumption, the local bond stress and slip relation obtained from isolated bars are used in this study.

Local bond-slip relationships of isolated bars have been proposed by a number of investigators in the past (Hawkins et al. 1982, Eligehausen et al. 1983, Ueda et al. 1987, Pochanart and Harmon 1989, Soroushian and Choi 1989, Soroushian et al. 1991, Harajli 1994, Harajli and Mabsout 2002). These and other studies have identified two types of bond failure between the reinforcement and concrete according to amount of confinement around the bar. If the surrounding concrete is large and the concrete is well confined by transverse reinforcement, bond failure occurs by pullout. On the other hand, if the surrounding concrete is small and the concrete is unconfined or poorly confined, bond failure occurs by splitting of surrounding concrete. Therefore, experimentally derived local bond stress-slip models are often composed of two separate equations for unconfined and confined concrete.

Previous researchers (Soroushian 1989, Popov 1984) have suggested the use of a one-dimensional multi-spring model to idealize the behavior of reinforcing bars embedded in concrete (Fig. 1). In this model, the reinforcing bar is divided into several small segments, where each bar segment is attached to a bond-slip spring that represents the local bond resistance on the bar surface. Knowing the stress-strain relationship for the bar and with the characteristic bond stress-slip relation, the pullout force P and anchorage slip Δ_{slip} can be calculated.

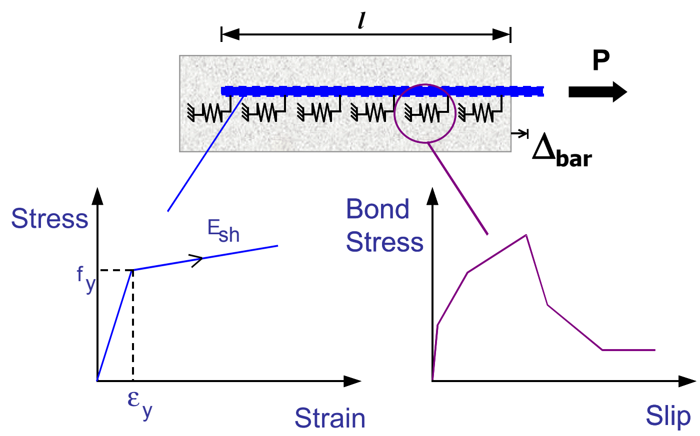

Fig. 1: Uniaxial multi-spring model of an isolated anchored bar

In this study, several local bond-slip relations found in the open literature (Hawkins et al. 1982, Eligehausen et al. 1983, Ueda et al. 1987, Pochanart and Harmon 1989, Soroushian and Choi 1989, Soroushian et al. 1991, Harajli 1994, Harajli and Mabsout 2002) were compared against experimental data obtained from well-documented tests conducted by other researchers (Eligehausen et al. 1983, Ueda et al. 1987, and Grundhoffer 1992). Based on this comparison, the model proposed by Harajli and Mabsout (2002), shown in Figure 2, was found to provide the best agreement between the calculated and measured response, and thus it was chosen for this study.

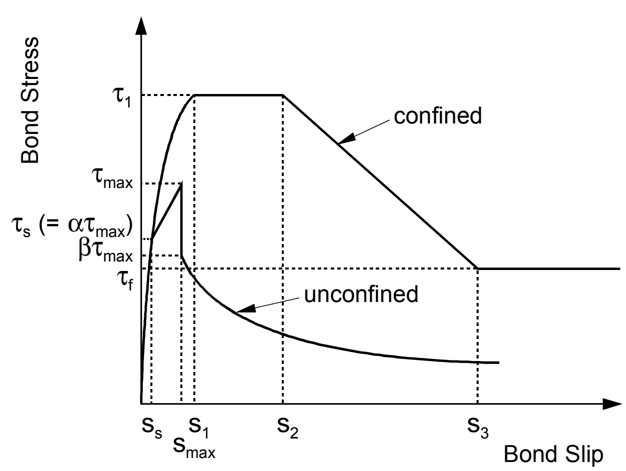

Fig. 2: Local bond stress-slip relation considered for modeling of columns with short lap splices (Harajli and Mabsout 2002)

2.1 Analysis Procedure

Three resistance mechanisms are used to describe the response of older reinforced concrete columns. These mechanisms are illustrated in Figure 3 and include the contributions from flexure, shear and anchorage slip of the spliced reinforcement. Figure 4 depicts the typical profile of the columns studied and the corresponding computer model. A main element, whose length was the same as the clear length of the column, was used to model the contributions of flexure and shear. This member consisted of an elastic beam-column element with a nonlinear rotational spring at the base and a shear spring. The additional deformations caused by bond-slip of the lap splices were modeled separately by a nonlinear rotational spring atop of a rigid element added at the base as shown in Figure 4.

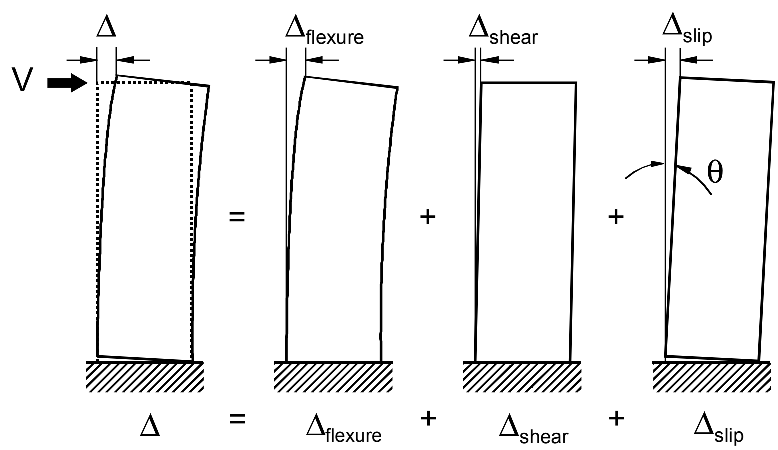

Fig. 3: Deformation mechanisms considered in this study

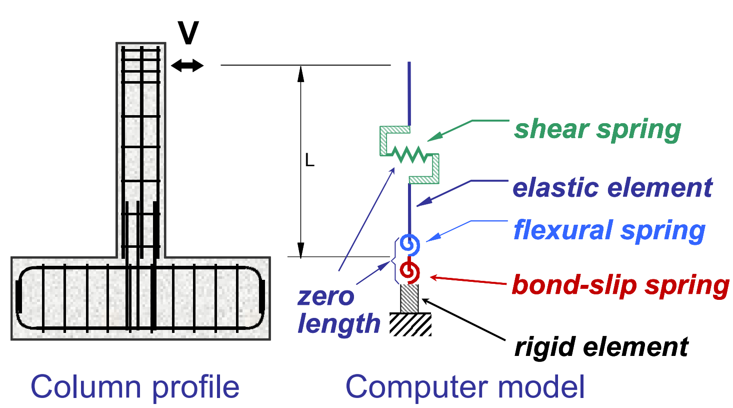

Fig. 4: Computer model of reinforced concrete column with short lap splices

Figure 5 shows the backbone and typical hysteretic laws of the flexural and bond-slip springs. Hysteretic laws include both stiffness and strength degradation with increasing deformation amplitude, and with repeated inelastic excursions. These laws were included in the program DRAIN2D and are described in more detail elsewhere (Pincheira et al. 1999, Barin and Pincheira 2002). In addition, the descending portion of the backbone curve was modified in this study by adding a trilinear relation in order to better represent the softening portion of the modified Harajli's unconfined, bond-slip model (Fig. 2).

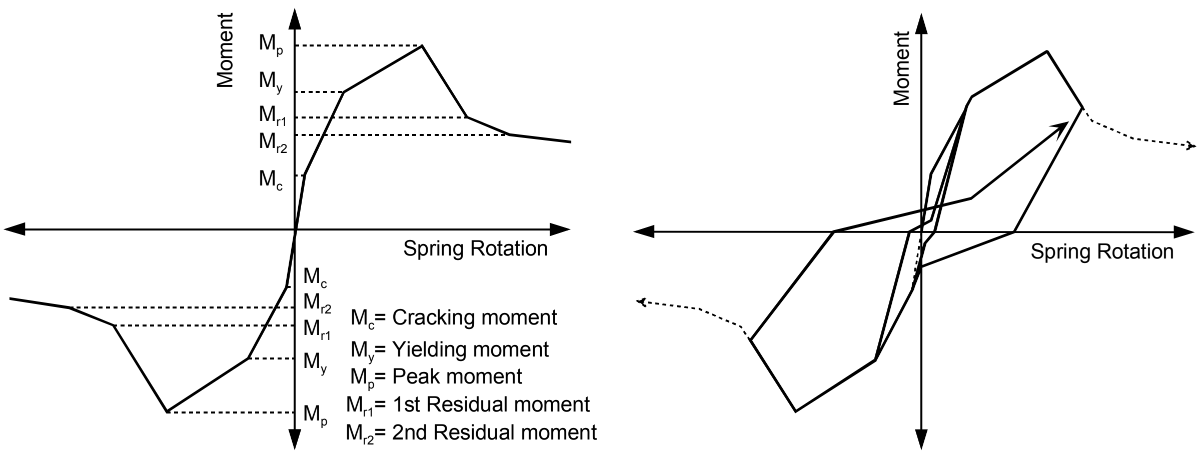

(a) backbone curve (b) hysteretic laws

Fig. 5: Typical hysteretic laws of the nonlinear rotational spring elements

Moment-rotation backbone curves for the nonlinear flexural spring were calculated from moment-curvature relationships including the effects of axial forces using the program BIAX (Wallace 1992). Although most of the columns studied had widely spaced ties that provided little confinement to the concrete core, the modified Kent and Park stress - strain relationship (1982), for both unconfined and confined concrete were used. A yield plateau followed by strain hardening characterized the stress-strain relations of the steel reinforcement. The material properties were based on measured values from laboratory tests. The continuous moment-curvature relationships were then approximated by a multi-linear curve to construct the backbone curves (Fig. 5).

While the columns studied here were not expected to exhibit a shear dominated behavior, a nonlinear shear spring was included in the models. The Modified Compression Field Theory (MCFT) (Vecchio and Collins 1986) provides a general approach for calculating the shear force and shear distortion response of reinforced concrete members, including the effects of flexure and axial force. Here, the shear force-shear distortion backbone curve of the studied columns were calculated using program RESPONSE 2000 (Bentz 2001).

Bar force and slip relationships of the lap splices were calculated using the multi-spring model described earlier (see Fig. 1). Based on these relationships, end rotations due to bar slip including bar extension at the base of the columns were calculated using the recommendations of Razvi and Saatciouglu (1996).

3. COMPARISON OF ANALYTICAL MODEL WITH EXPERIMENTAL RESULTS

In this section, the calculated response was compared with experimental data obtained from three independent investigations (Aboutaha et al. 1996, Lynn et al. 1996, Melek and Wallace 2004). The dimensions and properties of the columns studied are presented and Table 1. Columns FC1, FC4, FC5, FC14, and FC15 were tested at the University of Texas at Austin, while columns 2SLH18, 3SLH18 and 3SMD12 were tested at the University of California at Berkeley. The rest of the columns studied were tested at the University of California at Los Angeles. The longitudinal reinforcement was lap spliced over a length of either 20 or 24 bar diameters, immediately above the foundation block. Transverse reinforcement consisted of No. 3 reinforcing bars spaced at 12 or 16 inches and had 90-degree, non-seismic hooks. In all columns, the provided area of transverse reinforcement along the lap splice region was not enough to assume bond - slip relations for confined concrete. Therefore, local bond - slip relations for unconfined concrete were employed for all columns. All of the columns considered, were subjected to unidirectional reversed cyclic loads of prescribed deformation amplitudes. Further details of the dimensions, reinforcing details and loading history of the columns can be found elsewhere (Aboutaha et al. 1996, Lynn et al. 1996, Melek and Wallace 2004).

3.1 Cyclic Loading Response

Figure 6 shows a comparison between the measured and calculated shear force and drift ratio for selected columns FC15, 3SMD12, and S10MI. It should be noted that the hysteretic laws of the flexural, shear, and bond-slip springs are controlled by several parameters that account for stiffness and strength decay with loading cycles. Here, no attempt was made to adjust these parameters so as to obtain the best possible agreement between the calculated and measured response for each individual column. Instead, a common set of intermediate parameter values was chosen to represent a moderate decay rate in all of the columns.

Table 1: Dimensions and properties of columns studied

Researcher	Column	Column Dimensions			Longitudinal Reinforcement			Transverse Reinforcement		Concrete	Axial Load
		b [in]	h [in]	l [in]	Amount	l_s [in]	f_y [ksi]	Amount	f_y [ksi]	f_c' [ksi]	
Aboutaha et al.	FC1	36	18	108	16-#8	24	63	#3@16	58	4.70	0
	FC4	36	18	108	16-#8	24	63	#3@16	58	2.85	0
	FC5	36	18	108	16-#8	24	63	#3@16	58	2.98	0
	FC14	27	18	108	12-#8	24	63	#3@16	58	4.17	0
	FC15	18	18	108	8-#8	24	63	#3@16	58	4.17	0
Lynn et al.	2SLH18	18	18	116	8-#8	20	48	#3@18	58	4.80	$0.12A_gf_c'$
	3SLH18	18	18	116	8-#10	25	48	#3@18	58	3.71	$0.12A_gf_c'$
	3SMD12	18	18	116	8-#10	25	48	#3@12	58	3.70	$0.35A_gf_c'$
Melek and Wallace	S10MI	18	18	72	8-#8	20	74	#3@12	69	5.26	$0.10A_gf_c'$
	S20MI	18	18	72	8-#8	20	74	#3@12	69	5.26	$0.20A_gf_c'$
	S30MI	18	18	72	8-#8	20	74	#3@12	69	5.26	$0.30A_gf_c'$
	S20HI	18	18	66	8-#8	20	74	#3@12	69	5.13	$0.20A_gf_c'$
	S20HIN	18	18	66	8-#8	20	74	#3@12	69	5.13	$0.20A_gf_c'$
	S30XI	18	18	60	8-#8	20	74	#3@12	69	5.13	$0.30A_gf_c'$

b: width of column cross-section, h: height of column cross-section, l: clear height of column, l_s: splice length, f_y: yield strength of reinforcing bar, f_c': compressive strength of concrete, A_g: gross area of column cross-section.

The data show that the general characteristics of the calculated response agree very well with the measured response for the columns. For the common set of parameter values chosen here, the model tends to overestimate the amount of strength decay after peak resistance for the columns, but both stiffness and strength decay is well represented by the calculated response. Also, the post-peak behavior is very well represented by the trilinear descending portion assumed for the bond-slip spring. The response of the rest of the columns not shown here follows the same trends.

In Table 2, the measured and calculated lateral strengths are shown for all columns. The ratio between the measured and the calculated peak lateral load is also shown in the table. These data show that the calculated maximum lateral loads are in very good agreement with the measured values. The average measured-to-calculated strength ratio was 1.03 with a standard deviation of 0.09.

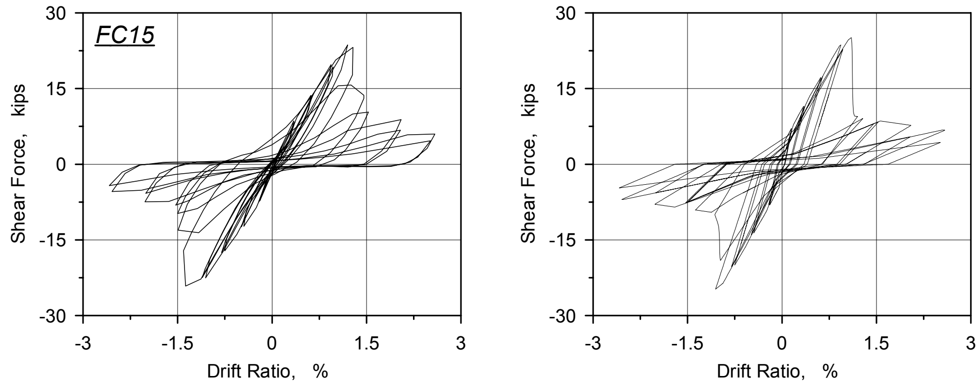

(a) measured – FC15 **(b) calculated – FC15**

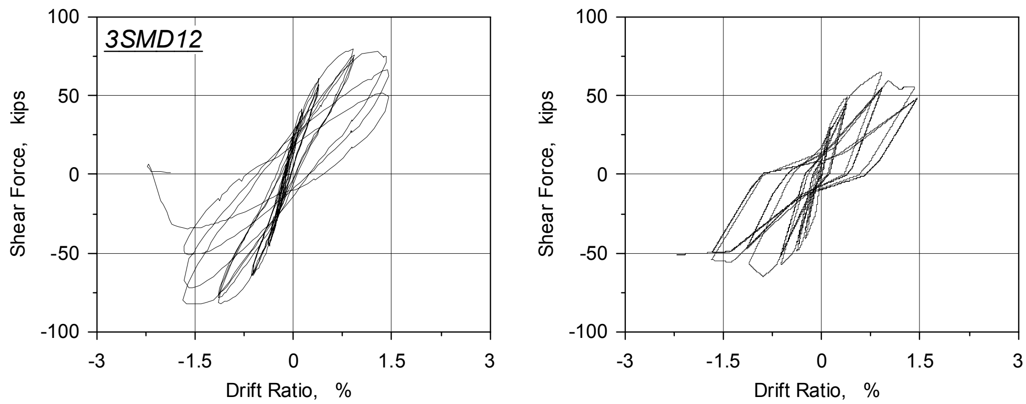

(c) measured – 3SMD12 **(d) calculated – 3SMD12**

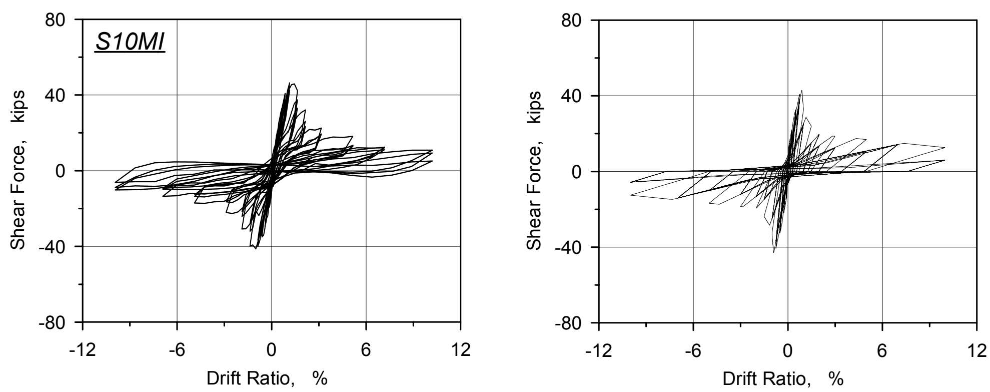

(e) measured – S10MI **(f) calculated – S10MI**

Fig. 6: Comparison of measured and calculated response of columns studied

Table 2: Measured and calculated strength and failure mode

Column Designation	Maximum Lateral Loads			Failure Modes	
	Measured $V_{meas,}$ [kips]	Calculated $V_{calc,}$ [kips]	V_{meas}/V_{calc}	Observed	Calculated
FC1	51	52.6	0.97	SpF	SpF
FC4	41	43.0	0.95	SpF	SpF
FC5	40	42.7	0.94	SpF	SpF
FC14	33	38.0	0.87	SpF	SpF
FC15	24	25.2	0.95	SpF	SpF
2SLH18	53	44.8	1.18	YiR, SpD, ShF	YiR, ShF
3SLH18	61	51.6	1.18	YiR, SpD, ShF	ShF
3SMD12	83	73.9	1.12	YiR, SpD, ShF	SpF
S10MI	46	43.2	1.06	SpF	SpF
S20MI	52	52.3	0.99	SpF	SpF
S30MI	64	60.6	1.06	SpF	SpF
S20HI	61	58.3	1.05	SpF	SpF
S20HIN	60	59.1	1.02	SpF	SpF
S30XI	77	70.9	1.09	SpF	ShF
Average(SD)			1.03(0.09)		

Also shown in the table are the observed and calculated failure modes. It may be noted that all calculated failure modes match those observed during the tests except for columns 3SMD12 and S30XI. Column 3SMD12 was reported to exhibit yielding of the longitudinal reinforcement followed by degradation of the splice region and to fail in shear (Lynn et al. 1996). The analysis showed, however, that splice failure would occur prior to a shear failure. Column S30XI was reported to exhibit splice failure as the dominant failure mode with visible shear damage (Melek and Wallace 2004). The calculated failure mode for this column was in shear.

3.2 Comparison with FEMA 356

In the United States, the current guidelines for seismic rehabilitation of buildings, FEMA 356 (2000), present generalized force–deformation relations for concrete elements or components to be used in nonlinear analysis procedures. For reinforced concrete elements with lap-spliced bars that do not meet the development requirements of ACI 318 (2002), the guidelines FEMA 356 2000) suggest that the capacity of the existing reinforcement be calculated as follows:

$$f_s = \frac{l_b}{l_d^{ACI}} f_y \tag{1}$$

where f_s = maximum stress that can be developed in the bar for the provided lap splice length l_b ; f_y = yield strength of reinforcement; and l_d^{ACI} = length calculated according to Equation (12-1) of ACI 318 (2002).

A comparison of Equation (1) with the experimental data and analysis results conducted here showed that Equation (1) consistently underestimated the splice strength of the columns by a large margin, and that there were two main reasons for this result. First, Equation (12-1) of ACI 318 (2002) for computing the development length, l_d^{ACI} , includes a resistance factor and thus it inherently leads to conservative estimates of the required development length for the bar. Second, the equation proposed in FEMA 356 (2000) uses a linear relationship between the bar stress and its development length whereas the actual relation is nonlinear.

Using a regression analysis of the bar stress and anchorage length relations obtained for various bar diameters, bar yield, concrete strengths and the results of this study, the following expression is proposed for estimating the bar stress for a given splice length,

$$f_s = \left(\frac{l_b}{0.8\, l_d^{ACI}} \right)^{2/3} f_y \qquad (2)$$

Equation (2) is a modified version of Equation (1) where the multiplier 0.8 in the denominator accounts for the conservatism of the development length equation of ACI 318 and it is based on the test data used here. The 2/3 power simply accounts for the nonlinear relation between the bar stress and the splice length.

Figure 7 shows the relationship between the bar stress and the anchorage length computed with uniaxial spring model for the bars in two columns (FC4 and S10MI). Also shown in the figure is the linear approximation proposed by FEMA 356 (2000) as well as the proposed relationship in Equation (2) for these bars. It may be seen that the combined conservatism of Equation (12-1) of ACI 318 (2002) and the linear approximation given by Equation (1) significantly underestimates the stress in these bars for a given development length. It can also be seen that the agreement between the proposed Equation (2) and the data is excellent except for very short development lengths which are outside of the range of practical interest. Although not shown in the figure, similar comparisons can be made for bars of different yield strengths embedded in concrete of various common strengths.

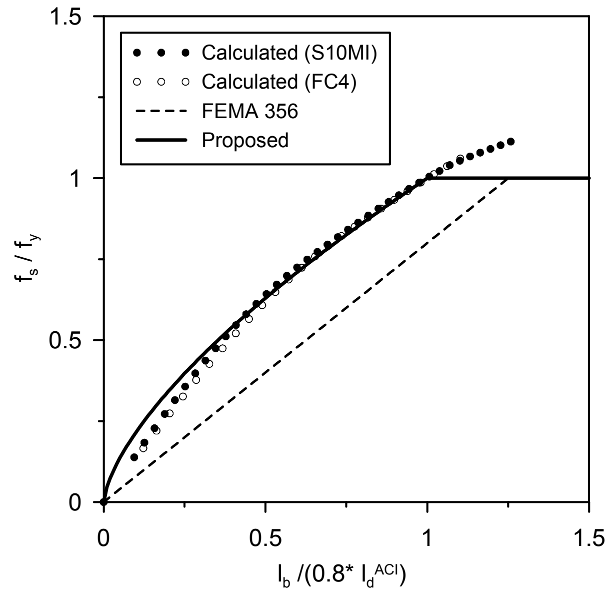

Fig. 7: Comparison between proposed Eq. (2) and calculated bar stress in columns FC4 and S10MI

In Figure 8, the measured moment at the base of the columns, M_{peak}^{meas}, is compared with the moment computed using the uniaxial spring model, M_{peak}^{model}, and proposed Equation (2), $M_{peak}^{proposed}$,at splice failure. Columns 2SLH18, 3SHL18 and 3SMD12 are excluded from this comparison because they were tested in double curvature. Thus, moment redistribution from the base (splice region) to the top of the column could have occurred prior to reaching the maximum lateral resistance. Therefore, the moment at splice failure was not known with certainty to the authors. It can be seen that the measured moment and that calculated based on the proposed equation are in excellent agreement. Clearly, the proposed equation provides as simpler alternative to the more refined spring model for calculating the bar stress at splice failure.

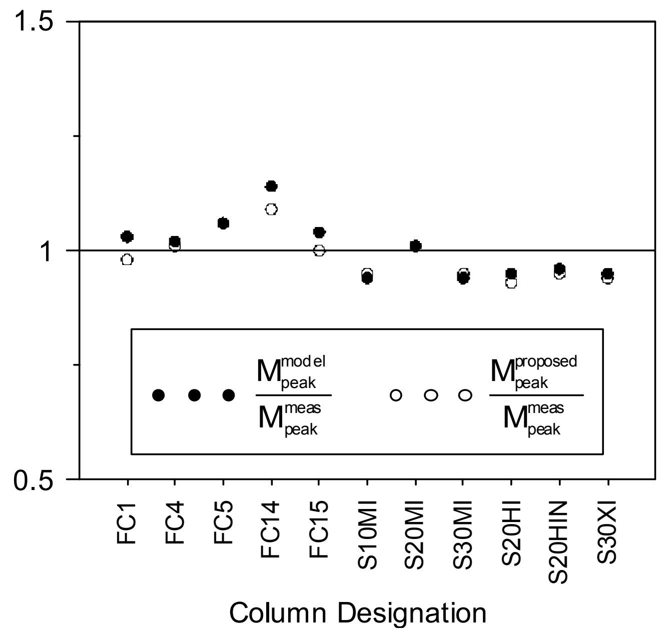

Fig. 8: Calculated-to-measured ratio of the moment corresponding to splice failure

4. CONCLUSIONS

A two-dimensional, nonlinear modeling and analysis procedure for the seismic assessment of reinforced concrete columns with short lap splices subjected to earthquake loading is presented. The reliability and goodness of the proposed procedure is evaluated by comparing the analytical results of the analyses with experimental data. Based on the results presented here, the following conclusions can be drawn:

(1) The strength of short lap splices can be predicted well using local bond-slip models derived from isolated anchored bars.

(2) The calculated lateral load resistance and calculated failure mode were in very good agreement with that observed in the experiments for the majority of the columns studied.

(3) The main aspects as well as the general characteristics of the measured response under cyclic loading were represented very well by the analytical model.

(4) The current equation presented in FEMA 356 significantly underestimates the bar stress at splice failure. Based on the results obtained in this study, a modified equation that results in improved estimates of the bar stress at splice failure is proposed.

5. ACKNOWLEDGEMENTS

The work presented in this paper was supported in part by a Post-doctoral Fellowship Program of Korea Science & Engineering Foundation (KOSEF) awarded to the second author. The authors wish to thank Messrs. Riyad S. Aboutaha, Michael D. Engelhardt, Abraham C. Lynn, Jack P. Moehle, Murat Melek and John W. Wallace for providing the experimental data used in this investigation. The opinions, findings and conclusions expressed in this paper are solely those of the authors and do not necessarily represent the views of the sponsor or the individuals mentioned here.

REFERENCES

Aboutaha, R.S., Engelhardt, M.D., Jirsa, J.O., and Kreger, M.E. (1996) Retrofit of Concrete Columns with Inadequate Lap Splices by the Use of Rectangular Steel Jackets. *Earthquake Spectra* 12(4):693-714.

ACI 318 (2002) Building Code Requirements for Reinforced Concrete American Concrete Institute, Detroit.

Azizinamini, A., Pavel, R., Hatfield, E., and Ghosh, S.K. (1999) Behavior of Lap-Spliced Reinforcing Bars Embedded in High-Strength Concrete *ACI Structural Journal* 96(5):826-835.

Barin, B., and J.A. Pincheira (2002) Influence of Modeling Parameters and Assumptions on the Seismic Response of an Existing RC Buildings M.S. Thesis, University of Wisconsin, Madison.

Bentz, E. (2001) Response-2000: User Manual University of Toronto, Toronto.

Darwin, D., and Graham, E.K. (1993) Effect of Deformation Height and Spacing on Bond Strength of Reinforcing Bars. *ACI Structural Journal* 90(6): 646-657.

Eligehausen, R., P.E. Popov, and V.V. Bertero (1983) Local Bond Stress-Slip Relationships of Deformed Bars under Generalized Excitations *UCB/EERC-83-23*, University of California.

FEMA 356 (2000) Prestandard and Commentary for the Seismic Rehabilitation of Buildings prepared by ASCE for Federal Emergency Management Agency, Washington D.C.

Grundhoffer, T.M., C.W. French, and R.T. Leon. (1992) Bond Behavior of Uncoated and Epoxy-Coated Reinforcement in Concrete *Structural Engineering Report No. 92-04*, University of Minnesota.

Harajli, M.H. (1994) Development/Splice Strength of Reinforcing Bars Embedded in Plain and Fiber Reinforced Concrete *ACI Structural Journal* 91(5):511-520.

Harajli, M.H., and Mabsout, M.E. (2002) Evaluation of Bond Strength of Steel Reinforcing Bars in Plain and Fiber-Reinforced Concrete. *ACI Structural Journal* 99(4):509-517.

Hawkins, N.M., Lin, I.J., and Jeang, F.L. (1982) *Local Bond Strength of Concrete for Cyclic Reversed Loadings*, Applied Science Publishers, London.

Lynn, A.C., Moehle, J.P., Mahin, S.A., and Holmes, W.T. (1996) Seismic Evaluation of Existing Reinforced Concrete Building Columns. *Earthquake Spectra* 12(4):715-739.

Melek, M. and Wallace, J.W. (2004) Cyclic Behavior of Columns with Short Lap Splices. *ACI Structural Journal* 101(6):802-811.

Park, R., Priestley, M.J. N., and Gill, W. D. (1982) Ductility of Square-Confined Concrete Columns *Journal of the Structural Division, ASCE.* 108(ST4):929-951.

Plizzari, G.A., Marchina, E., and Giuriani, E. (1996) Experimental Study of Splitting and Flexural Cracks in a RC Beams with Overlapped Splices *RILEM, Material and Structures* 29:19-27.

Pincheira, J.A., Dotiwala, F.S., and D'Souza, J.T. (1999) Seismic Analysis of Older Reinforced Concrete Columns *Earthquake Spectra* 15(2):245-272.

Pochanart, S., and Harmon, T. (1989) Bond-Slip Model for Generalized Excitation Including Fatigue *ACI Material Journal* 86(5): 465-474.

Popov, E. P. (1984) Bond and Anchorage of Reinforcing Bars under Cyclic Loading," *ACI Journal* 81(4):340-348.

Razvi, S.R., and Saatcioglu, M. (1996) Design of R/C Columns for Confinement Based on Lateral Drift *OCEERC 96-02*, University of Ottawa, Ottawa.

Souroushian, P., and Choi, K.B. (1989) Local Bond of Deformed Bars with Different Diameters in Confined Concrete *ACI Structural Journal* 86(2):217-222.

Souroushian, P., Choi, K.B., Park, G.H., and Aslani, F. (1991) Bond of Deformed Bars to Concrete: Effects of Confinement and Strength of Concrete. *ACI Material Journal* 88(3):227-232.

Ueda, T., Lin, I.J., and Hawkins, N.M. (1986) Beam Bar Anchorage in Exterior Column-Beam Connections *ACI Structural Journal* 83(3): 412-422.

Vecchio, F.J., and Collins, M.P. (1986) The Modified Compression-Field Theory for Reinforced Concrete Elements Subjected to Shear *ACI Journal* 83(2):219-231.

Wallace, J.W. (1992) BIAX: Revision 1 A Computer Program for the Analysis of Reinforced Concrete and Reinforced Masonry Section *CU/CEE-92/4*, Clarkson University, Potsdam.

KEYWORDS: lap splices, columns, strength decay, stiffness decay, bond-slip, cyclic loads, seismic excitation

SESSION 4: PRELIMINARY ANALYSIS OF THE FULL-SCALE TEST

Chaired by

♦ Ken Elwood and Taiki Saito ♦

NONLINEAR DEFORMATION MODE IN EARTHQUAKE RESPONSES OF ASYMMETRIC REINFORCED CONCRETE STRUCTURES

Toshikazu KABEYASAWA[1] and Toshimi KABEYASAWA[2]

ABSTRACT

In this paper, general characteristics for nonlinear earthquake responses of asymmetric reinforced concrete structures are investigated based on nonlinear deformation modes. The static and dynamic analyses of the specimen for full-scale table at E-Defense test are carried out to examine the effect of torsion on expected responses. Preliminary shaking table test of one-third scale six-story eccentric reinforced concrete wall-frame structures are also analyzed, by which a fair correlation was observed between the test and equivalent SDF response analysis. Several other types of wall-frames were designed to simulate asymmetric responses in case that 2nd mode is dominant. The dominant modes were decomposed from the nonlinear dynamic responses, by which general characteristics were discussed in terms of effective mass ratio. It was found that the effective mass ratio converges approaches a constant value when the inelastic response is large. The constant could be derived from nonlinear pushover analysis considering the first mode and the second mode in the assumed load vectors. Dynamic responses assuming different hysteresis models indicated that the general characteristics might be due to inelastic unloading stiffness, which induces a correlation in the phases of relative acceleration response and input acceleration. Three-dimensional shaking table tests of one-fourth-scale four-story eccentric reinforced concrete wall-frame structures were also analyzed by which change in principal direction was discussed.

1. INTRODUCTION

A new design procedure has been introduced into seismic design at the revision of the Building Standard Law of Japan in 2000. The inelastic displacement responses are estimated from linear response spectrum of the design earthquake by equivalent linearization in single-degree-of-freedom (SDF) system based on Nonlinear Pushover Analysis (NPA) under 1st mode force vector. However, in case of asymmetric structures, at least two modes in horizontal responses, translational mode and rotational mode, should generally be considered in estimation and reduction to SDF, and a rational method of introducing the two modes has not yet been established. In this paper, general characteristics in inelastic torsional responses are discussed based on the dynamic deformation modes expressed in terms of effective mass ratio. Various types of asymmetric wall-frames are analysed, such as six-story specimens for the preliminary shaking table test under series, other types of designed specimens, and four-story specimens

[1] *Master, Dept. of Architecture, Faculty of Engineering, University of Tokyo; Email: tosikazu@eri.u-tokyo.ac.jp*
[2] *Professor, Earthquake Engineering Research Inst., University of Tokyo; Email kabe@eri.u-tokyo.ac.jp*

under three-dimensional dynamic loadings, as well as the full-scale specimen designed for shaking table test at E-Defence.

2. METHODS OF ANALYSIS

2.1 Nonlinear Pushover Analysis

A method of estimating nonlinear maximum response of asymmetric multi-story structure has been proposed using simple Nonlinear Pushover Analysis (NPA), considering the effects of higher modes. The static pushover analysis is carried out under a force vector, which combines the 1st mode and 2nd mode each weighing by the mode participation factor (1+2 mode force vector) [1]. When the eigenvector of i-th mode is given as $\{u\}_i = \{\phi_{dxi}, \phi_{dyi}, \phi_{\theta i}\}$, and i-mode participation factor as β_i, the lateral force vector can be denoted by the equations (1) and (2).

$$\{F\} = [M]\sum_i \beta_i \{u\}_i = [M]\sum_i \beta_i (\phi_{dxi}\ \phi_{dyi}\ \ \phi_{\theta i})^T \qquad (1)$$

$$\beta_i = \frac{(\phi_{dxi}\ \phi_{dyi}\ \ \phi_{\theta i})\ \ [M]\{\alpha\}}{(\phi_{dxi}\ \phi_{dyi}\ \ \phi_{\theta i})\ \ [M](\phi_{di}\ \ \phi_{dyi}\ \phi_{\theta i})^T} \qquad (2)$$

ϕ_{dxi}: i-th mode lateral deformation component in X-direction

ϕ_{dxi}: i-th mode lateral deformation component in Y-direction

$\phi_{\theta i}$: i-th mode story rotation component

β_i: i-th mode participation factor

$[M]$ Mass matrix

α: $(1\ldots\ ,1\ldots\ ,0\cdots)^T$ Acceleration action vector

The formula has commonly been used for estimating the responses of symmetric building structures including higher mode deformations based on static analysis empirically as well as Modal Pushover Analysis[2], performed by the summation of time-history response of each modes. Dynamic responses of two modes replaces the summation of SDF response against each mode force, so that this is based on the assumption that maximum response of each mode deformation occurs simultaneously, although the assumption has not yet been verified generally.

2.2 Effective Mass Ratio

In past research[3] representing the index to express the participation of i-th mode in dynamic response, the effective mass ratio M_i has been used, which gives a specific value depending on the dynamic characteristics of a structure in elastic response. The index is given by the equation

(3), which is equivalent to the level of the external forces subjected the unit input acceleration in a certain component, which is defined by the vector {α}. The equation of motion reduced to SDF in i-th mode is given by the equation (4). The index has been adopted as a general criteria, for example, in the guidelines for the new BSL procedure[4, 5], to give the scope of SDF reduction process for the vertical mass and stiffness distributions in symmetric building structures. It is also pointed out that the reduction to SDF should be limited in case that the index of the 1st mode is not less than 0.8 based on nonlinear response analyses of asymmetric structures[6].

$$M_i = (\beta_i \{u\}^T{}_i [M]\{\alpha\}) / M_{all} \tag{3}$$

M_{all} : Total mass of the

M_i : i-th mode effective mass

$$M \ddot{q}(t) + C \dot{q}(t) + K q(t) = -\beta_i \{\phi_i\}^T [M]\{\alpha\} Ag \tag{4}$$

$M = \beta_i{}^2 \{\phi_i\}^T [M]\{\phi_i\}$: Equivalent mass in SDF

$C = \beta_i{}^2 \{\phi_i\}^T [C]\{\phi_i\}$: Equivalent damping in SDF

$K = \beta_i{}^2 \{\phi_i\}^T [K]\{\phi_i\}$: Equivalent stiffness in SDF system

2.3 Procedure for Decomposition of Deformation Mode in Nonlinear Response

A modal decomposition method[7, 8] has been proposed and used to derive a basic or dominant mode shape vector {X} and time-history scalar q(t) from a vector of inelastic time-history responses of a structure {f(t)}. If the mode shape {X} is defined so as to minimizes E, which is time history summation of square of the errors between the given responses and the mode vectors as given by the equation (6), it is proved mathematically that the mode vector {X} can be drawn as the first eigenvector $\{u\}_{1d}$ against ([m], [R]) as shown in the formulae (7) and (8). The second mode can also be drawn from the residual component of f(t) reiteratively. In the following analysis, the decomposed modes as above are assumed to be the first and second mode in nonlinear dynamic response.

$$\{f(t)\} \sim \{X\} q(t) \tag{5}$$

$$E = \int_{t_2}^{t_1} [\{f(t)\} - \{X\}q(t)]^T [m][\{f(t)\} - \{X\}q(t)]\, dt \tag{6}$$

$$[R] = \int_{t2}^{t1} \{f(t)\}\{f(t)\}^T\, dt \tag{7}$$

$$([m][R][m])\{u\}_{1d} = \lambda_1 [m]\{u\}_{1d} \tag{8}$$

2.4 Procedure for NPA and Nonlinear Earthquake Response Analysis

The nonlinear pushover analysis and dynamic earthquake response analysis are carried out using a three-dimensional frame analysis program "CANNY 99"[9]. In the analysis, the structures are idealized using one-component model for columns and beams, and three-vertical line element (TVL) model for structural wall. The cracking force, yielding force of members in the member hysteresis model, Takeda model, are calculated in accordance with AIJ guidelines[10]. The effect of the slab on the flexural strength of the beam is considered as well. The secant yielding stiffness is calculated by an empirical formula and stiffness after yielding is 0.1% of elastic stiffness for beams and columns, 0.03 for bending spring, and 0.02 for shear spring of walls. Basically, the hysteresis models for bending, axial and shear spring are Takeda model with unloading exponent constant γ=0.5, axial-stiffness model and linear model, respectively. However, the stiffness degradation after shear cracking is considered in the shear spring of the wall model, for which Takeda model is used. Damping coefficient is 0.02 of critical, which is proportional to the tangent stiffness matrix. The beam column joint is assumed to be rigid zone. Modelling the full-scale test specimen, the rigid zone of the short column is assumed up to the height of the standing wall attached to the beam.

3. ANALYSIS OF THE FULL-SCALE SPECIMEN

Nonlinear Pushover Analysis of the full-scale specimen for the shaking table test at E-Defence is carried out [11]. The relations between lateral deformation on top floor and base shear are shown in Figure 1. The analysis is conducted in X and Y direction under the lateral forces of uniform and inverted triangular distribution. At the maximum lateral deformation angle of 0.02, the base shear coefficient marks almost 0.6 under uniform and 0.45 under triangular in X direction, and almost 0.75 and 0.60 in Y direction. Shear forces carried by the central wall-frame (X2-frame) is almost half of the total base shear in Y-direction. The elastic periods of three modes are 0.260s in X-direction, 0.257s in Y-direction, and 0.182s in rotation.

Nonlinear Dynamic Analysis is carried out to investigate torsional response of the test specimen. The input earthquake record is JMA_Kobe, and input scale factor for the original earthquake intensity is changed to generalize the analysis results against different ductility level. The effective mass ratios of 1st and 2nd deformation modes discomposed in NDA are compared as shown in Figure 2 (a) to those in NPA where the force vectors are assumed as the first mode or the sum of the 1st and 2nd modes weighted by participation factors. Effective mass ratios in NDA approximates to those in NPA well in inelastic range more than deformation of 0.15m. It may be concluded that the nonlinear response can be simplified with 1st mode SDF response, and not influenced by higher mode deformation in large deformation.

To evaluate the effect of torsional response directly, lateral drift increment of the outer frame to the centre in the 1st story is shown in Figure 2(b). The increment in Y-direction is 10 % at KOBE (0.6), which gradually decreases with the increase of deformation. On the other hand, the increment in X-direction is exponentially increasing, and finally up to 50 % under KOBE (1.0). These two results indicate that story rotation influences response more in X-direction, and not so much in Y-direction, therefore the main collapse mechanism in Y-direction would not change due to the effect of torsion.

The input direction of the earthquake motion in Nonlinear Dynamic Analysis is changed in order to examine the effect on the responses. The responses of the drift and the shear force of the wall in the 1st story vs. the input direction of NS-component of the original record, JMA_Kobe is shown in Figure 3. The deformation and wall shear in Y-direction attained the maximum value when the input direction turns 45 degrees from X-direction, which was selected in above analysis. Although the analysis model can not simulate the shear collapse, the maximum lateral deformation angle and the shear force in the wall reached 1/50 (rad), and almost 3000 (KN) in Y-direction, by which the specimen would collapse associated with shear failure of structural wall.

The relation between lateral deformation on top floor and base shear in Y-direction is shown in Figure 4. The maximum shear coefficient attained 0.8 at maximum, which is larger by 0.2 than that in the decomposed mode and NPA, due to the effect of higher mode responses.

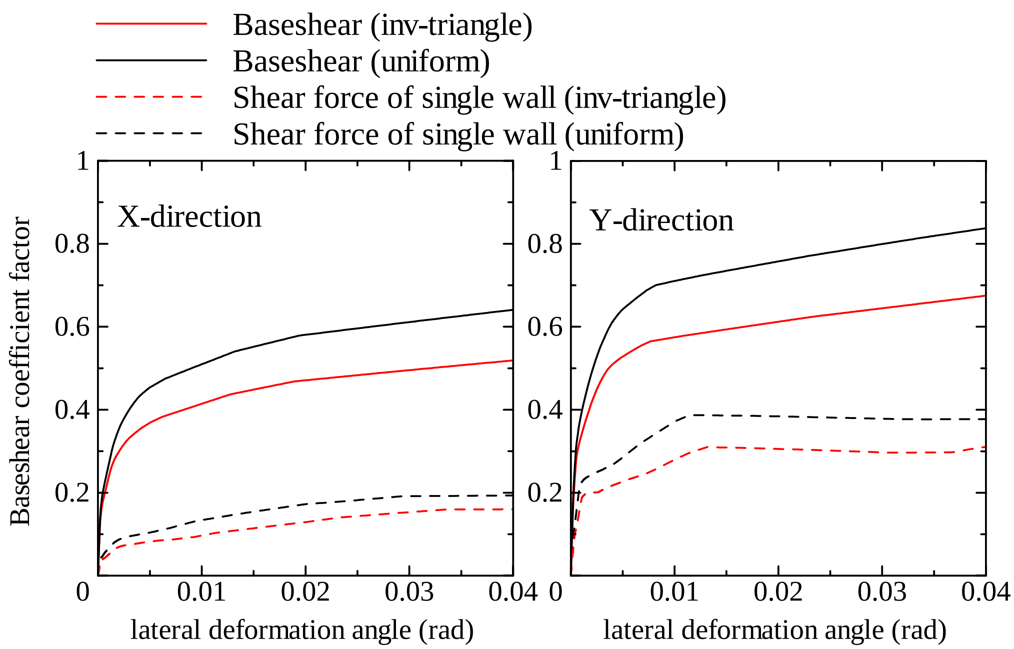

Fig. 1: Pushover analysis of the full-scale specimen for testing at E-Defense

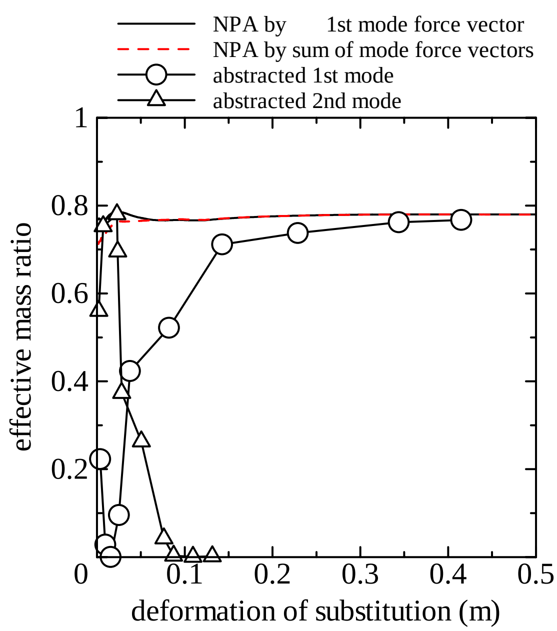

(a) Effective mass ratio of 1st and 2nd modes

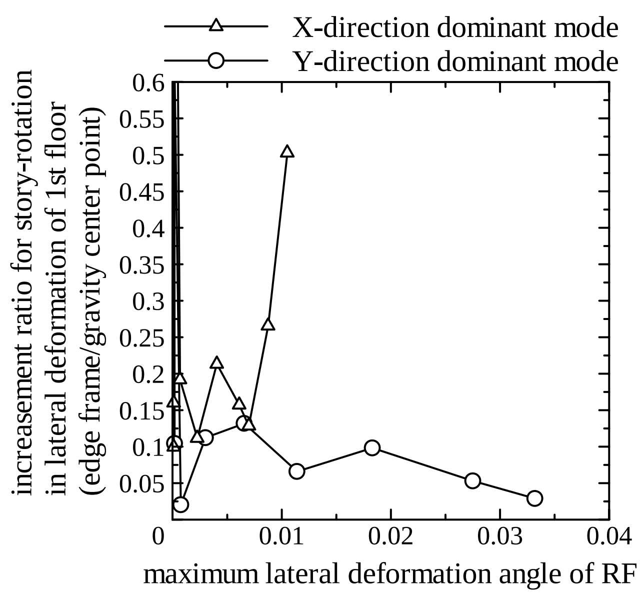

(b) Effect of torsion on 1st story responses

Fig. 2: Torsional responses in nonlinear dynamic analysis

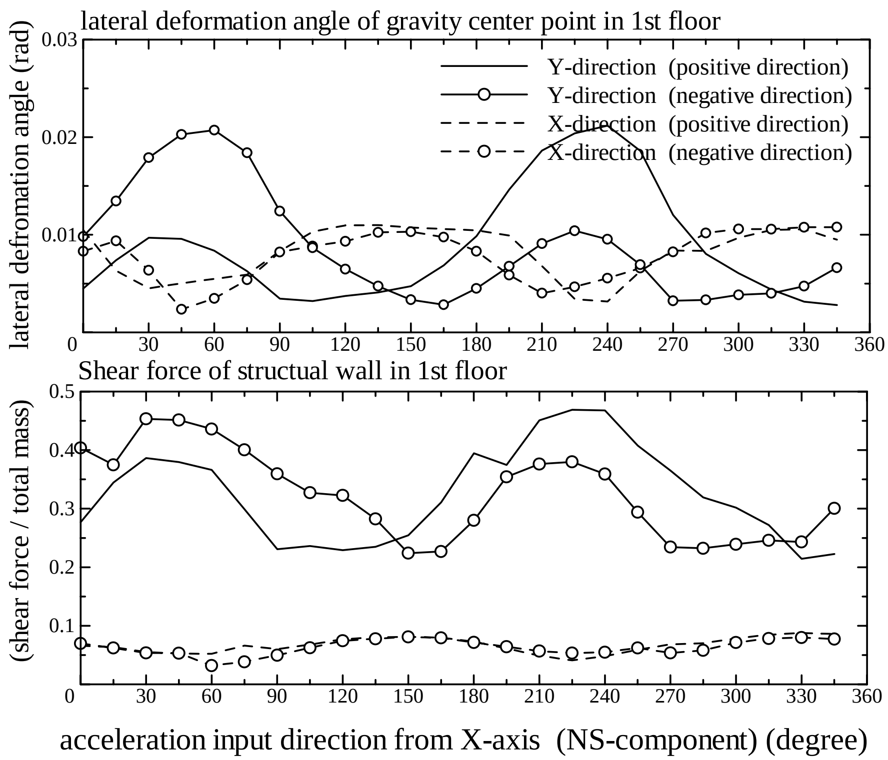

Fig. 3: Relation between acceleration input direction and response

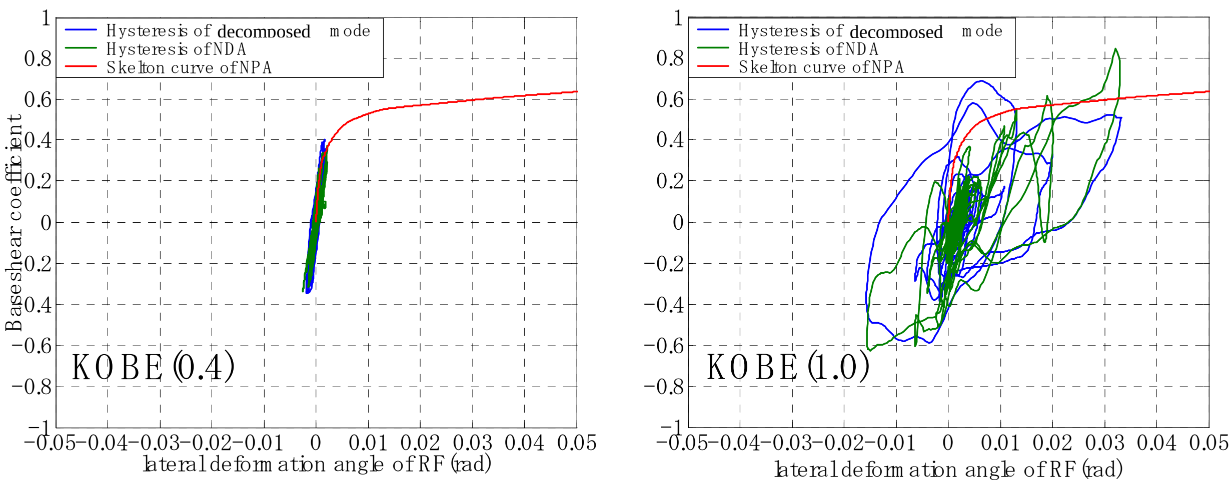

Fig. 4: Hysteresis of decomposed 1st mode and Nonlinear Dynamic Analysis

4. ASYMMETRIC SPECIMENS FOR TESTS AND ANALYSES

4.1 Six-Story Specimens for 1-D Shaking Table Test

One-third-scale six-story asymmetric reinforced concrete structures were tested as the preliminary shaking table test[12], which has two walls located eccentrically in each direction as shown in Figure 5. The total height of the specimen is 6450 mm, which is the sum of base (450 mm) and each story height of 1000 mm. Details of wall and column sections are illustrated in Table 1. In the test, called as test I below, two identical specimens were subjected to different input motions as shown in Table 3(a). Acceleration was input only in one direction, X-direction. For the first Specimen A, far field earthquakes, such as CHILE (1985 Chile earthquake), TOH (1978 Miyagi-ken-oki earthquake) were used and the intensity was gradually increased. On the other hand, near field earthquake motions, such as JMA (1995 Hyougo-ken-Nanbu earthquake recorded at Kobe ocean metrological observatory), TAK (1995 Hyougo-ken-Nanbu earthquake recorded at JR Takatori station) were used and the intensity was made high enough for collapse in less times of input.

4.2 Four-Story Specimens for 3-D Shaking Table Test

Two identical one-fourth scale four-story reinforced concrete specimens were tested under three-dimensional earthquake motions where the direction of motions input to the structure was changed between the two specimens (Specimen A-3D, Specimen B-3D). The input table is shown in Table 3(b) and the specimen is shown in Figure 5, while the details are described elsewhere[13]. Here, the torsional responses under three-dimensional motion were analysed and discussed.

Table 1: Section details of members (Test I)

Columns	B×D	200×200	Beams	B×D	150×250
	Main bars	12-D10		Main bars	2-D10
	Hoops	D4@50		Hoops	D6@75
Walls	Width	80 mm	Wall	B×D	240×250
	Steel bars	D6@100 W		Main bars	4-D10
Mass in each floor		9.75 ton		Hoops	D6@75

Table 2: Properties of specimens

	T1(s)	T2(s)	M1	M2	(M1)	(M2)	Re1	Re2
Specimen for test I	0.203	0.074	0.573	0.019			0.884	0.215
Specimen for test II	0.095	0.089	0.748	0.037	0.041	0.776		
Specimen 1 for analysis	0.178	0.109	0.261	0.503			0.396	0.134
Specimen 2 for analysis	0.185	0.131	0.365	0.366			0.384	0.097

※ Effective mass ratio of 1st mode M_1 calculated in acceleration principal axis (test A)
Effective mass ratio of 1st mode (M_1) calculated in acceleration principal axis (test B)

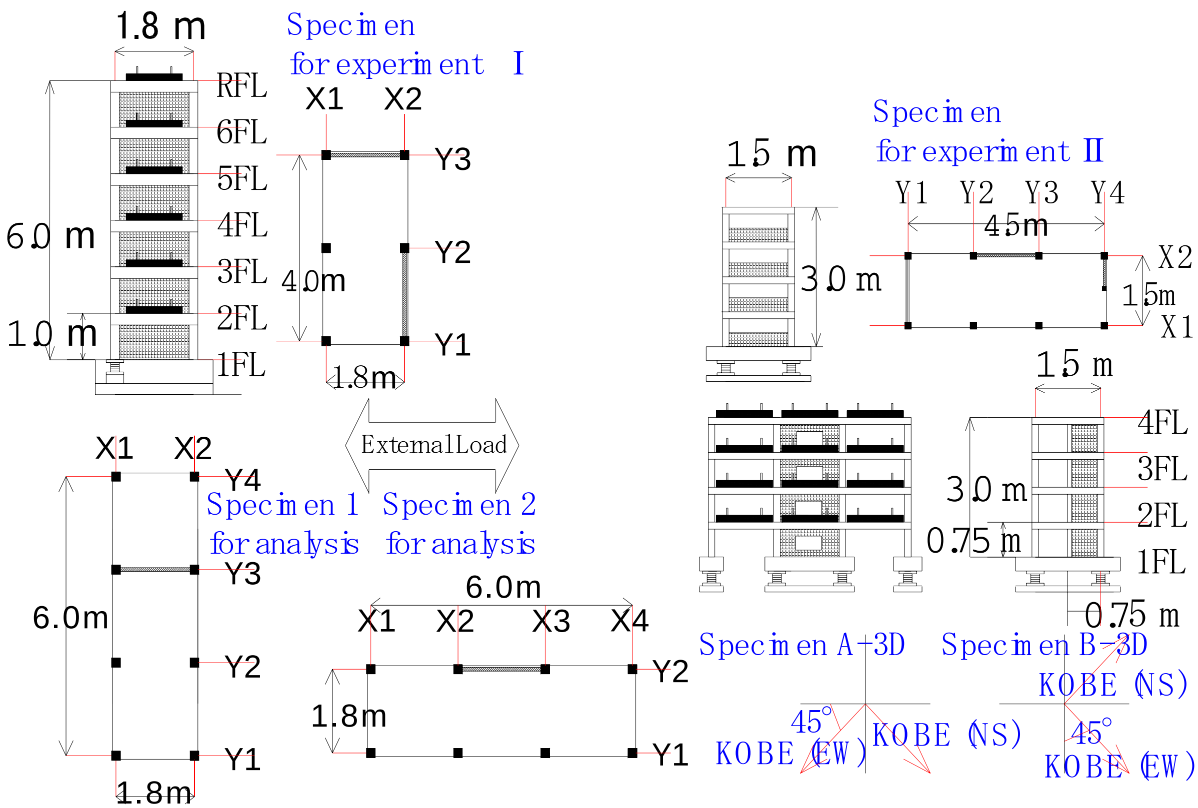

Fig. 5: Plan and elevation of each specimens

Table 3: Run table of shaking table test

(a) Shaking table test I						(b) Shaking table test II		
Specimen A			Specimen B			Specimen A, B		
Run	EQ record	Amp	Run	EQ record	Amp	Run	EQ record	Amp
1	TOHOKU	0.15	1	TAKATORI	0.06	1	KOBE	0.05
2	TOHOKU	0.30	2	KOBE	0.10	2	KOBE	0.20
3	TOHOKU	0.60	3	KOBE	0.20	3	KOBE	0.40
4	CHILE	0.25	4	KOBE	0.20	4	KOBE	0.60
5	CHILE	0.35	5	KOBE	0.60	5	KOBE	0.80
6	CHILE	0.45	6	TAKATORI	1.10	6	KOBE	1.00
7	CHILE	0.60				7	KOBE	1.25
8	CHILE	0.90				8	KOBE	1.25
9	CHILE	1.10				9	KOBE	1.25
10	CHILE	1.10				Time axis is shorten in Run 9 ($1/\sqrt{1.25}$)		
11	CHILE	1.20						

4.3 Six-Story Specimens for Modal Analysis

Based on the result of shaking table test I, nonlinear earthquake response analysis of several six-story asymmetric building structures are also carried out. In these specimens, plan and location of walls are varied to simulate the general cases of torsional behavior. In this paper, the analytical results are shown for only two cases, Specimens 1 and 2 shown in Figure 5, out of 12 specimens, where almost the same effective mass ratios are calculated for elastic the 1st and then 2nd mode and two modes would be dominant in dynamic responses. The general characteristics derived below were common for all other specimens.

5. ANALYSIS OF THE SIX-STORY SPECIMENS

5.1 The Response of the Decomposed 1st Mode

The modal decomposition by the equations (5) through (8) is applied to time-history responses of the displacement and the force vectors calculated from NDA, which was conducted before the test, and also those measured in the shaking table test I. for the six-story Specimens A and B. The hysteresis relations of the decomposed 1st mode are shown in Figure 6 with the skeleton curves by NPA under the elastic 1st mode. The hysteresis relations of the analysis and the test are quite similar for the Specimen A, while the analysis overestimates the maximum deformation after the large deformation at run 6 for the Specimen B, because higher yielding force and stiffness were measured in the test. The reason is not clear but it might be due to the effect of higher strain rate and also higher mode in vertical direction because of higher acceleration input to collapse.

These decomposed 1st deformation modes are analysed for both specimens as shown in Figure 7. The change of maximum deformation in decomposed mode against dynamic response of the structure is shown in Figure 7(a). In these specimens, the 1st mode dominates dynamic response with high effective mass ratio in X-direction, and the disposition doesn’t change up to large deformation. The drift ratios of the 1st mode to structure are similar for both specimens in spite of different input level. Values of the effective mass ratios and the ratios of the story rotation to the lateral drift on roof floor in the decomposed mode are shown in Figure 7(b), (c). From these results, it may be concluded that the nonlinear dynamic response of the specimens, with high effective mass ratio in the 1st mode, can accurately be estimated by NPA simply using the 1st mode force vector.

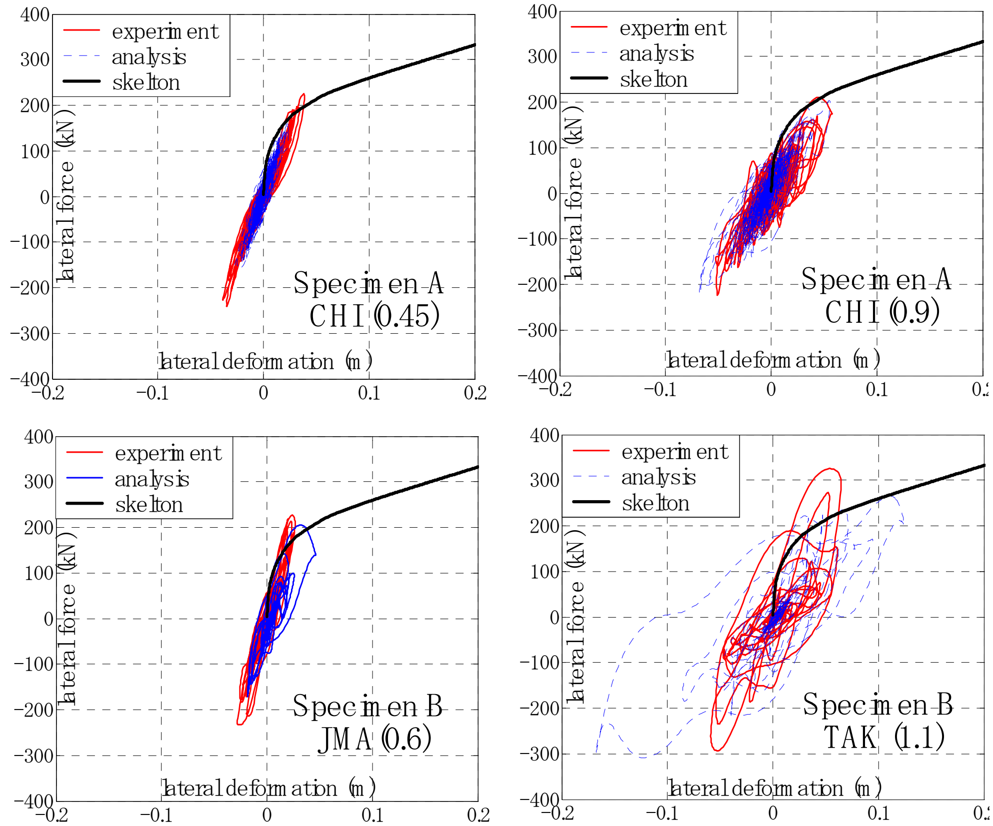

Fig. 6: Hysteresis of 1st mode in analysis and experimental results

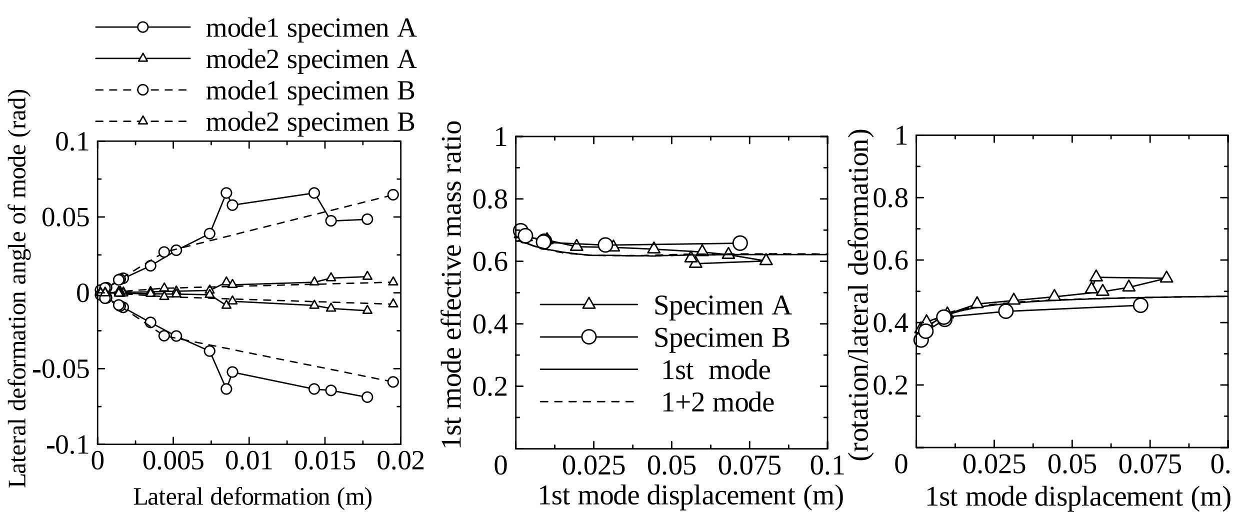

Fig. 7: The change of nonlinear 1st deformation mode

5.2 Estimation of Response by Equivalent Linear SDF System

Maximum roof displacements in each run are estimated by NDA and equivalent SDF response as shown in Figure 8 for Y1 open-frame and Y2 gravity centre.

In NPA for estimation, two types of he deformation mode, 1st mode and 1+2 mode force vectors are assumed. The equivalent period T_e and equivalent damping h_e in SDF system are determined at the maximum deformation from the tests.

The test could be simulated basically well by NDA except for run 6 of Specimen B. The error may be due to the modelling of the hysteresis shapes. The error between NDA and the SDF estimation is relatively small and the effect of the force vectors in NPA is small. Therefore, the nonlinear response of the asymmetric test structures with high effective mass ratio can be estimated accurately by the equivalent SDF system under the 1st mode.

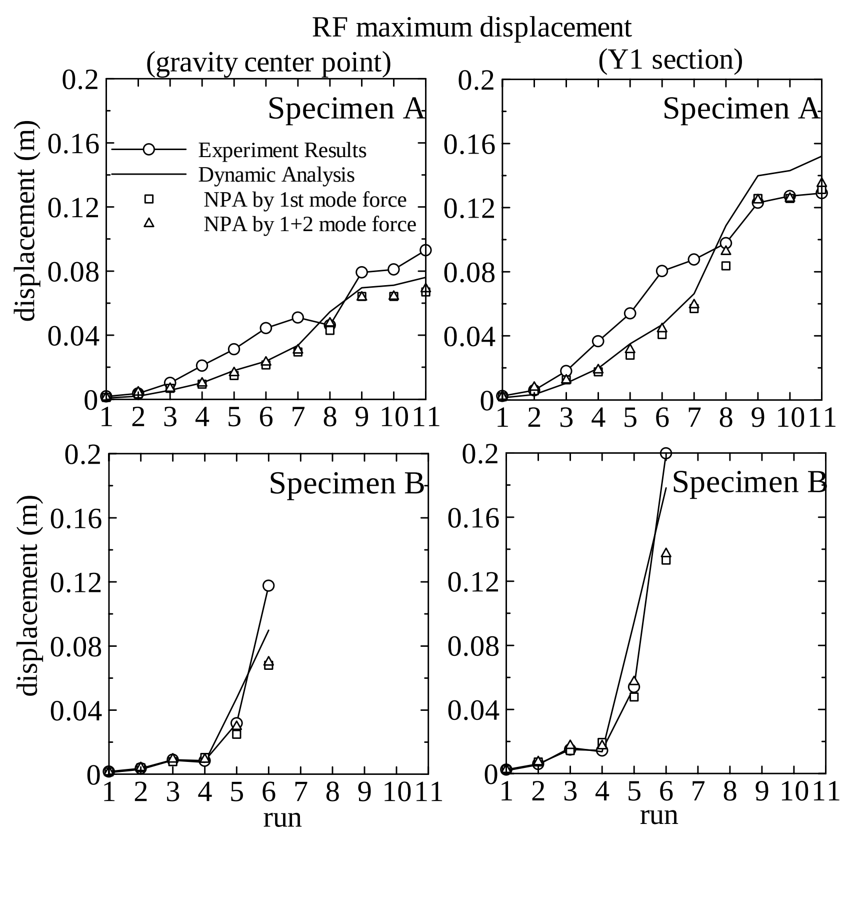

Fig. 8: Maximum response of shaking table Test Ⅰ

6. DEFORMATION MODES OF MULTI-STORY ASYMMETRIC STRUCTURES

6.1 Modal Decomposition from the Waves by NDA

Nonlinear dynamic analyses of the six-story asymmetric structures shown in 4.3 are carried out to investigate generally the responses using the NPA and the modal decomposition shown in 2.1 through 2.3. These structures are specially selected for the analysis and estimation here where the effective mass ratio for the 1st mode is less than 0.5 and that for the 2nd mode is relatively larger, so that both modes would be dominant in the responses. The input motions used for the analyses are two earthquake records (KOBE, CHILE), and an artificial earthquake record (BCJL2). The input scale factor was changed from the original earthquake intensity to generalize the analytical responses from elastic to well inelastic regions with the increments of 0.5 for BCJL2 and 0.25 for KOBE and CHILE. Two different force vectors, the 1st mode force vector and the 1+2 mode force vector, are used in NPA, where the 1+2 mode vector is a modal sum of the 1st and 2nd modes as given by equation (1).

The effective mass ratios in the deformation modes decomposed from dynamic analysis and derived from NPA under the two different force vectors are compared as shown in Figure 9(a). The maximum modal deformation is taken for abscissa-axis in the figure. The effective mass ratio in dynamic analysis is in between those by NPA under two different force vectors. The value changes with the maximum deformation from close to the value by the 1st mode force vector to that by the 1+2 mode force vector for NPA, and became constant a little larger than the latter. This characteristic change with the inelastic deformation is generally common in all cases of the earthquakes and the specimens, and the deformations at the change of the mode seem to be specific to the specimens and regardless of the input earthquakes. This indicates that the decomposed deformation mode can be estimated as the deformation mode by NPA under the 1+2 mode force vectors well in inelastic range. This is the same as the past empirical results although the reason has not yet been made clear, which will be discussed further in 6.2.

The change of effective mass ratio in the 2nd deformation mode decomposed from the residual component is shown in Figure 9(b). The value decreases corresponding to the maximum 1st mode deformation, and finally becomes almost zero. Based on the definition of the effective mass ratio, these results indicate that the mode force vectors by unit acceleration turn to be 0 after large deformation except for the decomposed 1st mode, which is close to the 1+2 mode, and

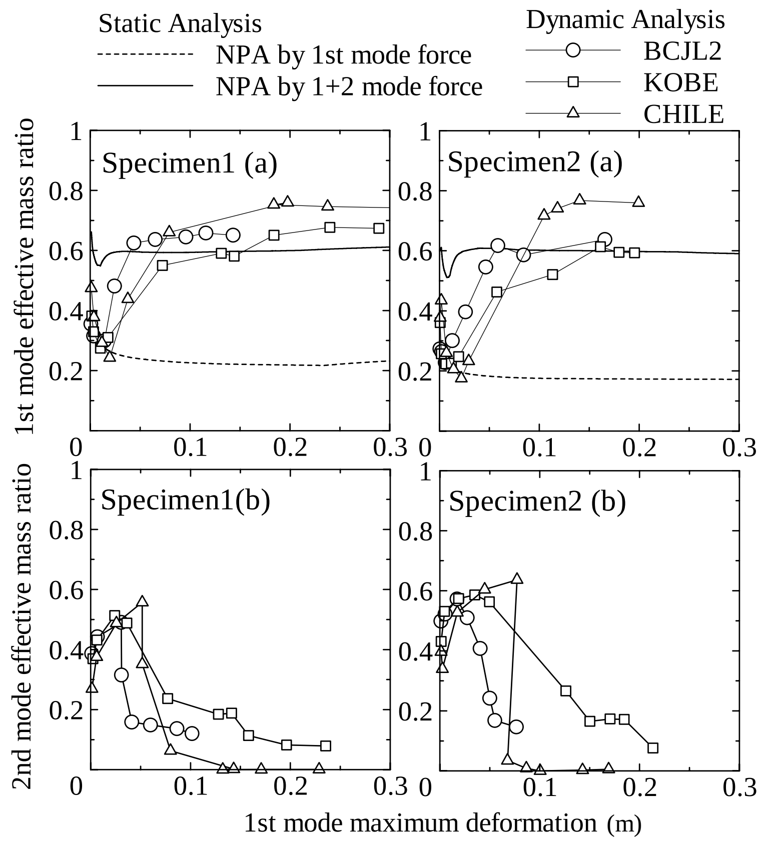

Fig. 9: Change of the effective mass ratio in Specimens 1 and 2

that the dynamic response may be estimated by the SDF response.

Based on these general characteristics, estimation of nonlinear responses of asymmetric structures using NPA and the equivalent SDF system can be improved rationally. The effects of torsional responses are considered using the rational force vectors in NPA corresponding to the decomposed mode shapes. The correction method and the results are is described in detail elsewhere, while the outline is shown below.

In elastic range or small inelastic range, dynamic response consists of two mode deformations, so that maximum deformation may be estimated by MPA, which sum up each mode deformations with NPA under elastic modes. On the other hand, well in inelastic range, the dynamic force vector may be approximated as those by the 1+2 mode force vector. The deformation mode can be estimated from NPA using the 1+2 mode force vector. In the intermediate region, a method of interpolation for the force vector is applied for the two approximations.

The first characteristic deformation where the mode changes could be derived by NPA as the yielding deformation of the first mode. The second characteristic deformation could be approximated at the deformation where the deformation mode becomes constant by NPA under the 1+2 mode force. By using these modified force vectors, the unified method from elastic to inelastic region is available for the estimation by NPA and SDF and the accuracy could be improved especially in the intermediate region.

6.2 Interpretation of the Characteristics in the Decomposed Deformation Modes

Additional NDA is carried out for a same asymmetric structure using two different hysteresis models to explicate the above characteristics in the response modes. The analysed structure is based on the six-story specimen A for the test although the structural wall in the orthogonal direction is removed for simplicity. Hysteresis of bending spring are all RC (Takeda) model (α =0.5) in Specimen A1, while tri-linear-elastic model in Specimen A2, the loading skeleton curves of which are identical for both, that is, only the unloading stiffness is varied between the two models. Input accelerations are KOBE with amplification factor of 0.1 and 3.5 for elastic and inelastic response respectively.

The time-history of the relative acceleration responses in the decomposed modes are compared with the input acceleration for the four cases in Figure 10. The amplitudes are normalized by each maximum value to compare only phase characteristics. The phases in the waves for the Specimen A1 and that in the Specimen A2 in elastic responses to KOBE (0.1) are independent to the input acceleration. On the other hand, the phase in the Specimen A1 under KODE (3.5) is correlated and inverse to that of the input acceleration. The force vector, the absolute acceleration, is sum of the relative and input accelerations. Therefore, this property is equivalent to the characteristics that in the decomposed deformation mode converging into the 1+2 mode forces. However, it should be noted that these correlation is observed only in the Specimen A1 with Takeda model and not in the Specimen A2 with the nonlinear elastic model. Therefore, the essential source of these characteristics might depend on stiffness branch to unloading direction.

The effective mass ratios in the 1st and 2nd decomposed deformation modes are compared in Figure 11 with different amplitudes of responses. The effective mass ratio in the Specimen A2 does not increase in the 1st mode deformation, which is consistent with the result of time-history relative acceleration.

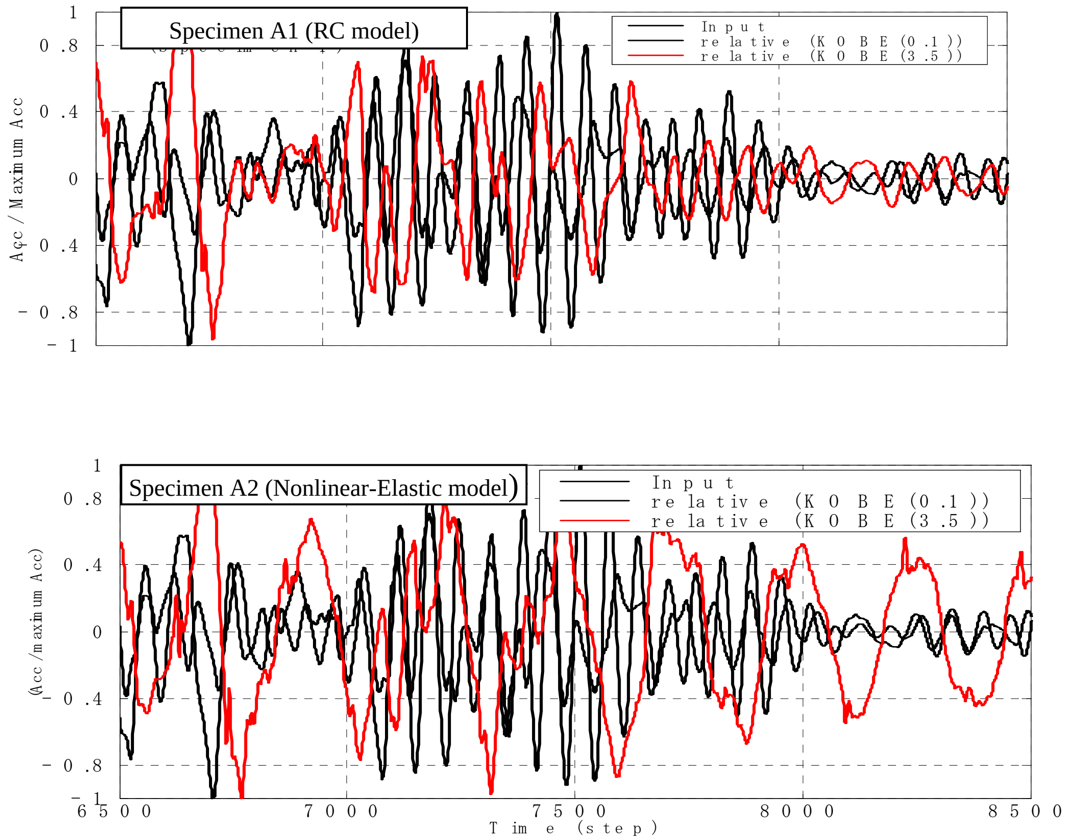

Fig. 10: Comparison with relative acceleration and input acceleration

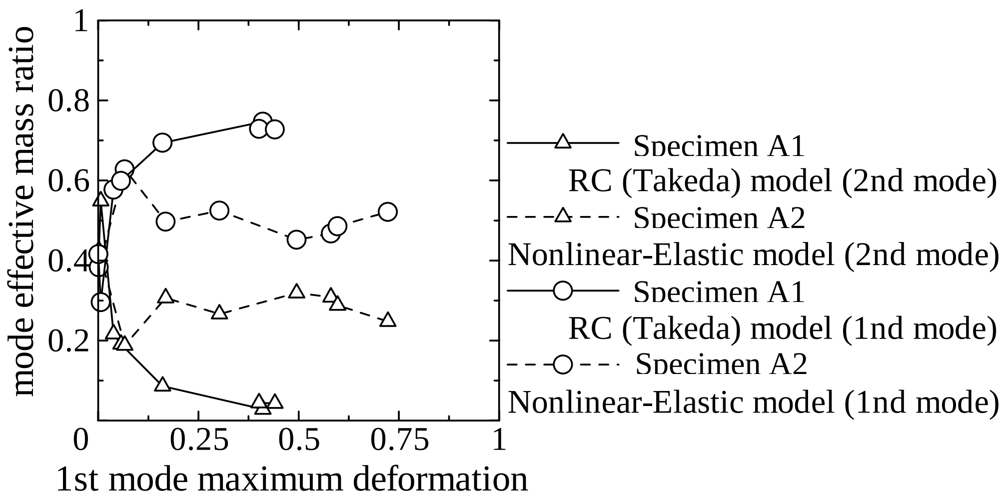

Fig. 11: The change of effective mass ratio in 2 Specimens

7. THREE-DIMENSIONAL RESPONSE OF THE FOUR-STORY SPECIMENS

The modal decomposition method was applied to three-dimensional torsional responses, that is, the measured responses in the shaking table test of Specimen A-3D and B-3D shown in Figure 5. The test was conducted under three-dimensional earthquake motion for the two specimens, where the direction of the input motion was varied. The effective mass ratios are calculated for the decomposed 1st mode and the 2nd mode of the observed deformation responses and compared as shown in Figure 12(a), where the direction of the reference external acceleration vector was rotation taken as the abscissa in the figure. The direction of the principal axis in the response deformation modes (PARD) is defined as that indicating the peak value of the mass ratio, which is shown for Run 1 and Run 7 in Figure 12(b). The principal axes of the input acceleration directions (PAID) are also shown in the figure, which is defined as the direction of the maximum value of the vector.

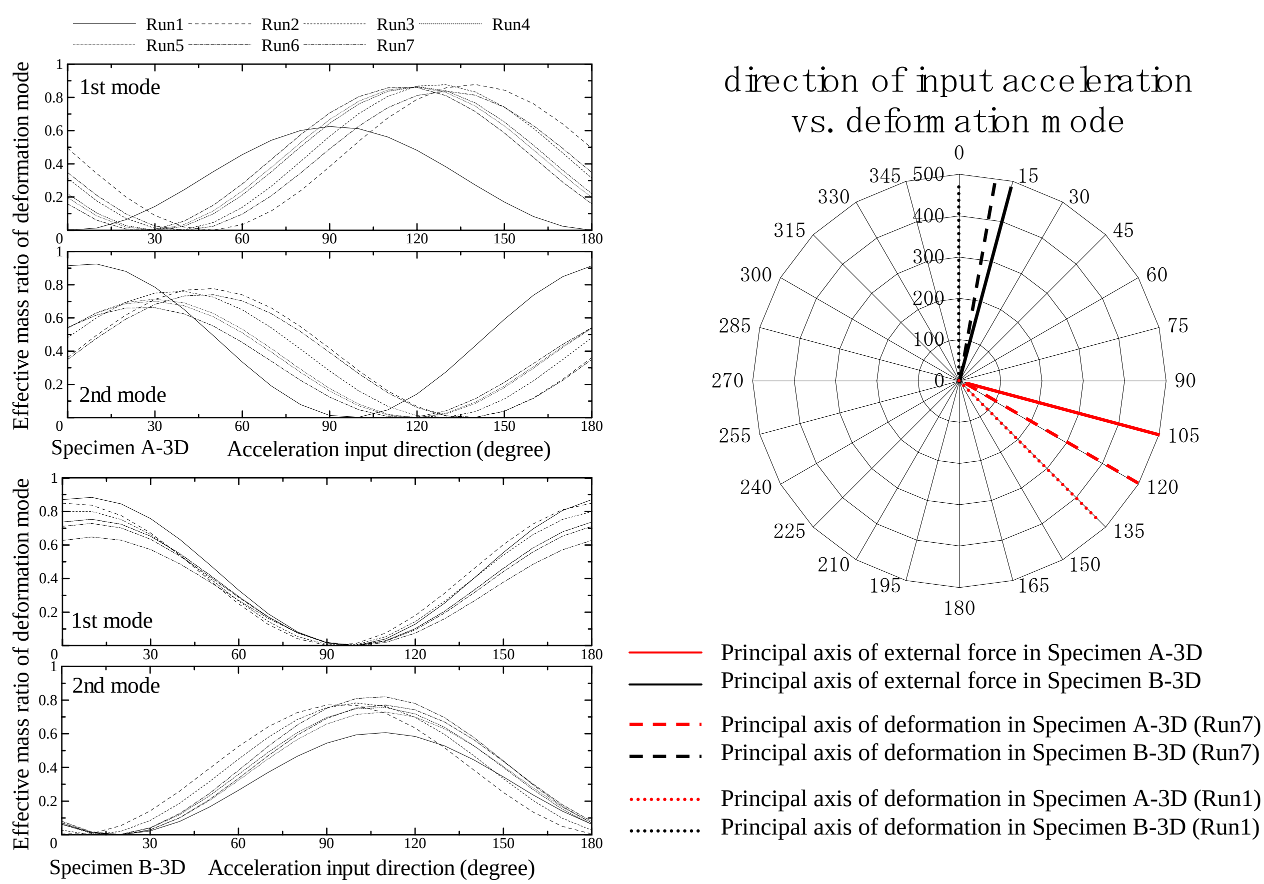

(a) **(b)**

Fig. 12: Change of effective mass ratio in test specimen

Compared with the main input direction (PAID), the main response direction (PARD) is different in elastic range, but becomes close in inelastic range of deformation for both specimens. This result can also be interpreted similarly to the characteristics above where the decomposed relative acceleration correlated with the input direction acceleration, which promote the dominant mode deformation in the three-dimensional mode.

Although it could be specific to the case of the test, the directivity for the decomposed deformation mode seems to converge into in parallel and orthogonal to the PAID. If this is general the case in all asymmetric structures, the yielding mechanisms could be specified in accordance with PAID, and the three-dimensional torsional responses of structure may be simulated by the independent two modes of deformations defined by the axis of PAID.

8. CONCLUSION

The following concluding remarks are derived from the modal decomposition procedure proposed for the analysis and the interpretation of the inelastic torsional behaviour of asymmetric reinforced concrete structures.

(1) The torsional behaviour of the full-scale shaking table test could be evaluated with a traditional procedure where the higher mode deformation and the story-rotation do not influence the responses much in inelastic range.

(2) As for asymmetric RC structures with high effective mass ratio in the 1st deformation mode, such as the six-story test specimens, the accuracy of the estimation with the equivalent SDF response analysis and NPA simply by the 1st mode force vector is verified experimentally as well as analytically.

(3) As for asymmetric RC structures with low effective mass ratio in the 1st deformation mode, the basic deformation mode in well inelastic range may be approximated generally with the 1+2 mode force vector.

(4) It is estimated from the correlation in the phases of the waveforms in the relative response acceleration and the input acceleration that the above characteristics may be ascribed to the branch at loading or unloading stiffness in inelastic range.

(5) From the measured responses in the 3-D shaking table test, the main response direction (PARD) is different in elastic range, compared with the main input direction (PAID), but

becomes close in inelastic range of deformation. Three-dimensional torsional responses of structures may be simulated by the independent two modes of deformations defined by the axis of PAID.

REFERENCES

1. Anil K. Chopra and Rakesh K. Goel: Modal Pushover Analysis symmetric and unsymmetric plans buildings, International Workshop on PBSD Concepts & Implementation, 2004.7.
2. Anil K. Chopra and Rakesh K. Goel: A Modal Pushover Analysis Procedure to Estimate Seismic Demands for Buildings, A report on research conducted under grant no.CMS-9812531, from the National Science PEER Report 2001.3.
3. Kouichi Oami and Masaya Murakami: The index of torsion effect in dynamic earthquake response for 1st story asymmetric buildings, AIJ annual report structure category 1999.7
4. Building Center of Japan: *Revised Building Standard Law of Japan(in Japanese)*, Building Center of Japan, 2000.7
5. Building Center of Japan: *The limit capacity design analysis, calculation, and examples(in Japanese)*, Building Center of Japan, 2002
6. Kenji Fujii: *A study on estimates the nonlinear earthquake response in multi-story asymmetric buildings(in Japanese)*, Doctor of Engineering theses, The University of Tokyo, 2003.2
7. Haruo Takizawa: Mode abstraction from dynamic response of ductile structures beams yielding precedes, Journal of Structural Engineering, AIJ, Vol.36B, pp245-pp258 1990.3
8. Akinori Watanabe and Toshimi Kabeyasawa: A study on earthquake response deformation of reinforced concrete frame structure, concrete engineering annual report, pp137-142, 1990
9. Li, Kangning: *A study on the nonlinear earthquake response of reinforced concrete frame structures*, Doctor of Engineering theses, The University of Tokyo, 1988.12
10. Architectural Institute of Japan: *Design Guidelines for Earthquake Resistant Reinforced Concrete Buildings Based on Inelastic Displacement Concept*, AIJ, 1997.7
11. Toshimi Kabeyasawa, Taizo Matsumori, Hideo Katsumata and Kazutaka Shirai: Design of the Full-Scale Six-Story Reinforced Concrete Wall-Frame Building for Testing at E-Defense, Proceedings of the NEES/E-Defense workshop on collapse simulation of reinforced concrete building structures, 2005
12. Toshikazu Kabeyasawa, Masaki Murase, Toshimi Kabeyasawa, Taizo Matsumori: Shaking table test of asymmetric RC wall frame structures subjected to different earthquakes input (in Japanese), Proceedings, Japan Concrete Institute, Vol.26, No.2, pp1159-1164 2004.7
13. Kazutaka Shirai, Toshikazu Kabeyasawa, Hideo Katsumata and Toshimi Kabeyasawa: Tri-Axial Shaking Table Test on Reinforced Concrete Buildings with Large Eccentricity, Proceedings of the NEES/E-Defense workshop on collapse simulation of reinforced concrete building structures, 2005

DYNAMIC ANALYSIS AND PERFORMANCE EVALUATION OF REINFORCED CONCRETE WALL-FRAMES WITH STRENGTH DETERIORATION

Tomoya MATSUI[1], Toshimi KABEYASAWA[2] and Hiroshi KURAMOTO[3]

ABSTRACT

In this study, response analysis of wall-frame structure modeled on level of member was carried out, results of that was compared with seismic performance in "the seismic screening standards of existing reinforced concrete building" in Japan, the effect that member with strength deterioration affects seismic performance was examined as basic study. As the results, although the effect of strength deterioration has looseness according to the earthquake wave, it is possible that seismic capacity of structure that have a lot of deformability and strength deterioration could be overestimated in the seismic screening standards. And that behavior can be attribute damage concentration at a specific story.

1. INTRODUCTION

In "the seismic screening standards of existing reinforced concrete building" that is applying practically in Japan, seismic performance of structure that have strength deterioration (consisting of one brittle and one ductile vertical member) is evaluated as the follows, to use the basic seismic index that is formulated based on results of response analysis of single degree of system, to evaluate excluding brittle members, to evaluate with the strength index at ultimate limit. Considering procedure of evaluation is intended to simplify, performance evaluation of reinforced concrete structure don't reach to evaluation including general behavior with strength deterioration. Accordingly, in this study, response analysis of wall-frame structure modeled on level of member was carried out, results of that was compared with seismic performance in the seismic screening standards in Japan, the effect that member with strength deterioration affects seismic performance was examined as basic study.

2. PRELIMINARY SIMULATION OF THE FULL-SCALE SHAKING TABLE TEST

2.1 Description of the Specimen

At first, preliminary simulation of reinforced concrete wall-frame structure of full-scale 3D shaking table test that is planned by "DaiDaiToku Research Project" is shown. Particularly, the

[1]*Department of Architecture and Civil Engineering, Toyohashi University of Technology, Aichi, Japan*
Email: matsui@tutrp.tut.ac.jp
[2]*Earthquake Research Institute, University of Tokyo, Tokyo, Japan*
Email: kabe@eri.u-tokyo.ac.jp
[3]*Department of Architecture and Civil Engineering, Toyohashi University of Technology, Aichi, Japan*
Email: kura@tutrp.tut.ac.jp

effect that multi-story shear wall of center of the structure affects behavior of the structure. Plan and elevation of the specimen are shown in Figure 1. Details of the specimen are omitted herein.

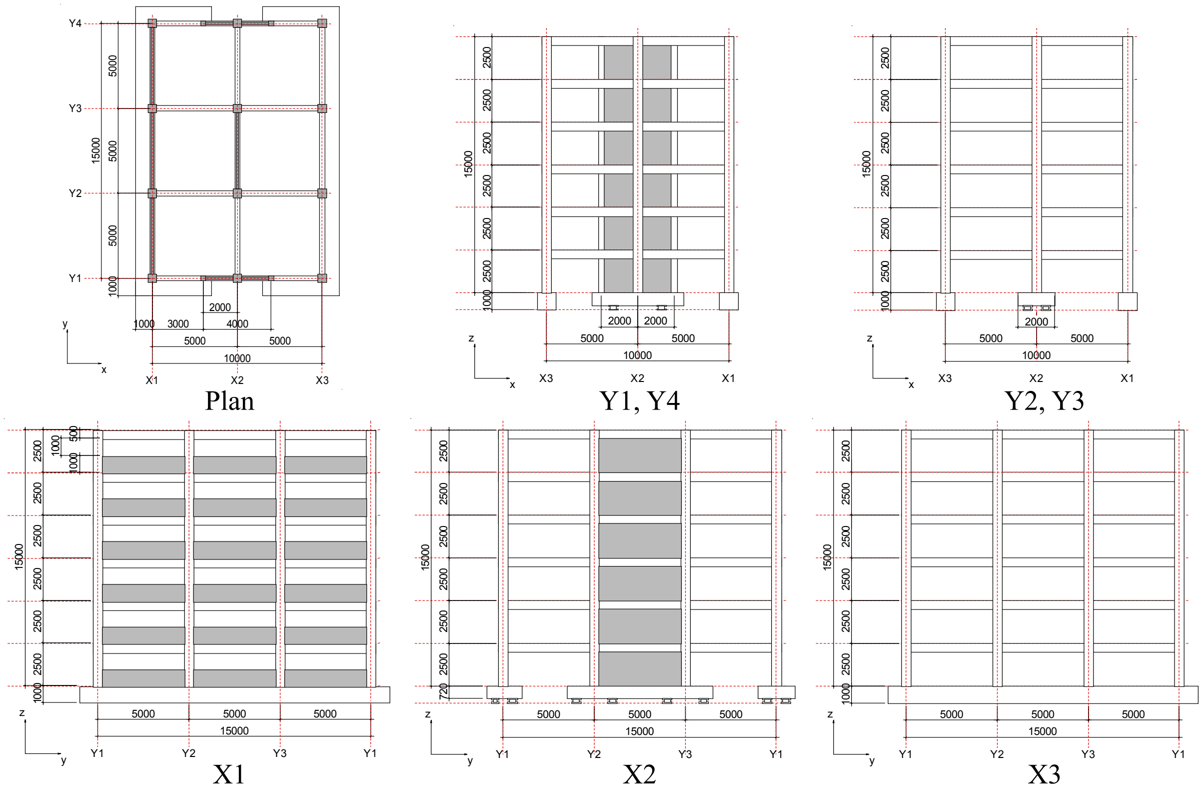

Fig. 1: Plan and elevation of specimen

2.2 Modeling of Structure

The specimen was modeled in 3 dimensions, floor slab was assumed to be rigid in plane, causing identical horizontal displacement of the entire joint in a floor level (component of horizontal displacement for rotation of slab are different). Strength deterioration was considered in only shear wall of center of the structure. In analysis, the yield strength of D10 and D19 reinforcing bars were assumed to be 354 N/mm^2 and 380 N/mm^2 respectively, the compressive strength was assumed to be 24 N/mm^2. Weights were given by the weight of effective areas to nodes as lumped mass, and considered component of horizontal of weight. Weight of a story was assumed 1225kN. The rotational inertia at node was ignored in this analysis. The foundation is considered fixed.

2.3 Modeling of Shear Wall

Shear wall is idealized isoparametric element to considering strength deterioration [1]. This wall model is composed of panel element, and line element of boundary column and boundary beam.

Boundary column is modeled by nonlinear spring, considering only axial stiffness. Rotational spring of boundary beam is rigid and axial spring of that is linear (Fig. 2). By using isoparametric element for panel element, it is possible to consider behavior of reinforced concrete panel under biaxial stress state. As for constitutive law for concrete, the rotating crack model was used, concrete stress-strain model considered the compression softening [2] and the tension stiffening effect [3] as shown in Figure 3. The steel hysteresis model used in this model is bi-linear type. The detailed theory and verification about this model are shown in [4], [5].

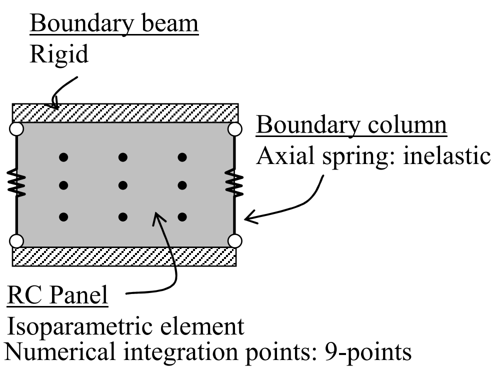

Fig. 2: Rough figure of shear wall model used isoparametric element

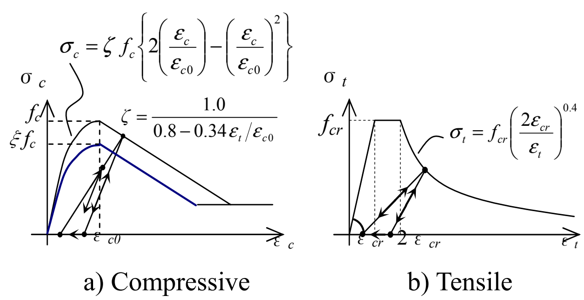

Fig. 3: Relationship of stress and strain of concrete at integration points

2.4 Modeling of Beam and Column

The One-component model was used for beams spandrel wall, wing wall and columns. The models have two nonlinear rotation springs at the two ends, and a nonlinear axial spring in this analysis. At rotation spring, Takeda model that included stiffness changes at flexural cracking and yielding was used (Fig. 4). The cracking and yielding point of skeleton curve were calculated according to reference [6]. The equations that were used to evaluation cracking moment M_c and yielding moment M_y of columns are shown in the following.

$$ {}_cM_c = 0.56\sqrt{F_c}\; Z_e + N\, D/6 \tag{1}$$

$$ {}_cM_y = 0.8 a_t\; {}_t\sigma_y\; D + 0.5\, N\, D\left(1 - \frac{N}{b\, D\, F_c}\right) \tag{2}$$

where F_c: compressive strength of concrete, Z_e: elastic section modulus, N: axial force on the section, D: depth of column, b: width of column, a_t: area of tensile reinforcement, ${}_t\sigma_y$: yielding strength of reinforcing bars.

The following equations were used to evaluation cracking moment M_c and yielding moment M_y of beam. The effective width of slab for beams were assumed 0.5 m (=0.1L:L is span of beam), ${}_GM_y$ of beam was obtained as the average ${}_GM_{yu}$ with tensile at upper end and ${}_GM_{yd}$ with tensile at lower end.

$$ {}_GM_c = 0.56\sqrt{F_c}\ Z_e \tag{3}$$

$$ {}_GM_y = \left({}_GM_{yu} + {}_GM_{yd}\right)/2 \tag{4}$$

$$ {}_GM_{yu} = 0.9\left(a_t\ {}_t\sigma_y + {}_{sr}a_t\ {}_{sr}\sigma_y\right)d \tag{5}$$

$$ {}_GM_{yd} = 0.9 a_t\ {}_t\sigma_y\ d \tag{6}$$

where d: effective depth, ${}_{sr}a_t$: area of reinforcement of slab, ${}_{sr}\sigma_y$: yielding strength of reinforcing bars of slab.

Yielding moment of the spandrel wall was evaluated the following equation, the average of yielding moment of tensile in beam side and that of tensile in spandrel wall.

$$ M_u = a_{te}\ \sigma_y\ (d_e - 0.5x_n) $$

$$ a_{te} = a_t + \sum a'_t\left(\frac{\sigma'_y}{\sigma_y}\right),\ \text{and}\ \ a_{te} \le \left(0.85F_c \cdot t \cdot x_{nb}/\sigma_y\right) - \sum a'_t\left(\frac{\sigma'_y}{\sigma_y}\right) \tag{7}$$

$$ x_n = a_{te} \cdot \sigma_y / (0.85F_c \cdot t),\quad x_{nb} = \frac{{}_c\varepsilon_B}{{}_c\varepsilon_B + {}_s\varepsilon_y} d_e \tag{8}$$

where, a_t: area of tensile reinforcement in beam, a_{te}: area of tensile reinforcement in spandrel wall, σ_y, σ'_y: yielding strength of beam and spandrel wall, t: thickness of spandrel wall or width of beam in compression side, d_e: center of tensile reinforcements, ${}_c\varepsilon_B$: strain at compression strength of concrete, ${}_s\varepsilon_y$: strain at yielding of reinforcement of beam.

The effective width of slab for beams were assumed 1.0 m, and elastic stiffness of beam were increased as 1.5 and 2.0 times for one side slab and two side slab. The post-yielding stiffness was assumed as 0.001 times the elastic stiffness. Transverse beams that connect to shear wall boundary columns and adjacent parallel frames were also modeled like the above.

Yielding moment of the wing wall was evaluated with the following equation.

$$ M_y = \left(a_t\ \sigma_y\ l_w + 0.5\sum\left(a_w\ \sigma_{wy}\right)l_w + 0.5N\ l_w\right) \tag{9}$$

where a_t: area of longitudinal reinforcement in tension-side boundary column, σ_y: yielding strength of longitudinal reinforcement in tension-side boundary column, a_{wv}: area of vertical reinforcement in wall, σ_{wy}: yielding strength of vertical reinforcement in wall, l_w: distance between centroids of boundary column, N: axial force on the section. Then a_t is equal to 0, longitudinal reinforcement of center column was included in a_{wv}.

The axial stiffness-model was used at axial springs (Fig. 5) of column. Stiffness in compression is elastic. Stiffness in tensile is reduced considering only reinforcements, the yielding strength were calculated for all main reinforcement bar of column. The post-yielding stiffness was assumed as 0.001 times the elastic stiffness.

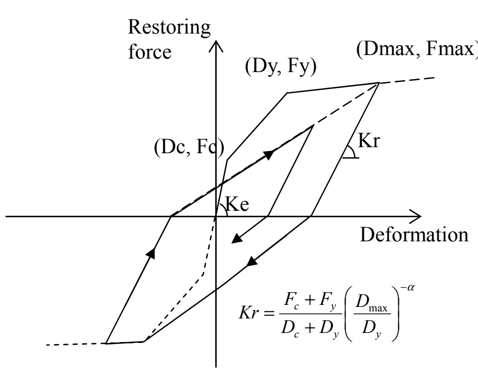

Fig. 4: Hysteresis model of rotational spring (TAKEDA-model)

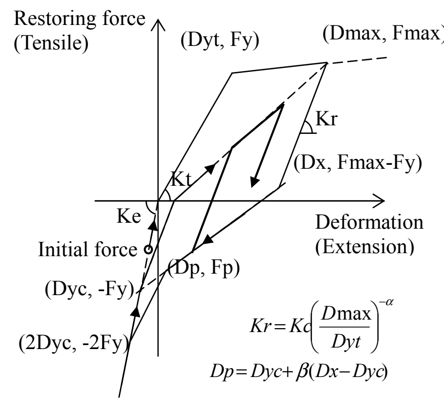

Fig. 5: Hysteresis model of axial spring

2.5 Method of Analysis

The equation of motion was solved numerically using Newmark-β method with β=0.25. Increment time for integrate was 0.002 sec. The damping factor was 0.02 in proportion to the tangential stiffness. Unbalanced forces due to change of stiffness were corrected in the next load step.

2.6 Input Ground Motion

The NS and EW component of Hyogo-ken Nanbu earthquake recorded at Japan Metrological Agency in 1995 (JMA) were used in this analysis. Considering that Input level in Y direction of structure become intense, direction of NS-component was corresponded to the direction rotated 45 degrees to the Y-axis as shown in Figure 6.

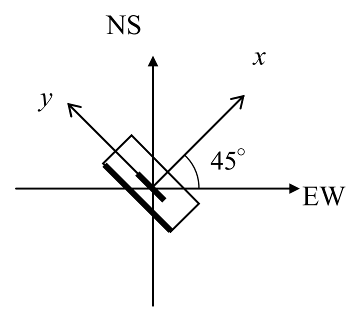

Fig. 6: Direction of input ground motion

2.7 Analytical Results

At first, results of planed specimen are shown. Relationships of base shear coefficient and drift angle at RF of X and Y direction are shown in Figures 7 and 8. Results of pushover analysis under inversed triangular and rectangular load distribution are plotted on these figures. Base shear coefficients of test structure in X and Y direction were 0.35 and 0.55 under inversed triangular load distribution, 0.43 and 0.7 under rectangular load distribution. Base shear coefficients of shear wall were 0.29 under inversed triangular load distribution, 0.38 under rectangular load distribution. In Y-direction considering strength deterioration, after yielding, base shear coefficient under rectangular load distribution declines at 0.015 rad steeply. The difference between rectangular and inversed triangular is seen in Figure 8. Maximum base shear coefficient in Y-dir. of response analysis reached 0.75, envelope curve of that show an agreement with skeleton curve under rectangular load distribution. Maximum base shear coefficient in X-direction of response analysis reached 0.32. Maximum displacement in X-direction reached 0.012 rad, it is one third times as much as that in Y-direction. Orbit of story drift angle at 2F and

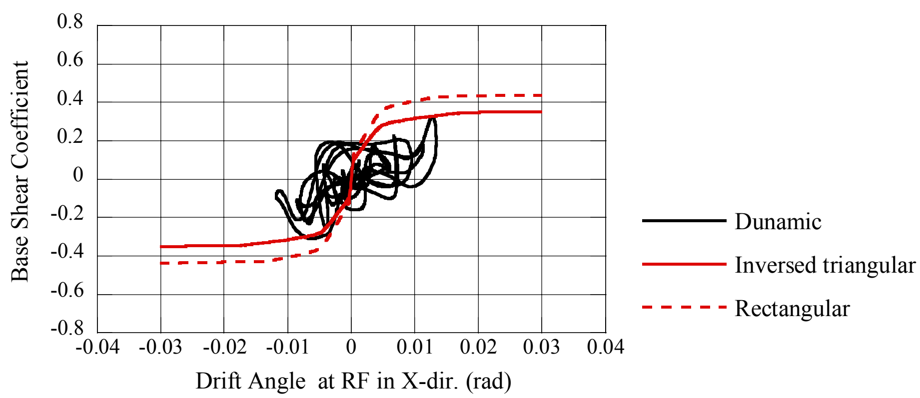

Fig. 7: Base shear coefficient vs. drift angle at RF of structure (X-direction)

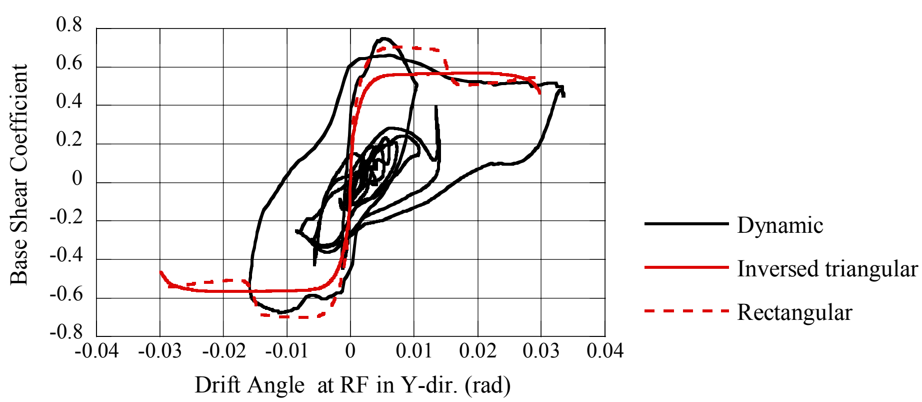

Fig. 8: Base shear coefficient vs. drift angle at RF of structure (Y-direction)

maximum story drift angle at each floors in Y-direction are shown in Figures 9–10. Response of structure is notable in Y-direction as Figure 9. And damage concentration in the first story is clearly seen from Figure 10. It is supposed that the structure collapse under 1.0 times input of JMA wave due to story collapse at first story in Y-direction.

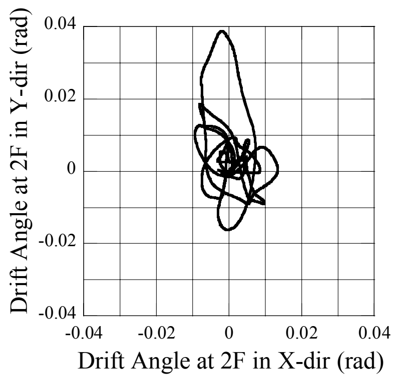

Fig. 9: Orbit of story drift angle at 2F

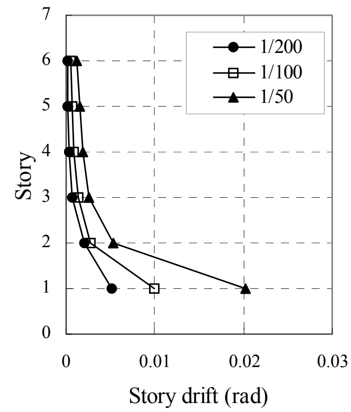

Fig. 10: Maximum story drift angle at each floors in Y-direction

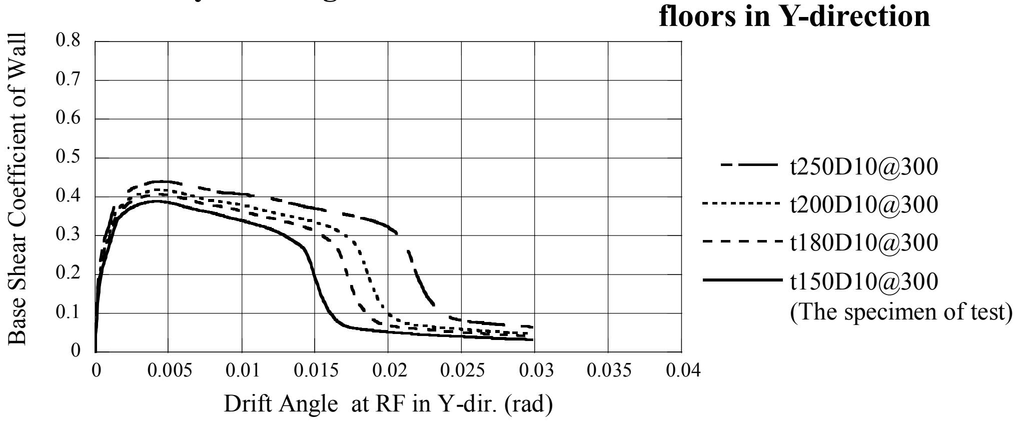

Fig. 11: Base shear coefficient vs. drift angle at RF of structure (Y-direction)
Under rectangular load distribution, Parameter is thickness of wall, t

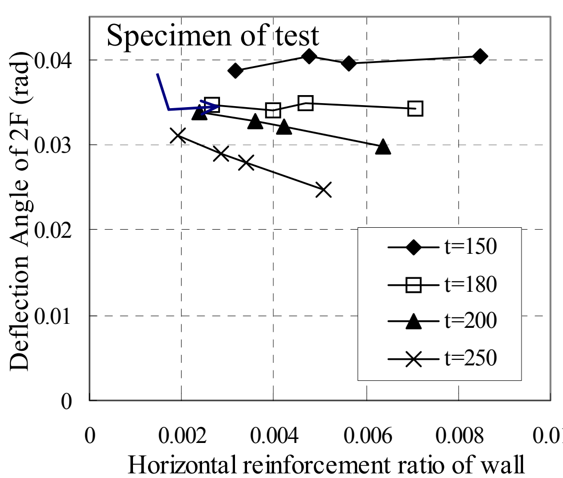

Fig. 12: Maximum story drift angle at 2F in Y-direction
t: thickness of shear wall

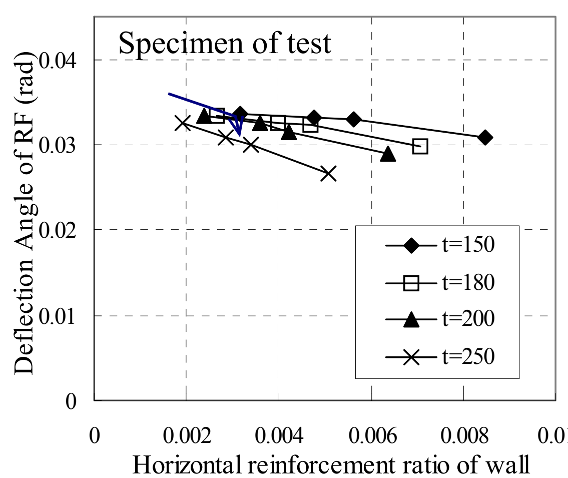

Fig. 13: Maximum story drift angle at RF in Y-direction
t: thickness of shear wall

Table 1 Section detail of members

Column	B×D (mm)		800×800
	Main bar		12-D25 (p_g =0.95%, p_t=0.32%)
	Hoop		4-D13@100
Beam	B×D (mm)		450×850
	Main bar	Top	5-D25 (p_t=0.66%)
		Bottom	3-D25 (p_t=0.4%)
Wall	Thickness		200
	Vertical and horizontal bar		2-D13@200 (p_w=0.635%)

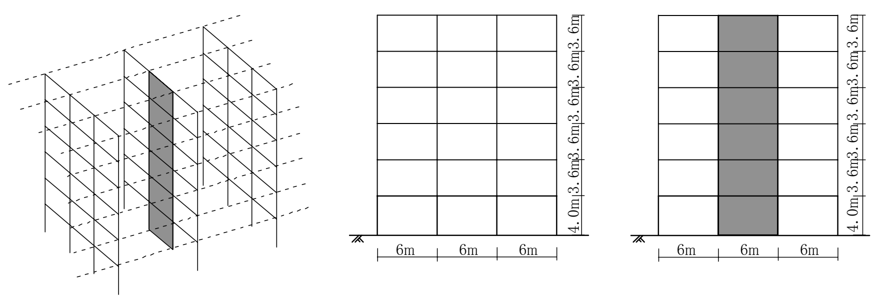

(a) Structure system (b) Frame plane (c) Wall-frame plane

Fig. 14: Analytical structure

3.2 Modeling of Structure

The structure in this analysis can be modeled by parallel combination of frame plane (Fig. 15) and wall frame plane (Fig. 16).

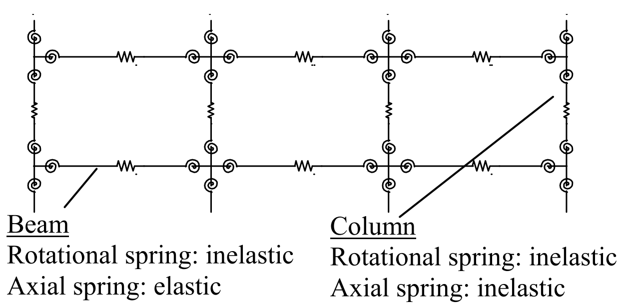

Fig. 15: Modeling of plane of frame plane

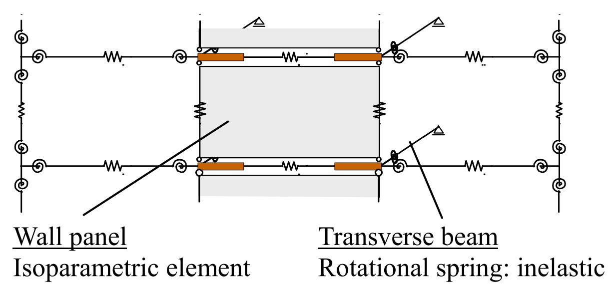

Fig. 16: Modeling of plane of wall-frame plane

3.3 Input Ground Motion

Five recorded earthquake motions were used in this study. The NS component of Miyagi-ken Oki earthquake recorded at Tohoku university in 1978 (TOH), the NS component of Imperial Valley earthquake recorded at EL Centro in 1940 (ELC), the NS component of Hyogo-ken Nanbu earthquake recorded at Japan Metrological Agency in 1995 (JMA), the EW component of Tokachi Oki earthquake recorded at Hachinohe in 1968 (HAC), the NS component of Hyogo-ken Nanbu earthquake recorded at JR Takatori Station in 1995 (TAK). Response acceleration spectrums and characteristics of are shown in Figure 17 and Table 2. The earthquake motions acceleration level of which are different were inputted to modeled structure. Duration of ground motions was inputted until the acceleration decline to 20% of peak of acceleration.

Table 2: characteristic of input ground motion (original level)

Earthquake data	Maximum acceleration (gal)	Maximum velocity (kine)	Duration time (sec)
ELC	341	34.8	0~20
HAC	186	42.9	0~30
JMA	836	85.4	1~15
TAK	612	124.2	0~18
TOH	262	40.9	5.6~25

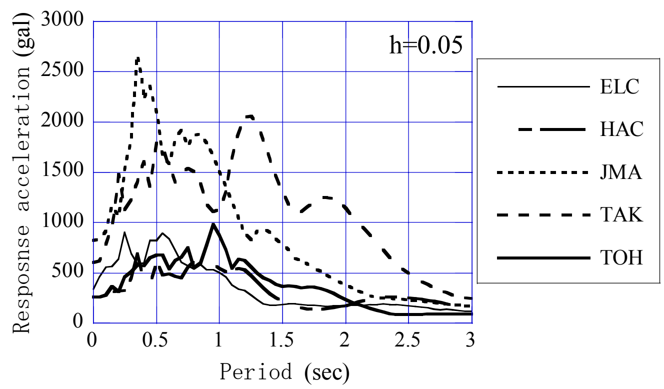

Fig. 17: Response acceleration spectrum (Original level of earthquake data)

3.4 Basic Seismic Index of the Seismic Screening Standards in Japan and Analysis Parameters

The basic seismic index E_0 in the "the seismic screening standards" of building in this study are defined as follows.

Wall-frame structure (vertical member have different deformation characteristic)

$$_{wc}E_0 = \frac{n+1}{n+i}\sqrt{(C_w F_w)^2 + (C_c F_c)^2} \tag{10}$$

Frame structure (vertical member have similar deformation characteristic)

$$_{c}E_0 = \frac{n+1}{n+i} C_c F_c \tag{11}$$

where, C_w, C_c: the strength index of wall and column, F_w, F_c: the ductility index of wall and column, n: the number of floor, i: the targeted floor. The strength index C is calculated by divided strength of vertical members by weight upper floors and the ductility index F is calculated with the deformation capacity and failure type of vertical members. As this study is intended for first story, $(n+1)/(n+i)$ is 1. Analysis parameter was established β, ratio of strength of wall to strength structure.

$$\beta = \frac{C_w}{C_w + C_c} \quad (0 \leqq \beta \leqq 0.65) \tag{12}$$

Then, C_c was constant (=0.28). The strength indexes of shear wall C_w were calculated using maximum shear force obtained from results of push over analysis. The ductility indexes of column were assumed 1.75, 2.1, 2.6, and 2.94. The ductility indexes of shear wall F_w were assumed values (F_w=1.4, 1.63, 1.82) corresponding to deflection angle when shear force declined to 80% of maximum from the results of analysis. Deflection angle and ductility factor corresponding to the ductility index are shown in Table 3. An example of push over analysis (ratio of wall-frame structure to frame structure is 1:2) is shown in Figure 18. Load distribution is inversed triangular. Fundamental period were 0.26 ～ 0.51. Although it is reported that seismic capacity variation is shown due to difference of natural period, this region is assumed to be almost applicable on the seismic screening standards.

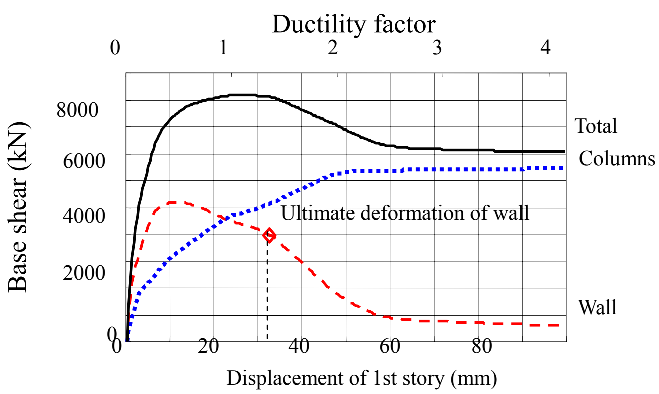

Fig. 18: Relationship of base shear and displacement of 1st story

Table 3: Deflection angle and ductility factor of Member corresponding to the ductility index

The ductility index	Deflection angle of member	Ductility factor
1	1/250	0.6
1.27	1/150	1
1.75	1/100	1.5
2.1	1/75	2
2.6	1/50	3
2.94	1/38	4
3.2	1/30	5

3.5 Results of Response Analysis

Relationship of β and ductility factor μ are shown in Figure 19. Where, ductility factor μ are calculated as maximum story drift angle of second floor to 1/150 of yielding deformation of column. β=0 represents frame structure. Although strength of structure rise with increasing β, ductility factor is increasing in a range more than about 2 under the same input acceleration level. While ductility factor is decreasing in a range less than μ=2 with increasing β. The same tendency is also shown under the other input earthquake motion except TAK.

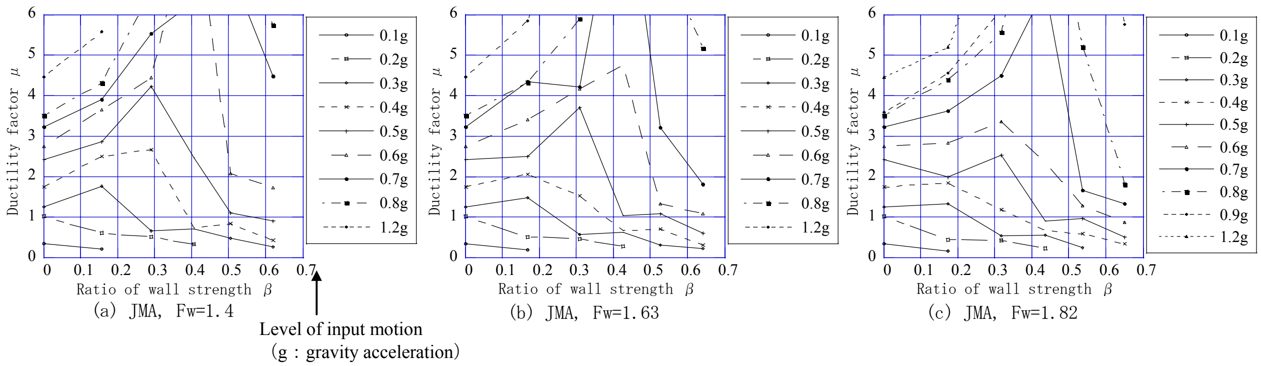

Fig. 19: Relationship of wall strength ratio β and ductility factor μ

Figure 20 is shown lateral displacement at each floor level of frame structure and wall-frame structure under the same input motion level. Displacement at the top floor of wall-frame structure is smaller than that of frame structure, while displacement at second floor of wall-frame structure is larger than that of frame structure. In Figure 20, wall-frame structure collapse at the first story due to strength deterioration with wall failure. It is thought that response ductility factor of wall-frame structure is larger than that of frame structure due to damage concentration in the first story.

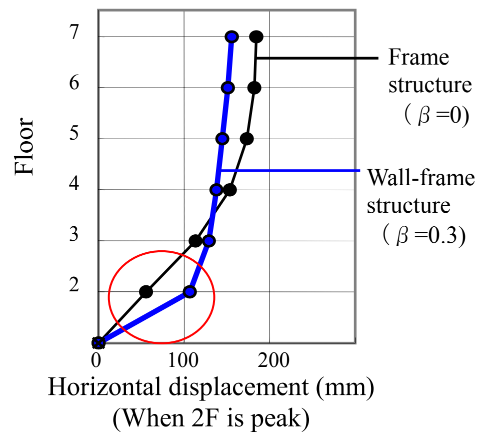

Fig. 20: Distribution of lateral displacement at each floor level

4. PERFORMANCE EVALUATION OF REINFORCED CONCRETE WALL-FRAMES WITH STRENGTH DETERIORAITION

Results of comparing analytical results with evaluation in the seismic screening standards are shown in Figure 22. Seismic capacity ratio, which is input motion level (maximum acceleration), k_{wc} when displacement at second floor reached ductility factor corresponding to the ductility

	Wall-frame structure	Frame structure	Seismic capacity ratio
Seismic capacity of the seismic screening standards	${}_{wc}E_0$	${}_{c}E_0$	${}_{wc}E_0/{}_{c}E_0$
Seismic capacity of analysis (Level of ground motion)	k_{wc}	k_c	k_{wc}/k_c

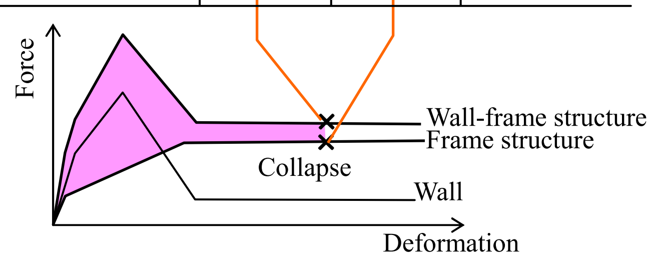

Fig. 21: Seismic capacities of response analysis and the seismic screening standards

indexes of column divided by that of frame structure (β =0), k_c is plotted in vertical axis. That is to say, seismic capacity ratio in this study represents how far is shear walls added on frame structure that is hatched in Figure 21 evaluated.

As for the structure whose ductility index of column F_c is relatively small, the evaluation in the seismic screening standards draw line including the minimum values of analytical results as shown in Figure 22. As for the structure whose ductility index of column F_c is relatively large, seismic capacity ratio based on the seismic screening standards is increasing with increasing β. However it can be seen that seismic capacity ratio on based response analysis could be becomes less than 1 from Figure 21, there is discrepancy between the seismic screening standards and response analysis. The larger F_c become, the more that tendency is specific. In other words, it is possible that seismic capacity of structure with strength deterioration could be overestimated in the seismic screening standards. In addition, as the strength index of wall F_w become large, seismic capacity ratio increase. Correlation of β, F_c and F_w, that express the level of strength deterioration up to collapse of structure.

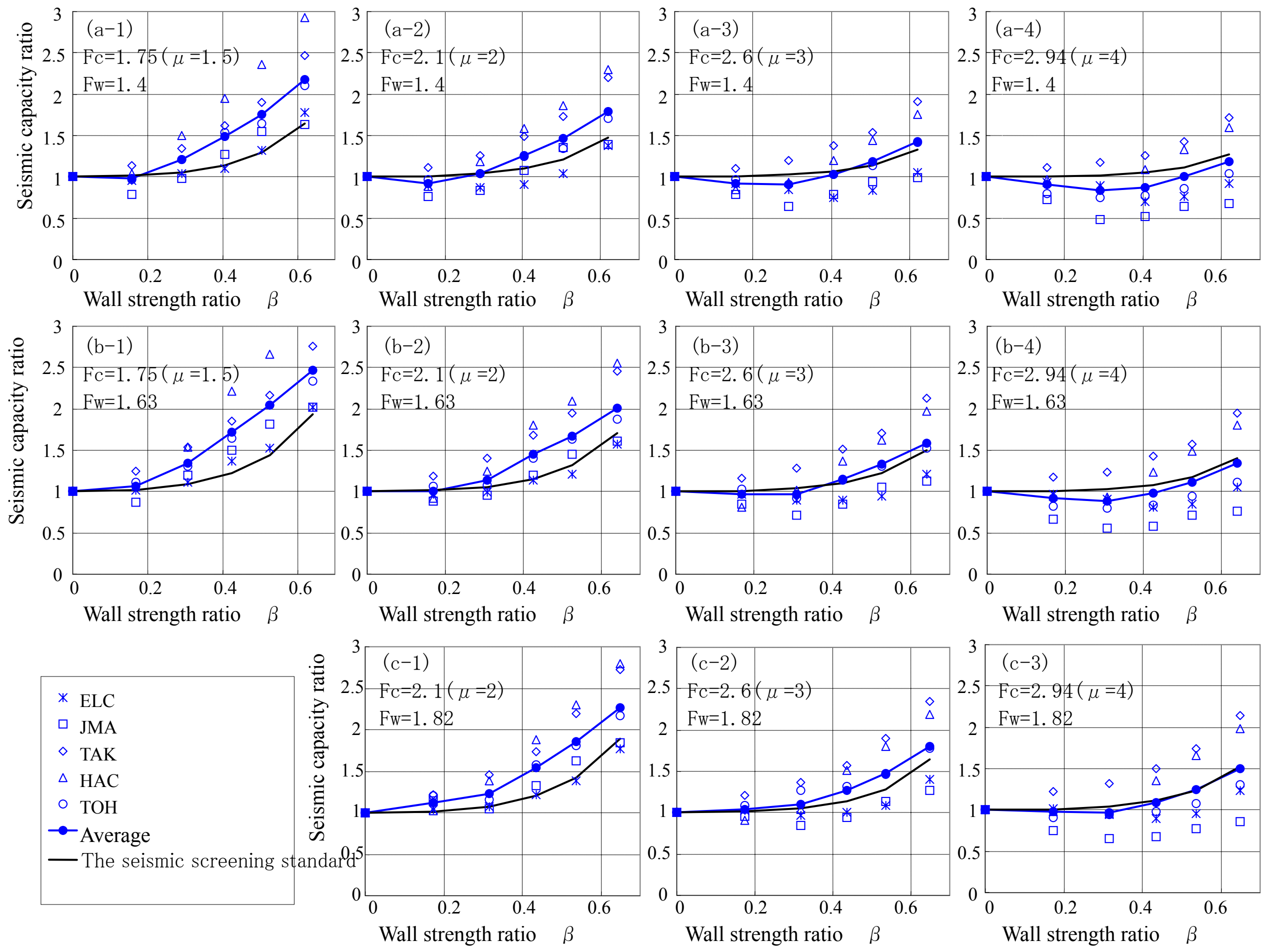

Fig. 22: Relationships of wall strength ratio, β, and seismic capacity ratio

5. CONCLUSIONS

1. The following conclusions can be drawn from the results of preliminary simulation of specimen of full-scale shaking table test.

- The specimen will be collapsed at first story in Y-direction by input motion of 1.0 time JMA wave.
- Even if thickness and reinforcement of wall increase, the specimen will be collapse by input motion of 1.0 times JMA wave.

2. Analytical results of wall-frame structure were compared with seismic performance in “the seismic screening standards of existing reinforced concrete building” in Japan, the effect that member with strength deterioration affects seismic performance was examined. The following conclusion can be drawn.

- Although the effect of strength deterioration has looseness according to the earthquake wave, it is possible that seismic capacity of structure that have a lot of deformability and strength deterioration could be overestimated in the seismic screening standards. And that behavior can be attribute damage concentration at a specific story.

REFERENCES

[1] Chen, S. and Kabeyasawa T. (2000). Modeling of reinforced concrete shear wall for nonlinear analysis. 12th World Conference on Earthquake Engineering, CD-ROM, Paper No.1596.

[2] Vecchio, F. and Collins, M. P. (1986). The Modified Compression Field Theory for Reinforced Concrete Elements Subjected to Shear, ACI Journal, Vol.83, pp.219-231.

[3] Okamura H. and Maekawa K. (1991). Nonlinear analysis and constitutive model of reinforced concrete, Gihodo.

[4] Matsui T. and Kabeyasawa T. (2004). Nonlinear analysis study on reinforced concrete walls subjected to cyclic load (in Japanese), Summaries of technical papers of annual meeting, Architectural Institute of Japan, C-Ⅱ, pp.291-292.

[5] Matsui T. and Kabeyasawa T. (2005). Analytical study on behavior of reinforced concrete shear walls (in Japanese), Proceedings of the 3d annual meeting of Japan association for earthquake engineering, Japan Association for Earthquake Engineering, pp.430-431.

[6] Design Guidelines for Earthquake Resistant Reinforced Concrete Buildings Based on Inelastic Displacement Concept (1997, in Japanese). Architectural Institute of Japan.

Keywords: Reinforced concrete, Full-scale shaking table test, Wall-frame structure, Strength deterioration, the seismic screening standards of Japan, seismic performance evaluation

DYNAMIC ANALYSIS OF REINFORCED CONCRETE WALL-FRAMES TO COLLAPSE

Yousok KIM[1] and Toshimi KABEYASAWA[2]

ABSTRACT

A non-linear analytical model developed for estimating the shear dominant behavior of non-ductile element is described. A salient feature of the proposed model is to represent strength degradation by incorporating the softening behavior in concrete constitutive law and the bending, shear and axial force interaction formulated from the plane stress resultants. Conventional analytical models for column and wall are also adopted, which are unable to simulate post peak behavior adequately. Using these two kinds of analytical models, preliminary analytical study on a full-scale shaking table test planned to conduct in January 2006 was carried out. Comparing the results obtained from these analytical methods show the difference in seismic responses and failure modes, which indicate the important role of realistic analytical model in assessing the performance and collapse process of the structure.

1. INTRODUCTION

A lot of efforts to understand the collapse process of RC structures under seismic loading have been devoted in both experimental and analytical studies. However, it is difficult to realize the realistic structural behavior expected during strong earthquake since there exist many restrictions in laboratory or field test. On the other hand, the trade-off between computational effort and accuracy of analytical procedures has posed a challenge in analytical study.

With the aim of simulating actual seismic behavior, an unprecedented shaking table test on a full-scale reinforced concrete building structure is planned at E-Defense of NIED, a new 3-D earthquake simulator, in January 2006. In this paper, characteristics of a full-scale specimen are described and analytical column model developed for estimating post peak behavior characterized by strength deteriorating feature is also introduced and validated by experimental results. The specific objective of the preliminary analytical study presented herein focus on predicting the collapse procedure of the full-scale specimen followed by strength deterioration of shear critical structural members. As well, the existing analytical models are also adopted and the difference in structural behavior with and without strength degrading feature is investigated.

[1] *Post-doctoral fellow, Earthquake Research Institute, University of Tokyo, Tokyo, Japan, Email: yskim@eri.u-tokyo.ac.jp*
[2] *Professor, Earthquake Research Institute, University of Tokyo, Tokyo, Japan, Email: kabe@eri.u-tokyo.ac.jp*

2. PROPOSED COLUMN MODEL

A column element in frame analysis is generally idealized by one line element with two-end nodes as shown in Figure 1(a). In the proposed model, however, the element is divided into three line elements by inserting two internal nodes (3,4) locating at αL_0 from two external nodes (1,2) (Fig. 1(b)). Furthermore, as shown in Figure 1(c), each line element is transformed to plate element with 4 nodes. The deriving procedure of member stiffness matrix is described below.

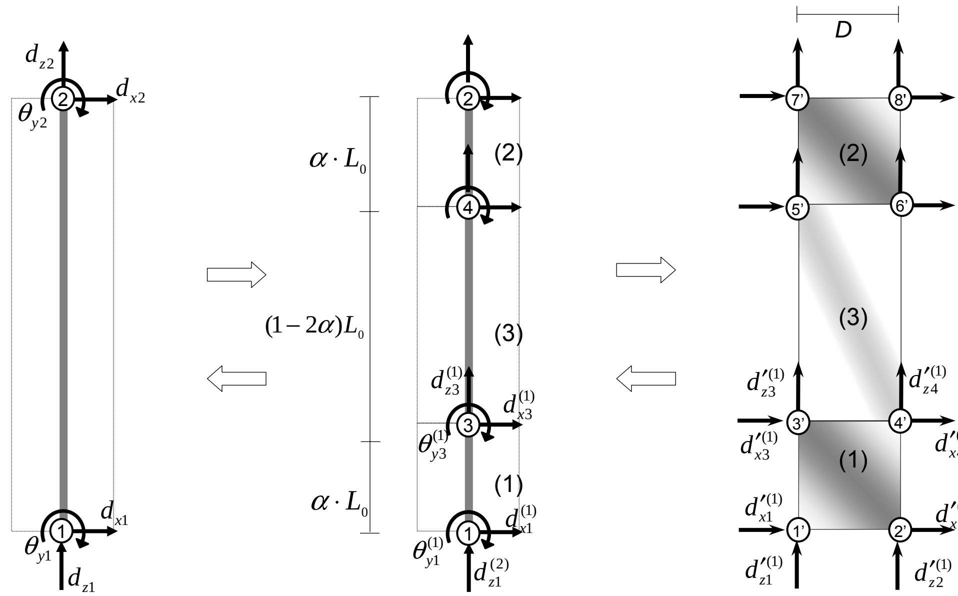

(a) Line element with two nodes (b) Subdivided line elements (c) Transformed plate elements

Fig. 1: Proposed column model

2.1 Deriving the Member Stiffness Matrix

The member stiffness matrix is derived from those of three line elements under the direct stiffness method enforcing the equilibrium and compatibility conditions at nodes (Eq. (1)).

$$\begin{Bmatrix} \{\Delta F_1\} \\ \{\Delta F_2\} \\ \{\Delta F_3\} \\ \{\Delta F_4\} \end{Bmatrix} = \begin{bmatrix} [k_{11}^{(1)}] & 0 & [k_{13}^{(1)}] & 0 \\ & [k_{22}^{(2)}] & 0 & [k_{24}^{(2)}] \\ & & [k_{33}^{(1)}]+[k_{33}^{(3)}] & [k_{34}^{(3)}] \\ symm. & & & [k_{11}^{(1)}]+[k_{44}^{(3)}] \end{bmatrix} \cdot \begin{Bmatrix} \{\Delta D_1\} \\ \{\Delta D_2\} \\ \{\Delta D_3\} \\ \{\Delta D_4\} \end{Bmatrix} \tag{1}$$

The superscripts in parenthesis and the subscripts denote the divided element number and node number, respectively. Expressed using internal (i) and external (e) node notation, Equation (1) becomes

$$\begin{Bmatrix} \{\Delta F_e\} \\ \{\Delta F_i\} \end{Bmatrix} = \begin{bmatrix} [K_{ee}] & [K_{ei}] \\ [K_{ie}] & [K_{ii}] \end{bmatrix} \cdot \begin{Bmatrix} \{\Delta D_e\} \\ \{\Delta D_i\} \end{Bmatrix} \tag{2}$$

On the basis of the assumption that no external force is applied to the internal nodes, Equation (3) is obtained.

$$\{\Delta D_i\} = [K_{ii}]^{-1} \cdot (\{\Delta F_i\} - [K_{ie}]\{\Delta D_e\}), \qquad \{\Delta F_i\} = 0 \tag{3}$$

By substituting Equation (3) into Equation (2) (static condensation method), we have reduced member stiffness matrix in the form of Equation (4), where only the external nodal displacements and forces are related.

$$\{\Delta F_{6\times1}\} = [K_{6\times6}]\{\Delta D_{6\times1}\} \tag{4}$$

2.2 Plate Element Formulation

Figure 1 (b) and (c) shows the relationship between line element and plate element, which have 6 and 8 DOF respectively. The line element can be transformed to plate element based on the two assumptions: one is plane section hypothesis and the other is the stress assumption that transverse stress is zero. The displacement relationship between two elements is, therefore, obtained as like Equation (5).

$$\left.\begin{aligned} d'^{(1)}_{x1} &= d^{(1)}_{x1}, \qquad & d'^{(1)}_{z1} &= d^{(1)}_{z1} + (D/2)\cdot\theta^{(1)}_{y1} \\ d'^{(1)}_{x4} &= d^{(1)}_{x3}, \qquad & d'^{(1)}_{z4} &= d^{(1)}_{z3} - (D/2)\cdot\theta^{(1)}_{y3} \end{aligned}\right\} \tag{5}$$

The plate element is considered as linear plane element with two nodes along an edge and based on the isoparametric formulation which uses the same shape functions to define the element shape as are used to define the displacements within element. A strain-displacement matrix $[B_{3\times8}]$ and a plane stress-strain relationship are shown in Equation (6) and (7), respectively. The assumption that the nodal displacements in lateral direction transformed from the line element are identical makes the transverse incremental strain $\Delta\varepsilon_x$ become zero in Equation. (6). Therefore, the lateral strain cannot be found in an explicit way using Equation (6), but instead evaluated from Equation (8) consistent with the assumption described above.

$$\{\Delta\varepsilon\} = [B_{3\times8}] \cdot \{\Delta d'_{8\times1}\} \tag{6}$$

$$\{\Delta\sigma\} = [D]\{\Delta\varepsilon\} = \begin{bmatrix} D_{11} & D_{12} & D_{13} \\ D_{21} & D_{22} & D_{23} \\ D_{31} & D_{32} & D_{33} \end{bmatrix} \begin{Bmatrix} \Delta\varepsilon_x \\ \Delta\varepsilon_z \\ \Delta\gamma_{xz} \end{Bmatrix} \tag{7}$$

$$\Delta\varepsilon_x = -\frac{D_{12}}{D_{11}}\cdot\Delta\varepsilon_z - \frac{D_{13}}{D_{11}}\cdot\Delta\gamma_{xz} + \frac{\Delta\sigma_x}{D_{11}}, \quad (\Delta\sigma_x = 0) \tag{8}$$

Once the incremental transverse strain is found, complete plane strain components are obtained and then plane stresses can be calculated. In this study, smeared rotating crack approach is adopted for evaluating stresses and material tangent stiffness matrix from given strains, which is based on averaged stress and strain including the effect of crack and coaxiality between principal stress and strain (Vecchio, 1986 and Stevens, 1991).

$$\{f'_{8\times1}\} = \int [B_{3\times8}]^T \{\sigma\} dV \ , \tag{9}$$

$$[k'_{8\times8}] = \int [B_{3\times8}]^T [D][B_{3\times8}] dV \tag{10}$$

Finally, the force and stiffness matrix of plate element can be evaluated by numerical integration with two-dimensional gaussian quadrature (Eqs. (9) and (10)).

2.3 Constitutive Model

The behavior of the plate element that is basic analytical unit in the proposed model is determined from the material constitutive laws and therefore the accuracy of the analytical results is, to a great extent, dependent on the material models. Figure 2 shows the constitutive laws for concrete, where the strength softening effect and the tension stiffening effect are considered.

The compressive strength reduction factor c_1 is adopted from Vecchio and Collins (1986) (Eq. 11) and the descending branch representing the tension stiffening effect is from Isumo and Shima (1989). For the constitutive law of longitudinal and transverse reinforcement, Ramberg-Osgood type model is used.

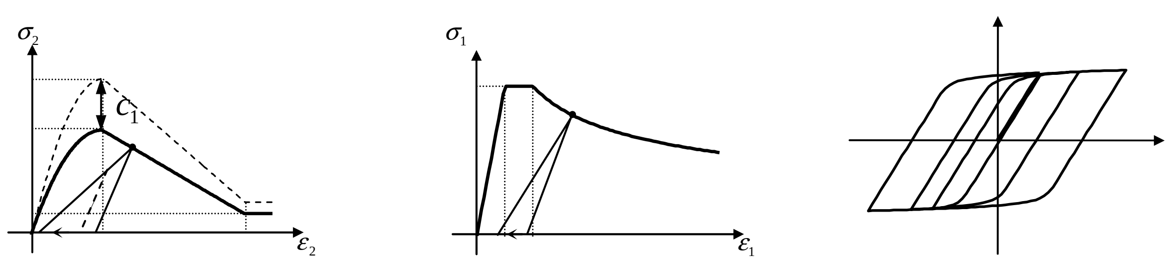

(a) Concrete compressive model (b) Concrete tension model (c) Steel mode

Fig. 2: Constitutive law for concrete and steel

$$c_1 = 1.0/(0.8 - 0.34\varepsilon_1/\varepsilon_{c0}) \tag{11}$$

2.4 Iterative Procedure for Numerical Solution

Two iterative schemes imposing internal force equilibrium (Eq. (12)) and transverse stress equilibrium condition (Eq. (13)) are introduced as the numerical solution. Both of the iterative procedures are continued until the predefined convergence tolerance is satisfied, and the updated material and element stiffness is used for evaluating the residual displacement in internal nodes and the transverse residual strain, respectively.

$$\{F_i^u\} = \{\{f_3^{(1)}\} + \{f_3^{(3)}\}, \{f_4^{(3)}\} + \{f_4^{(2)}\}\}^T \tag{12}$$

$$\sigma_x^u = \sigma_{cx} + \rho_{sx} \cdot \sigma_{sx} (= 0) \tag{13}$$

However, the displacements assigned at external nodes should not be changed in the iteration loop, because the displacement compatible condition at the external nodes should be ensured. In a same manner, explicitly calculated strains (i.e., longitudinal and shear strain) are not updated in the iteration loop, but the lateral strains at each integration point are computed using renewed material stiffness and residual stress obtained by imposing the equilibrium condition between transverse steel stress and concrete one.

2.5 Model Validation

For the purpose of verifying the proposed model, column tests under reversed cyclic loading were simulated using the proposed model. The main experimental parameter of specimens adopted herein is the level of axial load stresses, 0.28, 0.3 and 0.16 (Ousalem and Kabeyasawa, 2002).

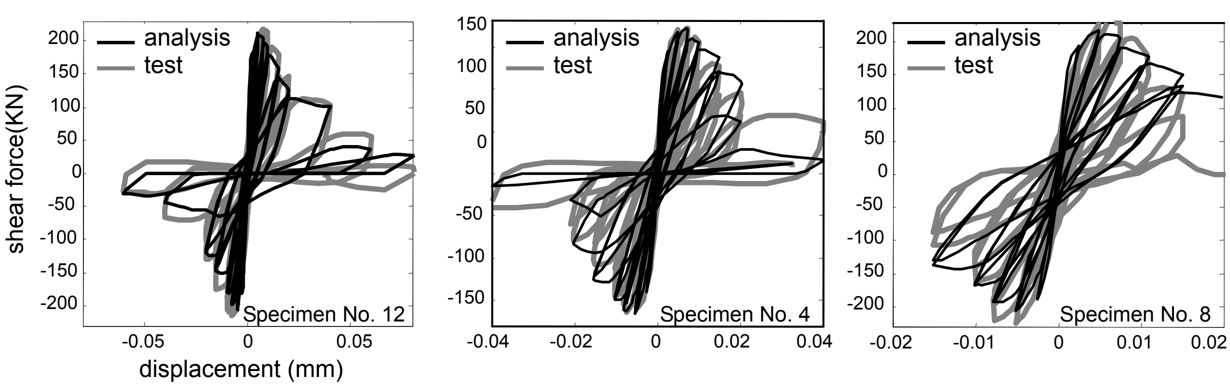

(a) $N_0 / bDF_c : 0.16$ (b) $N_0 / bDF_c : 0.28$ (c) $N_0 / bDF_c : 0.3$

Fig. 3: Experiment vs. analysis

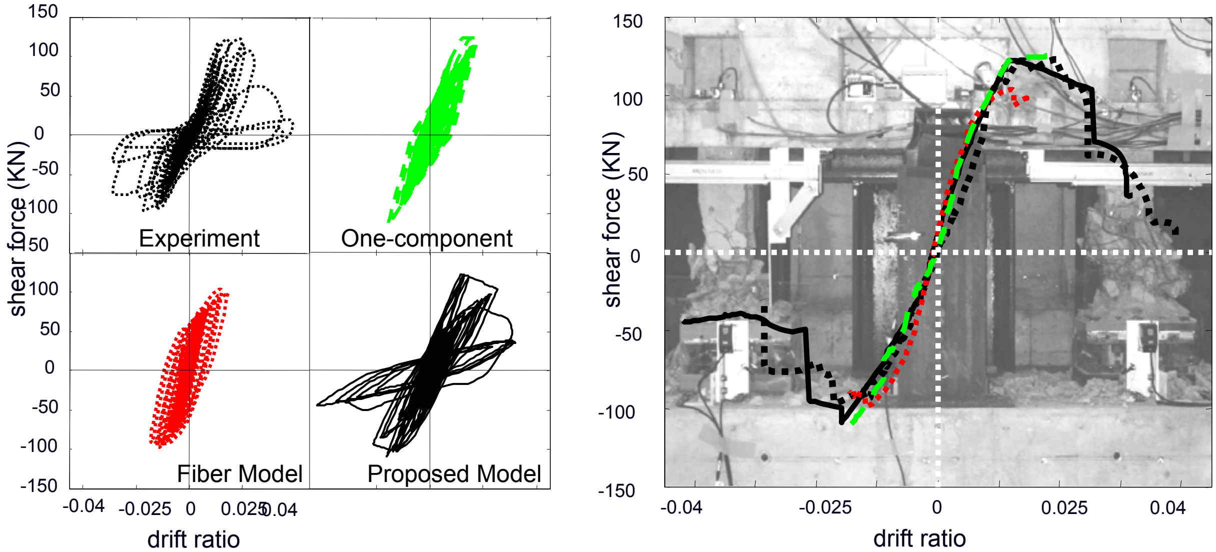

(a) Shear force-drift ratio hysteretic relationship (b) Envelope curves

Fig. 4: Correlation between test and analytical results

The analytical results are compared with the experimental ones in Figure 3. Good correlation between the predicted and the observed load-displacement relationship was obtained, although less accuracy has been observed in relatively high axial load conditions (Fig. 3(c)) where strength degradation in test is more outstanding compared to that of calculated ones.

In addition to the static test described above, shaking table test (Kim and Kabeyasawa, 2002) also analysed by proposed model and existing analytical models (One-component model and fiber model). Figure 4 shows the load-deflection relationships between observed and simulated results during Chile earthquake (1985) input with a scaled maximum velocity of 28.3cm/sec corresponding to 50cm/sec for prototype structure. As shown in Figure 4, only the proposed model could simulate the strength degrading behavior observed in experimental results, although the load-deformation backbone curves of conventional models also showed acceptable agreement with the experimental one before the initiation of strength deterioration.

3. ANALYTICAL METHODOLOGY

3.1 Full-Scale Specimen

The full-scale specimen, designed in accordance with 1970's design practice in Japan, has a six-story in height and 3-span and 2-bay in plan (Fig. 5). Longitudinal direction (Y-direction) in plan comprises open frames, a shear wall frame and a spandrel beam frame with short columns, which generate moderate uniaxial eccentricity in whole plans. And the transverse direction (X-direction) with symmetric plan consists of open frames and wing walls that provide considerable strength and stiffness.

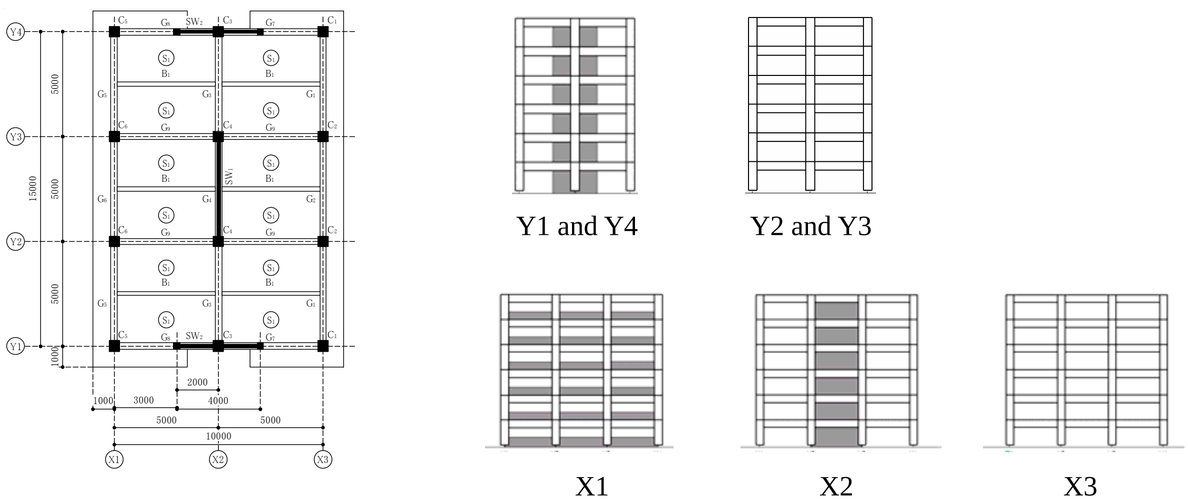

Fig. 5: Plan and elevation of full-scale specimen

3.2 Analytical Model

In order to predict the collapse procedure of the specimen, the post peak response characterized by strength deterioration of shear critical members should be simulated in analytical models. Preliminary analytical study presented herein focused on the structural behaviour and the failure mode that are dependent on the analytical member models.

Two shear wall models (**T**hree **V**ertical **L**ine **E**lement model and **I**so-**P**arametric **M**odel) and three column models (**O**ne-**C**omponent model, **F**i**B**er model and **P**roposed **M**odel) are adopted as the analytical models in this study. These models are mainly different in the ability to simulate the strength deteriorating feature. Table 1 summarize the combination of analytical member models investigated in this analytical study.

Table 1: Matrix of analytical model combination

Column / Wall	One-Component model	Fiber model	Proposed model
Three Vertical Line Element	TVLE-OC	TVLE-FB	TVLE-PM
Iso-Parametric Element	IPE-OC	IPE-FB	IPE-PM

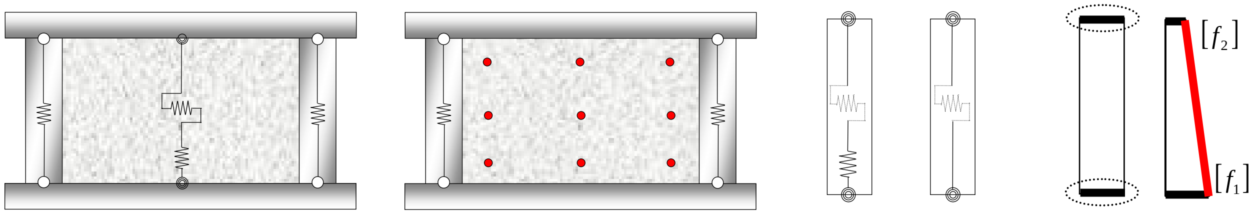

(a) TVLE (b) IPE (c) OC (d) FB

Fig. 6: Member models

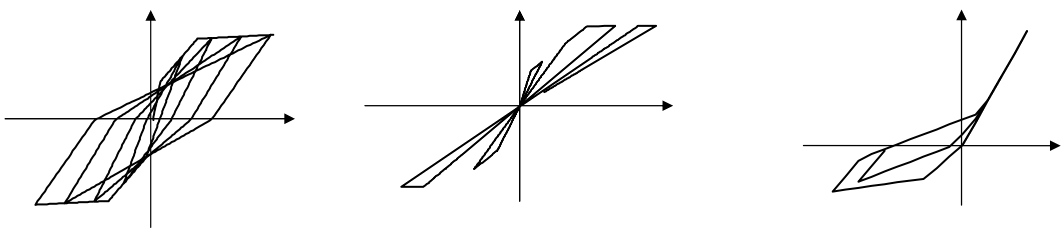

(a) Takeda model (b) Origin-Oriented model (c) Axial stiffness model

Fig. 7: Hysteretic models for force-displacement relation

The conceptual illustration of wall models and line element models are shown in Figure 6. All girders of specimen are modelled by one-component model irrespective of model combination. The girder sections are calculated taking into account the contribution of effective slab width. Slab and beam-column connection were assumed to be rigid in all cases.

Three Vertical Line Element model

Wall panel is idealized by rotational, shear and axial spring, and two side columns attached to the panel are represented by axial component using one-component model or fiber model. The flexural and the axial behavior of boundary beams are assumed to be rigid. Origin-Oriented model (Fig. 7(b)) is used as the hysterical model for both flexural bending and shear component, and axial stiffness model (Fig. 7(c)) is for the axial hysteretic model. In this model, the interaction between flexural bending and shear component in panel cannot be expected because the shear response is determined from the second-order effect of flexural one.

Iso-Parametric Element model (Chen and Kabeyasawa, 2000)

Shear panel consists of one isoparametric element based on the smeared-rotating crack approach. The force-displacement relation of the shear panel is obtained from the plane stress-plane strain relationship estimated at the gauss integration points, which enable this model to consider N-M-V interaction in a rational manner. Constitutive laws for concrete and steel are identical to those used in PM model (Fig. 2(a)(b)) and the boundary line elements, columns and beams, are modelled in the same manner as TVLE model.

One-Component model

Flexural bending behavior is idealized by implementing rotational springs at the end of member and axial behaviour is represented by axial spring. On the other hand, shear flexibility coefficient is assumed to be proportional to that of flexural bending instead of incorporating shear spring. For girders, flexural bending and shear component are same to those of column but the axial component is not considered. Takeda model and axial stiffness model are adopted as the hysterical model for the rotational and the axial spring, respectively (Fig. 7).

Fiber model

Fiber model used in this analysis is based on the force method (flexibility method) and only two end sections are taken into account for element formulation. In this model, the flexibility distribution along the member axis is assumed to be linear, which can be formulated by flexibility matrix relationship between two end sections (Eq. 14). Therefore, the analytical integration is used for calculating the member flexibility matrix instead of numerical integration, which result in efficiency of computational effort. Figure 8 shows end sections of column and wing wall subdivided by concrete and reinforcement fibers.

$$f(z) = (1 - z/L_0) \cdot [f_1] + z/L_0 \cdot [f_2] \tag{14}$$

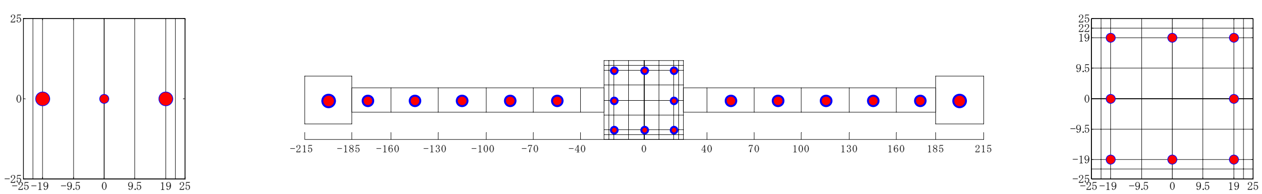

(a) Attached column to the shear wall (b) Wing wall (c) Independent column

Fig. 8: Section division

Table 2 summarizes the characteristics of each column model into three categories: plasticity distribution (strength degrading feature), X-Y-Z axis coupling and N-M-V coupling. It is seen from these descriptions that all of these three models have the limitation for evaluating the response expected to occur in full-scale specimen.

Table 2: Characteristics of column models

	Plasticity distribution	X-Y-Z axis coupling	N-M-V coupling
One-Component Model	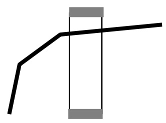	$\begin{Bmatrix}\{M_x\}\\ \{M_y\}\\ \{N_z\}\end{Bmatrix}=\begin{bmatrix}[K_{xx}] & [0] & [0]\\ & [K_{yy}] & [0]\\ sym. & & [K_{zz}]\end{bmatrix}\cdot\begin{Bmatrix}\{\theta_x\}\\ \{\theta_y\}\\ \{d_z\}\end{Bmatrix}$	$\begin{Bmatrix}\{M\}\\ \{N\}\\ \{V\}\end{Bmatrix}=\begin{bmatrix}[K_{MM}] & [0] & [0]\\ & [K_{NN}] & [0]\\ sym. & & [K_{VV}]\end{bmatrix}\cdot\begin{Bmatrix}\{\theta\}\\ \{u\}\\ \{v\}\end{Bmatrix}$
Fiber Model	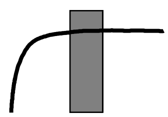	$\begin{Bmatrix}\{M_x\}\\ \{M_y\}\\ \{N_z\}\end{Bmatrix}=\begin{bmatrix}[K_{xx}] & [K_{xy}] & [K_{xz}]\\ & [K_{yy}] & [K_{yz}]\\ sym. & & [K_{zz}]\end{bmatrix}\cdot\begin{Bmatrix}\{\theta_x\}\\ \{\theta_y\}\\ \{d_z\}\end{Bmatrix}$	$\begin{Bmatrix}\{M\}\\ \{N\}\\ \{V\}\end{Bmatrix}=\begin{bmatrix}[K_{MM}] & [K_{MN}] & [0]\\ & [K_{NN}] & [0]\\ sym. & & [K_{VV}]\end{bmatrix}\cdot\begin{Bmatrix}\{\theta\}\\ \{u\}\\ \{v\}\end{Bmatrix}$
Proposed Model	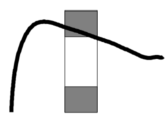	$\begin{Bmatrix}\{M_x\}\\ \{M_y\}\\ \{N_z\}\end{Bmatrix}=\begin{bmatrix}[K_{xx}] & [0] & [0]\\ & [K_{yy}] & [K_{yz}]\\ sym. & & [K_{zz}]\end{bmatrix}\cdot\begin{Bmatrix}\{\theta_x\}\\ \{\theta_y\}\\ \{d_z\}\end{Bmatrix}$	$\begin{Bmatrix}\{M\}\\ \{N\}\\ \{V\}\end{Bmatrix}=\begin{bmatrix}[K_{MM}] & [K_{MN}] & [K_{MV}]\\ & [K_{NN}] & [K_{NV}]\\ sym. & & [K_{VV}]\end{bmatrix}\cdot\begin{Bmatrix}\{\theta\}\\ \{u\}\\ \{v\}\end{Bmatrix}$

4. PUSHOVER ANALYSIS

Non-linear pushover analyses were conducted on six cases of model combinations (Table 1) by applying increasing lateral force representing uniform and inverted triangular distribution over the height.

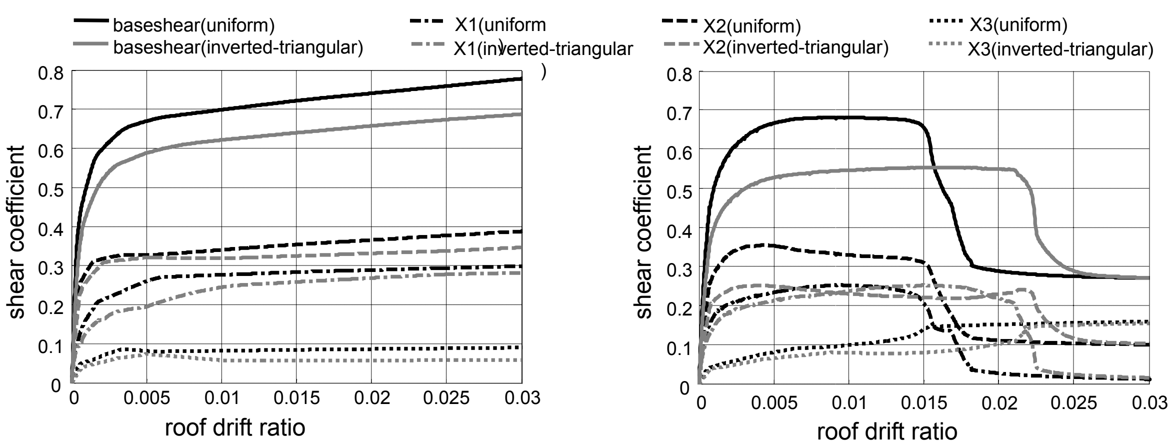

(a) TVLE-OC (b) IPE-PM

Fig. 9: Pushover analysis results

For two cases of TVLE-OC and IPE-PM, Figure 9 shows the relationship between roof drift ratio and shear coefficient of each frame on loading direction (Y-direction). The effect of force distribution type on shear coefficient is outstanding in IPE-PM combination case where strength deterioration feature is considered both in wall and in column model.

In Figure 10, the relationship between 1F inter-story drift ratio and shear coefficient of X1 and X2 frame is presented with the deformed shape of specimen when the roof drift ratio is 0.015.

It can be seen from this figure that the displacement concentration on the 1st story and load-carrying capacity between X1 and X2 frame are varied according to the column models.

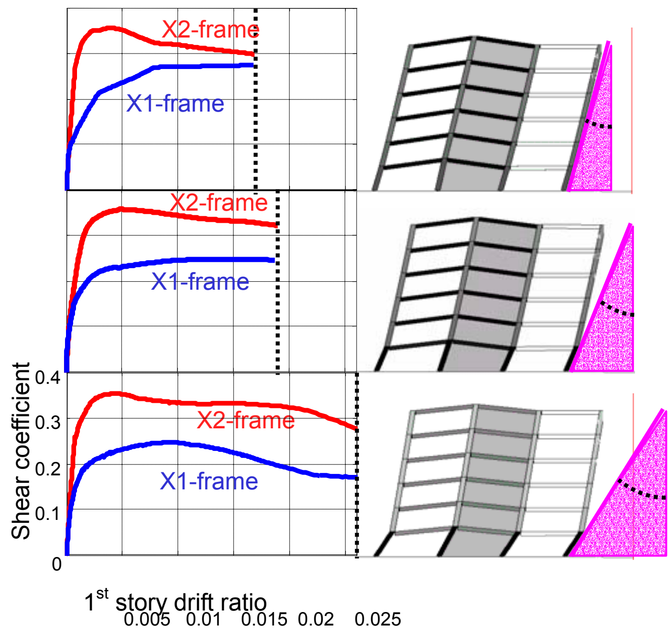

Fig. 10: Drift ratio vs. shear coefficient

Figure 11 shows the collapse process of specimen before onset of strength degradation in shear wall by illustrating the yielding sequence of members adjacent to the shear wall. It should be noted that the magnitudes of member responses, except for the shear wall, were scaled arbitrarily for the convenience of comparing each response. Tensile yield of boundary column in tensile side occurred first and then the flexural yielding of girders in loading direction was followed. Strength degradation in shear wall was initiated shortly after the transverse girder yielded.

Figure 11(b) and (c) show the yielding state of the other girders when the longitudinal and the transverse girder yielded, respectively. A similar process was observed irrespective of the model combinations.

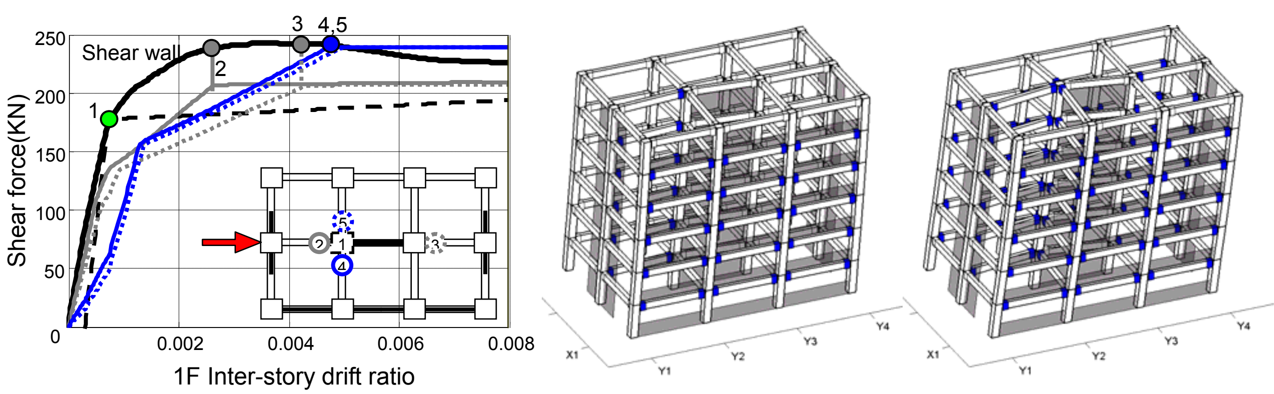

(a) Yielding sequence of members (b) Stage 2 (c) Stage 4

Fig. 11: Collapse process of specimen

5. DYNAMIC ANALYSIS

5.1 Earthquake Data Input Plan

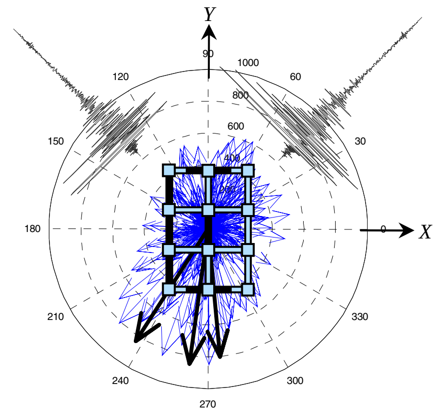

Fig. 12: Earthquake input direction

Kobe earthquake (JMA, 1995) is chosen for the input ground motion. North-south and east-west components are subjected to the specimen with an angle 45 degree and 135 degree rotated from the X-axis, respectively (Fig. 12), and vertical component is also applied.

The solid and the dashed arrows in Figure 12 indicate the direction of acceleration resultant composed of NS and EW components when the maximum acceleration is recorded in NS and EW components, respectively.

And maximum acceleration resultant of two components is shown by solid thick arrow. As can be seen from this figure, the earthquake input resulted from two components is roughly directed along the axis of shear wall (Y-axis).

5.2 Torsional Response

Figure 13 shows the mode shapes (from 1st to 3rd) calculated from the initial stiffness and the stiffness when the roof drift ratio is 0.015. At initial state, we can see that torsional mode is coupled with translational one in 2nd and 3rd mode, but in inelastic range, translational response become dominant. This change in dynamic characteristics can be attributed from the fact that spandrel beam frame yielded in early stage as shown in Figure 11and consequently the difference in stiffness between X1 and X3 frame, which generate the stiffness eccentricity in plan, become small. In addition, it can be inferred that torsional response was resisted by Y1 and Y4 frame with high stiffness and strength.

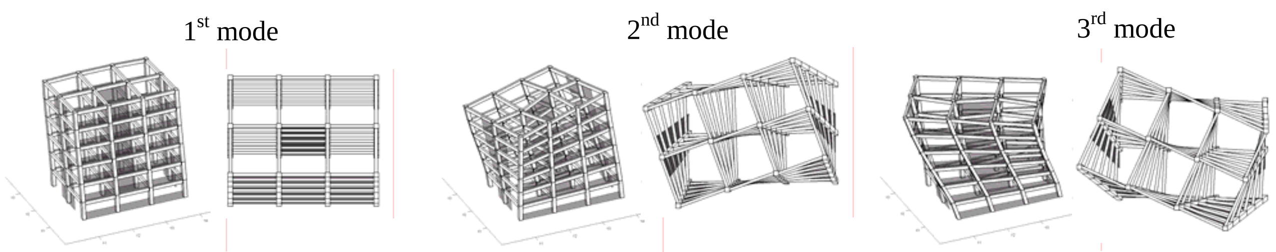

(a) Initial state

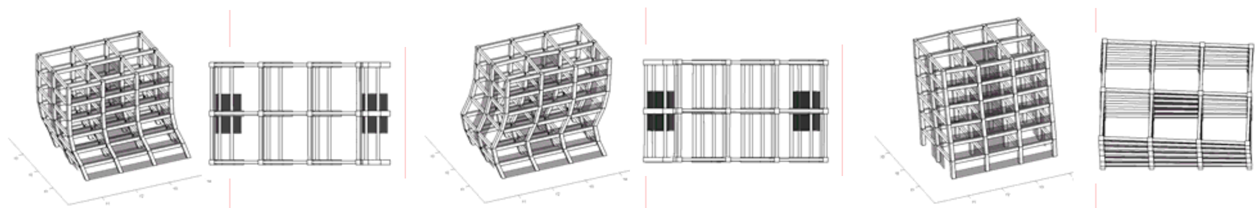

(b) Inelastic range (roof drift ratio: 0.015)

Fig. 13: Mode shape

This result could also be observed by comparing the index of torsional response degree in elastic range with that in inelastic range. This index indicates the distance of the response center from the center of gravity (Kim and Kabeyasawa, 2002, Figure 14(a)).

The relationship between rotating angle and translational displacement at a gravity center is illustrated in Figure 14, where the lines are fitted from the dynamic analysis results of full-scale specimen subjected Kobe NS component in the Y-direction. It is apparent from this figure that the torsional response is more distinguishable in elastic range rather than in inelastic one.

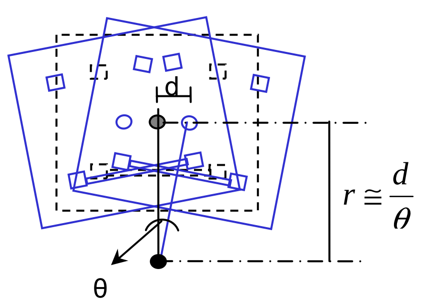

(a) Response center

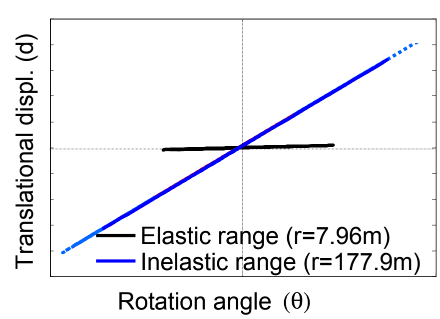

(b) Rotation angle-translational displ.

Fig. 14: Torsional response degree in elastic and inelastic range

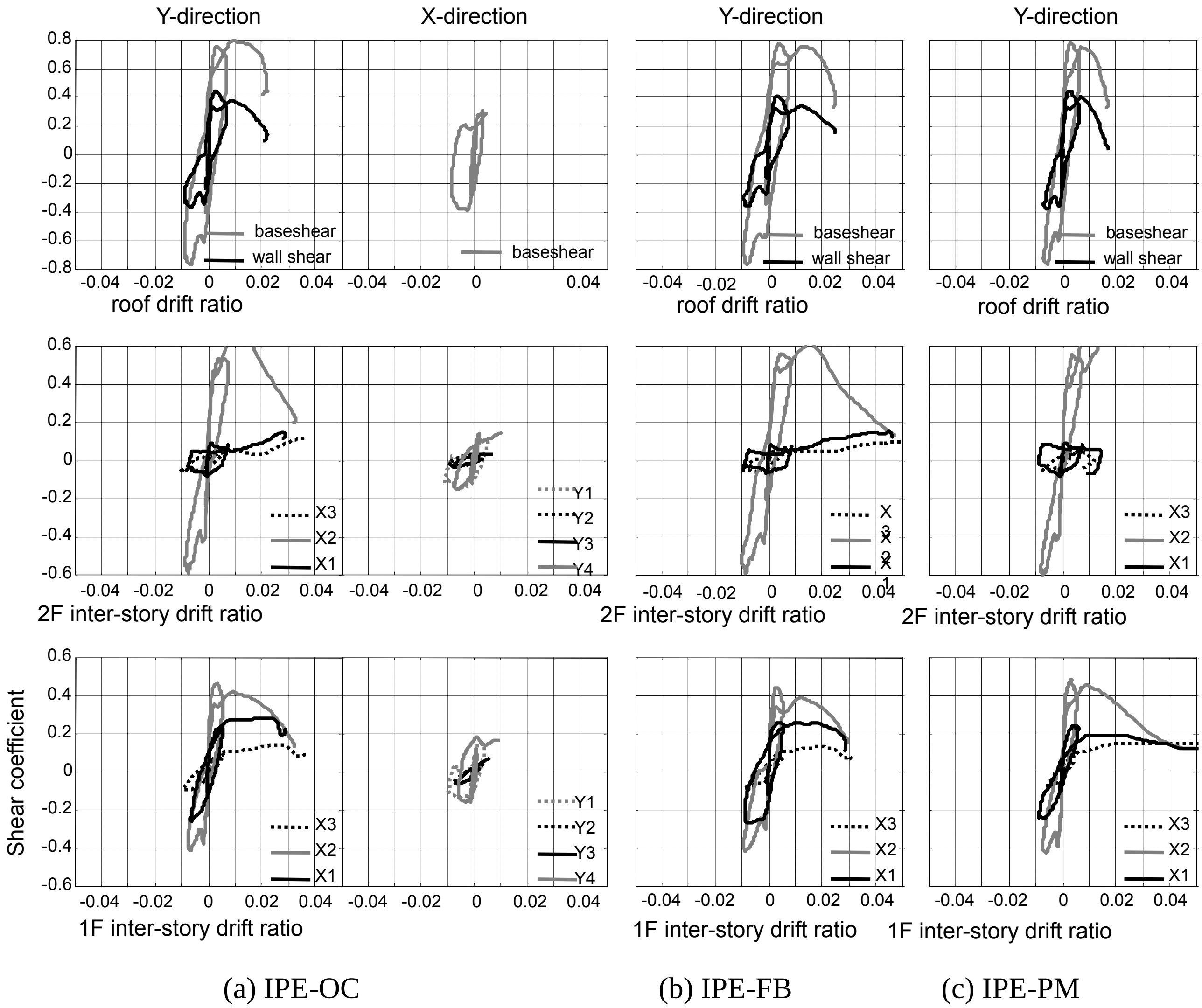

Fig. 15: Dynamic analysis results

5.3 Dynamic Analysis Results

Figure 15 shows the dynamic analysis results of three model combination cases: IPE-OC, IPE-FB and IPE-PM. The response in X-direction shown at Figure 15(a) is smaller than that in Y-direction, which arise from the fact that the base motion input is concentrated in Y-direction as shown previously (Fig. 12). This was consistent with the results obtained from the other analytical cases although not presented herein. As well, the maximum base shear coefficient in Y-direction is almost same in all of three model combination cases, and somewhat higher than that of pushover analysis results.

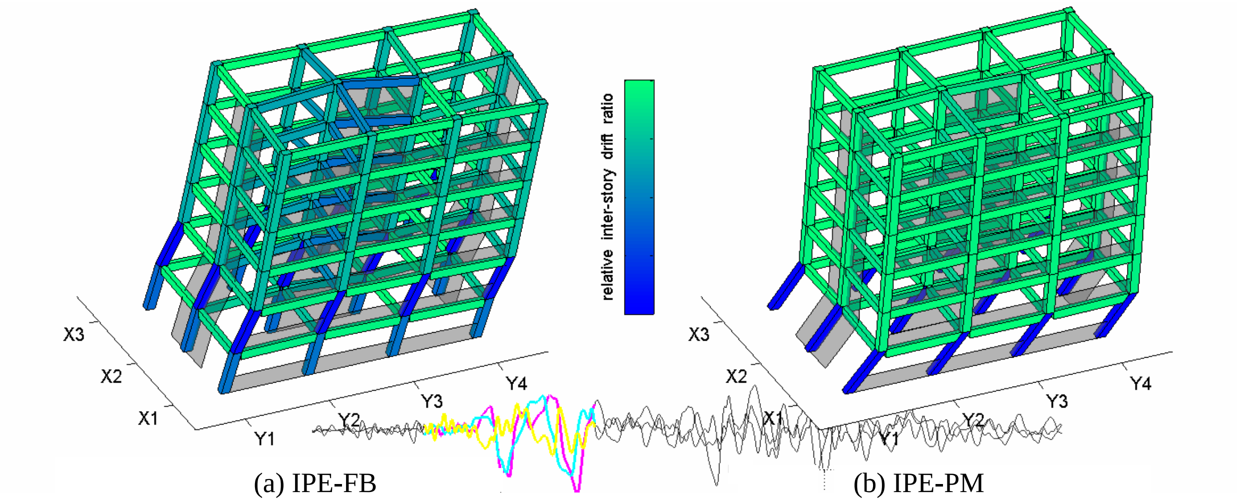

Fig. 16: Deformed shape of specimen

However, it is interesting to note that the displacement concentration at the 1st and the 2nd story is quiet different depending on the kind of column model. For IPE-OC case, the displacements at 1stand 2nd story are almost same, but the other two cases show the opposite results in the amplitude of each inter-story drift (Fig. 15 (b), (c)).

Figure 16 shows the deformed shapes of specimen when maximum inter-story displacement was recorded in the 2nd story. This different behavior between IPE-PM and IPE-FB case can be attributed mainly to the column model involved by strength degrading feature that causes and enhances the displacement concentration in the 1st story.

In addition to the strength degrading features of column model, axial force-biaxial moment interaction introduced in fiber model may account for these different failure modes related with the shear wall response. That is, strength degradation in shear wall model is governed by softening behavior of concrete that is a function of tensile strain in orthogonal direction. And the tensile strain is directly determined from the nodal displacements of shear wall by simply applying isoparametric formulation and rotating crack approach. Since the rigid diaphragm not allowing for in-plane deformation in the slab is assumed in this analysis, strength degradation in shear wall model is highly dependent on the axial displacement of side columns.

As a result, relatively large axial displacement of boundary columns induced by the biaxial bending behavior may decrease the shear wall strength and consequently increase the deformation of 2nd story in IPE-FB case.

6. SUMMARY

Preliminary analyses on the full-scale specimen were carried out using conventional analytical models and proposed column model that are mainly different in capability of reproducing the post- peak behaviour. It is revealed from this study that

1. Before onset of strength degradation in shear wall, it was shown that the yielding sequence of the structural members connected to the shear wall and overall yielding process of specimen was quietly similar irrespective of the analytical models.
2. Elastic torsional behaviour induced by different stiffness between open frame and spandrel beam frame was changed to be less dominant in inelastic range, which might be attributed from the facts that the spandrel beam frame yielded in early stage and relatively strong wing wall frame in orthogonal direction resisted against the torsional response.
3. After strength deterioration initiated in shear wall, inter-story displacement was strongly dependent on the analytical model. That is, displacement concentration in the 1^{st} story was pronounced in the analytical results obtained using proposed column model with strength degrading feature.
4. The effect of multi-directional earthquake input appeared in the analytical results simulated by fiber model in which biaxial bending and flexural bending-axial force interaction are incorporated.

REFERENCES

Chen, S and Kabeyasawa, T. (2000). Modeling of reinforced concrete shear wall for nonlinear analysis. *Proceedings of the 12th World Conference on Earthquake Engineering, New Zealand, Paper No. 1596.*

Izumo, J., Shima, H. and Okamura, H. (1989). Analytical Model for RC Panel Elements Subjected to In-plane forces. *Concrete Library International, JSCE*, No.12:155-181.

Kim, Y. and Kabeyasawa, T. (2002). Shaking Table Test of Reinforced Concrete Frames with/without Strengthening for Eccentric Soft First Story. *Proceedings of the Fourth US-Japan Workshop on Performance-Based Earthquake Engineering Methodology for Reinforced Concrete Building Structures*:119-134.

Ousalem, H. and Kabeyasawa, T. et al. (2002). Experimental Study on Seismic Behavior of Reinforced Concrete Columns Under Constant and Variable Axial Loadings. *Proceedings of the Japan Concrete Institute Annual Conference*, Vol.24, No.2:229-234.

Stevens, NJ., Uzumeri, SM. and Collins, MP. (1991) Reinforced Concrete Subjected to Reversed Cyclic Shear – Experiments and Constitutive Model. *ACI Structural Journal* 88(2): 135-146.

Vecchio, F. and Collins, MP. (1986) Modified Compression Field Theory for Reinforced Concrete Elements Subjected to Shear. *ACI Journal, Proceedings.* 83(2): pp.219- 231.

SESSION 5: SEISMIC BEHAVIOR OF SHEAR WALLS

Chaired by

♦ Shyh-Jiann Hwang and Kazutaka Shirai ♦

PRELIMINARY ANALYSES OF FULL-SCALE REINFORCED CONCRETE WALL-FRAME SPECIMEN IN DAIDAITOKU PROJECT

Yasushi SANADA and Toshimi KABEYASAWA[1]

ABSTRACT

This paper describes preliminary analyses of a 6-story reinforced concrete wall-frame structure, which is a full-scale specimen for a shaking table test using E-Defense in the DaiDaiToku Project. Seismic performances of the test specimen were numerically evaluated. An isoparametric element model for shear walls and a fiber model for columns were used for the analyses. The specimen formed an overall yield mechanism with flexural yielding at the wall bottom. After that, however, the system mechanism changed into a story yield mechanism with shear failure of the shear wall, which was caused by the shear softening of shear wall.

1. INTRODUCTION

A shaking table test of a full-scale 6-story reinforced concrete wall-frame structure is planned using E-Defense, NIED (National Research Institute for Earth Science and Disaster prevention) by the DaiDaiToku Project. As a part of the research project, preliminary analyses of the test specimen were conducted to evaluate seismic performances of the specimen. This paper describes the outlines of the specimen, numerical models for the analyses, and the results obtained from pushover analyses.

2. ANALYSED STRUCTURE

An analysed structure is a full-scale, 6-story, 2x3-bay reinforced concrete wall-frame structure, which was designed for a shaking table test using E-Defense in the DaiDaiToku Project. The 3-D image and the first-floor plan of the specimen are shown in Figures 1 and 2. The details of the columns and the shear walls are also shown in Table 1. The compressive strength of concrete was assumed to be 24MPa and the tensile strength of steel was 380MPa for D19 bars and 354MPa for D10 bars in the following analyses.

[1] *Earthquake Research Institute, University of Tokyo, Tokyo, Japan*
Email: ysanada@eri.u-tokyo.ac.jp

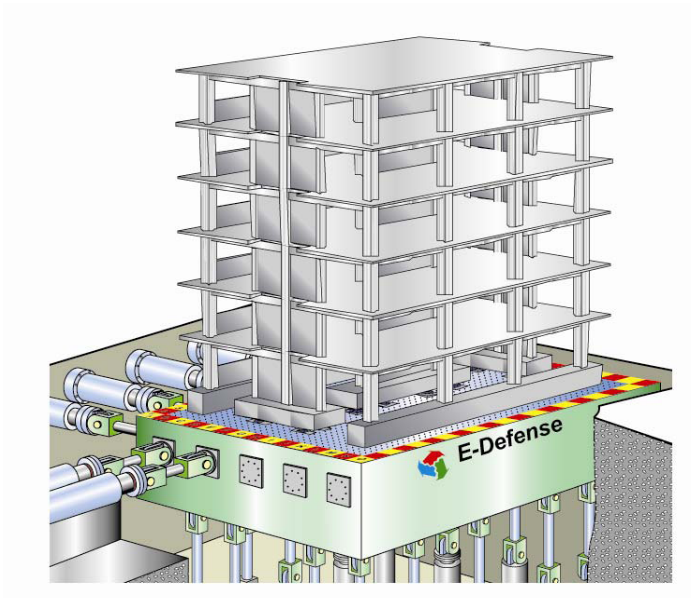

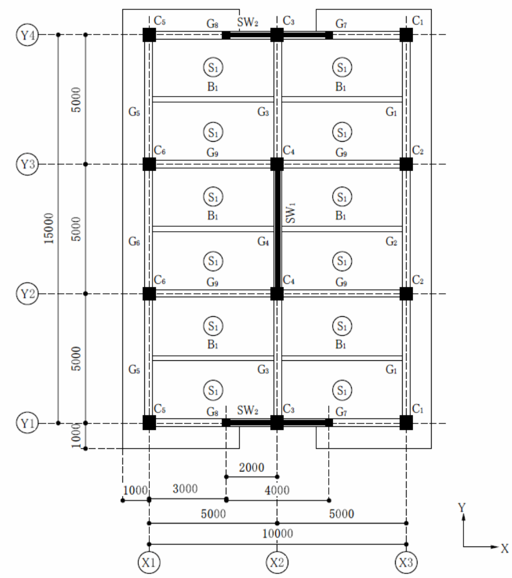

Fig. 1: 3-D image of the specimen **Fig. 2: First-floor plan of the specimen**

Table 1: Details of the columns and the shear walls

Column		Shear wall	
B x D	500 x 500	Thickness	150
Longitudinal bars	8-D19	Vertical bars	D10@300double
Horizontal reinforcements	D10@100	Horizontal bars	D10@300double

Unit: mm

3. NUMERICAL MODELING FOR ANALYSES

A fiber model was used for the columns to consider interactions between bending moment and axial force. Figure 3 shows the details of the column model. The flexibility distributions for flexure and axial deformation were assumed to be linear from the column ends to the inflection point. The fiber slices at the member ends consisted of 9 concrete elements and 8 steel elements. The stress-strain relationships of concrete and steel used in the column model are shown in Figure 4. The Bauschinger's effect was considered in the steel model. More details of the fiber model are described in Kabeyasawa (2000).

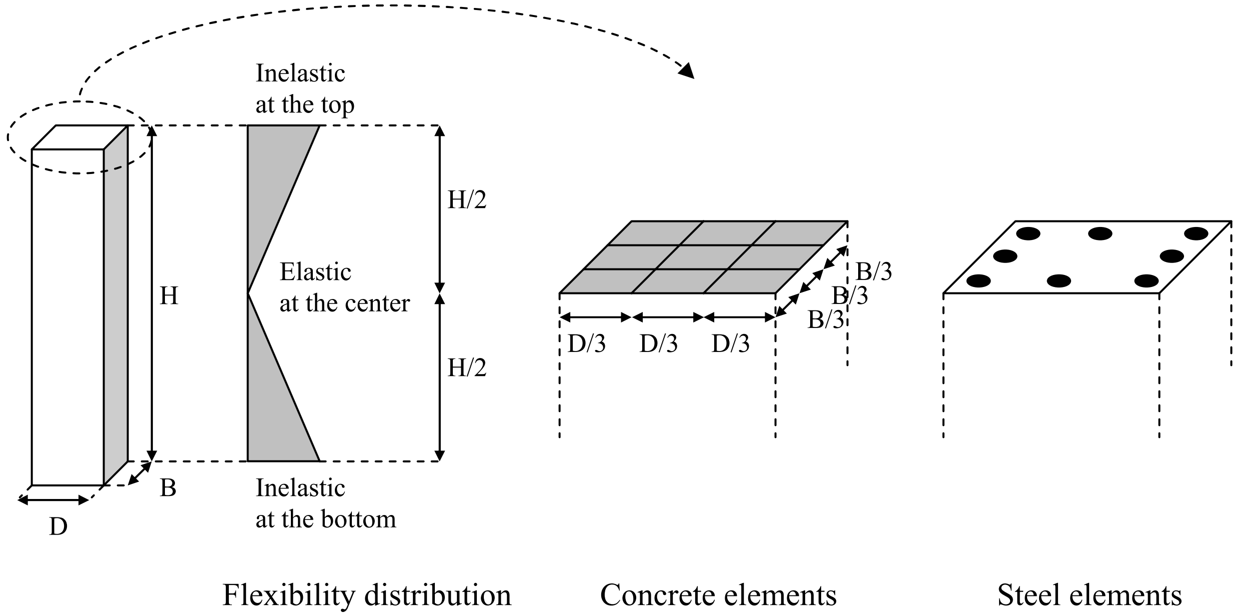

Fig. 3: Column model

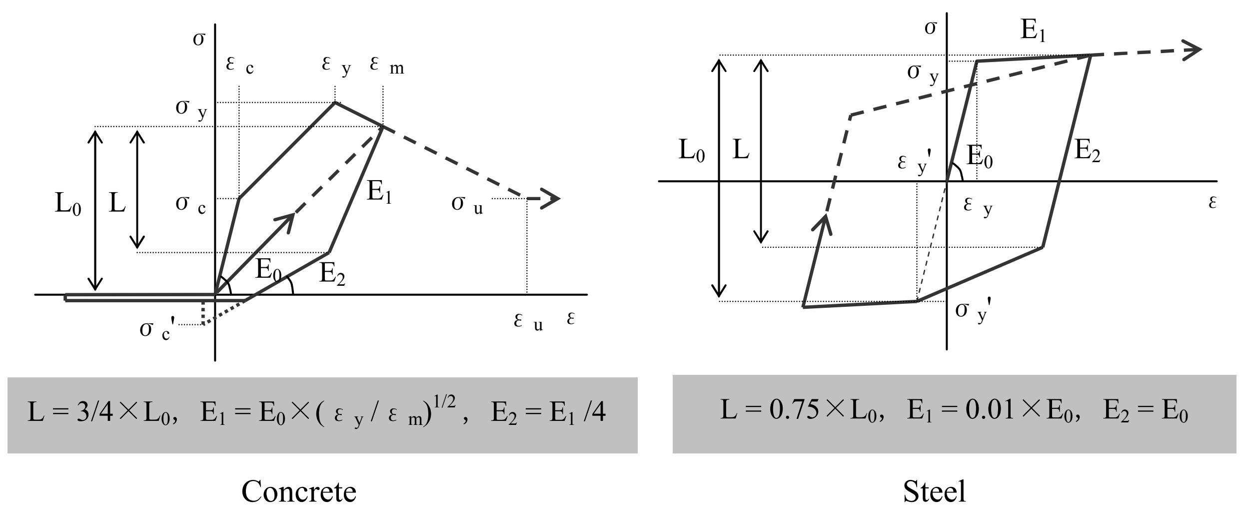

Fig. 4: Stress-strain relationships in the column model

A 4-node isoparametric element model (Chen, 2000) was used for the shear walls. This model consists of one panel element, two vertical elements representing boundary columns, and two beam elements, as shown in Figure 5. The upper and lower beam elements were assumed to be rigid in flexure, but flexible in axial deformation. Nine integration points were assumed in the panel element for evaluating the stress-strain relationships of concrete and steel. Figure 6 shows the concrete model used in the panel element. The stress-strain relationship of concrete up to the peak was defined by Eq. (1), and the degradations on stiffness and strength of concrete under two-dimensional stress fields were evaluated by Eq. (2) (Vecchio, 1986). Therefore, the shear softening of shear wall can be rationally considered in this model.

$$\sigma_c = \beta\ \sigma_{c0}\{2(\varepsilon_c/\varepsilon_{c0})-(\varepsilon_c/\varepsilon_{c0})^2\} \tag{1}$$

$$\beta = 1.0/\{0.8-0.34(\varepsilon_t/\varepsilon_{c0})\} \tag{2}$$

where, σ_c: compressive stress, β: reduction factor on stiffness and strength, σ_{c0}: uniaxial compressive strength, ε_c: compressive strain, ε_{c0}: strain at peak compressive strength, ε_t: orthogonal tensile strain.

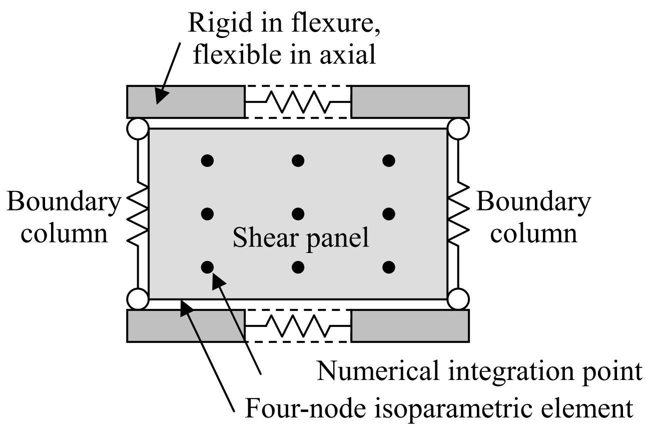

Fig. 5: Shear wall model

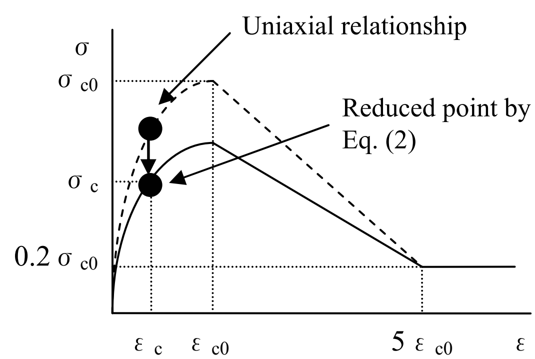

Fig. 6: Concrete model in the panel element

The beams and slabs were replaced using the one component model and isoparametric elements used in the shear wall model, respectively.

4. RESULTS OF PUSHOVER ANALYSES

Pushover analyses were carried out in the Y-direction, shown in Figure 2, to evaluate the seismic performances of the specimen. The assumed load distributions were an inverted triangular mode shape and a uniform one. The lateral force loaded on each floor was distributed to each node in proportion to its tributary floor area.

The relationships between the base shear coefficient and the overall drift ratio of the specimen are shown in Figure 7. The specimen formed an overall yield mechanism with a flexural yielding of the wall bottom in both analyses. Although the overall yield mechanism was maintained up to the overall drift ratio of 0.02rad, then the system mechanism changed into a story yield mechanism due to the softening of shear wall. The strength degradation was also observed in the analysis under uniformly distributed loads. Figure 8 shows the displacement distributions along the height of the specimen. The displacement concentrated in the first- or second-story at the large deformation. The shear forces carried by the first-story columns, and the first- and second-story walls, from the analysis under uniformly distributed loads, are shown in Figure 9. The shear force in the second-story wall was much larger than that in the first-story up to the drift ratio of 0.02rad., which caused the shear failure of the second-story wall and the drift concentration in the second story around the drift ratio of 0.02rad.

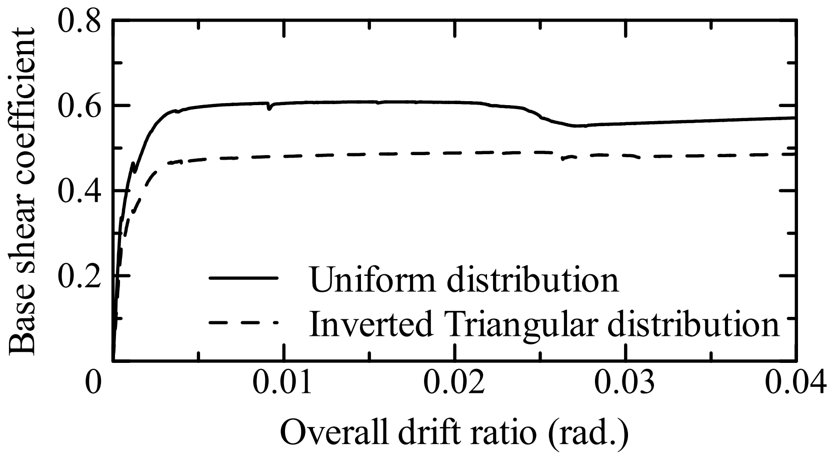

Fig. 7: Base shear coefficient vs. overall drift ratio

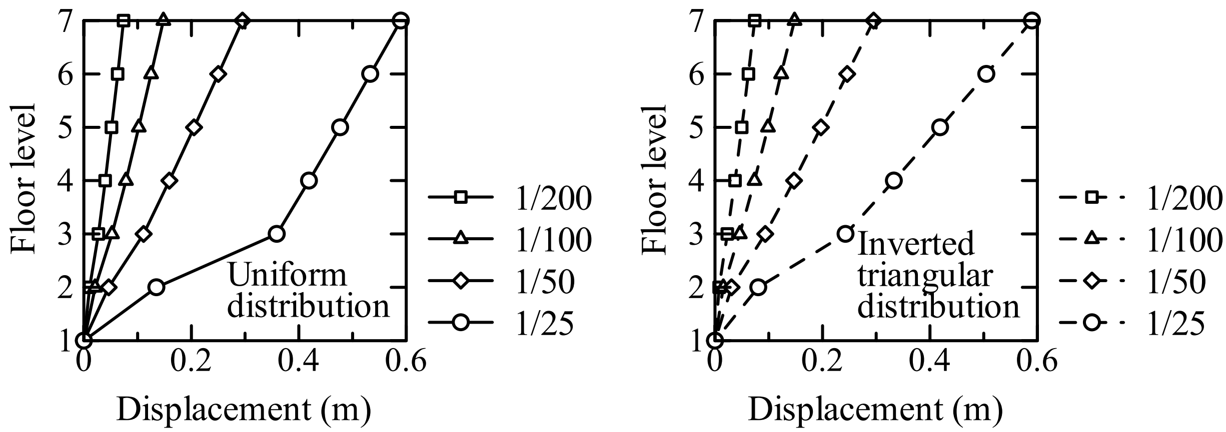

Fig. 8: Displacement distributions along the height

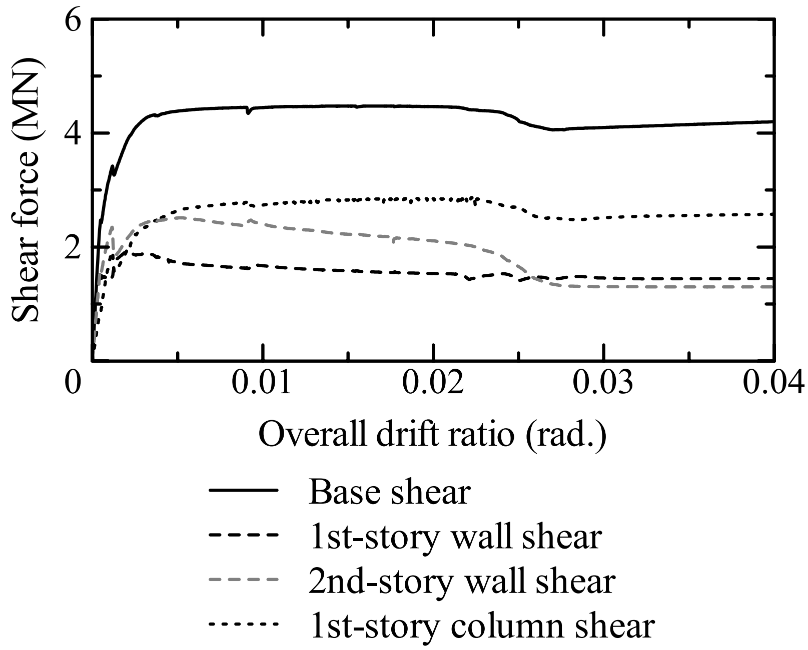

Fig. 9: Shear force vs. overall drift ratio under uniformly distributed loads

Figure 10 shows the shear forces of the first-story columns. The shear strength calculated by the AIJ equation is also shown in this figure. Although the shear behaviours of the columns were assumed to be elastic in this analysis, the input shear forces of the short columns exceeded the calculated strength, which means that the first-story short columns may fail in shear. The shear failure of the first-story short columns can trigger the drift concentration in the first story, in spite of the analytical results shown in Figures 7 to 9, in which the drift concentrated in the second story.

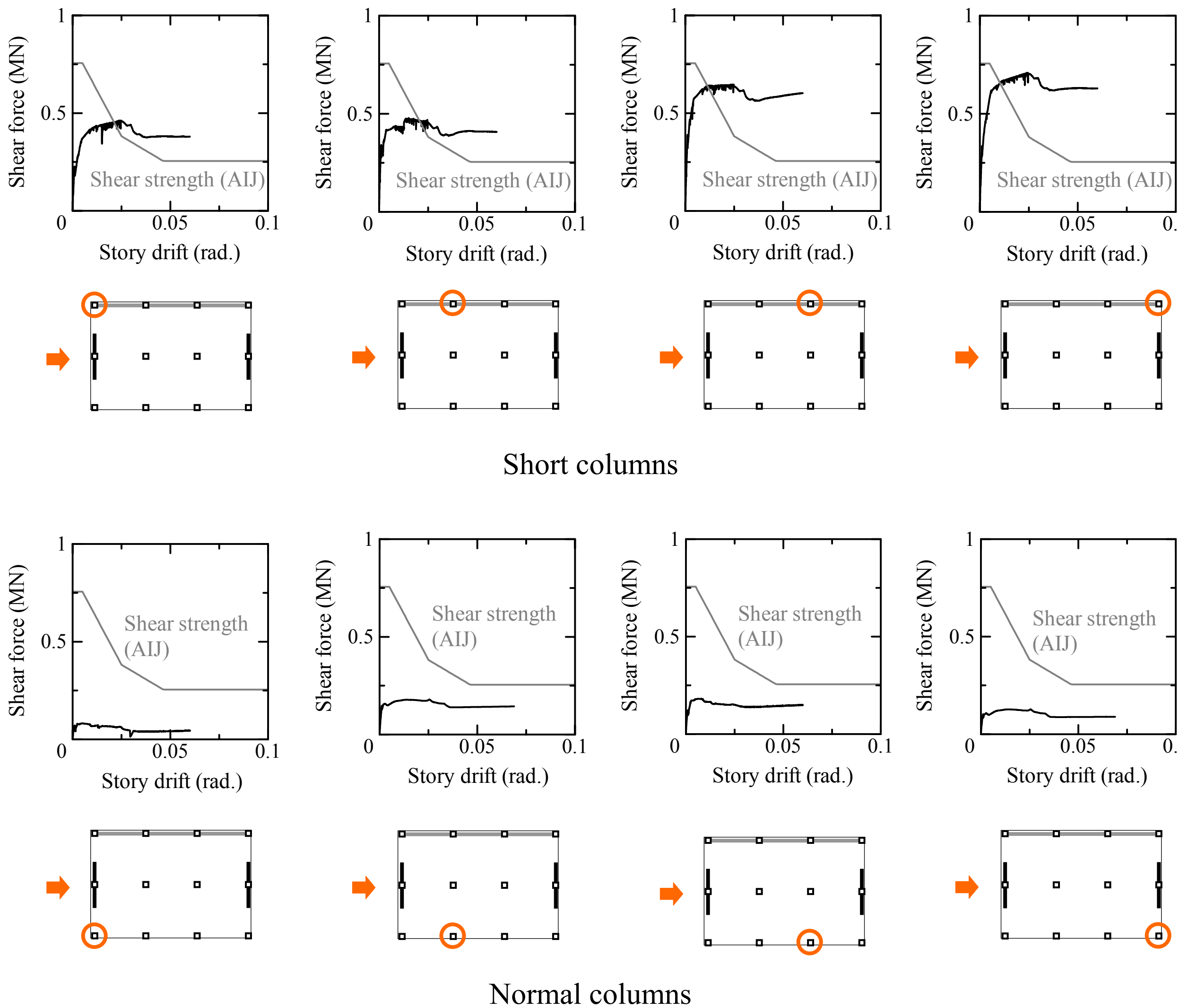

Fig. 10: Shear forces in the 1st-story columns

5. CONCLUDING REMARKS

Pushover analyses of a reinforced concrete wall-frame structure, designed as a specimen for a shaking table test using E-Defense by the DaiDaiToku Project, was carried out herein. The specimen formed an overall yield mechanism with a flexural yielding at the wall bottom, the system mechanism, however, changed into a story yield one. This was caused by the shear failure of the second-story wall due to its shear softening after the flexural yielding. Further analyses are needed to investigate inelastic shear responses of the first-story short columns.

REFERENCES

Chen, S., and T. Kabeyasawa. (2000). Modeling of reinforced concrete shear wall for nonlinear analysis. *12th World Conference on Earthquake Engineering*, CD-ROM, Paper No. 1596.

Kabeyasawa, T., Y. Sanada, and M. Maeda. (2000). Effect of beam axial deformation on column shear in reinforced concrete frames. *12th World Conference on Earthquake Engineering*, CD-ROM, Paper No. 1017.

Vecchio, F. J., and M. P. Collins. (1986). The modified compression field theory for reinforced concrete elements subjected to shear. ACI Journal, Vol. 83, No. 2, pp. 219-231.

Keywords: drift concentration, fiber model, isoparametric element model, pushover analysis, shear softening of shear wall, three-dimensional analysis.

HYSTERESIS MODELS BASED ON STATIC TEST AND SIMULATION OF DYNAMIC BEHAVIOR FOR *RC* SHEAR WALLS

Hiroshi KURAMOTO, Tomofusa AKITA and Tomoya MATSUI[1]

Toshimi KABEYASAWA[2]

ABSTRACT

The main objective of this series of study is to grasp the difference between dynamic and static behaviors of RC shear walls. This paper shows a static loading test on RC shear walls carried out to compare with the dynamic loading test using the uni-directional shaking table conducted in 2002. Using the static analysis, a model of the restoring force characteristics of RC shear walls is constructed. The restoring force characteristic model is based on the existing research presented by Umemura et al. in which capacity degradation caused by cyclic loadings is considered. The hysteresis of RC shear walls in the dynamic test are compared with those calculated using the constructed model to examine the possibility of simulating the dynamic behaviors by the static restoring force characteristics model.

1. INTRODUCTION

A dynamic loading test on a full-scale 6 story RC building will be conducted in January 2006 using a huge shaking table, which is capable of the tri-directional earthquake wave inputs, at a new testing facility called “the E-Defense” constructed in Miki City of Hyogo Prefecture, Japan. Currently, fundamental studies toward the full-scale test are being carried out by many researchers involved in the project. As one of them, a dynamic loading test on RC shear walls of one-third scale using the uni-directional shaking table was conducted by National Research Institute for Earth Science and Disaster Prevention (NIED) and Earthquake Research Institute (ERI) of the University of Tokyo in 2002 (Matsui et al., 2004). And then, a static loading test on RC shear walls of one-third scale was also conducted by the authors to compare with the dynamic loading test.

In this paper, the static loading test is outlined as compared with the dynamic loading test and hysteresis models of RC shear walls are proposed based on the existing research in which

[1] *Department of Architecture & Civil Engineering, Toyohashi University of Technology, Toyohashi, Japan*
Email: kura@tutrp.tut.ac.jp
[2] *Earthquake Research Institute, the University of Tokyo, Tokyo, Japan*

capacity degradation caused by cyclic loadings is considered (Umemura et al., 2002). Moreover, through earthquake response analysis using the hysteresis models, the possibility of simulating the dynamic behavior by the static restoring force characteristics model is discussed.

2. OUTLINE OF DYNAMIC LOADING TEST

The outline and conclusions of the dynamic loading test conducted in 2002 by NIED and ERI (Matsui et al., 2004) are briefly shown below.

The purpose of this dynamic test is to grasp the dynamic behavior and restoring force characteristics of RC shear walls. Two specimens, Specimen WALL-A expected to fail in shear before flexural yielding and Specimen WALL-B expected to occur flexural failure, were tested using the uni-directional shaking table in NIED. The specimens are designed to simulate the

Table 1: Concrete stress (dynamic test)

Specimen	Part	Age (days)	fc (N/mm^2)
WALL-A	first story	40	26.4
	second story	32	30.0
WALL-B	first story	48	25.2
	second story	40	29.6

Table 2 Properties of bar (dynamic test)

Sort and Part		Yield strength (N/mm^2)	Young's modulus (kN/mm^2)	Ultimate strength (N/mm^2)	Extension (%)
D6 (SD295A)	wall reinforcement, tie, stirrup	377	196	493	29.4
D10 (SD295A)	beam reinforcement	366	181	503	28.0
D13 (SD390)	column reinforcement	434	186	605	22.8

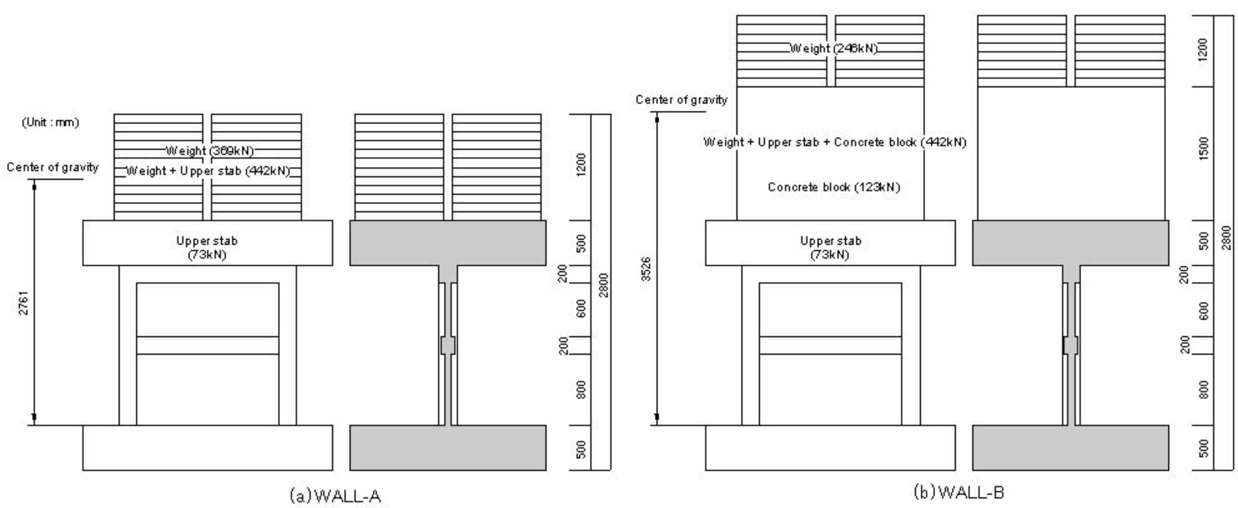

Fig. 1: Specimens (dynamic test)

Table 3: Earthquake motions

Earthquake motion	Target velocity (kine)	Magnification ratio for original earthquake motion	Maximum acceleration (gal)	WALL-A	WALL-B
TOH	25	0.6	154.9	○	○
ELC	37	1.1	375.9	○	○
JMA	50	0.6	492.4	○	○
JMA	75	0.9	738.5	○	○
CHI	60	0.9	796.0	○	○
JMA	100	1.2	984.7	○	○
CHI	50	0.7	619.1	○	×
TAK	125	1.0	605.5	○	×
CHI	70	1.0	884.4	○	×

lower two story of multi-story shear walls in a six-story RC building and scaled to one-third of the prototype walls, as shown in Figure 1. The variable investigated is shear span ratio, which are 1.38 for Specimen WALL-A and 1.76 for Specimen WALL-B, respectively. The mechanical properties of concrete and reinforcing bars used are listed in Tables 1 and 2, respectively.

Table 3 shows the earthquake motion used in the dynamic test. Five earthquake motions, TOH (Miyagiken-oki Earthquake, Tohoku University 1970 NS), ELC (Imperial Valley Earthquake, El Centro 1940 NS), JMA (Hyogoken-nambu Earthquake, JMA Kobe 1995 NS), CHI (Chile Earthquake, Vina del Mar 1985 NS) and TAK (Hyogoken-nambu Earthquake, JR Takatori 1995 NS) are used. As shown in Table 3, the target maximum input velocity is set for each earthquake motion and the tests are sequentially carried out from the upper line in the table. Circle marks in Table 3 designate that the earthquake motion is applied for the specimens, while x marks indicate that the earthquake motion is not applied. Hereafter, the earthquake motions are called, for example, TOH25 or ELC37 which consists of the combination of earthquake motion name and target maximum input velocity.

The results of the dynamic test are summarized as follows:

(1) According to the calculation of shear and flexural strengths using existing design equations, Specimen WALL-A will fail in shear after flexural yielding, and Specimen WALL-B will have flexural failure. However, both specimens failed in shear after flexural yielding in the test, although the failure mode of Specimen WALL-B, which had compressive failure at the bottom of the boundary column and wall, differed a little from that of Specimen WALL-A.

(2) It is thought that the maximum strengths of both specimens should agree with the calculated flexural strengths because the specimens failed in shear after flexural yielding. However, the measured maximum strengths exceeded the calculated flexural strengths due to the increase

in the yield strength of reinforcing bars that are caused by the strain hardening, strain velocity effect, etc.

(3) Both specimens showed S-shape hysteresis loops which have little plastic deformation and little energy dissipation capacity until flexural strength, and showed reverse S-shape hysteresis loops after the flexural strength.

3. OUTLINE OF STATIC LOADING TEST

3.1 Specimens

The specimens used in the static test had the same configuration and bar arrangements as those used in the dynamic test. Similar to the specimens used in the dynamic test, two specimens are prepared in the static test, Specimen WALL-AS expected to fail in shear after flexural yielding and Specimen WALL-BS expected to occur the flexural failure. Their shear span ratios are 1.38 for Specimen WALL-AS and 1.76 for Specimen WALL-BS, respectively. The configurations and bar arrangements of the specimens are shown in Figure 2, and the details of the section are listed in Table 4. The mechanical properties of concrete and reinforcing bars are shown in Tables 5 and 6, respectively.

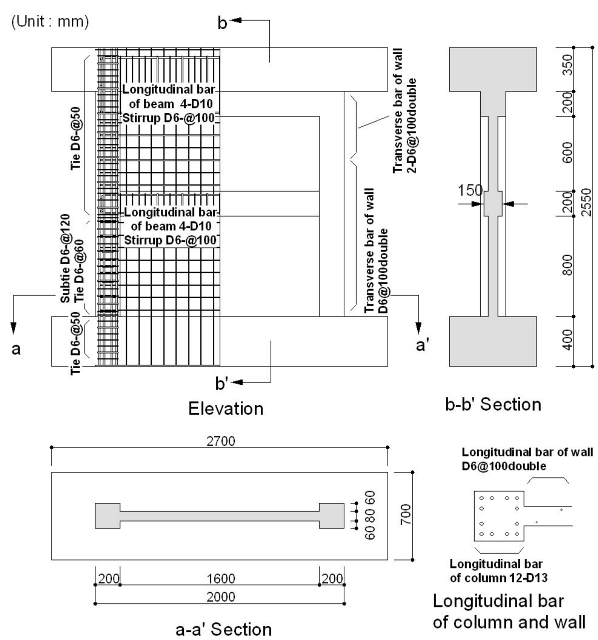

Fig. 2: Cross section and bar arrangement

Table 4: Specification of section

		First story	Second story
Column	Section	200×200	
	Longitudinal bar	12-D13 (pg=3.8%)	
	tie	2-D6@60 (pw=0.53%)	2-D6@50 (pw=0.64%)
	subtie	2-D6@120 (pw=0.27%)	—
Beam	Section	150×200	200×500※1
	Longitudinal bar	4-D10 (pt=0.54%)	
	stirrup	2-D6@100 (pw=0.42%)	
Wall	Thickness	80	
	Longitudinal bar	D6@100double (ps=0.4%)	2-D6@100double (ps=0.8%) D6@100double (ps=0.4%)
	Transverse bar	D6@100double (ps=0.4%)	

Unit mm

Fc=27N/mm^2, Longitudinal bars of columns (SD390), Others (SD295A)

※1 Upper 300mm of beam depth 500mm has combined with an upper stub (Refer Fig.2)

Table 5: Concrete stress (static test)

Specimen	Part	Age (days)	fc (N/mm^2)
WALL-AS	first story	39	26.0
	second story	34	27.9
WALL-BS	first story	46	27.4
	second story	41	30.2

Table 6: Properties of bar (static test)

Sort and Part		Yield strength (N/mm^2)	Young's modulus (kN/mm^2)	Ultimate strength (N/mm^2)	Extension (%)
D6 (SD295A)	wall reinforcement, tie, stirrup	371	199	495	12.9
D10 (SD295A)	beam reinforcement	378	199	473	28.0
D13 (SD390)	column reinforcement	485	192	615	18.5

3.2 Loading Method and Measuring Procedure

The loading apparatus used in the static test is shown in Photo 1. The wall specimens were loaded horizontal shear reversals by a manual jack of 1,000kN capacity with applying a constant axial force of 442kN by two vertical manual jacks of 2,000kN capacity for each. During the testing, the additional moment was also applied to the top of the specimens using the vertical jacks to keep the prescribed shear span ratio.

The loading was conducted by controlling the relative wall rotation angle, R, given by dividing the height corresponding to the measuring point of horizontal displacement at the top of the specimen, h_m (2,000mm), into the horizontal deformation, δ_T , i.e. $\mathrm{R} = \delta_T / h_m$.

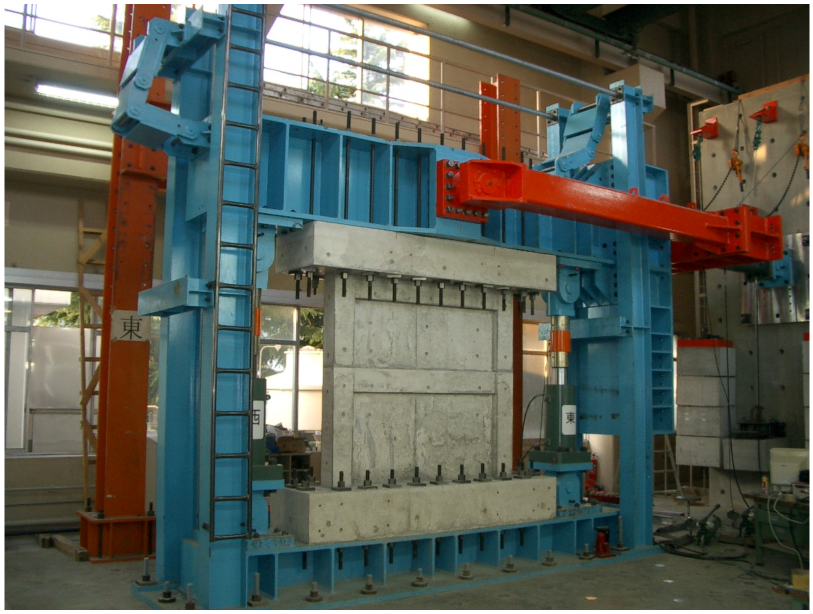

Photo 1: Loading apparatus

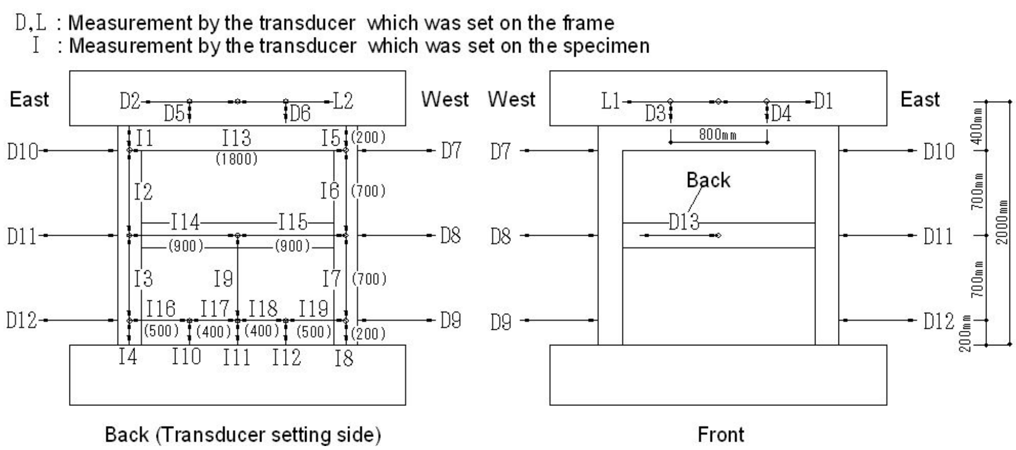

Fig. 3: Measuring plan

As a rule, the measuring system and points in the static test are the same as those in dynamic test. Figure 3 indicates measuring points of displacements.

4. RESULTS OF STATIC LOADING TEST

4.1 Failure Modes

Cracking patterns of both specimens at the loading cycle of R=1/100 radian and after the loading are shown in Figures 4 and 5. The loading toward the west is defined as the positive loading while the loading toward the east is the negative loading.

Specimen WALL-AS with smaller shear span ratio occurred the initial cracking at the bottom of wall and columns in the first story at the loading cycle of 1/800 radian, and attained the calculated yield strength at the first cycle loading of 1/200 radian. After the flexural yielding, the spalling of cover concrete in the west bottom side of the wall occurred at the loading cycle of 1/100 radian, exhibiting sign of compressive failure. Significant capacity degradation was observed at the same time, after that, the west bottom side of the wall failed in compression at the second cycle loading of 1/100 radian. Resulting in shear failure of the west column, Specimen WALL-AS failed in shear at the first cycle of 1/67 radian. Although the longitudinal bars of the wall finally ruptured, Specimen WALL-AS didn’t collapse because the east column sustained the axial load.

Specimen WALL-BS with larger shear span ratio had flexural cracks at the bottom of the wall and columns in the first story at the loading cycle of 1/800 radian, and developed the yield strength at the first cycle of 1/200 radian. The cracks in the column were connected with the cracks in the wall at the loading cycle of 3/400 radian, at the same time, a large flexural crack appeared at the bottom of the wall. Thus, significant flexural failure mode was observed. However, signs of compressive failure were observed in the west bottom side of the wall and columns at the loading cycle of 1/67 radian. Compressive failure occurred on the wall near the bottom of west column at the loading cycle of 1/50 radian, flexural cracks on the west bottom side of the wall and flexural shear cracks on the east side of the wall were extended quickly simultaneously, and then sliding shear failure occurred on the wall.

From Figure 4, the sign of compressive failure was observed on the west bottom side of the wall at the loading cycle of 1/100 radian for Specimen WALL-AS, while it is not found at the loading cycle of 1/100 radian for Specimen WALL-BS. Moreover, it is found that significant flexural failure mode was observed in Specimen WALL-BS because the inclination of shear cracks of Specimen WALL-BS is smaller than that of Specimen WALL-AS and many flexural cracks occurred on the columns.

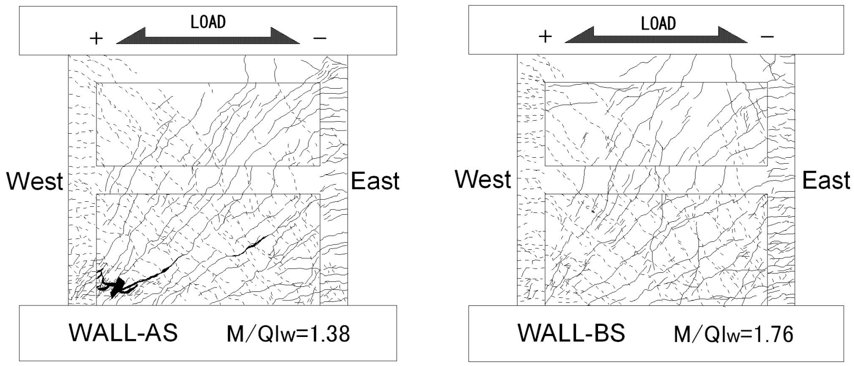

Fig. 4: Cracking situation after loading of R=1/100rad

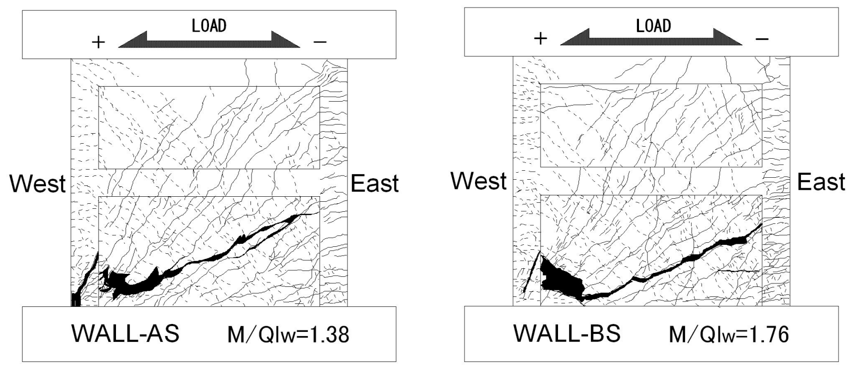

Fig. 5: Cracking situation after final loading

As described above, the failure process of Specimen WALL-AS is different from that of Specimen WALL-BS, however, the failure types of both specimens are the same, that is shear failure caused by the compressive failure of the wall near the west side bottom of the column after flexural yielding. This result agreed with result (1) of the dynamic test shown in Chapter 2. Thus, differences are not found between the dynamic and the static loading.

4.2 Shear-Displacement Relationship

The shear force versus rotation angle relationships of both specimens are shown in Figure 6 with the calculated flexural strength given by and Eq. (1) (AIJ, 1987) and shear strength given by Eq. (2) (AIJ, 1998).

$$Q_{mu} = \left(a_t \cdot \sigma_y \cdot l_w + 0.5 a_w \cdot \sigma_{wy} \cdot l_w + 0.5 N \cdot l_w\right)/h \tag{1}$$

$$Q_{su} = t_w \cdot l_{wb} \cdot p_s \cdot \sigma_{wy} \cdot \cot\phi + \tan\theta(1-\beta) \cdot t_w \cdot l_{wa} \cdot \nu \cdot \sigma_B / h \tag{2}$$

Both specimens showed elastic behavior until the relative rotation angle, R, of 1/800 radian, their stiffness were degraded due to flexural cracks at R of 1/400 radian, and they almost reached the

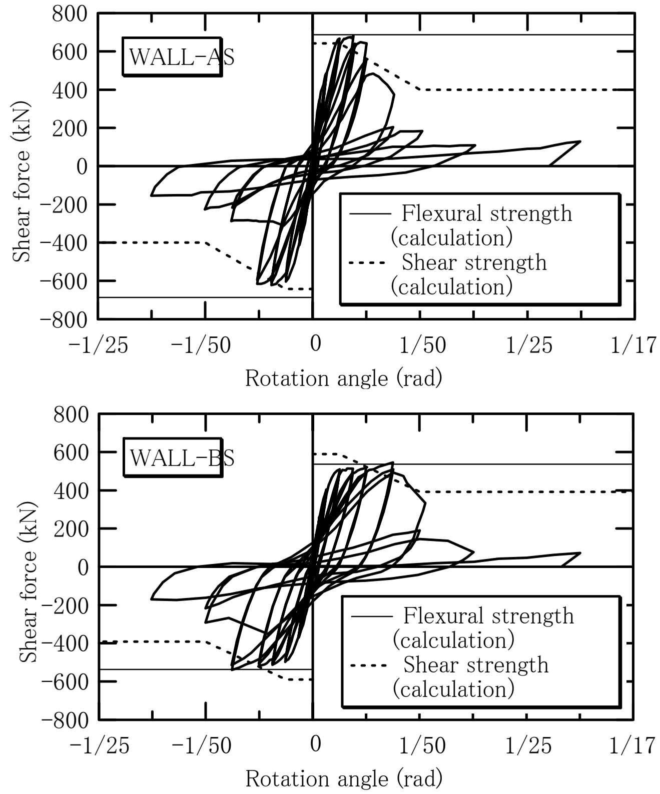

Fig. 6: Shear versus rotation angle relationships

maximum strength due to yielding of longitudinal bars in tensile column at R of 1/200 radian. The maximum strengths were 681kN for Specimen WALL-AS and 545kN for Specimen WALL-BS, and also almost agreed with their ultimate flexural strengths. The maximum strength of Specimen WALL-BS was about 0.8 times that of Specimen WALL-AS. In comparison with result (2) of the dynamic test, it is agreed that the maximum strengths of the specimens WALL-B and WALL-BS with larger shear span ratio are about 0.8 times smaller than those of the specimens WALL-A and WALL-AS with smaller shear span ratio. Moreover, from the results that the flexural strengths agreed with the calculated flexural strengths in the static test and it exceeded the calculated flexural strengths in the dynamic test, influences of dynamic effects are found clearly in the dynamic test.

4.3 Comparison of the Hysteresis Loops of the Dynamic and the Static Test

Figure 7 shows the comparison of dynamic and static hysteresis loops. In the figure, the hysteresis loops of Specimen WALL-B in the dynamic test are shown when JMA50 and CHI60 were inputted, while those of Specimen WALL-BS in the static test are drawn for the second

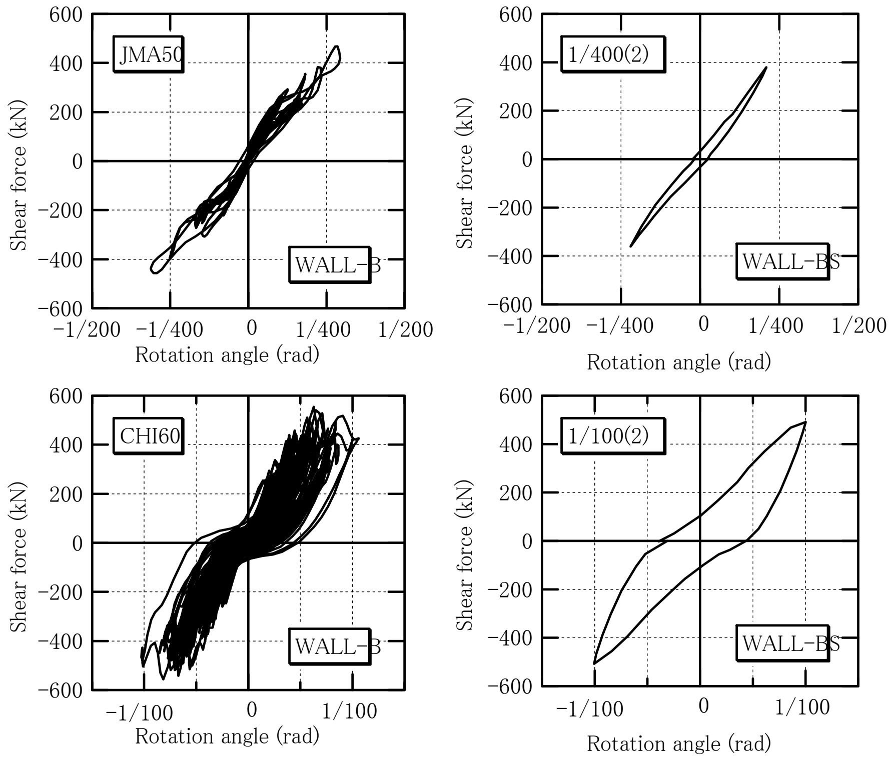

Fig. 7: Comparison of the hysteresis loops of the dynamic and the static tests

cycles of the loading cycle of 1/400 radian and 1/100radian because the maximum displacements are almost the same as those in the dynamic test.

As described in the result (3) in the dynamic test, Specimen WALL-B showed the S-shaped hysteresis loops when JMA50 was inputted in which the specimen didn't reach the flexural yield strength, although it showed the reverse S-shaped hysteresis loops for CHI60 input before which the flexural yielding occurred. In the static test, on the other hand, Specimen WALL-BS showed the reverse S-shaped hysteresis loops even if the specimen didn't reach the flexural yield strength. Furthermore, the hysteresis loops were reverse S-shape after the yielding in the static test, but it has a less slip characteristic than the dynamic hysteresis loops. Therefore, the differences between the dynamic and the static behavior are found.

5. HYSTERESIS MODELS OF RC SHEAR WALLS

As described in Chapter 4, the capacity degradation of RC shear walls after flexural yielding due to cyclic loadings was observed in the static test. Similar test results were also reported on RC members in existing researches (i.e., Kinugasa et al. 1994). Considering these results, the effect of the capacity degradation should be taken into account in constructing the restoring force characteristic models of RC shear walls which is used for the earthquake response analysis.

In order to simulate the responses of RC shear walls in the dynamic test shown in Chapter 2 by the earthquake response analysis, a restoring force characteristic model of RC shear walls is constructed based on the static test results. However, since the capacity degradation due to cyclic loadings is not considered in Takeda model or Takeda-slip model which is usually used for the hysteresis models of RC members, an existing research (Umemura et al. 2002) explained below is referred in constructing the restoring force characteristic model.

(1) Existing research

In order to evaluate more accurately the seismic performance of buildings by earthquake response analysis, Umemura et al. (2002) proposed a hysteresis model which can express the capacity degradation or deterioration of deformability, as shown in Figure 8. The hysteresis model uses modified TAKEDA model that the effect of the capacity degradation is considered by making the stiffness decrease due to moving oriented point. In the original Takeda model, the stiffness is decided by the slope of the line from origin to the oriented point that is the maximum point until the last loop. In the modified Takeda model, on the other hand, the capacity degradation and restoration due to increment of deformation are considered by using the stiffness derived from new oriented point that is larger than the last maximum point, as shown in Figure 8. The increment of the oriented point is estimated by the following equation.

$$d_n = d_p + \left(d_{\max} - d_{\min}\right) \times \chi \tag{3}$$

Where, d_n = new oriented point, d_p = last oriented point in the same direction as the new point, $d_{\max}$ = the last maximum displacement in the same direction as the new point, and $d_{\min}$ = the last maximum displacement in the opposite direction of the new point. χ is the stiffness degradation factor given by Eq. (4).

$$\chi = 0.12 + 0.00069 f_c - 0.039 p_w + 0.016 n_o - 0.019 \lambda \tag{4}$$

Where, f_c = concrete compressive strength (N/mm^2), p_w = transverse reinforcement ratio (%), n_o = axial force ratio, and λ = shear span ratio.

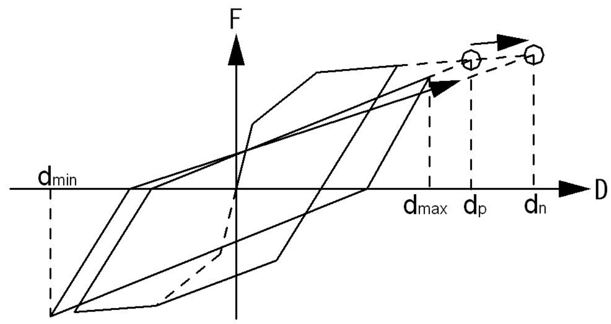

Fig. 8: Restoring characteristics model proposed by Umemura et al

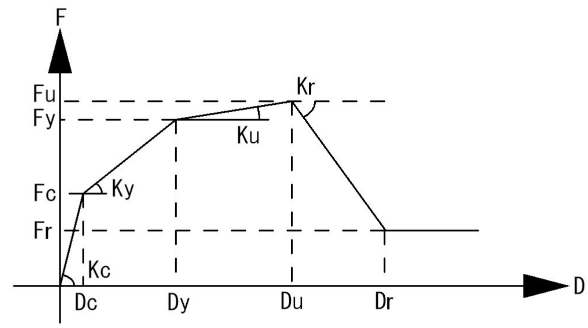

Fig. 9: Backbone curve

(2) Proposed hysteresis model

In constructing the hysteresis model of RC shear walls, the penta-linear backbone curves are assumed to consider capacity deterioration after the shear failure and the large deformation with low capacity, as shown in Figure 9. The backbone curves are determined based on the static test.

TAKEDA-slip model shown in Figure 10, which can express from the slip characteristic with small hysteretic area to the spindle shape characteristic with large hysteretic area by four parameters, unloading stiffness degradation factor α and α', slip stiffness degradation factor β and slip-hardening factor γ, is used as the hysteresis rule of the model.

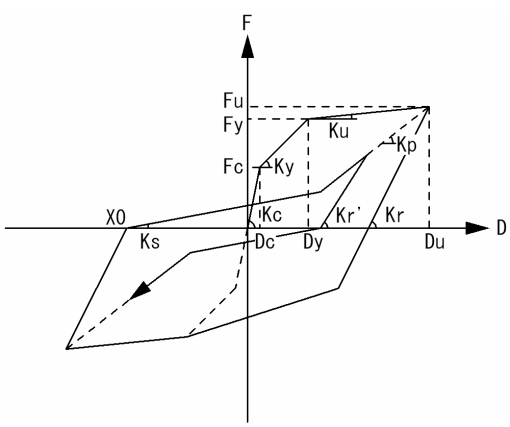

$$K_r = \frac{F_c + F_y}{D_c + D_y} \left| \frac{D_y}{D_u} \right|^{\alpha}$$

$$K'_r = \alpha' \cdot K_r$$

$$K_s = \frac{F_u}{D_u - X_0} \left(\frac{D_u}{D_u - X_0} \right)^{\beta}$$

$$K_p = \gamma \cdot \frac{F_u}{D_u}$$

Fig. 10: Takeda-slip model

Table 7: Values of backbone curve

	Kc	Ky	Ku	Kr	Fc	Fy	Fu	Fr	Dc	Dy	Du	Dr
WALL-AS	214.3	48.7	1.4	-19.0	300.0	670.0	680.0	130.0	1.4	9.0	16.0	45.0
WALL-BS	200.0	48.5	1.8	-15.3	180.0	500.0	540.0	80.0	0.9	7.5	30.0	60.0

Stiffness :kN/mm Shear force :kN Deformation :mm

Table 8: Values of parameter

	α	α'	β	γ	χ
WALL-AS	0.6	1.0	1.0	1.0	0.02
WALL-BS	0.4	1.0	1.0	0.9	0.02

Moreover, the stiffness degradation rule by moving oriented point is applied for the model to consider the capacity degradation due to cyclic loadings as well as the research by Umemura et al. However, since the applicability of Eq.(4) for RC shear walls and dynamic analysis is unknown, the stiffness degradation factor, χ, is treated as a parameter in constructing the hysteresis model.

6. STATIC ANALYSIS

Static analysis for the specimens WALL-AS and WALL-BS in the static test is carried out using the hysteresis model shown in Chapter 5. The purpose of this analysis is to determine four parameters of TAKEDA-slip model and the stiffness degradation factor, χ. Therefore, while the values of the parameters are changed and the analytical results are compared with the hysteresis loops of the static test, the static analysis is repeated by trial and error until good agreement is obtained between the analytical and test results.

The values of the backbone curves obtained from the static analysis and the parameters of Takeda-slip model are listed in Tables 7 and 8, respectively. The difference between the specimens WALL-AS and WALL-BS was found in the unloading stiffness degradation factor α and the slip-hardening factor γ. The hysteresis loops of each specimen in the static test obtained from the static analysis are shown in Figure 11 with the static test results. From the figure, it can be found that almost good agreement is obtained between the analytical and test results.

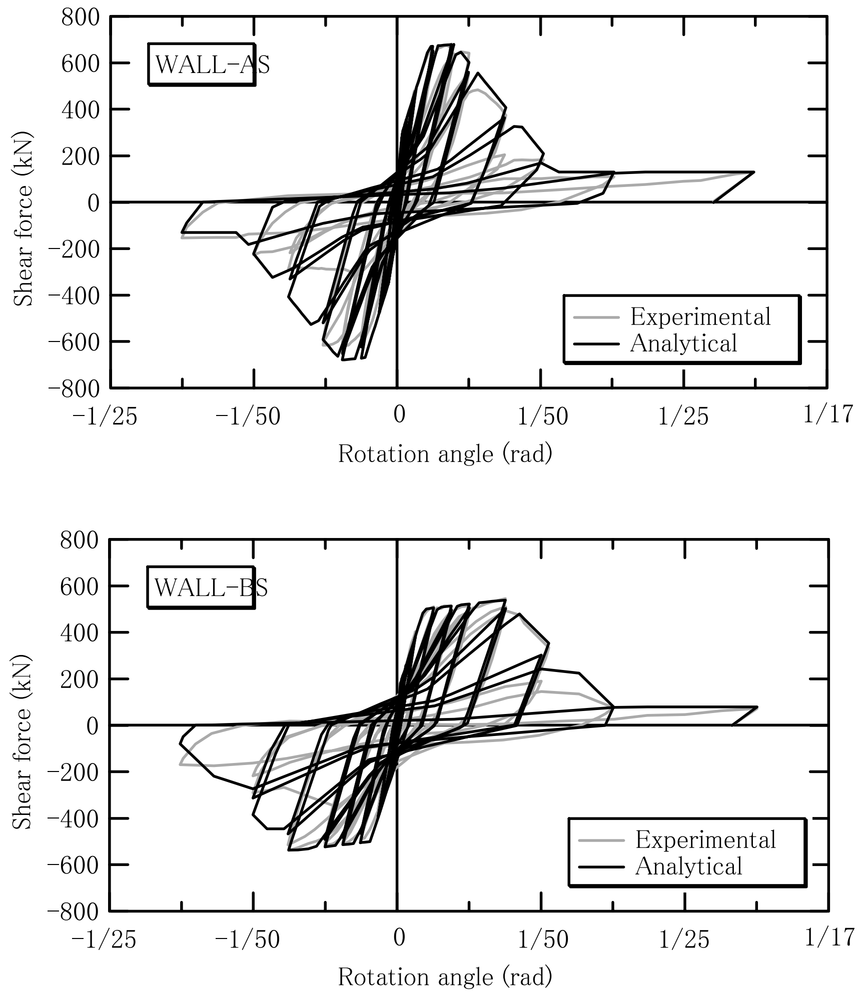

Fig. 11: Result of the static analysis

7. SIMULATION OF DYNAMIC TEST BY EARTHQUAKE RESPONSE ANALYSIS

Earthquake response analysis using the hysteresis models constructed in Chapter 6 is conducted for specimens in the dynamic test to examine the possibility of simulating the dynamic behaviors by the static hysteresis model. A SDOF model was substituted for the specimen, assuming its mass is on the center of gravity. The integration interval is set to 0.005 second and Newmark-β method (β=1/4) is used for the numerical integration of the equation of motion. Moreover, assuming the coefficient of damping is proportional to the stiffness at the moment, the damping factor is equal to 3%. In addition, the parameters of the hysteresis model that were determined by the static analysis are used in the earthquake response analysis.

For Specimen WALL-A, the hysteresis loops and the time history of displacement response for the main 5 seconds obtained from the earthquake response analysis are shown in Figure 12 with the results of the dynamic test. The analytical results show the elastic response for JMA50 input, the inelastic response before yielding for JMA75 and CHI60 inputs and the inelastic response after yielding for JMA100, respectively. It is found that the hysteresis loops and the time history show good agreement with the results of the dynamic test for JMA50 input.

Before yielding, although the analytical result for JMA75 input underestimates the displacement response, that for CHI60 input shows good agreement with the result of the dynamic test. Thus, it is found that the analytical results until JMA100 input can approximately simulate the results of the dynamic test. On the other hand, the analytical result for JMA100 input where the yielding occurred underestimates the displacement response. Moreover, the analytical result shows that the displacement response increases after yielding by considering the capacity degradation due to cyclic loading as well as that in the dynamic test, while it causes the one side drift of displacement. It is thought that the underestimation of the displacement is caused by what the energy dissipation of hysteresis loops in the analysis is larger than that of the test result.

Figure 13 shows the comparison of the hysteresis loops and the time history of displacement response between the analytical and test results for Specimen WALL-B. The analytical result for TOH25 input which is the elastic response agrees well with the result of the dynamic test. Before yielding, although the analytical result for ELC37 input almost agrees with the test result, that for JMA50 input underestimates both capacity and displacement responses, similar to the case of JMA75 input for Specimen WALL-A. For JMA75 input in which flexural yielding occurred, the time that the maximum displacement response occurred in the analysis is different from that in the dynamic test. Thus, it is found that the accuracy of simulation by the analysis for Specimen WALL-B is somewhat worse than that for Specimen WALL-A in larger earthquake motion inputs.

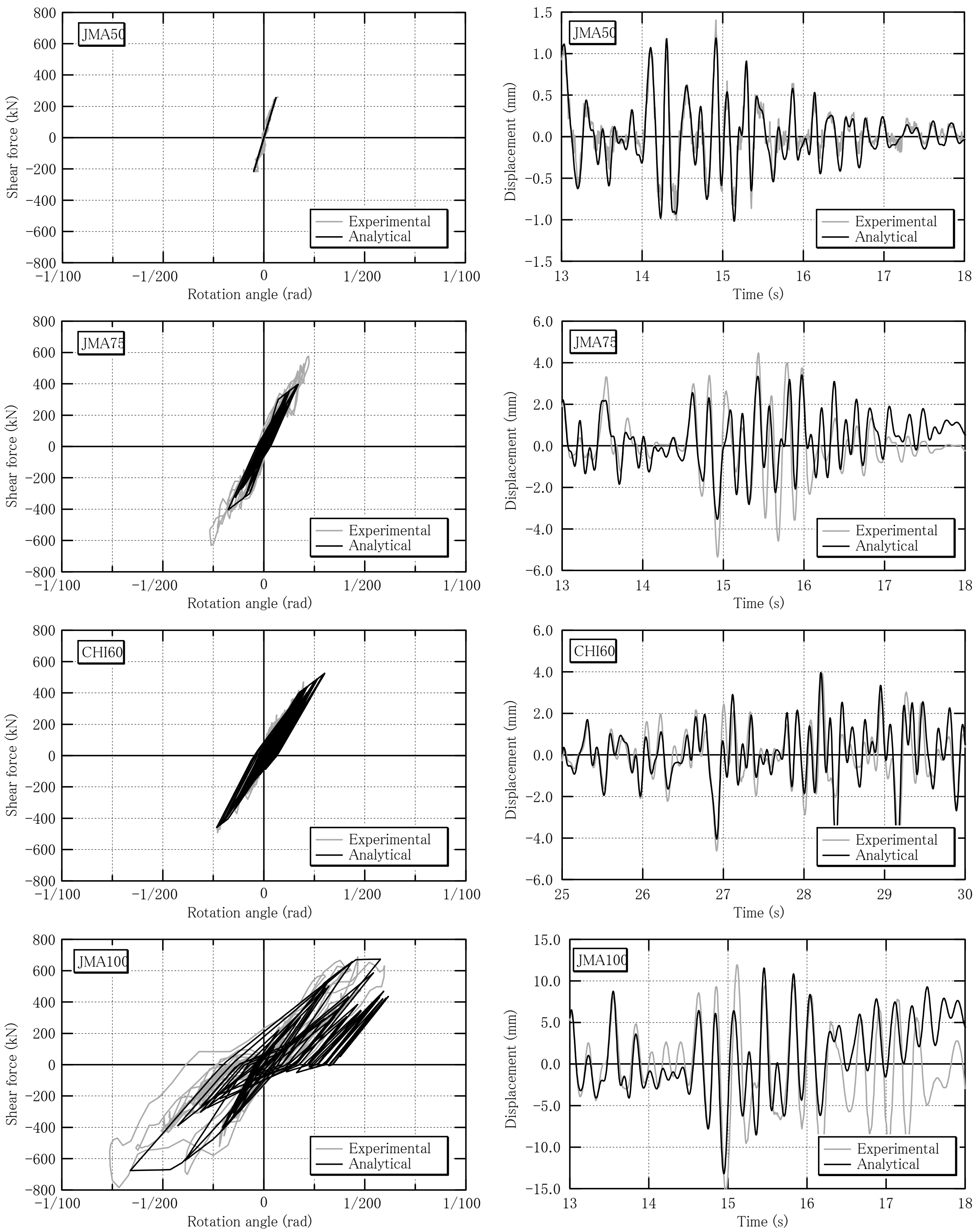

Fig. 12: Hysteresis loop and time history of displacement by the earthquake response analysis (WALL-A)

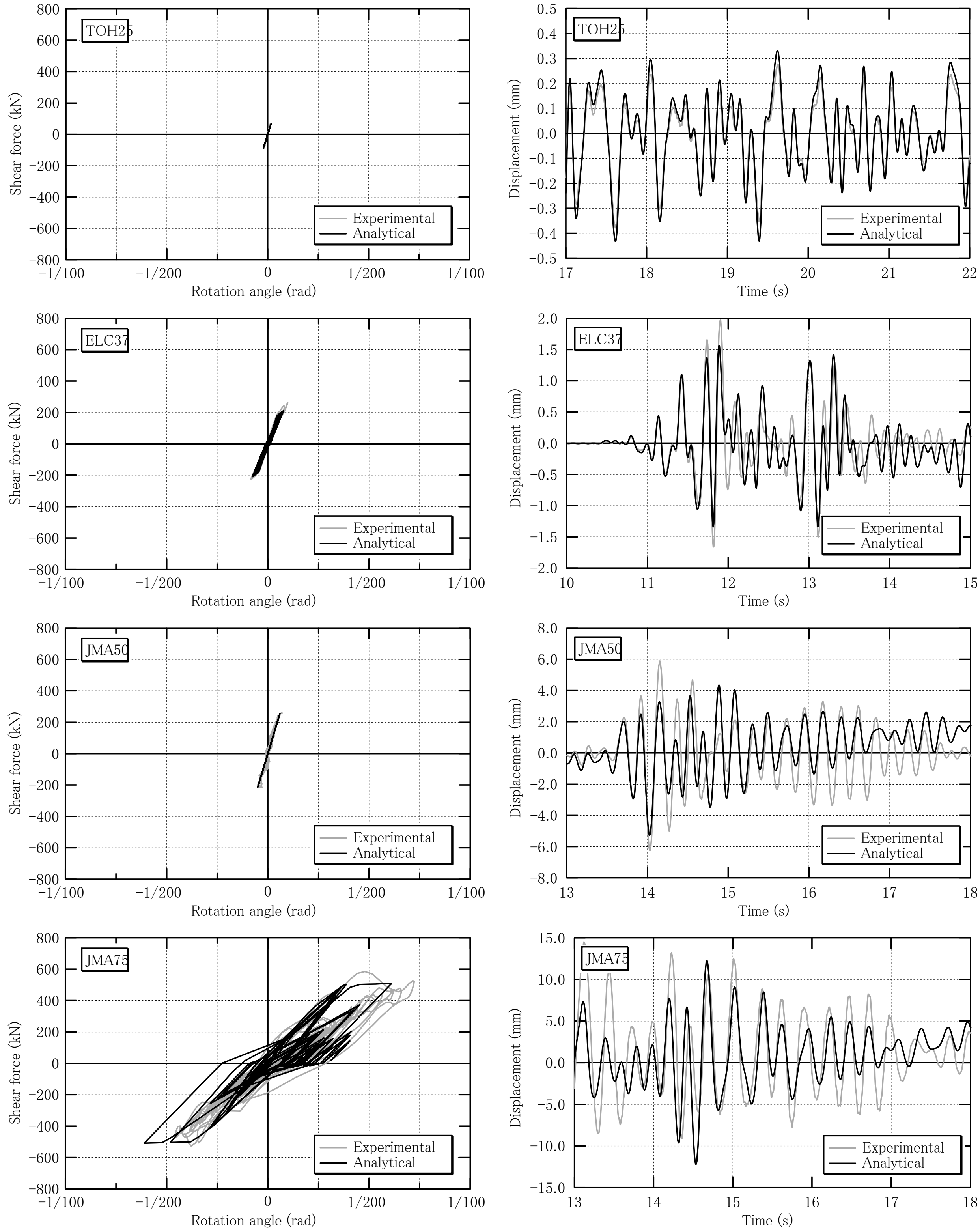

Fig. 13: Hysteresis loop and time history of displacement by the earthquake response analysis (WALL-B)

8. CONCLUSIONS

The main results obtained from this study can be summarized as follows:

(1) Based on the calculated strengths of RC shear walls by the existing design equations, the specimens WALL-AS and WALL-BS were expected to occur shear failure and flexural failure, respectively. However, both specimens failed in shear after flexural yielding.

(2) Before reaching the flexural yield strength, RC shear walls in the dynamic test showed S-shaped hysteresis loops, while those in static test had reverse S-shaped hysteresis loops. After reaching the flexural yield strength, on the other hand, the walls in both the dynamic and static tests showed S-shaped hysteresis loops. However, the hysteresis loops in the dynamic test showed more larger slip characteristic than those in the static test.

(3) A hysteresis Model of RC shear walls considering the capacity degradation due to cyclic loadings was proposed based on the static test. The model consists of Takeda-slip typed hysteresis loops with penta-linear backbone curves.

(4) From the time history earthquake response analysis using the proposed model for RC shear walls in the dynamic test, it is shown that the dynamic behavior can be approximately simulated by the analysis until the walls attain to the ultimate strength.

REFERENCES

Architectural Institute of Japan (1987). *Data on Ultimate Strength Design of Reinforced Concrete*. AIJ (in Japanese).

Architectural Institute of Japan (1998). *Design Guidelines for Earthquake Resistant Reinforced Concrete Buildings Based on Inelastic Displacement Concept*. AIJ (in Japanese).

Kinugasa H. and S. Nomura (1994). Failure Modes in Flexural yield Hinge Region of RC Members Subjected to Lateral Load Reversals, *Journal of Japan Concrete Institute*, Vol.6, No.2: 21-32 (in Japanese).

Matsui, T., T. Kabeyasawa, A. Kato, H. Kuramoto and I. Nagashima. (2004). Shaking Table Test and Analysis of Reinforced Concrete Walls. *Proceedings of Thirteenth World Conference on Earthquake Engineering*, Paper No. 419 (CD-ROM).

Umemura H., T. Ichinose, K. Ohashi and J. Maekawa (2002). Development of Restoring Force Characteristic Models for RC Members Considering Capacity Degradation, *Proceedings of Japan Concrete Institute*, Vol.24, No.2: 1147-1152 (in Japanese).

LATERAL LOAD RESISTING MECHANISM OF A MULTI-STORY SHEAR WALL CONSIDERING THE INTERACTION BETWEEN A SHEAR WALL AND PERIPHERAL ELEMENTS

Susumu KONO[1], Masanobu SAKASHITA[1], and Hitoshi TANAKA[2]

ABSTRACT

Two 15% scale specimens were constructed as basic structural assemblage models extracted from a practical 20-story monolithic shear wall system and precast shear wall system. The specimens consisted of the lowest three-story of a shear wall, a foundation beam, slabs of the first floor, and two piles. Static lateral load was applied with proportionally varying vertical load to simulate loading conditions of the prototype 20-story shear wall system under earthquakes. Shear cracking spread extensively over the foundation beam. Transition of shear transfer mechanisms at the shear wall base was observed from the strain distribution of longitudinal reinforcement in foundation beams and the strain distributions of different loading stages were predicted using a simple model taking into account the degree of crack opening at the wall base.

1. INTRODUCTION

In current design procedures [1][2], cantilever structural walls are normally assumed to stand on a solid foundation, and the foundation beams, slabs and piles are designed separately without considering their interactions. This is because their interactions have not been thoroughly studied for its complexity. Also neglected in the practical design is the fact that shear transfer mechanisms along the wall base vary depending on the crack patters and inelastic deformation levels at the shear wall base. This study aims to experimentally clarify the variation of the lateral load resisting mechanisms considering the interaction between a shear wall, foundation beams, slabs and piles, and to establish more rational design procedures for each structural component.

In the experimental, the specimen configuration was determined from typical Japanese twenty story residential buildings which normally have multiple spans of a RC moment resisting frame in the longitudinal direction and a single span of shear wall system in the transverse direction. In this study, the assemblage consisting of the lowest three story of shear wall with a foundation beam, the first floor slab, and two piles in the transverse direction was scaled to 15%. The shear wall was designed to fail in flexure and the contraflexure point of the piles was fixed at 750 mm

[1] *Dept. of Architecture, Kyoto University, Japan, Email: kono@archi.kyoto-u.ac.jp and rc.sakashita@archi.kyoto-u.ac.jp*
[2] *Disaster Prevention Research Institute, Kyoto University, Japan, Email: tanaka@sds.dpri.kyoto-u.ac.jp*

from the top of them although the depth of the contraflexure point in practice varies depending on various conditions such as the soil and intensity of axial force and lateral force.

2. EXPERIMENTAL SETUP

2.1 Specimens

Figure 1 shows 15% scale specimen configuration to simulate a cantilever wall on a foundation beam supported by two piles. The first floor slab extended 450 mm on either side of the wall and the total width was 900mm. The shear wall and the slab had the same thickness of 50mm. The square piles were designed to be elastic throughout the test so that the lateral load can increase to the failure of the shear wall. The piles extended to the midheight of the foundation beam without the pile caps for simplicity although piles in practice are circular and have solid pile caps on their top. The center-to-center distance of the piles was 1800 mm. The distance between the supporting pins and the top surface of the pile was 750 mm. Two specimens were identical except that the wall panel of Specimen PCW at each floor had four vertical slits filled with mortar to simulate a precast wall system. The horizontal joints of the precast wall were not modeled to simplify the specimen construction. Specimen MNW was cast monolithically. Material properties are shown in Table 1.

Table 1: Material properties

(a) Concrete

Location	Compressive strength (MPa)	Tensile strength (MPa)	Young's modulus (GPa)
Foundation beam, Pile	36.9	3.84	25.3
Wall, Column, Beam	41.3	3.77	27.6
Joint mortar	52.7	3.04	23.5

(b) Reinforcement

Type	Yield strength (MPa)	Young's modulus (GPa)	Tensile strength (MPa)
ϕ4	499	226	587
D6(S)	375	182	534
D6(K)	1084	176	1183
D10	377	188	524
D22	324	172	514
D25	319	183	491

Table 2: Reinforcing bars in MNW and PCW

Member (Section size)	Bar Type		Steel ratio (%)
Column (160×160mm)	Longitudinal	4-D10	1.11
	Transverse	2-D6(K)@50	0.79
Beam (100×120mm)	Upper Long.	4-D6(S)	0.65
	Lower Long.	4-D6(S)	0.65
	Transverse	2–ϕ4@100	0.25
Shear Wall (Thickness 50mm)	Vertical	ϕ4@100	0.25
	Horizontal	ϕ4@100	0.25
Pile (350×350mm)	Longitudinal	8-D22	2.53
	Transverse	4-D10@100	0.82
Foundation beam (100×540mm)	Upper Long.	8-D10	1.23
	Lower Long.	8-D10	1.23
	Shear rebar	2-D6(S)@100	0.63
Transverse Foundation beam (100×540)	Upper Long.	3-D10	0.25
	Lower Long.	3-D10	0.25
	Shear rebar	2-D6(S)@100	0.40
Slab (Thickness 50mm)	Both direction	ϕ4@100	0.25
Loading beam (400x600 mm)	Upper Long.	8-D25	1.80
	Lower Long.	8-D25	1.80
	Shear rebar	2-D10@100	0.36

D6(S) and D6(K) had different mechanical properties as shown in Table 1.

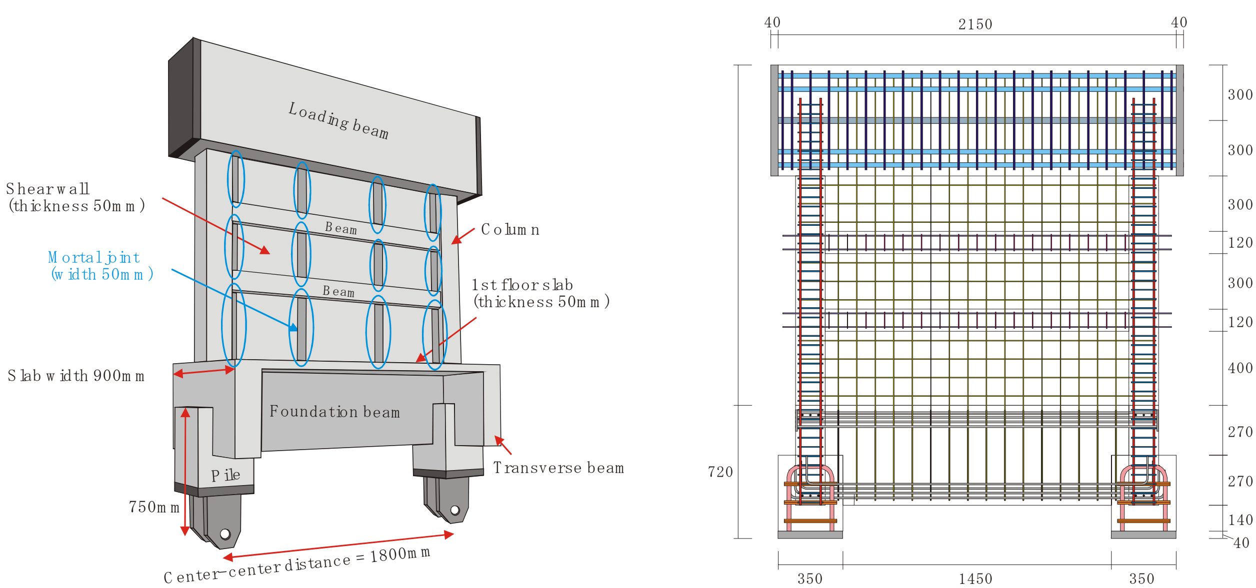

(a) Perspective (b) Dimensions and reinforcement

Fig. 1: Specimen configuration and reinforcement arrangement (unit: mm)

2.2 Loading System

As shown in Figure: 2, lateral load, Q, was applied statically through a 1000kN horizontal jack to the loading beam. Two vertical jacks were adjusted to create appropriate column axial forces, N1 and N2, which were liner functions of Q to simulate loading conditions of the prototype twenty-story shear wall system under earthquakes.

$$N_1 \text{ and } N_2 = 133 \pm 3.10 \cdot Q \qquad (kN) \tag{1}$$

At the roller support, horizontal force was applied to the pile by a 500kN jack so that the pile on the tension side carry 30% of Q and the pile on the compression side carry the rest, that is, the south pile carry 30% of Q for positive loading and 70% of Q for negative loading. The load was applied two cycles at each prescribed loading stage until crushing of the core concrete of the column.

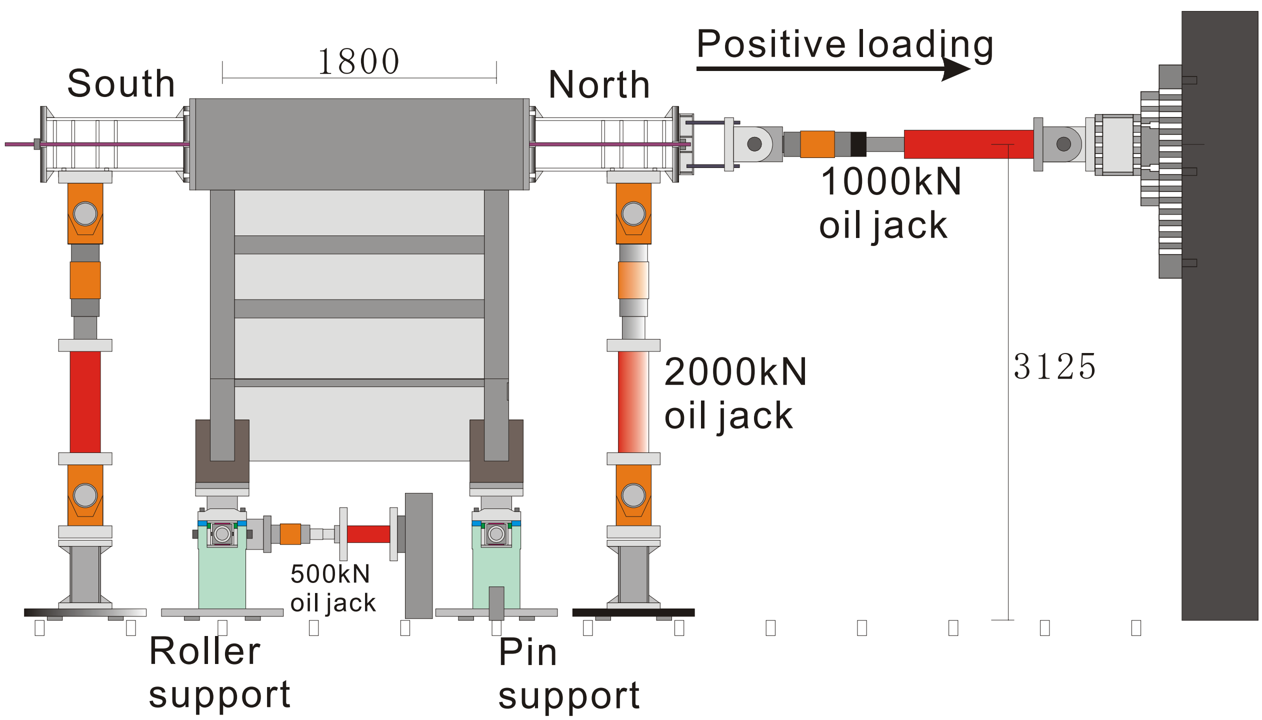

Fig. 2: Loading system (unit: mm)

3. TEST RESULTS

3.1 Observed Damage

Figure 3 shows the damage of specimens after the test. Wall cracks of both specimens were dominated by flexure as designed. Specimen PCW had some diagonal cracks running down along the vertical slit to the bottom of each story after cracks reached the slits. Because of this crack pattern, Specimen PCW had wall cracks more concentrated along the slits and beam interfaces compared with Specimen MNW. Foundation beams of both specimens similarly had large amount of shear cracks after the crack at the wall base opened due to the rotation of the shear wall. In addition, large gaps due to flexural action were found at the interface between the foundation beam and the piles. Before the experiment was carried out, it was expected that the foundation beam would resist monolithically with the shear wall, piles, and slabs and the damage would be minimal until the ultimate stage since vertical reinforcement of the shear wall was well anchored to the foundation beam and the longitudinal reinforcement of foundation beam was well anchored to the pile as specified in the design guidelines by AIJ [1]. The observed damage indicated that the foundation beam did not resist the external force monolithically with the peripheral members after the rotation of shear wall increased and the crack between the wall and foundation beam opened to a certain extent.

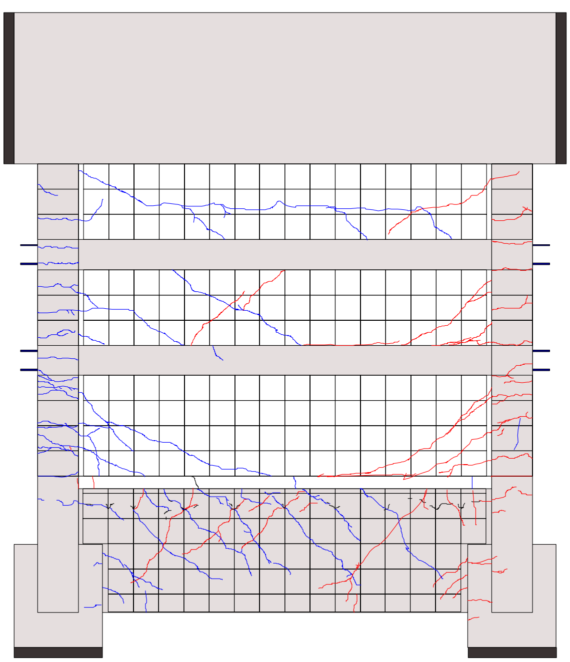

(a) MNW

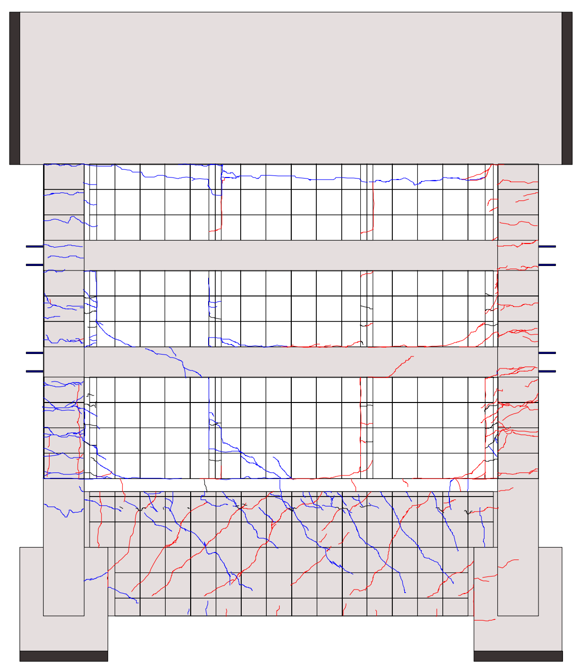

(b) PCW

Fig. 3: Observed damage of the east face after testing

3.2 Load-Displacement Relations

Figure 4 shows the lateral load-first story drift relations. Both specimens showed the ductile behavior up to drift angle (Called R hereafter) of R=2%. After R=2%, the lateral load carrying capacity degraded since the concrete of the compressive column base started to crush. Loads and drift angles at cracking and yielding of shear wall can be seen in Table 3. Flexural cracking loads, Qcr, were close to the flexural yielding loads, Qy, for both specimens. Drift angles at Qcr or Qy varied by large amount and it shows the difficulty of measuring deformation of this stiff system.

In order to confirm the validity of the experiment, the wall was modeled by superposing two types of spring elements which possessed tri-linear load-displacement relations. One spring represented the flexural behavior and the other represented the shear behavior. Two springs were set parallel to obtain the total response. The spring properties were derived using the Hirata et al. model [3] as shown in Figure 5. Original paper needs to be referred for details. The envelope curves of the flexural element and the shear element were assumed tri-linear. Figure 4 and Table 3 compares the analytical and experimental results. The computed flexural cracking strengths were about half as small as the experimental results but the computed flexural yielding loads agreed well with the experimental results. Figure 4 shows that the computed envelop curves have enough accuracy up to R=2% for MNW and R=1% for PCW.

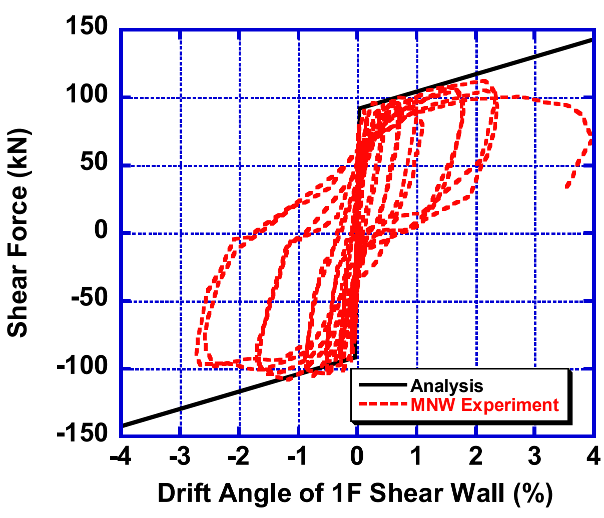

(a) MNW

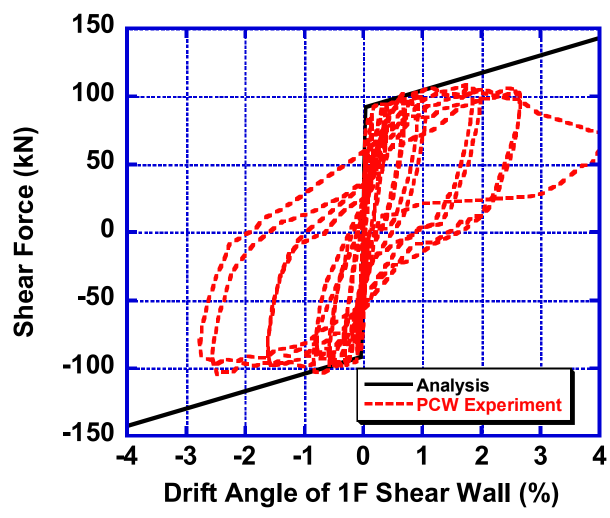

(b) PCW

Fig. 4: Lateral load - first story drift angle relations

Table 3: Load and drift angle at cracking and yielding of shear wall

		Analysis	MNW		PCW	
			Positive	Negative	Positive	Negative
Flexural cracking	Load Qcr (kN)	49.3	78.9	-76.0	84.8	-83.8
	Drift (%)	0.0082	0.0093	-0.0201	0.0517	-0.0053
Flexural yielding	Load Qy (kN)	91.8	84.3	-94.1	86.3	-88.7
	Drift (%)	0.0398	0.0514	-0.0751	0.0936	-0.0419

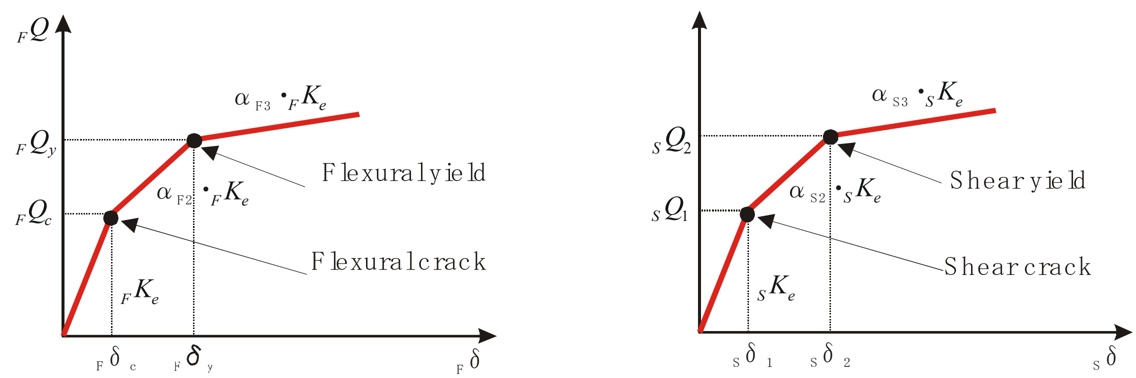

(a) Flexural element (b) Shear element

Fig. 5: Shear force – drift relations for the flexural element and shear element

3.3 Strain Distributions of Longitudinal Reinforcement in Foundation Beams

Figure 6 shows the strain distributions of longitudinal bars in foundation beams. Location in the foundation beam was measured from the center of the specimen and the north side is expressed positive. Multiple lines in each figure show the distribution at different loading stages. Strain of upper longitudinal reinforcement near the midspan tended to be larger than that of beam ends up to Stage 4. After Stage 5, the strain at the tensile side increased to catch up the value at the midspan. Strain distributions of the lower longitudinal reinforcement were nearly linear for any loading stages.

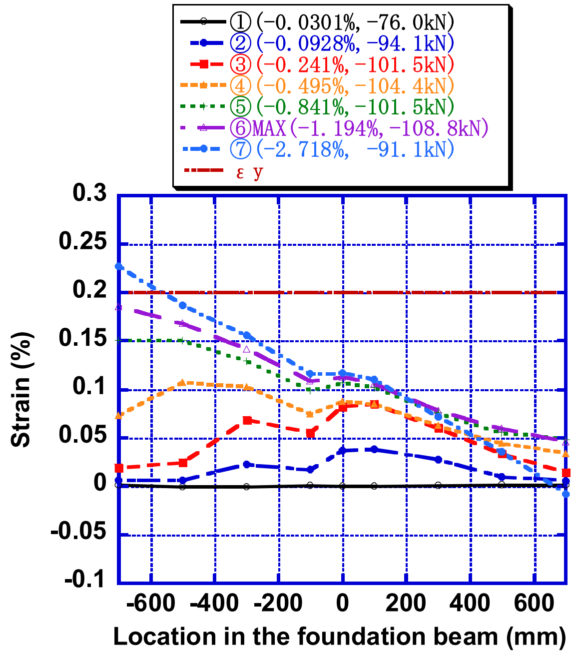

(a) Upper longitudinal bar in MNW

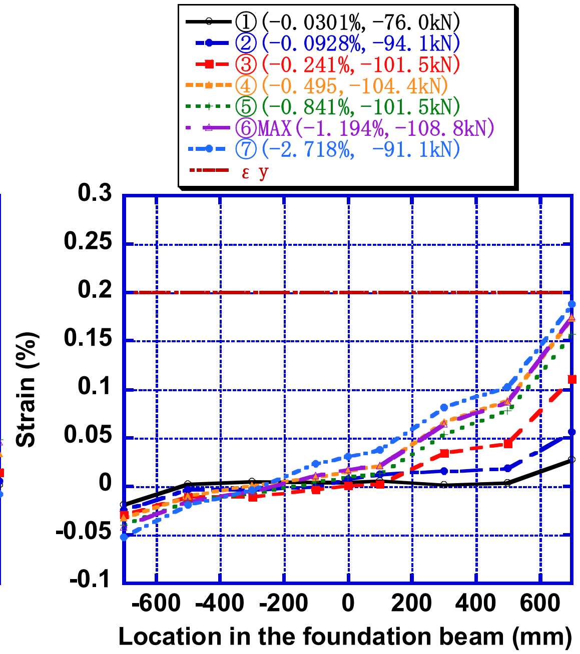

(b) Lower longitudinal bar in MNW

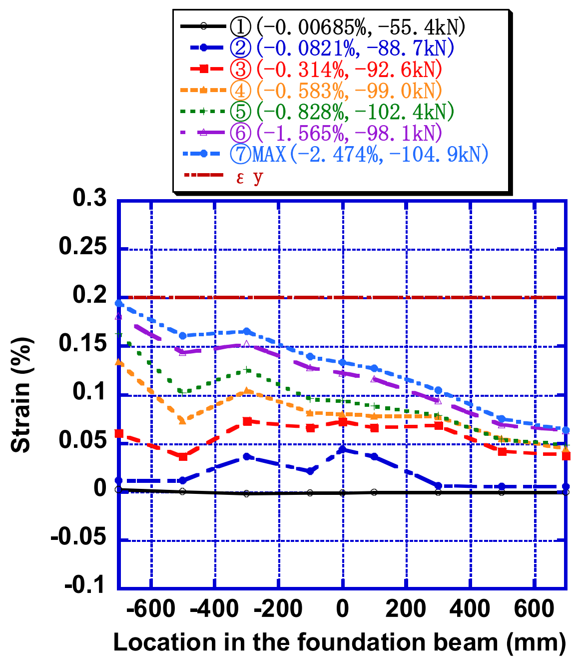

(c) Upper longitudinal bar in PCW

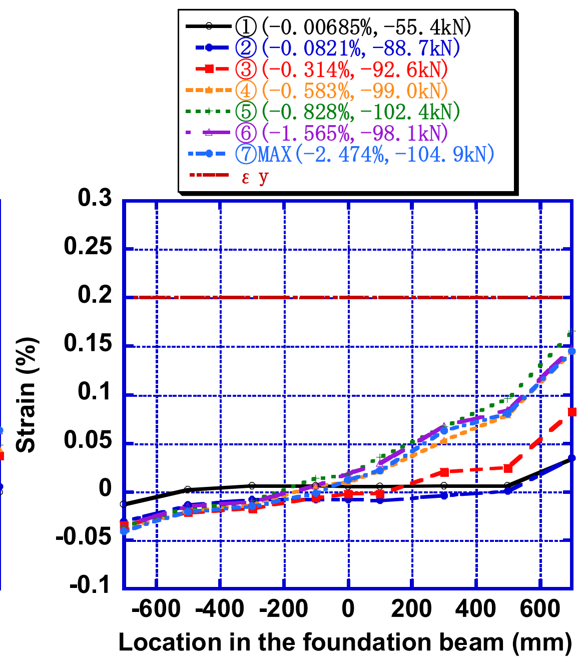

(d) Lower longitudinal bar in PCW

Fig. 6: Strain distributions of longitudinal reinforcement in foundation beams

4. MODELING LATERAL LOAD RESISTING MECHANISM OF FOUNDATION BEAMS

4.1 Simulation of Strain Distributions of the Foundation Beam

Figure 7 shows moment distributions of the foundation beam due to three types of forces acting on it. It was assumed that the forces acting on the foundation beam came from the piles and shear wall, the axial force of the pile directly transferred to the column and only moment and shear of piles transferred to the foundation beam as shown in Figure 7(a). Vertical tensile force at the wall base activates due to the vertical reinforcement. The reinforcement tries to lift up the foundation beam as the wall rotates and the moment distributes as Figure 7(b). Tangential force at the wall base, that is the shear force, comes from a dowel action of vertical reinforcement and concrete shear at the interface. Concrete shear consists of aggregate interlock at a cracked interface and elastic/plastic shear at a remaining ligament. The moment due to these shear force was assumed to distribute as Figure 7(c). Since the largest crack width between the wall base and the foundation beam became as large as a few centimeters, the crack width must have affected the stress transfer mechanisms at the interface. Hence a region with a large crack opening was separated from the rest of the wall base and expressed as detached region as shown in Figure 8. Assuming that the lateral force acts from left to right, the detached portion increases as the wall rotates. Although there is no quantitative definition of detachment, it is conceptually the interface with large crack opening. It was assumed that

- Vertical reinforcement has yielded at the detached region. Tensile stress of the reinforcement in the remaining ligament distributes linearly to zero at the compressive column.
- No shear force transfers at the detached interface. The shear force distributes evenly at the remaining ligament.

Figure 9 shows a moment distribution due to the interface shear force at the wall base for five different degree of detachment. Using the model, the strain distributions of the longitudinal reinforcement in the foundation beam were computed with section analysis. The computed results at three loading stages are shown in Figure 10. Degree of detachment was assumed so that the computed strain distribution best matched the experimental results. Although there are some local discrepancies between computed and experimental results, the simple model assuming the degree of detachment can be used to predict the force acting on the foundation beam. Discrepancy near the end of the foundation beam can be explained from the behavior of knee joints and the combined resistance from the upper story.

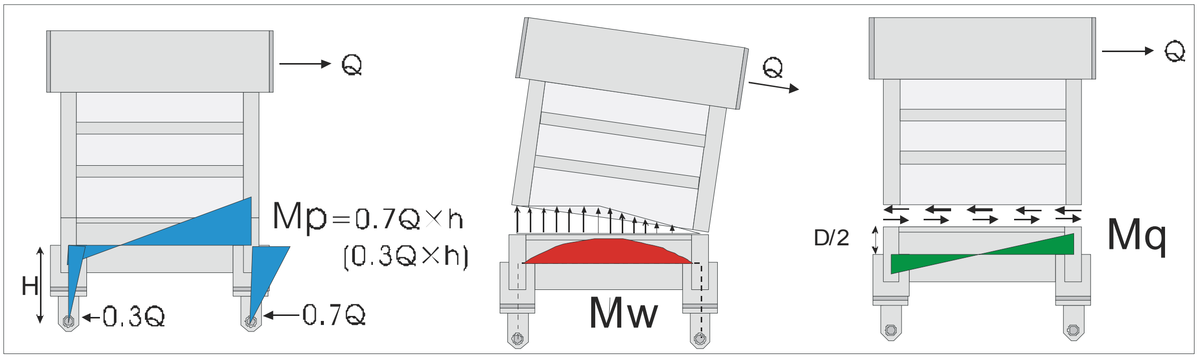

(a) Shear and moment from piles (b) Vertical tension from wall (c) Shear from wall

Fig. 7: Forces acting on the foundation beam and the resulting moment distributions

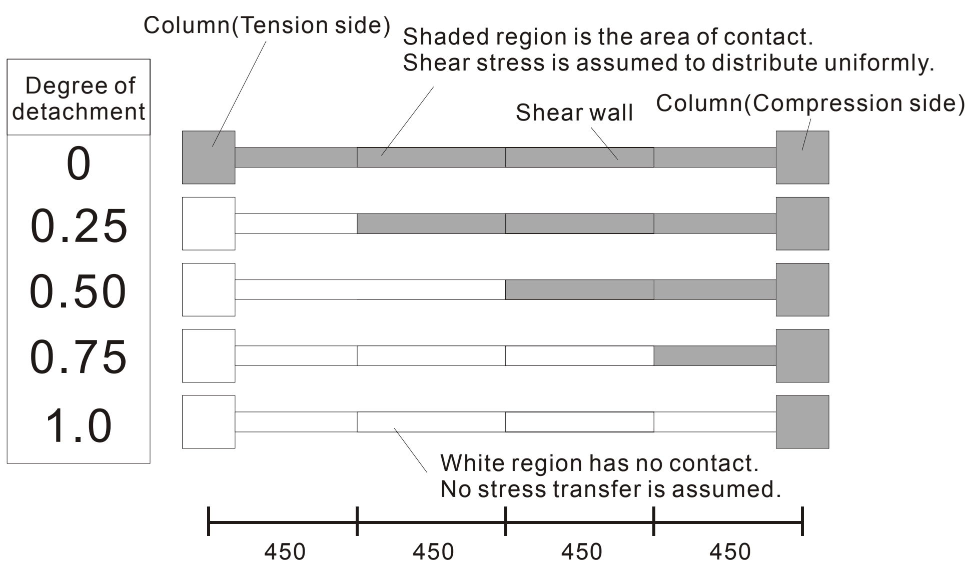

Fig. 8: Degree of detachment at the wall base due to the rotation of wall

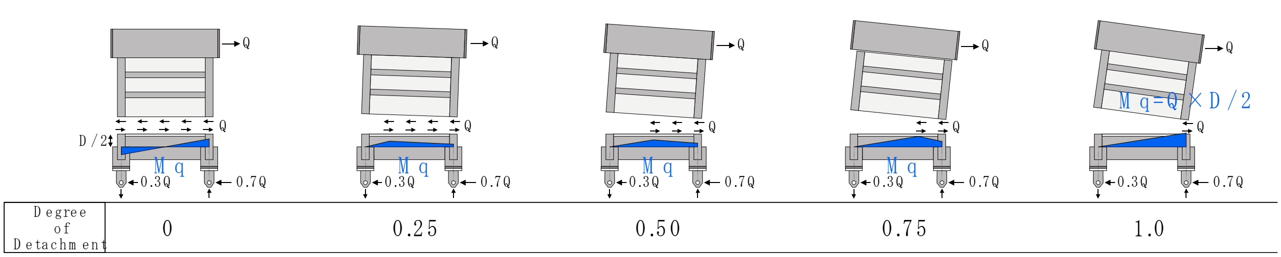

Fig. 9: Moment distribution in the foundation beam at different level of detachment

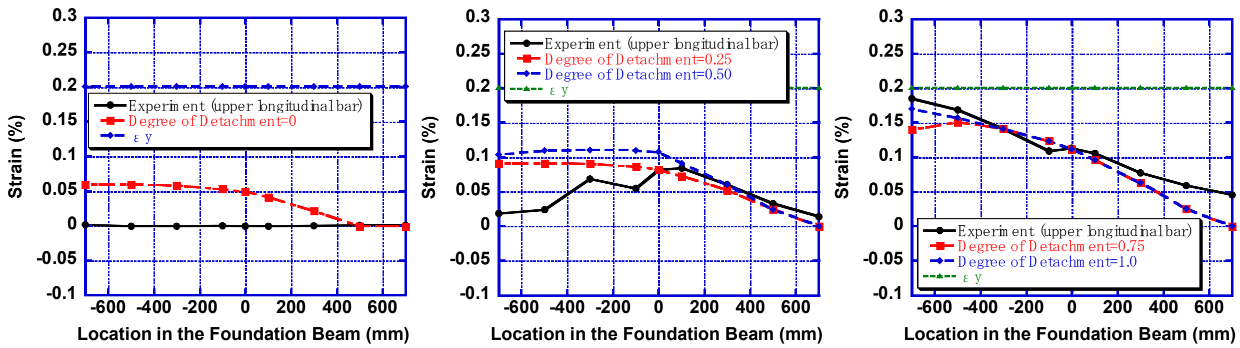

(a) Before yielding of wall (Stage 1)

(b) After yielding of wall (Stage 3)

(c) Ultimate stage (Stage 6)

Fig. 10: Strain distribution of the upper longitudinal reinforcement in the foundation beam

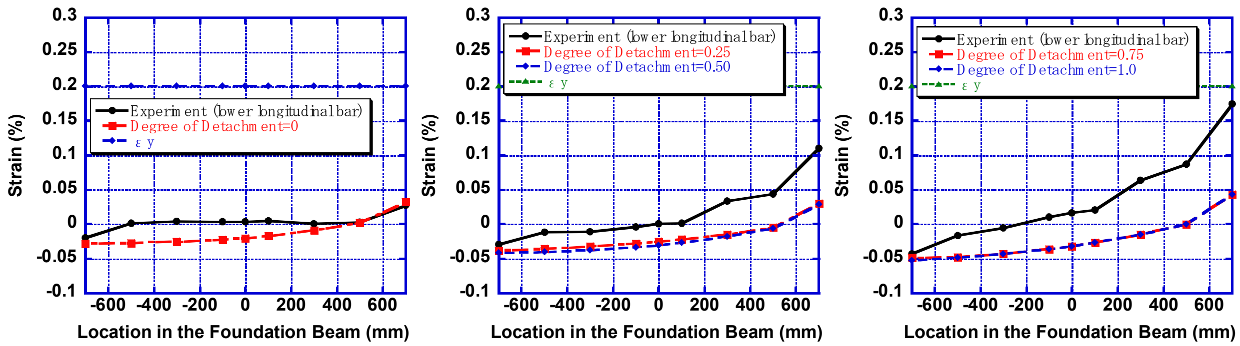

(a) Before yielding of wall (Stage 1)

(b) After yielding of wall (Stage 3)

(c) Ultimate stage (Stage 6)

Fig. 11: Strain distribution of the lower longitudinal reinforcement in the foundation beam

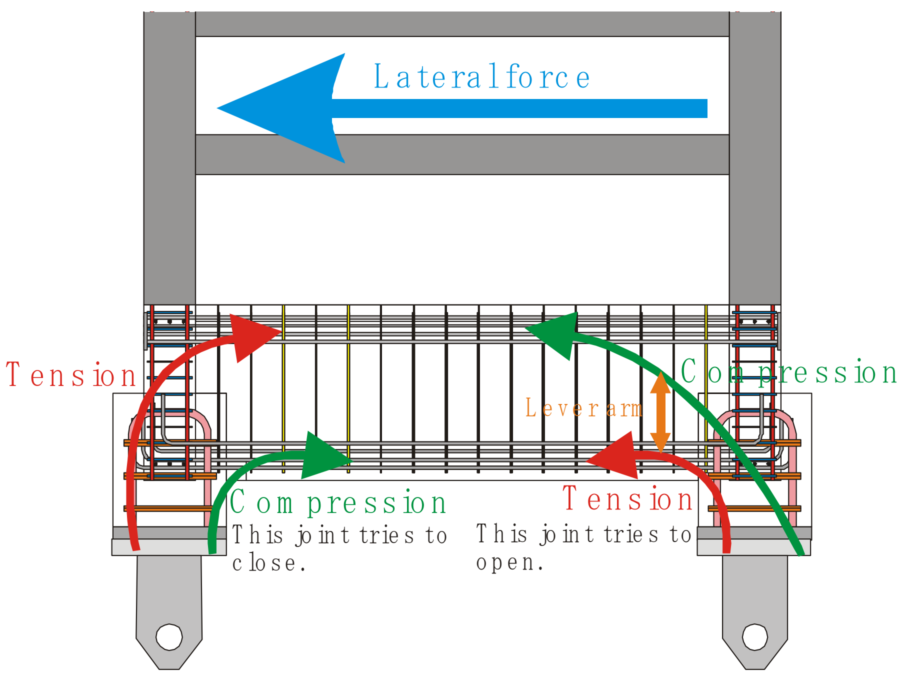

Fig. 12: Compressive force acting on the foundation beam

5. CONCLUSIONS

Two 15% scale cantilever structural walls were tested to clarify lateral load resisting mechanisms considering the interaction between the shear wall, foundation beams, slabs and piles. Main conclusions can be summarized as follows.

- Monolithic action between foundation beam and peripheral members, such as shear wall and piles, was much less than expected and unexpected shear cracking spread extensively over the foundation beam. However, effective width of slab was as wide as the half span.
- Forces acting on the foundation beam can be summarized as shear and moment from piles, and stresses transferred at the wall base interface. Stresses transferred at the wall base can be quantified by assuming the degree of detachment. Determination of degree of detachment is under study.
- Lateral loads for cracking and yielding was simulated well with a simple superposition of flexural and shear elements but displacements at cracking and yielding varied in experiment and prediction was not very precise.

REFERENCES

[1] Architecture Institute of Japan, “AIJ Standard for Structural Calculation of Reinforced Concrete Structures Based on Allowable Stress Concept,” 1999, pp 218-241.

[2] Paulay, T. and Priestley, M.J.N., “Seismic Design of Reinforced Concrete and Masonry Buildings,” John Wiley & Sons, 1992, pp. 362-499.

[3] Hirata, M., Naraoka, S., Kim, Y., Sanada, Y., Matsumoto, K., Kabeyazawa, T., Kuramoto, H., Hukuda, T., Kato, A., Ogawa, M., “Dynamic Test of Reinforcement Concrete Wall-Frame System with Soft First Story Part 1-Part 4” Summaries of technical papers of annual meeting architectural institute of Japan, 2001,pp705-712 (in Japanese).

SESSION 6: AXIAL FAILURE OF STRUCTURAL MEMBERS

Chaired by

♦ Chiun-lin Wu and Susumu Kono ♦

ASSESSMENT OF EXPECTED FAILURE MODE FOR REINFORCED CONCRETE COLUMNS

Ling ZHU, Kenneth J. ELWOOD, and Terje HAUKAAS[1]

ABSTRACT

For the seismic assessment of existing reinforced concrete buildings, it is important to be able to reliably predict the column failure modes. Using a database of 111 columns, this paper demonstrates that the common practice of comparing the plastic-shear demand to the shear strength of the column does not provide a reliable estimate of the observed failure mode. Two alternate methods are proposed. The first method provides an estimate of the probability of observing a particular failure mode through the development of a probabilistic failure mode model. This model identifies most critical parameters influencing the observed failure mode; namely, the transverse reinforcement ratio, the aspect ratio, and the plastic shear to shear strength ratio. The second method classifies a column based on these parameters and provides a simple means to determine if a column is expected to exhibit a flexure-dominated or shear-dominated response at failure.

INTRODUCTION

When subjected to large lateral drift demands, reinforced concrete columns frequently experience degradation in the lateral-load capacity as a result of several different failure modes. Three failure modes are considered in this study: (1) flexure failure, where degradation in the lateral-load capacity occurs *after* yielding of the longitudinal reinforcement due to damage related to flexural deformations (i.e. spalling of concrete, buckling of longitudinal bars, concrete crushing, etc.); (2) shear failure, where degradation in the lateral-load capacity occurs *before* yielding of the longitudinal reinforcement due to shear distress (i.e. diagonal cracking) in the column; and (3) a combined flexure-shear failure, where degradation in the lateral-load capacity occurs *after* yielding of the longitudinal reinforcement but results from shear distress in the column.

When designing retrofit strategies for existing reinforced concrete buildings, it is frequently not possible to limit the drift demands on all columns to avoid lateral-strength degradation. If a shear or flexure-shear failure is anticipated, then axial failure of the column can occur prior to P-delta

---

[1] *Department of Civil Engineering, University of British Columbia, Vancouver, Canada*
Email: lzhu@civil.ubc.ca, elwood@civil.ubc.ca, terje@civil.ubc.ca

instability due to sliding along the critical shear-failure plane (Elwood and Moehle 2005). Considering the general preference for flexure failures, it is important that an engineer be able to assess the expected failure mode for columns experiencing lateral-strength degradation. Furthermore, empirical models developed to estimate the capacity of reinforced concrete columns (e.g. drift capacity at lateral-strength degradation) should be developed based on a database of specimens with common attributes in their response and failure modes. Hence, a reliable assessment procedure to determine the expected failure mode is desired. In engineering practice, the expected failure mode is commonly assessed by comparing the plastic-shear capacity of the column to the shear strength. Using a large database of column tests, this study indicates that this strength-based approach does not provide a reliable prediction of the failure mode.

This paper presents two approaches to assess the expected failure mode of reinforced concrete columns. First, a probabilistic failure mode index model is proposed to determine the probability of observing a specific failure mode for a given column. The model is developed based on a Bayesian-updating methodology (Gardoni et al. 2002; Zhu et al. 2005) and a selected database of column specimens. The probabilistic model is employed to assess the probability of observing a flexure, flexure-shear, or shear failure mode for a column damaged during the Northridge earthquake. Second, a deterministic column classification method is proposed to categorize columns into two zones based on three column parameters. This classification method enables an engineer to approximately distinguish shear-dominated columns and flexure-dominated columns.

EXPERIMENTAL DATABASE

A database (UW-PEER database) containing results of cyclic lateral-load tests of reinforced concrete columns was compiled by researchers at the University of Washington under the support of the Pacific Earthquake Engineering Research Center (Berry et al. 2004). Based on the UW-PEER database, Camarillo (2003) provides yield displacements and the displacements at 80% maximum effective lateral force for 230 rectangular columns. Herein the maximum effective lateral force, V_{eff}, is calculated as the maximum moment (considering test configuration and $P-\Delta$ effect) divided by the shear span. For this study, selected tests have been excluded to focus on typical columns from older reinforced concrete buildings (i.e., 80 columns are excluded because of the usage of high strength concrete ($f_c' > 60\text{MPa}$); 15 columns are excluded because of unusual reinforcement details (e.g., spiral hoops or extra longitudinal bars in the column center); 9 specimens are excluded because of their special test setup is inconsistent with the expected loading and deformation of columns; and 1 column is excluded because of its very high shear span to depth ratio ($a/d \approx 9$)). In total, 125 columns are considered in this study. These 125 columns have properties within the following ranges:

- Aspect ratio: $1.2 \le a/d \le 7.0$
- Hoop spacing to depth ratio: $0.1 \le s/d \le 1.2$
- Concrete compressive strength: $16 \le f_c' \le 56.2\text{MPa}$
- Longitudinal reinforcement yield stress: $318 \le f_{yl} \le 587\text{MPa}$
- Longitudinal reinforcement ratio: $1.2\% \le \rho_l \le 3.3\%$
- Transverse reinforcement yield stress: $249 \le f_{yt} \le 616\text{Mpa}$
- Transverse reinforcement ratio: $0.06\% \le \rho'' \le 2.2\%$
- Normalized shear stress: $0.2 \le v\Big/\left(\sqrt{f_c'}\Big/6 + \rho'' f_{yt}\right) \le 3.1$
- Axial load ratio: $0.0 \le P\big/A_g f_c' \le 0.8$

where a is the shear span; d is the depth to the centerline of the outermost tension reinforcement; s is the hoop spacing; $\rho_l = A_{sl}/bh$ denotes the longitudinal reinforcement ratio; A_{sl} denotes the total area of longitudinal reinforcement; b is the width of column section; h is the depth of column section; $\rho'' = A_{st}/bs$ denotes the transverse reinforcement ratio; A_{st} denotes the area of transverse reinforcement; $v = V_{eff}/bd$ denotes the maximum nominal shear stress; P is the axial load; and $A_g = bh$ denotes the gross cross-sectional area of the column. Further details on the column database can be found elsewhere (Zhu 2005).

Recall that three failure modes are considered in this study: flexure failure, shear failure, and flexure-shear failure. The failure mode for each of column in the selected database is based on the failure modes identified by Camarillo (2003), with adjustments made to less than 10% of the columns based on further review of the references. Note that 14 column specimens tested by Pujol (2002) are not classified in any failure mode because the drift capacity, and perhaps the failure mode, was strongly affected by the unique loading routine (i.e., a large number of cycles to a selected maximum displacement until failure was observed). The tests by Pujol (2002) illustrate that loading routine (i.e. number of cycles and the amplitude of cycles) is expected to impact the observed column response; however, given the limited number of data available to assess the impact of loading routine, and the difficulty of determining the expected loading routine for columns in real buildings, the differences in the loading routines for specimens within the column database was not considered in this study. Excluding 14 specimens tested by Pujol, the selected database contains 64 flexure failure columns, 36 flexure-shear failure columns and 11 shear failure columns.

COLUMN CLASSIFICATION BASED ON SHEAR STRENGTH MODEL

It is well recognized that the relation between plastic shear demand and shear strength provides useful information in the determination of column failure modes. Here, the column shear demand is determined by its maximum moment capacity divided by the shear span, $V_p = M_{\max}/a$. The maximum moment capacity, $M_{\max}$, is computed through a moment-curvature analysis for the column's cross section. The column shear strength, V_n, is calculated according to a shear strength model proposed by Sezen and Moehle (2004). This model estimates the column shear strength as the summation of shear carried by concrete, V_c, and shear carried by transverse reinforcement through a 45° truss model, V_s.

$$V_n = kV_o = k(V_c + V_s) = k\frac{0.5\sqrt{f_c'}}{a/d}\sqrt{1+\frac{P}{0.5\sqrt{f_c'}A_g}}0.8A_g + k\frac{A_{st}f_{yt}d}{s}$$

$$k = \begin{cases} 1.0, & \mu_\delta \le 2.0 \\ 1.15 - 0.075\mu_\delta, & 2.0 < \mu_\delta < 6.0 \\ 0.7, & \mu_\delta \ge 6.0 \end{cases} \qquad \text{(MPa units)} \qquad (1)$$

where the coefficient k defines the shear strength degradation with increasing displacement ductility, μ_δ. Figure 1 illustrates the conceptual definition of the three failure modes based on the shear strength model. As suggested in the figure, columns with $V_p/V_o \ge 1.0$ are expected to fail in shear (S), columns with $V_p/V_o \le 0.7$ are expected to fail in flexure (F), and columns with $0.7 < V_p/V_o < 1.0$ are expected to experience a flexure-shear failure (FS). Therefore, according to this strength-based approach, $V_p/V_o = 0.7$ and $V_p/V_o = 1.0$ can be selected as boundaries for each failure mode.

Figure 2(a) compares the observed column failure mode and the value of V_p/V_o for the selected database (note that the 14 Pujol columns are excluded). The plot shows relatively high dispersion for all three failure modes. The results are further summarized in the form of a histogram, as shown in Figure 2(b). Only 32% of columns with $V_p/V_o \geq 1.0$ experienced pure shear failures as expected. Only 33% of columns with $0.7 < V_p/V_o < 1.0$ experienced flexure-shear failures as expected. In contrast, 91% of columns with $V_p/V_o \leq 0.7$ experienced flexure failures as expected. It is apparent that the boundaries of $V_p/V_o = 1.0$ and $V_p/V_o = 0.7$ are not sufficient to distinguish the three failure modes. Hence, the classification of column failure modes based only on the shear strength model is not adequate; other column parameters, which may also influence the observed failure mode, should be considered. A probabilistic failure mode index model incorporating not only the column shear demand-strength ratio but also several other column parameters is developed in the next section.

It should be noted that the Sezen and Moehle shear strength model was developed using a database of columns experiencing only flexure-shear failures. Since this model was developed to estimate the mean strength of such columns, some of the original database columns produced $V_p/V_o \geq 1.0$ or $V_p/V_o \leq 0.7$, similar to the results shown in Figure 2(a).

PROBABILISTIC FAILURE MODE MODEL

Figure 3 demonstrates the effect of eight key parameters on the column failure modes for the database described above (the relationship between V_p/V_o and the observed failure mode is shown in Figure 2(a)). It is apparent from the plots that there is considerable variability in the results, and no clear relationship between the failure modes and any one parameter. However, Figure 2(a) does suggest that columns with low shear demand-strength ratios, V_p/V_o, tend to fail in flexure, while columns with high shear demand-strength ratios tend to fail in shear. A similar trend is observed for normalized maximum shear stress, $v / \left(\sqrt{f_c'} / 6 + \rho'' f_{yt} \right)$ (MPa units), and longitudinal reinforcement index, $\rho_l f_{yl} / f_c'$, as shown in Figure 3. In contrast, columns with high aspect ratios, a/d, tend to fail in flexure while columns with low aspect ratios tend to fail in shear. Such trend is also shown in the relationship between the failure modes and transverse reinforcement ratio, ρ'', and transverse reinforcement index, $\rho'' f_{yt} / f_c'$. Based on the plots, the axial load ratio, $P / A_g f_c'$, hoop spacing ratio, s/d, and longitudinal reinforcement ratio, ρ_l, have no apparent relationship with the column failure modes.

Three integers, '1', '2' and '3', are assigned as failure mode indices to represent flexure failure, flexure-shear failure and shear failure, respectively. The goal of the probabilistic model is to develop an expression to predict the appropriate failure mode index (FM) and the probability of observing each failure mode. In order to investigate the dependence of the column failure modes on key parameters, the nine parameters in Figures 2(a) and 3 are considered in the initial formulation of probabilistic failure mode index model. The initial model takes the form

$$\begin{aligned} \mathrm{FM} = {} & \theta_1 + \theta_2 \rho_l + \theta_3 \frac{\rho_l f_{yl}}{f_c'} + \theta_4 \left(\rho'' \right)^{\frac{-1}{4}} + \theta_5 \frac{\rho'' f_{yt}}{f_c'} + \theta_6 \frac{s}{d} + \ldots \\ & \theta_7 \left(\frac{a}{d} \right)^{-2} + \theta_8 \frac{v}{\sqrt{f_c'} / 6 + \rho'' f_{yt}} + \theta_9 \frac{P}{A_g f_c'} + \theta_{10} \frac{V_p}{V_o} + \sigma \varepsilon \end{aligned} \tag{2}$$

where $\theta_1, \ldots, \theta_{10}$ are random variables denoting unknown model coefficients; ε is a random variable with zero mean and unit variance, and σ is a random variable representing the standard deviation of the model error. Note that all the θs in Equation (2) are dimensionless. Powers have been applied to some of the column parameters to obtain better model prediction consistent with the experimental observations.

A stepwise deletion procedure (Gardoni et al. 2002) was employed to assess the probabilistic model in Equation (2) and determine the most critical parameters affecting the observed failure mode. (The assessment and simplification of Eq. (2) is described in detail in Zhu (2005).) The final models take the form:

$$\mathrm{FM} = \theta_1 + \theta_4 (\rho'')^{\frac{-1}{4}} + \theta_7 \left(\frac{a}{d}\right)^{-2} + \theta_{10} \frac{V_p}{V_o} + \sigma\varepsilon \tag{3}$$

Table 1 lists the posterior statistics of the model coefficients in Equation (3). This probabilistic model identifies the most important parameters affecting the column failure mode, namely, transverse reinforcement ratio, aspect ratio, and shear demand-strength ratio. Note that the parameters, which have no clear relationship with column failure modes as shown in Figure 3 (e.g., the axial load ratio, $P/A_g f_c'$; hoop spacing ratio, s/d; and longitudinal reinforcement ratio, ρ_l), are all eliminated through the model assessment procedure. The mean prediction of FM is given by (with $\varepsilon = 0$ and $\theta_i =$ posterior mean value listed in Table 1)

$$(\mathrm{FM})_{mean} = 0.80 - 0.13(\rho'')^{\frac{-1}{4}} + 1.75\left(\frac{a}{d}\right)^{-2} + 1.33\frac{V_p}{V_o} \tag{4}$$

Figure 4(a) compares the observed FM and the mean calculated FM for the test columns. For a perfect model, the data would lump points around (1, 1), (2, 2) and (3, 3). However, the plot shows relatively high bias and dispersion for all three failure modes. If $\mathrm{FM} = 1.5$ and $\mathrm{FM} = 2.5$ (shown as dash dot lines in Fig. 4(a)) are selected as boundaries for each failure mode, Figure 4(b) summarizes the results of $(\mathrm{FM})_{mean}$ for the 111-column database in the form of a histogram. Within this database, the failure modes of 94% (=60/64) of flexure failure specimens, 92% (=33/36) of flexure-shear failure specimens, and 73% (=8/11) of shear failure specimens can be correctly predicted using Equation (4). The results of Figure 4(b) show considerable improvement over the strength-based approach (Fig. 2(b)).

The probabilistic failure mode model (Eq. (3)) is actually a probability density function for FM; hence it can be used to assess the probability of each failure mode for a given column through a reliability analysis. As an example, the failure mode probability is estimated for a column damaged during the Northridge earthquake. The seven-story moment frame building, shown in Figure 5 and located in Van Nuys, California, experienced significant ground shaking during both the San Fernando earthquake and the Northridge earthquake. Extensive literature on this structure is available elsewhere (Browning et al. 2000; Trifunac and Hao 2001). One of the damaged fourth-story exterior columns (C4, circled in Fig. 5) is assessed here.

Based on Equation (3), the distribution of FM for column C4 is constructed, as shown in Figure 6. Note that the marginal distributions for $\boldsymbol{\theta}$ and σ in Equation (3) are selected as normal and lognormal, respectively, with the posterior statistics given in Table 1. The assumed distributions and coefficients of variation (COV) for the material properties and applied loads of column C4 are summarized in Table 2. If FM = 1.5 and FM = 2.5 (shown as dashed lines in Fig. 6) are selected as boundaries for each failure mode, the probabilities of three failure modes can be determined by calculating the corresponding area under the probability density function. For column C4, the probability of flexure failure ($\text{FM} \le 1.5$) is 18%, the probability of shear failure ($\text{FM} \ge 2.5$) is 3%, and the probability of flexure-shear failure ($1.5 < \text{FM} < 2.5$) is 79%. The flexure-shear failure mode has the highest probability, and this failure mode classification is consistent with the observed column damage: severe shear distress at the top of the column, as shown in Figure 5.

TWO-ZONE COLUMN CLASSIFICATION METHOD

In order to identify the column failure modes using the probabilistic model, it is necessary to subjectively select boundaries for each failure mode. In order to avoid the difficulty in boundary selection for the probabilistic model, an alternative method is proposed to approximately separate the flexure-dominated columns from the shear-dominated columns. Recall that three parameters were identified as the most critical parameters affecting the column failure mode through the assessment of probabilistic failure mode model. The column classification method is based on these three column parameters, namely, the plastic-shear demand to shear strength ratio (V_p/V_n), aspect ratio (a/d), and transverse reinforcement ratio (ρ'').

Figure 7 plots V_p/V_n versus the aspect ratios for the 125-column database (V_n is determined based on Eq. 1). Note that the ratios V_p/V_n are greater than 1.0 for all shear failure columns and the majority of flexure-shear failure columns, while the values of V_p/V_n are less than 1.0 for most flexure failure columns. Moreover, all column specimens fail either in shear or flexure-shear when their aspect ratios are less than 2, while column specimens fail in flexure when their aspect ratios are greater than 4. Note that columns with large aspect ratios (a/d) will necessarily have a small plastic-shear demand (V_p), and hence V_p/V_n is expected to be less than 1.0.

Columns are classified according to the following criteria: (1) Columns satisfying $\rho'' \le 0.002$ are categorized into "Zone S" regardless of their V_p/V_n and a/d; (2) Columns satisfying either $a/d \le 2.0$ or $V_p/V_n \ge 1.05$ are categorized into "Zone S"; (3) Columns satisfying both $a/d > 2.0$ and $V_p/V_n < 1.05$ are categorized into "Zone F". Figure 8 summarizes the two-zone column classification results for the 125-column database. Zone S includes all shear failure columns and most of the flexure-shear failure columns; hence is referred to as the shear-dominated zone. Zone F includes nearly all flexure failure columns and only a few flexure-shear failure columns; hence is referred to as the flexure-dominated zone. Note that the 14 column specimens tested by Pujol (2002) are also included in Zone F. The two zone classification method provides a simple means to estimate the failure mode of a column and segregates the data for further model development. Two sub-databases are compiled based on this two-zone classification method, with each database containing columns experiencing similar failure modes. These sub-databases are used to develop new probabilistic drift capacity models (Zhu 2005).

CONCLUSION

In order to provide engineers with information on the expected column failure mode (or column response), two approaches are proposed in this study to classify columns. First, a probabilistic failure mode model is developed based on the Bayesian updating methodology and a database of 111 column specimens. This model identifies the most important parameters affecting the column failure mode, namely, transverse reinforcement ratio, aspect ratio and shear demand-strength ratio. Second, based on the aforementioned three critical parameters, a deterministic two-zone column classification method is proposed to approximately separate the shear-dominated columns (Zone S) from the flexure-dominated columns (Zone F). This straight-forward approach allows an engineer estimate the column failure mode and enables the separation of data into sub-databases for further model development (Zhu 2005). Both methods provide a better estimate of the column failure modes compared with the commonly used strength-based approach.

ACKNOWLEDGMENTS

This research was conducted under the support of a Discovery Grant from the Natural Sciences and Engineering Research Council of Canada. This funding is gratefully acknowledged.

REFERENCES

Berry, M., M. Parrish, and M. Eberhard, 2004, PEER Structural Performance Database User's Manual, (www.ce.washington.edu/~peera1), Pacific Earthquake Engineering Research Center, University of California, Berkeley.

Browning, J., Y.R. Li, A.C. Lynn, and J.P. Moehle, 2000, Performance Assessment of a Reinforced Concrete Frame Building, *Earthquake Spectra*, Vol. 16, No. 3, pp. 541-555.

Camarillo, H.R., 2003, Evaluation of Shear Strength Methodologies for Reinforced Concrete Columns, Department of Civil and Environmental Engineering, University of Washington.

Elwood, K.J. and J.P. Moehle, 2005, Axial Capacity Model for Shear-Damaged Columns, *ACI Structural Journal*, Vol. 102, No. 4, pp 578-587.

Gardoni, P., A. Der Kiureghian, and K.M. Mosalam, 2002, Probabilistic Capacity Models and Fragility Estimates for Reinforced Concrete Columns based on Experimental Observations, *Journal of Engineering Mechanics*, Vol. 128, No. 10, pp. 1024-1038.

Pujol, S., 2002, Drift Capacity of Reinforced Concrete Columns Subjected to Displacement Reversals, *Ph.D. Dissertation*, School of Civil Engineering, Purdue University.

Sezen, H., and J.P. Moehle, 2004, Shear Strength Model for Lightly Reinforced Concrete Columns, *Journal of Structural Engineering*, Vol. 130, No. 11, pp. 1692-1703.

Trifunac, M.D., and T.Y. Hao, 2001, 7-Storey Reinforced Concrete Building in Van Nuys, California: Photographs of the Damage from the 1994 Northridge Earthquake, *Report No. CE 01-05*, Department of Civil Engineering, University of Southern California.

Zhu, L., K.J. Elwood, T. Haukaas, and P. Gardoni, 2005, Application of a Probabilistic Drift Capacity Model for Shear-Critical Columns, *Journal of the American Concrete Institute (ACI)*, Special Publication.

Zhu, L., 2005, Probabilistic Drift Capacity Models for Reinforced Concrete Columns, *Masters Thesis*, Department of Civil Engineering, University of British Columbia.

Table 1: Posterior statistics of coefficients in probabilistic FM model (Eq. (3))

Coefficients	Mean	Standard Deviation	Correlation Coefficient				
			θ_1	θ_4	θ_7	θ_{10}	σ
θ_1	0.80	0.201	1.000	-0.733	-0.223	0.493	0.023
θ_4	-0.13	0.065	-0.733	1.000	0.251	-0.736	-0.013
θ_7	1.75	0.316	-0.223	0.251	1.000	-0.519	-0.038
θ_{10}	1.33	0.141	0.493	-0.736	-0.519	1.000	-0.011
σ	0.32	0.023	0.023	-0.013	-0.038	-0.011	1.000

Table 2: Assumed distributions for some material properties and applied loads of column C4 damaged during Northridge earthquake

Parameter	Distribution	Mean	COV
f'_c	lognormal	27.6MPa	0.05
f_{yt}	lognormal	345MPa	0.05
s	lognormal	305mm	0.02
P	lognormal	648KN	0.10

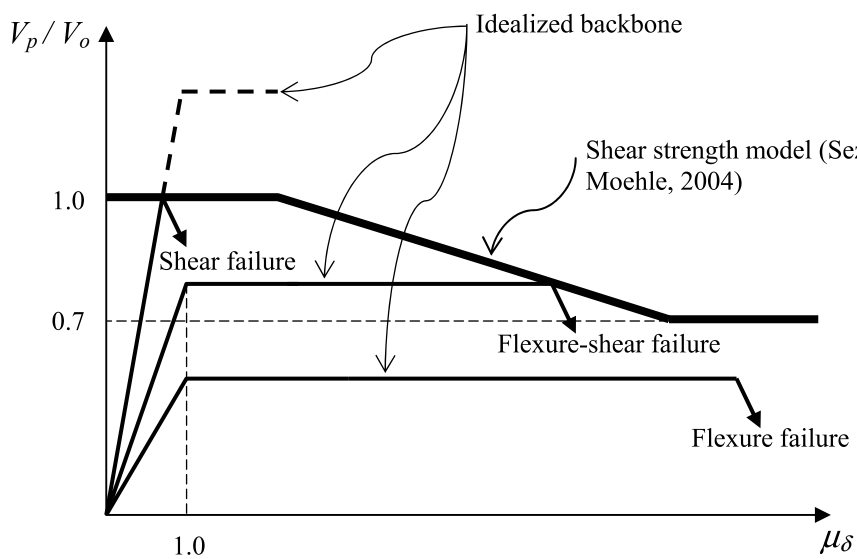

Fig. 1: Conceptual definition of column failure modes

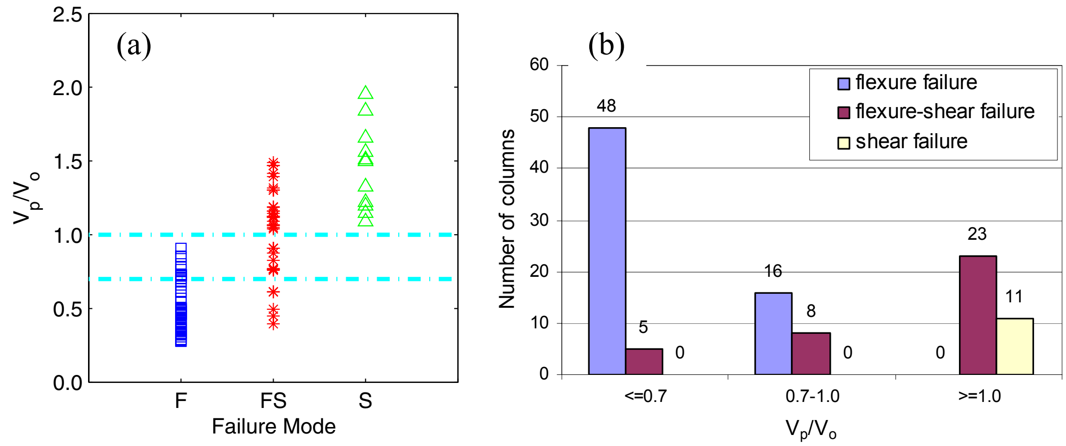

Fig. 2: Relation of observed column failure modes and V_p/V_o
(F—flexure failure; FS—flexure-shear failure; S—shear failure)

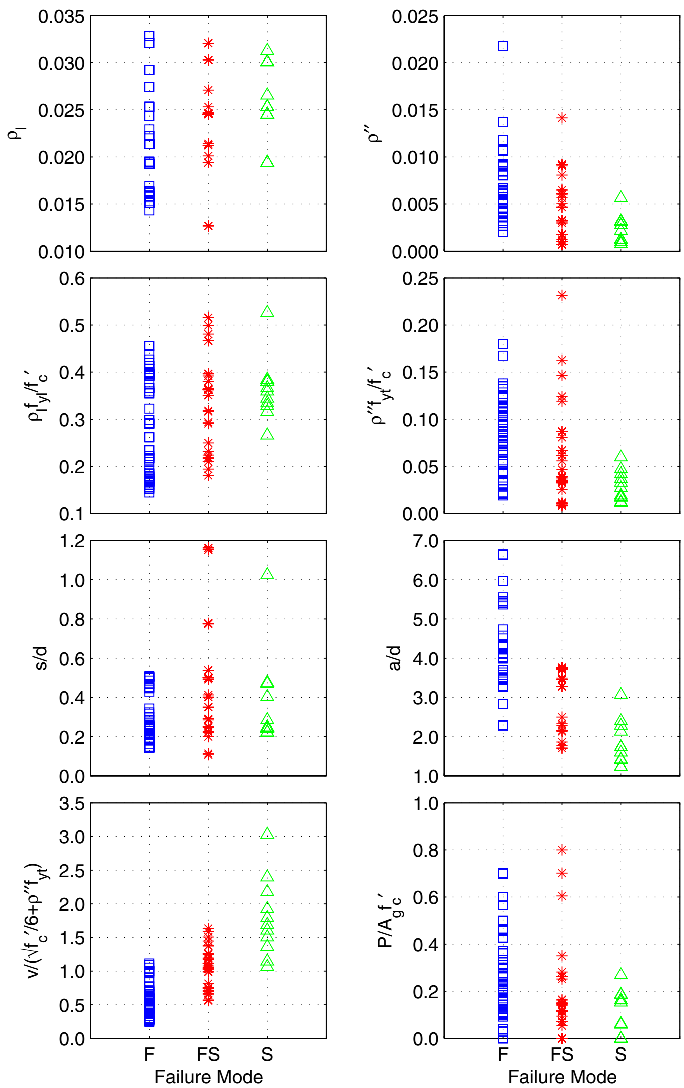

Fig. 3: Effect of key parameters on column failure modes

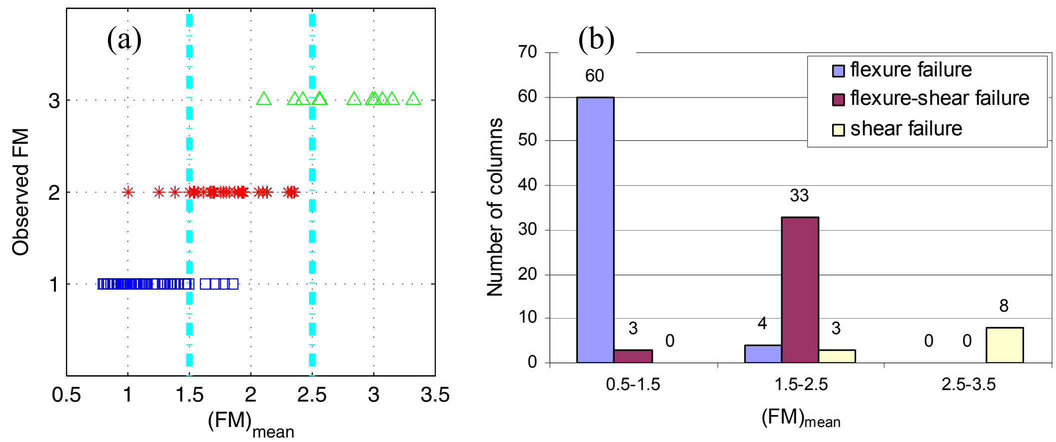

Fig. 4: Comparison of observed FM and calculated $(FM)_{mean}$ (Eq. (4))

Fig. 5: Building frame with columns damaged during Northridge earthquake

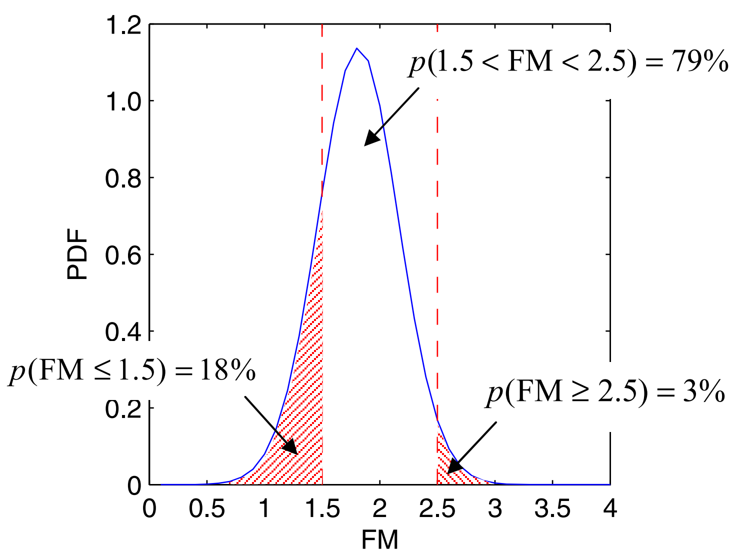

Fig. 6: Illustration of the distribution of FM for column C4

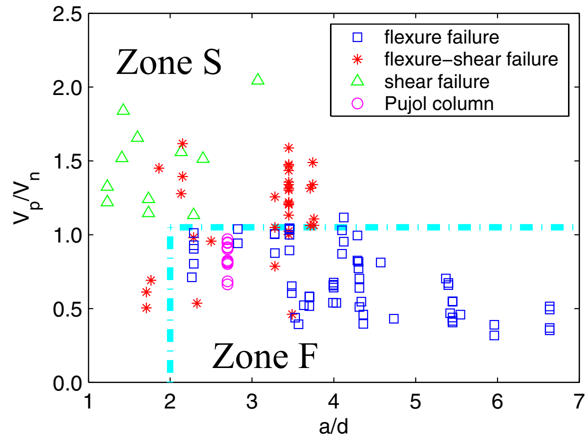

Fig. 7: Relationship between V_p/V_n and aspect ratio

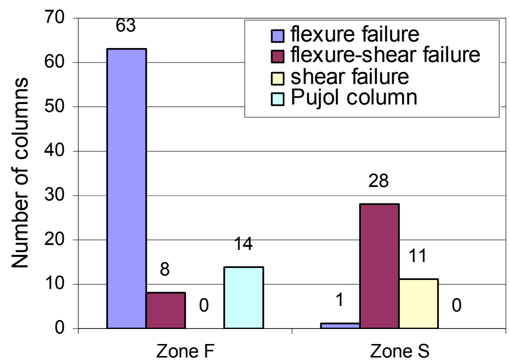

Fig. 8: Two-zone column classification method applied to column database

ESTIMATING THE DRIFT RATIO AT AXIAL LOAD FAILURE OF REINFORCED CONCRETE COLUMNS ON THE BASIS OF A MODEL TO CALCULATE SHEAR STRENGTH

Adolfo B. MATAMOROS[1] and Malte von RAMIN[2]

ABSTRACT

Experiments of columns subjected to repeated load reversals have shown that axial load failure in columns occurs after the loss of shear carrying capacity. This paper investigates the use of a method to estimate the effect of drift demand, transverse reinforcement, and axial load on the shear strength of columns in order to establish a relationship between these parameters at axial load failure. The methodology was evaluated on the basis of 11 columns tested to axial load failure at the University of California. The proposed model indicates that in slender members with light amounts of transverse reinforcement, the main parameters that affect the drift ratio at axial load failure of columns are the amount of transverse reinforcement and the axial load demand relative to the capacity of the column under concentric axial loading. An equation is proposed to estimate the drift at axial load failure on the basis of these two parameters.

1. INTRODUCTION

Experimental observations show that the shear capacity of columns becomes negligible prior to axial load failure (Elwood and Moehle 2005; Kato and Ohnishi, 2002; Kabeyasawa and Tasai 2002; Tasai 1999; Tasai 2000; and Yoshimura and Yamanaka 2000). The analysis presented in this paper explores the use of a model to calculate the reduction in shear strength with cyclic loading in reinforced concrete members to obtain estimates of the drift demand at which axial load failure is expected to occur. The method presented was previously derived and calibrated using experimental results from shear critical specimens subjected to monotonic loading, and flexure-critical specimens with various amounts of transverse reinforcement subjected to load reversals (von Ramin and Matamoros, 2005; von Ramin and Matamoros, 2004).

The method to calculate shear strength discussed in this paper is applicable to members with a wide range of geometric configurations, concrete compressive strengths, and amounts of transverse reinforcement (von Ramin and Matamoros, 2005). For this reason the proposed methodology has the potential of being used with a wide range of reinforced concrete member configurations. Because the experimental data set available is very small, the analysis presented

[1] *Department of Architectural, Civil, and Environmental Engineering, University of Kansas, Lawrence, Kansas*
Email: amatamor@ku.edu

[2] *O'Reilly Brothers Ltd., Kingscourt Co. Cavan, Ireland*
Email: maltevr@zinctone.de

focuses on estimating the drift demand at axial load failure for flexure-critical members with relatively low amounts of transverse reinforcement, and that are relatively slender (shear span-to-depth ratios greater than 2.5). In the United States 11 column specimens with these characteristics were tested at the University of California at Berkeley by Lynn (2001) and Sezen (2002).

2. DESCRIPTION OF MODEL TO CALCULATE SHEAR STRENGTH UNDER MONOTONIC LOADING

The shear strength of members subjected to load reversals is calculated on the basis of the shear strength under monotonic loading. The "initial" or "monotonic" shear strength is reduced as a function of the drift demand to account for the effects of load reversals causing the member to deform into the nonlinear range of response.

The monotonic shear strength is calculated as the combination of components related to arch action, V_a , truss action, V_t , the strength of compression zone, V_{cz} , and friction or aggregate interlock, V_f .

2.1 Shear Strength of Deep Members

In the case of deep members the shear strength afforded by the concrete is derived primarily from arch action, so the nominal shear strength is given by

$$V_n = V_a + V_t \tag{1}$$

The strength of the arch component is a function of the cross sectional area of the strut and the effective compressive strength of concrete of the strut, and is given by (von Ramin and Matamoros, 2005):

$$V_a = \underbrace{R_a}_{\substack{\text{Truss Mechanism} \\ \text{Factor}}} \cdot \underbrace{k_s}_{\substack{\text{Shear Span-to-depth} \\ \text{Ratio Factor}}} \cdot \underbrace{\beta_s f'_c}_{\substack{\text{Effective strut} \\ \text{strength}}} \cdot \underbrace{w \cdot b}_{\text{Strut Area}} \cdot \sin\theta \tag{2}$$

A detailed description of the terms in Eq. (2) is presented elsewhere (von Ramin and Matamoros, 2005). The term β_s , which is relevant to the analysis presented in this paper, is a function of the compressive strength of concrete, f'_c. The following expression for β_s was proposed by von

Ramin (2005) based on test results from members with concrete compressive strengths ranging between 15 and 140 MPa (Fig. 1):

$$\beta_s = 0.85 - 0.004 f_c' \geq 0.5 \tag{3}$$

A similar parameter proposed by Watanabe and Kabeyasawa (1998) is presented in Figure 1 for reference.

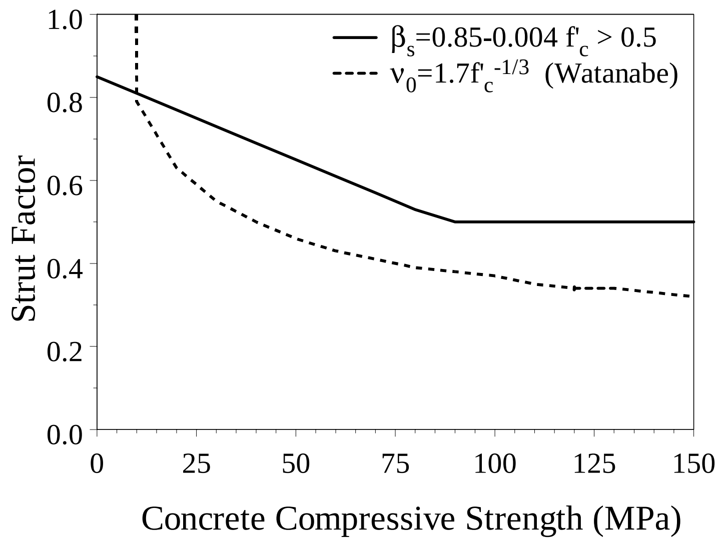

Fig. 1: Strut factor vs. concrete compressive strength

The strength provided by the truss mechanism is calculated on the basis of a variable-angle truss model.

$$V_t = \rho_w \ f_w \cdot b \cdot jd \cdot \cot\phi \tag{4}$$

Equation (4) can be derived from equilibrium based on the assumption of a uniform compression field (Collins and Mitchell, 1991). The term ρ_w is the transverse reinforcement ratio, f_w is the stress in the transverse reinforcement, *b* is the width of the member, *jd* is the lever arm between tension and compression resultants, and ϕ is the angle of inclination of the compression field with respect to the longitudinal axis of the member. The angle of inclination of compression field is a function of the shear span-to-depth ratio, with a minimum of 30° for slender members. The force carried by the transverse reinforcement is proportional to the stress induced in the compression field f_t, which can be derived also using principles of equilibrium as

$$f_t = \frac{\rho_w \ f_w}{\sin^2\phi} \tag{5}$$

The interaction between the arch and truss mechanisms is addressed by reducing the contribution of the arch component as the demand on the compression field increases, behavior which is reflected by the parameter R_a in Eq. (2). The contribution of the arch component decreases also with the shear span-to-depth ratio, and it becomes negligible for slender members. This behavior is reflected in Eq. (2) through the term k_s (von Ramin and Matamoros, 2005).

2.2 Shear Strength of Slender Members

In slender members the contribution of the arch component is negligible, and the shear strength provided by the concrete is related to the strength of the compression zone and aggregate interlock or friction through the crack interfaces. The nominal strength of slender members is given by

$$V_n = V_t + V_c \tag{6}$$

where V_c is the strength provided by compression zone and friction

$$V_c = V_{cz} + V_f \tag{7}$$

The magnitude of these two terms is derived based on equilibrium after inclined cracking takes place in a member without transverse reinforcement (von Ramin and Matamoros, 2005)

$$V_c = 0.4 \cdot \sqrt[3]{f'_c}\, b \cdot d \left[k + (1-k) \underbrace{\left(1 - \frac{\Delta w}{\Delta w_u}\right)}_{\substack{\text{Reduction in strength due to}\\ \text{loss in aggregate interlock}}} \right] \tag{8}$$

where k is the depth of the neutral axis at failure, Δw is the width of the crack at failure, and Δw_u is the critical crack width at which aggregate interlock is totally lost.

3. FAILURE MODES UNDER REPEATED LOAD REVERSALS

Damage to the concrete in the compression zone of flexure-critical members subjected to load reversals results in a gradual reduction of the flexural strength of the member. Similarly, cracks that propagate through the plastic hinge region result in progressive damage to the shear resistance mechanisms described in Section 2 (Matamoros and Sozen, 2003, von Ramin and Matamoros, 2005). The limit state corresponding to the loss of lateral load carrying capacity is commonly defined in the literature as that corresponding to a 20% reduction in the maximum lateral force carried by the member (Elwood and Moehle, 2005; and Matamoros and Sozen, 2003). It follows from the previous discussion that this limit state may be reached as a result of either a reduction in the flexural or the shear strength of the member. This concept is illustrated in Figure 2, where the broken line represents the variation in shear strength with drift demand and the solid line represents the variation in flexural strength with drift demand. In the case illustrated in Figure 2, the shear corresponding to 80% of the maximum shear demand defines two limiting drift ratios, one corresponding to the reduced flexural strength and the other corresponding to the reduced shear strength. In the case of flexure critical members, if the limiting drift ratio corresponding to the reduced flexural strength is greater than the limiting drift ratio corresponding to the reduced shear strength, a shift from flexure-critical to shear-critical behavior takes place at the drift ratio where both lines intercept (Fig. 2).

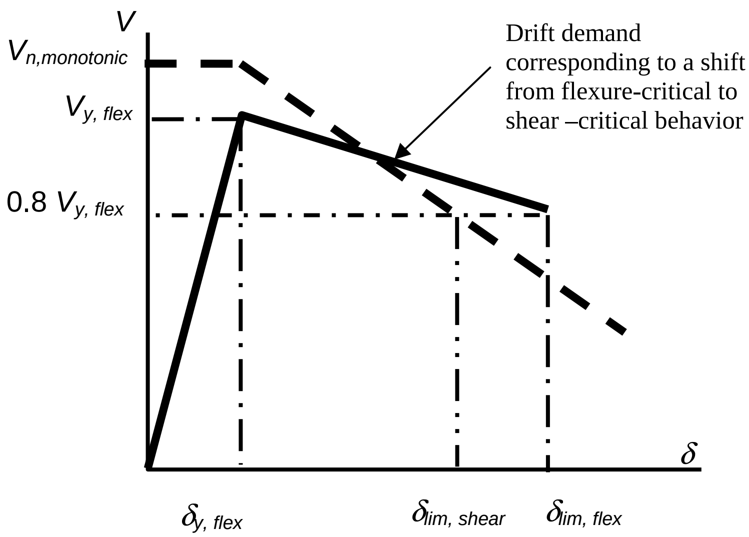

Fig. 2: Relationship between flexural strength, shear strength and drift demand

The model presented in this paper was calibrated originally to find the limiting drift corresponding to loss in lateral load capacity by relating section properties to the drift at yielding of the transverse reinforcement (von Ramin and Matamoros, 2004). This paper explores the use of this model to calculate the drift at axial load failure.

4. REDUCTION OF SHEAR STRENGTH COMPONENTS WITH CYCLIC LOADING

Experiments of columns subjected to repeated load reversals have shown that the strain demand in the transverse reinforcement within the plastic hinge region increases with increasing damage to the concrete, although the shear demand decreases due to a reduction in the flexural strength of the member (Wight and Sozen, 1973, Ichinose et al., 2001, Matamoros and Sozen, 2003). This observation suggests that as the level of damage increases, the component of the shear strength carried by the concrete tends to decrease, increasing the demand placed on the truss mechanism. The shear strength is calculated on the basis of the components of the nominal shear strength under monotonic loading V_n. As indicated in Section 2, the strength of slender members under monotonic loading is given by the sum of the concrete component V_c and the component associated with the truss mechanism V_t (Eq. 7). The strains demands in the longitudinal reinforcement of column members in the nonlinear range of response lead to crack widths expected to exceed the critical crack width at which aggregate interlock is lost. For this reason the contribution of the component associated with aggregate interlock is neglected. The reduced shear strength corresponding to a given drift demand $V_{n,\delta}$ is given by

$$V_{n,\delta} = (1-\eta)(V_{cz}) + \chi V_t \tag{9}$$

where η is a reduction parameter for the concrete component and χ is a reduction parameter for the truss component which are a function of the drift demand. When a member is subjected to repeated load reversals, no reduction in strength due to the effect reverse loading takes place during the initial incursion into the inelastic range of response. The reduction occurs when the drift demand in subsequent cycles causes damage to concrete. Because it is not possible to establish this point without prior knowledge of the loading history, a simple assumption for the purpose of design is that a reduction in strength takes place for drift demands exceeding the drift at yield.

The original calibration of the reduction parameters χ and η was performed using a significant number of members with intermediate and large amounts of transverse reinforcement. This type of members is able to withstand relatively large drift demands prior to loss in lateral load carrying capacity, and the inelastic drift demand at the limit state is significantly larger than the drift demand at yield. For this reason, von Ramin (2004) made the simplifying assumption of relating the reduction in shear strength to the total drift demand. In members with relatively small amounts of transverse reinforcement this assumption is not accurate because the drift demand at yield is a large fraction of the total drift demand. Consequently, in this paper the inelastic drift demand is used instead of the total drift demand as originally developed in the equations by von Ramin.

4.1 Reduction in Strength of Concrete Component

The reduction parameter η was calibrated on the basis of strain readings from tests by Ichinose (von Ramin and Matamoros, 2004). The following expression, which is a function of drift ratio and confinement ratio was proposed by von Ramin:

$$\eta = \frac{8 \cdot \delta_p}{\rho_w f_{wy} / f'_c + 0.01} \tag{10}$$

The relationship between the reduction parameter η and the inelastic drift ratio δ_p is presented in Figure 3. A similar expression proposed by Watanabe is presented for reference. Figure 3 shows that according to the model, a significant amount of confinement is needed to prevent rapid deterioration of the strength components related to the concrete. In members with low amounts of confining reinforcement the model indicates that strength afforded by the concrete is lost at relatively low drift ratios. This is reflected by Eq.(11), which was obtained by solving Eq. (10) for the drift ratio at which η = 1, which signifies a 100% reduction of concrete component.

$$\delta_p = \frac{\rho_w f_{wy} / f'_c + 0.01}{8} \tag{11}$$

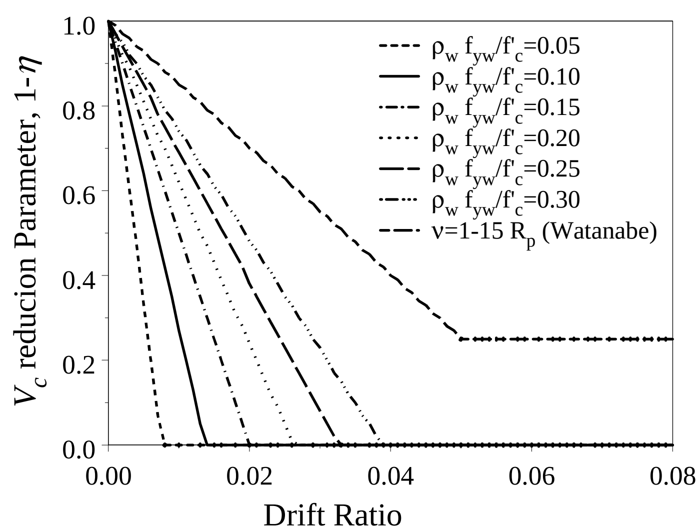

Fig. 3: Reduction parameter for V_c vs. drift ratio

Because the column set analyzed consists of members with very light amounts of transverse reinforcement, it is expected that at drift demands associated with axial load failure the only shear carrying mechanism available is the truss mechanism.

4.2 Reduction in Strength of the Truss Mechanism

While strain gage data from column tests clearly shows that the fraction of the total shear carried by the truss mechanism increases with damage to the concrete, it cannot be inferred from this information whether a reduction in the strength of the truss mechanism takes place also. This effect is illustrated in Figure4. The vertical axis in Figure 4 corresponds to the ratio of the shear carried by the truss at yielding of the transverse reinforcement to the strength of the truss under monotonic loading conditions, and the horizontal axis corresponds to the drift ratio at yielding of the transverse reinforcement. This figure shows that the reduction in strength of the concrete component is not enough to account for the total loss in shear strength.

Consequently, the strength of the truss mechanism must decrease with increasing drift demand also, as the concrete in the compression field degrades under load reversals.

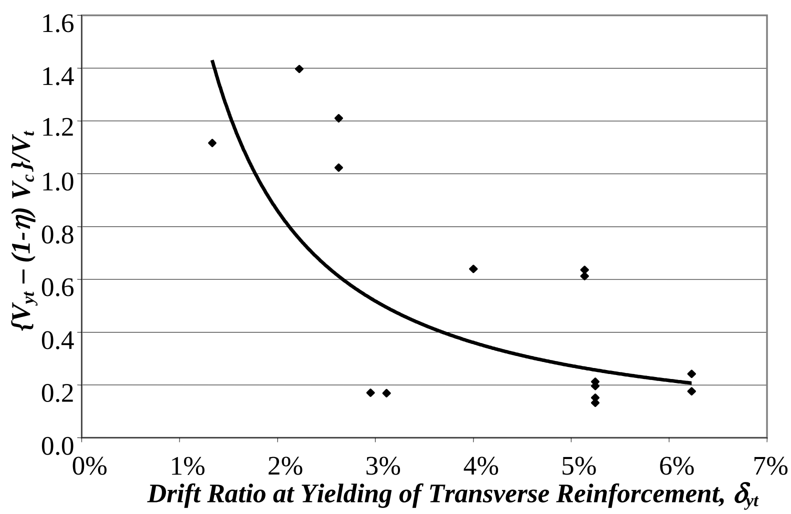

Fig. 4: Reduction parameter for V_c vs. drift ratio

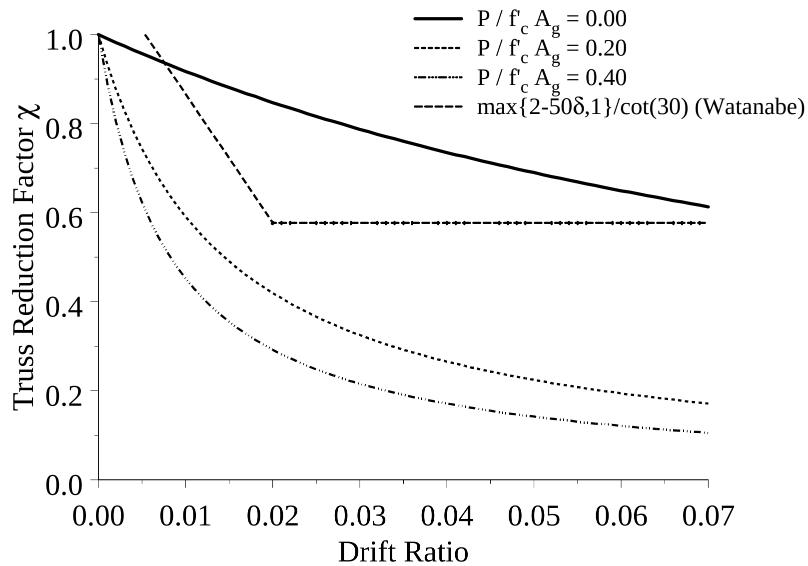

Fig. 5: Reduction parameter for V_t vs. drift ratio

After examining the effect of several parameters on the strength of the truss components, von Ramin (2004) proposed the following equation for the parameter χ

$$\chi = \frac{1}{1+1.5\delta_{yt} \cdot 6^{\lambda}} \tag{12}$$

where

$$\lambda = 1+2(P/f'_c A_g)^{0.35} \tag{13}$$

The relationship between χ and the drift ratio is presented in Figure 5. A reduction parameter for the truss component proposed by Watanabe is presented also for reference.

Figure 6 shows the measured and calculated response for specimen 2CLD12 tested by Sezen (2002). According to the shear model by von Ramin the strength associated with the concrete is lost soon after the maximum drift demand of the first cycle is exceeded, and the reduction in the strength of the truss component with drift ratio is much less. Figure 6 shows also that according to the proposed model there is a residual truss strength when axial load failure takes place.

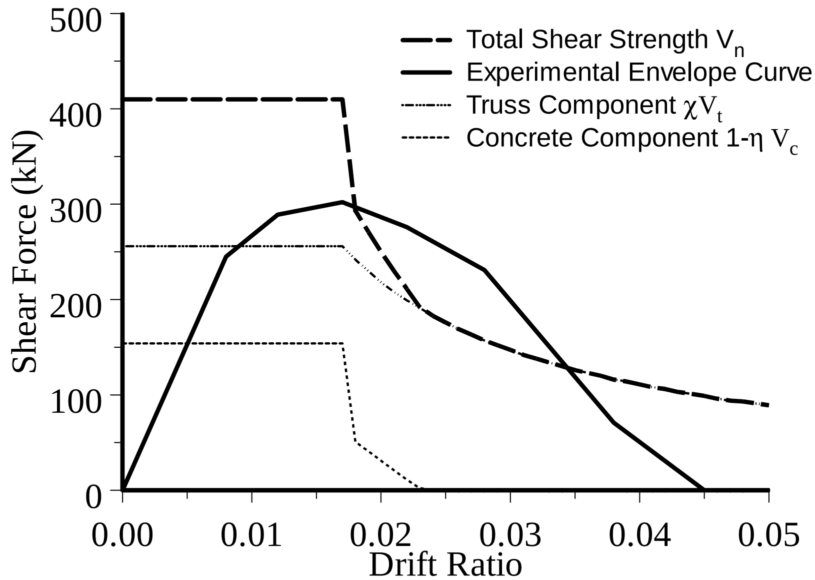

Fig. 6: Measured and calculated strength for specimen 2CLD12 by Sezen (2002)

5. ESTIMATES OF DRIFT RATIO AT AXIAL LOAD FAILURE

The main difficulty in using Eq. (12) and (13) to estimate the drift ratio at axial collapse is that the slope of the reduction factor χ decreases with increasing drift demand, such that at axial load failure the strength of the truss component is not zero. A simple solution was investigated by analyzing the magnitude of the residual strength of the truss mechanism at axial load failure.

From equilibrium the stress in the compression field at axial load failure can be calculated based on the reduced strength as:

$$f_t = \frac{\chi V_t}{b \cdot jd} \frac{1}{\sin\phi \cos\phi} \tag{14}$$

The reduction factor χ in Eq. (14) was calculated based on Eq. (12) as:

$$\chi = \frac{1}{1 + 1.5(\delta_a - \delta_y) \cdot 6^{\lambda}} \tag{15}$$

where δ_a is the drift ratio at axial load failure and δ_y is the drift ratio at yield. The ratio of compression field stress to effective strut strength calculated with Eq. (14) and (15) is plotted in Figure 7 against the transverse reinforcement ratio for the specimens tested by Lynn and Sezen.

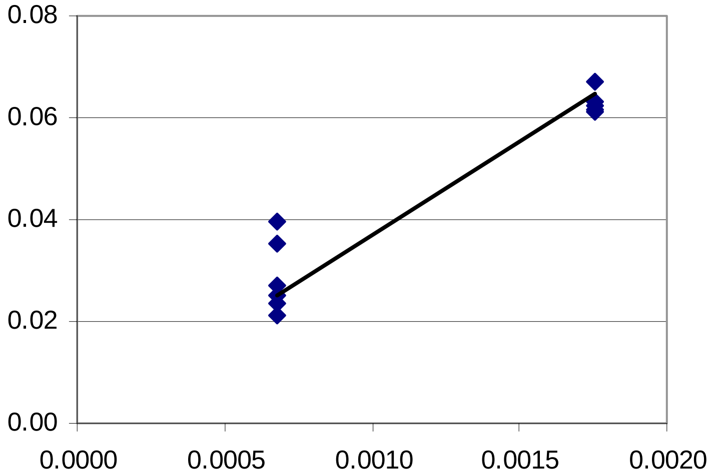

Fig. 7: Ratio of mean compressive stress in compression field to effective compressive strength vs. transverse reinforcement ratio

Figure 7 shows that for the data set examined the demand in the compression field at axial failure was proportional to the amount of transverse reinforcement.

Adopting the following expression for the limiting stress in the compression field:

$$\frac{f_t}{\beta_n \ f'_c} = 40\rho_w \tag{16}$$

The strength of the truss component at axial load failure is given by:

$$\chi V_t = 40 \ \rho_w \ \beta_n \ f'_c \, b \ jd \ \sin\phi \cos\phi \tag{17}$$

The reduction in truss strength at axial load failure can be calculated as:

$$\chi = 40 \frac{\beta_n \ f'_c}{f_{wy}} \sin^2\phi \tag{18}$$

and the drift ratio at axial load failure can be calculated as:

$$\delta_a = \frac{1-\chi}{\chi} \frac{1}{1.5\square 6^{\lambda}} + \delta_y \tag{19}$$

Table 1: Evaluation of test results

Specimen	$P/A_g f'_c$	Drift Ratio at Yield, δ_y	Drift Ratio at Collapse, δ_a				
				Eq. (21)		Eq. (19)	
			Measured	Calculated	Meas/Calc	Calculated	Meas/Calc
Lynn (2001)							
3CLH18	0.09	0.0065	0.0207	0.041	0.51	0.032	0.65
2CLH18	0.07	0.0051	0.0310	0.033	0.93	0.024	1.31
3SLH18	0.09	0.0053	0.0310	0.041	0.76	0.031	1.02
2SLH18	0.07	0.0044	0.0362	0.033	1.09	0.023	1.57
2CMH18	0.28	0.0056	0.0103	0.019	0.53	0.017	0.59
3CMH18	0.26	0.0077	0.0207	0.018	1.12	0.019	1.10
3CMD12	0.26	0.0066	0.0207	0.018	1.12	0.018	1.17
3SMD12	0.28	0.0077	0.0207	0.019	1.07	0.020	1.06
Sezen (2002)							
2CLD12	0.15	0.0089	0.0500	0.050	1.00	0.043	1.18
2CHD12	0.61	0.0068	0.0190	0.016	1.22	0.017	1.10
2CVD12	0.34	0.0071	0.0293	0.027	1.08	0.025	1.16
				Average	0.95		1.08
				Sigma	0.24		0.27
				COV	0.26		0.25

Calculated and measured drift ratios at axial load failure for the columns tested at the University of California are summarized in Table 1. The ratio of measured to calculated drift ratio had a mean value of 1.08 with a coefficient of variation of 0.25. The previous procedure can be further simplified by assuming a lower threshold for the limiting stress in the compression field of

$$\frac{f_t}{\beta_n\ f'_c} = 30\rho_w \tag{20}$$

and calculating the drift ratio at axial load failure using Eq. (18) and (21).

$$\delta_a = \frac{1-x}{x}\frac{1}{1.5 \bullet 6^{\lambda}} \tag{21}$$

The effect is an increase in the coefficient of variation of the measured to calculated drift ratio at axial failure from 0.25 to 0.26.

6. CONCLUSIONS

Although a significant number of test of columns subjected to load reversals have been carried out and reported in the literature, there are very few experimental data sets available that allow a thorough evaluation of the interaction between various shear resistance mechanisms in members subjected to load reversals. The method presented addresses such interaction in a very simple manner, at various stages of loading.

The equations that were derived based on the shear model by von Ramin provided reasonable estimates of the drift ratio at axial load failure for the data set evaluated. However, the amount of data available for calibrating the method was very limited and more experimental results are needed for a better assessment of the methodology.

There are several limitations inherent to the analysis that was conducted. All test data used in the evaluation had normal-strength concrete and similar loading protocols. Also, because the method was calibrated based on data from columns in which the transverse reinforcement yielded, failure at lower drift demands can occur in members in which the transverse reinforcement is not properly anchored.

REFERENCES

Collins, M. P., and D. Mitchell, (1991). Prestressed concrete structures. Prentice Hall, Englewood Cliffs, NJ, 766 pp.

Elwood, K., and Moehle, J. (2005). Axial Capacity Model for Shear-Damaged Columns, *ACI Structural Journal*, V. 102, No. 4, July-August 2005, pp. 578-587.

Ichinose, T., et al., (2001). Three-Dimensional Shear Failure of RC Columns after Cyclic Loading, *Modeling of Inelastic Behavior of RC Structures under Seismic Loads*, B.P. Shing, Editor, ASCE, Reston, VA, pp. 546-561.

Kabeyasawa, T.; Tasai, A.; and Igarashi, S. (2002). An Economical and Efficient Method of Strengthening Reinforced Concrete Columns Against Axial Load Collapse during Major Earthquake, *PEER Report 2002/02, Third US-Japan Workshop on Performance-Based Earthquake Engineering Methodology for Reinforced Concrete Building Structures*, Pacific Earthquake Engineering Research Center, University of California, Berkeley, Calif., pp. 399-412.

Kato, D., and Ohnishi, K. (2002). Axial Load Carrying Capacity of R/C Columns under Lateral Load Reversals, *PEER Report 2002/02, Third US-Japan Workshop on Performance-Based Earthquake Engineering Methodology for Reinforced Concrete Building Structures*, Pacific Earthquake Engineering Research Center, University of California, Berkeley, Calif., pp. 247-255.

Lynn, A. C., (2001). Seismic Evaluation of Existing Reinforced Concrete Building Columns, PhD dissertation, Department of Civil and Environmental Engineering, University of California, Berkeley, Berkeley.

Matamoros, A., Sozen, M., (2003). Drift Limits of High-Strength Concrete Columns Subjected to Load Reversals, *Journal of Structural Engineering, ASCE*, V. 129, No. 3, March 2003.

Sezen, H., (2002). Seismic Response and Modeling of Reinforced Concrete Building Columns, PhD dissertation, Department of Civil and Environmental Engineering, University of California, Berkeley.

Tasai, A. (1999). Residual Axial Capacity and Restorability of Reinforced Concrete Columns Damaged due to Earthquake, *PEER Report 1999/10, US-Japan Workshop on Performance-Based Earthquake Engineering Methodology for Reinforced Concrete Building Structures*, Pacific Earthquake Engineering Research Center, University of California, Berkeley, Calif., pp. 191-202.

Tasai, A. (2000), Residual Axial Capacity of Reinforced Concrete Columns during Shear Deterioration, *PEER Report 2000/10, Second US-Japan Workshop on Performance-Based Earthquake Engineering Methodology for Reinforced Concrete Building Structures, Pacific Earthquake Engineering Research Center*, University of California, Berkeley, Calif., pp. 257-267.

von Ramin, M., and Matamoros, A. (2004). Shear Strength of Reinforced Concrete Members subjected to Monotonic and Cyclic Loads, *SM Report No. 72*, University of Kansas Center for Research, Inc., Lawrence, Kansas, June 2004, 517 pp.

von Ramin, M., and Matamoros, A. (2005). Monotonic Shear Strength of Reinforced Concrete Members, accepted for publication in *ACI Structural Journal*.

Wight, J. K., and Sözen, M. A., (1973). Shear strength decay in reinforced concrete columns subjected to large deflection reversals, *Structural Research Report No. 403*, University of Illinois at Urbana-Champaign, Urbana-Champaign, Ill., 290 pp.

Yoshimura, M., and Yamanaka, N. (2000), Ultimate Limit State of RC Columns, *PEER Report 2000/10, Second US-Japan Workshop on Performance-Based Earthquake Engineering Methodology for Reinforced Concrete Building Structures*, Pacific Earthquake Engineering Research Center, University of California, Berkeley, Calif., pp. 313-326.

KEYWORDS: axial load failure, shear strength, columns, reinforced concrete, drift ratio, drift limit, collapse, shear critical

LATERAL LOAD RESPONSES AND AXIAL LOAD CAPACITY OF RC WALLS AND WALL PIERS

J. W. WALLACE[1], L. M. MASSONE[1], K. ORAKCAL[1], and K. J. ELWOOD[2]

ABSTRACT

Use of slender, stout, or perforated structural walls to resist earthquake actions is very common; therefore, robust modeling approaches which have been verified by comparison with results from well-instrumented tests are essential if comprehensive performance-based design approaches are to be implemented. To address these needs, modeling approaches for both axial load – moment interaction (P-M) and axial load – moment – shear (P-M-V) interaction are summarized and model results are assessed by comparing with available test results. Overall, the model results compare very favorably with test results, except for very low aspect ratios walls (< 0.5). To assess to potential for collapse during strong shaking, it is necessary to estimate when a structural wall loses its capacity to support tributary gravity loads. A shear – friction model developed for columns is modified and used to assess the lateral drift that results in the loss of a wall piers capability to sustain vertical loads. The model results indicate that typical wall piers with relatively low levels of gravity stress ($< 0.10 A_g f_c^{'}$) are capable of sustaining relatively large lateral drift ratios prior to loss of vertical load-carrying capacity. The proposed methodology provides an approach to assess axial load capacity of wall piers, produces results that are consistent with post-earthquake observations, and may allow for substantially more economical seismic rehabilitation schemes. Finally, details of an ongoing experimental study of wall piers are summarized. The experimental study will provide valuable data to validate the P-M-V model for low aspect ratios as well as provide vital data that will be used to assess the axial capacity model.

1. INTRODUCTION

Reinforced concrete (RC) structural walls are commonly used to resist the actions imposed on buildings due to earthquake ground motions. To resist such actions, properly proportioned and detailed slender walls are typically designed to yield in flexure, and to undergo inelastic flexural deformations without loss of lateral load capacity. Therefore, the ability to model the cyclic behavior and failure modes of structural walls is an important aspect of engineering design, particularly as the profession moves forward with design and evaluation approaches that emphasize performance based seismic design.

Recent research has shown that the lateral force versus deformation response of slender walls in flexure can be captured reasonably well using simple analytical models (e.g., Thomsen and

[1] *Department of Civil and Environmental Engineering, 5731 Boelter Hall, UCLA, Los Angeles, CA 90095-159, USA*
Email: wallacej@ucla.edu
[2] *Department of Civil Engineering,* University of British Columbia, Vancouver, BC, Canada V6T 1Z4

Wallace 2004), and improved predictions can be obtained using more detailed models (e.g., Orakcal et al. 2004; Orakcal and Wallace 2005). However, such models usually consider uncoupled shear and flexural responses, which is inconsistent with experimental observations, even for relatively slender walls (Massone and Wallace 2004).

Analytical models have been proposed to consider the observed coupling between flexural and shear components of RC wall response. One approach involves implementing the finite element method together with a constitutive RC membrane model that follows a rotating-angle modeling approach (e.g., Modified Compression Field Theory, Vecchio and Collins 1986; Rotating Angle Softened Truss Model, Pang and Hsu 1995). A methodology based on concept for a fiber model was proposed by Petrangeli et al. (1999) to couple shear with flexural and axial responses.

The analytical model summarized in this study is based on applying the methodology developed by Petrangeli to a macroscopic fiber-based model (Multiple-Vertical-Line-Element-Model, Vulcano et al. 1988). A summary of the proposed modeling approach to incorporate coupling of wall flexural and shear responses is presented. Preliminary model results are compared with test results obtained from tests on a slender wall and four short wall specimens to evaluate the modeling approach. The accuracy and limitations of the model are emphasized to identify model capabilities as well as ways to improve the model.

2. MODELING APPROACH (P-M and P-M-V)

2.1 P-M Base Model: Multiple-Vertical-Line-Element Model (MVLEM)

The Multiple Vertical Line Element Model (MVLEM) resembles a two-dimensional fiber model, simplified such that element rotations (curvatures) are concentrated at the center of rotation defined for each element. In the MVLEM, a single average value of curvature is assumed for each model element, as opposed to a generic displacement-based fiber model implementation where a linear curvature distribution (displacement interpolation function) is used between element nodes and the curvature distribution is integrated at Gauss points to obtain element rotations and displacements. A structural wall is modeled as a stack of MVLEs, which are placed one upon the other, and the coupled axial-flexural response of each MVLE is simulated by a series of uniaxial elements (or macro-fibers) connected to infinitely rigid beams at the top and bottom (e.g., floor) levels, that enforce a plane section assumption. A horizontal spring placed at the center of rotation (at relative height *ch*) of each MVLE, with a prescribed nonlinear force-deformation behavior, is commonly used to simulate the shear response of the element. Shear and flexural responses are considered uncoupled in the original formulation of the MVLEM. The constitution and kinematics of the MVLEM are explained in detail by Orakcal et al. (2004). As well, detailed material models are presented and recommendations for appropriate model and material parameters are recommended.

The ability of the model to capture experimentally observed behavior of the slender walls tested by Thomsen and Wallace (2004) was assessed by Orakcal and Wallace (2005). Analytical results for overall load – top displacement responses and lateral drift versus story height (Fig. 1), as well as first-story deformations (Fig. 2), indicate the model, with the detailed material relations implemented, captures the experimental responses quite well. Results for a slender T-shaped wall cross section (Fig. 3) are not quite as good for negative loads, which is an artifact of the model assumptions (plane section assumption, which is violated for negative loads).

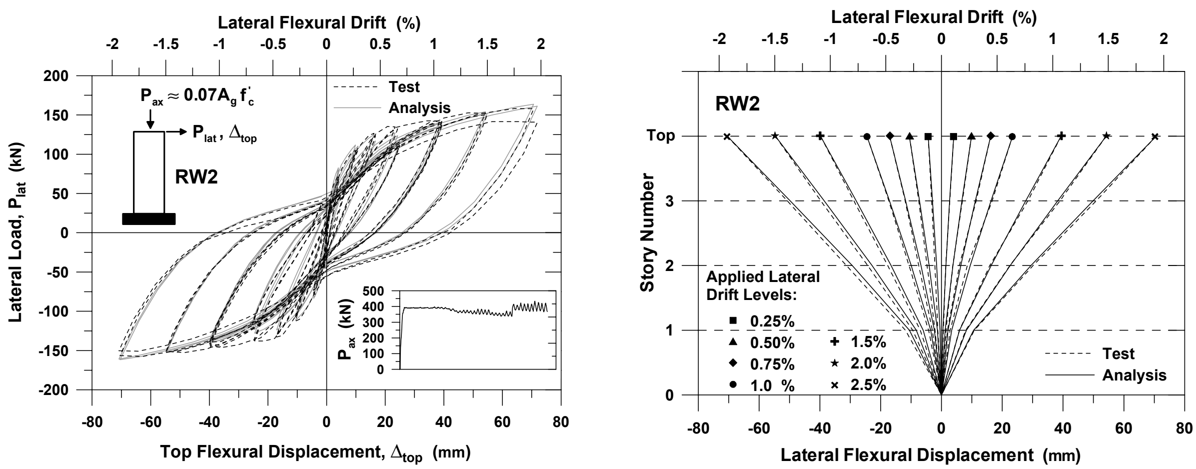

Fig. 1: Measured vs. predicted Responses (RW2)

2.2 P-M-V (Coupled) Model

The analytical model summarized in this study to couple axial load – moment behavior with shear behavior incorporates RC panel behavior into the Multiple-Vertical-Line-Element-Model, in order to capture the experimentally observed interaction in RC walls (Massone and Wallace 2004). The proposed wall model involves modifying the MVLEM by assigning a shear spring for each uniaxial element (Fig. 4). Each uniaxial element is then treated as a RC panel element, with membrane actions, i.e., uniform normal and shear stresses applied in the in-plane direction.

Therefore, the interaction between flexure and shear is incorporated at the uniaxial element (fiber) level. To represent constitutive panel behavior, a rotating-angle modeling approach (RA-STM, Pang and Hsu 1995) is used; however, a more refined constitutive stress-strain model for concrete in compression, which is calibrated with a large set of experimental results, is implemented (Orakcal and Wallace 2005). Constitutive stress-strain models for materials are applied along the principal directions of the strain field (i.e., principal strain directions 1 and 2), to obtain the stress field associated with the principal directions. It is assumed that the principal stress and strain directions coincide (as suggested by Vecchio and Collins 1986; Pang and Hsu 1995). Accordingly, the axial and shear responses of each uniaxial (panel) element are coupled, which further allows coupling of flexural and shear responses of the MVLEM, since the axial response of the uniaxial elements constitute the overall flexural response of each MVLE. Model details are presented by Massone et al (2005).

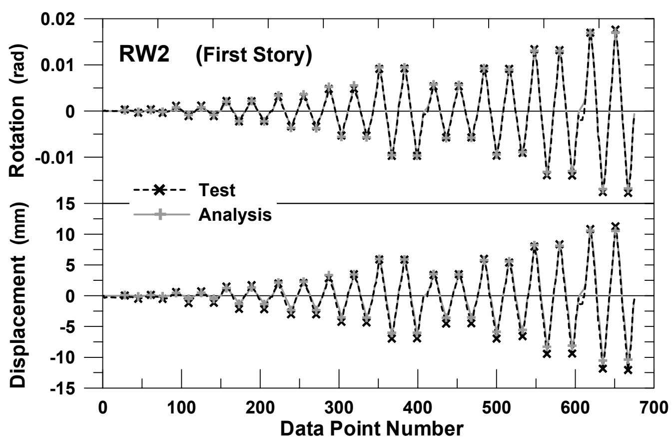

Fig. 2: First-story deformations (RW2)

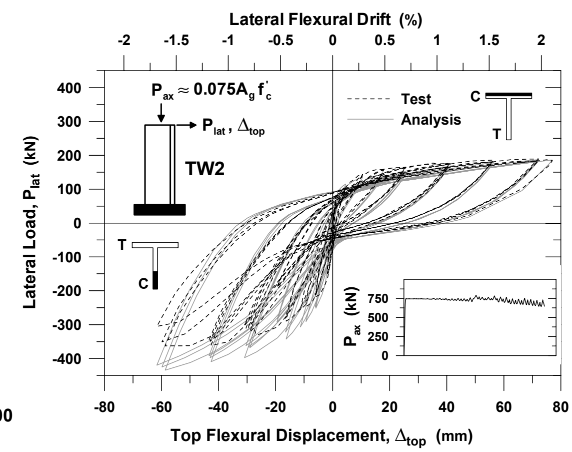

Fig. 3: Load – displacement response (TW2)

Model results are compared with reported test data to assess the ability of the model to capture observed behavior. Model and test results are compared depicted in Figure 5 are for panel tests by Pang and Hsu (1995) and indicate that the model represents the test results quite accurately. Although these results are encouraging, it is noted that the RA-STM implemented in the model was developed, at least in part, based on the test results reported in Figure 5. As well, the results presented are for pure shear loading conditions, versus for generalized loading conditions.

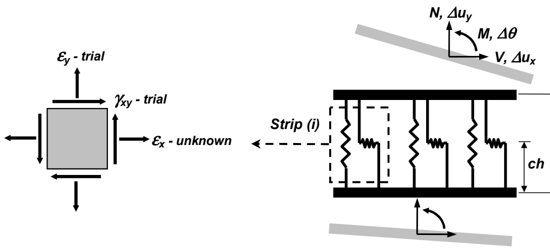

Fig. 4: Modeling approach (P-M-V)

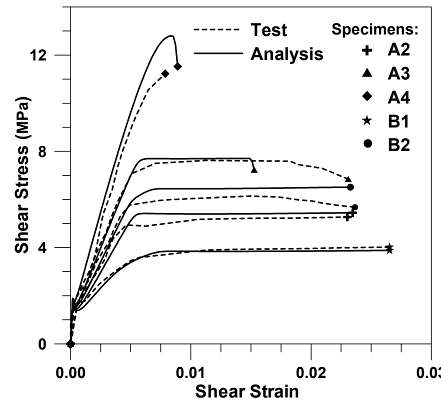

Fig. 5: Model assessment (panel tests)

A more comprehensive assessment of the model is conducted by using test results for low-aspect ratio walls; specimen 16 tested by Hidalgo et al. (2002) and specimen 74 reported by Hirosawa (1975). For both specimens, the amount of shear reinforcement provided was greater than or equal to the minimum specified in ACI 318-02 (2002), i.e., ρ_{min}=0.0025. Shear span ratios (*M/(Vl)*) were 1.0 for specimen 74 and 0.35 for specimen 16.

As observed in Figure 6(a), a very good correlation is obtained between test results and results of the proposed coupled shear-flexure model for Specimen 74 (*M/(Vl)*=1.0). Since the design flexural and shear capacities of the specimen are close, Figure 6(a) also includes an analytical flexural response prediction (with shear deformations not considered) obtained using a fiber model. The load-displacement response obtained by the flexural model is significantly different than the measured response and the coupled model response. After a lateral load of 450 kN, significant lateral stiffness degradation is observed in both the test results and results of the coupled model, but not in with the flexural model. This result demonstrates how the proposed model, which couples shear and flexural responses, is able to simulate observed responses with substantially greater accuracy than a flexural model, particularly for wall specimens where the nominal shear and flexural capacities are nearly equal. However, the correlation for Specimen 16 (*M/(Vl)* = 0.35) is far from being reasonable, where the analytical model under predicts the measured lateral load capacity of the wall by up to 50% for the entire loading history (Fig. 6(b)). The discrepancy is attributed to the variation in the shear span (Massone et al. 2005).

Overall, the correlations indicate that the accuracy of the proposed model in predicting wall response is progressively impaired as the shear span ratio of the wall modeled is reduced. The best correlation is obtained for Specimen 74 (*M/(Vl)* = 1.0), whereas results for intermediate ratios (*M/(Vl)* = 0.69 and 0.56, Massone et al. 2005) were generally good, and results for Specimen 16 (*M/(Vl)* = 0.35) are not representative. Therefore, it is apparent that the validity of the modeling approach and the model assumptions are violated as wall shear span ratios decrease. In a wall with a small shear span ratio, stresses and strains can follow significantly nonlinear distributions as opposed to the assumptions incorporated in the present model (uniform shear strain distribution and zero horizontal stress along wall length). Ongoing work, including experimental studies, focuses on improving the modeling methodology and assumptions, as well as conducting more extensive correlation studies with the existing and new test data.

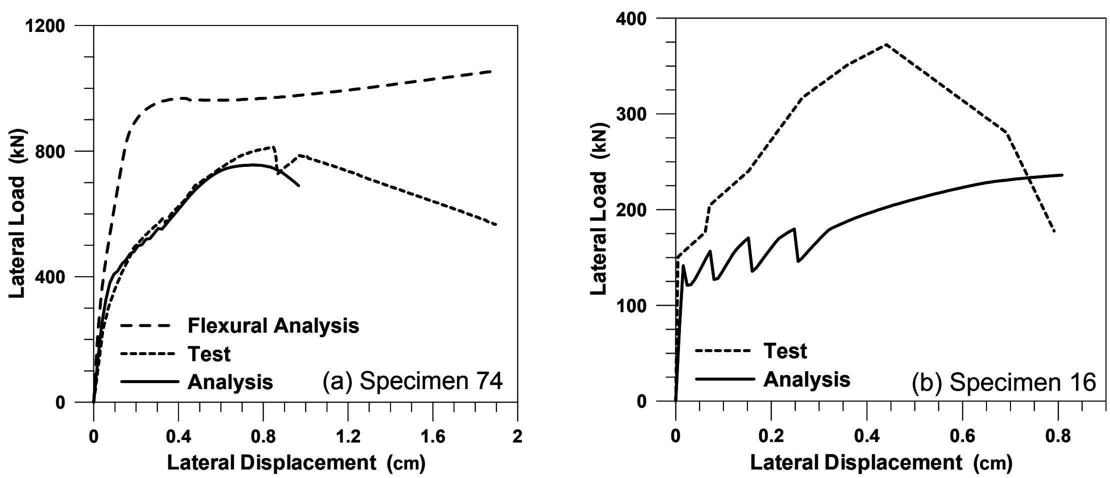

Fig 6: Lateral load–displacement responses for the short wall specimens

3. AXIAL CAPACITY MODEL

3.1 Model

Research conducted by Elwood and Moehle (2005) suggests that the axial load capacity of a shear critical column can be investigated using a shear friction model, where the axial load supported by a column must be transferred across the diagonal crack plane through shear friction. An analogous model for a vertical wall pier is shown in Figure 7, where the critical crack is assumed to extend diagonally over the clear height of the pier. Axial load failure results as sliding occurs along the critical crack plane when the shear friction demand exceeds the shear friction capacity. Dowel forces are shown for vertical boundary reinforcement; however, consistent with ACI 318-02 ("Building" 2002.) approach, dowel forces for distributed web reinforcement are assumed to be included implicitly in the shear friction force V_{sf} along the inclined plane. It is noted that walls tend to have more reinforcement distributed along the crack plane than columns; therefore, it is plausible that the shear friction coefficient should be higher given that the dowel action of the wall distributed reinforcement is implicitly included in the friction coefficient. Vertical and horizontal equilibrium for the free body diagram result in the following equations:

$$V + N\sin\theta = V_{sf}\cos\theta + A_{st}f_{st}\frac{d_c}{s_v}\tan\theta + n_{bars,boundary}V_{d,boundary} \tag{1}$$

$$P = N\cos\theta + V_{sf}\sin\theta + \frac{d_c}{s_h}P_{s,web} + n_{bars,boundary}P_{s,boundary} \tag{2}$$

where V and P = the shear and axial load demand on the wall, respectively, $n_{bars,boundary}$ = the total number of vertical boundary bars, $V_{d,boundary}$ = the dowel force developed in a single vertical boundary bar, V_{sf} = the shear friction force developed along the critical crack, N = the force developed normal to the critical crack, $A_{st}f_{st}$ = the force developed in the horizontal web bars crossing the critical crack, s_v = the vertical spacing of the horizontal web bars, s_h = the horizontal spacing of the vertical web bars, d_c = the depth of the core measured center line to center line of the ties, $P_{s,web}$ and $P_{s,boundary}$ = axial load supported by a single vertical web bar and boundary bar, respectively, and θ is the angle of the critical crack relative to the horizontal.

Although dowel action is shown in Figure 7 for the boundary vertical bars, the axial load resistance provided by this dowel action is not likely to be significant; hence, the dowel action and axial resistance of the boundary bars ($V_{d,boundary}$, and $P_{s,boundary}$) is ignored. The shear force resisted by the wall pier is set to a residual value (i.e., V=V_r) based on the assumption that the wall pier has lost most of its lateral load resistance at the onset of axial load failure. A review of column test data reveals that axial load capacity is typically lost when the shear force degrades to zero (Nakamura and Yoshimura 2002). The sensitivity of the axial capacity model to the assumed residual shear force can be assessed by setting the residual shear capacity of the wall pier to a fraction of the nominal capacity, as is commonly done in FEMA 356 (e.g., Table 6-18 and 6-19).

Based on the assumptions for the shear force and boundary bars, (1) and (2) are rewritten as (3) and (4):

$$N\sin\theta = V_{sf}\cos\theta + A_{st}f_{st}\frac{d_c}{s_v}\tan\theta - V_r \tag{3}$$

$$P = N\cos\theta + V_{sf}\sin\theta + \frac{d_c}{s_h}P_{s,web} \tag{4}$$

Alternatively, given that the crack is likely to extend the full pier height, (3) is rewritten as:

$$N\sin\theta = V_{sf}\cos\theta + A_{st}f_{st}\frac{h}{s_v} - V_r \tag{5}$$

The critical crack angle for wall piers is generally defined by the wall pier geometry. Common aspect ratios *h/l* vary between 1:2 and 2:1, with critical crack angles varying between 27 and 63 degrees for these cases, which are approximately the limits set for strut-and-tie models for D regions (e.g., see ACI 318-02, Appendix A). For piers with $h/l > 2$, the wall pier includes a B-region and a constant critical crack angle of 65 degrees as suggested by Elwood and Moehle (2005) for columns is appropriate. For piers with $h/l < 1/2$, a constant crack angle of approximately 25 degrees is assumed as use of a smaller angle would result in larger shear friction capacity. As well, for $h/l < 1/2$, shear friction is not important, as the contribution of shear friction to axial load transfer is small (Fig. 7).

3.2 Shear Friction

According to a classical shear friction model, shear is transferred across a crack based on the force normal to the crack plane N and an effective coefficient of friction μ (see Fig. 7):

$$V_{sf} = \mu N \tag{6}$$

The coefficient μ includes aggregate interlock and dowel action, in addition to pure friction; therefore, values of μ higher than that for pure friction are needed to match test data using (6). Substitution of (6) into (4) and (5), neglecting the contribution of the web reinforcement, and solving for the shear friction results in:

$$\mu = \frac{P - \frac{A_s f_{yt} h}{s_v}\frac{1}{\tan\theta} + \frac{V_r}{\tan\theta}}{\frac{P}{\tan\theta} + \frac{A_s f_{yt} h}{s_v} - V_r} \tag{7}$$

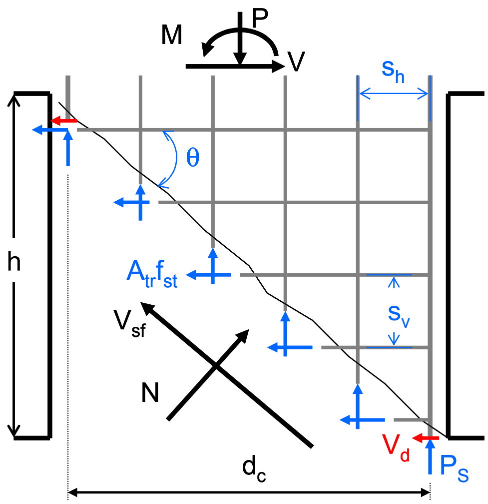

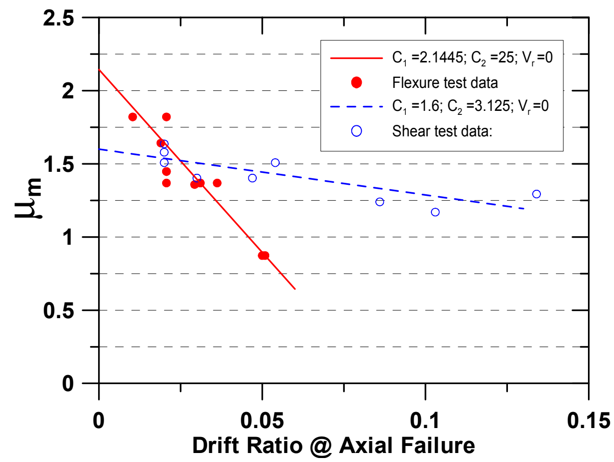

Fig. 7: Cracked pier free body diagram

Fig. 8: Shear friction relations derived from column tests

For columns, Elwood and Moehle (2005) were able to develop a relationship between coefficient of friction and drift based on a limited set of available column test data for cases where flexural yielding occurred prior to shear failure. For each column test, the axial load at axial failure (along with other information that is readily available) was substituted into (8), with V_r set to zero and $\theta = 65°$, and the resulting shear friction was plotted versus the drift observed at axial load failure as shown in Figure 8. The data reveal that shear friction decreases as the drift ratio increases, which is reasonable, and that a trend is captured by a linear fit of the form:

$$\mu = C_1 - C_2\left(\frac{\Delta}{h}\right)_{Axial} \geq 0 \qquad (8)$$

where the coefficients C_1 and C_2 were selected as 2.14 and 25, respectively, to achieve a close approximation to the data. Note that C_1 is the shear friction at zero drift (Fig. 8).

Although test data are not available for walls, the relationship between shear friction and the lateral drift at axial failure was reexamined using data from tests conducted in Japan (Yoshimura et al. 2004; Nakamura and Yoshimura 2002; Yoshimura and Yamanaka 2000) where the test columns failed in shear (no flexural yielding). Data from such tests may be considered more appropriate for estimating the response of walls since damage is typically concentrated at only a few principle cracks, similar to observed damage for wall piers. Tests results and a best-fit relation for shear friction versus lateral drift are shown in Figure 8. The shear friction at zero drift is less than the value for columns studied by Elwood and Moehle (2005), i.e., C_1 = 1.6

versus 2.14; however, the slope of the best-fit line is substantially less (i.e., C_2 = 3.1 versus 25). The availability of data from wall tests would be helpful to develop a relationship specific to the geometry and reinforcement of lightly-reinforced wall piers.

3.3 Model Predictions

The preceding sections developed expressions to assess the drift ratio at axial failure in terms of axial load and distributed web vertical and horizontal reinforcement. Results are presented to investigate overall trends for the drift ratio expected when axial load collapse occurs for lightly reinforced wall piers. Substitution of (8) into (7), and rearranging, results in the following:

$$\frac{\Delta}{L}=\frac{(1+C_1\tan\theta)+\left(P/C_3\right)(C_1-\tan\theta)}{C_2\left(P/C_3+\tan\theta\right)} \qquad C_3=\left(A_{st}f_{yt}h/s_v-V_r\right) \tag{9}$$

Results obtained with (9) can be presented in an alternate format if the following substitution is employed:

$$\frac{P}{C_3}=\frac{P/P_0}{\left(\dfrac{A_{st}f_{yt}h/s_v}{P_0}\right)-\left(\dfrac{V_r}{P_0}\right)} \tag{10}$$

Given the preceding information, the influence of various parameters, such as the critical crack angle, pier properties (materials, reinforcement, axial load level), residual shear strength, and the relationship for shear friction versus drift, on the lateral drift capacity at axial failure are investigated using (9) and (10). Only limited results are presented due to space limitations. In subsequent results presented, the shear friction versus drift relation at axial failure for columns derived by Elwood and Moehle (2005) is used.

Results are plotted in Figure 9(a) for V_r = 0 to assess the influence of the critical crack angle on pier lateral drift ratio at axial failure. The plot reveals that the drift at axial load failure decreases for increasing axial load and that smaller critical crack angles result in larger drift capacities. For the typical piers presented in Table 1, results plotted in Figure 9(a) indicate that relatively large drift capacities (Δ/h > 0.04) can be reached prior to loss of axial load capacity. The vertical axis can be modified to present results in a slightly different format, as shown in Figure 9(b), where the value of $(A_{st}f_{yt}h/s_v)/P_0$ is set to a constant value (*0.05*). Results from Figure 9(b) indicate that for typical axial load levels for buildings with lightly reinforced perimeter walls (generally 5 to 20% of P_0), very large lateral drift capacities are noted, generally exceeding 4%.

Figures 10(a) and 10(b) address the sensitivity of the axial load capacity to the quantity of transverse reinforcement crossing the critical crack plane, as well as pier geometry, material properties, and residual shear capacity. Figure 10(a) reveals that typical, lightly reinforced wall piers (e.g., wall piers with $(A_{st}f_{yt}h/s_v)/P_0$ = 0.025 to 0.075 and $P < 0.10A_gf'_c$; Table 1) are expected to reach a lateral drift ratio approaching 0.05 prior to loss of axial load capacity. A significant reduction is noted for $(A_{st}f_{yt}h/s_v)/P_0$ = 0.025 when residual shear strength is considered, as the assumed residual shear capacity of $0.02P_0$ is very close to this value.

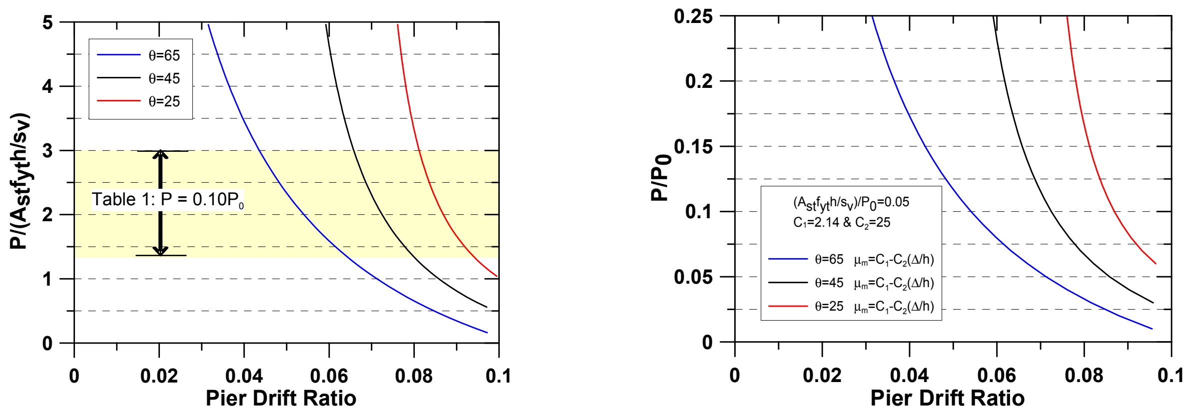

(a) Influence of pier properties and crack angle (b) Influence of axial load and crack angle

Fig. 9: Lateral drift at axial failure

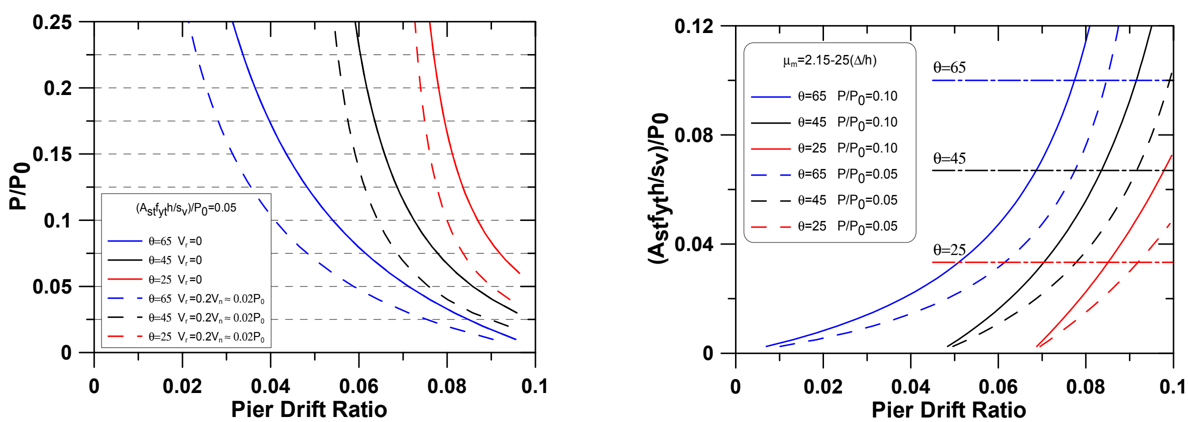

(a) Influence of crack angle and residual capacity (b) Influence of crack angle and axial load

Fig. 10: Lateral drift ratio at axial failure

4. APPLICATION AND TESTING

The approaches presented are being used to assess a 6-story building constructed in 1962, in which the lateral system consists of lightly-reinforced perimeter walls with openings. The Nonlinear Static Procedure of FEMA 356 is being used, and experimental studies of representative spandrels and piers of the building are being conducted to support the analytical work. The testing program will provide vital data that will be used to validate the analytical models being used for the piers and spandrels (i.e., backbone relations) as well as the axial capacity model presented. It is noted that the lack of hooks on the horizontal web reinforcement (the hooks shown in Fig 11(a) were cut off) might significantly impact lateral strength degradation and the ability to sustain axial load to large deformations (e.g., boundary reinforcement is susceptible to buckling). Additional studies may be conducted to assess behavior where better detailing is provided.

The test specimens are three-quarter scale replicas of typical wall segments created by window openings of the perimeter walls. A photo of a wall pier specimen prior to concrete placement is shown in Figure 11(a) and wall spandrel prepared for testing is shown in Figure 11(b). The test setup allows the level of axial load to be controlled (e.g., zero for spandrels) and the rotation at the top of the beam to be controlled (i.e., held at zero). Lateral load is applied through an L-shaped reaction frame as shown in Figure 11(b) such that the moment at the mid-height of the test panel is zero. Approximately 100 sensors are used to collect loads, displacements, rebar strain, and average concrete strains during testing.

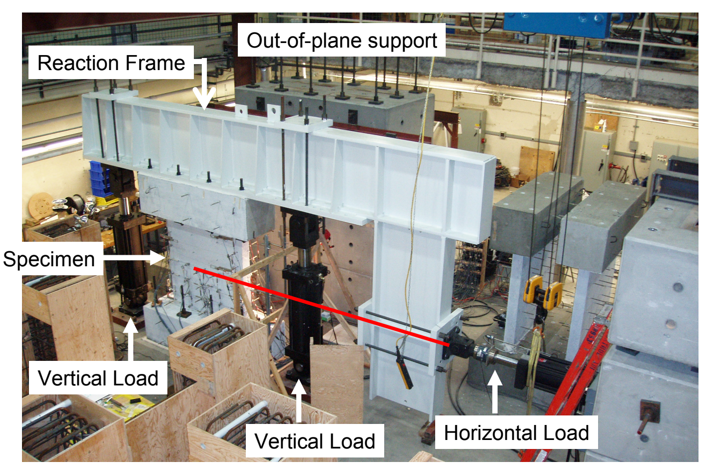

Fig. 11: (a) Wall pier reinforcement **(b) Test setup with spandrel specimen**

5. CONCLUSIONS

An overview of modeling approaches to account for P – M – V interaction for walls is presented. Model results are compared with test results to validate the modeling approaches. In general, model results for slender walls agree closely with test results. For low-rise walls, including P-M-V interaction resulted in significant improvements between model and test results. However, for walls with shear span ratio less than approximately 0.5, model assumptions are violated and significant discrepancies existed between model and test results.

A shear friction model developed to estimate the lateral drift at loss of column axial load capacity was modified and applied to wall piers. The model suggests that wall piers with modest axial load can sustain relatively large lateral drift ratios prior to loss of axial load capacity. Test results for wall piers are needed to assess and validate and improve the model.

Use of comprehensive nonlinear analyses procedures coupled with component testing is an effective strategy for developing rational and economical rehabilitation measures. Use of this approach for a 1962 building with lightly-reinforced, perimeter walls suggests that substantial savings will be achieved relative to use of simplified procedures that rely on linear analysis procedures. The test results will provide data that will be useful for validating both the P-M-V interaction model and the axial capacity model.

6. ACKNOWLEDGMENTS

The work presented in this paper was supported by funds from the National Science Foundation under Grants CMS-9632457 and CMS-9810012, as well as in part by the Earthquake Engineering Research Centers Program of the National Science Foundation under NSF Award Number EEC-9701568 through the Pacific Earthquake Engineering Research (PEER) Center. The authors would like to acknowledge the valuable input provided by John Gavan, Ayse Kulahci, Aaron Reynolds, and Dr. Luis Toranzo at KPFF Consulting Engineers, Los Angeles. Any opinions, findings, and conclusions or recommendations expressed in this material are those of the authors and do not necessarily reflect those of the National Science Foundation.

REFERENCES

"Building Code Requirements for Structural Concrete – ACI 318-02", *American Concrete Institute*, Farmington Hills, Michigan, 2002.

Elwood, K.J., and J. P. Moehle, "An Axial Capacity Model for Shear-Damaged Columns", *ACI Structural Journal*, Vol. 102, No. 4, pp. 578 – 587, July – Aug. 2005.

Nakamura, T., and M. Yoshimura, "Gravity Load Collapse of Reinforced Concrete Columns with Brittle Failure Modes". *Journal of Asian Architecture and Building Engineering*, 1(1): 21-27, 2002.

Hidalgo, P.A., C. A. Ledezma, R. M. Jordan, "Seismic Behavior of Squat Reinforced Concrete Shear Walls", *Earthquake Spectra*, V. 18, No. 2, pp. 287-308, 2002.

Hirosawa, M., "Past Experimental Results on Reinforced Concrete Shear Walls and Analysis on Them", *Kenchiku Kenkyu Shiryo*, No. 6, BRI, Ministry of Construction, Japan, 1975.

Massone, L. M., K. Orakcal, J. W. Wallace, "Modeling flexural/shear interaction in RC walls, *ACI Structures Journal*, SP- Seismic Shear, American Concrete Institute, Farmington Hills, MI, (Nov. 2005, expected).

Massone, L.M. and J. W. Wallace, 2004, "Load – Deformation Responses of Slender Reinforced Concrete Walls", *ACI Structural Journal*, V. 101, No. 1, pp. 103-113.

Orakcal, K., Conte, J. P., Wallace, J. W., "Flexural Modeling of Reinforced Concrete Walls – Model Attributes," *ACI Structural Journal*, Vol. 101, No. 5, pp. 688 – 698, Sept. – Oct. 2004.

Orakcal, K. and Wallace, J. W., "Flexural Modeling of Reinforced Concrete Walls – Model Calibration," *ACI Structural Journal*, Vol. 103, No. 1, Jan. – Feb. 2006 (expected).

Pang, X.D. and T. T. C. Hsu., "Behavior of Reinforced Concrete Membrane Elements in Shear", *ACI Structural Journal*, V. 92, No. 6, pp. 665-679, 1995.

Petrangeli, M., P. E. Pinto, and V. Ciampi, "Fiber Element for Cyclic Bending and Shear of RC Structures. I: Theory", *Journal of Engineering Mechanics*, ASCE, V. 125, No. 9, pp. 994-1001, 1999.

Thomsen IV, J.H. and J. W. Wallace, "Experimental Verification of Displacement-Based Design Procedures for Slender Reinforced Concrete Structural Walls", *Journal of Structural Engineering*; ASCE, Vol. 130, No. 4, pp. 618-630, 2004.

Vecchio, F.J. and M. P. Collins, "The Modified Compressional-Field Theory for Reinforced Concrete Elements Subjected to Shear", *Journal of the American Concrete Institute*, V. 83, No. 22, pp. 219-231, 1986.

Vulcano, A., V. V. Bertero, and V. Colotti, "Analytical Modeling of RC Structural Walls", *Proceedings*, 9th World Conference on Earthquake Engineering, V. 6, Tokyo-Kyoto, Japan, pp. 41-46, 1988.

Yoshimura, M., Y. Takaine, and T. Nakamura, "Axial Collapse of Reinforced Concrete Columns", Proceedings of the 13th World Conference on Earthquake Engineering, Vancouver, BC, Paper No. 1699, 2004.

Yoshimura, M., and N. Yamanaka, "Ultimate Limit State of RC Columns", Second US-Japan Workshop on Performance-Based Earthquake Engineering Methodology for Reinforced Concrete Building Structures, Sapporo, Japan, PEER report 2000/10. Berkeley, Calif.: Pacific Earthquake Engineering Research Center, University of California, pp. 313-326, 2000.

Keywords: reinforced concrete; wall; pier; cyclic; nonlinear; flexure; shear, model; experimental, axial load, collapse, shear friction.

SESSION 7: DYNAMIC LOADING TESTS

Chaired by

♦ JULIO RAMIREZ AND TAKUYA NAGAE ♦

DYNAMIC LOADING TEST OF REINFORCED CONCRETE COLUMNS FOR IDENTIFICATION OF STRAIN RATE EFFECT

Jun TAGAMI, Norio SUZUKI, Takashi KANEKO, and Makoto MARUTA

ABSTRACT

To identify the effect of strain rate on the mechanical properties of reinforced concrete columns during an earthquake, dynamic and static loading tests were conducted by applying axial force and flexural shear simultaneously. Test variables were loading rate, shear span ratio, axial force ratio and the number of cycles at given amplitude. For the wave in the dynamic loading test, a sinusoidal wave of a maximum angular velocity of the member of approximately 0.15 rad./sec was used considering the strain rate level during a large earthquake. In the static loading test conducted for comparison, time history waveform of horizontal displacement and axial force obtained in the dynamic loading was input multiplying the time base by 1000. As a result of the tests, it was found that the flexural yield strength in the dynamic loading test was 6.9% to 9.5% greater than that in the static loading test, and that the shear strength under dynamic loading was 11.3% greater than that under static loading. The equivalent damping factor in the area with small amplitude range was greater under dynamic loading than in static loading. No significant difference was found in failure mode under dynamic or static loading. The effect of loading rate on the accumulated energy dissipation was not clearly determined.

1. INTRODUCTION

Existing studies (Hosoya, 1997 etc.) have shown that the flexural yield strength and the maximum strength of reinforced concrete columns increase with the increase in strain rate. No agreement has, however, been reached among existing studies on the effects of strain rate on the failure mode, deformation capacity and energy dissipation capacity. In this study, dynamic and static loading tests were conducted on reinforced concrete columns to identify the effects of strain rate on their mechanical properties during a large earthquake.

2. TEST DESCRIPTION

2.1 Specimens

Table 1 shows the specifications for specimens, mechanical properties of materials and calculated static strengths of specimens. Figure 1 shows the dimensions of specimens and arrangement of reinforcing bars. Five specimens (D-1 through -5) were used in the dynamic loading test and four (S-1 through -4) in the static loading test. All the specimens had the same cross section (250 mm x 250 mm) and arrangement of reinforcing bars (longitudinal reinforcement: 8-D13, lateral reinforcement: 2-D6@50mm). Test variables were loading rate (dynamic or static), shear span ratio (1.2 or 1.8), axial force ratio (0.1, 0.3 or 0.3 ± 0.2) and the

[1]*Building Structure Group, Kajima Technical Research Institute, 182-0036 Chofu, Tokyo, Japan*

number of loading cycles at given amplitude (1 or 3 cycles). D-1 and S-1 were designed so that the flexural yield is predominant. D-3 and S-3 were designed so that the shear failure is predominant. All of the other specimens were designed so that the flexural yield strength is close to the shear strength in order to confirm the presence of the change in failure mode due to loading rate.

2.2 Test Method

The loading equipment is shown in Figure 2. The specimen was fixed at the sliding device inside the loading frame. Axial force and enforced horizontal displacement were applied using dynamic actuators. The horizontal actuator controlled the relative displacement between the horizontal slide block and the reaction block on the specimen. The axial force was also applied vertically using another dynamic actuator through the vertical slide block.

The lateral loading program is shown in Figure 3. For loading, an incremental sinusoidal wave was used with a constant frequency f of 2.5 Hz in the small-amplitude area (deflection angle R: 1/800 to 1/200) and with a constant maximum angular velocity of member $Vmax$ of 0.15 rad./sec in the large-amplitude area (R: 1/100 or more). The frequency and angular velocity were set based on the assumption of the response of a six-storied reinforced concrete building with a height of approximately 20 m to a maximum ground-motion velocity of 50 cm/sec.

In actual loading, the waveform of loading shown in Figure 3 was applied in four to six sections. Cracking was observed between each loading section. Each time loading was started in a section, operating actuators at a stable speed was difficult. Therefore before applying a load at inexperienced amplitude, a cycle of loading at the maximum amplitude in the previous sections was additionally applied in the preliminary stage. This resulted in a total of three cycles of loading at the same amplitude except specimen D-5.

For specimens D-4 and S-4, varying axial force was imposed assuming the condition of exterior columns. The relationship between the axial force and the horizontal deformation of the column was defined as shown in Figure 5. The axial force ratio initially set at 0.3 was varied from 0.1 to 0.5 so as to decrease under horizontally positive loading and increase under negative loading.

For specimen D-5, another loading program shown in Figure 6 was applied using. To examine the effect of frequent cyclic loading at a small amplitude range, a set of loading was repeated five times. The set constituted three cycles of loading at R=1/1600, 1/800 and 1/400 respectively. Thus, loading was repeated a total of 15 cycles (3 cycles times 5) at each small amplitude. In the region with a large amplitude exceeding R=1/100, one cycle of loading was applied at each amplitude. The difference between D-2 and -5 is only the number of loading cycles. Other factors were common to both specimens.

The dynamic loading test was followed by the static loading test. This is because a waveform for input in the static loading test was created from the time history of horizontal displacement and axial force obtained in the dynamic loading by multiplying the time base by 1000. This enabled the use of the same amplitude of loading and acting axial force both in the dynamic and static loading tests.

Measured items were the horizontal and axial forces acting on the specimen, horizontal and vertical deformations of the specimen and the strain of longitudinal and lateral reinforcing bars. Four two-component force transducers were used to measure the horizontal and axial components of force and moment acting on the specimen. A personal computer with an analog-to-digital converter and a dynamic strain gauge were used for data acquisition. The sampling frequency for measurement was 500 Hz under dynamic loading and 1.0 Hz under static loading.

3. TEST RESULTS

3.1 Accuracy of Loading Control

Figure 7 shows the relationship between the ratio of test result to target loading rate, and the deflection angle. At a deflection angle R of less than 1/400 (2.5×10^{-3}), the actual loading rate was 62% to 95% of the target because the specimen was highly rigid in the small amplitude range. In the large-amplitude range with a deflection angle R of 1/100 or more, the actual loading rate was 89% to 105% of the target, nearly achieving the goal.

In the tests, dynamic actuators were used also for controlling the axial force. As a result, the fluctuation of axial force could be held within ±30 kN (axial force ratio of ±0.018) in D-1, -2, -3 and -5 to which a fixed axial force was applied. In D-4 to which a varying axial force was applied, the axial force in the test was in good agreement with the target.

3.2 Damage of the Specimen

In the specimen S-3 and D-3, shear failure occurred before flexural yielding. All of the other specimens in which the shear capacities were more than 0.9 suffered flexural yielding regardless of the loading rate. Damage in D-2 and S-2 that experienced flexural yielding, after the loading at a deflection angle R of 1/25 is shown in Photograph 1. In other specimens than D-3 and S-3, flexural cracks at the upper and lower edges, and concrete spalling at compressive edge were observed. No significant difference was found in damage in the dynamic or static loading test.

Detailed explanations are given below about the process of damage to specimen D-2 that suffered typical flexural yielding. Flexural cracks occurred at the critical section at a deflection angle R of 1/400. At R=1/100, shear cracks occurred and the yielding of longitudinal reinforcement in tension was confirmed. At R=1/50, concrete spalled on the corners of the specimen, and cracks occurred along the longitudinal reinforcement of the specimen splitting the bond. At R=1/25, large-scale concrete spalling was observed on the corners of the specimen. At R=1/16, the 135-degree hook of horizontal reinforcement was opened, and no axial force could be carried any longer and the specimen failed.

In specimens D-3 and S-3 that failed in shear, shear cracks occurred and restoring force suddenly decreased nearly at R=1/100. At R=1/50, concrete spalling was observed at midpoint of the specimen. At R=1/25, the 135-degree hook of hoops was opened, resulting in failure. Also in this case, no significant difference was found in damage in the dynamic or static loading test.

3.3 Lateral Force-Deformation Relationship

The test results are shown in Table 2. Lateral force-deformation relationships are shown in Figure 8. The mean of positive and negative flexural yield strength was greater than in the static loading test by 6.9% in D-1, 8.8% in D-2, 9.5% in D-4 and 9.4% in D-5. In specimen D-3 that failed in shear, the mean of positive and negative maximum strength was 11.3% greater than in the static loading test.

In S-1 and S-2 used in the static loading, the flexural yield strength increased 30% as the axial force ratio increased from 0.1 to 0.3. In D-1 and D-2 that were used in the dynamic loading, the flexural yield strength increased 31% as the axial force ratio increased from 0.1 to 0.3. This suggests that an increase in axial force had similar influence on the increase in flexural yield strength either under static or dynamic loading.

The hysteresis loops of specimens that suffered flexural yielding were nearly like a spindle until large amplitude of approximately R=1/25 both in the dynamic and static loading. Loading rate had no significant effect on the shape of the hysteresis loop. No significant difference was found in loop shape between D-3 and S-3, both of which failed in shear.

Table 2 lists the limit deflection angles of the member that is the deflection angle when the lateral force of the specimen lowered to 80% of its maximum strength. The limit deflection angle was nearly the same in each pair of specimens whether under dynamic or static loading.

Solid circles in Figure 8 indicate the points where the specimen lost its axial bearing capacity (referred to as the point of axial failure below). For most specimens, axial failure occurred nearly at the same loading cycle both under dynamic and static loading. The axial compressive deformation when the axial failure was occurred was approximately 1% of the length of the specimen regardless of the loading rate.

4. DISCUSSION OF TEST RESULTS

4.1 Increase of Flexural Yield Strength

The effect of strain rate on the yield strength of the member was examined in specimens that suffered flexural yielding under constant axial force. First, the longitudinal reinforcement strain rate at the time of flexural yielding of the specimen was obtained from the time-history data collected by the strain gauge attached to the longitudinal reinforcement. As a result, the mean longitudinal reinforcement strain rate was found to be 3.9 to 9.7 x 10^4 μ/sec ($\mu=10^{-6}$) during the time between no loading to reinforcement yielding.

The strain rate was substituted in equation (1) for the relationship between the strain rate and yield point that was obtained by the test using a fixed strain rate (Hosoya, 1996), to estimate the yield point of longitudinal reinforcement in the dynamic loading test in this study.

$$_d\sigma_y = \left(0.9 + 0.05 \cdot \log\left(\dot{\varepsilon}\right)\right) \cdot {}_S\sigma_y \tag{1}$$

where, ${}_d\sigma_y$: yield strength under dynamic loading, ${}_s\sigma_y$: yield strength under static loading, and $\dot{\varepsilon}$: strain rate (μ/sec). As a result, the rate of increase in yield strength of longitudinal reinforcement under dynamic loading was estimated to be 13.0% to 14.9%. Then, to re-calculate the flexural yield strengths of specimens used in the dynamic loading test, fiber element analysis was made at critical section using the yield strength under dynamic loading. The results are listed in Table 3. In the specimens subjected to dynamic loading, increases of yield point of longitudinal reinforcement owing to the effect of strain rate were reflected in increases in calculated flexural yield strength. As a result, the flexural yield strengths of specimens obtained in the dynamic loading test were 1.08 to 1.16 times the values calculated where the effect of strain rate was taken into consideration. The flexural yield strengths of specimens obtained in the static loading test were 1.10 to 1.11 times the calculated static strengths. Thus, consideration of the strain rate effect as described above enables the estimation of flexural yield strength under dynamic loading as accurately as under static loading.

4.2 Increase of Shear Strength

For specimens S-3 and D-3 that failed in shear, the effect of strain rate on the shear strength of the member was examined. First, the mean strain rates of main and horizontal reinforcing bars at the point of no loading through the point of maximum strength during cyclic loading at R=1/100, were obtained from the time-history data collected by the strain gauges attached to the longitudinal and lateral reinforcing bars. The mean strain rate was 1.24 x 10^4 μ/sec for longitudinal reinforcement and 8.0 x 10^3 μ/sec for lateral reinforcement. The rates of increase in yield strength of longitudinal and lateral reinforcement near the point of the maximum force were calculated by equation (1) to be 10.5% and 9.6%, respectively. The strain rate of concrete under dynamic loading was assumed to be identical to that of longitudinal reinforcement based on the study (Hosoya, 1996). Concrete strength was obtained by equation (2) representing an existing relationship between concrete strength and strain rate.

$$_d\sigma_B = \left(0.94 + 0.06 \cdot \log\left(\dot{\varepsilon}\right)\right) \cdot {}_S\sigma_B \tag{2}$$

where, ${}_d\sigma_B$: compressive strength of concrete under dynamic loading, ${}_s\sigma_B$: compressive strength of concrete under static loading, and $\dot{\varepsilon}$: strain rate (μ/sec). The rate of increase in concrete strength at the time of shear failure was estimated by equation (2) to be 18.6%. Shear strengths were obtained using the increased material strength and based on reference 3) (for unhinged members), and shown in Table 3. The calculated shear strength under dynamic loading was 1.28 times that obtained in the test. Under static loading, the test result was 1.3 times the calculated value. The results were more or less the same either under dynamic or static loading. If the effect of strain rate is considered properly, shear strength under dynamic loading can be estimated as accurately as under static loading.

4.3 Equivalent Stiffness

In order to examine the characteristics of the stable hysteresis loop, equivalent stiffness (Keq) and equivalent damping factor (Heq) were calculated (Fig. 9). Figure 10 shows the relationship between Keq and the deflection angle for D-2 and S-2 in the second cycle at respective loading amplitudes. Keq decreased as displacement amplitude increased both under dynamic and static loading. Keq in D-2 is higher than that in S-2 at any loading amplitude.

Figure 11 shows the relationship between the ratio of dynamic-to-static equivalent stiffness and the deflection angle at the second cycle in the same loading amplitude. In the specimens under dynamic loading, restoring force increased due to loading rate, so equivalent stiffness ratio also was generally higher than 1.0. Under large-amplitude dynamic loading cycle of R=1/25, Keq in dynamic loading was 6% to 17% higher than that in static loading.

4.4 Equivalent Damping Factor

Figure 12 shows the relationship between Heq and the deflection angle in the second cycle at respective amplitudes in D-2 and S-2. In both specimens, Heq of D-2 was approximately 5% around R=1/200. With subsequent increase of deflection angle, it increased to 9% at R=1/100 and 25% at R=1/25. Heq of S-2 is generally a little lower than Heq of D-2. Heq of D-5 in typical loading cycles is shown in Figure 13. D-5 was subjected to fifteen-cycle loading in total under small-amplitude area of R=1/1600, 1/800 and 1/400. Heq was nearly constant at 2% to 4% except for the case in the first loading cycle of R=1/400. The result in D-5 shows that the value of Heq in small-amplitude area is hardly affected by multiple cyclic loading.

Figure 14 shows the relationship of the ratio of dynamic-to-static equivalent damping factors and the deflection angle. Heq at small deflection angles was generally higher under dynamic loading than under static loading. The difference, however, decreased at larger deflection angles. Little difference was found beyond R=1/50.

4.5 Accumulated Energy Dissipation

Accumulated energy dissipation (= total amount of hysteresis loop areas) until the axial failure is shown in Table 4. In D-1, which failed one cycle earlier than S-1, accumulated energy dissipation was smaller than in S-1. In cases where axial failure in dynamic loading occurred in the same cycle in static loading, accumulated energy dissipation was larger under dynamic loading than under static loading.

D-2 and D-5, which were identical to each other except the loading program used, failed at the same loading amplitude range. The accumulated energy dissipation of D-5 until axial failure was only 62% of that in D-2 because smaller number of cyclic loading was imposed on D-5 than on D-2 in the large loading amplitude. This suggests that the accumulated energy dissipation greatly depends on the loading hysteresis until the axial failure.

5. CONCLUSIONS

Dynamic loading (maximum angular velocity of the member: 0.15 rad./sec) and static loading (1/1000 of loading rate in dynamic loading) tests were conducted on reinforced concrete columns subjected to axial and lateral loading. The following conclusions were obtained.

(1) In the tests, no significant difference was observed in failure mode under dynamic or static loading as long as the shear span and axial force were the same.

(2) The flexural yield strength was 6.9% to 9.5% greater in the dynamic loading test than that in the static loading test. The shear strength under dynamic loading was 11.3% greater than that under static loading.

(3) The limit deflection angle (deflection angle when the lateral force of the specimen lowered to 80% of the maximum force) was nearly the same under dynamic or static loading. No outstanding difference was found either in timing of axial failure.

(4) Equivalent stiffness obtained from the hysteresis loop in the second cycle of loading was greater in specimens under dynamic loading than under static loading by approximately 10% in the small- through large-amplitude areas.

(5) Equivalent damping factor obtained from the hysteresis loop in the second cycle of loading was much larger under dynamic loading than under static loading in small-amplitude areas. Small difference was observed in large-amplitude areas.

(6) Properly evaluating the increase in material strength owing to the effect of strain rate, and using an existing static strength evaluation equation enabled the estimation of flexural yield strength and shear strength of specimens under dynamic loading as accurately as under static loading.

(7) In these tests, the effect of loading rate on the accumulated energy dissipation was not clearly determined. On the other hand, a pair of dynamic loading test result of D-2 and D-5 suggests that the accumulated energy dissipation greatly depends on the loading hysteresis until the axial failure.

ACKNOWLEDGMENTS

This experimental study was conducted as part of "DaiDaiToku" special project, which the Ministry of Education, Culture, Sports, Science and Technology is promoting.

Keywords: Reinforced concrete; Columns; Dynamic loading test, Strain rate effect; Seismic performance

REFERENCES

Hosoya, H., T. Okada, T. Kitagawa, Y. Nakano and F. Kumazawa (1996). Fiber Model Analysis of Reinforced Concrete Members with Consideration of the Strain Rate Effect. *Journal of Structural and Construction Engineering.* Architectural Institute of Japan. No.482: pp. 83-92.

Hosoya, H., T. Okada, T. Kitagawa, Y. Nakano and F. Kumazawa (1997). Relationship Between the Increase of Strength and Failure Mode of Reinforced concrete Members by the Strain Rate Effect in an Earthquake. *Journal of Structural and Construction Engineering.* Architectural Institute of Japan. No.492: pp. 69-77.

Architectural Institute of Japan. (1999). Design Guidelines for Earthquake Resistant Reinforced Concrete Buildings Based on Inelastic Displacement Concept.

Table 1: Test specimens

	D-1	S-1	D-2	S-2	D-3	S-3	D-4	S-4	D-5
Cross Section (mm x mm)	b x D = 250 x 250								
Longitudinal Bar (σ_y : N/mm^2)	SD345 8-D13 Pt = 0.61% (σ_y = 391)								
Lateral Bar (σ_{wy} : N/mm^2)	SD295 2-D6@50 P_w = 0.51% (σ_{wy} = 400)								
Shear Span Ratio	1.8		1.8		1.2		1.8		1.8
Axial Force Ratio N/bDσ_B	0.1 (170kN)		0.3 (510kN)		0.3 (510kN)		0.3±0.2		0.3
Concrete Strength σ_B(N/mm^2)	29.6	29.4	29.7	29.9	30.7	31.3	30.9	31.4	30.2
Young's Modulas of Concrete (N/mm^2)	26200	27400	27200	27600	27500	26700	27000	27800	27000
Calculated Static Flexural Yield Strength (Qf)*1	123		164		246		174		164
Calculated Static Shear Strength (Qs)*2	158		158		158		158		158
Shear Capacity (= Qs/Qf)	1.27		0.96		0.64		0.91		0.96

*1 Based on a fiber model analysis. *2 Based on ref.3) where Rp = 0.01rad.

Table 2: Test results

	D-1	S-1	D-2	S-2	D-3	S-3	D-4	S-4	D-5
Flexural Strength (kN)	145	136	193	177	—	—	187	170	194
Deflection Angle at Flexural Strength (rad.)	1/68	1/68	1/128	1/109	—	—	1/105	1/89	1/86
Maximum Strength (kN)	148	137	193	179	271	244	191	173	194
Deflection Angle at Maximum Strength (rad.)	1/42	1/30	1/123	1/74	1/119	1/108	1/56	1/54	1/85
Limit Deflection Angle (rad.)	1/24	1/17	1/26	1/25	1/50	1/56	1/34	1/34	1/26
Failure Mode *1	F	F	F	F	S	S	F	F	F

*1 F: Flexural Yielding, S: Shear Failure

Table 3: Comparison of calculated and observed yield/maximum strength*1 considering strain rate effect

	S-1	S-2	S-3	D-1	D-2	D-3	D-5
Calculation (kN)	123	164	188	135	170	212	170
Test Result (kN)	136	177	244	145	193	271	194
Test / Calculation	1.10	1.11	1.30	1.08	1.16	1.28	1.14

*1 For D-3 and S-3, the values show the maximum strength. For the other specimens, the values show flexural yield strength.

Table 4: Accumulated energy dissipation

Accumulated Energy Dissipation (x10^4 kN・mm)	**S-1**	**S-2**	**S-3**	**S-4**	—
	5.14	4.20	1.12	2.45	—
	D-1	**D-2**	**D-3**	**D-4**	**D-5**
	4.56	4.86	1.49	3.44	3.04

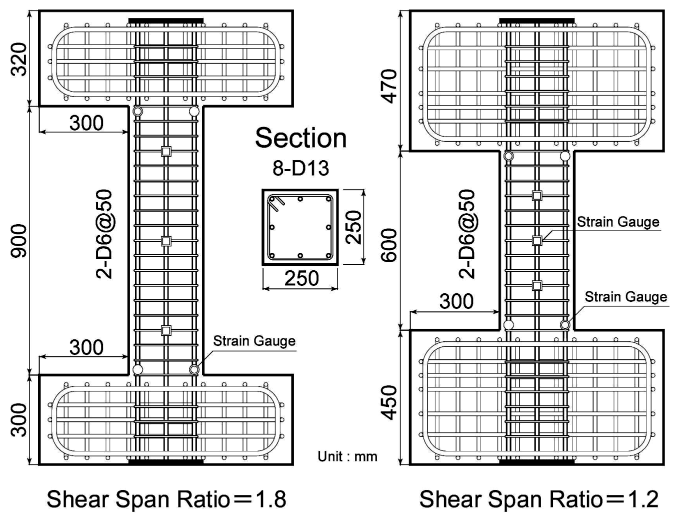

Fig. 1: Dimensions of test specimens

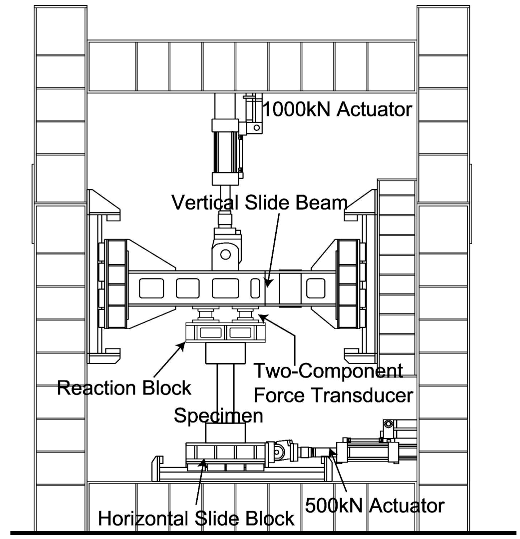

Fig. 2: Loading setup

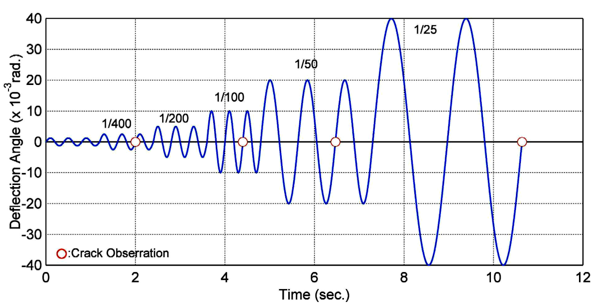

Fig. 3: Lateral loading program for D-1 to D-4

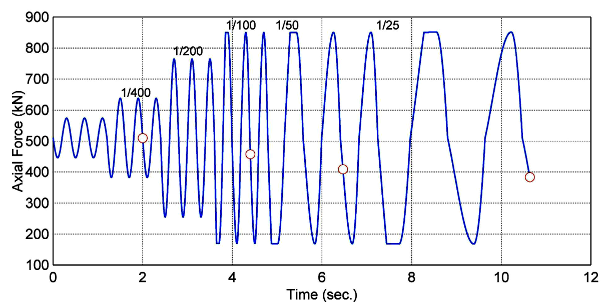

Fig. 4: Axial loading program for D-4

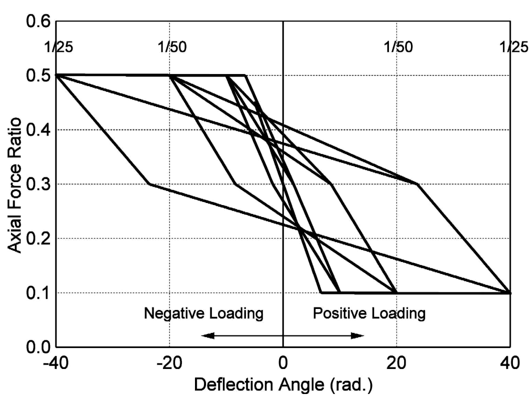

Fig. 5: Axial force - lateral displacement relationship for D-4 and S-4

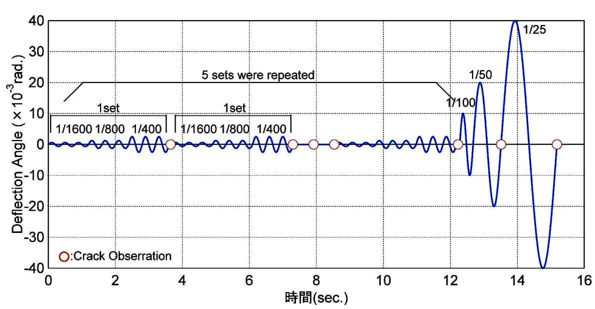

Fig. 6: Lateral loading program for D-5

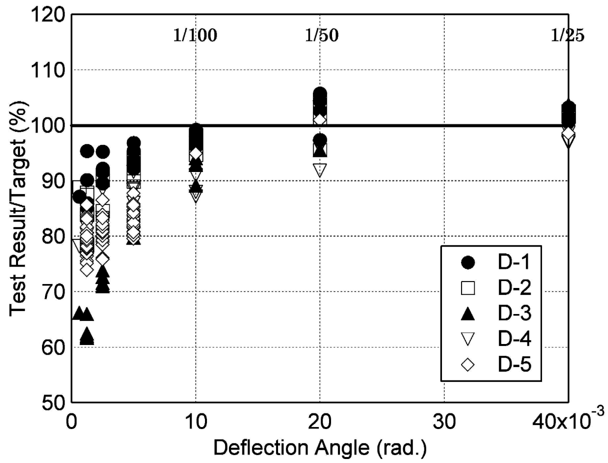

Fig. 7: Comparison of test result and target loading rate

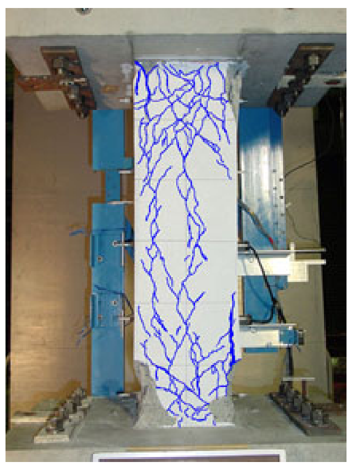

Specimen D-2

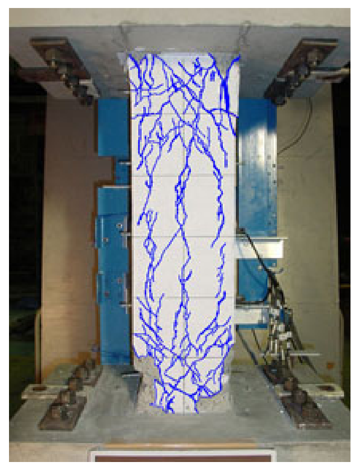

Specimen S-2

Photo 1: Damage in specimen D-2 and S-2 after loading of 1/25 rad.

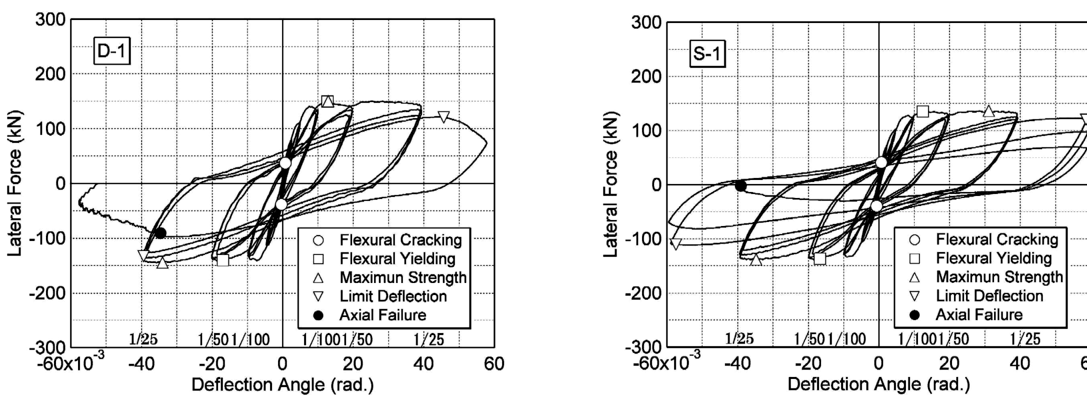

Fig. 8(a): Lateral force - deflection angle relations

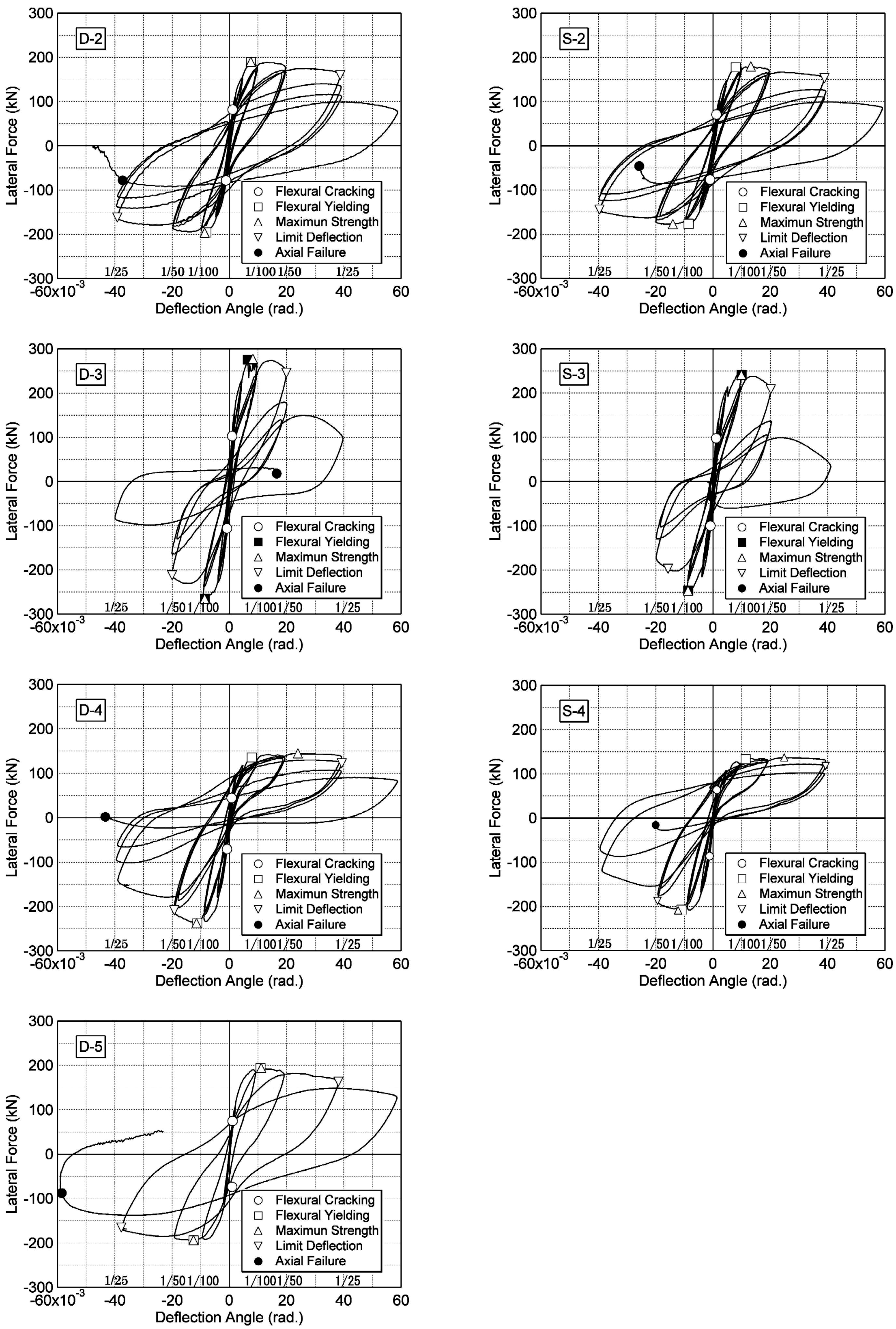

Fig. 8(b): Lateral force – deflection angle relations

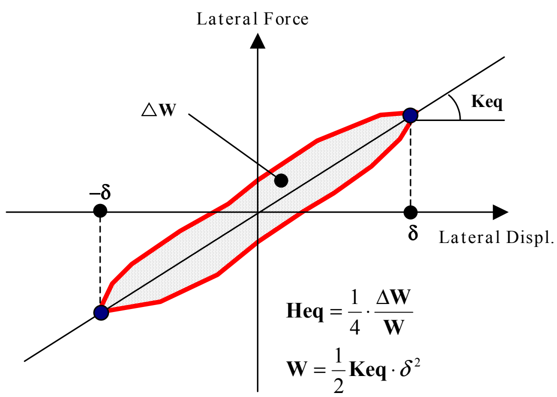

Fig. 9: Definition of Keq and Heq

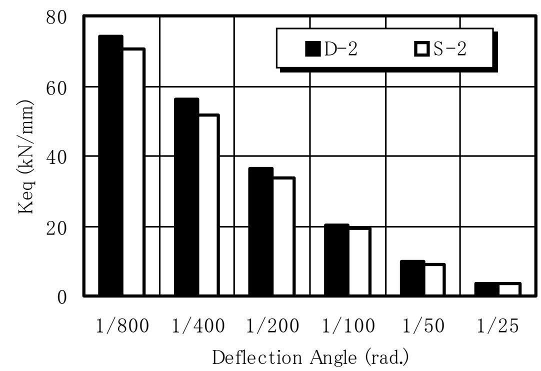

Fig. 10: Keq of D-2 and S-2

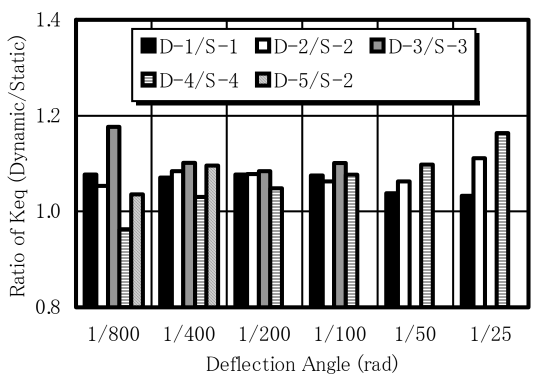

Fig. 11: Ratio of Keq (dynamic/static)

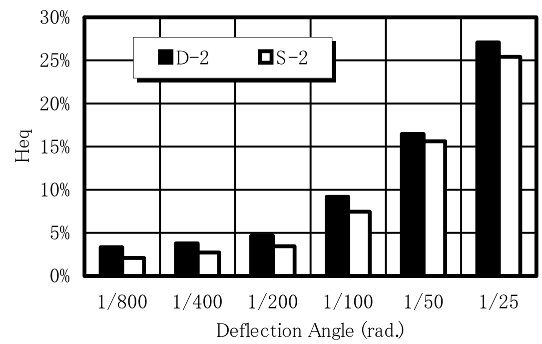

Fig. 12: Heq of D-2 and S-2

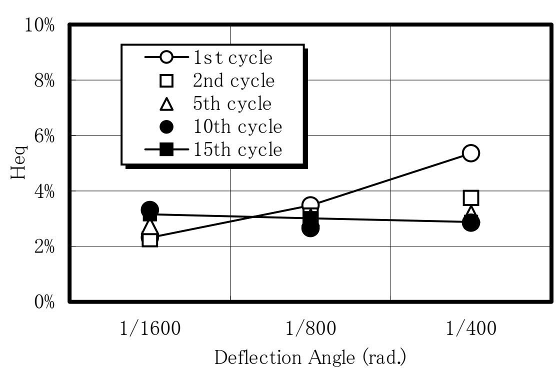

Fig. 13: Heq of D-5 for small amplitude

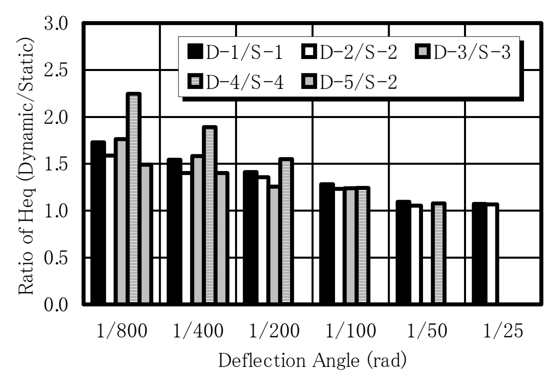

Fig. 14: Ratio of Heq (dynamic/static)

TRI-AXIAL SHAKING TABLE TEST ON REINFORCED CONCRETE BUILDINGS WITH LARGE ECCENTRICITY

Kazutaka SHIRAI[1], Toshikazu KABEYASAWA[2], Hideo KATSUMATA[3] and Toshimi KABEYASAWA[4]

ABSTRACT

To examine the response and damage behaviour of reinforced concrete buildings subjected to multi-directional input motions, and to obtain the preliminary know-how for the Dai-Dai-Toku E-Defense full scale experiment, tri-axial shaking table tests of wall-frame specimens were conducted. In the tests, input directions of principle axis of earthquake waves were rotated to two specimens. Thus, "Quantity of the input" by the earthquake motions was kept equivalent, and the influence of the difference of "Direction of the input" was examined. From the test results, following findings were obtained. (1) Comparing in same input level, two specimens showed difference response and damage behaviour. (2) Finally, both specimens failed at the shear wall with opening and the standing wall. (3) By the failure at the end of the standing wall, the short column changed into the long column, so the torsional vibration was excited remarkably. For shaking table control, the conventional input compensation technique using by inverse transfer function was adopted. As a result, it was confirmed that shaking table was controlled with sufficient fidelity by the technique.

1. INTRODUCTION

Dynamic behaviour of reinforced concrete (RC) buildings subjected to multi-directional input motion is not well known. Therefore investigation by shaking table tests and accumulation of test data are needed. So in this study, in order to discuss the response and damage behaviour of RC buildings subjected to multi-directional input motions, and to obtain the preliminary know-how for the following Dai-Dai-Toku E-Defense full scale experiment, tri-axial shaking table tests of RC wall-frame specimens were conducted. In the tests, input directions of principle axis of earthquake waves were rotated to two specimens. Thus, "Quantity of the input" by the earthquake motions was kept equivalent, and the influence of the difference of "Direction of the input" was examined. This paper describes mainly about methods and results of the tests.

[1] *Hyogo Earthquake Research Center, National Research Institute for Earth Science and Disaster Prevention, Miki, Hyogo, Japan*
Email: shirai@bosai.go.jp
[2] *Earthquake Research Institute, The University of Tokyo, Bunkyo, Tokyo, Japan*
Email: toshikazu@eri.u-tokyo.ac.jp
[3] *Technical Research Institute of Obayashi Corporation, Kiyose, Tokyo, Japan*
Email: katsumata.hideo@obayashi.co.jp
[4] *Earthquake Research Institute, The University of Tokyo, Bunkyo, Tokyo, Japan*
Email: kabe@eri.u-tokyo.ac.jp

2. TEST METHOD

2.1 Specimen

General view of the specimen is shown in Photo 1, and concept view of the specimen is shown in Figure 1. Standard floor plan and Elevations of each street are shown in Figure 2. The specimen was 1/4 scaled 4 storied RC wall-frame model. Plane span of the specimen was 1500mm x 1500mm (1 x 3 spans), and floor height is 750mm.

A total of two specimens (same specification, same size) were prepared. Test parameter was the shaking direction of the principle axis of the input earthquake motions.

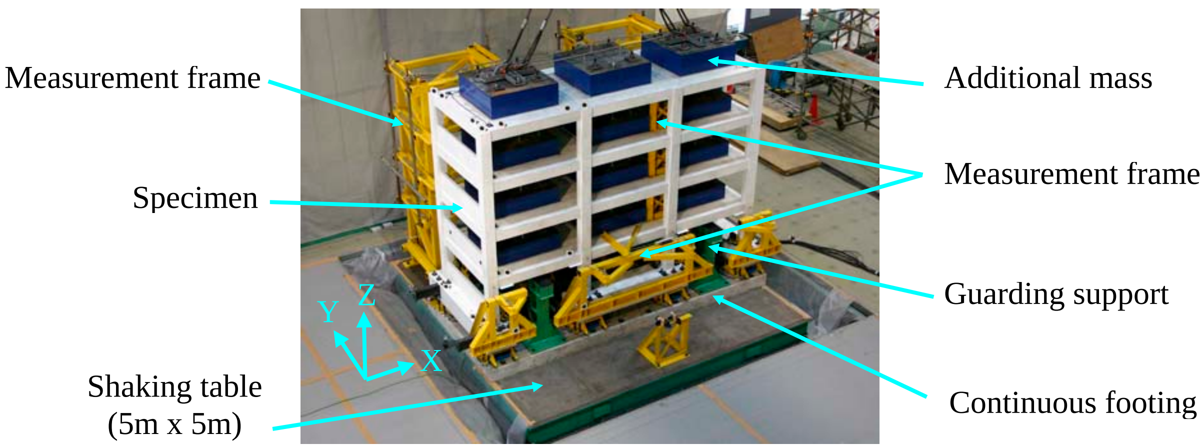

Photo 1: General view of the specimen

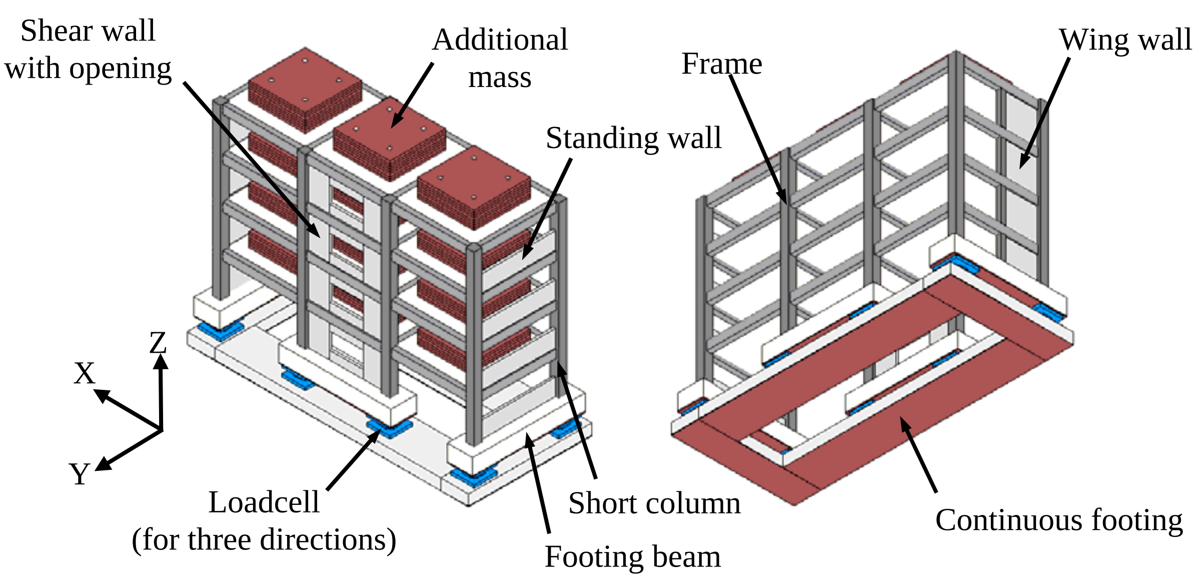

Fig. 1: Concept view of the specimen

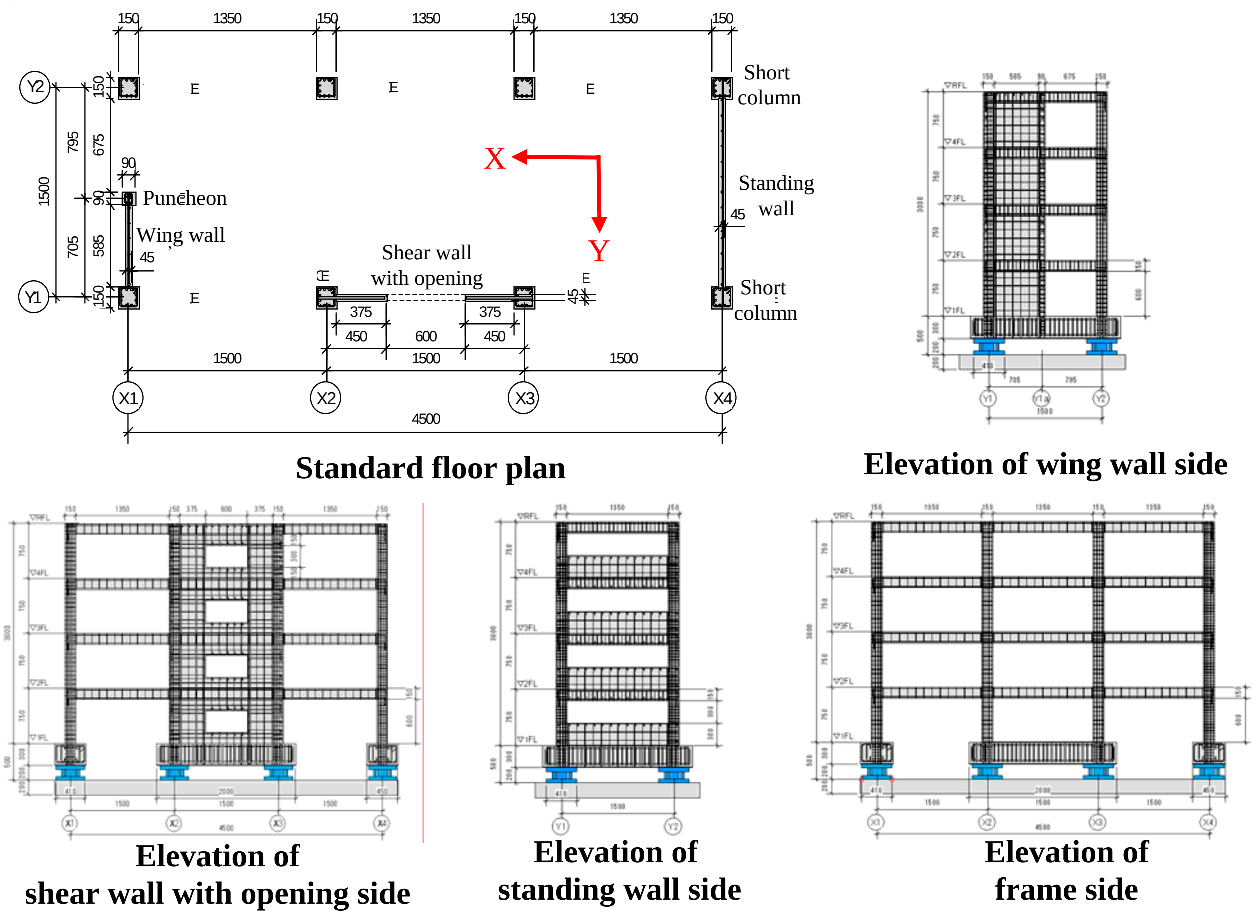

Fig. 2: Plan and elevations of the specimen

Various components and elements (frame, shear wall, standing wall, short column, wing wall, footing beam, and loadcell) were built in the specimen. These elements are assumed to the three-dimensional shaking table test of full scale RC structure using E-Defense in 2005 fiscal year.

Assuming buildings designed in 1980s in Japan, as a rule, arrangement of bar was applied to AIJ (1982). The structural dimensions of the specimen are shown in Table 1. The material properties are shown in Tables 2 and 3. The weight of each floor is shown in Table 4.

Final failure of the specimen was supposed occur at the shear wall with opening of Y1 St. as for X-direction, and at the short columns with standing wall of X4 St. as for Y direction. The shear wall with opening of Y1 St. was decentered from the center of gravity. But it was assumed that torsional response is not large because the wing wall and the short columns have almost the same and sufficient elastic rigidity. Actually, the elastic eccentricity of Y-direction is small as described later.

Table 1: Structural dimensions of the specimen

Portion	Section (mm)	Arrangement of bar	
		Main bar, Slab, Wall	Hoop, Stirrup, Remarks
Column	150 x 150	12-D6 (pg=1.71%)	2-D4@60 (pw=0.29%)
Short column	150 x 150	ditto	2-D4@40 (pw=0.44%)
Puncheon	90 x 90	4-D6 (pg=1.58%)	2-D4@60 (pw=0.49%)
Girder (Y1, Y2 St.)	b90 x D150	Top 2-D6 (pt=0.54%) Bottom 2-D6 (pt=0.54%)	2-D4@110 (pw=0.27%)
Girder (X2, X3 St.)	b90 x D150	Top 3-D6 (pt=0.81%) Bottom 2-D6 (pt=0.54%)	ditto
Girder (X1, X4 St.)	b90 x D150	ditto	2-D4@55 (pw=0.53%)
Footing beam	b450 x D300	Top 6-D19 (pt=1.41%) Bottom 6-D19 (pt=1.41%)	4-D10@60 (pw=1.05%) PL9 is set up at the bottom
Slab	t80	D4@80 double	--
Shear wall with opening	t45	D4@110 single (ps=0.27%)	Opening w600 x h300 Reinforcement of opening: 1-D6 (horizontal and vertical)
Standing wall, Wing wall	t45	D4@110 single (ps=0.27%)	Standing wall : h300

Table 2: Material properties (steel)

Steel bar	Yield strength (MPa)	Young's modulus (MPa)
D4	371 (0.2% offset value)	1.95×10^5
D6	374	2.03×10^5

Table 3: Material properties (concrete)

Specimen	Story	Compressive strength (MPa)	Young's modulus (MPa)
Case1	1st Story 2nd - 4th Story	31.2 30.5 (Average value)	2.19×10^4 2.14×10^4
Case2	1st Story 2nd - 4th Story	33.2 32.2 (Average value)	2.19×10^4 2.11×10^4

Table 4: Weight of each floor

RF	92kN (13.6 kN/m^2)
4F-2F	Each 76kN (11.2 kN/m^2)
Minor total	320kN (11.8 kN/m^2)

Footing beam	36 kN
Total payload (on shaking table)	450 kN

It was expected that valuable data can be obtained, because example of the shaking table tests using RC structure with large irregularity as this study was few in the past.

2.2 Preliminary Analysis

Results of preliminary analysis are shown in Figures 3 and 4. From the result of static analysis, base shear coefficient was 0.96 in X-direction, and 0.66 in Y-direction. Because the number of stories and spans of the specimen were little, the shear force coefficient of each story has increased compared with general actual buildings. The elastic eccentricity of the specimen was 0.12 in X-direction, and 0.02 in Y-direction.

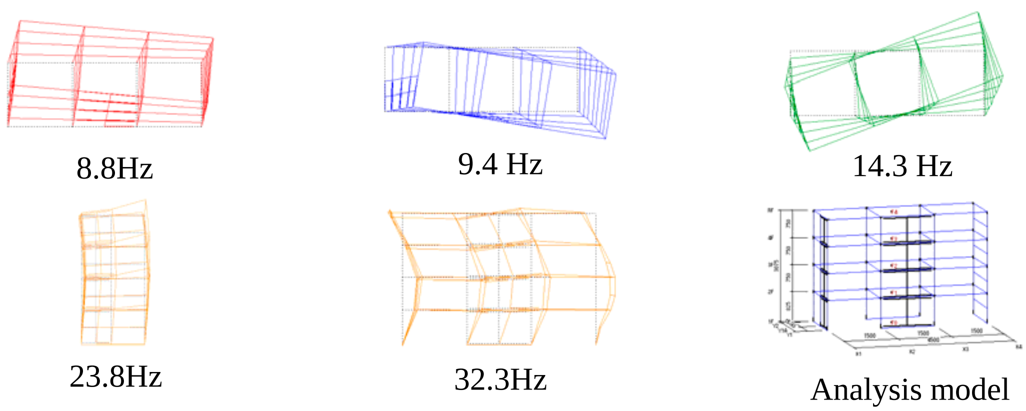

Fig. 3: Result of eigenvalue analysis

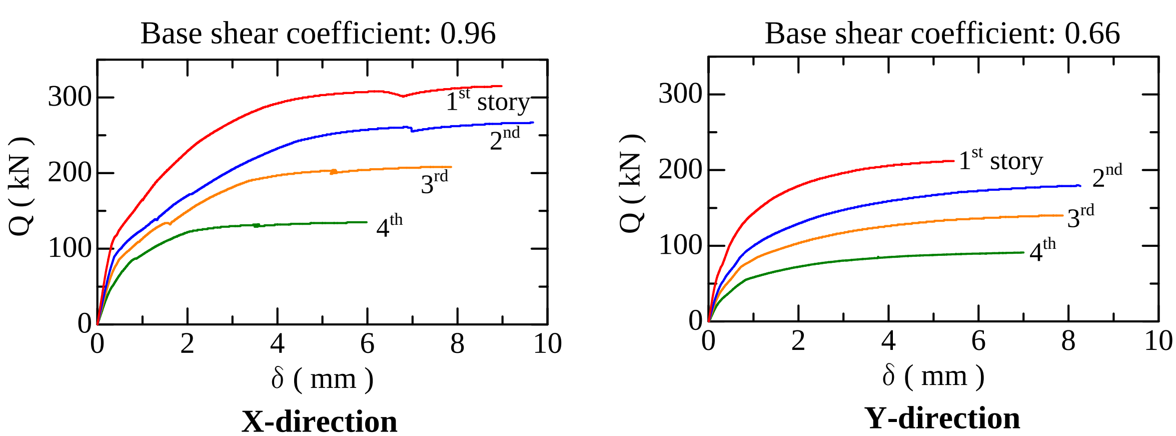

Fig. 4: Result of static loading analysis (shear force - displacement relationship)

2.3 Input Program

In the tests, input directions of the principle axis of input earthquake motions were rotated to two specimens. Thus, "quantity of the input" such as maximum input acceleration, maximum input velocity, total input energy, was kept equivalent, and the influence of the difference of "direction of the input" became comparable.

The input motions were based on acceleration record of the JMA Kobe NS, EW, UD (1995), and compressed the time axis into 1/2 times in consideration of the similarity rule.

In Case 1, the principle axis of the input motions was rotated +45 degrees around Z axis corresponding to the direction of broad side of the specimen (X-direction). And in Case 2, the principle axis of the input motions was rotated -45 degrees corresponding to the direction of narrow side of the specimen (Y-direction).

Further more, magnification of acceleration amplitude of the input motions were increased gradually, and plural runs (Run 1-7 in Case 1, Run 1-9 in Case 2) were conducted.

The input motions of Case 1 and Case 2 (when input magnification is 100%) are shown in Figure 5.

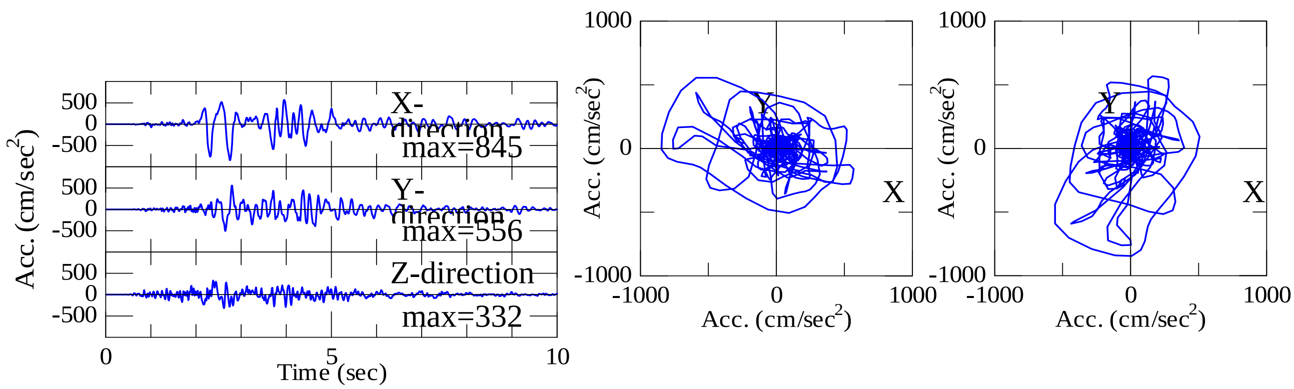

Time history of acceleration (Case 1)

Orbit of horizontal acceleration (Case 1)

Orbit of horizontal acceleration (Case 2)

Fig. 5: Input motions

To examine the influence of the input direction beforehand, non-linear 3D-frame dynamic analysis (input magnification 100%, input angle of the principle axis rotated from 0 degree up to 360 degrees) was carried out.

The result of analysis is shown in Figure 6. Here, the horizontal axis is the input rotation angle of the principle axis. The longitudinal axis is displacement ratio (defined as ratio of 1^{st} story Y-direction displacement at short column and 1^{st} story X-direction displacement at shear wall with opening). The displacement ratio was small at 30 or 210 degrees of the input rotation angle. On the one hand, the displacement ratio was large at 100 or 280 degrees of rotation angle.

It was shown that the response of the structure changes remarkably depending on the direction of the principle axis of the input motions. The rotation angle of the principle axis in each case was decided in consideration of this preliminary examination.

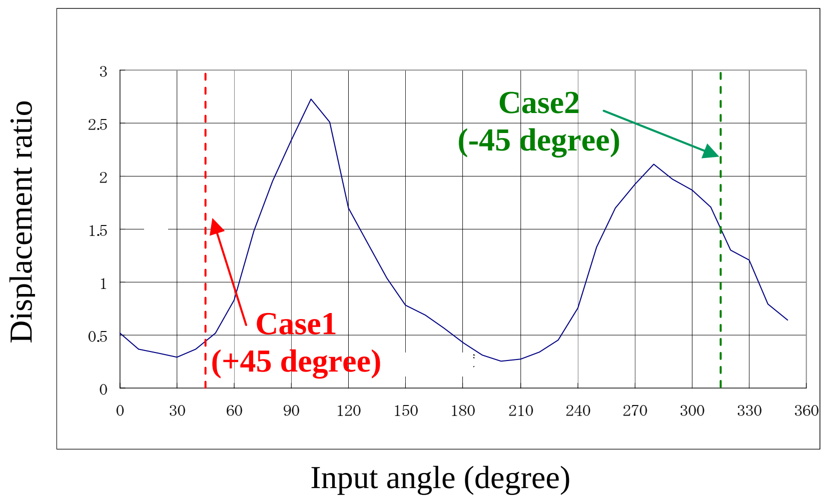

Displacement ratio
= (Short column, 1^{st} story, X-direction) / (Shear wall with opening, 1^{st} story, Y-direction)

Fig. 6: Result of the preliminary dynamic analysis

3. TEST RESULT

3.1 Shaking Process

The outline of the shaking process and test result is shown in Table 5. In Case 1, it resulted in shear failure at the bottom of the shear wall with opening of Y1 street after flexural yielding. On the contrary, the wing wall of X1 street did not fail to the last. This result agreed with the final failure mode predicted initially.

However, as for the standing wall of X4 street, it resulted in different damage situation from prior assumption. That was, the failure at the end of the standing wall progressed gradually from middle runs, and the short column changed into the long column. Thus, torsional vibration around Z-axis has increased remarkably because the rigidity of the frame of standing wall side decreased.

On the other hand, in Case 2, the damage of the standing wall was intensive, and the tendency of increase of the torsional vibration was shown in Case 1 or more. As for the short column of X4 street, shear crack was observed (Run 4). However, it did not result in shear failure because the short column changed into long column to the last, shear failure at the shear wall with opening of Y1 street occurred (Run 8, Run 9). The failure of the standing wall and the other parts were different from prior prediction.

Table 5: Outline of shaking process and test result

Run	Input ratio*1	Case1		Case2	
		R_W*2	Remarkable damage	R_C*3	Remarkable damage
Run1	5%	1/8500	—	1/3710	—
Run2	20%	1/1550	Crack at shear wall with opening and standing wall	1/1540	Crack at standing wall and wing wall
Run3	40%	1/615	Crack at shear wall with opening	1/472	Crack at shear wall with opening
Run4	60%	1/381	Crack at shear wall with opening	1/155	Shear crack at short column, Yielding of short column rebar,
Run5	80%	1/209	Yielding of vertical bar at shear wall with opening	1/71	Chipped at standing wall end
Run6	100%	1/124	Failure at standing wall end	1/22	Crush at column bottom, Failure at standing wall end
Run7	125%	1/32	Shear failure at shear wall with opening	1/23	
Run8	125%			1/21	Chipped at short column, Shear failure at shear wall with opening
Run9	125%			1/26	Shear failure at shear wall with opening

*1 Magnification of input motion
*2 Drift angel at shear wall with opening, 1st story, X-direction (rad.)
*3 Drift angel at standing wall and short column, 1st story, Y-direction (rad.)

Change of natural frequency (1st mode) obtained from the white noise shaking after each run is shown in Figure 7. The natural frequency has decreased finally down to about 2 Hz from about 8

Hz before shaking. Therefore, decrease in the rigidity because of the progress of damage was confirmed.

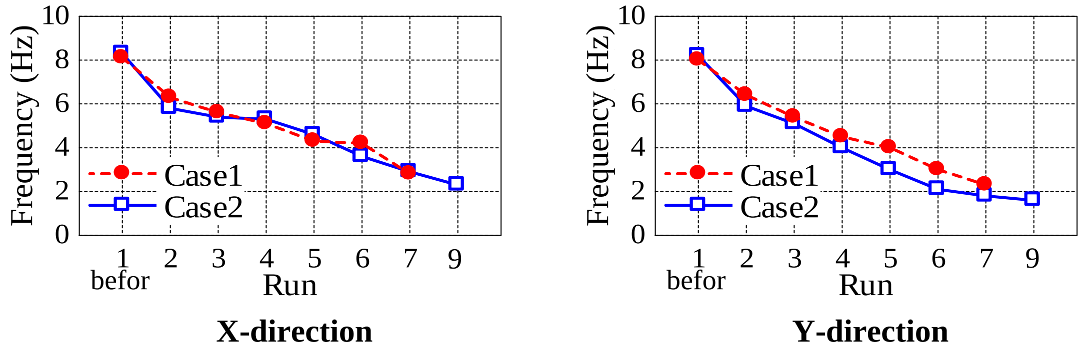

Fig. 7: Change of natural frequency obtained after each run

3.2 Response of Shear Force and Deformation

Hysteresis loops of 1st story is shown in Figure 8. Here, the vertical axis is base shear calculated from response acceleration and mass of each story at the center of the figure. The horizontal axis is relative story displacement at the center of the figure. In Case 2, the tendency was observed which to show the irregular loops by the torsional vibration in X-direction.

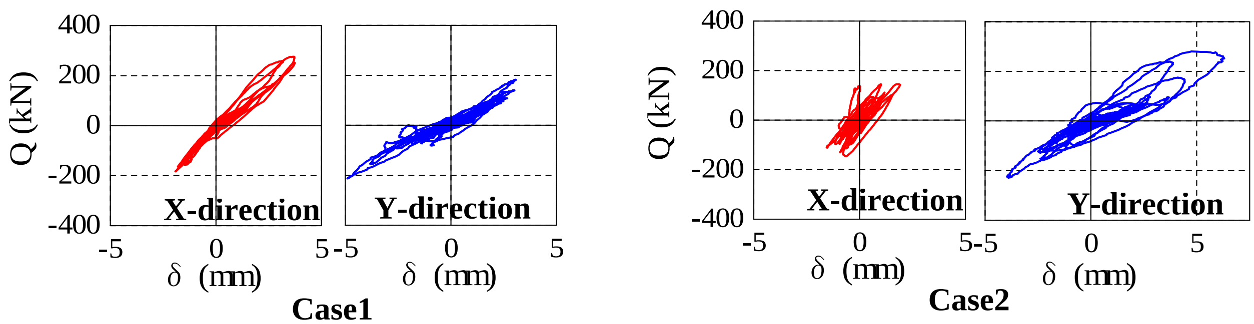

Fig. 8: Comparison of P-D Loops (Run 5 80% input)

The P-D Loops of all runs in Case 1 are shown in Figure 9. Moreover, the result of a prior static analysis (one direction pushover) is shown in Figure 9. The result of a static analysis roughly agreed with the skeleton curve of the test results of Case 1.

The example of assumed base shear (Q_L: total reaction force measured by all loadcells) and assumed wall shear (Q_{LW}: reaction force measured by two loadcells under the shear wall with opening) are shown in Figure 10. From the comparison of $Q_L$peak (maximum value of Q_L) and Q_{LW}peak (maximum value of Q_{LW}), ratio of wall shear / base shear was approximately figured out.

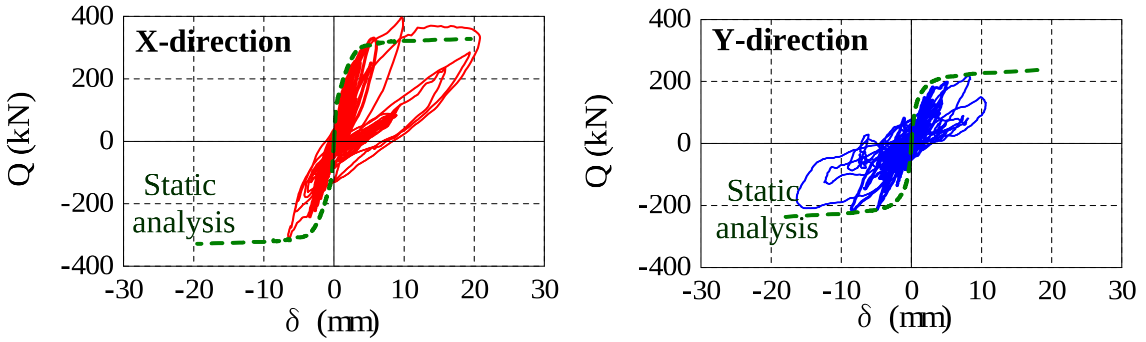

Fig. 9: Comparison of P-D Loops (Case 1 all Runs)

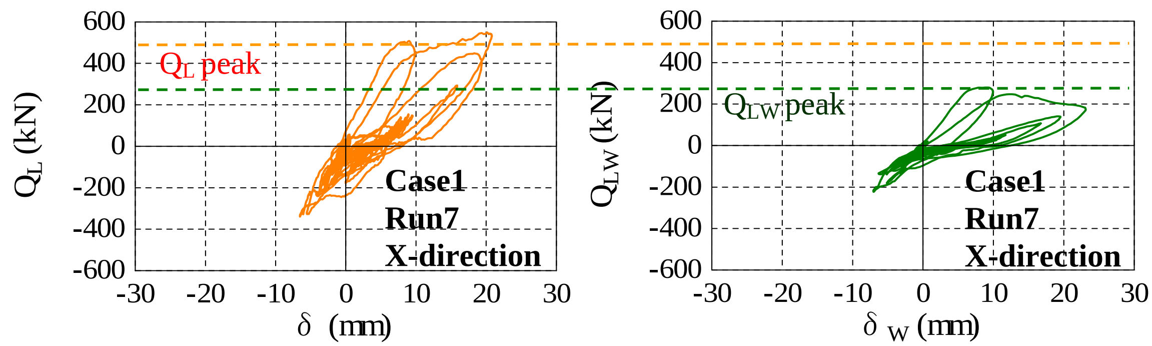

Fig. 10: Comparison of P-D Loops (Measured by Loadcell)

3.3 Damage in Final Stage

Damage diagrams of Case 1 and Case 2 after Run 6 are shown in Figure 11. In Case 1, which X-direction was the main axis of the input motions, damages were observed at the shear wall with opening. On the other hand, in Case 2, which Y-direction was the main axis, damages concentrated on the wing wall, the standing wall, and the short column. Thus, different damage and failure situation was shown when comparing with same run of Case 1 and Case 2. However, finally, it resulted in failure of the shear wall with opening and the standing wall about both specimen (Case 1 Run 7, Case 2 Run 9).

Final collapsing view of Case 2 is shown in Photo 2. As for Case 2, considering damage process on the way, it was guessed that the shear wall with opening failed by reduction of in-plane (X-directional) restraint for wall panel, after damage progress at the bottom of boundary columns by out-of-plane (Y-directional) forces.

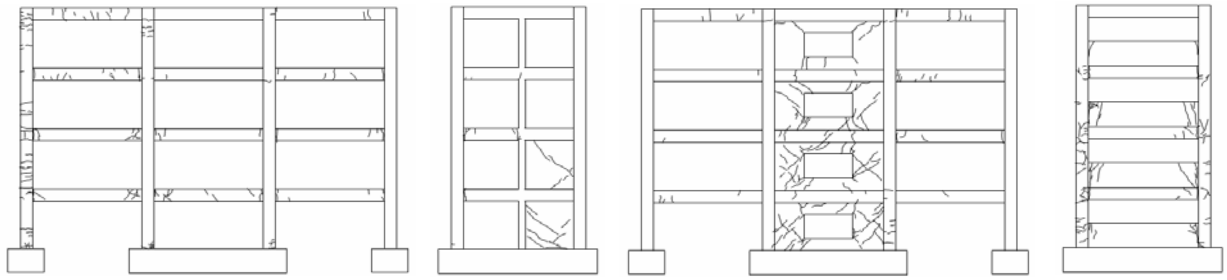

Frame side Wing wall side Shear wall with opening Standing wall side

Case1

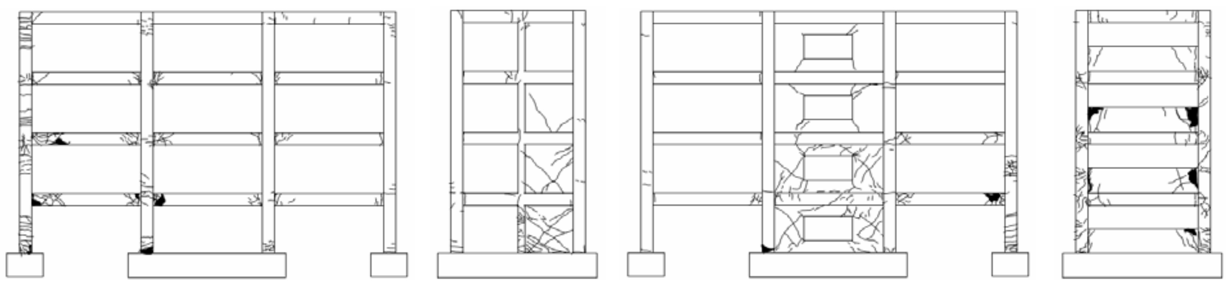

Frame side Wing wall side Shear wall with opening Standing wall side

Case2

Fig. 11: Comparison of damage situation (Run 6 100% input)

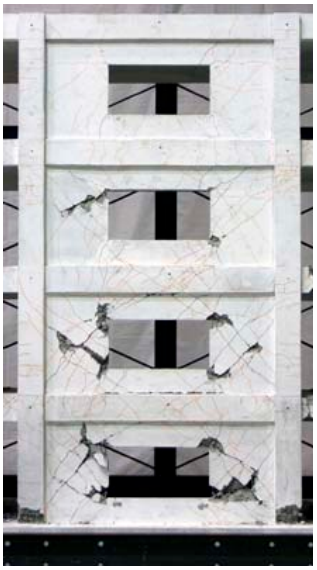

Shear wall with opening

Standing wall side

Photo 2: Final collapsing view (Case 2, Run 9)

3.4 Maximum Response

As for Case 1, maximum response acceleration of each story at the center of the figure is shown in Figure 12, and maximum shear force of each story is shown in Figure 13. Here, shear force was calculated by acceleration at the center of the figure and mass of each story. Generally, in the range of small runs, the maximum response acceleration showed about intermediate shapes of rectangular and Ai distribution.

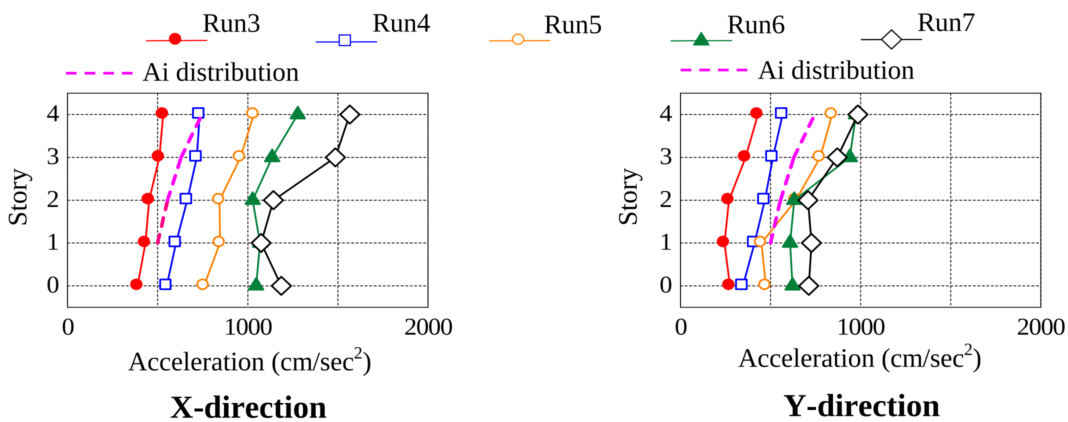

Fig. 12: Maximum response acceleration of each story (Case 1)

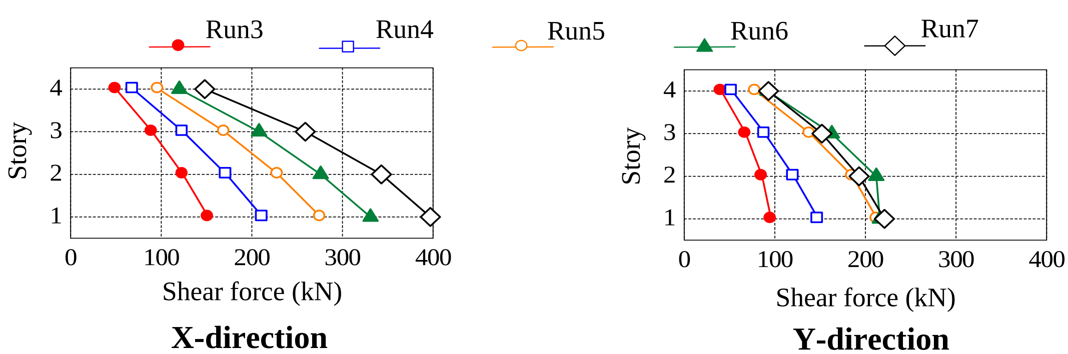

Fig. 13: Maximum shear force of each story (Case 1)

Comparison of maximum relative displacement of each story and each side is shown in Figure 14. In general, as for X-direction, the maximum deformation of the frame side was larger than that of the shear wall with opening side. And as for Y-direction, the maximum deformation of the standing wall side was larger than that of the wing wall side. From this, it was confirmed that the frame side and the standing wall side were oscillated remarkably by the torsional vibration. Especially, the relative increase of the maximum deformation value of the standing wall side was larger than the other side as runs progressed. It was understood that the short column became as the long column by the failure of the end of the standing wall, the rigidity and the strength of each component became not uniform, and the torsional vibration increased.

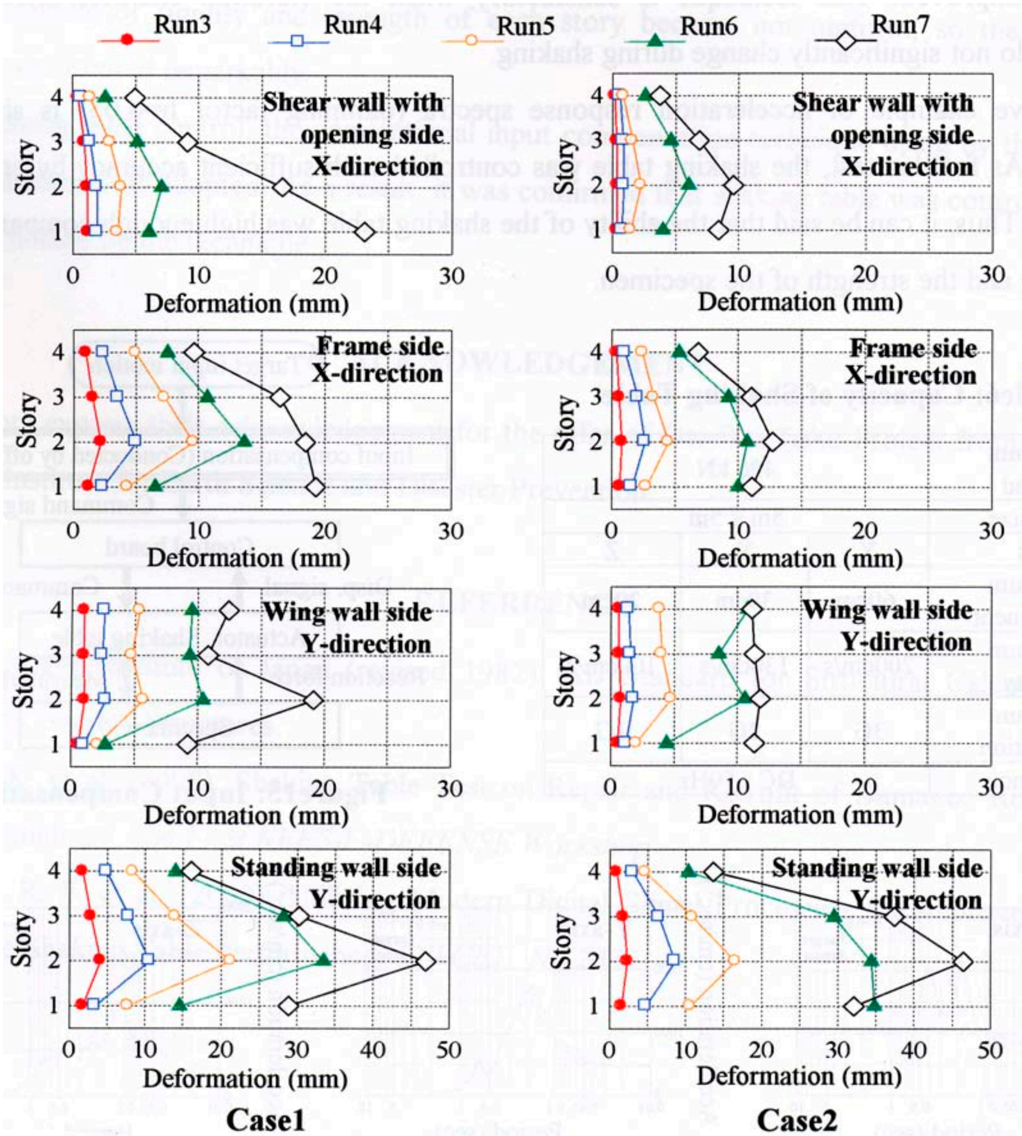

Fig. 14: Maximum deformation of each story and each side

4. FIDELITY OF SHAKING TABLE CONTROL

Capacity of the shaking table used in this study is shown in Table 6. To improve control accuracy during non-linear shaking, this study employed input compensation technique (Nowak 2000) which is one of the techniques used widely now. Block diagram of input compensation in control system of the shaking table is shown in Figure 15. In the case of input compensation, transfer function of a over-all system of the shaking table and the specimen is obtained in advance. Next, using the inverse of the transfer function, the command signal is adjusted by the tuning shaking. Finally, the influence of the specimen is reduced, and the characteristics of the shaking table are improved. This technique is satisfactory when the vibration characteristics of the specimen do not significantly change during shaking.

Comparative example of acceleration response spectra (damping factor h=0.05) is shown in Figure 16. As for this test, the shaking table was controlled with sufficient accuracy by employed technique. Thus, it can be said that the ability of the shaking table was high enough compared with the rigidity and the strength of the specimen.

Table 6: Capacity of shaking table

Maximum payload	490 kN		
Table size	5m x 5m		
Axis	X	Y	Z
Maximum displacement	60cm	30cm	20cm
Maximum velocity	200cm/s	130cm/s	100cm/s
Maximum acceleration	3G	2G	1G
Frequency	DC - 50Hz		

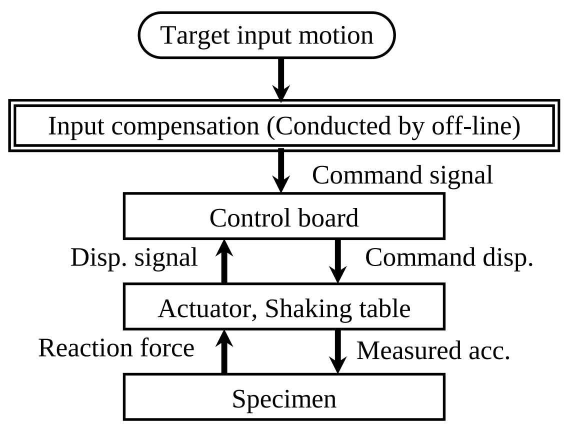

Fig. 15: Input compensation

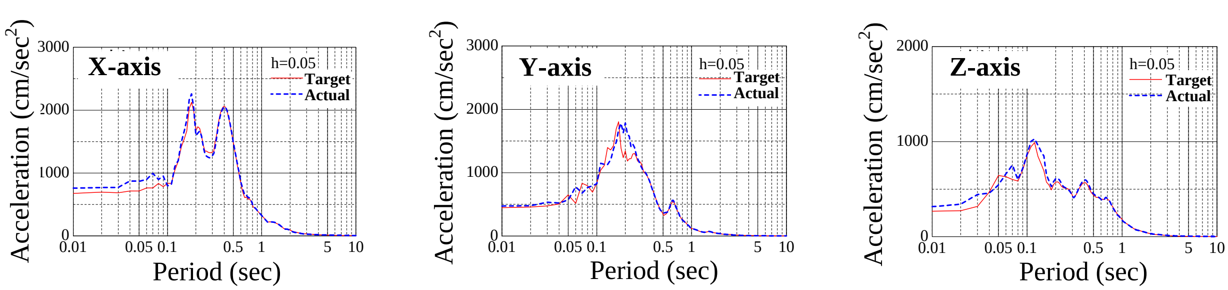

Fig. 16: Acceleration response spectra of input motions (Case 1, Run 5 80% input)

5. SUMMARY

To grasp the response and damage behaviour of RC buildings subjected to multi-directional input motions, and to obtain the preliminary know-how for the E-Defense Dai-Dai-Toku full scale experiment, tri-axial shaking table tests of RC wall-frame specimens were conducted. From the test results, the following findings were obtained.

(1) Comparing in the same input level, two specimens showed difference response and damage behaviour.

(2) Finally, both specimens failed at the shear wall with opening and the standing wall.

(3) By the failure at the end of the standing wall, the short column changed into the long column, the distributions of rigidity and strength of each story became not uniform, so the torsional vibration was excited remarkably.

(4) For shaking table control, the conventional input compensation technique using by the inverse transfer function was adopted. As a result, it was confirmed that shaking table was controlled with sufficient fidelity by the technique.

6. ACKNOWLEDGEMENT

The authors express their acknowledgement for the offer of Dai-Dai-Toku Project from National Research Institute for Earth Science and Disaster Prevention.

REFERENCES

Architectural Institute of Japan (revised 1982): AIJ Standard for Structural Calculation of Reinforced Concrete Structures.

Hideo, K. et al. (2005): Shaking Table Test on Repair and Retrofit of Damaged Reinforced Concrete Buildings. *The First NEES-E-DEFENSE Workshop*

Nowak, R. F. et al. (2000): Utilizing Modern Digital Signal Processing for Improvement of Large Scale Shaking Table Performance. *12WCEE, No.2035*

Keywords: Shaking table test, multi-directional input motion, reinforced concrete, wall-frame model, shear wall with opening, standing wall, wing wall, short column, loadcell, torsional vibration, control fidelity, input compensation

SHAKING TABLE TEST ON REPAIR AND RETROFIT OF DAMAGED REINFORCED CONCRETE BUILDINGS

Hideo KATSUMATA[1], Kazutaka SHIRAI[2], Yasuhiko MASUDA[3], Hiroya HAGIO[3]

Takeshi SANO[3], Kouhei KURITA[3] and Kozoh KIMURA[3]

Toshikazu KABEYASAWA[3] and Toshimi KABEYASAWA[4]

ABSTRACT

To discuss seismic performance of repair and retrofit techniques for damaged buildings during an earthquake shock, a shaking table test is carried out, employing a 1/4 scaled and 4 storied reinforced concrete building model. Applied retrofit techniques are wall installation using precast concrete blocks or fiber reinforced plastic (FRP) blocks, addition of a steel frame with friction slip damper, and column jacketing with carbon fibers. Comparing with the as-built test result against the same level input, the retrofit result shows improvement of performance, that is, increase in capacities or base shear, decrease in maximum response deformation, and reduction of damage. Namely, the employed techniques are verified to be useful for repair and retrofit. And also, it is shown that for the damaged buildings, adequate design and work of repair and retrofit can provide seismic performance equal to or more than the non-damaged state.

1. INTRODUCTION

To reduce earthquake disaster, it is important to grasp the failure mechanism of buildings against earthquake shocks and to establish seismic retrofit techniques as the practical countermeasure before such an earthquake attack. Moreover, repair and retrofit of damaged buildings should be considered to obtain total seismic safety. Therefore, it is necessary to establish techniques of repair and retrofit for continuous use of such damaged buildings.

In this paper, a test on repair and retrofit of such damaged buildings is described. A shaking table test, which is one of Dai-Dai-Toku Project, was carried out (Shirai 2005), employing 1/4 scaled and 4 storied reinforced concrete building models. One of the damaged test specimens was

[1] *Technical Research Institute, Obayashi Corporation, Kiyose, Tokyo, Japan*
Email: katsumata.hideo@obayashi.co.jp
[2] *Hyogo Earthquake Research Center, National Research Institute for Earth Science and Disaster Prevention, Miki, Hyogo, Japan (formerly, Technical Research Institute, Obayashi Corporation, Tokyo, Japan)*
Email: shirai@bosai.go.jp
[3] *Technical Research Institute, Obayashi Corporation, Kiyose, Tokyo, Japan*
[4] *Earthquake Research Institute, The University of Tokyo, Bunkyo, Tokyo, Japan*
Email: toshikazu@eri.u-tokyo.ac.jp
[5] *Earthquake Research Institute, The University of Tokyo, Bunkyo, Tokyo, Japan*
Email: kabe@eri.u-tokyo.ac.jp

repaired and retrofitted to be used for such a shaking table test as the original test, to discuss effectiveness of repair and retrofit techniques. The applied retrofit techniques are wall installation using precast concrete blocks or fiber reinforced plastic (FRP) blocks, addition of a steel frame with friction slip damper (FSD), and column jacketing with carbon fibers (Katsumata 2005).

It is noted that since these techniques are already applied for retrofit before an earthquake shock. Another aim of this study is to reflect obtained results to usual retrofit projects.

2. TEST METHOD

2.1 Specimen and Repair / Retrofit Method

The test specimen was a 1/4 scaled and 4 storied reinforced concrete building model and consisted of 3 bays for the X direction and 1 bay for the Y direction (Fig. 1 and Photo 1).

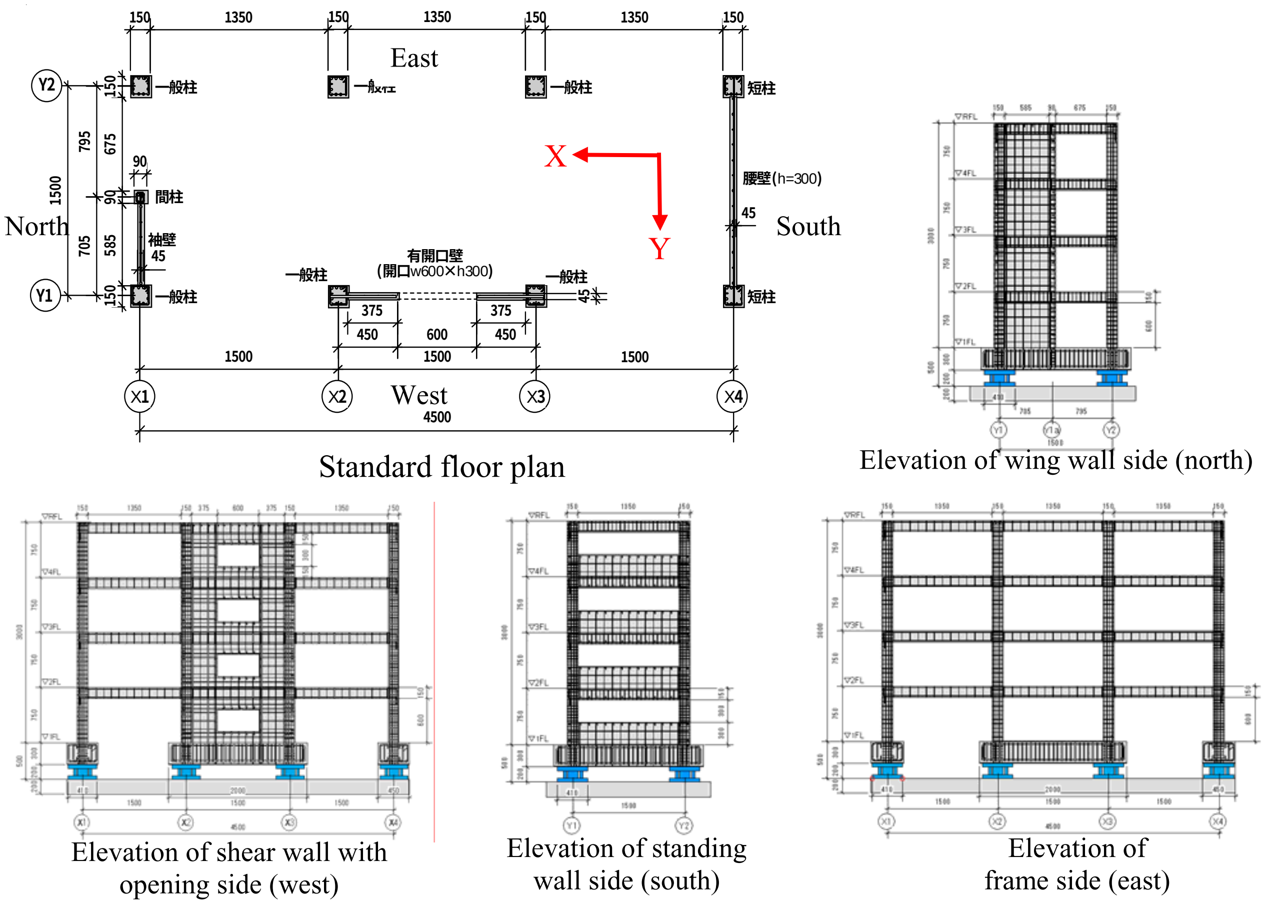

Figure 1 Plan and Elevation of Specimen Case 1 (Original)

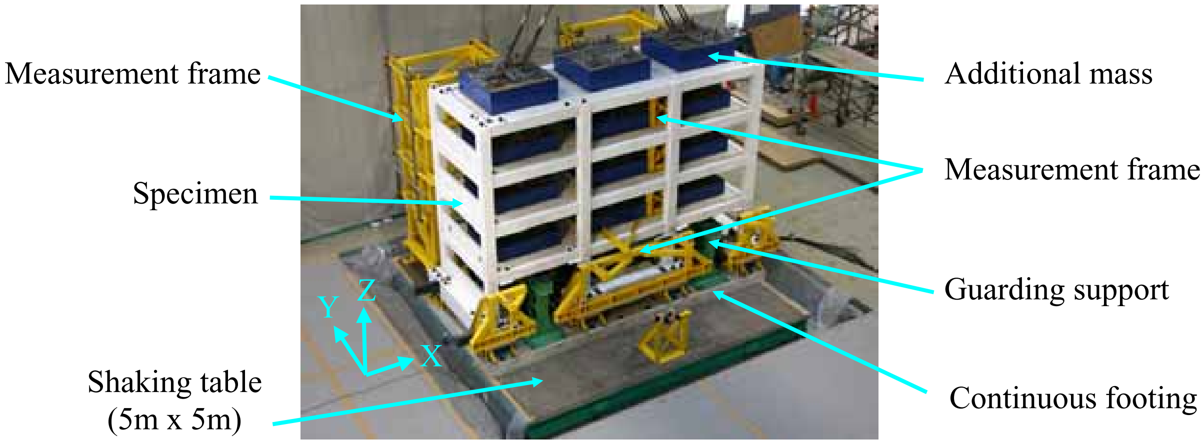

Photo 1 General View of the Specimen Case 1 (Original)

The major structural element for the X direction was a multi-story shear wall placed in the west frame. For the Y direction, the south outside frame consisted of short columns with standing walls and the north outside frame contained a multi-story wing wall. In the original shaking table test (Shirai 2005), the input ground motion was horizontally rotated so that the principal axis of the input was corresponding to the X direction of the specimen. The original test result showed heavy torsional vibration due to the failure of the standing walls and the eccentric wall arrangement. Although the major input direction was X, the south outside frame in the Y direction was heavily damaged as well as the multi-story wall in the X direction (Photo 2).

The employed repair and retrofit methods are shown in Fig. 2 and Photo 3. Considering constraints of practical retrofit works for actual buildings, retrofit methods and arrangement of such retrofit elements were determined.

West wall South frame

Photo 2 View after Test
(The Specimen Case 1 (Original))

Photo 3 View after Retrofit

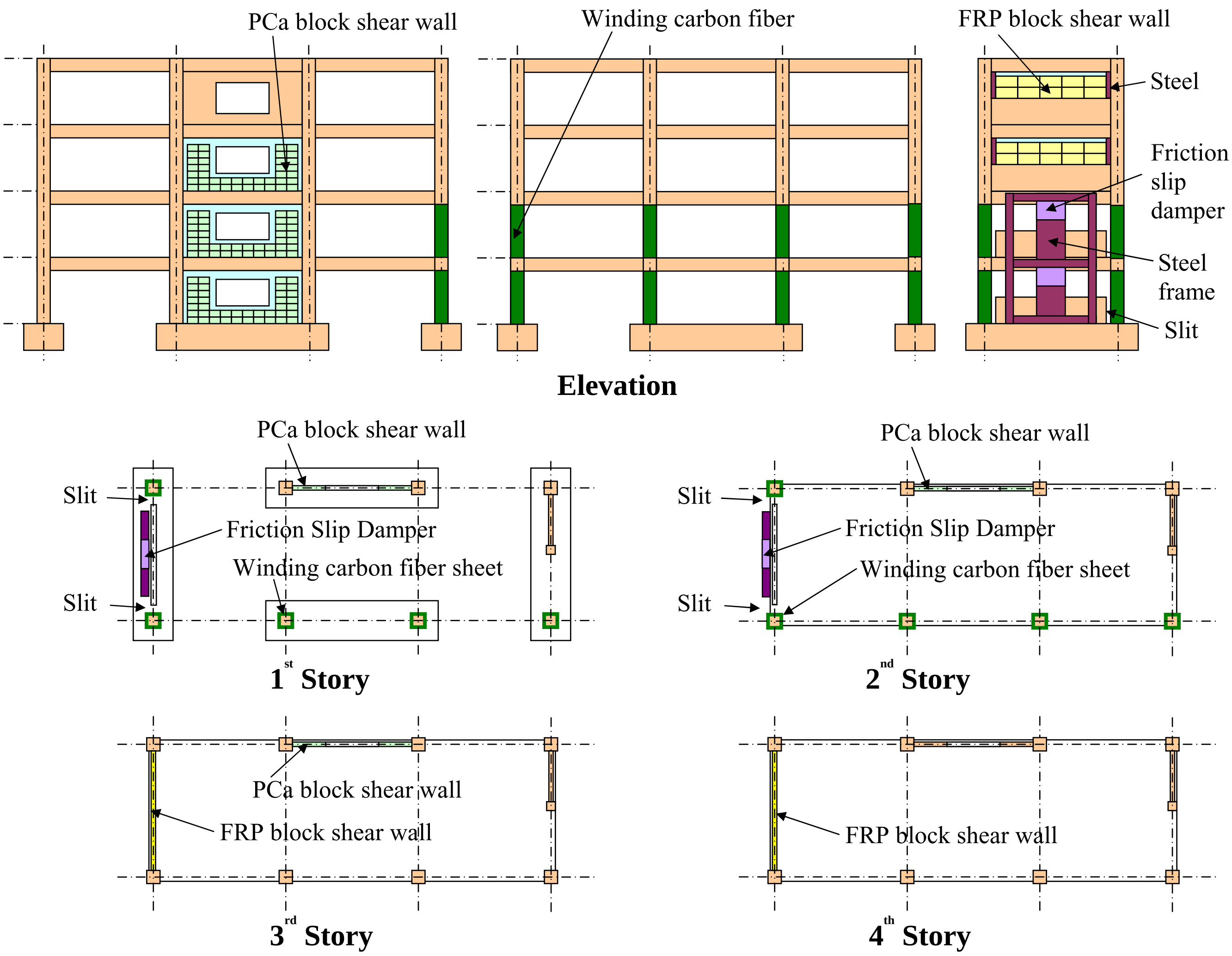

Figure 2 Outline of Retrofit

2.1.1 Repair

The following three methods were employed.

(1) For the small width cracks (crack width < 0.3mm), epoxy resin with very low viscosity was painted along the cracks. Dirt of this resin can be wiped out (Photo 4).

(2) For the large width cracks (crack width ≥ 0.3mm), epoxy resin was injected to the crack sealed by another type of resin under constant low pressure (Photo 5).

(3) For the crushed or heavily cracked concrete, such damaged concrete was removed and epoxy mortar was put to the broken part.

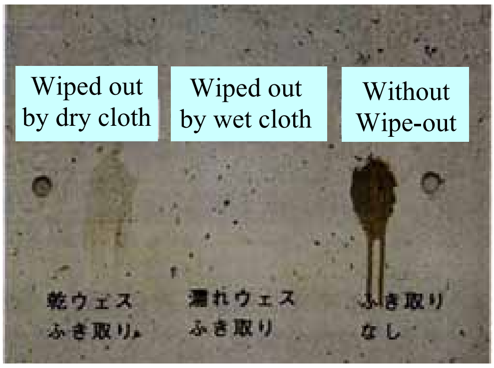

Photo 4 Wipe Out Test

Photo 5 Epoxy Injection

2.1.2 Installation of Precast Concrete Block Wall

The multi-story shear wall in the west frame was the lateral resisting elements for the major shaking direction. Since the 1st and 2nd stories of the wall were heavily damaged, the wall panels of these parts were removed and precast concrete block masonry walls (Photos 6 and Fig. 3) were installed to the removed portion. The 3rd story part of the wall was also retrofitted by the same manner to consider the continuity of the vertical direction.

This technique, called "3Q-Wall", saves construction time and makes no construction noise with good seismic performance, which are strongly required for retrofit of existing buildings in Japan. Details are shown elsewhere (Katsumata 2005 and Masuda 2004). This technique uses adhesive for connecting between blocks themselves or between block, guide steels and the existing concrete frame. The guide steel with welded bars is located between the concrete frame and precast blocks. The blocks are reinforced with bars. The void of blocks and the gap between guide steels and blocks are grouted with non-shrinkage mortar.

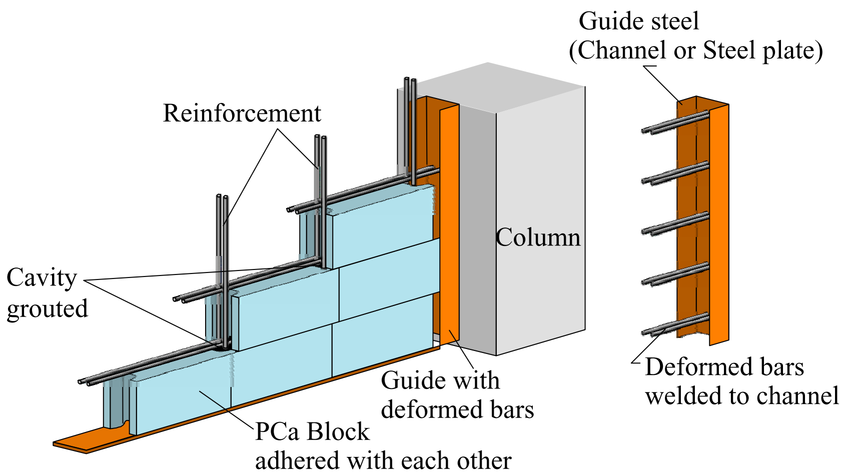

Figure 3 Conceptual View of 3Q Wall

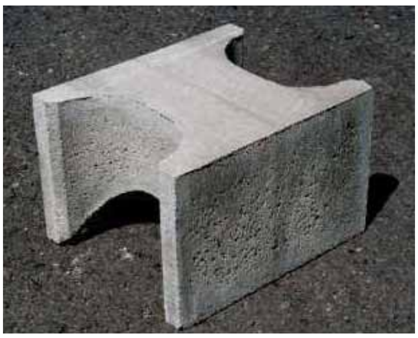

Photo 6 PCa Block Sample

Fig. 4 shows dimensions and block arrangement. The wall thickness was increased from 45mm of the original to 75mm of the new. However, past test results show that stiffness and strength of the wall is slightly decreased from that of monolithic walls. Generally speaking, the crack repairing is seldom successful in contributing the recovery of building stiffness, so stiffness of the specimen was estimated to be almost same as the original. The strength of the wall was determined by bending capacity, that is, longitudinal bar area of the wall side columns which were not retrofitted. Thus, strength of the specimen was considered to be almost same as the original. However, shear strength of the wall was increased up to 1.4 times of the original, so ductility of the wall was improved.

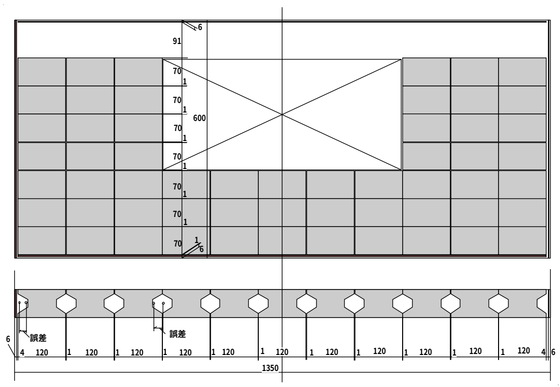

PCa Block

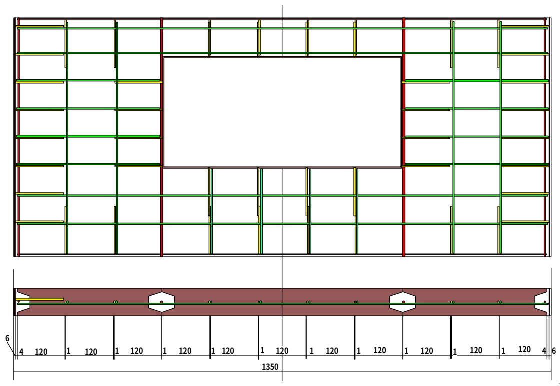

Reinforcing Bar and Guide Steel Plate

Figure 4 Arrangement of PCa Block Masonry Wall (1st – 3rd Story)

2.1.2 Addition of Outside Steel Frame with Friction Slip Damper

Damage of the south frame was heavy due to the failure of standing walls. Especially, the short columns in the 1st and 2nd stories and the beam end portions of the 2nd floor suffered much damage. From this result, it was determined to provide stable bearing capacity. The both ends of standing wall of the 1st and 2nd floor were removed to form structural slits. And also, a steel frame with friction slip damper (FSD) was added outside the south frame (Fig. 5). This method is preferable because construction area is located outside buildings and building occupancy was not disturbed. The steel frame consisted of the central column, outside columns and connecting beams. Diagonal brace was not applied because Japanese building clients did not like such diagonal members.

To the central column of the steel frame, the FSD called Brake Damper (Sano 2001) was installed. This FSD is one of vibration control devices and consists of friction slip materials (brake pad), disc springs, a high strength bolt, and so on (Fig. 6 and Photo 7). The disc springs, which have geometric nonlinearity, can keep the tension of the bolt constant under an adequate use. The friction slip material is the same type for brake pad of automobiles and has constant and stable friction coefficient between this pad and stainless plate. Consequently, this FSD shows and keeps ideal friction hysteresis behaviour for a long term.

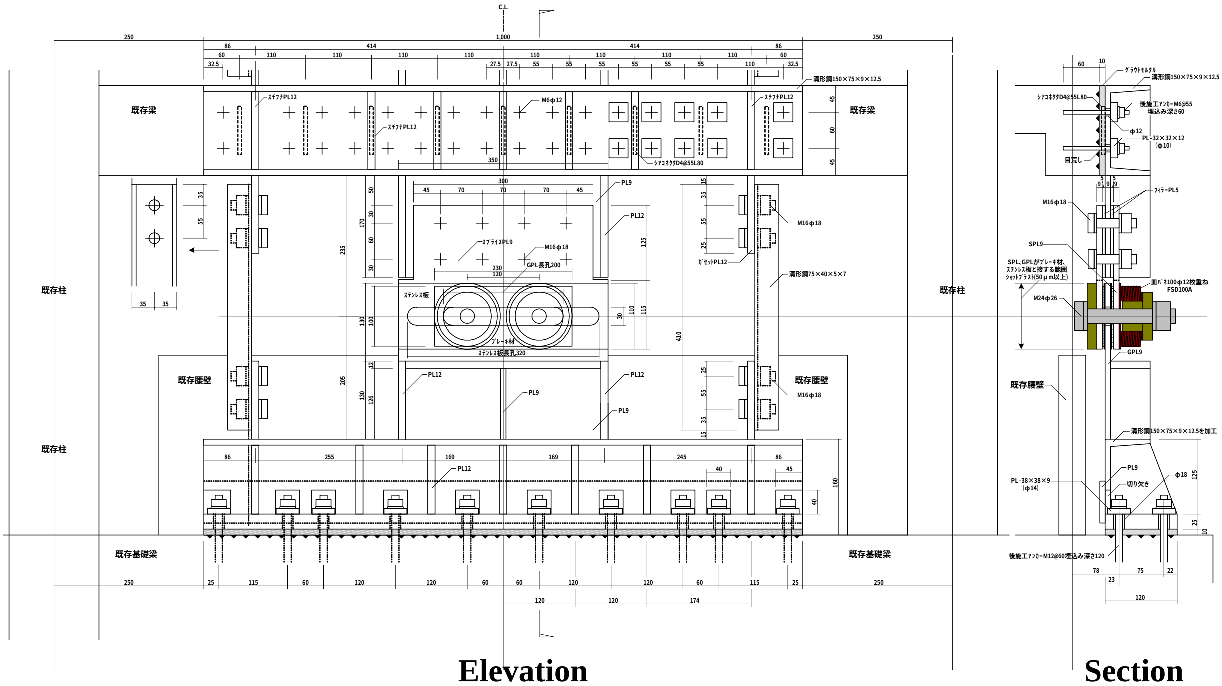

Figure 5 Detail of Friction Damper (1st Story)

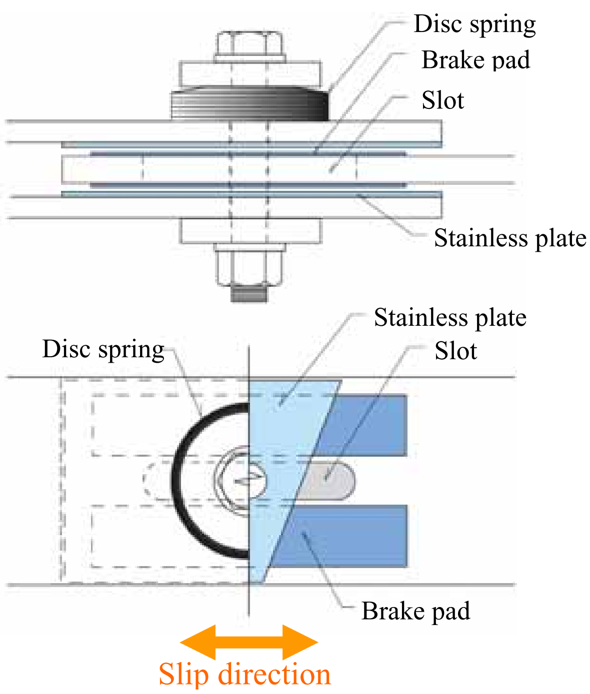

Figure 6 Conceptual View

Photo 7 Example of Friction Slip Damper

The outside columns of the steel frame (see Fig. 5) resisted the overturning moment induced by shear force of the central column. The existing beam ends were heavily broken and were considered not to resist the large shear from the overturning moment though the beams were repaired. Since the steel frame was eccentrically fixed outside the existing concrete frame, stress state of the joint part between the steel and concrete frames was severe. Therefore, sufficient amount of adhesive anchors was provided to the joint to transfer shear and tension. Moreover, shear keys were provided for the steel beam and the concrete surface of the existing frame was roughened.

2.1.4 Installation of FRP Block Masonry Wall

Damage of the 3rd and 4th stories of the south frame was slight, that is, stress state of these parts was mild. Therefore, FRP block masonry walls (Katsumata 2005, Sugimoto 2003, and Hagio 2003) were constructed on the standing wall of the 3rd and 4th stories (Fig. 7).

The FRP block does not have high strength, however, the FRP blocks passed light and wind, which is appreciated in the architectural side. An FRP masonry wall and blocks are illustrated in Fig. 8 and Photo 8. Construction procedure of the FRP block masonry walls is almost same as precast concrete block masonry. However, mortar grout is not employed and into the gap between blocks and an existing frame, connecting steel materials are inserted.

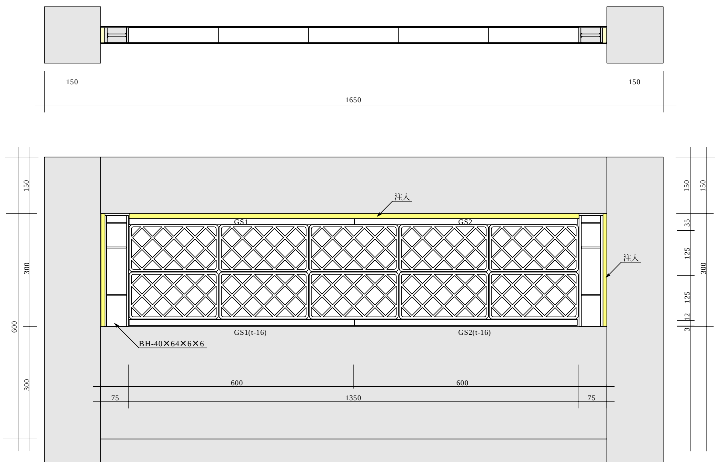

Figure 7 Retrofit Portion of GFRP Block Shear Wall (4th Story)

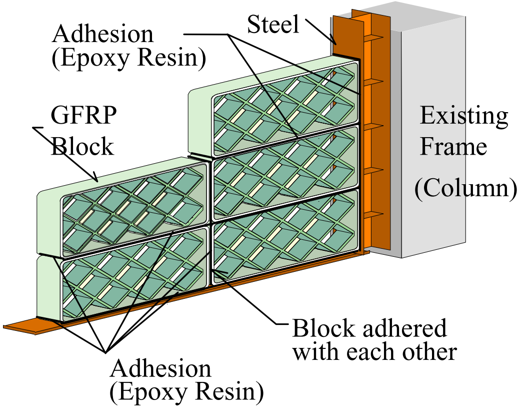

Figure 8 Conceptual View of FRP masonry

Photo 8 GFRP Block Sample

2.1.5 CFRP Jacketing

To the east and the north frames, any new wall and column was not connected, assuming an actual retrofit condition that an open frame is preferred.

However, the columns in the 1st and 2nd stories, except for the side columns of walls, were retrofitted by carbon fiber jacketing (Katsumata 2005) because of heavy or medium damage during the original test. Retrofit detail is shown in Figs. 9 and 10. Carbon fiber jacketing is superior to steel plate jacketing due to low cost and easy handling. The carbon fibers sheets are employed usually in Japan. The sheet was impregnated with epoxy resin and cured on site. The jacket of the cured CFRP (Carbon Fiber Reinforced Plastic) improves shear strength and ductility. It is required to make round corners of the column section by chamfering.

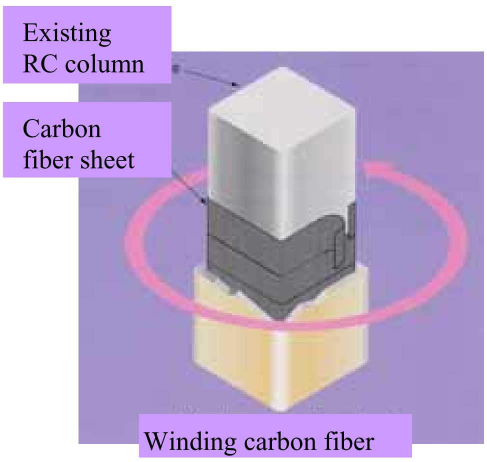

Figure 9 Conceptual View of CFRP Jacketing

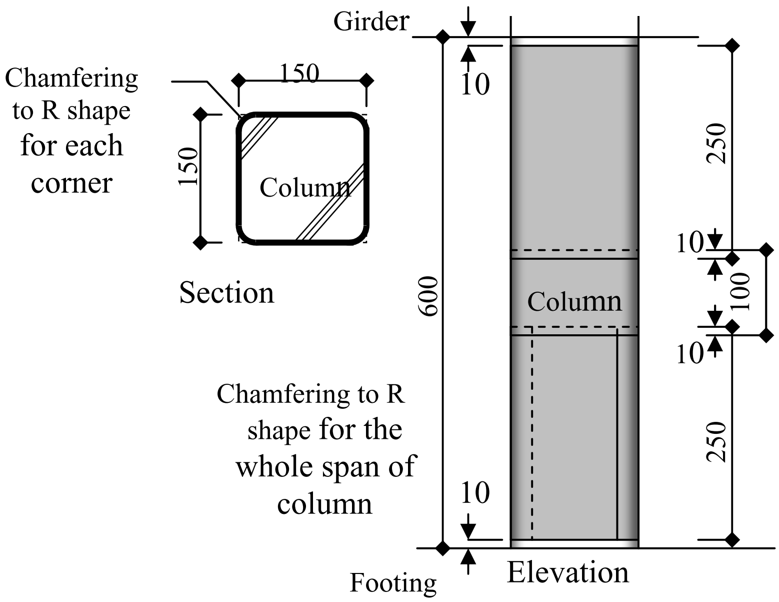

Figure 10 Column Jacketing Detail (1st –2nd Story)

2.2 Shaking Program

The shaking program was almost same as the original test. Detail is shown in the companion paper (Shirai 2005). The shaking table of Obayashi Corporation was employed for tri-axial and simultaneous shaking and the input ground motion was JMA Kobe 1995. However, the input was horizontally rotated so that the principal axis of the input was corresponding to the X direction of the specimen (Fig. 11). The amplitude of the input was gradually enlarged for each shaking run from 20 to 150 % of the original wave. Time scale of the input was reduced to 1/2 of the original wave due to the 1/4 scaled specimen. For the last run, the time scale was slightly extended to 1/2 x 1.22, aiming to collapse the specimen. The period of specimen was elongated by damage propagation and it was necessary for realizing the collapse to tune the frequency characteristics of the input motion.

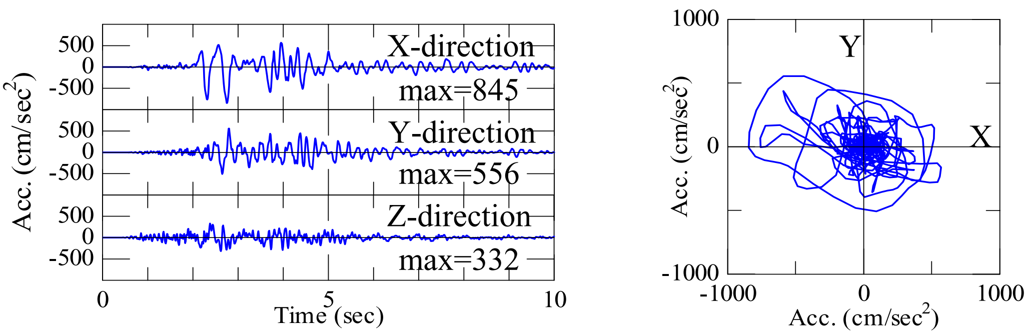

Time history of acceleration   Orbit of horizontal acceleration

Figure 11 Input Motions

3. TEST RESULT

3.1 Outline of Shaking

Summary of each shaking run is shown in Table 1.

For the small level input, the response deformation of the retrofit specimen was almost same as the original one although the wall thickness was increased. This is because that epoxy resin was not completely fulfilled in all cracks. Cracks applied with the painting method, which is developed for upgrading durability, opened again. However, cracks applied with injection method did not open. This repair method was suitable for a structural purpose.

For the large level input, the response deformation of the retrofit specimen was smaller than the original one. The damage, especially of the south frame, was also slight. For the 125% input, the original specimen reached ultimate range however the retrofitted specimen still remained in a usable range. For the larger inputs, namely 150% and 150%-2, the retrofitted specimen reached ultimate state and collapsed, respectively. Since the retrofitted specimen resisted the larger input, it is summarized that the employed retrofit methods were effective to improve seismic performance.

Table 1 Comparison of Shaking Process

Run	Input ratio*1	Case1 (Original)		Case3 (Retrofitted)	
		R_W*3	Remarkable damage	R_W*3	Remarkable damage
Run1	5%	1/8500	—	1/11000	—
Run2	20%	1/1550	Crack at shear wall with opening and standing wall	1/1700	Crack at PCa block shear wall
Run3	40%	1/615	Crack at shear wall with opening	1/605	Crack at wing wall
Run4	60%	1/381	Crack at shear wall with opening	1/355	Shear crack at wing wall
Run5	80%	1/209	Yielding of vertical bar at shear wall with opening	1/204	Crack at PCa block shear wall and wing wall
Run6	100%	1/124	Failure at standing wall end	1/107	Crack at standing wall
Run7	125%	1/32	Shear failure at shear wall with opening	1/51	Large crack between GFRP block and standing wall
Run8	150%			1/17	Shear failure at PCa block shear wall
Run9	150%*2			1/11	Shear failure at wing wall

*1 Magnification factor of input motion
*2 Drift angel at shear wall with opening, 1st story, X-direction (rad.)
*3 Time axis of input motion was extended 1.22 times

3.2 Damage in final stage

Damage diagrams of the original and retrofitted specimens are compared in Fig. 12. The final collapsing view is shown in Photo 9.

Weak-beam-strong-column mechanism was observed for the retrofitted test, as the original test. The final input of the original test was the 125% input and the wall of the west frame was crushed and heavy damage of the deep beams with standing walls and the short columns in the south frame was observed. However the retrofitted specimen was damaged in the walls of the west and north frames for the same 125% input, damage level was not so severe.

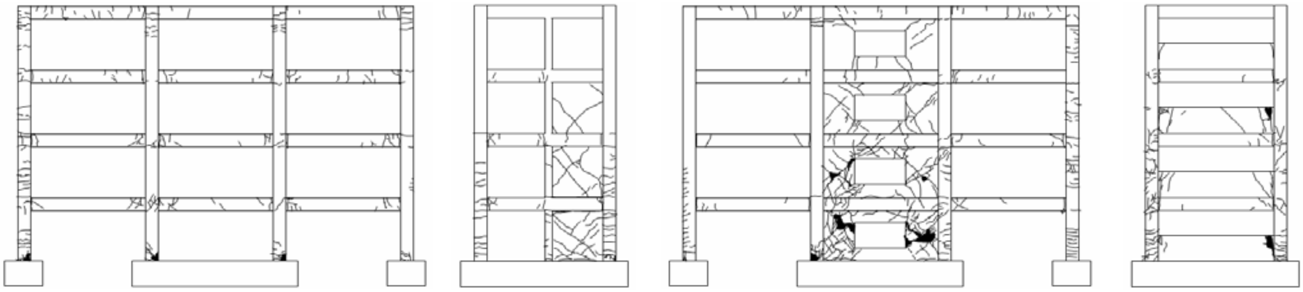

Case 1 (Original) Run7 (125% input)

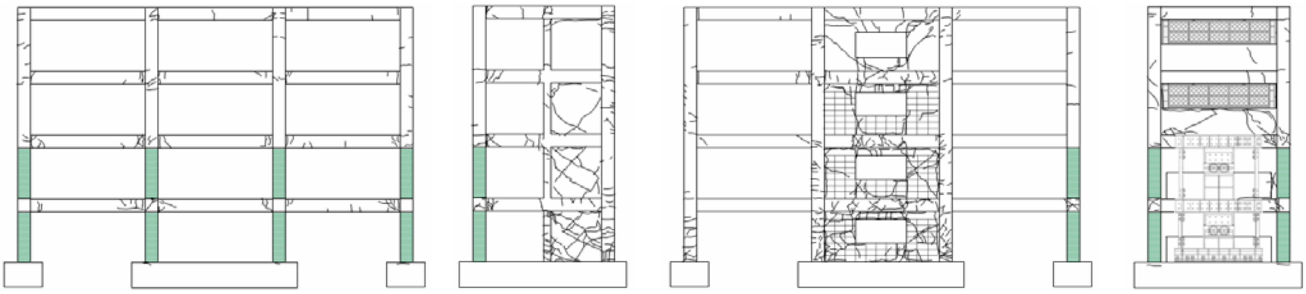

Case 3 (Retrofitted) Run7 (125% input)

Figure 12 Comparison of Damage in the Same Input Level

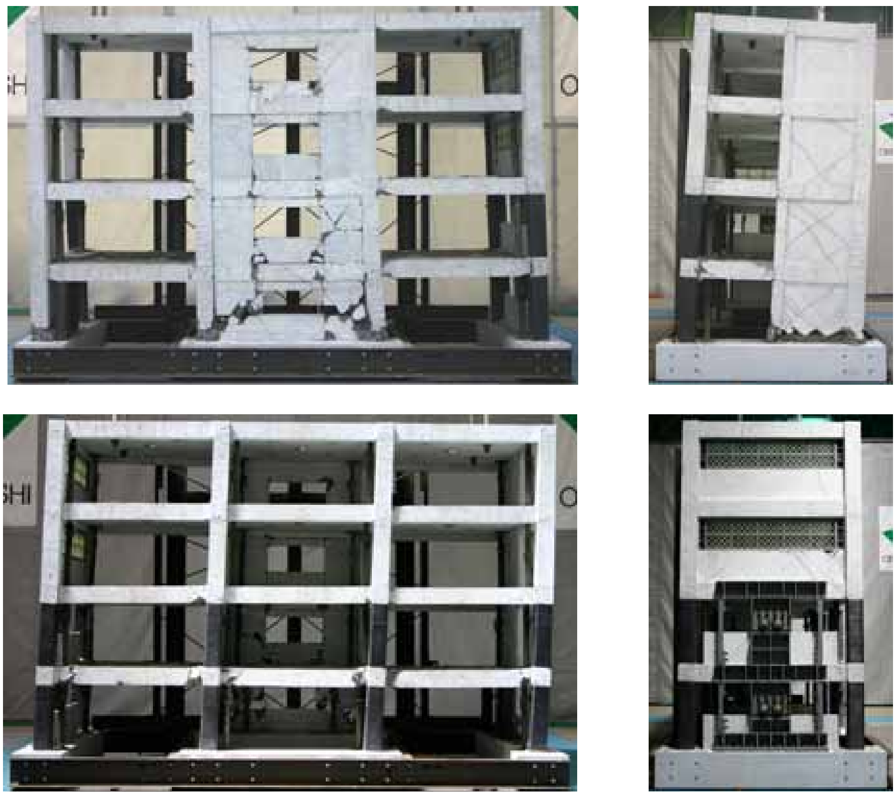

Photo 9 Final View of Case 3 (Retrofitted) (Run9 150% Input-2)

For the 150% input to the retrofitted specimen, damage was observed in the beams and the standing and hanging walls between wall openings in the precast block wall. This damage was a general problem for multi-story walls with openings located regularly, which is a future task to be considered in a structural design. The side column of the wall in the north frame was slightly crushed. This is because that the input of the north frame was increased due to the retrofit of the south frame. In the last run, the unretrofitted columns adjacent to walls in the west and north area were collapsed and this induced failure of the retrofitting precast concrete block masonry wall. The retrofitted columns by CFRP jacketing did not have damage, except for the bending cracks of the end regions. This shows that the column retrofit gives high safety margin. An alternative is considered that all beams and columns adjacent to walls are strengthened, however this concept does not seem practical. It is thought that this range of retrofit for this model is the best.

For example, a tentative damage analysis of the original and retrofitting tests is shown in Fig. 13. The damage was evaluated from a push-over analysis with 3-dimensional frame models and a prediction technique of crack propagation and width (Katsumata 2005 and Sugimoto 2004). Such a software "DREAM 3D" developed by Obayashi Corporation was employed. Heavily damaged potions of the analysis were almost similar to that of the test although there were still some differences. To improve the analytical precision is one of future works.

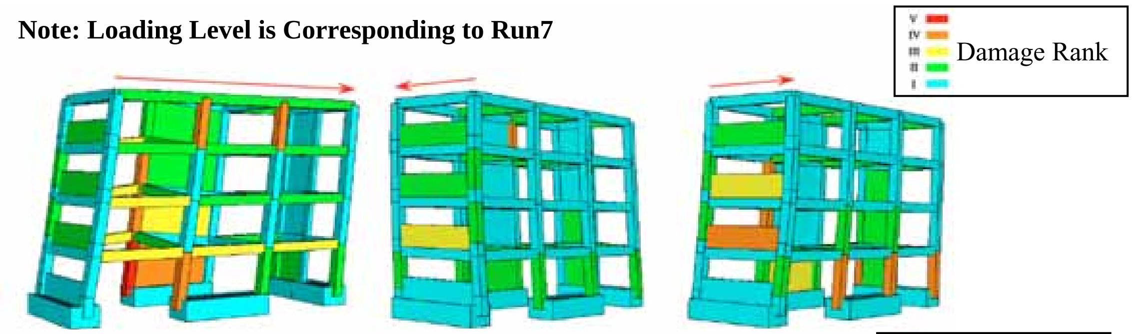

Case1 (Original)

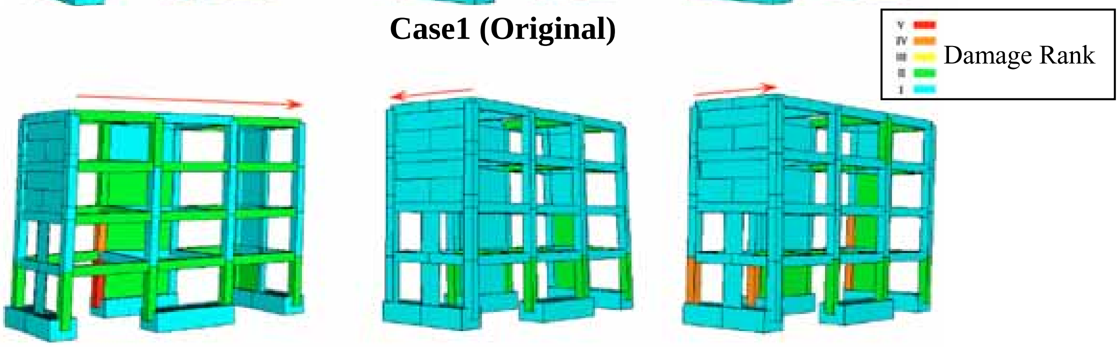

Case3 (Retrofitted)

Figure 13 Example of Damage Evaluation by Push-Over Analysis

3.3 Response of Shear Force and Deformation

Hysteresis loops of the 1st story are shown in Fig. 14. The retrofitted specimen showed yielding in the 100% input and stable plastic deformation in the 125% input. This shows that the employed methods had good behaviour. Each contribution was still unknown though the reaction forces from the table were measured. This may be one of future tasks.

In Fig. 14, a result of push-over analysis of the test structure is also shown. A single directional and monotonic loading was employed. The analysis shows that the bending capacity of members (beams, columns, and walls) was critical and that the load of the test was higher than the analytical loading capacity. It is pointed out that the material strengths of the analysis were acquired from the test piece and may be conservative, considering strain hardening of reinforcing bars experienced during the original test. The reinforcing bar strength strongly influenced on the bending capacity.

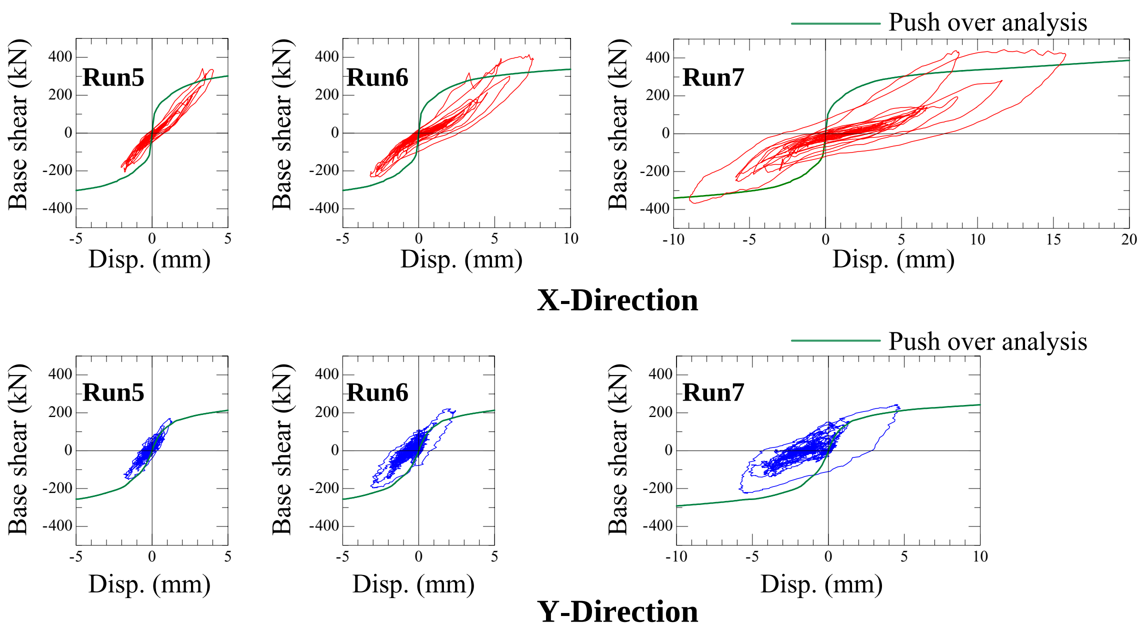

Figure14 Base Shear – 1st Story Displacement Relationship of Case3 (Retrofitted)

The skelton curves of the original and retrofitted specimens are compared in Fig. 15. The maximum shear of the retrofitted specimen was larger than the original one. This reason may be strain hardening of existing reinforcement, especially, in the side columns which governed the strength of walls and the strength of the building model.

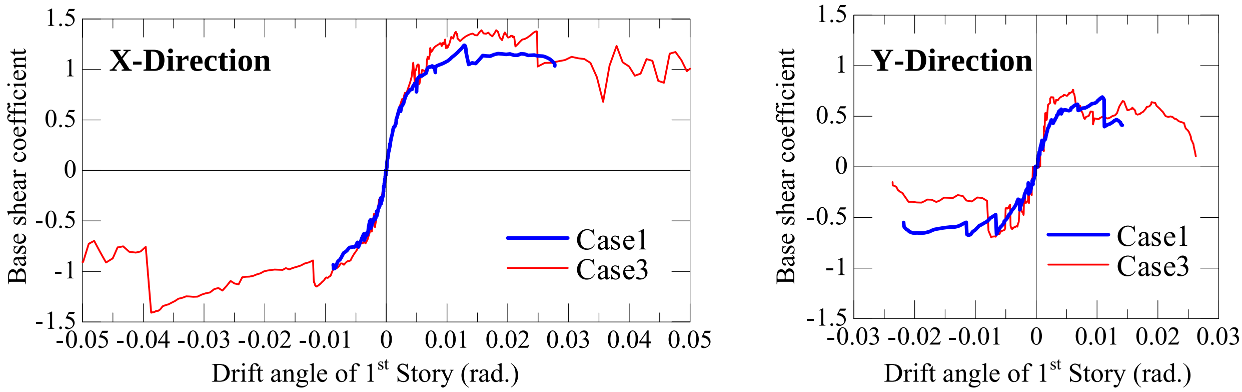

Note: case 1 = original, case 3 = retrofitted

Figure 15 Comparison of Skelton Curve

Orbit loops of displacement of the 1st story are compared in Fig. 16. The major vibration direction of the original was the Y direction however the retrofitted one was the X direction. This shows that the retrofit by the steel frame for the Y direction was effective for reduction of translation and torsional vibration by upgrading of stiffness and strength of the building model.

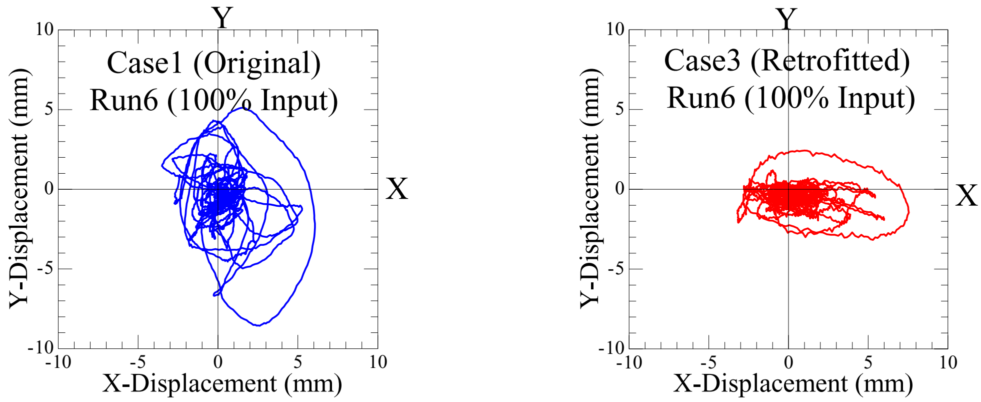

Figure 16 Comparison of X-Y Orbit of 1st Story Displacement in the Same Input Level

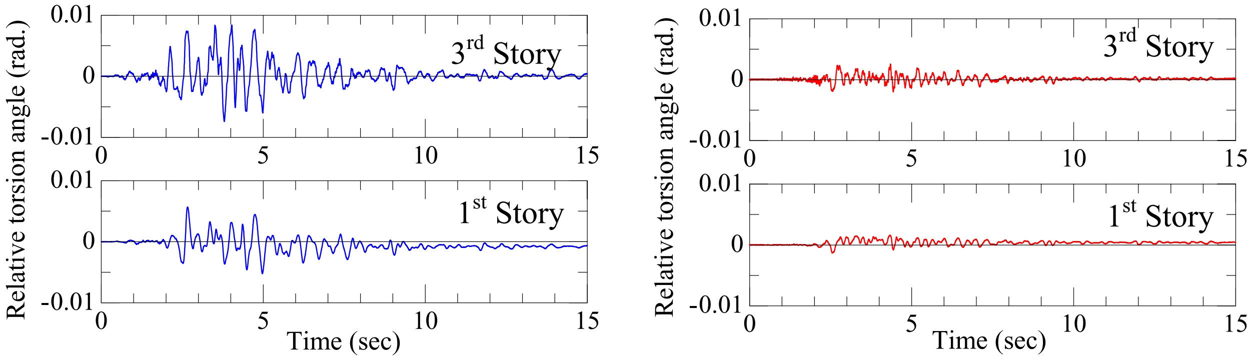

Case1 (Original) Run7 (125% Input) Case3 (Retrofitted) Run7 (125% Input)

Figure 17 Comparison of Relative Torsion Angle in Same Input Level

The torsional deformation was clearly reduced by retrofit as shown in Fig. 17. The steel frame with FSD in the 1st story was useful as mentioned below and the FRP block masonry wall in the 3rd story was also effective for retrofit.

The assumed hysteresis loop of the FSD is shown in Fig. 18. The vertical axis indicates shear force of the 1st story of the south frame from measurement of reaction forces, and is not the load acting FSD itself. However, this graph provides information on behaviour of the FSD. It is found that the FSD made slip deformation in the large shaking stage and absorbed vibration energy. However, the FSD deformation was smaller than the one expected before the test.

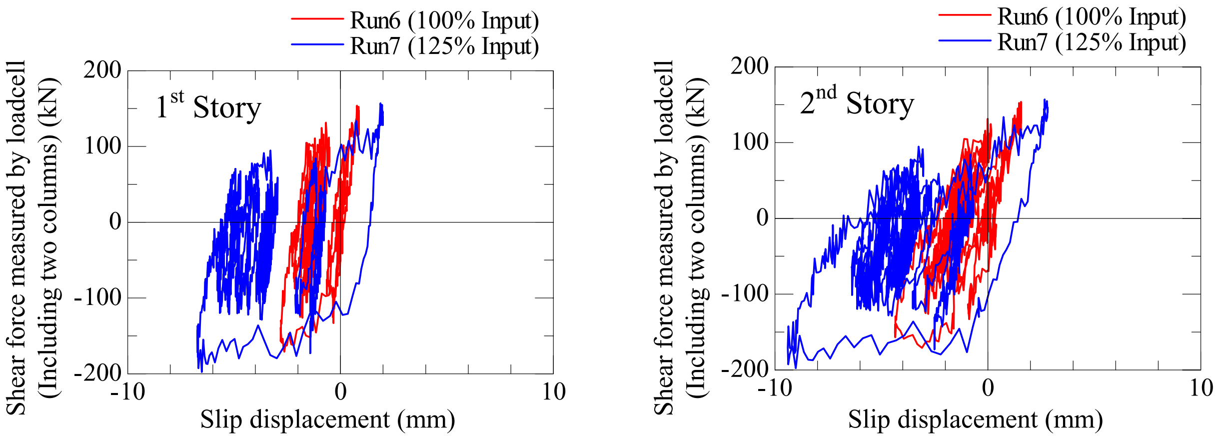

Figure 18 P-D Loops of Friction Slip Damper (Run6 and 7)

Maximum responses in each shaking run are shown Fig. 19. Generally, the retrofitted one was smaller than the original one. The south frame responses were quite different by retrofit and the south response was smaller than the north response. Considering this response distribution and the damage distribution mentioned before, an alternative design can be proposed that the strength of the south frame is reduced to increase in deformation of the south frame and decrease in deformation of the north frame. The reason is that the south frame was expected to have stable behaviour by the retrofitting FSD. However, this design concept on damage and response distribution should be discussed strictly because the input direction may influence the behaviour of the buildings.

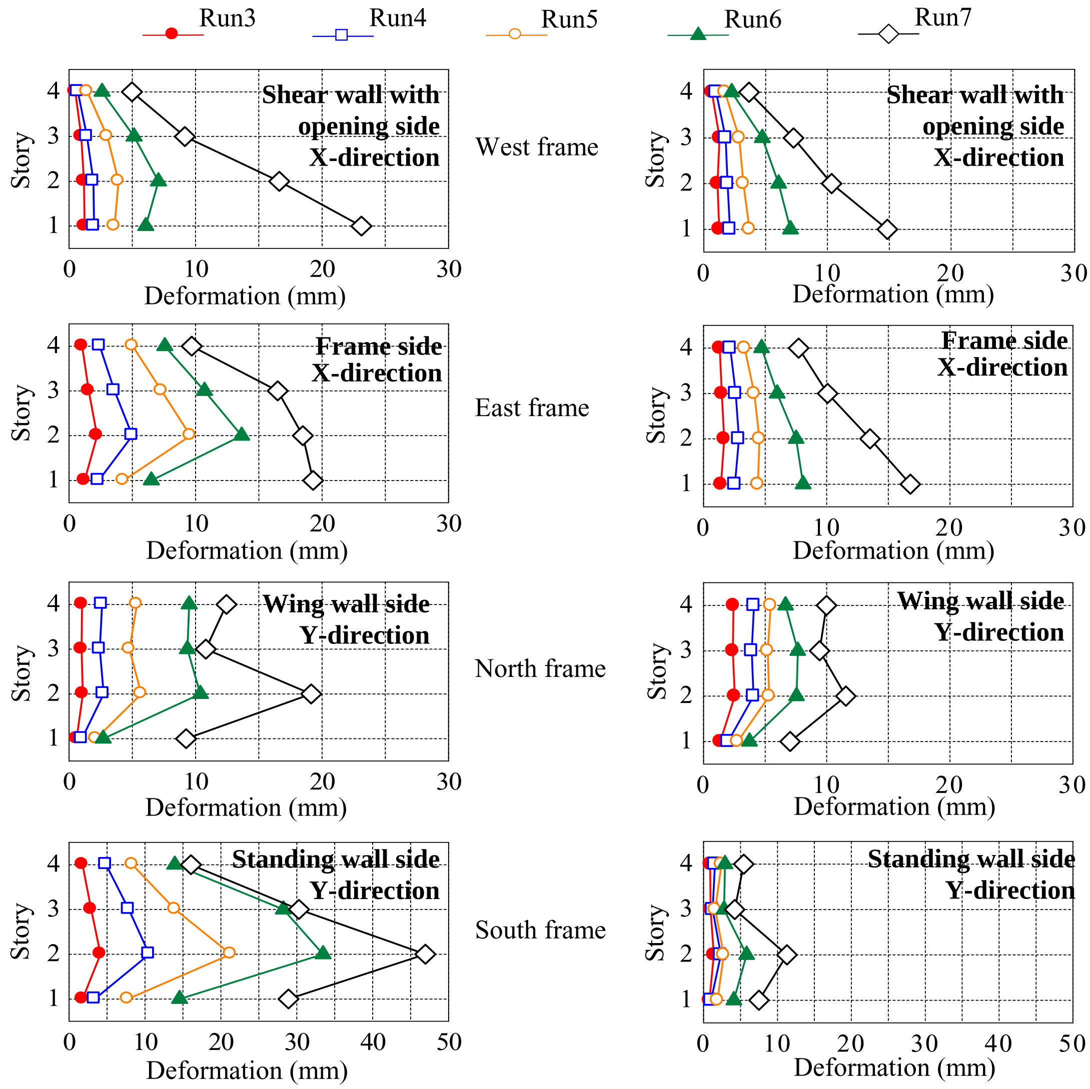

Case 1 (Original) **Case 3 (Retrofitted)**

Figure 19 Comparison of Maximum Response

4. SUMMARY

Employing the 4 storied reinforced concrete building model damaged by a previous shaking table test, a test on repair and retrofit was carried out through shaking table. The building specimen was retrofitted by precast concrete and FRP block masonry walls, a steel frame with friction slip dampers, and carbon fiber jacketing of column. The retrofitted specimen did not fail against the larger input than the original test. The torsional response was distinguished in the original test however it was reduced by adequate resisting elements (friction slip damper) in the perpendicular direction. The model collapsed finally induced by the failure of unretrofitted columns adjacent to walls. It can be said that retrofit elements had sufficient strength and ductility.

In the future, there are many problems to be solved, for example, emergency strengthening just after an earthquake shock, residual seismic performance of damaged buildings, and retrofit before an earthquake shock.

5. ACKOWLEDGEMENT

The authors express their acknowledgement for the offer of the tested specimen of Dai-Dai-Toku Project from National Research Institute for Earth Science and Disaster Prevention.

6. REFERENCE

Hagio, H., Sugimoto, K., Okuda, A., Kurita, K., Masuda, Y., Kimura, K., Itohiya, G., and Tazawa, H. (2003). An Experimental Study on Shear Walls Constructed by Laying GFRP Blocks into Existing Rigid Frames. *Proc. 8th Japan International SAMPE Symposium*, 2:1269-1273

Katsumata, H., Masuda, Y., and Tsuda, K. (2005). Development of Practical and Advanced Techniques of Performance Evaluation and Retrofit of Existing Reinforced Concrete Buildings. *ISEE Kobe 2005*

Masuda, Y., Hagio, H., Kurita, K., Kimura, K., Miura, K. and Yamamoto, S. (2004). Development of Low Noise and Low Shake Retrofitting Method “3Q-Wall”. *Report, Technical Research Institute, Obayashi Corporation*, 68 (in Japanese).

Sano, T., Suzui, Y., Hino, Y., and Takahashi, Y. (2001). Development of Friction Slip Damper using High Strength Bolts – Experiment on Brake Damper and Application to Building-. *Report, Technical Research Institute, Obayashi Corporation*, 62:13-20 (in Japanese)

Shirai, K., Katsumata, H., Kabeyasawa, T., and Kabeyaswa, T. (2005). Tri-Axial Shaking Table Test on Reinforced Concrete Buildings with Large Eccentricity. *The First NEES-EDEFENSE Workshop*

Sugimoto, K., Hagio, H., Okuda, A., Kurita, K., Masuda, Y., Kimura, K., Furuyama, N., Itohiya, G., and Tazawa, H. (2003). An Experimental Study on Shear Walls Constructed by Laying Concrete or GFRP Blocks into Existing Rigid Frames. *STRUCTURAL FAULTS and REPAIR 2003*, ECS Publications

Sugimoto, K., Tsuda, K., Nagahara, K., Kashiwase, T., Eto, H., Ichikawa, K. and Kawabata, T. (2004). Performance Evaluation Method for Reinforced Concrete Buildings. *Proceeding of 13WCEE*, 1137

7. KEYWORDS

Shaking table test, repair, retrofit, concrete block masonry wall, FRP block masonry wall, friction slip damper, carbon fiber jacketing, torsional deformation, response reduction

SESSION 8: PERFORMANCE OF EXISTING BUILDINGS

Chaired by

♦ John Wallace and Jun Tagami ♦

IN-SITU TEST OF SCHOOL BUILDING STRUCTURE IN TAIWAN

Yi-Hsuan TU,[1] Wu-Wei KUO,[2] and Shyh-Jiann HWANG[3]

ABSTRACT

The 1999 Chi-Chi earthquake revealed the poor performance of the RC school buildings in Taiwan. It also indicated an urgent need for the seismic evaluation and retrofit of the remaining schools. In order to realize the behavior of a typical school building subjected to lateral load, an in-situ test for an existing 2-story school building was carried out. Two experiments were conducted: a static pushover test to identify the strength, stiffness and toughness of the building, and a vertical load test to study the vertical load-carrying mechanism after failure of some members. In the static pushover test, a 6-classroom building constructed in 1964 was cut in the middle where a jack was set for monotonic loading along the longer axis of the building. One half of this building was reinforced by steel bracings to provide reaction support, while the other half was pushed to failure. The vertical load test employed only one of the classrooms. Inner columns of 1F of the classroom were cut off in the middle to simulate that they failed prior due to the short-column effect. The remaining frames with thick brick in-filled walls as partitions were expected to carry the weight of and prevent collapse. Water was added into two tanks set at the 2F and RF slabs as vertical loading. Results of these tests are reported, analyzed and interpreted in this paper.

INTRODUCTION

In Taiwan, many typical school buildings suffered severe damage by the Chi-Chi earthquake, 1999. Most of old school buildings were designed according to a standard plan that is functional for getting natural light and ventilation. The typical plan has all the openings and a corridor in the longitudinal direction and many partition walls in the transverse direction. Some common failure patterns were found because of the typical type of school buildings, such as failure in the longitudinal direction due to lack of walls, short-column effect due to constrain by windowsills, and strong-beam-weak-column effect due to non-ductile reinforcement and slabs that connect with the beams. For preventing possible damage in the future, it is urgent to develop the seismic assessment and retrofit technology for the existing schools. Although there are already some assessment methods developed by international researchers, usually they are verified by small-scale or partial structural assemblages but not full-scale structure. It is still questionable that if test results in the laboratory can represent the true behavior of actual buildings. Therefore, an in-situ pushover test of an existing school building is carried out for realizing the real structural behavior.

---

[1] *Post-doctoral research fellow of National Center for Research on Earthquake Engineering*
[2] Ph.D. *candidate of National Taiwan University of Science and Technology*
[3] *Professor of National Taiwan University of Science and Technology Division Head of National Center for Research on Earthquake Engineering*

Indebted to the Hualien County Government and Hsin-Cheng junior high school, the research team composed of crews of the National Center for Research on Earthquake Engineering (NCREE), the National Taiwan University of Science and Technology (NTUST), the Dahan Institute of Technology (DHIT) and the National Taiwan University (NTU) were allowed to use an old school building that is about to be demolished as the subject of pushover test. Except for providing verification for seismic assessment and retrofit technology, this test also gives further understanding of seismic ability of existing school buildings.

DESCRIPTION OF THE TEST

The site plan of Hsin-Cheng junior high school is shown in Figure 1. The specimen is one of the buildings parallel to each other. The building with 2 floors contains 6 classrooms and a hallway in the middle. Longitudinal axis of the building is in North-South direction. The oldest part of the test building was originally built in 1966. Its main structure is made of reinforced concrete (RC), but the partitions and windowsills are made of 1-brick-thick brick walls. The building had no visible damage before the test, as shown in Figure 2.

There are two primary tests: pushover test and vertical load test, prepared and executed from January 20th to 29th, 2005. The north half of the building was used as the specimen of pushover test. After the pushover test, one classroom of the south half was then used as the specimen of vertical load test. Details of description of the two tests are as below.

PUSHOVER TEST

Test Description

Figure 3 shows the layout of the pushover test. Three classrooms at the north half of the subject building was cut apart from the south half to be pushed over. Figure 4 shows the structural plan of the specimen. Each 10m wide classroom is consist of 3 spans, lies along the longitudinal direction. About half of the columns in B-frame and all the columns in D-frame have 90-110cm high windowsills that usually cause the short-column effect besides them. Short-column effect happens because the column constrained by windowsills that were not considered in design, effective height of the column is then shortened and cause larger shear stress or even shear failure. However, since the specimen is higher (1F: 3.9m, 2F: 3.6m) then ordinary school building, the effects of short columns here are not really severe.

Three 150t and three 300t hydraulic actuators were set at the cut beam end of A, B, and D frames of 1F and 2F, respectively. They were designed to push the specimen in its weak axis. Behind the actuators, 2 spans of the south classroom were reinforced by added steel bracings to provide reacting support. Figure 5 shows the actuator and steel bracings.

During the test, the actuators were controlled through their cylinder areas to keep the loading put on 1F and 2F being 1:2, which is the proportion of lateral load distributed by the fundamental mode. The loading was monotonic, but in every 0.05% drift, the actuators were hold for 15-20 minutes, so that the staff can mark cracks and record the damage condition. The specimen was loaded until it's strength descended to 67% of the maximum strength. For preventing doing any harm to the neighbor in the north side and safety of the staff, two steel supports were set in the classrooms in 1F to prevent complete collapse of the specimen.

Instrumentations for story displacement, member rotation, and shear deformation at beam-column joints were set. Figure 6 shows the position of primary displacement gauges, they were set at both side of specimen and actuators in case of the reacting part moves contrarily.

Test Results

Figure 7 shows the final scene of the specimen at a roof drift ratio of about 4%. However, most deformation happened at 1F, while the 2F seemed remain undamaged, so the drift ratio at 1F was actually nearly 8%. Figure 8 shows the pushover curve of the specimen. The maximum base shear P is 2915kN when the roof displacement Δ_2 reached 150mm. Some indentations showed when the actuators were hold for recording damages, however the shape of curve is still smooth and shows very good ductility.

As shown in Figure 7, the normal columns at A-frame obviously failed by flexural bending and concrete at the compressive side crushed. Other normal columns in B-frame showed the same failure pattern. Otherwise, the short columns mostly failed by both bending and shear. Both horizontal and diagonal cracks showed in these columns' ends, as shown in Figure 9. The diagonal cracks caused by shear stress show that the short-column effect did happened. While all of the columns had failed, the beams and slab still remained almost undamaged. This phenomenon, so-called strong-beam-weak-column, was also found in those school buildings damaged by the Chi-Chi earthquake.

Strengths of the materials sampled from different height of columns were found to be scattered and irregular. The average compressive strengths of concrete are 23.3MPa in 2F and 21.8MPa in 1F, while yielding strength of steels are distributed between 314 and 480MPa.

VERTICAL LOAD TEST

Test Description

Objective of vertical load test is to know that if a school building still has vertical sustainability after the prior failure of short columns. So as shown in Figure 10(a), a classroom of the south half of the subject building was chosen to be the specimen. Six inner columns were cut off in the middle, and the other 6 ones with the partitions were left to simulate the situation that part of columns has been failed by short-column effect. The vertical load is supposed to be carried by the beams and passed on to the remaining partition walls and columns, as shown in Figure 10(b).

Two tanks were set on top of 1F and 2F, where water would be added as vertical loading. A draw-line gauge was set under the center of 1F slab to measure its sag.

Test Results

It took two days to fill the tanks, but even though the two tanks were both filled, beams and slab of 1F were only slight cracked, as shown in Figure 11. Most cracks closed after unloaded; apparently the steels in them still remained elastic. Figure 12 shows the progress of loading and sag of 1F slab. Because of errors in water line reading, the curve is not very smooth. But it's clear that loading at 2F top has less influence on the sag of 1F slab then loading at 1F top does, probably due to the participation of 2F beams and columns. The specimen sustained 105 tons of extra loads, which are about 1.5 times of its self-weight. The test result shows that brick partition walls may be a useful support against vertical failure.

COMPARISON OF TEST RESULTS AND ANALYTICAL METHOD

An analytical method, simplified pushover method (Tu 2004), is employed to calculate the analytical pushover curve for comparison with test result. This method was developed according to the strong-beam-weak-column behavior of typical low-rise RC buildings in Taiwan. Base on the behavior, it is assumed that the beam and slab are rigid and seldom fail. So the structure deforms like a shear building, and the story shear strength is provided by vertical members only, as shown in Figure 13. Since a rigid slab means all the vertical members connected to the slab must have a common deflection at the same time, the story shear can be obtained by superposing shear forces of every vertical member at a certain deflection. Then, by assuming that the vertical distribution of horizontal load and shear building deformation, base shear and roof displacement can be get.

Figure 14 shows the comparison between test and analytical result. The analytical prediction about failure mode of columns corresponds with the test result. But the analytical pushover curve obviously underestimates the strength and stiffness of the specimen. A possible reason of the error is the out-of-plane contribution by the partition brick walls. As shown in Figure 15, the brick partition walls connected to the columns tightly and seemed provide some out-of-plane strength. But the out-of-plane behavior of brick wall still remains to be studied.

CONCLUSIONS

In-situ test provides a precious chance to realize the behavior of a real building and to verify the analytical methods. The pushover test result confirmed the damaging behavior of school buildings observed in the Chi-Chi earthquake. Typical failing characteristics of school buildings, such as short-column effect and strong-beam-weak-column behavior, did happen to the specimen. The experimental pushover curve shows well ductility and strength more than expected. An analytical method is compared to the test result and shows conservative outcome. The vertical load test result shows that beam and slab are strong enough to sustain the vertical load after part of columns failed and pass the load on to the remaining partition frames. Results of the two tests show that the brick partition walls might be able to provide not only vertical support but also out-of-plane strength.

Further research subjects would include study on out-of-plane behavior of brick walls, retrofit measures for resisting horizontal and vertical loads, and improving the analytical method.

ACKNOWLEDGMENTS

The authors appreciate the National Science Council and Ministry of Education for sponsoring the test, the Hualien County Government, and Hsin-Cheng junior high school for providing so much help, and the staff and students from NCREE, NTUST, DHIT and NTU for their contributions.

REFERENCE

Tu, Y. H.(2004). “Shaking Table Test and Seismic Analysis of RC School Building Structures,” Ph.D. dissertation, National Cheng-Kung University, Tainan, Taiwan.

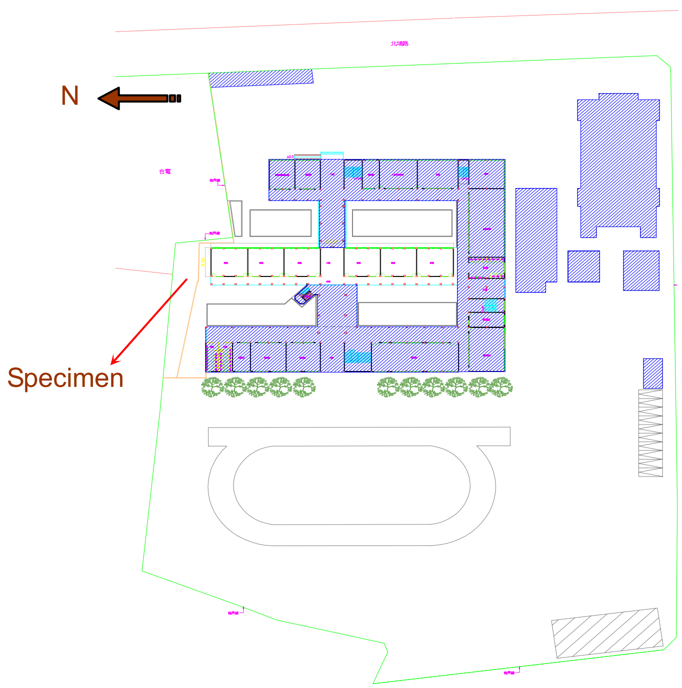

Fig. 1: Site plan of Hsin-Cheng Junior High School, Hualien

Fig. 2: Pictures of the subject building

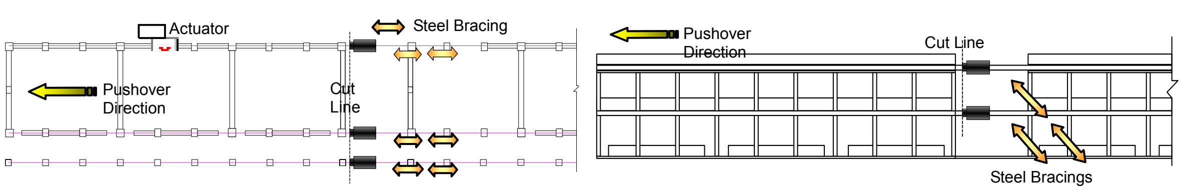

(a) Plan (b) Elevation

Fig. 3: Test layout

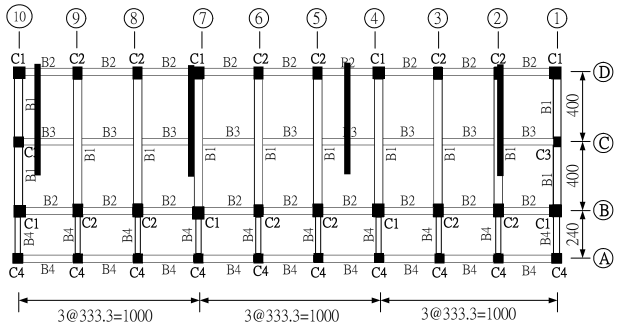

Fig. 4: Structural plan of the specimen of pushover test

(a) Set up of actuator

(b) Steel bracings

Fig. 5: Actuator and steel bracings

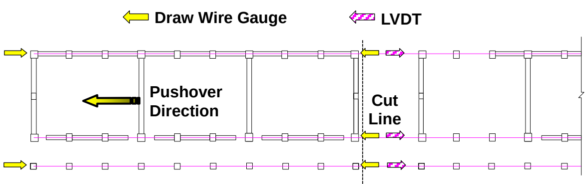

(a) Plan

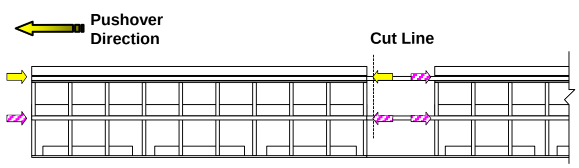

(b) Elevation

Fig. 6: Layout of instrumentation

Fig. 7: Specimen: after the test

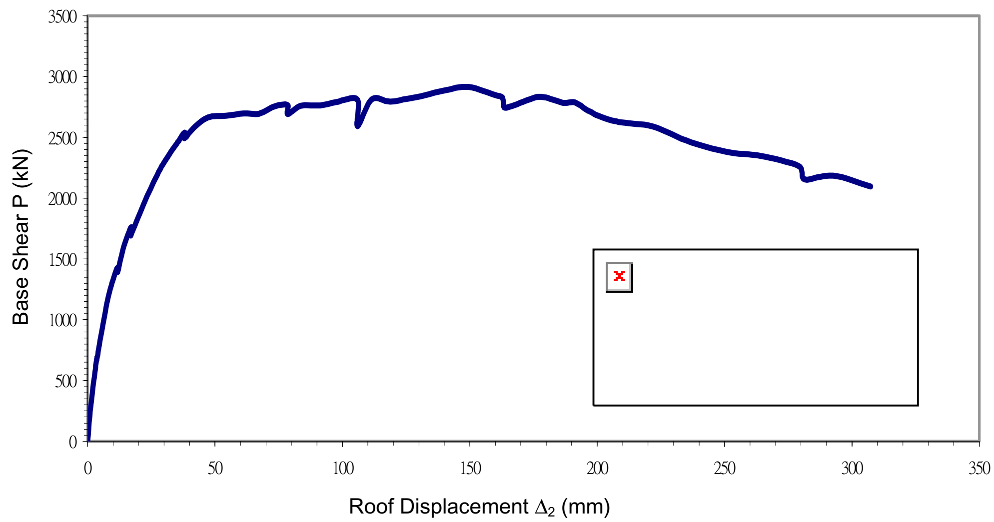

Fig. 8: Pushover curve of the specimen

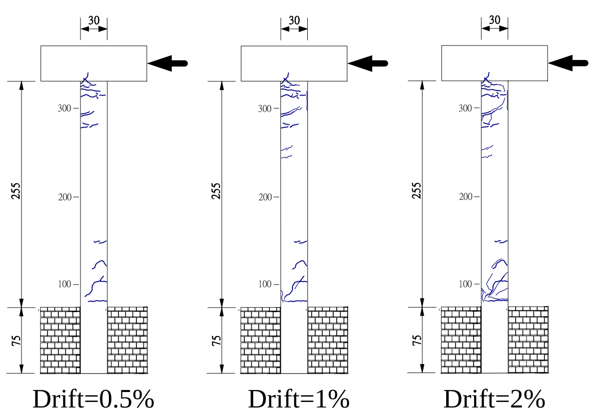

(a) Crack development

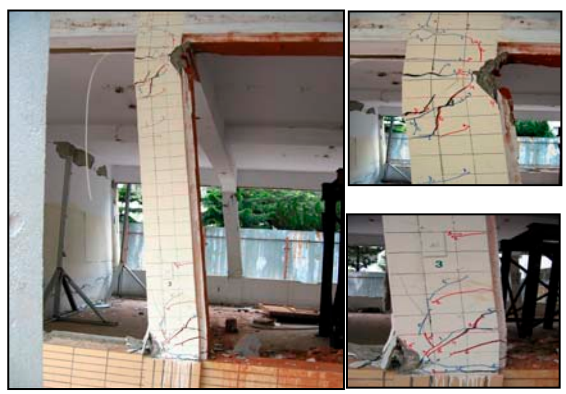

(b) Picture of final stage

Fig. 9: Column failed by bending-shear

(a) Specimen

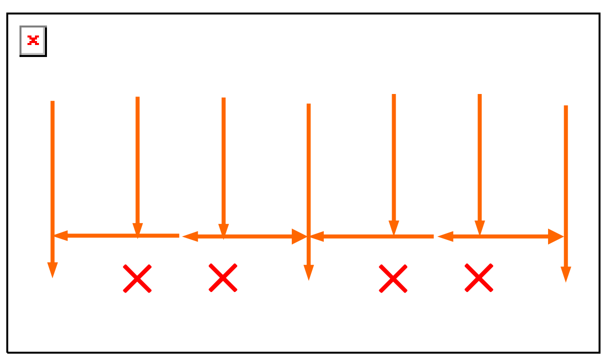

(b) Expected vertical stress flow

Fig. 10: Vertical load test

Fig. 11: Cracked beams after the vertical load test

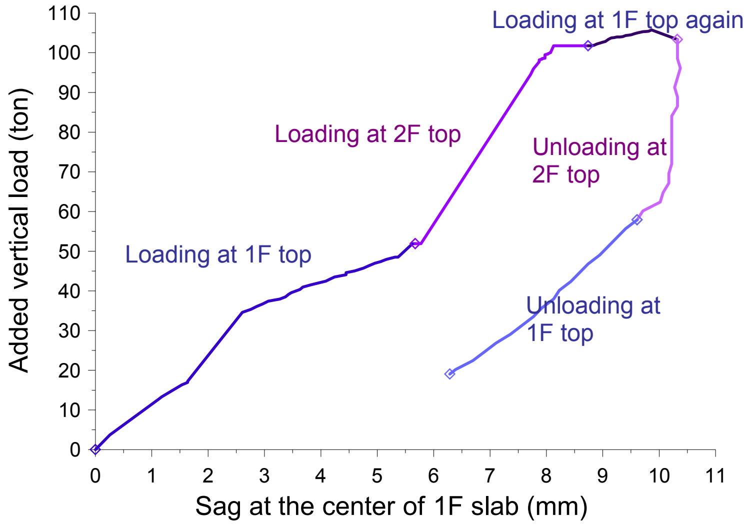

Fig. 12: Relationship between vertical loading and sag at the center of 1F slab

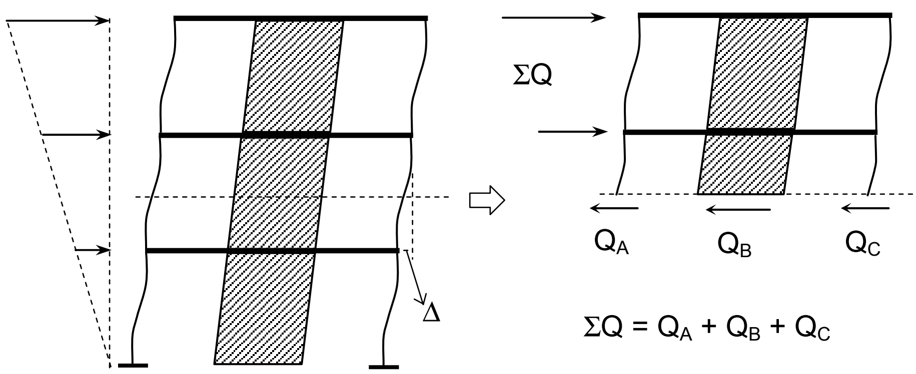

Fig. 13: Concept of calculation story shear by simplified pushover method

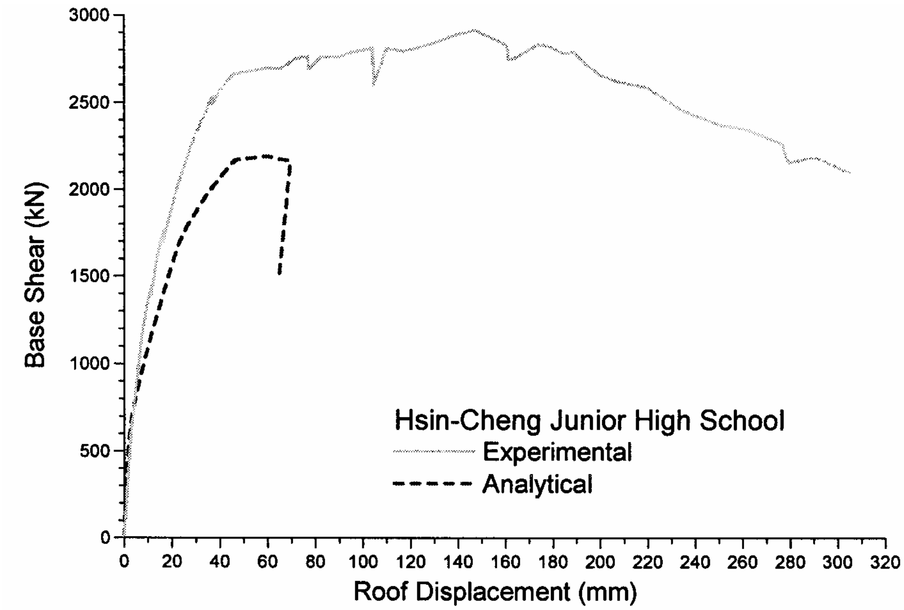

Fig. 14: Comparison of test and analytical pushover curve

Fig. 15: Brick partition wall deflected in out-of-plane direction

PERFORMANCE OF SCHOOL BUILDINGS IN TURKEY DURING THE 1999 DÜZCE AND THE 2003 BINGÖL EARTHQUAKES

Turel GUR[1], Ali Cihan PAY[1], Julio A. RAMIREZ[1], Mete A. SOZEN[1], Arvid M. JOHNSON[2]

ABSTRACT

Teams of researchers from various institutions and organizations in the USA led by Purdue University (USA) in collaboration with researchers from the Middle East Technical University (Turkey) made two surveys of damage to concrete structures in the cities of Düzce, Kaynaşlı and Bolu following the 1999 Marmara (M_w=7.4) and Düzce (M_w=7.2) earthquakes and in Bingöl and its vicinity after the 2003 earthquake (M_w=6.4) in Turkey. The 1999 earthquakes devastated northwestern Turkey. The 2003 event damaged mostly the eastern province of Bingöl. The full reports of these surveys, including geological, geotechnical and structural observations in detail, are available at www.anatolianquake.org. The combined building inventory after the surveys in Turkey includes 35 school and dormitory buildings. This paper focuses on the findings of the survey of 21 of these buildings with the same floor plan developed by the Ministry of Education of Turkey.

1. DAMAGE RATING

The damage ratings (Table 1) are based on the condition of the ground story of the buildings. With the exception of building D02, if damage occurred, the ground story showed the largest extent. The damage to the reinforced concrete structures was rated using a three-level system.

- SEVERE DAMAGE: Structures containing columns with inclined cracks. We note that inclined cracking in columns represents severe damage if the amount of transverse reinforcement is light. Observations in the field as well as information obtained from typical structural plans indicated that 8-mm bars with yield strength of 220 MPa were used commonly for transverse reinforcement. The tie spacing in the columns was typically 200 to 250 mm. In some school buildings, the tie spacing was observed to be reduced to 100 to 120 mm at the end regions.
- MODERATE DAMAGE: Structures with shear and flexure cracks on beams, spalling of concrete on columns and hairline cracks in shear walls.
- LIGHT DAMAGE: Damage limited to hairline flexural cracks in the beams.

The damage to masonry infill walls, composed of hollow bricks, was also rated using a three level system:

---

[1] *School of Civil Engineering, Purdue University, 550 Stadium Mall Drive, W. Lafayette IN 47907*
[2] *School of Earth and Atmospheric Sciences, Purdue University*

- SEVERE DAMAGE: continuous cracking at boundaries, loss or crushing of masonry units (Fig.1).
- MODERATE DAMAGE: fine cracks in walls and at boundaries with flaking of large pieces of plaster (Fig. 2).
- LIGHT DAMAGE: hairline cracks on plaster and at boundaries.

2. SEISMIC CONDITIONS AT THE SCHOOL SITES

2.1 Strong Motions

The November 12, 1999 Düzce earthquake was associated with a 40-km surface rupture running in the east-west direction. The ground motion was recorded at stations in Düzce and Bolu. The peak horizontal components of the records are listed in Table 2. There was no strong motion record available for Kaynasli, which is located at the eastern end of the surface rupture. The strong-motion station in Bingöl recorded the May 1, 2003 earthquake. The peak horizontal components of the record are included in Table 2 as well. The displacement spectrum of all three records for 2% of critical damping is given in Figure 3. Comparison of the displacement spectra obtained from the records shows it is plausible to state that buildings in Bingöl were not subjected to a ground motion with higher displacement demand than those in Düzce and Bolu.

2.2 Ground Conditions

The results of the team's investigation of soil and rock foundation materials at the school sites in the Bingöl area suggest that differences in damage to school buildings from place to place in Bingöl due to the 1 May 2003 earthquake were a result of characteristics of the structures, not of foundation conditions or gross ground deformation. The soil and granular alluvial deposits are quite uniform and the distance between the epicenter of the main shock and the schools is similar. The shaking should have been reasonably uniform throughout Bingöl. Düzce and Bolu in NW Anatolia and Bingöl in SE Anatolia are all in Pleistocene basins. Most of the school sites of our study were on valley fill. The ground conditions in all school sites would be expected to be similar.

3. STRUCTURAL PROPERTIES OF THE SCHOOL BUILDINGS AND THEIR DAMAGED STATES

3.1 Schools with Moment-Resisting Frames

Eleven of the schools with moment-resisting frames were in and around Bingöl. The number of stories of the buildings ranged from 2 to 4. A typical column layout of these buildings is seen in Figure 4. The lateral load resisting system in these buildings can be categorized as regular in plan. The majority of the columns were aligned in regular bays, and most of the beams framed into columns. The dimensions of the columns in the buildings were typically 0.3 x 0.5 m. The typical dimensions of the beams are 0.3 x 0.7 m. The locations of the masonry infill walls varied depending on the use of the space in each school. The masonry infill was typically thicker in exterior walls than in interior walls. The thickness of the masonry infill, including the plaster, was estimated to be 0.25 m and 0.38 m, respectively, for interior and exterior walls.

The total column area of buildings where the lateral load resisting system consisted only of moment-resisting frames was approximately 1% of the floor area, regardless of the number of floors. Consequently, the performance of these structures during the earthquake was influenced significantly by the number of floors. The level of damage assigned to the lateral load resisting system with respect to the number of floors was categorized as follows:

- 4 two-story school buildings: 3 were moderately damaged and 1 lightly damaged
- 11 three-story school buildings: 3 collapsed, 6 were severely damaged and 2 were moderately damaged
- 1 four-story school building: It was severely damaged.

The columns of all three collapsed buildings appeared to have failed in shear (Fig. 5). Figure 6 reveals the extent of the shear damage on the columns in one of the severely damaged buildings (C14-01).

Damage to the masonry walls was rated separately. The three- and four-story buildings typically sustained severe masonry wall damage (Table 3).

3.2 Schools with Dual Systems

Of the five school buildings with dual systems, three are in Düzce, one in Bolu and one in Kaynasli. The buildings have the same floor plan as the buildings of Bingöl with moment-resisting frames except that two bays in each orthogonal direction are occupied by reinforced concrete walls. The thickness of these walls was established to be 0.2 m. The total concrete wall area is 0.4% of the floor area in the long direction and 0.5% in the short direction of the building. The buildings range from two-story to four-story.

The most severely damaged dual system was one of the four-story buildings (D02) in Düzce (Fig. 7). Its damage was concentrated at the half-buried basement surrounded by earth-retaining concrete walls. These walls do not cover the full height from the floor to the ceiling of the basement. There are windows between the earth-retaining walls and the beams of the basement. The exterior columns in the basement, that were captive along their weak axis because of the windows next to them, failed in shear (Fig. 8). Neither the columns of the other stories nor the shear walls suffered any damage. There were moderately damaged masonry infill walls in the basement. Unlike the other buildings, the damage rating of building D02 was based on the damage state of the basement rather than of the ground floor. The ground floor and the other floors did not suffer severe damage to the structural or non-structural components.

The columns of the rest of the dual-system buildings had no visible damage. The structural system of the other four-story building (D03) in Düzce was rated to be lightly damaged because of the damage to its beams. The masonry walls of building D03 were moderately damaged. There was no damage observed to the structural and nonstructural elements of the two-story school buildings (D01 and K01) in Düzce and Kaynasli and the three-story school building (B01) in Bolu. Building K01 was only 50 m away from (south of) the main surface rupture of the Düzce earthquake.

4. DAMAGE COMPARISON

One of the most significant structural deficiencies observed commonly in the school buildings was the presence of captive columns formed by openings for the small windows in the masonry infill walls by the columns. There were at least two captive columns adjacent to the windows in the bathrooms and around the stairwells in all the schools. In addition, in seven of the schools in

Bingöl, there was a furnace room on the ground floor level where the small windows increased the number of captive columns from 2 to 8.

The observed difference in the performance of the dual systems and that of the moment-resisting frame systems is not to be attributed to defects arising from construction quality. The construction quality was quite uniform in all the buildings. There were also common detailing problems. The ends of the transverse reinforcement were typically not anchored in the concrete core. "Sufficient confinement" was not observed in the end regions of the columns.

Comparison of the performance of the dual and moment-resisting systems during the earthquakes has been organized on the basis of number of stories in the buildings:

- *Two-story buildings:* The two structures with dual systems showed no signs of visible damage. The moment-resisting frame structures survived without any damage to their columns. The displacement demand on these structures by the earthquakes was not high enough to damage the captive columns and the masonry walls severely. The masonry walls remained intact and contributed to the stiffness of the structures. In buildings C13-07 and C14-06 there was moderate damage to the walls.
- *Three- and four-story buildings:* The three dual-system structures suffered almost no damage to their concrete structural walls. Of the three buildings, only building D02 was rated as severely damaged. Unlike the other buildings in the inventory, building D02 suffered damage to its basement. The exterior columns in the basement were captive columns due to the discontinuity of the concrete earth-retaining walls, which did not extend the full height of the columns. The structural walls prevented collapse. The columns above the basement level were not damaged. Of the twelve schools with moment-resisting frames, ten of them were either severely damaged or collapsed. Only two survived without any damage to the columns. The displacement demand was high enough to result in severe damage to the masonry infill walls. The damage to the masonry walls appears to have affected the structural response in two ways: (1) The stiffness of the system was reduced, and (2) Crumbling of the masonry at the wall corners resulted in additional captive columns.

5. CONCLUSIONS

The damage survey of the school buildings in two earthquake areas in Turkey has re-emphasized a well-known principle of earthquake-resistant design. The collapse of multistory, non-ductile reinforced concrete moment-resisting frame buildings with hollow-brick infill walls, which are typical of construction throughout Turkey, can be prevented by including a few properly-located structural walls.

The performance of the buildings with moment-resisting frames only seemed to be correlated with the number of floors in the buildings because the column size is uniform in all the schools. The two-story buildings could survive the earthquake without any damage to their columns. The three- and the four-story buildings, however, did not perform satisfactorily. Of the 12 buildings with three stories or higher, ten buildings suffered shear damage to their columns. Three of them collapsed because of the columns failed in shear.

The efficacy of the structural walls to prevent building collapse is demonstrated by the fact that all school buildings in the inventory with dual-system frame structures, with the exception of one, were lightly damaged or not damaged at all. The sole severely damaged structure was damaged not by failure in the ground story, as all the other school buildings, but by failure of captive columns at basement level as a result of discontinuity of the foundation walls in height. The structural walls of the building, which were not damaged at all, prevented the collapse of the building by providing sufficient lateral strength as well as maintaining gravity load carrying capacity.

6. ACKNOWLEDGMENTS

This work was conducted with support by the U.S. National Science Foundation (NSF) under Grant No. 85270-CMS and Grant No. 0334950 to Purdue University. Opinions, findings, conclusions, and recommendations included in the paper are those of the authors listed and do not reflect the views of the National Science Foundation.

Table 1: List of the schools and their damage states after the events

	School Name	Location	Building No.	Structural System	Damage to RC System	Damage to Masonry	No. of Stories
Duzce Earthquake	Dariyeri Hasanbeyi Ilkogretim Okulu	Kaynasli	K01	Dual System	None	None	2
	Andolu Ticaret Lisesi	Bolu	B01	Dual System	None	None	3
	Yunus Emre Ilkogretim Okulu	Duzce	D01	Dual System	None	None	2
	Necmi Hosver Ilkogretim Okulu	Duzce	D02	Dual System	Severe *(Basement)*	Moderate *(Basement)*	4
	Azmi Milli Ilkogretim Okulu	Duzce	D03	Dual System	Light	Moderate	4
Bingol Earthquake	75. Yil Ilkogretim Okulu	Bingol	C13-01	Moment-resisting frame	Severe	Severe	3
	Sehit Mustafa Gundogdu Ilkogretim Okulu	Bingol	C13-05	Moment-resisting frame	Moderate	Light	2
	Kazim Karabekir Ilkogretim Okulu	Bingol	C13-06	Moment-resisting frame	Moderate	Light	2
	Vali Kurtulus Sismanturk Ilkogretim Okulu	Bingol	C13-07	Moment-resisting frame	Light	Moderate	2
	Kaleonu Ilkogretim Okulu	Bingol	C13-08	Moment-resisting frame	Collapsed	Collapsed	3
	Saricicek Koyu Ilkogretim Okulu	Saricicek	C13-09	Moment-resisting frame	Collapsed	Collapsed	3
	Celtiksuyu Ilkogretim Okulu	Celtiksuyu	C13-10	Moment-resisting frame	Collapsed	Collapsed	3
	Karaelmas Ilkogretim Okulu	Bingol	C14-01	Moment-resisting frame	Severe	Severe	3
	Mehmet Akif Ersoy Ilkogretim Okulu	Bingol	C14-03	Moment-resisting frame	Severe	Severe	3
	Ataturk Lisesi	Bingol	C14-04	Moment-resisting frame	Moderate	Moderate	3
	Vali Guner Orbay Ilkogretim Okulu (Main Building)	Bingol	C14-05	Moment-resisting frame	Moderate	Moderate	3
	Vali Guner Orbay Ilkogretim Okulu (2nd Building)	Bingol	C14-06	Moment-resisting frame	Moderate	Moderate	2
	Ataturk Ilkogretim Okulu	Bingol	C14-07	Moment-resisting frame	Severe	Moderate	3
	Sarayici Ilkogretim Okulu	Bingol	C15-01	Moment-resisting frame	Severe	Severe	4
	Murat Ilkogretim Okulu	Bingol	C15-02	Moment-resisting frame	Severe	Severe	3
	Ekinyolu Koyu Ilkogretim Okulu	Ekinyolu	D16-01	Moment-resisting frame	Severe	Severe	3

Table 2: The maxima of the ground motions recorded near the school sites during the Düzce and Bingöl earthquakes

Station	Earthquake	Max. Ground Acc. (m/s^2)	
		EW	NS
Duzce	Duzce Eq.	5.04	4.00
Bolu	Duzce Eq.	7.91	7.25
Bingol	Bingol Eq.	2.71	5.35

Table 3: Basic structural parameters of the buildings

	Bldg No.	Damage to RC System	Damage to Masonry	N_{floor}	A_{floor} (m^2)	A_{sw} EW (m^2)	A_{mw} EW (m^2)	A_{sw} NS (m^2)	A_{mw} NS (m^2)	A_c (m^2)	CI (%)	WI (%)
Duzce Earthquake	K01	None	None	2	595	2.9	12.5	2.4	6.8	5.1	0.21	0.26
	B01	None	None	3	595	2.9	12.5	2.4	6.8	5.1	0.14	0.17
	D01	None	None	2	595	2.9	12.5	2.4	6.8	5.1	0.21	0.26
	D02	Severe	Moderate	4	595	2.9	12.5	2.4	6.8	5.1	0.11	0.13
	D03	Light	Moderate	4	595	2.9	12.5	2.4	6.8	5.1	0.11	0.13
Bingol Earthquake	C13-01	Severe	Severe	3	595	0.0	16.0	0.0	10.6	6.5	0.18	0.06
	C13-05	Moderate	Light	2	585	0.0	18.7	0.0	11.7	6.5	0.28	0.10
	C13-06	Moderate	Light	2	589	0.0	15.7	0.0	11.0	6.5	0.27	0.09
	C13-07	Light	Moderate	2	589	0.0	16.8	0.0	11.9	6.5	0.27	0.10
	C13-08	Collapsed	Collapsed	3	595	0.0	18.3	0.0	7.4	6.5	0.18	0.04
	C13-09	Collapsed	Collapsed	3	595	0.0	16.0	0.0	9.3	6.5	0.18	0.05
	C13-10	Collapsed	Collapsed	3	595	0.0	16.0	0.0	9.3	6.5	0.18	0.05
	C14-01	Severe	Severe	3	595	0.0	15.7	0.0	9.4	6.5	0.18	0.05
	C14-03	Severe	Severe	3	595	0.0	5.4	0.0	12.7	6.5	0.18	0.03
	C14-04	Moderate	Moderate	3	595	0.0	12.5	0.0	11.4	6.5	0.18	0.06
	C14-05	Moderate	Moderate	3	595	0.0	7.4	0.0	17.1	6.5	0.18	0.04
	C14-06	Moderate	Moderate	2	595	0.0	16.0	0.0	10.7	6.5	0.27	0.09
	C14-07	Severe	Moderate	3	595	0.0	16.0	0.0	8.9	6.5	0.18	0.05
	C15-01	Severe	Severe	4	595	0.0	14.9	0.0	7.3	6.5	0.14	0.03
	C15-02	Severe	Severe	3	595	0.0	14.4	0.0	10.6	6.5	0.18	0.06
	D16-01	Severe	Severe	3	595	0.0	14.8	0.0	7.7	6.5	0.18	0.04

N_{floor} :Number of floors
A_{sw}EW: Total shear wall area in the east-west direction
A_{sw}NS: Total shear wall area in the north-south direction
A_{mw}EW: Total masonry infill wall area in east-west direction
A_{mw}NS: Total masonry infill wall area in east-west direction
A_c: Total column area
CI: Column index
WI: Wall index

Fig. 1: Examples of severe masonry-wall damage

Fig. 2: A moderately-damaged masonry wall

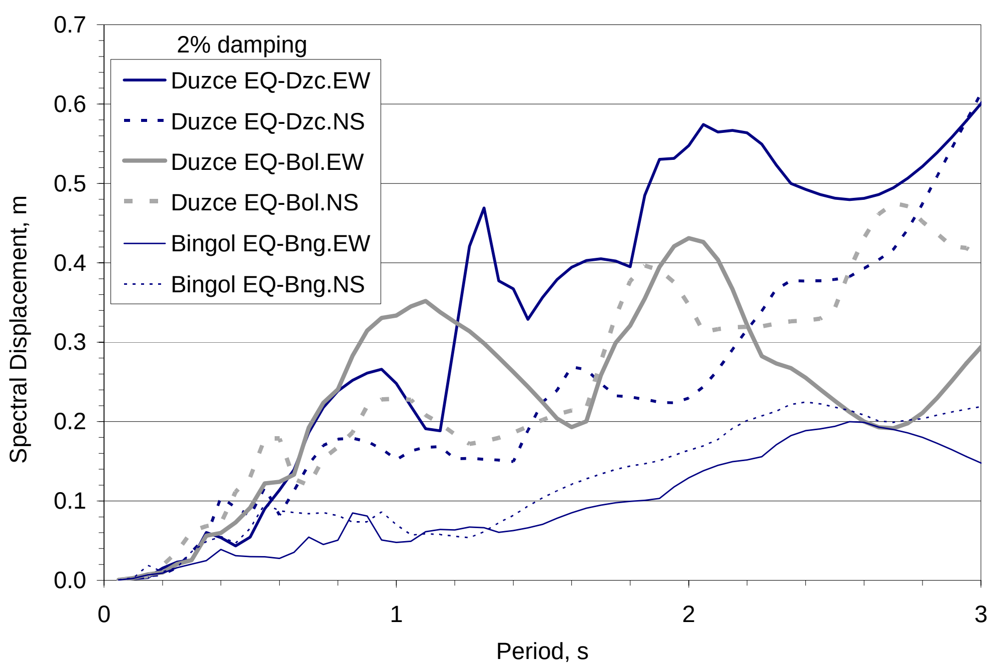

Fig. 3: The displacement spectra of the ground motions recorded near the school sites during the Düzce and Bingöl earthquakes

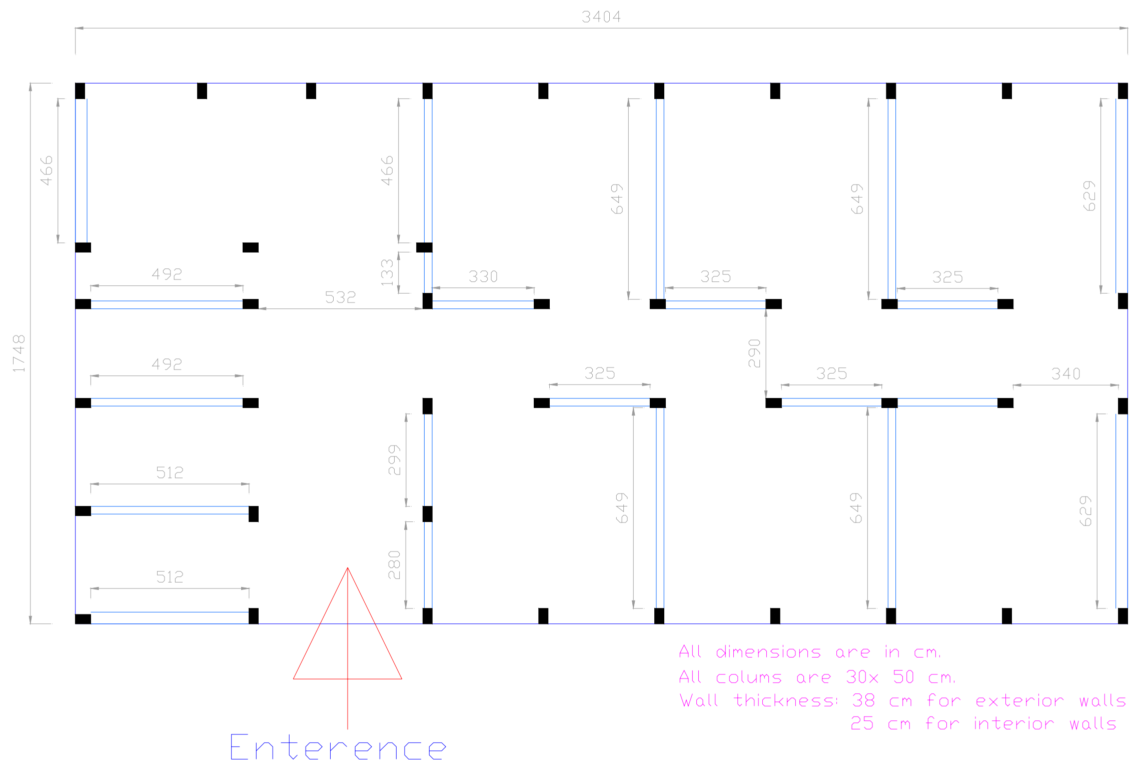

Fig. 4: Typical floor plan for moment-resisting frame systems

Fig. 5: The remains of the corner column of the ground floor of the building shown in Fig. 5 (Building C13-09). The corner column failed in shear.

Fig. 6: A captive column in Building C14-01 created by the crushing of the corner regions of infill walls

Fig. 7: The four-story dual-system building in Düzce (Building D02)

Fig. 8: The view of the captive exterior columns in the basement of Building D02 from outside and inside. The columns are captive in their weak axis.

SESSION 9: NONLINEAR BEHAVIOR OF FRAMES

Chaired by

♦ Marc Moore and Shaohua Chen ♦

AN EXPERIMENTAL STUDY ON 6-STORY R/C STRUCTURE WITH MULTI-STORY SHEAR WALL (PART 1)

Taiki SAITO[1], Masaomi TESHIGAWARA[2], Hiroshi FUKUYAMA[1], Hiroto KATO[1], K oichi KUSUNOKI[1], and Tomohisa MUKAI[1]

ABSTRACT

Using a Large Scale Testing Laboratory in the Building Research Institute, a series of pseudo dynamic tests are planned to examine the nonlinear behaviour of a reinforced concrete frame structure with a continuous shear wall along the height of the building changing the condition of the rigidity of the basement of the wall. The test and a computer analysis of a six-story wall-frame structure were conducted and the mechanism to carry the seismic force was examined in detail. Also, a sub-structure pseudo dynamic test of a specimen which represents the lower part of the six-story structure, consisting of one story shear wall and transversal base beams, is planned to see the effectiveness of the testing method by comparing with the full structure test.

1. INTRODUCTION

A pseudo-dynamic test of a two-span-one-bay-six-story reinforced concrete structure with a multi-story shear wall was conducted at the Large Scale Testing Laboratory in the Building Research Institute (BRI), Japan. The main purpose of this test is to examine the effect of the rigidity at the bottom of the shear wall to the distribution of lateral forces and axial forces carried by the wall and columns of the structure and develop reasonable design procedures for reinforced concrete structures that have wall and open frames. The results of the test are discussed in detail in this paper and the subsequent paper.

This paper also introduces a new sub-structure pseudo dynamic testing system recently developed in BRI to test only the most important part of a building and analyze the rest part mathematically in a computer. Using this system, the lower part of the six-story structure, consisting of one story shear wall and transversal base beams, is planned to be tested to simulate the behaviour of the full structure and compare the results with those of the previous full structure test. A preliminary test was conducted using a steel specimen with the similar configuration to see the accuracy and effectiveness of substructure pseudo dynamic testing system.

1 *Building Research Institute, Tachihara 1, Tsukuba, 305-0802, Japan*

2 *Nagoya University, Furo-cho, Chigusa-ku, Nagoya, Aichi 464-8603, Japan*

2. PSEUDO DYNAMIC TEST

2.1 Test Specimen

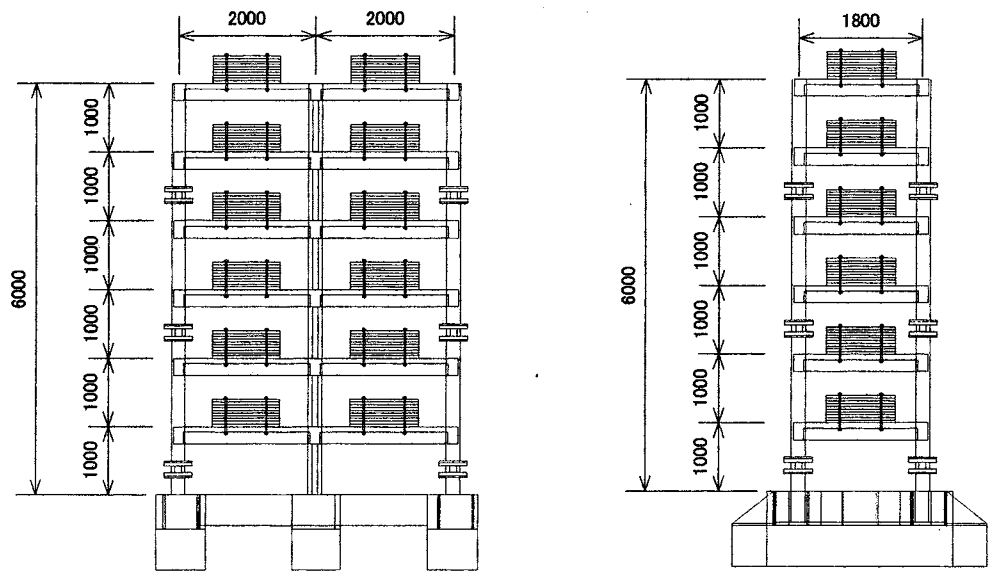

Figure 1 Elevation view (UNIT: mm)

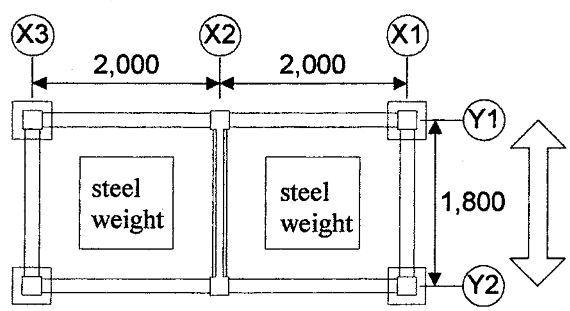

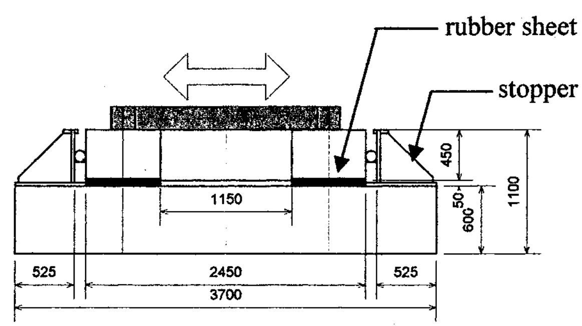

Figure 2 Plan view (UNIT: mm)

Figure 3 Basement of X2 frame

Figures 1 and 2 show the elevation and the plan of the test specimen. The specimen is designed to be 1/3 scale of a real size structure. It has six-stories, one-bay in the loading direction and two-bays in the perpendicular direction. The basements of X1 and X3 frames are fixed on the floor. The basement of X2 frame is placed on the rubber sheet as shown in Figure 3 to allow the lift up of the basement due to rocking movement of the wall. The lateral movement of the basement is restrained by the steel devices arranged at the both sides of the basement. After conducting a series of pseudo dynamic tests using this specimen (hereafter referred to as *rocking specimen*), we fixed the basement of X2 frame using PC steel bars and continued another series of tests using the same specimen (hereafter referred to as *fixed specimen*) to see the difference of shear and axial force distributions in wall and column elements between two test series.

The story weight of the structure is 90.5 kN at the Roof floor, 94.0 kN at the second to sixth floors, and 27.5 kN at the basement floor, including 61.5 kN supplemental weight on each floor slab. The size and rebar arrangement of each member are presented in Table 1, and material properties based on material test results are listed in Table 2.

Table 1 Member size and rebar arrangement

	Beam					
	1 Floor (X1, X2)		1 Floor (Y1, Y2)		2-R Floor	
Section (mm)	B×D	200×450	B×D	200×450	B×D	150×250
	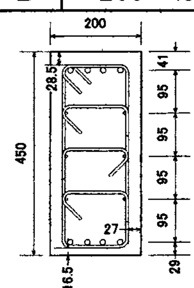		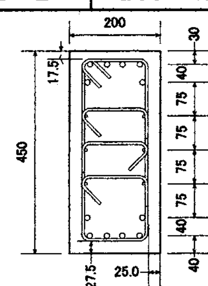		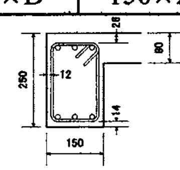	
Rebar	Lateral	4-D10	Lateral	6-D10	Lateral	3-D10
	Side	6-D6	Side	6-D6		
	Stirrup	2-D6@100	Stirrup	2-D6@50	Stirrup	2-D6@60
	Column		Wall			
	1-6 Story		1-6 Story			
Section (mm)	B×D	200×200	t		80	
	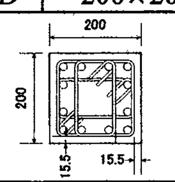		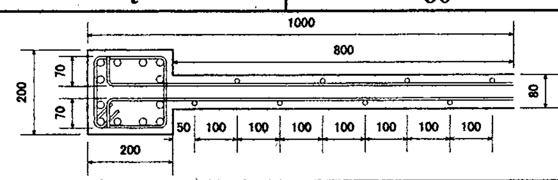			
Rebar	Lateral	12-D13	Vertical		D6@100	
	Hoop	2-D6@60	Horizontal		D6@100	
	Slab					
	1-6 Story					
Section (mm)	t	80				
	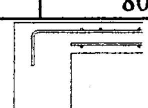					
Rebar	Upper	D6@100				
	Lower	D6@200				

Table 2 Material parameters

Rebar	Young's Modulus (N/mm^2)	Yield Strength (N/mm^2)	Break Strength (N/mm^2)
D6	1.66×10^5	349	501
D10	1.76×10^5	353	496
D13	1.76×10^5	345	472
Concrete	Young's Modulus (N/mm^2)	Compression Strength (N/mm^2)	
(average)	2.66×10^4	37.1	
Rubber	Young's Modulus (N/mm^2) (from the compression test in displacement range [0.2-0.5mm])		
(average)	51.1		

2.2 Test Setting

In the beginning of the pseudo dynamic test, seven actuators were arranged as shown in Figure 4; one actuator at each floor and two actuators at the top floor. Floor displacements were measured by the magnetic scales from the steel tower built next to the specimen. In total 72 displacement transducers were used to measure the deformations of beams and columns, the relative story displacements, and sway and rocking displacements of the basement. Strains of rebar inside structural elements were measured by 275 strain gauges. And the axial and shear forces carried by the columns at first, third and fifth floor were measured by the load cells embedded in the middle of the columns.

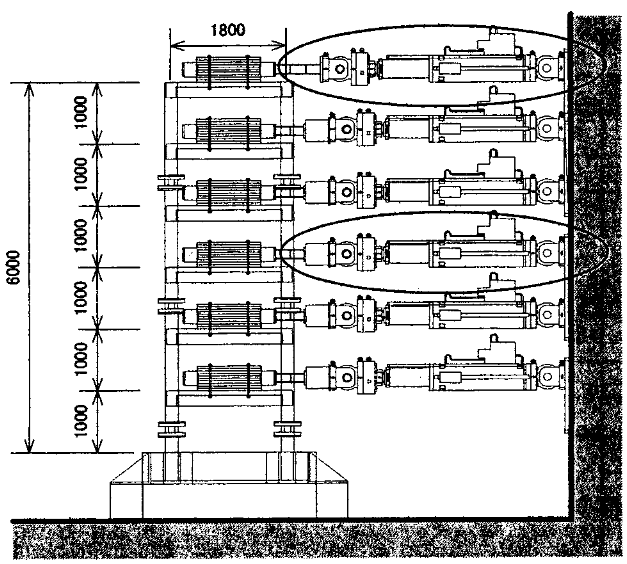

(a) Elevation ◯ adopted actuators

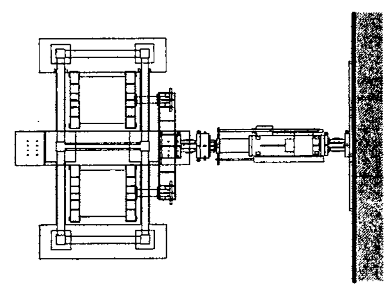

(b) Plan (2F-6F)

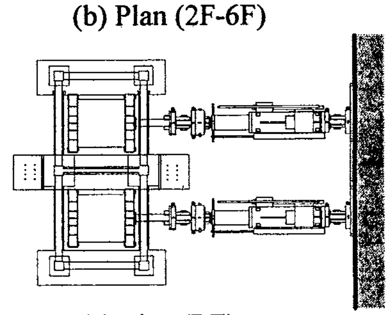

(c) Plan (RF)

Figure 4 Test setting

Before starting the test, a unit load was applied on each floor to obtain the stiffness matrix of the six-degree-of-freedom lumped mass system, and the natural period and the mode shape were obtained as shown in Table 3 for the rocking specimen and the fixed specimen, respectively. The lateral story stiffness was measured as 1,470kN/mm from the unit loading of the rocking specimen. Taking the minimum controllable displacement of the actuator of 0.01mm into account, such high story stiffness leaded large force controlling error. To avoid the divergence of displacement caused by the control error, we reduced the freedom of the model to be second-degree-of-freedom system. Consequently, the number of actuators were also reduced to be three; one actuator at the fourth floor and two actuators at the top floor. The effective masses for the second-degree-of-freedom system were calculated so that the first and second natural periods and mode shapes match those of six-degree-of-freedom system. The values of effective masses are also presented in Table 3.

Table 3 Vibration modes from the unit loading

	Mode shape and natural period			Effective mass for 2-DOF system
Rocking specimen	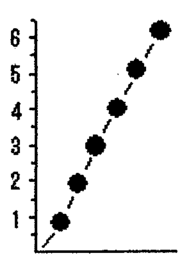 $T_1 = 0.157$sec	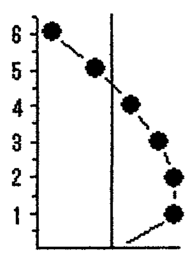 $T_2 = 0.05$sec	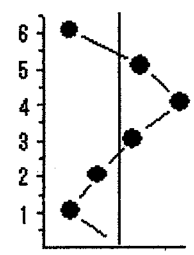 $T_3 = 0.018$sec	m_1 (fourth floor) 350.84kN m_2 (top floor) 148.96kN
Fixed specimen	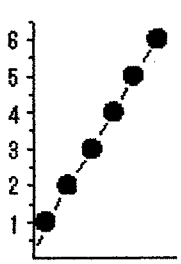 $T_1 = 0.269$ sec	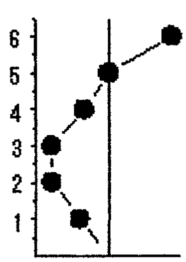 $T_2 = 0.07$sec	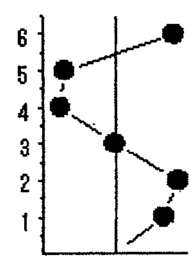 $T_3 = 0.039$sec	m_1 (fourth floor) 312.62kN m_2 (top floor) 147.98kN

2.3 Input Ground Motions

Four different input earthquake ground motions were used for the pseudo dynamic test as listed in Table 4. The time interval of the input acceleration data was scaled down to be $1/\sqrt{3}$ of that of the original record according to the scale of the specimen. Also, the amplitude of the input acceleration data was scaled to have a certain maximum velocity level from the original one as listed in Table 4. The duration of input motion was around seven seconds determined so that it included the major portion of the earthquake record. Since the fixed specimen still held the resistance capacity after the loading of TAKA250, the static loading test was conducted at the end of the test series until the specimen reached the collapse mechanism. The ratios of static force at the fourth and top floors were 1 and 1.5.

Table 4 Loading history

Date of Experiment	Name	The Maximum Velocity Level (cm/s) *	Original Record
Rocking specimen			
2003.8.29			Unit loading
2003.9.19	TOH25	25	Tohoku University, 1978 Miyagi-ken-oki earthquake
2003.9.20	ELC37	37	Imperial Valley, 1940 El Centro earthquake
2003.9.22	KOBE50	50	JMA Kobe, 1995 Hyogo-ken-Nanbu earthquake
2003.9.23	KOBE75	75	ditto
Fixed specimen			
2003.9.27			Unit loading
2003.9.29	KOBE50	50	JMA Kobe, 1995 Hyogo-ken-Nanbu earthquake
2003.9.30	KOBE75-1	75	ditto (terminated due to a problem in the loading system)
2003.10.9	KOBE75-2	75	ditto
2003.10.10	TAKA250	250	JMA Takatori, 1995 Hyogo-ken-Nanbu earthquake
2003.10.10			Static loading

* scaled from the original records

2.4 Test Results

Relations between the top displacement and base shear of the structure obtained in each loading are presented in Figure 6 and 7, and crack distributions and locations of rebar yielding are presented in Figures 8 and 9 for the rocking specimen and fixed specimen, respectively.

2.4.1 Damage process of the rocking specimen

For the rocking specimen, rebar yielding did not happen in the loading of TOH25 and ELC37, however, the natural period of the specimen measured by the free vibration test changed to be T=0.18 second after the loading of TOH25 and T=0.23 second after the loading of ELC37. Rebar yielding was observed in the loading of KOBE50 at the beam ends on the second, third and fourth floors in X1 and X3 frames and at the basement beams of Y1 frame. The range of rebar yielding was extended to the beams at the top floor in X1 and X3 frames and at the shear walls at the first and second stories in the loading of KOBE75.

Flexural cracks appeared first on the base beams in the loading of ELC37. In the loading of KOBE50, shear cracks appeared on the shear walls from the first to fourth stories and flexural cracks appeared on all the columns and beams in X1 and X3 frames. The maximum base shear reached 495kN in the positive side and -513kN in the negative side in the loading of KOBE75. As shown in Figure 7, amount of cracks on shear walls in the second and third stories are larger than those on the shear wall in the first story. The location of rebar yielding is also shown in Figure 7. Rebar yielding appeared at the ends of beams from the second to top floors in X3 frame.

2.4.1 Damage process of the fixed specimen

For the fixed specimen, all of the vertical rebar in the shear wall in the first story yielded in the loading of KOBE50 and flexural cracks appeared on the side columns at the first and second stories in X2 frame. In the loading of KOBE75-2, cracks appeared on the cross sections in X1 frame. Also, rebar in the first and second story columns in X2 frame yielded. In the loading of TAKA250, the maximum base shear reached ~~563~~ 757kN in the positive side and -~~563~~ 782kN in the negative side. Crack distributions after TAKA250 are shown in Figure 8. It can be seen that the shear walls at the first, second and third stories severely damaged and shear cracks reached on the shear wall at the top story. The location of rebar yielding is also shown Figure 8. All rebar at the ends of the beams in Y1 frame from the second to top floors yielded. Also rebar yielding happened at the second floor slab near the side of X2 frame.

In the static loading, the maximum base shear reached 795kN in the positive side and -697kN in the negative side. As shown in Figure 9, the specimen deformed largely in the loading direction. After the static loading, a wide shear crack appeared from the right top of the wall to the middle left into the side column (see Figure 10). From the result, it can be concluded that the shear wall yielded by flexure first and finally collapsed by shear.

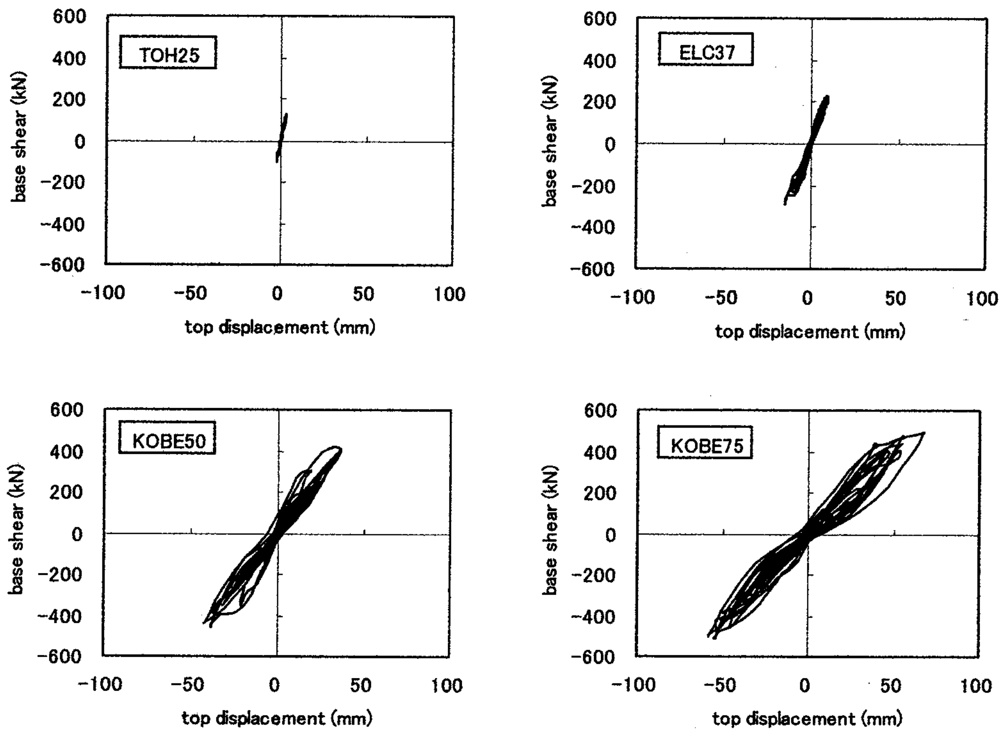

Figure 5 Top displacement and base shear relationship (the rocking specimen)

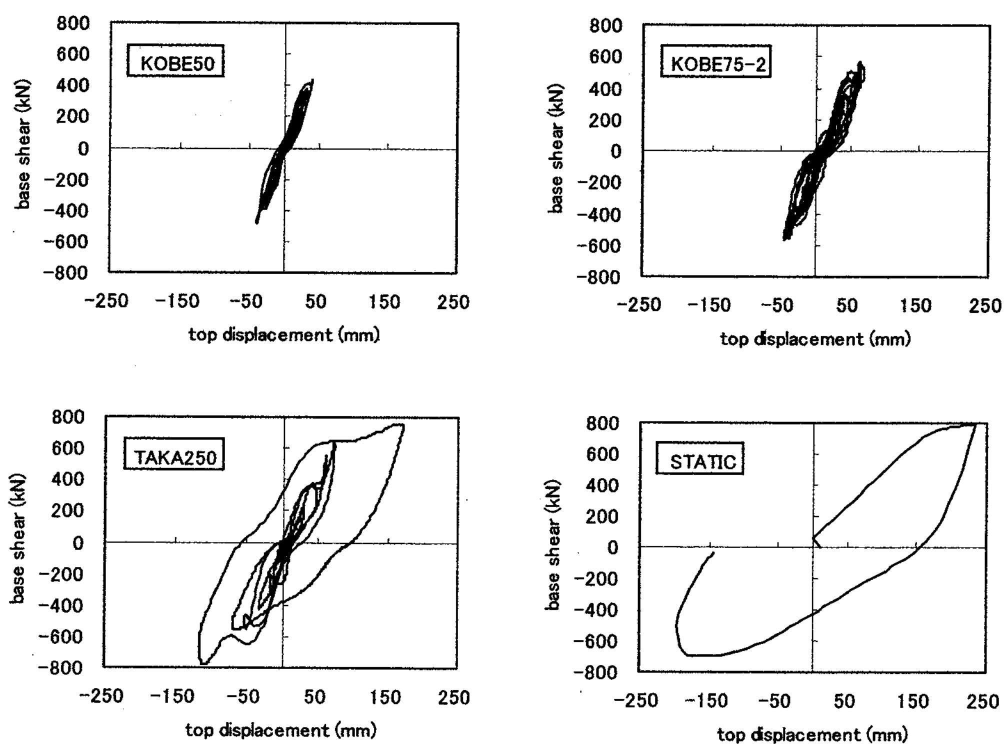

Figure 6 Top displacement and base shear relationship (the fixed specimen)

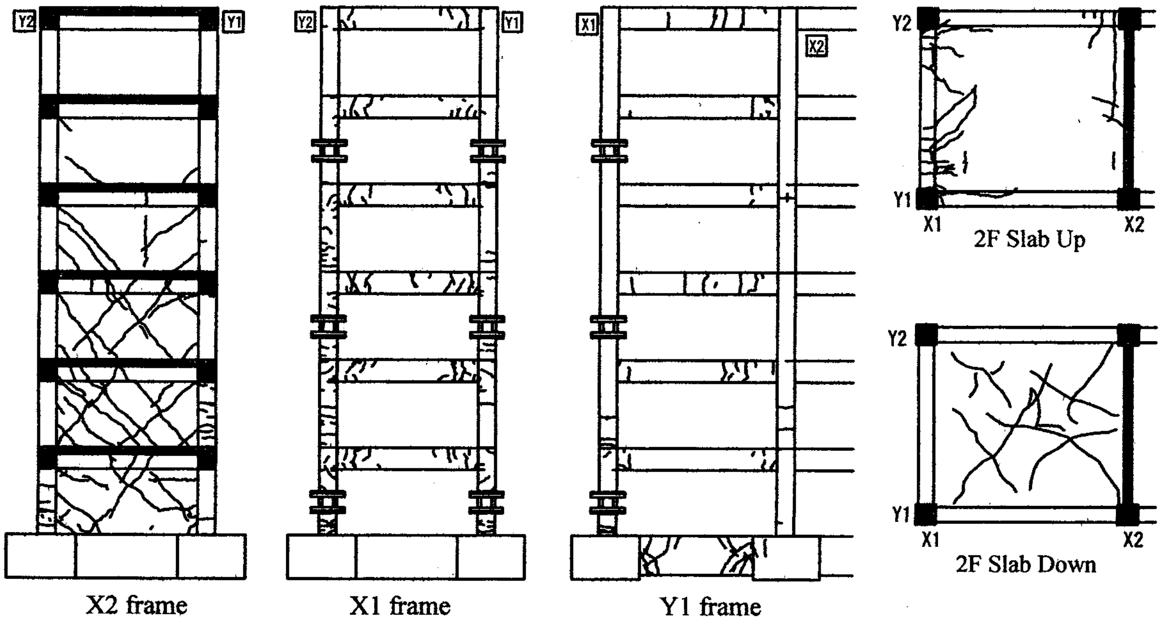

(a) Crack distributions (after KOBE 75)

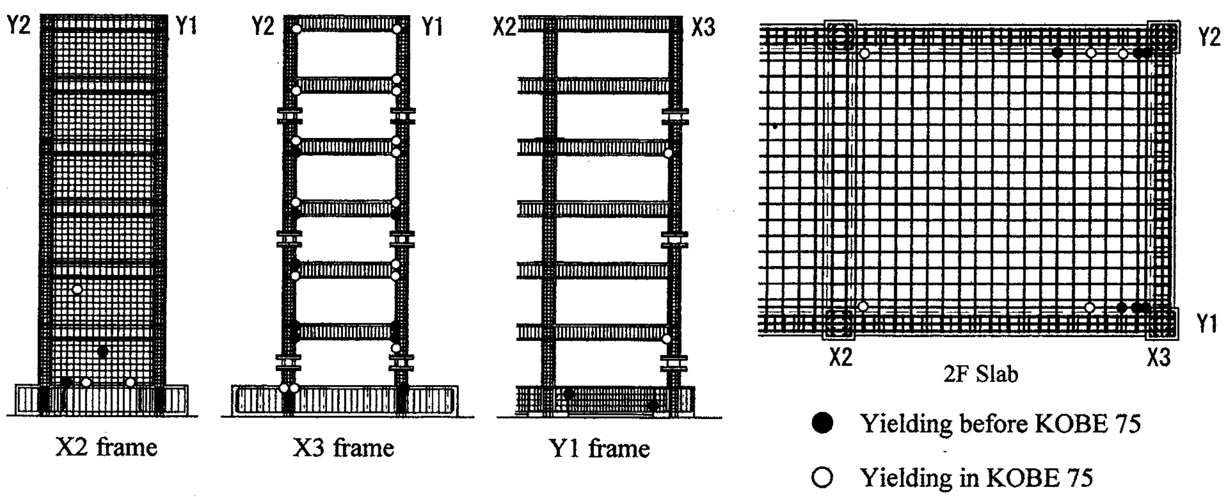

(b) Locations of rebar yielding

Figure 7 Crack distributions and rebar yielding (the rocking specimen)

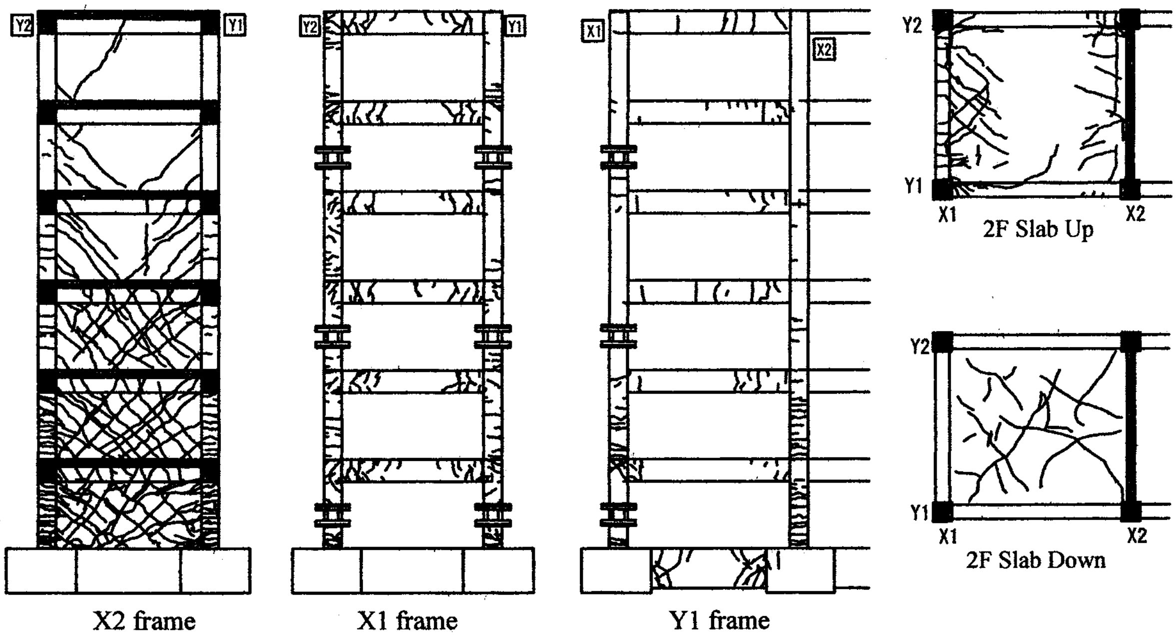

(a) Crack distributions (after TAKA 250)

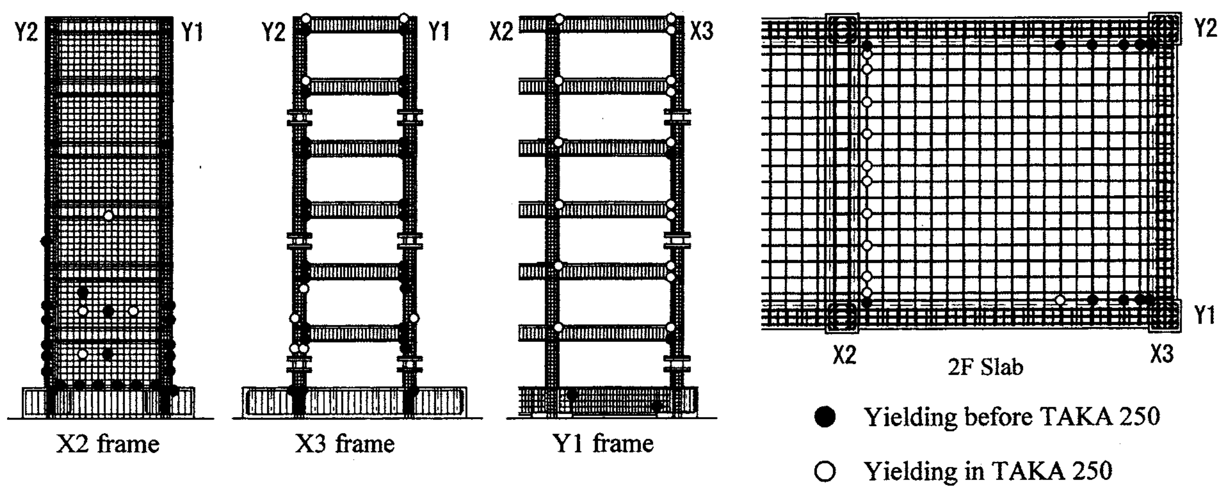

(b) Locations of rebar yielding

Figure 8 Crack distributions and rebar yielding (the fixed specimen)

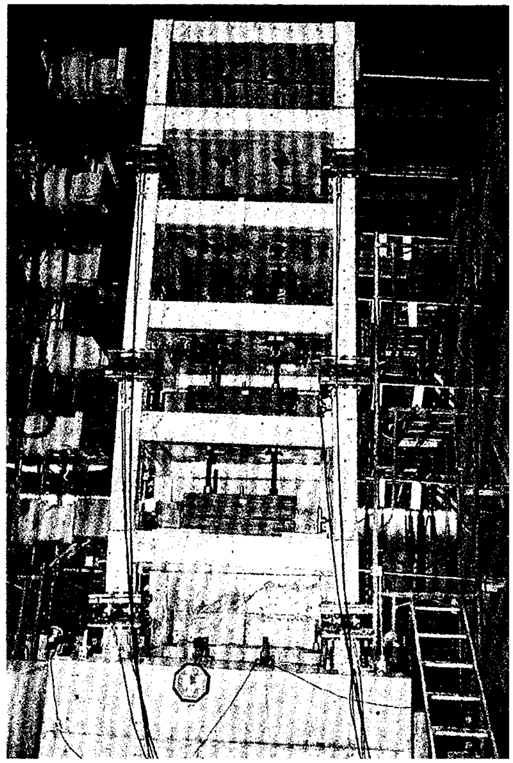

Figure 9 Static loading of the fixed specimen

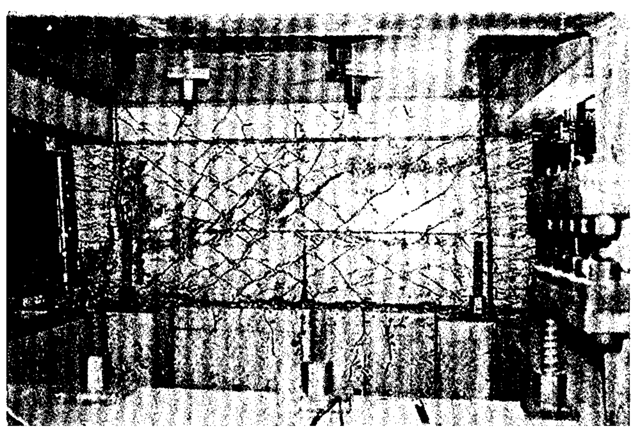

Figure 10 Damage at the first story shear wall after the static loading (the fixed specimen)

3. NONLINEAR PUSH OVER ANALYSIS

3.1 Nonlinear element models

Figure 11 shows the nonlinear element models in the computer program "STERA-3D", which was developed in BRI to analyse three-dimensional behaviour of reinforced concrete structures. The parameters of element models for the test specimen were calculated based on the member properties listed in Tables 1 and 2. In the calculation of flexural capacity of beams, full width of slab reinforcement was taken into consideration. The yield rotations of beam and column elements were evaluated by the following formula (Sugano, 1970):

$$\frac{M_y}{\theta_y} = \alpha_y K_0 \tag{1}$$

$$\alpha_y = \left(0.043 + 1.63 n p_t + 0.043 \frac{M}{QD} + 0.33 \frac{N}{bDF_c}\right)\left(\frac{d}{D}\right)^2, \quad K_0 = \frac{6EI}{l} \tag{2}$$

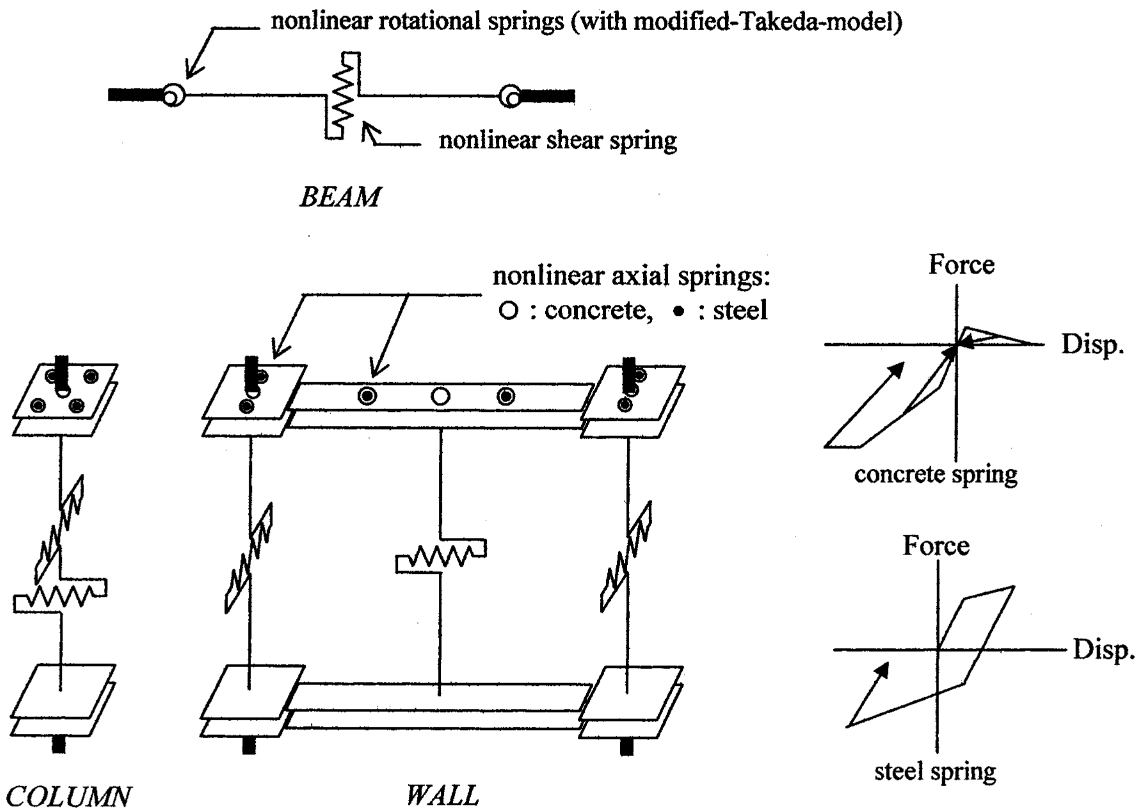

Figure 11 Nonlinear element models

in which, M_y: yield moment at member ends, θ_y: yield rotation at member end, *n*: Young's modulus ratio ($= E_s / E_c$), : tensile reinforcement ratio, *M/QD*: shear span-to-depth ratio, *N*: axial force, *b*: width of the section, *D*: depth of the section, F_c: compression strength of concrete, and l : total length of member. The yield rotation of wall element was calculated assuming $\alpha_y = 0.2$ and $K_0 = 2EI/l$ in Equation (1). Nonlinear interaction between moment and axial force of the column element was modelled by the Multi-Spring Model (Li and Otani, 1993), where nonlinear axial springs for concrete and steel were arranged in the sections of member ends. A similar model was developed for the wall element (Saito et.al., 1991). Since the specimen was designed to have flexural yielding at the member ends and have enough shear strength, shear springs in the element models were assumed to be elastic throughout the analysis.

3.1 Nonlinear push-over analysis

A nonlinear push-over analysis of the frame model of the rocking specimen was carried out applying lateral static forces in the loading direction. The distribution of the lateral forces over the height of the structure was determined assuming the triangular shape of the seismic coefficient. The static force was applied at the center of gravity in each floor, and increased until the displacement at the top floor reached 1/80 of the total height of the structure. Figure 12 shows the yield mechanism and the relation between the top displacement and base shear force. The frame reached the yield mechanism with large deformation of perpendicular beams attached to the shear wall. The largest base shear was 450kN at the end of the loading and the shear wall carried 40.4 % of the total amount of shear force. It was found out that after the perpendicular beams yielded, the shear force carried by the wall didn't change so much. On the contrary, the shear force carried by the columns increased as the external force increased.

Figure 13-(a) shows the comparison between the distributions of seismic coefficient obtained from the pseudo dynamic test and triangular shape used for the push-over analysis. The seismic coefficient of the pseudo dynamic test was calculated from the force of actuators at the maximum shear in each loading divided by the weight of the floor. It can be seen that the seismic coefficients at the fourth floor of the pseudo dynamic test are slightly larger than 0.5 of the triangular shape. Figure 13-(b) shows the comparison of the top displacement and base shear relationship between the pseudo dynamic test and push over analysis. It can be seen that the force-displacement curve of the push over analysis relatively well envelops the hysteresis loop of the pseudo dynamic tests.

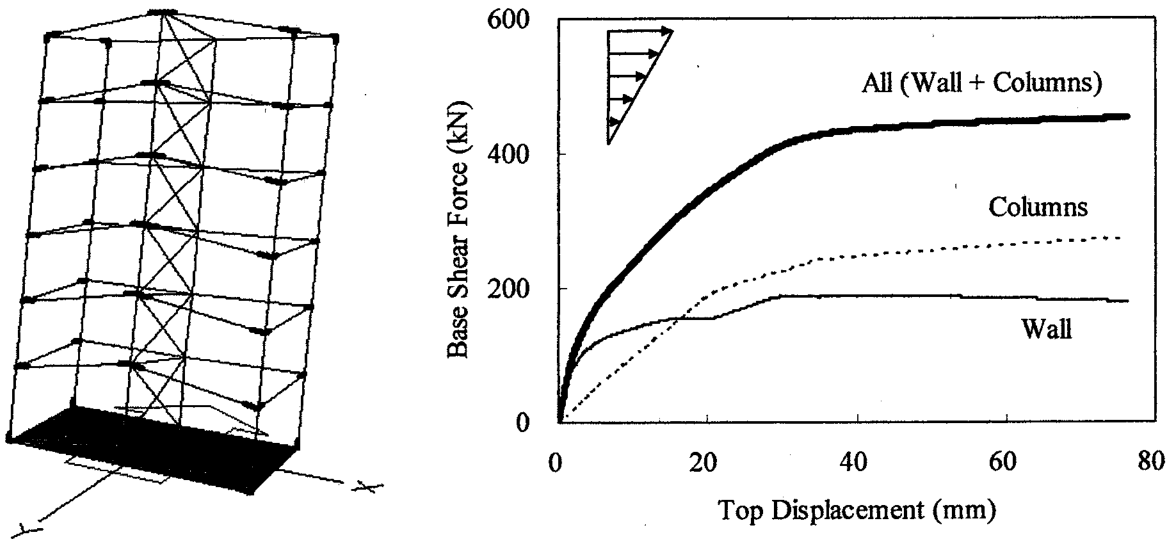

(a) Yield mechanism

(b) Top displacement and base shear relationship

Figure 12 Nonlinear push over analysis (the rocking specimen)

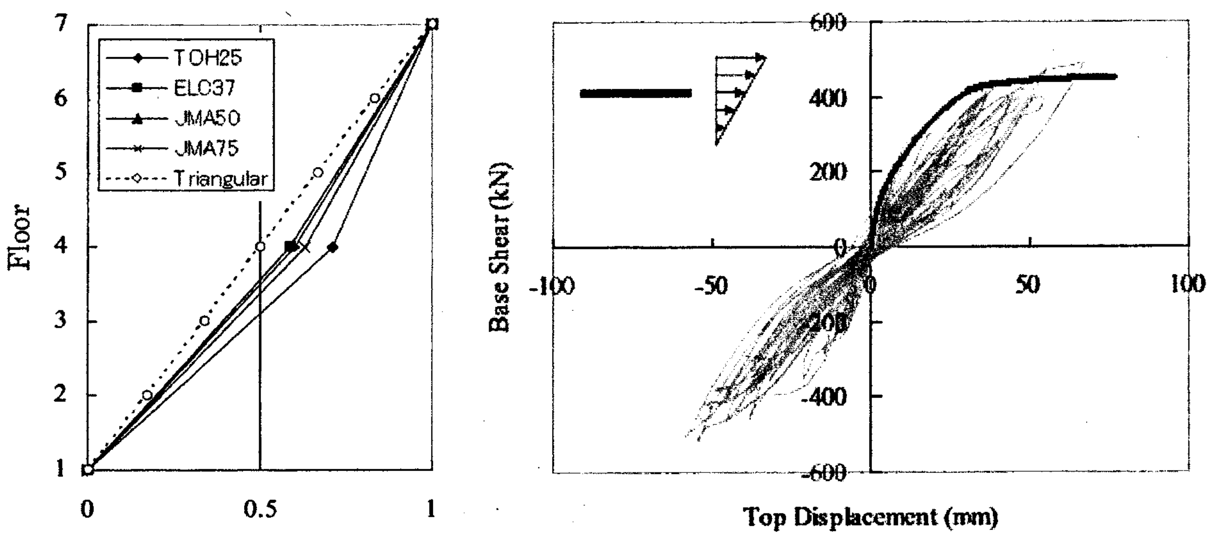

(a) Seismic Coefficient Distribution

(b) Top Displacement and Base Shear Relationship

Figure 13 Comparison between the pseudo dynamic test and push over analysis (the rocking specimen)

Shear forces of the columns at the first, third, and fifth stories were measured by the load cells embedded in the columns. By subtracting them from the forces of actuator, the shear forces of the wall were obtained. Table 5 shows the ratios of shear forces carried by the columns and wall at the first story at the maximum base shear in each loading. The ratio of the shear force carried by the wall is changed from 26% (in TOH25) to 42.2% (in KOBE75).

Table 5 Shear force distribution in the pseudo dynamic test (the rocking specimen)

Input Earthquake	Time (sec)	Base Shear (kN)	Columns (%)	Wall (%)
TOH25	4.42	128.3	74.0	26.0
ELC37	2.52	-288.9	65.7	34.3
KOBE50	0.89	-460.5	62.9	37.1
KOBE75	1.03	513.0	57.8	42.2

An alternative way to evaluate the distribution of lateral shear force among wall and columns is to apply the principle of virtual work method to each frame. In the case of X2 frame, as shown in Figure 12-(a), the force from the perpendicular beams on the lift up side, Qy, can be calculated as $Qy=(My_P+My_N)/l_B$; where My_P and My_N are the yield moments of positive and negative bending, and l_B is the length of beam. Figure 12-(b) shows the yield mechanisms of X1 and X3 frames. From the principle of virtual work method, the base shear forces carried by the wall and columns are calculated as $\sum P_W$ =150.8kN and $\sum P_C$ =274.7kN, respectively. Therefore, the total base shear is 425.4kN and the ratio of shear force carried by the wall is 35.5%, which is consistent with the results of the push over analysis and the pseudo dynamic test.

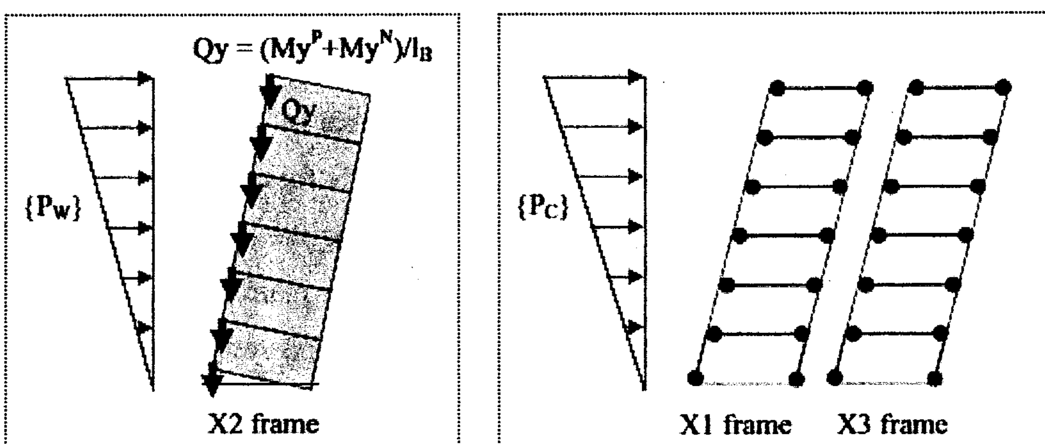

(a) Wall (b) Columns

Figure 14 Principle of virtual work method

4. SUB-STRUCTURE PSEUDO DYNAMIC TEST

4.1 Specimen for preliminary test

A new system for sub-structure pseudo dynamic test was recently introduced to the existing test operation system of the Large Scale Structural Testing Laboratory in BRI. In the new system, a part of the structure which is critical for the structural behaviour is extracted as a physical model to be tested (the physical sub-structure). The rest part is modeled numerically in a computer using the "STERA-3D" program (the numerical sub-structure). The data of displacements and forces at the interface between the physical and numerical sub-structures are exchanged between the actuator control system and computer system through the internet connection using TCP/IP. It offers the possibility to combine an advanced testing facility in one place and a high-class computer simulation system in another place to solve complicated behaviour of a large scale structures.

To confirm the accuracy and stability of the new testing system, a preliminary test was conducted using a steel specimen which represents the lower part of a six-story steel frame structure with braces in the middle frame. As shown in Figure 15, the full structure is decomposed into the numerical sub-structure and physical sub-structure. The test specimen (the physical sub-structure) consists of one-story brace frame with two transversal base beams. There are three freedoms at the interface between two sub-structures; two vertical freedoms, *V1, V2*, and one horizontal freedom, *H*.

The elevation views of the test specimen are shown in Figure 16. Similar to the reinforced concrete specimen, the basement of the brace frame of the specimen is not fixed on the floor to allow its lift up by rocking movement. Also the lateral displacement of the basement is restrained by the steel devices. The sizes of steel elements are listed in Table 16. The grade of steel is SS400 with nominal yield strength of 235kN. The story weight is 98kN for each story. The elements of the test specimen are designed strong enough to be elastic during the loading so that the test can be repeated to check the performance of the testing system. The main concern of this test is to capture the behaviour of the physical sub-structure with rocking and sway of the basement of the brace frame.

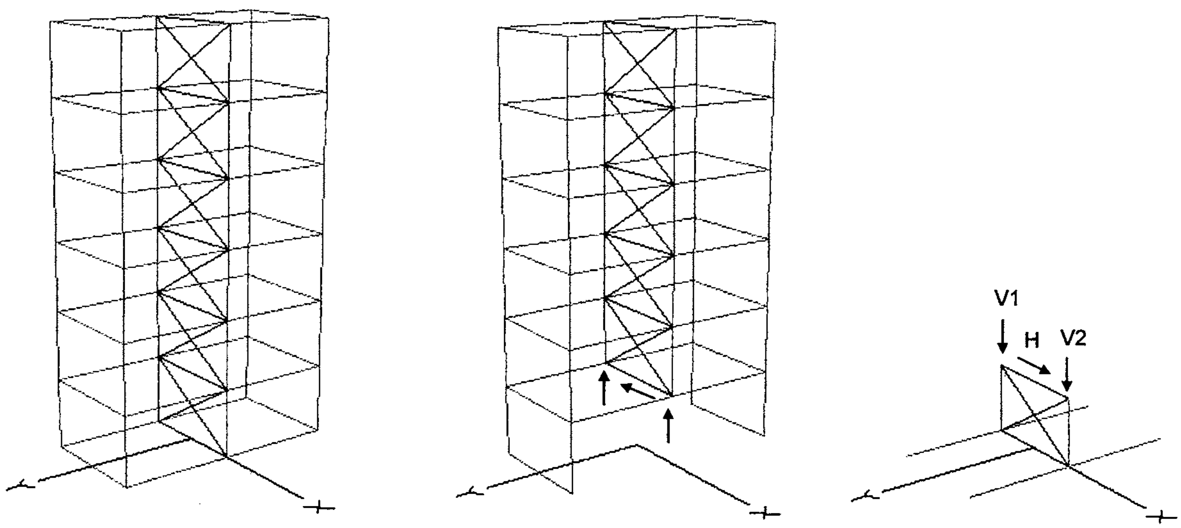

(a) Full structure (b) Numerical sub-structure (c) Physical sub-structure

Figure 15 Sub-structure model for the 6-story frame specimen

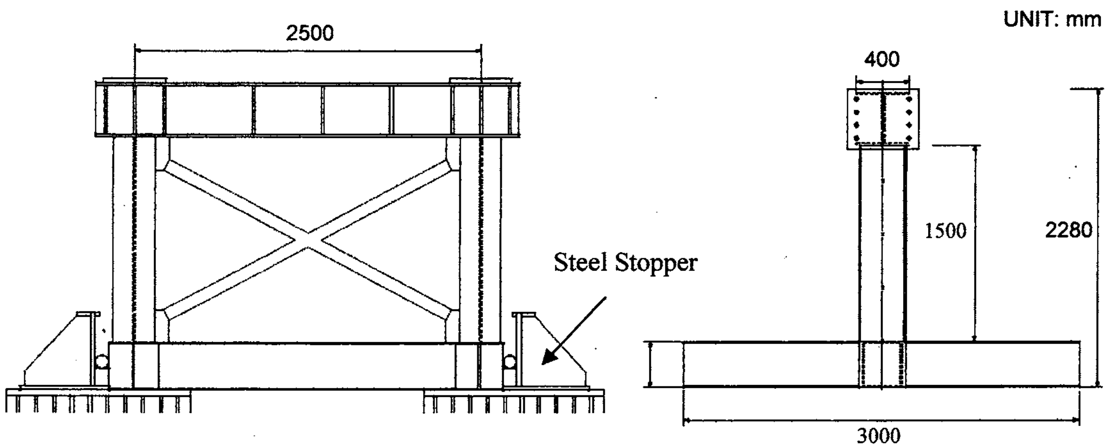

Figure 16 Elevation views of the test specimen (the physical sub-structure)

Table 6 Member size of steel elements

	Beam		
	1-R Floor (X1, X3, Y1, Y2)	1 Floor (X2)	2-R Floor (X2)
Section (mm)	H-350×350×12×19		H-400×400×13×21

	Column	Brace
	1-6 Story	1-6 Story
Section (mm)	H-350×350×12×19	2L-75×75×9

4.2 Numerical algorithm for sub-structure pseudo dynamic test

The numerical algorithm for the sub-structure pseudo dynamic test is the operator splitting method of stepwise integration (Nakashima et al. 1990). The algorithm is depicted in the followings:

(1) Predictor of displacement vector

The predictor of displacement vector in (n+1) step, $\{y_{n+1}*\}$, is calculated in the computer from the Newmark-β algorithm assuming zero input ground accelerations:

$$\{y_{n+1}*\} = \{y_n\} + \{\dot{y}_n\}\Delta t + (\frac{1}{2} - \beta)\{\ddot{y}_n\}\Delta t^2 \qquad (3)$$

Where $\{y_n\}$ and $\{\dot{y}_n\}$ are displacement and velocity vectors of the full structure at (n) step. Δt is the integration time interval. The factor β is set to be 0.25 (average acceleration scheme). Among the components of the predictor vector, $\{y_{n+1}*\}$, the displacements at the interface between two sub-structures, D_{V1}^*, D_{V2}^*, D_H^*, are selected as control displacements.

(2) Restoring force vector from the numerical sub-structure

Imposing the displacements of the predictor vector to the numerical sub-structure, restoring force vector, $\{f_{n+1}*\}_{analysis}$, is calculated in a computer, and the forces at the interface between two sub-structures, F_{V1}^*, F_{V2}^*, F_H^*, are selected as control forces.

(3) Restoring force vector from the physical sub-structure

Since the vertical stiffness of the specimen is quite high, control error of the vertical displacements, $D_{V1}^*$and D_{V2}^*, may leads large force error. Therefore, only horizontal displacement, D_H^*, is used for displacement control of the horizontal actuator, and other two vertical actuators are controlled by the vertical forces, $-F_{V1}^*$ and $-F_{V2}^*$, which are already calculated from the numerical sub-structure. As a result, three actuators are controlled in different ways using force and displacement controls. From the test results, the restoring force vector, $\{f_{n+1}*\}_{test}$, is then obtained for the physical sub-structure.

(4) Corrector of displacement vector

The restoring force vector of the full structure is obtained by adding the restoring force vectors of two substructures, that is:

$$\{f_{n+1}*\} = \{f_{n+1}*\}_{analysis} + \{f_{n+1}*\}_{test} \tag{4}$$

The corrector of displacement vector is then calculated in a computer from the following formula:

$$\begin{aligned}
\{\ddot{y}_{n+1}\} &= \left[[M] + \frac{1}{2}[C]\Delta t + \beta[K_0]\Delta t^2\right]^{-1}\left[-[C]\left(\{\dot{y}_n\} + \frac{1}{2}\{\ddot{y}_n\}\Delta t\right) - \{f_{n+1}*\} - [M]\{\ddot{y}_{0n+1}\}\right] \\
\{\dot{y}_{n+1}\} &= \{\dot{y}_n\} + \frac{1}{2}(\{\ddot{y}_n\} + \{\ddot{y}_{n+1}\})\Delta t \\
\{y_{n+1}\} &= \{y_{n+1}*\} + \beta\{\ddot{y}_{n+1}\}\Delta t^2
\end{aligned} \tag{5}$$

Where $[M]$, $[K_0]$, and $[C]$ are the mass, initial stiffness, and damping matrices. $\{\ddot{y}_{0n+1}\}$ is the ground acceleration at the (n+1) step. The damping matrix $[C]$ is calculated as:

$$[C] = \frac{2h_1}{\omega_1}[K_0] \tag{6}$$

Where h_1 is the damping factor for the first mode (to be 0.02 for the steel specimen), ω_1 is the first natural circular frequency obtained from the initial structure. The flow of the sub-structure pseudo dynamic test is summarized in Figure 17.

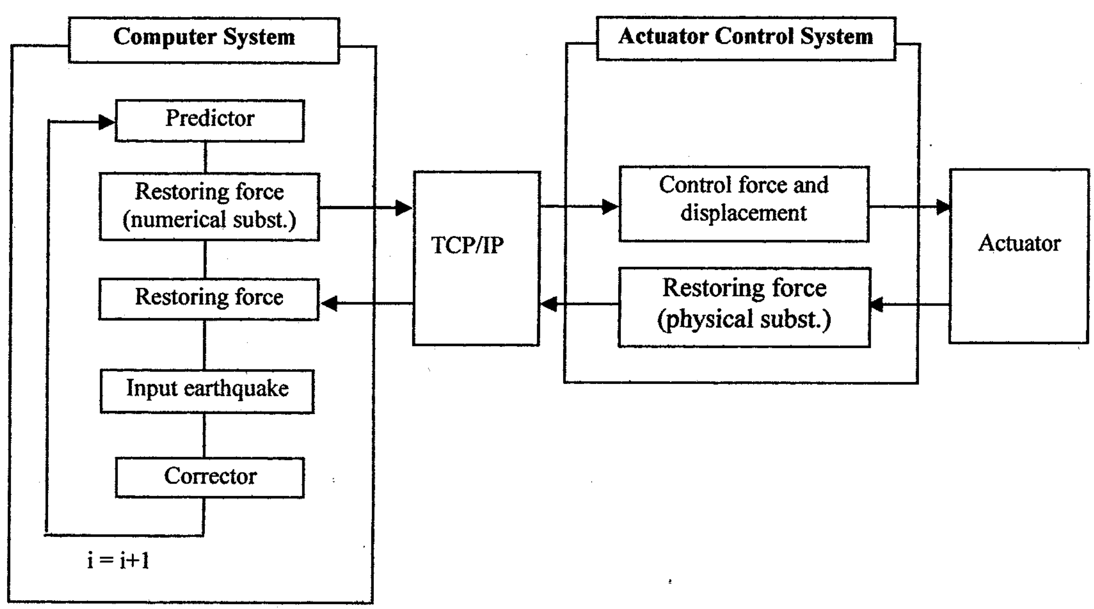

Figure 17 Flow of the sub-structure pseudo dynamic test

4.3 Test results

Figure 18 shows the setup of actuators in the testing system. Two actuators were arranged in vertical direction, and one was in horizontal direction.

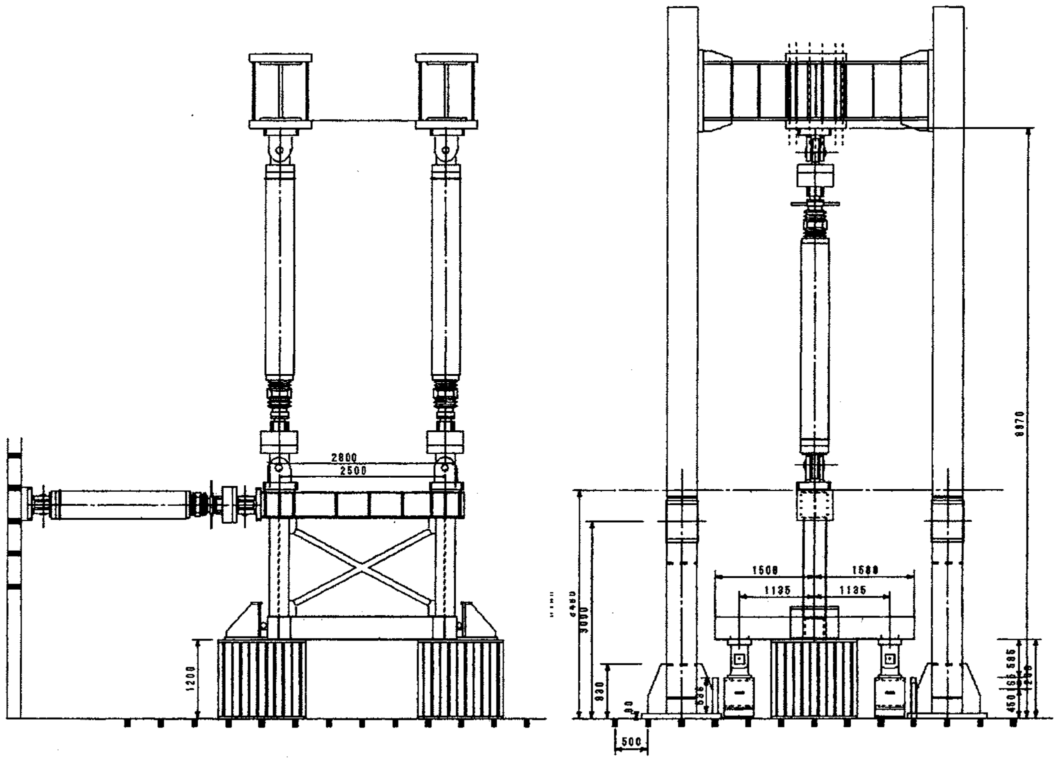

Figure 18 Test setting for sub-structure pseudo dynamic test

The input earthquake ground motion was KOBE50. The time interval of numerical integration was 0.002 second. Figure 19 shows the lateral force-displacement relationship at the first story. It can be seen in Figure 19-(a) that the force-displacement relationship of the brace frame presents a complicated loop shape. Most of the shear force at the first story is carried by the four corner columns in the numerical sub-structure (Figure 19-(b)).

To understand the behaviour of the brace frame, a mathematical model was constructed as shown in Figure 20. There were vertical and lateral springs attached at the basement to simulate rocking and sway behaviour. Stiffness of each spring was determined after trial and error. Applying the same interface forces obtained from the sub-structure pseudo dynamic test, the displacement of the model was calculated. Figure 21 shows the comparison of lateral force-displacement relationships between the model and test specimen. It can be seen that the loop shape of the test specimen is well traced by the model.

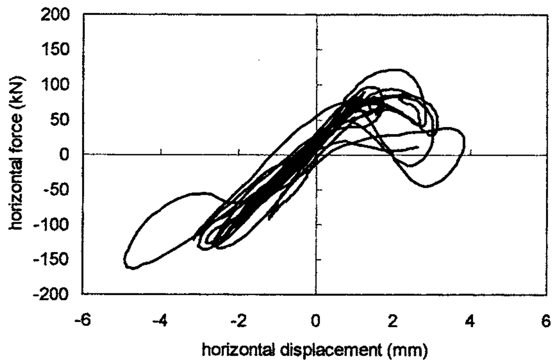

(a) Brace frame

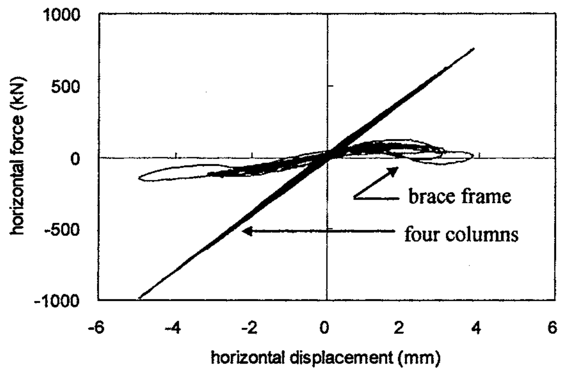

(b) Brace frame and four corner columns

Figure 19 Shear force and displacement relationship at the 1st story

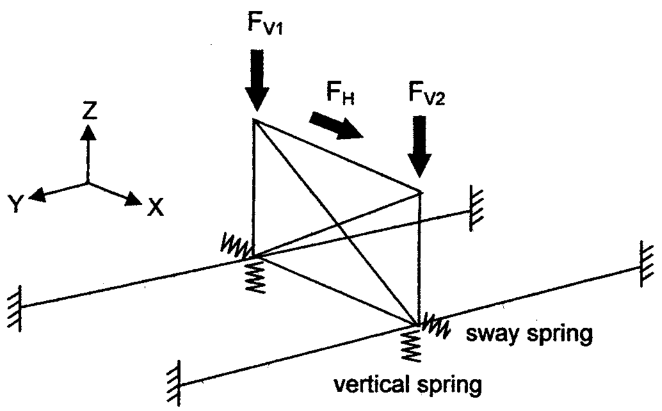

(a) mathematical model of brace frame

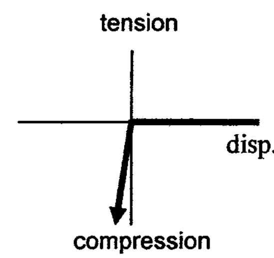

(b) characteristic of vertical spring

Figure 20 Mathematical model of the physical sub-structure

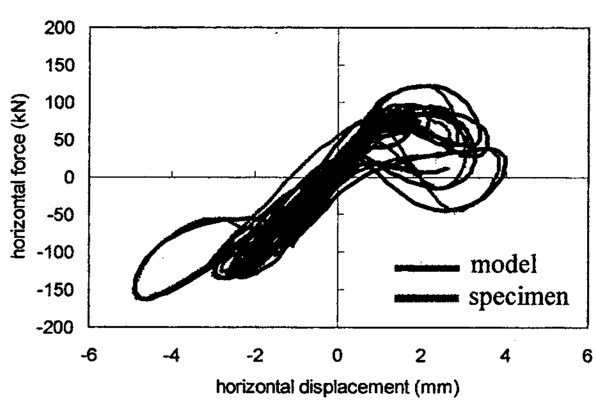

Figure 21 Comparison of hysteresis loops between model and specimen

CONCLUSIONS

This paper presented the outline of the pseudo dynamic test of a 6-story reinforced concrete wall-frame structure conducted in the Large Scale Testing Laboratory in BRI. The lateral shear force distributions among wall and column elements are examined in detail by comparing with the results of the push-over analysis and the virtual work method.

A new system of the sub-structure pseudo dynamic test is also introduced with the results of the preliminary test of a steel specimen. After confirming the effectiveness of the testing method, a reinforced concrete sub-structure is planned to be tested subsequently and the result will be compared with the previous full structure test.

ACKNOWLEDGEMENTS

This research was carried out as a part of Special Project for Earthquake Disaster Mitigation in Urban Areas under the support of Ministry of Education, Culture, Sports, Science and Technology, Japan.

REFERENCES

Saito, T. , Ogawa, J., Shibuya, J and Fu, J. (1991). Analysis of Inelastic Behaviour of Wall-Frame Structures", *Proceedings of the Japan Concrete Institute*, Vol.13, No.2, pp.613-618 (in Japanese).

Sugano, S. (1970). Experimental Study on Restoring Force Characteristics of Reinforced Concrete Members, *Doctor of Engineering Thesis, University of Tokyo* (in Japanese).

Nakashima, M., Ishii, K. and Ando, K. (1990). Integration techniques for substructure pseudo-dynamic test, *Proc. fourth National Conference of Earthquake Engineering,* Vol.2, pp.515-524.

Li, K-N. and Otani, S. (1993). Multi-Spring Model for 3-Dimensional Analysis of RC Members, *Journal of Structural Engineering and Mechanics.* Vol. 1.

AN EXPERIMENTAL STUDY ON 6-STORY R/C STRUCTURE WITH MULTI-STORY SHEAR WALL
PART 2: LATERAL FORCE CARRIED BY WALL AND OPEN FRAMES

Koichi KUSUNOKI[1], Tomohisa MUKAI[1], Masaomi TESHIGAWARA[2], Hiroshi FUKUYAMA[1], Hiroto KATO[1], and Taiki SAITO[1]

ABSTRACT

In order to study what amount of lateral force and varied axial force are carried by the wall frame in reinforce concrete buildings with multi-story shear wall, the pseudo-dynamic test with 2-span-1-bay-6-story reinforced concrete structure with a multi-story shear wall was conducted with the parameter of the rigidity at the bottom of shear wall. The test results were discussed with the numerically calculated strengths in terms of the varied axial force borne by the wall frame, lateral force carried by the wall frame, lateral force distribution mode, and the equivalent height of the specimen and the wall frame.

1. INTRODUCTION

In the reinforced concrete structure that has multi-story shear wall frame (hereafter referred to as wall frame) and open frame, the stiffness and strength of the wall frame are gererally much larger than those of the open frame. Therefore, the amounts of horizontal force and varied axial force due to overturning moment carried by the wall and open frames are quite different. Furthermore, the wall frame makes rocking vibration according to the details and characteristics at the bottom of the wall frame, such as the vertical stiffness of ground and stiffness of transverse ground girders. Thus, the vertical stiffness of the ground and stiffness of transverse ground girders affect the bending stiffness of the wall frame.

In order to develop a more sophisticated seismic design method for reinforced concrete structures that have wall and open frames, it is inevitable to figure out how much horizontal force and varied axial force are carried by the wall frame, and to clarify the effect of details and

[1] *Structural Engineering Department, Building Research Institute, Tsukuba, Japan*
E-mail: kusunoki@kenken.go.jp
[2] *Department of Architecture, School of Engineering, Nagoya University, Nagoya, Japan*
E-mail: teshi@corot.nuac.nagoya-u.ac.jp

characteristics at the bottom of the wall frame on the behavior of the structures. Experimental test to study these topics has, however, not been conducted before, because it requires relatively large specimen. As a part of Dai-Dai-Toku project, a pseudo-dynamic test with 1-span-2-bay-6-story reinforced concrete structure, which has a multi-story shear wall at the center of the structure was conducted in Building Research Institute. The parameter of the test was the detail at the bottom of the wall frame; the wall frame was fixed to the reacting wall for one test series (hereafter referred to as rigid specimen), and not fixed for the other test series (hereafter referred to as rocking specimen). The differences of the amount of horizontal force carried by the wall frame between the rigid and rocking specimens will be discussed in this paper.

2. OUTLINE OF THE PSEUDO-DYNAMIC TEST

Figure 1 shows the dimension of the specimen and the loading system. The specimen has one span of 1.8m in the loading direction, two spans of 2.0 m in the perpendicular to the loading direction, and six stories. In order to prevent torsional response, the wall frame was installed in the mid frame (X2 frame). The specimen was 1/3-scaled model, and the additional weight of 61.5kN was loaded on each floor. Total weight of each floor was 87.9kN for roof, 91.8kN for 2 to 6 floors, and 26.8kN for the basement.

The X1 and X2 frame basements were fixed rigidly to the reacting floor with R/C mass. On the other hand, a rubber sheet (t=50mm, K_v=423kN/mm) was installed between the X2 frame basement and R/C mass so that the wall frame can rotate (refer Fig. 1 (d)) for the rocking specimen. The lateral movement of the X2 frame basement was restrained with the steel angle shown in Figure 1. The weight of the X2 frame basement was 11.4 kN. For the rigid specimen, the X2 frame basement and R/C mass was bound with PC steel bars.

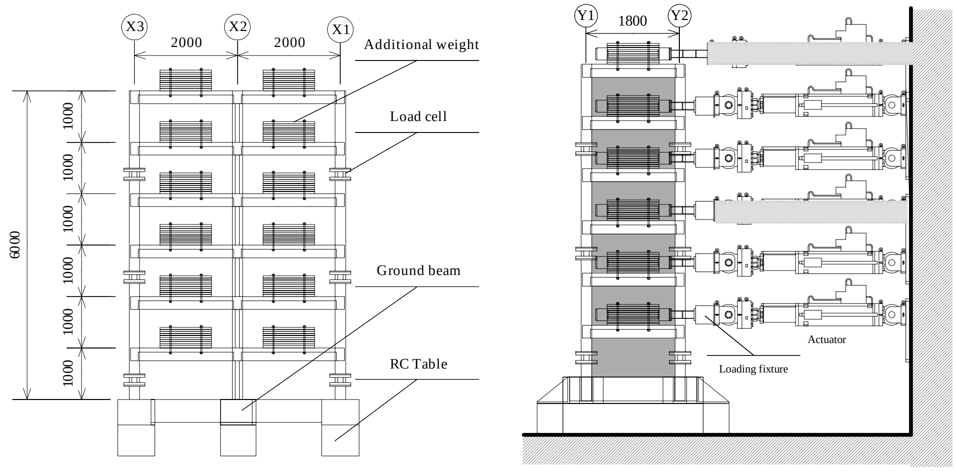

(a) Elevation for the perpendicular to the loading direction **(b) Elevation for the loading direction**

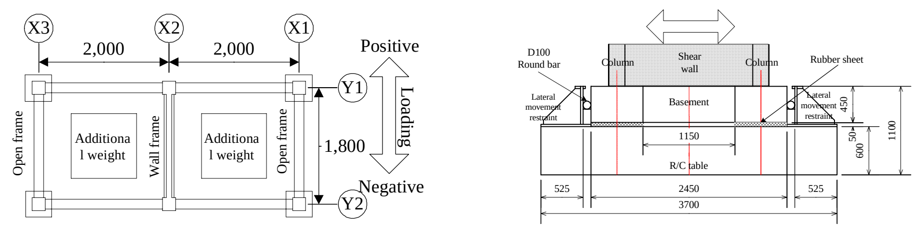

(c) Plan **(d) Basement of X2 frame**

Fig. 1: Specimen and loading system

The elevation of the loading system is shown in Figure 1 (b). Each floor had one actuator except roof floor. Actuators were attached to the additional steel weight on the floors with the loading fixture. Only the roof floor had two actuators to prevent torsional response.

The six-degree-of-freedom shear vibration model with lumped mass was applied for the pseudo-dynamic test. The OS integral method [Nakashima et. Al., 1990] was adopted to solve equation of motion. The damping was modeled proportional to the initial stiffness, and the damping coefficient of 2% to the first elastic resonant period was used.

First, the unit loading, which is to load small force to each floor, was conducted to measure the stiffness matrix of the specimen. The lateral story stiffness was measured as 1,470kN/mm from the unit loading. With the minimum controllable displacement of the actuator of 0.01mm, such high story stiffness leaded large force controlling error. Therefore, it was predicted that the motion of equation cannot be solved and tended to diverge. Therefore the degree-of-freedom of the specimen was reduced again down to second-degree-of-freedom for the pseudo-dynamic test. The lumped masses were assumed to locate at 4th and roof floor. The masses were decided so that the first mode shape of the second-degree-of-freedom system coincides with that of the six-degree-of-freedom system (obtained from the unit loading). The ratios of the base-shear and overturning moment of the second-degree-of-freedom system to those of six-degree-of-freedom system were 0.96 and 0.995 for the rocking specimen and 0.97 and 0.98 for the rigid specimen respectively. They agreed very well with each other. Thus, only the hatched actuators in Figure 1 were used for the pseudo-dynamic test.

The earthquakes recorded at Tohoku University during the 1978 Miyagi-Ken-Oki Earthquake (hereafter referred to as Tohoku), at El Centro during the 1940 Imperial Valley earthquake (NS component, hereafter referred to as El Centro), at Kobe Marine Observatory and Takatori during the 1995 Kobe Earthquake (hereafter referred to as JMA Kobe and Takatori, respectively) were applied for the input motions. They were normalized so that the maximum velocities of the records became 0.25 to 2.50 m/sec in full scale. The durations of input motion were about 7 seconds, which included principal portion of the records. Since the Takatori, the last input motion, did not make a total collapse of the specimen, static cyclic loading was conducted until the specimen collapsed. The lateral force distribution mode for the static loading was roof floor : 4th floor = 1.5 : 1.0, which was the mode at the maximum response displacement during Takatori input. The loading history was summarized in Table 1.

Table 1: Loading history

Date	Input motion	Velocity in full scale(m/sec)
rocking specimen		
8/29	Unit loading	
9/19	Tohoku	0.25
9/20	El Centro	0.37
9/22	JMA Kobe	0.50
9/23	JMA Kobe	0.75
Rigid specimen		
9/27	Unit loading	
9/29	JMA Kobe	0.50
9/30	JMA Kobe*	0.75
10/9	JMA Kobe	0.75
10/10	Takatori	2.50
10/10	Static loading	

*Terminated along the test due to a problem in the loading system

Seventy-two transducers were instrumented into the specimen to measure lateral story deformation, beam and column deformation, rocking and sway at the basement. The forces induced by actuators were measured by the load cells attached to the actuators. Strains of main bars, hoops, shear reinforcements in beams, columns, and walls were measured with 275 strain gauges. Specially prepared load cells to measure vertical and lateral forces were also installed into the mid-height of the columns on the first, third, and fifth stories (Fig. 1 (a)).

3. STRENGTH OF THE SPECIMEN CALCULATED WITH THE METHOD OF VIRTUAL WORK

Because of the capacity of the loading system, the capacity of the specimen was expected as small as possible. Because of that, beams were designed only to resist the gravity force with the assumption that the structure has infinite uniform span. Then columns were designed so that the structure achieves the weak-beam-strong column total yielding system. As the result, 3-D10 was arranged for upper and bottom of beams, and 12-D13 was arranged for columns. The design material strengths were 30N/mm^2 for concrete and 295 N/mm^2 for steel bars

Calculated yield strengths of beams with design material strength and material test result are listed on Table 2. Yield strengths of column and shear wall are listed on Table 3. The ultimate horizontal strength of specimen was calculated with the method of virtual work and strengths on Table 2 and Table 3. Considered yield mechanisms of the specimen are shown in Figure 2. That is total yield mechanism of beam-yield type for the open frames ((a) in Fig. 2), yield at the bottom of the wall frame ((b) in Fig. 2), and yield at both ends of transverse beams ((c) in Fig. 2) for the rigid specimen. For the rocking specimen, the effect of lifting ((b) in Fig. 2) was considered instead of yield at the bottom of wall frame. The inverse triangular distribution shape and uniform distribution shape were applied for the lateral force distribution shape. Calculated ultimate horizontal strength and its base-shear coefficient are listed on Table 4. The lateral forces carried by the columns in the open frames were also listed on Table 5.

Axial force N acts in the tensile column due to the effect of lifting and yield of transverse beams as shown in Figure 3. The lateral force Q due to the overturning moment M by N must be carried by some structural members. For the rocking specimen, Q can be carried by (1) horizontal stopper, (2) friction between R/C table and basement, (3) columns in the first story, and/or (4) directly going to the reacting floor through the transverse ground beams. For the rigid specimen, Q can be carried by (1) shear wall and/or (2) columns in the first story. When Q is carried by the shear wall or columns in the first story, their inflection heights get lower than the heights when they resist to the lateral force due to the mechanism shown in Figure 2 (a) and (b) in order to increase the horizontal strength. If shear wall fails in shear and columns fails in shear or yields at both ends, the effect of lifting and yield of transverse beams cannot be counted any more, since no structural member can carry Q any more. The horizontal resistance due to lifting and yield of transverse beams are listed on Table 6.

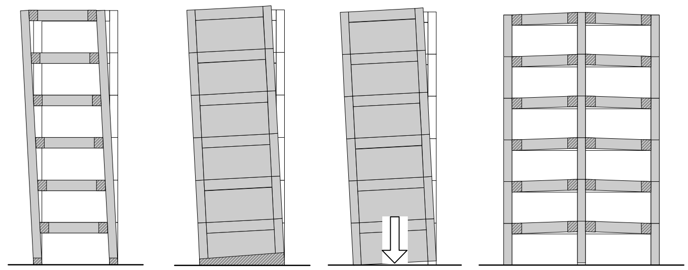

(a)Open frame (b)Wall frame (c)Lift-up (d)Transverse beam

Fig. 2: Yield mechanism considered to the virtual work method

Table 2: Yield strength of beams (kN*m)
Design material strength/Material test result

Effective width of slab		Beams	Transverse beams	Ground beams	Transverse ground beams
Tension at upper end	0.1ℓ	17.0/20.3	16.2/19.4	32.3/38.7	47.2/56.5
	Whole width	32.7/39.1	29.3/35.0	32.3/38.7	47.2/56.5
Tension at bottom end		12.3/14.8	13.0/15.6	31.4/37.5	48.3/57.9

Table 3: Yield strength of columns and shear walls
Design material strength/Material test result

	Column		Shear wall
	X1 and X3 frame	X2 frame	
Yield strength	35.9/40.9	41.9/47.2	1071.1/1233.1

Table 4: Ultimate horizontal strength (upper: kN, lower: base shear coef.)
Design material strength/Material test result

		Rocking specimen		Rigid specimen	
Effective width of slab		0.1ℓ	Whole width	0.1ℓ	Whole width
Mode shape	Triangular	340.5/383.0 0.59/0.67	424.0/483.0 0.74/0.84	493.7/565.4 0.90/1.03	583.7/673.1 1.07/1.23
	Uniform	419.4/471.8 0.73/0.82	522.4/595.1 0.91/1.04	611.4/700.3 1.12/1.28	722.9/833.7 1.32/1.52

Table 5: Ultimate horizontal strength of open frame
kN / Ratio to the total strength

	Effective width of slab	Rocking specimen		Rigid specimen	
		0.1ℓ	Whole width	0.1ℓ	Whole width
Triangular	Compressive	22.84/0.06	128.76/0.27	31.60/0.06	142.18/0.21
	Tensile	91.10/0.24	45.86/0.09	91.10/0.16	45.86/0.07
	Total	113.94/0.30	174.62/0.36	122.70/0.22	188.04/0.28
Uniform	Compressive	49.27/0.10	169.27/0.28	60.87/0.09	187.04/0.22
	Tensile	91.10/0.19	45.86/0.08	91.10/0.13	45.86/0.06
	Total	140.37/0.29	215.13/0.36	151.97/0.22	232.90/0.28

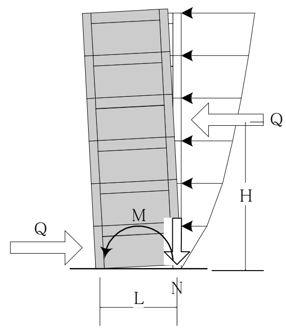

Fig. 3: Resistance mechanism due to lift and transverse beams

Table 6: Ultimate horizontal strength due to lift and transverse beams

kN / Ratio to the total strength

		Rocking specimen		Rigid specimen	
Effective width of slab		0.1ℓ	Whole width	0.1ℓ	Whole width
Mode shape	Triangular	269.0/0.70	308.4/0.64	156.8/0.28	199.2/0.30
	Uniform	331.4/0.70	379.9/0.64	194.2/0.28	246.7/0.30

4. VERTICAL AND LATERAL FORCE CARRIED BY THE WALL FRAME

4.1 Method to Calculate Vertical and Lateral Force Carried by the Wall Frame

As shown in Figure 1, load cells were installed into the mid-height of four columns in first, third and fifth stories to measure the restoring forces in the vertical and loading horizontal directions. The initial values for the vertical load cells were recorded when they were on the ground without any load on them. The initial values for the lateral load cells and transducers were recorded just after the unit loadings. As a trouble occurred in the loading system during the JMA Kobe 75 kine input to the rigid specimen, some transducers were re-installed. Therefore, the initial values were recorded again before inputting the JMA Kobe 75 again for the rigid specimen.

The lateral force carried by each floor, $Q_{1\sim6}$, is calculated as follows with the actuator forces measured on the 4th and roof floor, F_4 and F_R.

$$\begin{cases} Q_{1\sim3} = \mathrm{F}_4 + \mathrm{F}_\mathrm{R} \\ Q_{4\sim6} = \mathrm{F}_\mathrm{R} \end{cases} \tag{1}$$

The lateral forces carried by the shear walls in the first, third, and fifth stories are calculated as the $Q_{1\sim6}$ subtracted by the lateral forces carried by columns measured with the load cells in columns. The overturning moment at the mid-height of each story, $M_{1\sim6}$, is calculated as follows with the height between each mid-height level to each actuators, $h_{1\sim6\,\mathrm{to\,R}}$ and $h_{1\sim3\,\mathrm{to}\,4}$.

$$\begin{cases} M_{1\sim3} = h_{1\sim3\,\mathrm{to}\,4} \cdot \mathrm{F}_4 + h_{1\sim3\,\mathrm{to\,R}} \cdot \mathrm{F_R} \\ M_{4\sim6} = h_{4\sim6\,\mathrm{to\,R}} \cdot \mathrm{F_R} \end{cases} \tag{2}$$

The varied axial force due to the overturning moment ΔN is calculated as $M_{1\sim6}$ divided by the span length of 1,800mm. The varied axial force borne by the columns in the first, third, and fifth stories, ΔN_{Column}, were calculated as the measured axial forces with the load cells subtracted by the gravity load, which was the initial values measured before Tohoku input. The varied axial force carried by the shear wall is calculated as ΔN subtracted by ΔN_{Column} of two columns in the compression and tension sides.

The axial and lateral forces carried by the wall and columns were studied at the points on the skeleton curve of the relationship between base-shear and representative displacement proposed by Kusunoki and Teshigawara [Kusunoki and Teshigawara, 2003]. The base-shear, Q_1, is calculated with Equation 1. The representative displacement, Δ, is calculated with Equation 3. The points on the skeleton curve are the largest or smallest displacement points among first to its data points.

$$\Delta = \frac{\sum m_i \cdot {}_M x_i}{\sum m_i} \tag{3}$$

where, m_i is the mass of each story and $\{{}_M x\}$ is the relative displacement vector to the basement. All input motions to the rigid specimen were assumed to be inputted consecutively. The input motions of second JMA Kobe 75 and after were also assumed to be inputted consecutively to the rocking specimen.

The skeleton curves of the relationship between base-shear and representative displacement of the rocking and rigid specimen were shown in Figures 4 and 5, respectively. The calculated horizontal strengths of the specimen with material test results, effective slab width of 0.1ℓ and whole width, and horizontal force distribution shapes of uniform distribution shape and inverse triangular distribution shape (refer section 2) are also superimposed into each figure. The base-shear reached the strength calculated with 0.1ℓ effective width and inverse triangular distribution shape during JMA Kobe 50 and strength calculated with whole slab width as effective and inverse triangular distribution shape during JMA Kobe 75 for the rocking specimen. According to the measured strains, the rocking specimen formed the total yielding mechanism at the maximum displacement. The base-shear reached the strength calculated with 0.1ℓ effective width during Takatori for the rigid specimen, but the horizontal force distribution shape was between uniform and inverse triangular.

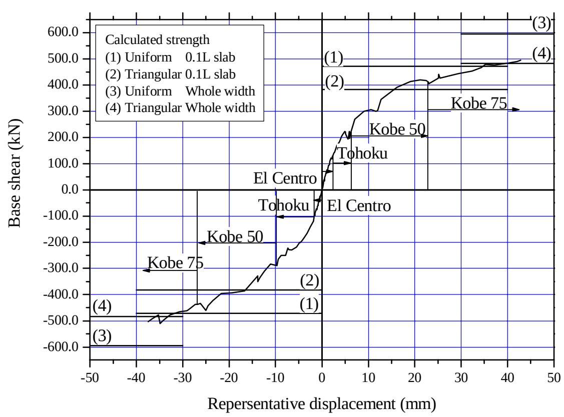

Fig. 4: Envelope curves of the relationship between base-shear and representative displacement of the rocking specimen

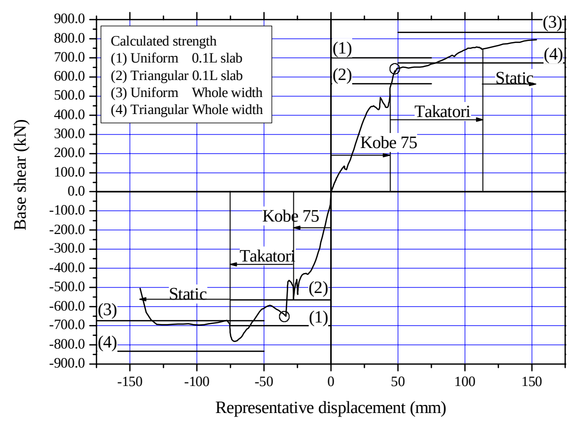

Fig. 5: Envelope curves of the relationship between base-shear and representative displacement of the rigid specimen

4.2 Lateral Force Carried by the Wall and Open Frames

Figure 6 shows the relationship between the lateral force carried by the wall and open frames and the representative displacement of the rocking specimen. The lateral forces carried by the open frame and the wall frame (the effect of lifting and yield of transverse beams) calculated with the method of virtual work when the whole slab width is effective and horizontal force distribution shape is uniform and inverse triangular. Here, the lateral force carried by the open frame was calculated as the lateral force at the total yielding mechanism of the open frame (Fig. 2 (a)), and then the lateral force carried by the wall frame was calculated as the total lateral force subtracted by the calculated lateral force carried by the open frame. At the maximum displacement when the total yielding mechanism was achieved, the measured lateral force carried by open frames was more than the calculated value, and the measured force carried by the wall frame was less than the calculated value. Since the horizontal ultimate strength coincided with the calculated strength as shown in Figure 4, the amount of differences of the measured and calculated lateral force of the open frame and wall frame were almost the same. It can be said that some of the lateral force due to the effect of lifting and yield of transverse beams went to the open frame through the slab and the transverse beams.

Figure 7 shows the relationship between the lateral force carried by the wall and open frames and the representative displacement of the rigid specimen. The lateral force carried by the open frame and wall frame calculated with the method of virtual work with whole slab width as effective and uniform distribution shape. The data point when the stiffness of the open frames degraded drastically (Point B on the figure) agreed with the calculated base shear in both positive and negative loading direction. The lateral force carried by the wall and open frames were almost constant after point B, but not after point C when the shear wall failed in shear. The secant stiffness to the data point when the stiffness of the wall frame degraded drastically (Point A on the figure) in the positive loading direction was smaller than the secant stiffness in the negative loading direction. Followings can be raised as reasons; the effect of damages during the rocking loading test, and the rigidity at the bottom of the wall frame. At the maximum displacement in the positive direction which did not show any resistance deterioration, some of the lateral force calculated to be carried by the wall frames was carried by the open frame as observed with the rocking specimen. The reason why the amount of difference of measured and calculated lateral force of the open frame and wall frame is that the actual horizontal force distribution shape was in between uniform and inverse triangular that will be shown in Section 0, while the uniform distribution shape was applied for the calculation.

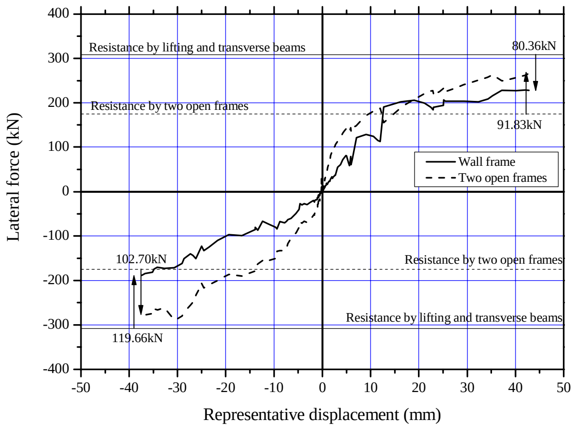

Fig. 6: Lateral force carried by shear wall and open frames (rocking specimen)

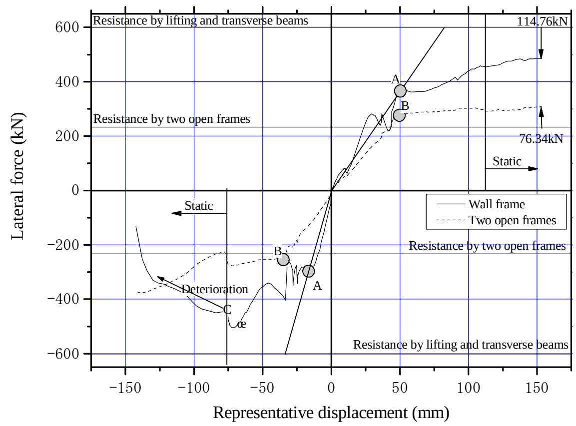

Fig. 7: Lateral force carried by shear wall and open frames (rigid specimen)

4.3 Lateral Force Carried by Columns in Compressive and Tensile Side

Figure 8 shows the relationship between the ratio of the lateral force carried by the columns in the Y1 and Y2 frame to the base shear and the representative displacement of the rocking specimen. The ratio calculated with the method of virtual work with whole slab width as effective and inverse triangular horizontal force distribution shape was also shown in the figure. The ratio in the tensile side gets smaller according to the deformation, and then the ratio reached the calculated ratio at the maximum displacement when the total yielding mechanism was achieved. On the other hand, the ratio in the compressive side increased even when the displacement was small, and then the ratio became constant, which was much higher than the calculated ratio. It shows that the lateral force due to the effect of lifting and yield of transverse beams was carried mostly by the column in the compressive side.

Figure 9 shows the relationship between the ratio of the lateral force carried by the Y1 and Y2 frame to the base shear and the representative displacement of the rigid specimen. The ratio calculated with the method of virtual work with whole slab width as effective and uniform horizontal force distribution shape was also shown in the figure. The ratio in the tensile side reached the calculated ratio when the displacement became large, and the ratio in the compressive side was much larger than the calculated ratio as observed in the rocking specimen.

It also shows that the lateral force due to the effect of lifting and yield of transverse beams was carried mostly by the column in the compressive side as the rocking specimen.

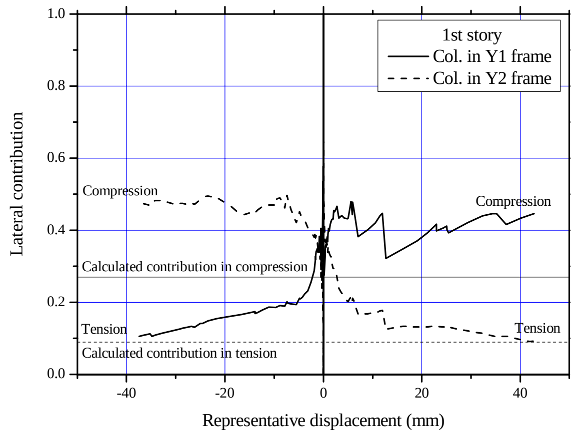

Fig. 8: Ratio of lateral force carried by columns in Y1 and Y2 frames (rocking specimen)

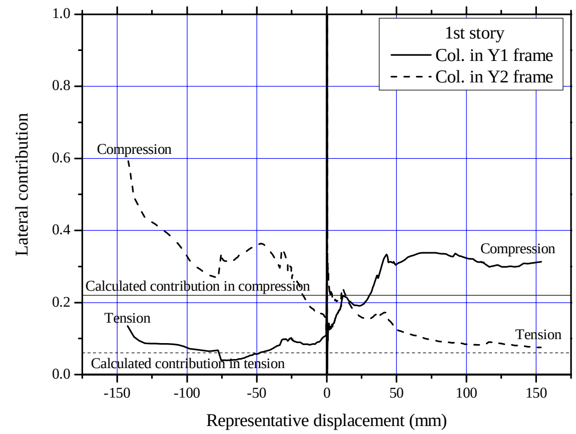

Fig. 9: Ratio of lateral force carried by columns in Y1 and Y2 frames (rigid specimen)

Figure 10 shows the relationship between the ratio of the inflection height to the clear height of the columns in the first story and representative displacement of the rocking specimen. The inflection height was calculated as *Mu/Q/h*, where *Mu* is the flexural strength, *Q* is the lateral force measured with the load cell installed in the column, and *h* is the clear height of the column. The flexural strength of the column *Mu* was calculated with Equation 4 [AIJ, 1990] with the axial force measured by the load cell. Note that the calculated inflection height ratio becomes larger than the actual ratio when the bottom of column has not yielded yet.

$$M_u = \begin{cases} \left(0.5 \cdot a_g \cdot \sigma_y \cdot g_1 \cdot D + 0.024(1+g_1)(3.6-g_1)b \cdot D^2 \cdot F_c\right)\dfrac{N_{\max}-N}{N_{\max}-N_b} & N_{\max} \geq N > N_b \\ 0.5 \cdot a_g \cdot \sigma_y \cdot g_1 \cdot D + 0.5N \cdot D \cdot \left(1 - N/(b \cdot D \cdot F_c)\right) & N_b \geq N > 0 \\ 0.5 \cdot a_g \cdot \sigma_y \cdot g_1 \cdot D + 0.5N \cdot g_1 \cdot D & 0 \geq N \geq N_{\min} \end{cases} \tag{4}$$

where;

a_g Total area of re-bars in column

σ_y Yield stress of re-bar

g_1 Ratio of distance between re-bars in compressive and tensile side to the depth of column

b Width of column

D Depth of column

F_c Concrete strength

N Axial force

$$N_{\max} = b \cdot D \cdot F_c + a_g \cdot \sigma_y$$

$$N_b = 0.22(1 + g_1) \cdot b \cdot D \cdot F_c$$

$$N_{\min} = -a_g \cdot \sigma_y$$

Figure 10 shows that the inflection height ratios for the compressive and tensile columns are almost the same for the rocking specimen, and they got smaller according tot the deformation. The inflection point was, however, at higher than mid-height of the column, and the top of the column had not yielded.

Figure 11 shows the relationship between the inflection height ratio to the clear height and the representative displacement of the rigid specimen. The inflection height ratio in both compressive and tensile sides was less than 1.0 when the representative displacement was larger than about +/- 50mm when the total yielding mechanism was supposed to be achieved (Point B in Fig. 7). The ratio for the compressive column was, however, more than 0.5 and then the top of the column did not yield. On the other hand, the ratio for the tensile column was less than 0.5 when the displacement was more than 50mm in the positive direction and less than -100mm in the negative direction. Therefore, the top of the column was supposed to yield under the tensile varied axial force.

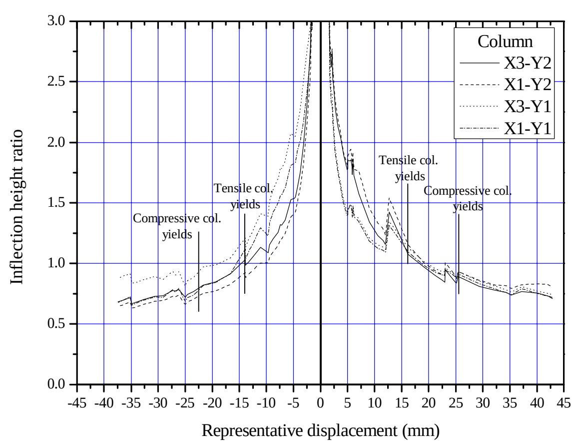

Fig. 10: Lateral force carried by columns in Y1 and Y2 frames (rocking specimen)

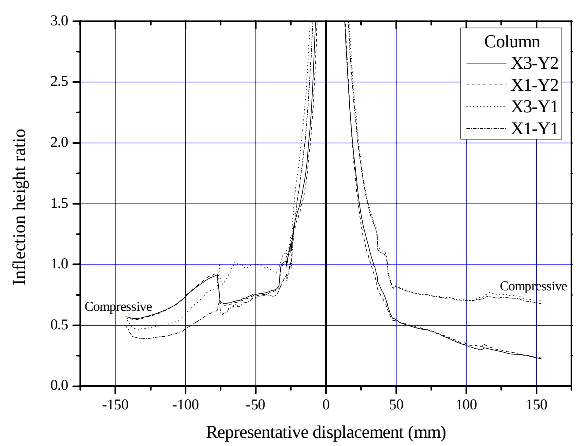

Fig. 11: Lateral force carried by columns in Y1 and Y2 frames (rigid specimen)

Figure 12 shows the lateral forces measured by the load cell installed into the mid-height of the columns. The horizontal strength of columns calculated with Equation 4 with axial force measured by the load cell and the assumption of the inflection height ratio of 0.5. This figure also shows that the top of the column in the tensile side yielded. The calculated strength in the tensile side underestimates from the figure. That is the reason why the inflection height ratio became less than 0.5 in Figure 11.

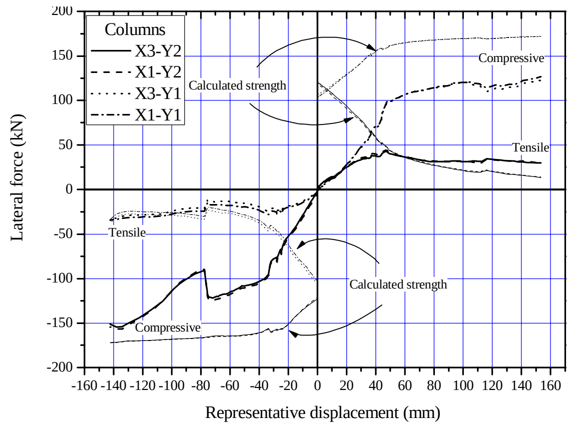

Fig. 12: Lateral force carried by the open frame and calculated lateral strength (rigid specimen)

5. OVERTURNING MOMENT AND LATERAL FORCE DISTRIBUTION SHAPE

The base shear, Q is calculated with Equation 1. If the horizontal force distribution shape is uniform (Fig. 13 (a)), the overturning moment, M, is calculated as Equation 5 with Q and each mass m_1 and m_2.

$$M = (m_1 \cdot h_1 + m_2 \cdot h_2)\frac{Q}{m_1 + m_2} \tag{5}$$

If the horizontal force distribution mode is inverse triangular (Fig. 13 (b)), the overturning moment, M, is calculated as Equation 6.

$$M = (m_1 \cdot h_1 + m_2 \cdot h_2^2/h_1)\frac{Q}{m_1 + m_2 \cdot h_2/h_1} \tag{6}$$

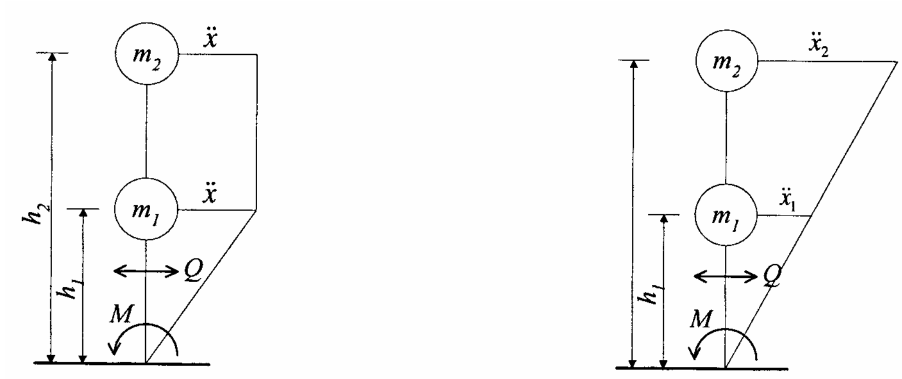

(a) Uniform distribution shape (b) Inverse triangular distribution shape

Fig. 13: Vibration mode and overturning moment

If the horizontal force distribution shape is uniform distribution shape or inverse triangular distribution shape, the overturning moment of the specimen calculated with Equation 2 coincides with the moment calculated with Equation 5 and Equation 6 respectively.

Figure 14 shows the relationship between the recorded overturning moment and the representative displacement of the rocking specimen. The overturning moments calculated with Equation 5 and 6 for the uniform and inverse triangular distribution shape are also superimposed to the figure. From the figure, the horizontal force distribution mode of the rocking specimen was closer to the inverse triangular shape than to the uniform shape. The upper part of the distribution shape became even larger than the inverse triangular shape when the representative displacement was larger than about 20mm.

Figure 15 shows the relationship between the recorded overturning moment and the representative displacement of the rigid specimen. As mentioned earlier, the distribution shape was fixed as roof floor : fourth floor = 1.5 : 1.0 during the static loading. Therefore, the ratios of recorded overturning moment to the moments calculated with Equation 5 and 6 were constant. Although there can be seen little fluctuation, the distribution shape was closer to the uniform distribution shape than to the inverse triangular distribution shape, but did not achieve the uniform distribution shape.

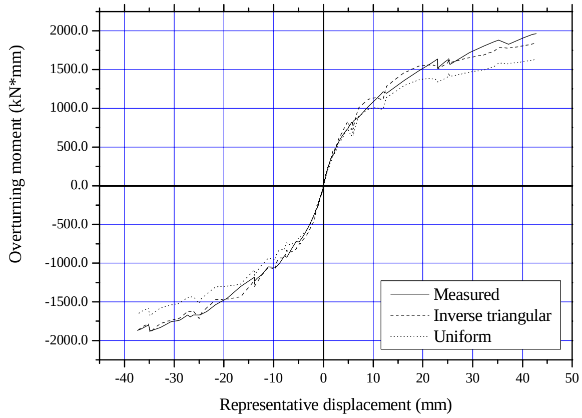

Fig. 14: Measured overturning moment (rocking specimen)

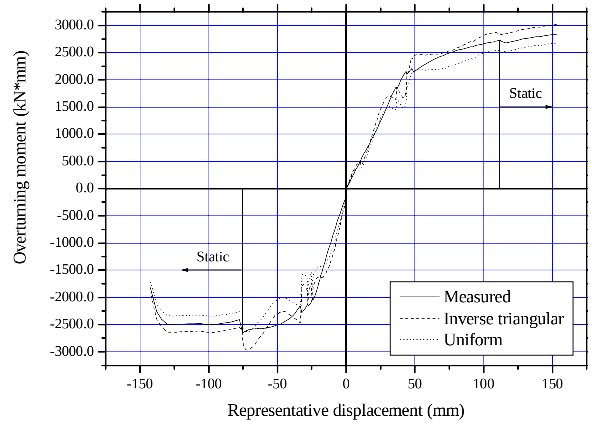

Fig. 15: Measured overturning moment (rigid specimen)

Figure 16 shows the relationship between the equivalent height of the specimen and the wall frame and the representative displacement. The equivalent height of the specimen was calculated as the overturning moment calculated with Equation 2, M, divided by the base shear calculated with Equation 1, Q. The overturning moment carried by the open frames, M_{open}, was calculated as $(N1+N2) \cdot L/2$, where N1 and N2 are varied axial forces and L is the clear span length as shown in Figure 17. The overturning moment carried by the wall frame, M_{wall}, was calculated as M- M_{open}. The equivalent height of the wall frame was calculated as the M_{wall} divided by the lateral force carried by the shear wall, Q_{wall}.

Figure 16 shows that the equivalent height of the specimen was constantly about 4m. On the other hand, the equivalent height of the wall frame in the very small deformation range was almost 10m, which was much higher than the height of the frame and showed the pure bending behavior. Figure 18 shows the relationship between the opening at the bottom of the wall on the Y1 and Y2 frame and the representative displacement. From Figures 16 and 18, the equivalent height of the wall frame dropped down drastically to the same as the equivalent height of the specimen at the opening of about 2mm.

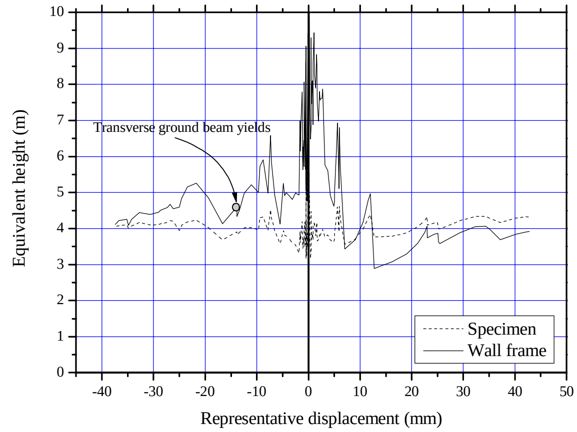

Fig. 16: Equivalent height of the specimen and shear wall (rocking specimen)

Figure 19 shows the relationship between the equivalent height and the representative displacement of the rocking specimen. The static loading result was not studied here, since the lateral force distribution shape was fixed during the static loading. Although the result was fluctuated, the equivalent height by the representative displacement of 50mm in the positive direction was about 4m. Then the equivalent height of the wall frame dropped down to 3m. The reason of the fluctuation came from the fluctuation of the story shear around peak displacements due to a higher mode effect as shown in Figure 20. In other words, the response displacement at the top was affected by the higher modes and became larger or smaller than the first mode. The equivalent height goes up when the response displacement at the top becomes larger than the first mode, and goes down when it becomes smaller. Thus, the equivalent height was fluctuated.

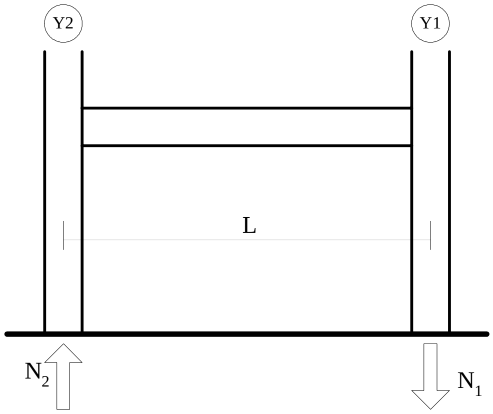

Fig. 17: Overturning moment of open frame

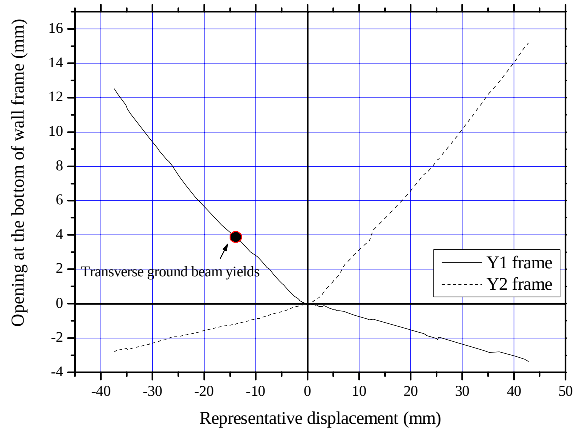

Fig. 18: opening at the bottom of the shear wall of the rocking specimen

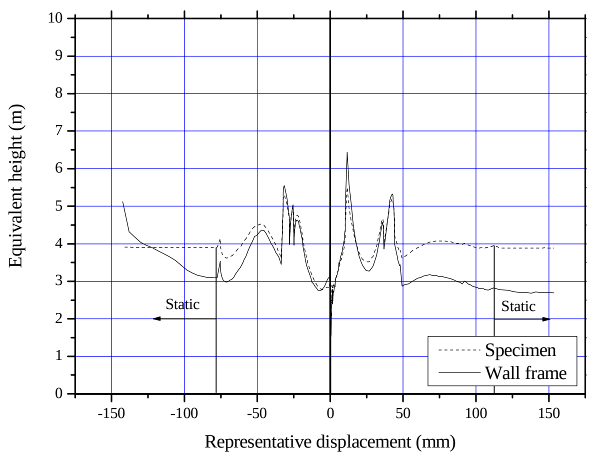

Fig. 19: Equivalent height of the specimen and shear wall (rigid specimen)

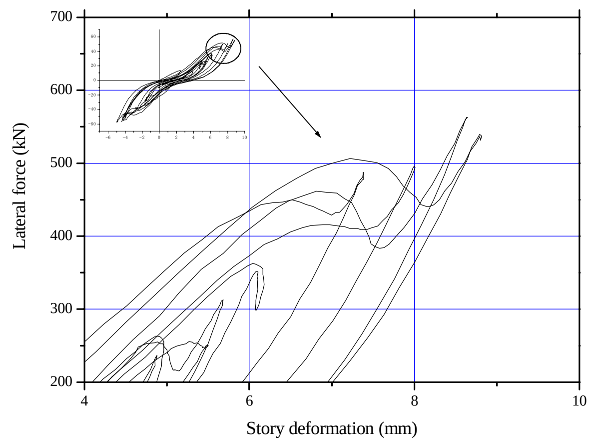

Fig. 20: Relationship between base-shear – first story deformation (rigid specimen : JMA Kobe75)

CONCLUDING REMARKS

In order to study what amount of lateral force and varied axial force are carried by the wall frame in reinforced concrete buildings with multi-story shear wall, the pseudo-dynamic test with 2-span-1-bay-6-story reinforced concrete structure with a multi-story shear wall was conducted with the parameter of the rigidity at the bottom of shear wall.

Results from the studies are summarized as follows;

- Some of the lateral force due to the effect of lifting and yield of transverse beams are carried by column in compressive side of the open frame. Therefore, the lateral force carried by the compressive column was recorded more than calculated with the method of virtual work.

- The top of the columns did not yield for the rocking specimen. The columns in the tensile side for the rigid specimen also yielded at both ends.
- The horizontal force distribution shape of the rocking specimen was closer to the inverse triangular distribution shape, while that of the rigid specimen was closer to the uniform distribution shape.
- The equivalent heights of the specimen and the wall frame of the rocking specimen were about 2/3 of the height of the specimen (4m) except very small response displacement region.
- The equivalent heights of the specimen and the wall frame of the rigid specimen were fluctuated, but about 2/3 to 1/1 of the height of the specimen (4m to 6m). The equivalent height of the wall frame was higher than of the specimen.

REFERENCES

Architectural Institute of Japan, Design Guideline for Earthquake Resistant Reinforced Concrete Buildings Based on Ultimate Strength Concept, November 1990

Koichi Kusunoki and Masaomi Teshigawara, A New Acceleration Integration Method to Develop A Real-Time Residual Seismic Capacity Evaluation System, Journal of Structural And Construction Engineering, No.569, pp.119-126, July 2003

Masaomi Teshigawara, Koichi Kusunoki, Hiroto Kato and Taiki Saito, Test Specimen and Method for Pseudo Dynamic Test on 6-Story RC Structure with Multi Story Shear Wall, Proceedings of the Japan Concrete Institute Vol.26, July 2004

Masayoshi Nakashima, Masatoshi Ishida and Kazuhiro Ando, Integration Techniques for Substructure Pseudo Dynamic Test (Pseudo dynamic test using substructuring techniques), Journal of Structural And Construction Engineering, No.417, pp.107-118, November 1990

DAMAGE PROCESS AND COLLAPSE CAPACITY OF RC FRAME STRUCTURE — FROM THE VIEWPOINT OF MECHANISM CONTROL

Takuya NAGAE[1], Shizuo HAYASHI[2], Luis IBARRA[3], and Helmut KRAWINKLER[4]

ABSTRACT

At present, the mechanism formed by strong columns and weak beams (i.e. complete mechanism) is strongly recommended as a design concept for multi-story frame structures. However, it is not easy to demonstrate quantitatively the advantages for the performance of the building, such as safety against collapse, even if the complete mechanism is guaranteed in a seismic event. From the viewpoint of reparability, it is generally difficult to repair all hinges in beams, in the case of complete mechanism. In addition, costs of downtime can be high because all of stories of the building become the target of repairing. In this paper, a concept of mechanism control is presented that intends to concentrate damages to the lower part of the frame structure and keep the rest of the structure (higher part) intact. The type of mechanism can be controlled by appropriately strengthening the upper part of the building. On the other hand, it is obvious that the extreme case, i.e. soft-first-story building can produce a poor collapse capacity. Thus, for this type of design, it becomes very important to show the balance between the reparability and the safety against collapse. In this paper at the first stage, damage process up to collapse is presented from the results of incremental dynamic analyses for reinforced concrete frame structures with different size of partial mechanisms. The response assessment for the structure is performed through probabilistic approaches, and eventually the probability of collapse is computed and compared.

1. INTRODUCTION

The mechanisms formed by strong columns and weak beams (i.e. complete mechanisms, Fig. 1) are now strongly recommended as a design concept for multi-story frame structures (AIJ 1990, Paulay 1986, et al.), because energy dissipation occurs in plastic hinges at both ends of many beams during a major seismic event. However, it is not easy to demonstrate quantitatively the advantages for the performance of the building, such as safety against collapse, even if the complete mechanism is guaranteed during an event. From the viewpoint of restoration, it is generally difficult to repair all hinges in many beams. In addition, costs in terms of downtime can be high because all of stories of the building become the target of repair.

The type of mechanism of a structure during earthquakes can be controlled by strength ratios of the upper part to the lower part, i.e. by relatively strengthening the members in the upper part of the building. As shown in Fig. 1, if a mechanism is located in a limited area, the rest of the

[1] *Researcher, Disaster Prevention Research Institute, Kyoto University, Japan, nagae@steel.mbox.media.kyoto-u.ac.jp*
[2] *Professor, Structural Engineering Research Center, Tokyo Institute of Technology, Japan*
[3] *Senior Research Engineer, Southwest Research Institute, USA*
[4] *Professor, Department of Civil and Environmental Engineering, Stanford University, USA*

building remains intact. Thus, repair work can be rationalized and also losses of downtime can be reduced.

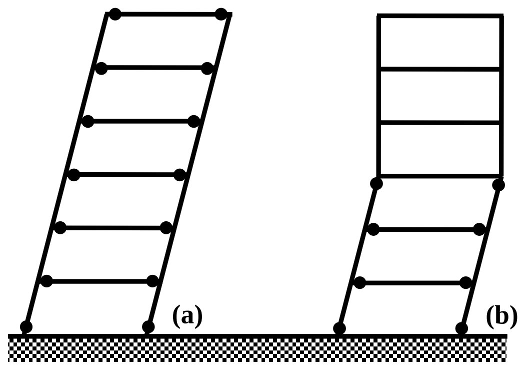

Fig. 1: (a) Complete mechanism and (b) partial mechanism

This concept also has benefits in the construction process. That is to say, though residential reinforced concrete (RC) buildings tend to have walls surrounding openings, which can contribute to the strength of building, all the walls are commonly separated from the main frame using slits in order to attain the complete mechanisms. This type of site work makes the process of construction inefficient. In the case of partial mechanism, the slits are not necessary anymore in the area where no plastic hinging occurs. Conversely, the strength provided by the walls becomes very important for the design based on the mechanism control.

Thus, the type of mechanism can be an option for performance based design, which should follow diverse demands from stakeholders or residents. On the other hand, it is obvious that a localized partial mechanism means the decrease in the number of members consuming energy. Thus, for a building designed based on mechanism control, it becomes very important to demonstrate adequate performances in terms of the damage process and the collapse capacity.

This paper demonstrates procedures to evaluate performance of RC frame structures with partial mechanism and considers the effects of the size of partial mechanism on the seismic performance. In regard to a procedure to evaluate performance of structures, a couple of studies systematically evaluated responses of buildings and highlighted the collapse capacities (Ibarra and Krawinkler 2004, Zareian and Krawinkler 2004). These studies computed collapse capacity by increasing the intensity measures related to hazard of a site, (i.e., incremental dynamic analysis, Vamvatsikos and Cornell, 2002) until the responses of the structure can be judged to have reached collapse, and statistically computed global collapse capacities to treat large scatter of output data.

2. APROACH FOR ESTIMATING THE PERFORMANCE OF STRUCTURE

2.1 Model of Analysis

In this study, twelve-story RC moment-resisting building shown in Figure 2 is considered. This building was designed in accordance with the Design Guideline Based on Ultimate Strength Concept (AIJ, 1990) in order to get a complete mechanism. That is to say, the yield strength of beam ends was decided to be larger than the moment from a static analysis assuming elastic members for the combination of the horizontal load shown in Figure 3, a dead load and a live load. Then, the strength of columns was decided to be larger enough than that of the connected

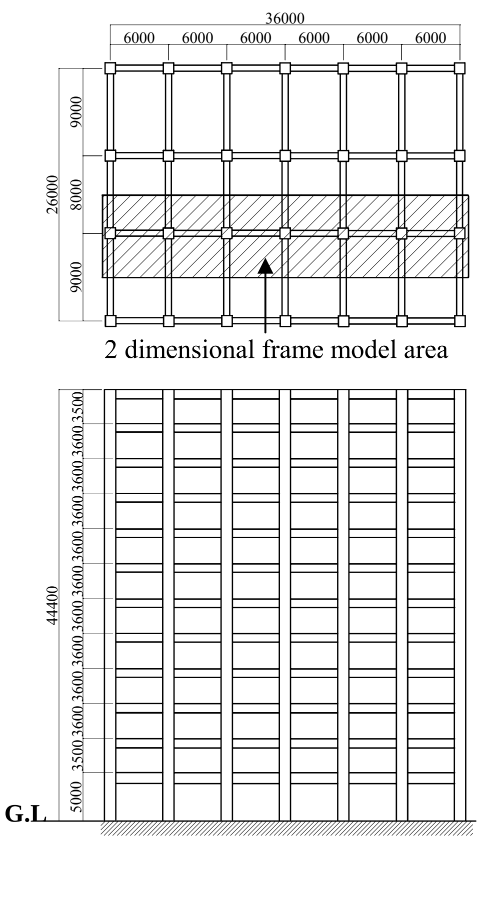

Fig. 2: Building analyzed in this study

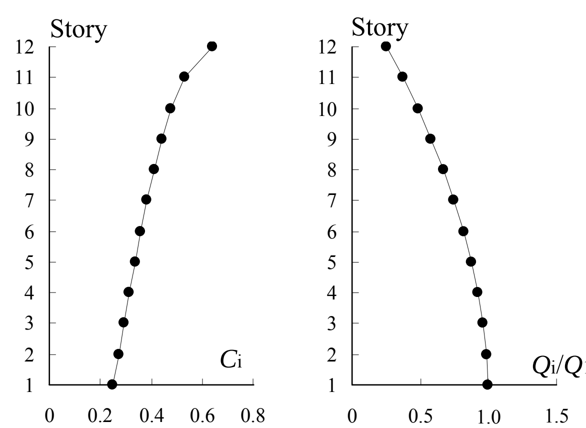

$C_i = Q_i/W_i$ Q_i: shear force of each story W_i: weight of a portion above the story Q_1: shear force of the first story

Fig. 3: Horizontal force condition for the original design

beams to attain plastic hinging in the beams. As a result, the strength distribution of beams almost corresponds to the horizontal load distribution in Figure 3.

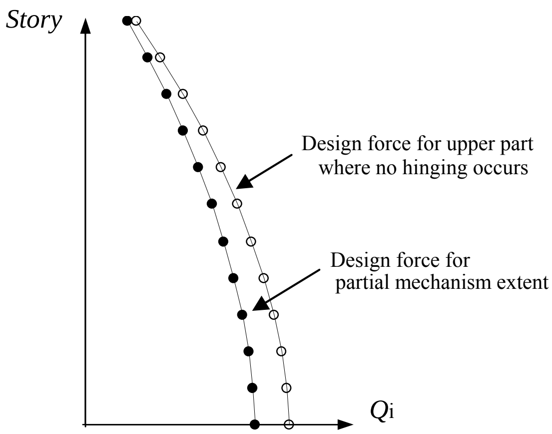

Fig. 4: Concept of story shear force *Q*i for mechanism control design

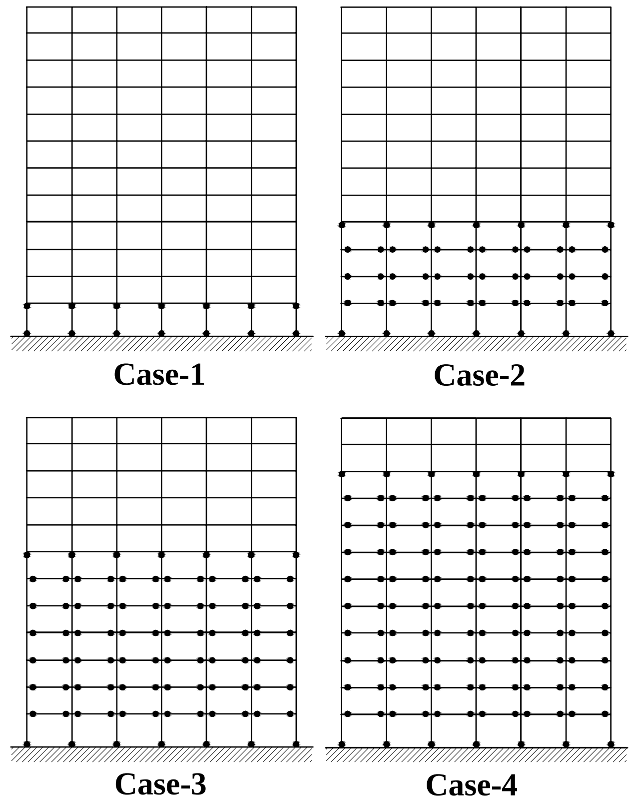

Fig. 5: Assumed partial mechanisms

The design concept to control the partial mechanism extent is depicted in Figure 4 that means the partial mechanism extent of the structure is limited by strengthening the upper part of the building appropriately. Thus, assuming that the upper part is strengthened enough, the four cases shown in Figure 5 are considered. One interior frame is realized as a two-dimensional frame model. For Case-1, the partial mechanism is located in only the first story, and for Case-2, Case-3, and Case-4, the mechanisms are extended from the first to fourth, the first to seventh and the first to tenth story, respectively.

The members in the partial mechanism extents have the same configurations as those given by the guideline's design. The beams and the top ends and the bottom ends of columns in the partial mechanism extents are modeled as inelastic members. The tops of columns in the partial mechanism extents are weakened in terms of the yield strengths because the guideline does not intend to let them yield. All members in the upper areas and the columns in the partial mechanism extents, where no plastic hinging occurs, are modeled as elastic members.

Flexural deformations of the line elements are concentrated to the ends and modeled using rotational springs. The initial stiffness of the spring K_1 is calculated using the Young modulus of concrete, the moment of inertia of gross section and the clear span. The hysteretic characteristics of the rotational spring in the partial mechanism extent are modeled by revising the Takeda Model (1970) to represent the strength deterioration after the peak strength as shown in Figure 6. The cracking moment and the yield moment are calculated by fiber section analysis. Rotations corresponding to the yield moments are calculated by the Sugano's equation (1973). The rotation at the peak moment θ_u and the rotation at zero moment θ_0 are assumed 0.03rad and 0.10rad respectively. That is to say, the members are assumed to be ductile based on the guideline's lateral reinforcing. To simplify the problem, the same pair of θ_u and θ_0 is used for all of members. The stiffness after yield is defined as K_1 times 0.001. The first-mode period T_1 of the structure from an eigen-value analysis is 0.813 sec. The structure is damped by 5 % coefficient for the first mode, but the damping force of each member is changed in proportion to the instantaneous stiffness of the member. The P-D effects are considered using a geometric stiffness formulation.

Figure 7 shows results of inelastic pushover analyses based on the horizontal load distribution given by the guideline's design. The pushover analyses do not incorporate either strength deterioration or P-D effects. The relationships between shear force ratio C_1 and inter-story drift

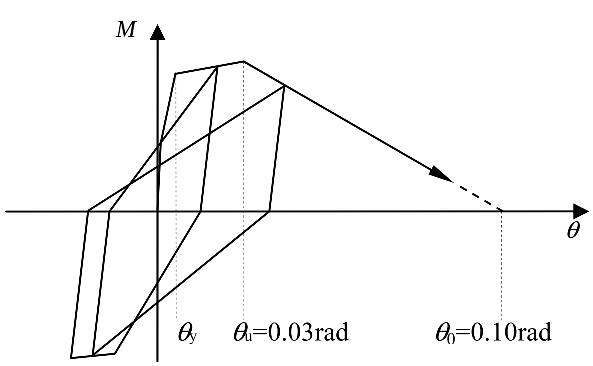

Fig. 6: Characteristics of rotational springs

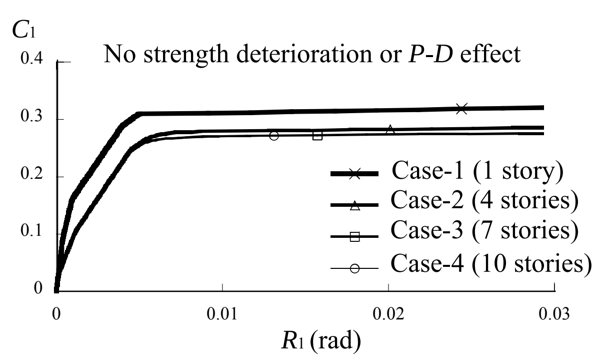

Fig. 7: Results of pushover analysis

ratio R_1 of the first story are very close in Case-2, Case-3 and Case-4. This means that the members of the partial mechanism extents reach yielding at the level of stress decided by the guideline's design. Case-1, which the columns of the fist story hinge at the two ends, is made as close as possible to other cases by adjusting the amount of main reinforcement of the columns.

2.2 Ground Motion and Hazard

A set of 40 ground motions (Medina 2003) is used for the incremental dynamic analyses. The ground motions were recorded in various earthquakes in California. The sites are categorized as Type-D site of NEHRP (183m/sec$<V_s<$366m/sec or 15$<N<$50, where V_s is shear wave velocity, N is N value of SPT test). The earthquake magnitudes are from 6.5 to 7.0, and the source-to-site distance ranges from 13 to 40 km. The selected intensity measure, IM, is the linear spectral acceleration at the first period of the structure using 5% damping, $S_a(T_1)$ (EERI 1989). For the site, this study assumes Van Nuys, which is located in Southern California and categorized as soil Type-D. The results of hazard analyses by PEER studies are available for Van Nuys. The use of $S_a(T_1)$ as IM implies that all the ground motions are scaled to a common $S_a(T_1)$ at the elastic period of the SDOF system. Thus, the frequency content of the ground motion cannot be considered explicitly. The large dispersion in spectral accelerations due to the different frequency content of the selected ground motions is illustrated in Figure 8, in which the ground motions are scaled to have the same spectral acceleration at T_1=0.813 sec. The dispersion increases with period, and response predictions may exhibit significant scatter depending on the extent of inelasticity, which leads to period elongation**.**

2.3 Incremental Dynamic Analysis (IDA) and Collapse Capacity

Figure 9 shows the concept of incremental dynamic analysis and collapse capacity. The left side of the figure represents the hazard curve for $S_a(T_1)$ and the right side represents the maximum inter-story drift ratio in all stories, IDR_{max}, which is computed for increments of $S_a(T_1)$.

Eventually, the system becomes unstable because of the large deformation that does not permit a further increase of $S_a(T_1)$. The $S_a(T_1)$ at the last stage is defined as the collapse capacity $S_{a,\ collapse}$. Note that IDR_{max} decreases several times as $S_a(T_1)$ increases. This return phenomenon occurs because during dynamic responses the pattern such as timing of yielding changes, or because the relationship between the positive value and the negative value in the time history changes in terms of the maximum.

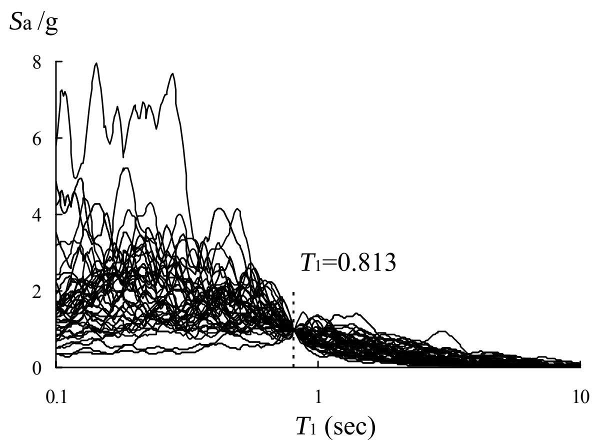

Fig. 8: Scaled acceleration spectra

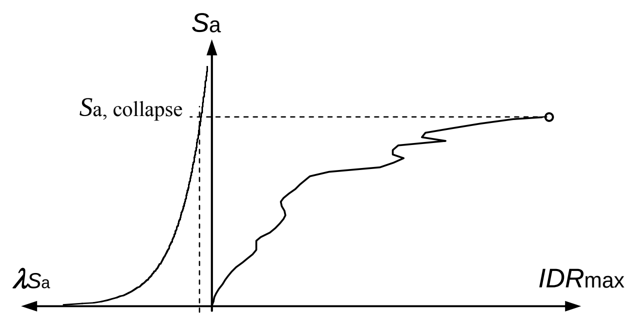

Fig. 9: Collapse capacity

2.4 Statistics of Results from Incremental Dynamic Analyses

Figure 10 shows the results of the incremental dynamic analyses for the set of 40 ground motions. The vertical axis is the intensity measure IM of the ground motion (i.e. $S_a(T_1)$) and the horizontal axis is the engineering demand parameter, EDP (in this case, the maximum inter-story drift ratio in all stories, IDR_{max}). In Figure 10, the individual incremental dynamic analyses are represented by gray lines, whereas the 50th and 84th curves are indicated with black lines.

For these dispersed data, EDP-direction statistics and IM-direction statistics can be conducted. For vulnerability curves (EDP given S_a) EDP-direction statistics is used, and for collapse statistics (probability of collapse given S_a) IM-direction statistics is used.

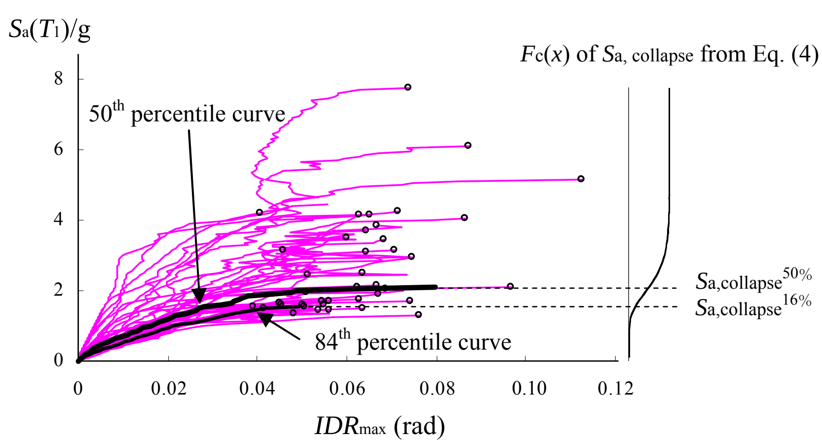

Fig. 10: A set of results from incremental dynamic analyses (Case-2)

2.4.1 Collapse Fragility Curve and Probability of Collapse

The collapse fragility curves $F_c(x)$ are obtained by IM-direction statistics for collapse capacity data. Thus, the fragility curve can be expressed by

$$F_c(x) = P\left[S_{a,\,collapse} \le x\right] \tag{1}$$

$F_c(x)$ can be defined as the probability that $S_{a,\,collapse}$ is less than or equal to x.

If the collapse fragility curve $F_c(x)$ for a given system has been determined, probabilistic collapse assessment can be carried out according to the following equation:

$$\lambda_{collapse} = \int_0^{\infty} F_c(x) \left| d\lambda_{Sa}(x) \right| \tag{2}$$

where $\lambda_{collapse}$ is mean annual frequency of collapse, $\lambda_{Sa(x)}$ is mean annual frequency of S_a exceeding x.

The fragility curve, $F_c(x)$, can be obtained by fitting a lognormal distribution to the collapse capacity data for the 40 ground motion. The lognormal distribution is a logical selection for several reasons: (a) most of the individual collapse capacity data has a skewed distribution with a longer tail for upper values, (b) collapse capacity values are always positive and, (c) previous studies have associated the distribution of spectral acceleration and the response of a nonlinear structure (in terms of EDP) to lognormal distributions (Shome and Cornell, 1999).

In general, the mean and the standard deviation of the natural logarithm of sample are used to define the entirely moderate shape. The result represents very close fitting around median but also represents errors in both sides of the median. In this case, because $F_c(x)$ is combined with the differentiated $\lambda_{Sa(x)}$ (i.e. d $\lambda_{Sa(x)}$, annual frequency of S_a of x) as expressed in Eq.(2), it can be reasonable to fit the portion for smaller percentile than median, which is combined with relatively large $d\lambda_{Sa(x)}$. Thus, in this study, the median of the natural logarithm of the data, $\mathrm{Ln}(S_{a,\,collapse})^{50\%}$ and the equivalent dispersion δ_{eq} of the sample are used as parameters, where $\mathrm{Ln}(S_{a,\,collapse})^{50\%}$ corresponds to the natural logarithm of the median $S_{a,collapse}^{50\%}$. By adopting the difference between $\mathrm{Ln}(S_{a,\,collapse})^{50\%}$ and $\mathrm{Ln}(S_{a,\,collapse})^{16\%}$ as δ_{eq}, δ_{eq} and $F_c(x)$, which focus on the portion for smaller percentile than median, can be calculated by

$$\delta_{eq} = \mathrm{Ln}\left(\frac{S_{a,\,collapse}{}^{50\%}}{S_{a,\,collapse}{}^{16\%}}\right) \tag{3}$$

$$F_c(x) = \Phi\left(\frac{\mathrm{Ln}(x) - \mathrm{Ln}(S_{a,\,collapse}{}^{50\%})}{\delta_{eq}}\right) \tag{4}$$

where Φ is the cumulative normal distribution function.

2.4.2 Vulnerability Curves for EDP

For the vulnerability curve, which means the EDP given $S_a(T_1)$, the "counted" EDP-direction statistics is adopted because of the incompleteness of the dataset after one or more ground motions produce collapse. For a set of 40 ground motions, the average of the 20th and 21st sorted value is taken as the median (50th percentile) and the 34th sorted value is taken as the 84th percentile. The median EDP curve at different intensity levels terminates when 50% of ground motions have led to collapse of the frame. In Figure 10, the percentile curves are also shown. The ends of the median EDP curve and the 84th percentile EDP curve are close to $S_{a,collapse}{}^{50\%}$ and $S_{a,collapse}{}^{16\%}$ that are produced by IM-direction statistics for the collapse capacity data, respectively.

Estimating statistically the EDP curves is useful for several purposes. It can be used to assess performances at a given hazard level, for example the relevant design basis calling for "the 84th percentile demand" etc., raging from EDP based damage control to collapse.

3. APPROACH FOR ESTIMATING THE PERFORMANCE OF STRUCTURE

3.1 Influences of Mechanism Control on EDP Curve

For all hinges in the mechanism extents, Figure 11 (1) shows the median (50th percentile) curves of the sum of hysteretic energy dissipation E_{sum} and Figure 11 (2) shows the median curves of the sum of the maximum plastic rotations ${}_p\theta_{max\_sum}$ (the maximum rotation θ_{max} minus the yielding rotation θ_y). The figures show that E_{sum} and ${}_p\theta_{max\_sum}$ are, respectively, going almost the same trace regardless of the size of the partial mechanism. This tendency suggests that the building consumes the same amount of energy during a seismic event regardless of the mechanism type, and then ${}_p\theta_{max\_sum}$ has a certain relationship with E_{sum} at a given hazard level.

However, collapse occurs at different $S_a(T_1)$ values. Although Case-2 deviates form Case-3 and Case-4 at the late stage, most of the plastic hinges of Case-2 are in the negative slope region of the skeleton curve at that stage. Figure 11 (3) shows the median IDR_{max} curves for the four cases. It is shown that, at a given hazard level, IDR_{max} of Case-1, which produces first-story mechanism, is the largest, and IDR_{max} decreases as the mechanism extent becomes larger. However, the differences tend to become small for Cases 3 and Case 4.

The average of the maximum plastic rotations ${}_p\theta_{max\_ave}$ can be expressed as ${}_p\theta_{max\_sum}/n$, where n is the number of the hinges. On the other hand, as shown in Figure 11 (2), ${}_p\theta_{max\_sum}$ is almost the same regardless of the size of the partial mechanism. Thus, it can be concluded that ${}_p\theta_{max\_ave}$ in the case of different extents of partial mechanisms can be inversely proportional to n, and then the tendency of IDR_{max} with different extents of mechanisms can be explained. That is to say, as the partial mechanisms are enlarged by three stories, the effect of the extent of partial mechanism on IDR_{max} decreases gradually.

An additional important observation can be made from Figure 12, which shows the distribution of the maximum inter-story drift ratio in each story IDR_i over the 12 stories. In Case-4 with the 10-story partial mechanism, the IDR_i values in the lower area are very close to those of Case-3, not only because the increase in the number of plastic hinges is small but also because the hinges in the upper area of the partial mechanism do not dissipate much energy. This phenomenon suggests that the energy dissipation concentrates in the lower area and is not being shared equally across the mechanism as the number of stories becomes large.

3.2 Influence of Mechanism Control on the Probability of Collapse

The collapse fragility curves are obtained from Eq.(4) by IM-direction statistics for collapse capacity data. Figure 13 shows the fragility curves of the four cases. At a given hazard level, i.e., $S_a(T_1)$, the probability of collapse becomes smaller as the partial mechanism extent becomes larger. However, the differences tend to become small, too, as the partial mechanism takes over a significant area of the structure (Cases 3 and 4).

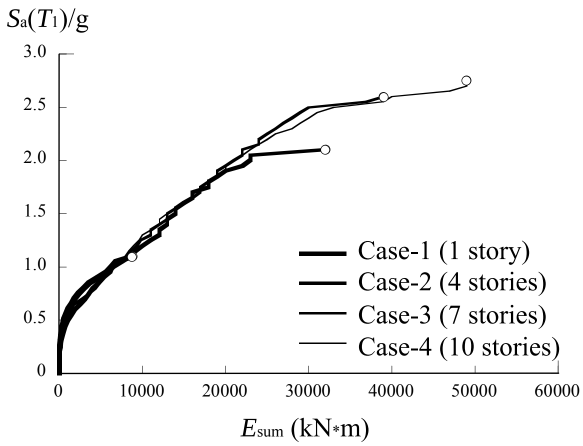

(1) Sum of hysteretic energy dissipation in all hinges

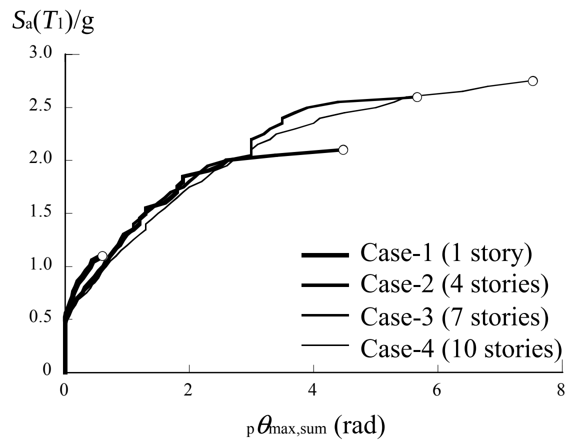

(2) Sum of maximum plastic rotations in all hinges

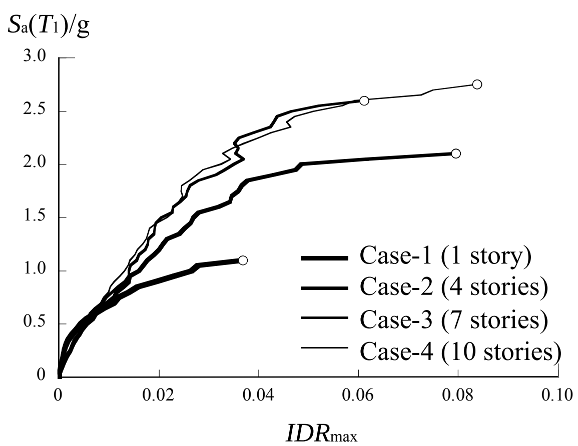

(3) Maximum inter-story drift ratio

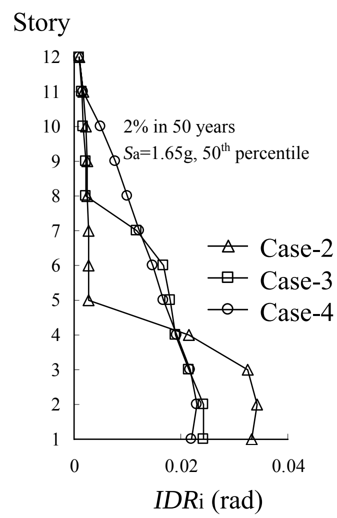

Fig. 11: Median 50th pecentile curves for EDP

Fig. 12: *IDR*i distributions

The fragility curves are combined with the spectral acceleration hazard curves to provide mean annual frequencies of collapse $\lambda_{\text{collapse}}$, as expressed in Eq.(2). The spectral acceleration hazard curve in Figure 14 is obtained using results of hazard analyses for Van Nuys (Somerville and Cornell 2002). Thus, the mean annual frequency of collapse, $\lambda_{\text{collapse}}$ in each case can be obtained by these conditions and numerical integration.

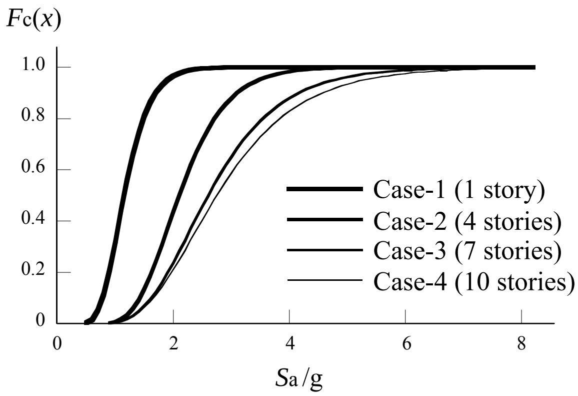

Fig. 13: Fragility curves of collapse capacity

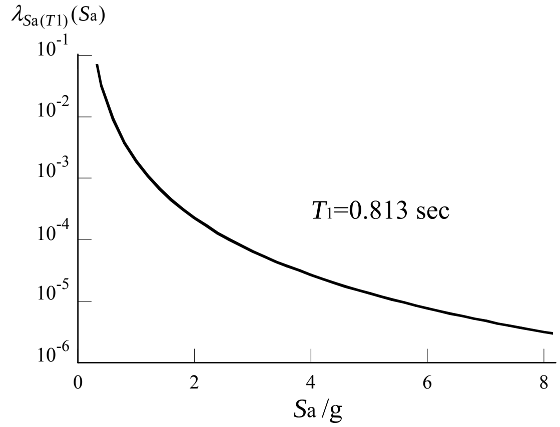

Fig. 14: Hazard curve at Van Nuys

In addition, assuming a Poisson process, the probability of collapse in t years is given by

$$P(\text{collapse}|\, t) = 1 - \exp(-\lambda_{\text{collapse}} \cdot t) \tag{5}$$

Figure 15 shows the probabilities of collapse in 1 year and 50 years for each case, where the probability in 1 year means the annual hazard. For Case-1 with fist-story mechanism, the probabilities in 1 year and 50 years are conspicuously high compared to other cases. For Case-2 with four-story mechanism, the risk of collapse is mitigated drastically. On the other hand, the collapse probability decreases only slightly as the extent of the partial mechanism grows beyond four stories. This can be explained by tendency of the collapse fragility curves combined with the site hazard curve.

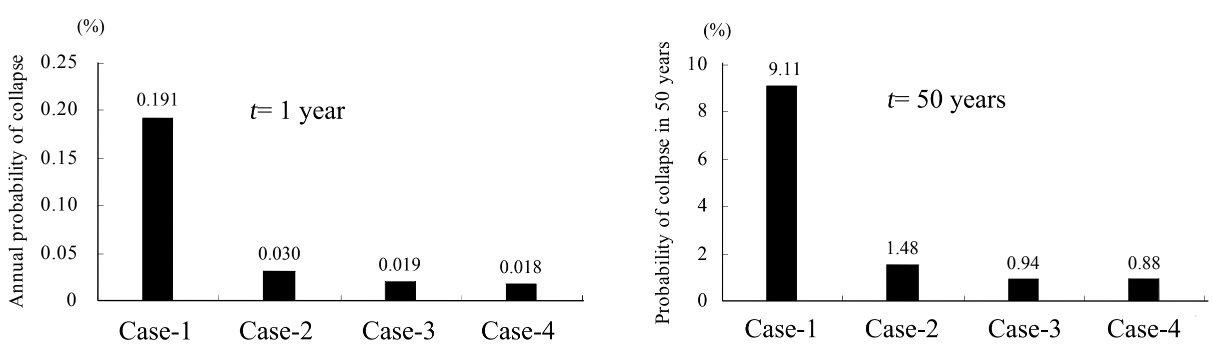

Fig. 15: Annual probabilities of collapse and probabilities of collapse in 50 years

4. CONCLUSIONS

In this study, twelve-story reinforced concrete frame structures were considered based on the mechanism control that intends to keep the upper part of building intact after earthquakes. The structure was originally designed by the ultimate strength concept and the procedures given by AIJ's guidelines (1990). For the analyses, assuming the additional strengthening for the upper part of this structure and using elastic members in the area, the partial mechanism was forced. From the results of these analyses, the following observations can be made.

(1) EDP-direction statistics

In this study, three EDP are considered as follows:

The sum of the hysteretic energy dissipations of all hinges E_{sum} and the sum of the maximum plastic rotations of all hinges ${}_p\theta_{max\_sum}$ at a given hazard level tend to be the same regardless of the size of the partial mechanism, respectively.

On the other hand, the maximum inter-story drift over all stories IDR_{max} decreases as the mechanism extent becomes large. However, simultaneously, the differences tend to become small. The reason can be explain from 1) the average of maximum plastic rotation ${}_p\theta_{max\_ave}$ is inversely proportional to the number of hinges n, and 2) in the case with the 10-story partial mechanism, the maximum inter-story drift in individual stories IDR_i becomes relatively large in the lower area of the partial mechanism. Thus, IDR_{max} of the case with the 10-story partial mechanism becomes very close to that of the case with the 7-story partial mechanism at a given hazard level, not only because the increase in the number of plastic hinges is small but also because the hinges in the upper area of the partial mechanism do not dissipate much energy.

(2) IM-direction statistics

A method was illustrated that evaluates the probability of collapse in t years by using the spectral acceleration hazard curve and the collapse fragility curve. The probabilities of the cases with different extents of partial mechanisms were compared.

As a result, it was shown that the probability of collapse is reduced as the mechanism extent becomes large. However, the collapse probability decreases only slightly as the extent of the partial mechanism grows beyond four stories.

Design based on mechanism control could become an option for performance based design, which should satisfy diverse demands from stakeholders and residents. Reducing the number of stories involved in the mechanism can produce benefits in terms of the repair process from earthquakes and even the construction process (see item 1). In this research, it is suggested that involving a certain number of stories in the mechanism is very important, but the impact on improving the seismic performance reaches a ceiling as concluded above. In the near future, performance based design procedure is expected to be developed that consider the balance between the seismic performance and the benefits from mechanism control.

ACKNOWLEDGEMENT

The authors acknowledge the suggestions of Farzin Zareian, Paul Cordova, Jorge Ruiz-Garcia, Hassameddin Aslani and Jack Baker of Stanford University. The helpful suggestions and assistance of Professor Masayoshi Nakashima of Kyoto University were also greatly appreciated.

REFERENCES

AIJ (1990), “Design Guidelines for Earthquake Resistant Reinforced Concrete Buildings Based on Ultimate Strength Concept”.

EERI Committee on Seismic Risk (1989), “The basics Risk Analysis”, Earthquake Spectra, 5 (4), 675-702.

Farzin Z., Ibarra, L.F., and Krawinkler, H. (2004), “Seismic Demands and Capacities of Single-Story and Low-Rise Multi-Story Woodframe Structures”, 13th WCEE, Paper No. 2144.

Federal Emergency Management Agency “Prestandard and Commentary for the Seismic Rehabilitation of Buildings (FEMA356/November2000)”.

Ibarra, L. F., and Krawinkler, H., (2004), “Global Collapse of Deteriorating MDOF Systems”, 13th WCEE, Paper No. 116.

Medina, R. (2003), ”Seismic Demands for Nondeteriorating Frame Structures and Their Dependence on Ground Motions”, Ph. D. thesis, Stanford University.

Paulay, T. (1986), “A Critique of the special Provisions for Seismic Design of the Building Code Requirements for Reinforced Concrete (ACI 318-83)”, TECHNICAL PAPER, ACI Journal, pp.274-283, March-April.

Shome, N., and Cornell, C.A. (1998), “Earthquakes, Records, and Nonlinear Responses”, Earthquake Spectra, 14 (3), 469-500.

Somerville P., Cornell, C.A. (2002), “Ground Motion time histories for the Van Nuys Building, PEER Methodology Testbeds Project, URS Corporation, Pasadena, CA.
Sugano, S. (1973), “Study on Hysteretic Behavior of Members of Reinforced Concrete Members”, Concrete Journal (in Japanese), Vol.11, No.2.
Takeda, T. , Sozen, M. A., and Nielsen, N. N. (1970), ”Reinforced Concrete Response to Simulated Earthquakes”, Journal of the Structure Division, ASCE, ST12, pp. 2557-2573.
Vamvatsikos, D., and Cornell, C.A. (2002), “Incremental Dynamic Analysis”, Earthquake Engineering and Structural Dynamics, 31, 3, 491-514.

SESSION 10: STATE OF DESIGN PRACTICE

Chaired by

♦ Jose Pincheira and Koichi Kusunoki ♦

SESSION 11: GENERAL DISCUSSIONS AND RESOLUTIONS

Chaired by

♦ Jack Moehle and Toshimi Kabeyasawa ♦

RESOLUTIONS

Existing hazardous buildings are the number one seismic safety problem in the world. Older-type reinforced concrete buildings represent a significant percentage of these structures that have yet to be addressed in a systematic way. Numerous earthquakes worldwide (e.g., 1994 Northridge, California; 1995 Hyogo-ken Nambu, Japan; 1999 Chi Chi, Taiwan; 1999 Duzce, Turkey) have demonstrated the collapse risk of this class of buildings. Numerous recent earthquakes in Japan, the U.S., and elsewhere are reminders of the need for research on the realistic simulation of predicting the collapse behavior of existing hazardous buildings under extreme motions so that at-risk buildings can be identified and upgraded.

The papers presented at The First NEES/E-Defense Workshop on Collapse Simulation of Reinforced Concrete Building Structures demonstrate the progress being made in experimental and analytical simulation of collapse behavior. Important outcomes of the Workshop include

(1) recognition that important research on seismic collapse simulation of reinforced concrete buildings is under way in the U.S., Japan, and other countries — in particular, participation of researchers from Canada and Taiwan in this workshop importantly enhanced knowledge transfer;

(2) better understanding of the present state of knowledge and practice of collapse simulation, and the research needs for the future;

(3) detailed understanding of the current test plans on relevant subjects worldwide;

(4) detailed understanding of past experimental and analytical research on structures and members, especially reinforced concrete columns, walls, and the dynamic behavior of structures to collapse;

(5) better understanding of the practical application of simulation or retrofitting methods; and

(6) identification of common areas of concern, and areas of needed advancement, such as realistic testing and rigorous analytical modeling on collapse behavior.

The Workshop was a successful continuation of the 1999–2003 U.S.-Japan Workshops on Performance-Based Earthquake Engineering Methodology for Reinforced Concrete Building Structures. The success at this Workshop suggests that the participating countries will benefit from continued cooperation. The reasons for continued cooperation are that

(1) the participating countries have a shared need to develop improved methods for seismic design and evaluation;
(2) in Japan and the U.S., and elsewhere, there is a need for integrated analytical and experimental approaches, which was promoted in this meeting format; and
(3) each side brings unique data, experience, knowledge, and facilities, the sharing of which benefits all.

These discussions are best accomplished through face-to-face meetings of extended duration such as occur in a workshop format. Therefore, the following recommendations are offered:

(1) Because of the rapid rate at which new information and applications are being achieved, the importance of advances to Japan, the U.S., and elsewhere, and the success of the first Workshop, the participants recommend that the second NEES/E-Defense Workshop on Collapse Simulation of Reinforced Concrete Building Structures be organized next year. Consideration should be given to convening the meeting to coincide with a major international conference or major scheduled test at E-Defense or a NEES laboratory.
(2) At the second workshop, several topics for focused discussion should be considered, including the following:
    (a) realistic experimental verification for simulating collapse behavior
    (b) simplified and rigorous analytical methods for simulating collapse behavior
    (c) ultimate safety in performance-based design against an extreme motion
    (d) seismic evaluation and retrofit of existing buildings emphasizing reduction of collapse risk
    (e) case studies of existing buildings, including applications of seismic assessment and upgrading in professional practice
    (f) observations from earthquakes
(3) Cooperative activities between individual participants from the U.S. and Japan and from other countries are encouraged to address problems of mutual concern. Efforts should be undertaken to facilitate exchange of personnel, including students, faculty, and professional researchers and practitioners, as well as of information on technical issues and applications. Funding agencies are encouraged to support these activities.

PEER REPORTS

PEER reports are available from the National Information Service for Earthquake Engineering (NISEE). To order PEER reports, please contact the Pacific Earthquake Engineering Research Center, 1301 South 46th Street, Richmond, California 94804-4698. Tel.: (510) 231-9468; Fax: (510) 231-9 461.

PEER 2005/10 *First NEES/E-Defense Workshop on Collapse Simulation of Reinforced Concrete Building Structures.* September 2005.

PEER 2005/06 *Global Collapse of Frame Structures under Seismic Excitations*. Luis F. Ibarra and Helmut Krawinkler. September 2005.

PEER 2005/01 *Empirical Characterization of Site Conditions on Strong Ground Motion.* Jonathan P. Stewart, Yoojoong Choi, and Robert W. Graves. June 2005.

PEER 2004/09 *Electrical Substation Equipment Interaction: Experimental Rigid Conductor Studies.* Christopher Stearns and André Filiatrault. February 2005.

PEER 2004/08 *Seismic Qualification and Fragility Testing of Line Break 550-kV Disconnect Switches.* Shakhzod M. Takhirov, Gregory L. Fenves, and Eric Fujisaki. January 2005.

PEER 2004/07 *Ground Motions for Earthquake Simulator Qualification of Electrical Substation Equipment.* Shakhzod M. Takhirov, Gregory L. Fenves, Eric Fujisaki, and Don Clyde. January 2005.

PEER 2004/06 *Performance-Based Regulation and Regulatory Regimes.* Peter J. May and Chris Koski. September 2004.

PEER 2004/05 *Performance-Based Seismic Design Concepts and Implementation: Proceedings of an International Workshop.* Peter Fajfar and Helmut Krawinkler, editors. September 2004.

PEER 2004/04 *Seismic Performance of an Instrumented Tilt-up Wall Building.* James C. Anderson and Vitelmo V. Bertero. July 2004.

PEER 2004/03 *Evaluation and Application of Concrete Tilt-up Assessment Methodologies.* Timothy Graf and James O. Malley. October 2004.

PEER 2004/02 *Analytical Investigations of New Methods for Reducing Residual Displacements of Reinforced Concrete Bridge Columns.* Junichi Sakai and Stephen A. Mahin. August 2004.

PEER 2004/01 *Seismic Performance of Masonry Buildings and Design Implications.* Kerri Anne Taeko Tokoro, James C. Anderson, and Vitelmo V. Bertero. February 2004.

PEER 2003/18 *Performance Models for Flexural Damage in Reinforced Concrete Columns.* Michael Berry and Marc Eberhard. August 2003.

PEER 2003/17 *Predicting Earthquake Damage in Older Reinforced Concrete Beam-Column Joints.* Catherine Pagni and Laura Lowes. October 2004.

PEER 2003/16 *Seismic Demands for Performance-Based Design of Bridges.* Kevin Mackie and Božidar Stojadinovi . August 2003.

PEER 2003/15 *Seismic Demands for Nondeteriorating Frame Structures and Their Dependence on Ground Motions.* Ricardo Antonio Medina and Helmut Krawinkler. May 2004.

PEER 2003/14 *Finite Element Reliability and Sensitivity Methods for Performance-Based Earthquake Engineering.* Terje Haukaas and Armen Der Kiureghian. April 2004.

PEER 2003/13 *Effects of Connection Hysteretic Degradation on the Seismic Behavior of Steel Moment-Resisting Frames.* Janise E. Rodgers and Stephen A. Mahin. March 2004.

PEER 2003/12 *Implementation Manual for the Seismic Protection of Laboratory Contents: Format and Case Studies.* William T. Holmes and Mary C. Comerio. October 2003.

PEER 2003/11 *Fifth U.S.-Japan Workshop on Performance-Based Earthquake Engineering Methodology for Reinforced Concrete Building Structures.* February 2004.

PEER 2003/10 *A Beam-Column Joint Model for Simulating the Earthquake Response of Reinforced Concrete Frames.* Laura N. Lowes, Nilanjan Mitra, and Arash Altoontash. February 2004.

PEER 2003/09 *Sequencing Repairs after an Earthquake: An Economic Approach.* Marco Casari and Simon J. Wilkie. April 2004.

PEER 2003/08 *A Technical Framework for Probability-Based Demand and Capacity Factor Design (DCFD) Seismic Formats*. Fatemeh Jalayer and C. Allin Cornell. November 2003.

PEER 2003/07 *Uncertainty Specification and Propagation for Loss Estimation Using FOSM Methods.* Jack W. Baker and C. Allin Cornell. September 2003.

PEER 2003/06 *Performance of Circular Reinforced Concrete Bridge Columns under Bidirectional Earthquake Loading*. Mahmoud M. Hachem, Stephen A. Mahin, and Jack P. Moehle. February 2003.

PEER 2003/05 *Response Assessment for Building-Specific Loss Estimation.* Eduardo Miranda and Shahram Taghavi. September 2003.

PEER 2003/04 *Experimental Assessment of Columns with Short Lap Splices Subjected to Cyclic Loads*. Murat Melek, John W. Wallace, and Joel Conte. April 2003.

PEER 2003/03 *Probabilistic Response Assessment for Building-Specific Loss Estimation.* Eduardo Miranda and Hesameddin Aslani. September 2003.

PEER 2003/02 *Software Framework for Collaborative Development of Nonlinear Dynamic Analysis Program.* Jun Peng and Kincho H. Law. September 2003.

PEER 2003/01 *Shake Table Tests and Analytical Studies on the Gravity Load Collapse of Reinforced Concrete Frames.* Kenneth John Elwood and Jack P. Moehle. November 2003.

PEER 2002/24 *Performance of Beam to Column Bridge Joints Subjected to a Large Velocity Pulse.* Natalie Gibson, André Filiatrault, and Scott A. Ashford. April 2002.

PEER 2002/23 *Effects of Large Velocity Pulses on Reinforced Concrete Bridge Columns.* Greg L. Orozco and Scott A. Ashford. April 2002.

PEER 2002/22 *Characterization of Large Velocity Pulses for Laboratory Testing.* Kenneth E. Cox and Scott A. Ashford. April 2002.

PEER 2002/21 *Fourth U.S.-Japan Workshop on Performance-Based Earthquake Engineering Methodology for Reinforced Concrete Building Structures*. December 2002.

PEER 2002/20 *Barriers to Adoption and Implementation of PBEE Innovations.* Peter J. May. August 2002.

PEER 2002/19 *Economic-Engineered Integrated Models for Earthquakes: Socioeconomic Impacts.* Peter Gordon, James E. Moore II, and Harry W. Richardson. July 2002.

PEER 2002/18 *Assessment of Reinforced Concrete Building Exterior Joints with Substandard Details.* Chris P. Pantelides, Jon Hansen, Justin Nadauld, and Lawrence D. Reaveley. May 2002.

PEER 2002/17 *Structural Characterization and Seismic Response Analysis of a Highway Overcrossing Equipped with Elastomeric Bearings and Fluid Dampers: A Case Study.* Nicos Makris and Jian Zhang. November 2002.

PEER 2002/16 *Estimation of Uncertainty in Geotechnical Properties for Performance-Based Earthquake Engineering.* Allen L. Jones, Steven L. Kramer, and Pedro Arduino. December 2002.

PEER 2002/15 *Seismic Behavior of Bridge Columns Subjected to Various Loading Patterns.* Asadollah Esmaeily-Gh. and Yan Xiao. December 2002.

PEER 2002/14 *Inelastic Seismic Response of Extended Pile Shaft Supported Bridge Structures.* T.C. Hutchinson, R.W. Boulanger, Y.H. Chai, and I.M. Idriss. December 2002.

PEER 2002/13 *Probabilistic Models and Fragility Estimates for Bridge Components and Systems.* Paolo Gardoni, Armen Der Kiureghian, and Khalid M. Mosalam. June 2002.

PEER 2002/12 *Effects of Fault Dip and Slip Rake on Near-Source Ground Motions: Why Chi-Chi Was a Relatively Mild M7.6 Earthquake.* Brad T. Aagaard, John F. Hall, and Thomas H. Heaton. December 2002.

PEER 2002/11 *Analytical and Experimental Study of Fiber-Reinforced Strip Isolators*. James M. Kelly and Shakhzod M. Takhirov. September 2002.

PEER 2002/10 *Centrifuge Modeling of Settlement and Lateral Spreading with Comparisons to Numerical Analyses***.** Sivapalan Gajan and Bruce L. Kutter. January 2003.

PEER 2002/09 *Documentation and Analysis of Field Case Histories of Seismic Compression during the 1994 Northridge, California, Earthquake.* Jonathan P. Stewart, Patrick M. Smith, Daniel H. Whang, and Jonathan D. Bray. October 2002.

PEER 2002/08 *Component Testing, Stability Analysis and Characterization of Buckling-Restrained Unbonded Braces™.* Cameron Black, Nicos Makris, and Ian Aiken. September 2002.

PEER 2002/07 *Seismic Performance of Pile-Wharf Connections.* Charles W. Roeder, Robert Graff, Jennifer Soderstrom, and Jun Han Yoo. December 2001.

PEER 2002/06 *The Use of Benefit-Cost Analysis for Evaluation of Performance-Based Earthquake Engineering Decisions*. Richard O. Zerbe and Anthony Falit-Baiamonte. September 2001.

PEER 2002/05 *Guidelines, Specifications, and Seismic Performance Characterization of Nonstructural Building Components and Equipment*. André Filiatrault, Constantin Christopoulos, and Christopher Stearns. September 2001.

PEER 2002/04 *Consortium of Organizations for Strong-Motion Observation Systems and the Pacific Earthquake Engineering Research Center Lifelines Program: Invited Workshop on Archiving and Web Dissemination of Geotechnical Data, 4–5 October 2001*. September 2002.

PEER 2002/03 *Investigation of Sensitivity of Building Loss Estimates to Major Uncertain Variables for the Van Nuys Testbed.* Keith A. Porter, James L. Beck, and Rustem V. Shaikhutdinov. August 2002.

PEER 2002/02 *The Third U.S.-Japan Workshop on Performance-Based Earthquake Engineering Methodology for Reinforced Concrete Building Structures*. July 2002.

PEER 2002/01 *Nonstructural Loss Estimation: The UC Berkeley Case Study.* Mary C. Comerio and John C. Stallmeyer. December 2001.

PEER 2001/16 *Statistics of SDF-System Estimate of Roof Displacement for Pushover Analysis of Buildings.* Anil K. Chopra, Rakesh K. Goel, and Chatpan Chintanapakdee. December 2001.

PEER 2001/15 *Damage to Bridges during the 2001 Nisqually Earthquake.* R. Tyler Ranf, Marc O. Eberhard, and Michael P. Berry. November 2001.

PEER 2001/14 *Rocking Response of Equipment Anchored to a Base Foundation.* Nicos Makris and Cameron J. Black. September 2001.

PEER 2001/13 *Modeling Soil Liquefaction Hazards for Performance-Based Earthquake Engineering.* Steven L. Kramer and Ahmed-W. Elgamal. February 2001.

PEER 2001/12 *Development of Geotechnical Capabilities in OpenSees.* Boris Jeremi . September 2001.

PEER 2001/11 *Analytical and Experimental Study of Fiber-Reinforced Elastomeric Isolators*. James M. Kelly and Shakhzod M. Takhirov. September 2001.

PEER 2001/10 *Amplification Factors for Spectral Acceleration in Active Regions.* Jonathan P. Stewart, Andrew H. Liu, Yoojoong Choi, and Mehmet B. Baturay. December 2001.

PEER 2001/09 *Ground Motion Evaluation Procedures for Performance-Based Design.* Jonathan P. Stewart, Shyh-Jeng Chiou, Jonathan D. Bray, Robert W. Graves, Paul G. Somerville, and Norman A. Abrahamson. September 2001.

PEER 2001/08 *Experimental and Computational Evaluation of Reinforced Concrete Bridge Beam-Column Connections for Seismic Performance*. Clay J. Naito, Jack P. Moehle, and Khalid M. Mosalam. November 2001.

PEER 2001/07 *The Rocking Spectrum and the Shortcomings of Design Guidelines.* Nicos Makris and Dimitrios Konstantinidis. August 2001.

PEER 2001/06 *Development of an Electrical Substation Equipment Performance Database for Evaluation of Equipment Fragilities*. Thalia Agnanos. April 1999.

PEER 2001/05 *Stiffness Analysis of Fiber-Reinforced Elastomeric Isolators.* Hsiang-Chuan Tsai and James M. Kelly. May 2001.

PEER 2001/04 *Organizational and Societal Considerations for Performance-Based Earthquake Engineering.* Peter J. May. April 2001.

PEER 2001/03 *A Modal Pushover Analysis Procedure to Estimate Seismic Demands for Buildings: Theory and Preliminary Evaluation.* Anil K. Chopra and Rakesh K. Goel. January 2001.

PEER 2001/02 *Seismic Response Analysis of Highway Overcrossings Including Soil-Structure Interaction.* Jian Zhang and Nicos Makris. March 2001.

PEER 2001/01 *Experimental Study of Large Seismic Steel Beam-to-Column Connections.* Egor P. Popov and Shakhzod M. Takhirov. November 2000.

PEER 2000/10 *The Second U.S.-Japan Workshop on Performance-Based Earthquake Engineering Methodology for Reinforced Concrete Building Structures.* March 2000.

PEER 2000/09 *Structural Engineering Reconnaissance of the August 17, 1999 Earthquake: Kocaeli (Izmit), Turkey.* Halil Sezen, Kenneth J. Elwood, Andrew S. Whittaker, Khalid Mosalam, John J. Wallace, and John F. Stanton. December 2000.

PEER 2000/08 *Behavior of Reinforced Concrete Bridge Columns Having Varying Aspect Ratios and Varying Lengths of Confinement.* Anthony J. Calderone, Dawn E. Lehman, and Jack P. Moehle. January 2001.

PEER 2000/07 *Cover-Plate and Flange-Plate Reinforced Steel Moment-Resisting Connections.* Taejin Kim, Andrew S. Whittaker, Amir S. Gilani, Vitelmo V. Bertero, and Shakhzod M. Takhirov. September 2000.

PEER 2000/06 *Seismic Evaluation and Analysis of 230-kV Disconnect Switches.* Amir S. J. Gilani, Andrew S. Whittaker, Gregory L. Fenves, Chun-Hao Chen, Henry Ho, and Eric Fujisaki. July 2000.

PEER 2000/05 *Performance-Based Evaluation of Exterior Reinforced Concrete Building Joints for Seismic Excitation.* Chandra Clyde, Chris P. Pantelides, and Lawrence D. Reaveley. July 2000.

PEER 2000/04 *An Evaluation of Seismic Energy Demand: An Attenuation Approach.* Chung-Che Chou and Chia-Ming Uang. July 1999.

PEER 2000/03 *Framing Earthquake Retrofitting Decisions: The Case of Hillside Homes in Los Angeles.* Detlof von Winterfeldt, Nels Roselund, and Alicia Kitsuse. March 2000.

PEER 2000/02 *U.S.-Japan Workshop on the Effects of Near-Field Earthquake Shaking.* Andrew Whittaker, ed. July 2000.

PEER 2000/01 *Further Studies on Seismic Interaction in Interconnected Electrical Substation Equipment.* Armen Der Kiureghian, Kee-Jeung Hong, and Jerome L. Sackman. November 1999.

PEER 1999/14 *Seismic Evaluation and Retrofit of 230-kV Porcelain Transformer Bushings*. Amir S. Gilani, Andrew S. Whittaker, Gregory L. Fenves, and Eric Fujisaki. December 1999.

PEER 1999/13 *Building Vulnerability Studies: Modeling and Evaluation of Tilt-up and Steel Reinforced Concrete Buildings.* John W. Wallace, Jonathan P. Stewart, and Andrew S. Whittaker, editors. December 1999.

PEER 1999/12 *Rehabilitation of Nonductile RC Frame Building Using Encasement Plates and Energy-Dissipating Devices.* Mehrdad Sasani, Vitelmo V. Bertero, James C. Anderson. December 1999.

PEER 1999/11 *Performance Evaluation Database for Concrete Bridge Components and Systems under Simulated Seismic Loads.* Yael D. Hose and Frieder Seible. November 1999.

PEER 1999/10 *U.S.-Japan Workshop on Performance-Based Earthquake Engineering Methodology for Reinforced Concrete Building Structures.* December 1999.

PEER 1999/09 *Performance Improvement of Long Period Building Structures Subjected to Severe Pulse-Type Ground Motions*. James C. Anderson, Vitelmo V. Bertero, and Raul Bertero. October 1999.

PEER 1999/08 *Envelopes for Seismic Response Vectors.* Charles Menun and Armen Der Kiureghian. July 1999.

PEER 1999/07 *Documentation of Strengths and Weaknesses of Current Computer Analysis Methods for Seismic Performance of Reinforced Concrete Members.* William F. Cofer. November 1999.

PEER 1999/06 *Rocking Response and Overturning of Anchored Equipment under Seismic Excitations.* Nicos Makris and Jian Zhang. November 1999.

PEER 1999/05 *Seismic Evaluation of 550 kV Porcelain Transformer Bushings.* Amir S. Gilani, Andrew S. Whittaker, Gregory L. Fenves, and Eric Fujisaki. October 1999.

PEER 1999/04 *Adoption and Enforcement of Earthquake Risk-Reduction Measures.* Peter J. May, Raymond J. Burby, T. Jens Feeley, and Robert Wood.

PEER 1999/03 *Task 3 Characterization of Site Response General Site Categories*. Adrian Rodriguez-Marek, Jonathan D. Bray, and Norman Abrahamson. February 1999.

PEER 1999/02 *Capacity-Demand-Diagram Methods for Estimating Seismic Deformation of Inelastic Structures: SDF Systems*. Anil K. Chopra and Rakesh Goel. April 1999.

PEER 1999/01 *Interaction in Interconnected Electrical Substation Equipment Subjected to Earthquake Ground Motions.* Armen Der Kiureghian, Jerome L. Sackman, and Kee-Jeung Hong. February 1999.

PEER 1998/08 *Behavior and Failure Analysis of a Multiple-Frame Highway Bridge in the 1994 Northridge Earthquake.* Gregory L. Fenves and Michael Ellery. December 1998.

PEER 1998/07 *Empirical Evaluation of Inertial Soil-Structure Interaction Effects.* Jonathan P. Stewart, Raymond B. Seed, and Gregory L. Fenves. November 1998.

PEER 1998/06 *Effect of Damping Mechanisms on the Response of Seismic Isolated Structures.* Nicos Makris and Shih-Po Chang. November 1998.

PEER 1998/05 *Rocking Response and Overturning of Equipment under Horizontal Pulse-Type Motions.* Nicos Makris and Yiannis Roussos. October 1998.

PEER 1998/04 *Pacific Earthquake Engineering Research Invitational Workshop Proceedings, May 14–15, 1998: Defining the Links between Planning, Policy Analysis, Economics and Earthquake Engineering.* Mary Comerio and Peter Gordon. September 1998.

PEER 1998/03 *Repair/Upgrade Procedures for Welded Beam to Column Connections.* James C. Anderson and Xiaojing Duan. May 1998.

PEER 1998/02 *Seismic Evaluation of 196 kV Porcelain Transformer Bushings.* Amir S. Gilani, Juan W. Chavez, Gregory L. Fenves, and Andrew S. Whittaker. May 1998.

PEER 1998/01 *Seismic Performance of Well-Confined Concrete Bridge Columns.* Dawn E. Lehman and Jack P. Moehle. December 2000.